15 July 2005

Science

Vol. 309 No. 5733
Pages 337–520 $10

The Trypanosomatid Genomes

125 YEARS OF GLOBAL Science

AAAS

When you take it off, things get interesting.

Study dephosphorylation with the SignalScout™ Phosphatase Profiling System.

Studying protein phosphorylation is critical to understanding the regulation of normal cell growth. Our new SignalScout™ Phosphatase Profiling System* allows you to study dephosphorylation by Protein Tyrosine Phosphatases (PTPs). This system includes mammalian expression clones of human PTPs and matched substrate trapping mutants. We also offer a line of highly specific antibodies against protein phosphatases to help you to detect a phosphatase of interest.

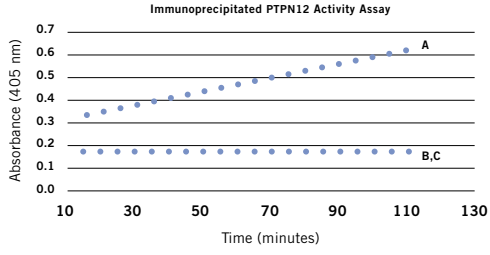

Trendlines and data points plotted for a pNPP phosphatase assay compare the activity of SignalScout™ PTPN12 Human Phosphatase Clone Vector (A, r^2=1.0) to a catalytically inactive mutant PTPN12 vector (B, r^2=.88) and to untransfected cells (C, r^2=0.95). The anti-c-Myc tag antibody was used for the immunoprecipitation.

Need More Information? Give Us A Call:

Stratagene USA and Canada
Order: (800) 424-5444 x3
Technical Services: (800) 894-1304

Stratagene Europe
Order: 00800-7000-7000
Technical Services: 00800-7400-7400

Stratagene Japan K.K.
Order: 03-5159-2060
Technical Services: 03-5159-2070

www.stratagene.com

Ask Us About These Great Products:

SignalScout™ ACP1v3 Human Phosphatase Vector	257001
SignalScout™ PTP4A2 (PRL2) Human Phosphatase Vector	257010
SignalScout™ PTP4A3v1 (PRL3) Human Phosphatase Vector	257013
SignalScout™ PTPN1 (PTP1B) Substrate Trapping Mutant Human Phosphatase Vector	257023
SignalScout™ PTPN12 Human Phosphatase Vector	257028
SignalScout™ PTPN12 Substrate Trapping Mutant Human Phosphatase Vector	257029
SignalScout™ PTPN7v2 (HePTPv2) Human Phosphatase Clone	257064
SignalScout™ PTPN7v2 (HePTPv2) Substrate Trapping Mutant Human Phosphatase Vector	257065

For a complete listing of anti-phosphatase antibodies, please visit: **www.stratagene.com/signaling**

*Patent pending.

STRATAGENE®

Now The Right Side Knows What The Left Side Is Doing.

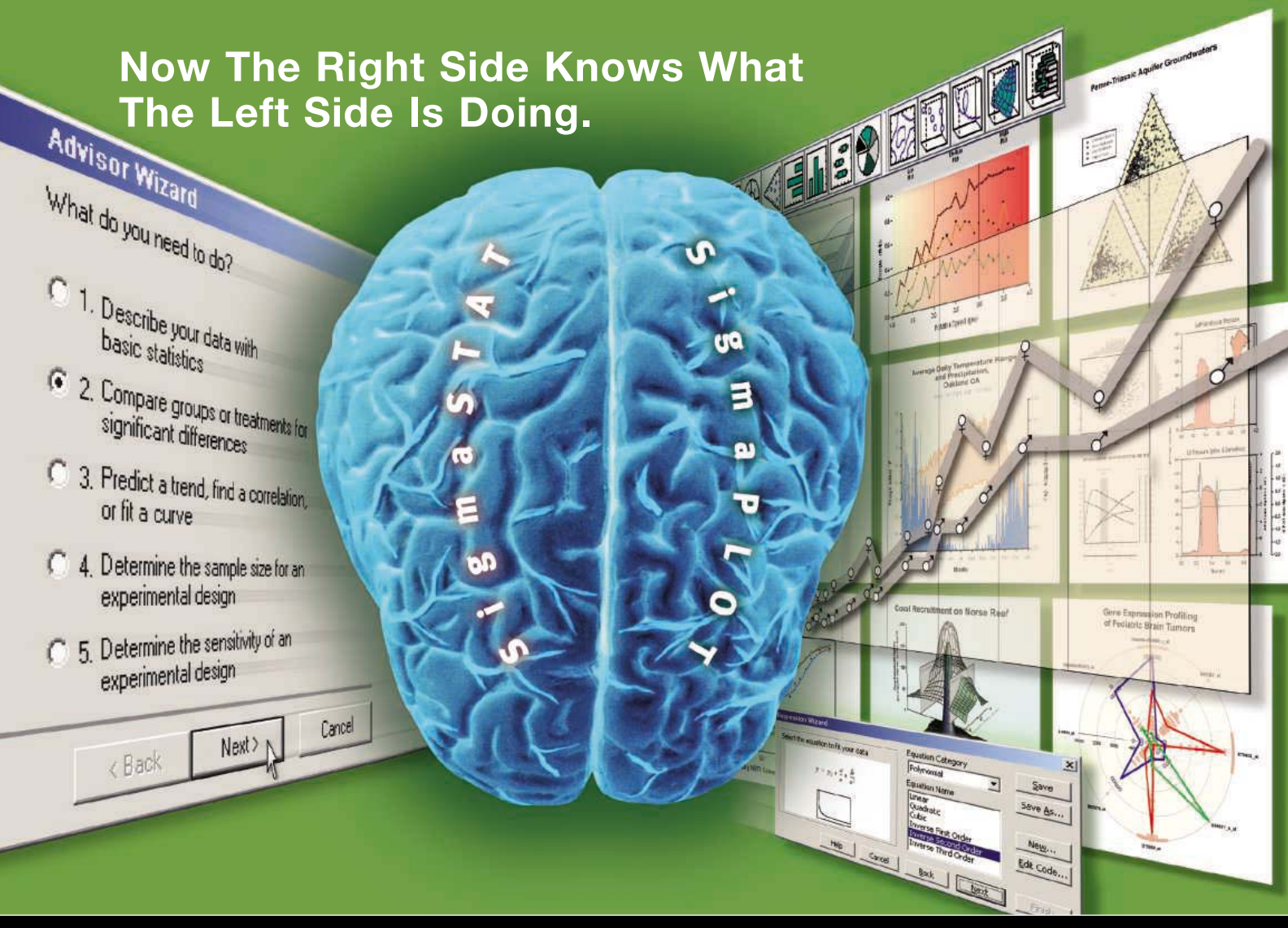

Combine the Powerful Statistical Output of SigmaStat with the Publication-quality Graph Creation of SigmaPlot

SigmaPlot is the award-winning technical graphing and data analysis software package used by more than 100,000 researchers worldwide who need to produce defensible research and create compelling graphs that clearly present their results for technical publications, presentations or the web. SigmaStat 3.1 now seamlessly integrates with SigmaPlot 9.0 for deeper statistical analysis within SigmaPlot's statistics menu.

SigmaPlot allows you to:

> Create graphs easily and publish your work anywhere
> Analyze and manage your data quickly and easily
> Choose over 80 different 2-D and 3-D graph types
> Customize every element of your graphs
> Instantly access SigmaPlot from Microsoft® Excel
> Streamline your work by automating repetitive tasks

SIGMAPLOT
Exact Graphs for Exact Science

Add SigmaStat 3.1 to get easy-to-use, expert statistical analysis within SigmaPlot!

SigmaStat guides you through your analysis:

> Suggests the appropriate statistical test
> Checks assumptions in the data to avoid statistical error
> If your data violates any of those assumptions, the Advisor Wizard suggests another test
> Generates an intelligent report that explains your results in plain English – not statistical jargon
> Even handles messy data with missing values

SIGMASTAT
Advisory Statistics for Scientists

With SigmaStat you'll have the expertise of a professional statistical consultant at your fingertips!

FREE ONLINE TUTORIALS & 30-DAY TRIAL SOFTWARE AVAILABLE AT WWW.SYSTAT.COM

SigmaScan®	TableCurve 2D	TableCurve 3D	PeakFit	SYSTAT
Automated Image Analysis	*Automated Curve Fitting Analysis*	*Automated Surface Fitting Analysis*	*Automated Peak Separation Analysis*	*Comprehensive Statistical Analysis*

adsci

graphic design by Guto Mesquita / castle photo: André Az

Fiocruz THE OSWALDO CRUZ FOUNDATION

Feet anchored in tradition, eyes turned to the future

Founded on May 25th 1900 under the name Federal Serum Therapy Institute, The Oswaldo Cruz Foundation (Fiocruz) was created with the mission of fighting Brazil's most important public health problems. It was in its laboratories in Rio de Janeiro that in 1909 Carlos Chagas discovered the disease that bears its name – Chagas disease, also known as American trypanosomiasis –, its pathogen (*Trypanosoma cruzi*) and the mechanisms of transmission by reduviid insects ("kissing bugs").

Nowadays, Fiocruz mission encompasses research, technological development and innovation; production of vaccines, drugs, reagents and diagnostic kits; clinical research; delivery of reference health services; education and training of human resources; information and communication; product and service quality control; and the implementation of social programs.

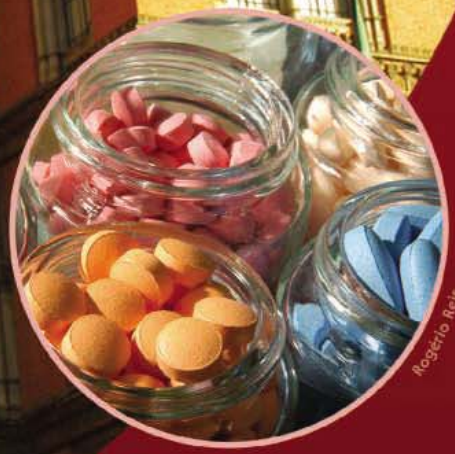

Colaborations

Fiocruz congratules the scientists, institutions and funding agencies that made the sequencing of the genomes reported in this issue of Science and is ready to collaborate in the development of new health interventions that are accessible, affordable and appropriate for developing countries.

Future directions

Fiocruz new Center for Technological Development in Health (CDTS in its Portuguese acronym) will start to be built in the Manguinhos campus in the end of 2005 and will be operational in 2008. Its facilities include technological platforms, animal experimentation facilities and flexible labs where Fiocruz will work in collaboration with public and private industrial sectors in the joint development of health products.

MOST CITED INSTITUTIONS IN CLINICAL MEDICINE
FIOCRUZ MS

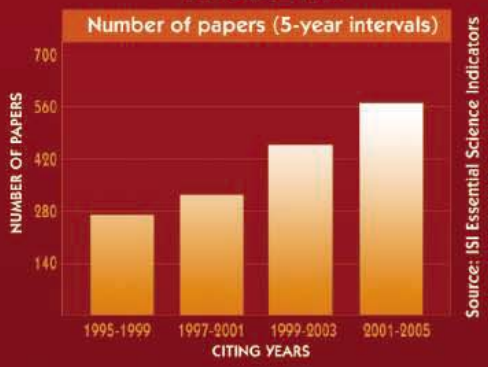

Research and development: high-quality

According to the Essential Science Indicators of the Institute for Scientific Information (ISI), Fiocruz is one of the most cited institutions in clinical medicine and publishes over 400 research papers per year in high-quality, peer-reviewed international journals.

Oswaldo Cruz Foundation (FIOCRUZ)
Av. Brasil 4365 – Manguinhos
Rio de Janeiro, RJ 21040-900 Brazil
Tel: +55-21- 2598-4242
Fax: +55-21-2260-6707
http://www.fiocruz.br

GE Healthcare

Why do 100,000 scientists trust GE Healthcare for all their protein purification needs?

Here's Ä clue.

To 100,000 scientists worldwide, the name ÄKTA™ has always meant outstanding protein purification, and now it's brought to you by GE Healthcare. With the ability to purify virtually 100% of all biomolecules, the ÄKTAdesign™ platform can handle the toughest of challenges. Whatever the scale, from laboratory, to process development and manufacturing, there's an ÄKTAdesign system to meet every need. All systems in the ÄKTAdesign family work with the intelligent UNICORN™ software, which makes it easy to control every stage of your purification processes. Accurate, reproducible results just take a little pure imagination.

Visit www.amershambiosciences.com/aktadesign

imagination at work

GE15-05

Science

Special Issue

Trypanosomatid Genomes

Volume 309
15 July 2005
Number 5733

Colored scanning electron micrograph of *Trypanosoma brucei* (blue) among red blood cells. A special section in this issue presents the genomes of three insect-transmitted trypanosomatid parasites that cause chronic and ultimately fatal infections in humans and livestock, for which few safe therapies exist. Several accompanying articles discuss trypanosomatid comparative biology and strategies for control. [Image: Eye of Science/Photo Researchers Inc.]

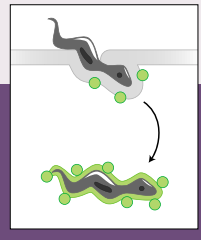

For related online content in STKE, see page 349 or go to www.sciencemag.org/sciext/tryp/

Departments

368

News of the Week

383

News Focus

Letters

Books *et al.*

Policy Forum

Contents continued

Systems Biology — Plasmid DNA Purification

Raising plasmid prep standards again — visual lysis control for greater confidence

New

Insufficient mixing of lysis buffer

Correct mixing of lysis buffer

Correct mixing of neutralization buffer

QIAGEN plasmid kits — now better than ever!

QIAGEN has consistently set the standard for plasmid purification, providing faster preps, higher throughput, more convenience, superior DNA quality for stringent applications, and contract production services. Now our enhanced plasmid prep kits offer even more:

- **Visual lysis control** — a simple color change during cell lysis (blue) and neutralization (colorless), ensures optimal mixing of buffers to give maximum yields of plasmid DNA
- **Color-coded buffer bottles** — easy identification of the correct buffer for added confidence
- **Streamlined handbooks and short protocols** — quickly find the information you need to get rapid results
- **Comprehensive plasmid resource site** — a one-stop Web site containing information on all aspects of plasmid purification at www.qiagen.com/goto/plasmidinfo

Purify your DNA with confidence — use QIAGEN plasmid kits with visual lysis control!

QIAGEN

Perspectives

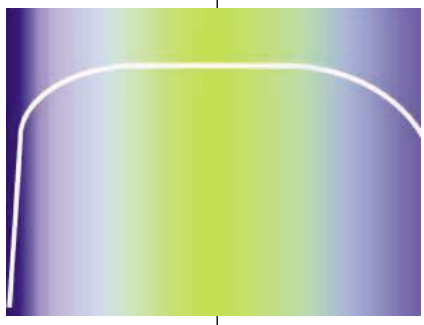

456

Science Express www.sciencexpress.org

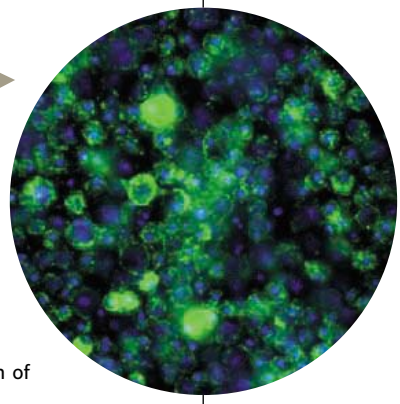

Brevia

Research Article

Reports

364 & 459

Contents continued

Shrimp Alkaline Phosphatase – My Requirements:

1. Must have high activity
2. 100% heat-inactivation...quickly
3. Cost effective and works in many different buffers and applications
4. An enzyme I can completely trust

Want proof? Visit www.getsapfacts.com

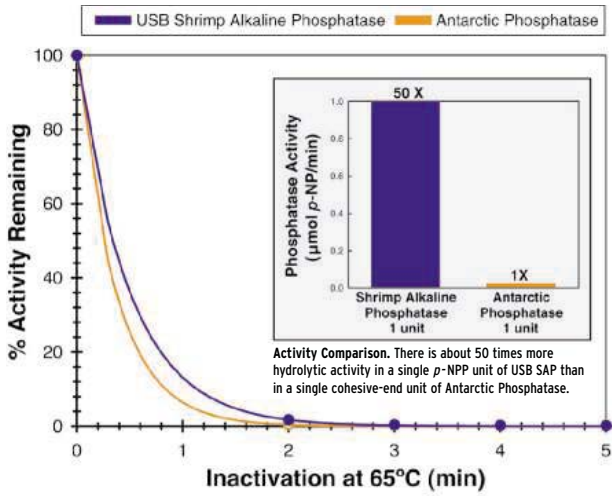

Activity Comparison. There is about 50 times more hydrolytic activity in a single *p*-NPP unit of USB SAP than in a single cohesive-end unit of Antarctic Phosphatase.

Heat inactivation of USB Shrimp Alkaline Phosphatase (SAP) and Antarctic Phosphatase. 20 cohesive-end units (0.2 *p*-NPP units) of each enzyme were diluted into assay buffer and incubated at 65°C. Percent activity remaining at indicated time points was measured by *p*-NPP assay. Complete heat-inactivation occurs within 5 minutes.

USB Shrimp Alkaline Phosphatase – The Benchmark Heat-Labile Alkaline Phosphatase.

Shrimp Alkaline Phosphatase was introduced by USB in the early 1990s as a novel enzyme that was every bit as active as calf intestinal alkaline phosphatase, but much easier to heat-inactivate. This feature of SAP made it the enzyme of choice because it is used directly in place of CIAP – with no need to change buffers or reaction conditions. SAP can be used directly in restriction enzyme digestions or with PCR products* prior to SNP analysis or DNA sequencing. Dephosphorylated vectors may be ligated without further purification. At USB, we know you need products made with integrity. Products that help you be more productive in the lab. Products like USB SAP. To get the facts on USB SAP, please visit www.getsapfacts.com.

usb
Fueling Innovation™

*ExoSAP-IT and the Exonuclease I/Shrimp Alkaline Phosphatase Method are covered by US Patent Nos. 5,741,676 and 5,756,285 and related patents. ExoSAP-IT is covered by US Patent Nos. 6,379,940 and 6,387,634.

800.321.9322 | www.usbweb.com

REPORTS CONTINUED

481

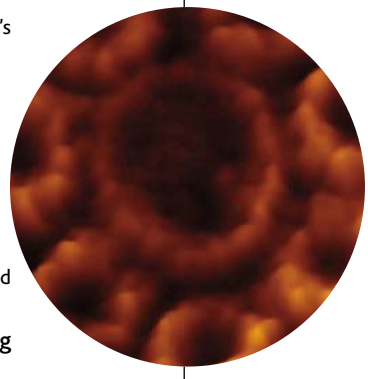

484

AAAS
ADVANCING SCIENCE, SERVING SOCIETY

SCIENCE (ISSN 0036-8075) is published weekly on Friday, except the last week in December, by the American Association for the Advancement of Science, 1200 New York Avenue, NW, Washington, DC 20005. Periodicals Mail postage (publication No. 484460) paid at Washington, DC, and additional mailing offices. Domestic individual membership and subscription (51 issues): $135 ($74 allocated to subscription). Domestic institutional subscription (51 issues): $550; Foreign postage extra: Mexico, Caribbean (surface mail) $55; other countries (air assist delivery) $85. First class, airmail, student, and emeritus rates on request. Canadian rates with GST available upon request, GST #1254 88122. Publications Mail Agreement Number 1069624. **Printed in the U.S.A.**

Change of address: allow 4 weeks, giving old and new addresses and 8-digit account number. **Postmaster:** Send change of address to *Science*, P.O. Box 1811, Danbury, CT 06813–1811. **Single copy sales:** $10.00 per issue prepaid includes surface postage; bulk rates on request. **Authorization to photocopy** material for internal or personal use under circumstances not falling within the fair use provisions of the Copyright Act is granted by AAAS to libraries and other users registered with the Copyright Clearance Center (CCC) Transactional Reporting Service, provided that $15.00 per article is paid directly to CCC, 222 Rosewood Drive, Danvers, MA 01923. The identification code for *Science* is 0036-8075/83 $15.00. *Science* is indexed in the *Reader's Guide to Periodical Literature* and in several specialized indexes.

Contents continued

amplification

The MJ Line of Amplification Products

Moto vs. Manual:
The advantages of a motorized lid

Simplified Automation of Sealing and Resealing

One requirement for optimal performance with very small volumes — especially in 384-well plates — is that pressure from the lid must be substantial, uniform, and reproducible. A Moto Alpha™ lid imparts three important benefits: 1) reduced vapor loss; 2) less variability among runs, cyclers, and users; 3) the option of using automation-friendly sealing pads. It is difficult to achieve the pressures necessary for 1–3 µl reactions using a manual lid. The Moto Alpha lid has two clamps that engage as it closes; these, along with the hinge, form a three-point hitch. Pressure is specified in software, and strain gauges provide feedback control to the DC motor.

The Moto Alpha unit, together with an auto-sealing microplate lid, allows uncomplicated automation of sealing, opening, and resealing plates — without the need to integrate costly automated sealing and unsealing workstations. Arched auto-sealing lids automatically release from microplates when the cycler is opened, and therefore are ideal for repeated access. To make plate retrieval fail-safe, ejectors push the plate from the lid and lift it from the block as the lid opens. The plate is then presented uncoupled from the cycler, exactly 5 mm above the block.

Plates of Two Plastics:
Rigid, yet reaction-friendly

Microplates may be middle-aged technology (circa 1962), but only now are they reaching levels of maturity that allow 1 µl reactions.

Refinements include enhanced precision in the z-axis and extreme flatness after thermal cycling, so that robots can deposit/remove tiny droplets reliably. Plates must be sufficiently rigid for robot fingers to get a good grip. The walls of wells must pass heat readily, and they can neither bind proteins nor inhibit DNA reactions. Lastly, the plates must seal well.

Bio-Rad has achieved these goals through a patented two-part Hard-Shell® molding process (U.S. patent 6,340,589). Thin-wall wells are made from a reaction-friendly soft plastic with polished rims for good sealing; an integral chassis of rigid plastic imparts structural strength while being very stable, both dimensionally and thermally.

Moto Sealing Minimizes Dropouts
Robust low-volume sealing

During cycling, large excursions in the partial pressure of water lead to 40–50% changes in total pressure; this pumping action tends to drive off water vapor. Progressive loss of water concentrates ions in the mix, and this can inhibit PCR and DNA sequencing reactions.

Now, the combination of high-pressure Moto Alpha lids and compliant sealers can give equal or better sealing performance than older "welded" seals while allowing easier access postcycling. Evaporative losses during dispensing also can be reduced 5-fold by placing an auto-sealing lid on the microplate as soon as it is filled. Sealing data (in table) show that Microseal® 'A' disposable film, reusable auto-sealing lids, and peelable (not welded) heat seals work equally well for low-volume reactions when used with a Moto Alpha lid. Thus the motorized lid can reduce dropouts and operating costs by making low-volume sealing reliable and reproducible.

One Microliter DNA Reactions Now Possible
Major milestone in cost reduction for genetic analysis

Investigators at the Sanger Institute have demonstrated that high-quality sequencing reactions can be reliably performed in volumes as low as 1 µl in 384-well plates. In reactions involving less pure templates, 3 µl volumes may be more practical.

This represents a significant milestone in reducing costs of high-throughput DNA sequencing. It also represents substantial progress toward the routine clinical use of sequencing technology — now, many more clinical determinations can be made from a single specimen.

This technological advance does not reflect any single development; rather, it comes from a combination of many small refinements to microplates, sealing technologies, thermal cyclers, and protocols. Indeed, the limiting factor now seems to be liquid handling, for it is difficult to reproducibly dispense reaction mix and specimens where the total volume equals only about 1/30th of a drop of water (i.e., 1 µl).

Sanger scientists performed 1 µl and 2 µl reactions using purified plasmid DNA. Volumes of 3 µl were used for production DNA because salts in the buffer would make a drying step inhibitory. All reactions involved reduced quantities of costly dyes; all gave long, high-quality reads.

Sequencing reactions in Hard-Shell 384 plates in a Tetrad™ 2 cycler with Moto Alpha units.

Type of Seal	Volume	DNA	Dropouts	Q20+ Reads
Disposable film Microseal 'A' (compliant)	1 µl	Plasmid	0%	739 bases
	2 µl	Plasmid	0%	840 bases
	3 µl	Production	3%	786 bases
Reusable pad Auto-sealing lid (compliant)	1 µl	Plasmid	2%	773 bases
	2 µl	Plasmid	0%	848 bases
	3 µl	Production	2%	802 bases
Heat-seal film Easy peel (thermal adhesion)	1 µl	Plasmid	2%	820 bases
	2 µl	Plasmid	0%	845 bases
	3 µl	Production	4%	792 bases

1 µl and 2 µl templates were purified plasmid DNA dried in wells, then resuspended to indicated volume with mix. 3 µl templates were 4–6 kb genomic fragments in pUC19, in 2 µl of buffer with 1 µl of mix added. Q20+ read lengths from four runs in ABI 3730 sequencer. Data from Anthony West PhD, Sanger Institute.

sciencenow www.sciencenow.org Daily News Coverage

Fake Sex Pays Off
Mounting without insemination keeps female fowl faithful.

Simplifying a Nutty Problem
Swirling marbles may give clues to why larger nuts tend to float to the top of the can.

The Blunder Down Under
What killed Australia's largest animals?

Bulking up your negotiation skills.

science's next wave www.nextwave.org Career Resources for Young Scientists

US: Negotiation Boot Camp—Tips and Techniques to a Universal Career Skill *D. Jensen*
Few job skills bring as much value to your life and career as the ability to negotiate well.

US: Careers in Molecular Diagnostics *M. Vacek*
Hundreds of molecular genetics labs are springing up across the country.

UK: How to Stop a Drift Away from Tenure *CareerDoctor*
An assistant professor feels that her precious time is spent on committee meetings and classes, not research.

Europe: Training Scientists as Managers *A. Forde*
Did a recent laboratory management course help participants find better ways to resolve conflict?

GrantsNet: July 2005 Funding News *Next Wave Staff*
Get the latest index of research funding, scholarships, fellowships, and internships.

science's sage ke www.sageke.org Science of Aging Knowledge Environment

Perspective: Aging Down Under *S. J. Olshansky*
New organization promotes aging-related research in Australia.

News Focus: Pathological Partnership *M. Leslie*
Study fingers p53 as an accomplice in Huntington's disease.

News Focus: Not Like the Other *R. J. Davenport*
Older identical twins acquire different chromosome marks.

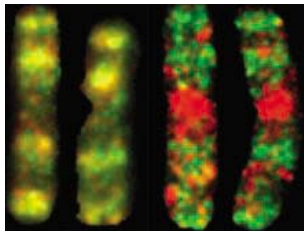

Twins don't match.

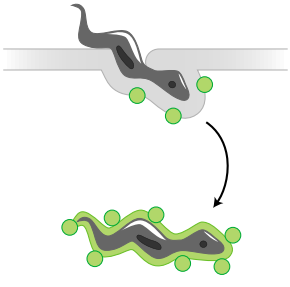

Cellular invasion by *T. cruzi*.

science's stke www.stke.org Signal Transduction Knowledge Environment

Related Trypanosomatid Genomes section page 399

Perspective: Host Cell Signaling and *Trypanosoma cruzi* Invasion—Do All Roads Lead to Lysosomes? *B. A. Burleigh*
Investigation of the role of PI3K signaling suggests that *T. cruzi* entry into host cells may be lysosome-independent.

Connections Map: Interleukin-13 (IL-13) Pathway *A. Kelly-Welch, E. M. Hanson, A. D. Keegan*
Signaling by IL-13 is implicated in asthma, inflammatory bowel disease, and parasitic nematode expulsion.

Connections Map: Interleukin-4 (IL-4) Pathway *A. Kelly-Welch, E. M. Hanson, A. D. Keegan*
IL-4 signaling is a target for treatment of asthma and allergy.

Separate individual or institutional subscriptions to these products may be required for full-text access.

Traditional Mini Preps are Over.

Start automating with the latest in plasmid DNA purification. The Mini Prep 96 can perform up to 96 preps in 1 hour of processing time. Up to 8 µg of plasmid DNA per lane at less than $1 a prep.

Start with easy operation. Disposable cassettes allow for direct loading of culture with no centrifugation.

Start the Mini Prep 96 with the push of a button. Remove high purity DNA and use in most microbiology protocols — including sequencing and cell transfection.

Start saving time and money with the Mini Prep 96.

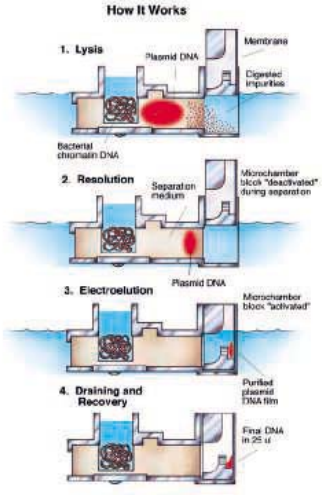

Four Easy Steps to
Plasmid DNA Purification

Stop Manual Mini Preps START ENTER Start the Mini Prep 96™

1-800-466-7949
www.macconnell.com

Mini-Preps at the Push of a Button.
6195 Cornerstone Court, San Diego, California 92121, Fax: 858-452-6753

MacConnell Research

A Field Day for Fast Computing

The Earth's magnetic field is produced by vigorous convection in its liquid iron outer core, and it is thought that many details of the field and its behavior over time, including reversals, are produced by the dynamics of these convections. However, it has been difficult to obtain the fluid state of the core in numerical simulations; in particular, the ratio of viscous to rotational forces is very small, so the core is in a Taylor state in which the axial magnetic torque vanishes. **Takahashi *et al.*** (p. 459; see the news story by **Kerr**) have now obtained these conditions in numerical experiments using a very fast supercomputer, the Earth Simulator. Their model reproduces many aspects of the current and past magnetic field and reveals how the field may vary during a reversal.

Some Wiggle Room

Below the glass transition temperature, T_g, of an amorphous material, large-scale molecular motions are no longer possible, and the material is thought of as being frozen. However, even below T_g, local atomic motions are still possible. **Priestly *et al.*** (p. 456) look at the roles of free, fixed, and internal surfaces on the relaxations in a polymer glass, by tagging the chains with fluorescent dyes so that their motion can be tracked. Relaxations are strongly influenced by the surfaces, and this effect extends considerably into the bulk of the material into regions where surface effects do not affect T_g.

The Virtual Synapse

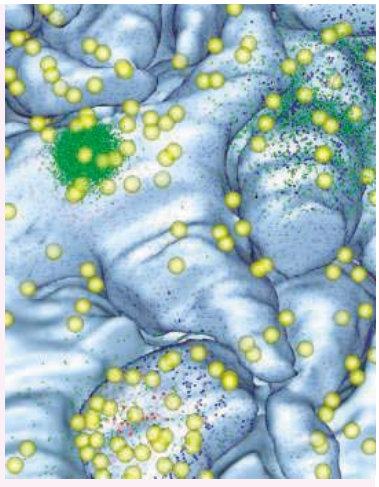

In a multiparameter, multidimensional system, building a quantitative and detailed model can be a helpful adjunct to experimental studies in exploring parameter space. **Coggan *et al.*** (p. 446, see the Perspective by **Lučić and Baumeister**) have taken a step toward describing dynamic events at a neuronal synapse by reconstructing the architecture of the pre- and postsynaptic membranes and underlying cytoplasmic vesicles, and incorporating kinetic measurements of neurotransmitter receptor properties as well as other physical and chemical parameters of neurotransmitters. At this simulated synapse, the known electrophysiology of transmitter release could not be explained by vesicle fusion only at the active zone, the classical region of membrane apposition between the pre- and postsynaptic neurons. Instead, the modeled electrophysiology fits better to observations if ectopic release by vesicle fusion outside of active zones is included.

A Threat to Tokyo from Below

The Philippine Sea Plate subducts to the north underneath Japan just south of Tokyo. Seismic hazards related to a subduction zone earthquake depend greatly on the depth to the fault. The plate boundary was thought to be about 20 to 40 kilometers (km) or more beneath the city, which is home to about 33 million people. Using seismic imaging, **Sato *et al.*** (p. 462) show that the boundary fault flattens and is no deeper than 25 km beneath Tokyo.

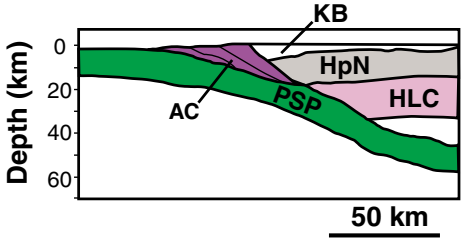

Not the First Stars We See Tonight?

The first stars born in the universe formed from primordial gases that contain no "metals"—astrophysical shorthand for carbon and heavier elements. Once these first-generation stars died in supernova explosions, second- and later-generation stars formed as the metal-enriched debris gravitationally coalesced. The recent discovery of "hyper metal poor" stars led to hopes that the earliest generation of stars, the so-called Population III, had been found. **Iwamoto *et al.*** (p. 451, published online 2 June 2005; see the Perspective by **Beers**) describe computer modeling that indicates these prime candidate stars are in fact second-generation objects that formed from the supernovae of an earlier population of stars. The results, which accurately reproduce the abundance of chemical elements in the hyper metal poor stars, will have important implications for identifying the true "first" stars.

Controlled Single-Photon Emission

The ability to deliver single photons on demand is an important requirement for quantum information processing and secure quantum communication. Reproducibility, in terms of the photon states from one to the other, as well as ease of implementation must also be considered for practical uses. Existing single photon sources generally meet one of these requirements, but not both. **Darquié *et al.*** (p. 454) present an approach, based on exciting a single, optically trapped rubidium atom with short laser pulses, that can meet both requirements. Each pulse stimulates the atom to emit a single photon.

Trypanosomes Beware

Recently, human serum apolipoprotein L-I (apoL-I) was found to lyse African trypanosomes, the parasite responsible for sleeping sickness. **Pérez-Morga *et al.*** (p. 469) have now elucidated the mechanism by which apoL-I kills trypanosomes. ApoL-I contains a membrane pore-forming domain that targets the lysosomal membrane of incoming trypanosomes. An ionic pore forms that triggers uncontrolled osmotic swelling of the lysosome and leads to trypanosome lysis. This function of apoL-I helps provide humans with an innate form of immunity against this pathogen. The parasite *Trypanosoma cruzi* goes through four life-cycle stages during its development in insects and humans; in humans, it causes Chagas disease. Complementing the sequencing of 3 kinetoplastid genomes reported in this issue, **Atwood *et al.***

CONTINUED ON PAGE 353

CREDITS (TOP TO BOTTOM): COGGAN *ET AL.*; SATO *ET AL.*

Roche Applied Science

Transcriptor First Strand cDNA Synthesis Kit

Bring Power and Sensitivity to Two-Step RT-PCR

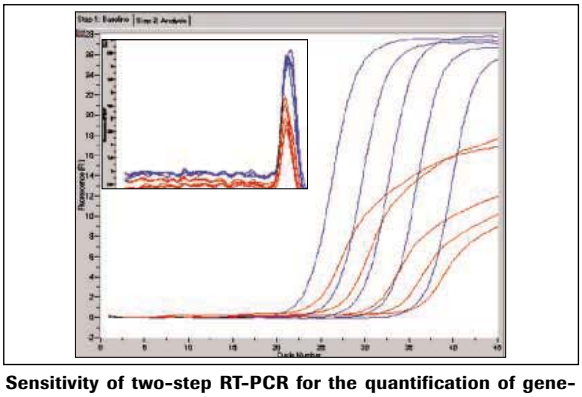

Sensitivity of two-step RT-PCR for the quantification of gene-expression levels on the LightCycler® 2.0 Instrument. Either the Transcriptor First Strand cDNA Synthesis Kit (blue curves) or another supplier's RNase H⁻ M-MuLV Reverse Transcriptase (red curves) was used to perform reverse transcription on 100 ng to 10 pg of total RNA from K-562 cells. LightCycler® FastStart DNA Master^{PLUS} SYBR Green I[‡,§] was then used with primers for G6PDH to quantify gene-expression levels on the LightCycler® 2.0 Instrument.

Transcriptor First Strand cDNA Synthesis Kit[†]	
Cat. No. 04 379 012 001	1 kit for 50 reactions

Transcriptor Reverse Transcriptase[†]	
Cat. No. 03 531 317 001	25 reactions
03 531 295 001	50 reactions
03 531 287 001	200 reactions

Choose the new **Transcriptor First Strand cDNA Synthesis Kit** for sensitive results from standard and difficult templates in two-step RT-PCR on blockcyclers and real-time PCR instruments (*e.g.*, the LightCycler® Instruments or ABI PRISM Instruments).

- **Increase sensitivity in quantitative RT-PCR**
  Improve gene-expression studies by increasing sensitivity (see figure) and simultaneously reverse transcribing rare and abundant RNA (over a 10^8-fold range of RNA)–without distorting gene-expression levels.
- **Power through challenging RNA secondary structures**
  Reverse transcribe at 55°C to obtain RT-PCR products from templates that M-MuLV reverse transcriptases can't handle.
- **Produce large quantities of full-length cDNA in qualitative two-step RT-PCR**
  Achieve high yields of cDNAs up to 12 kb using the kit's anchored-oligo$(dT)_{18}$ primer, which prevents mispriming within the poly(A) tail.

To maximize power and sensitivity in two-step RT-PCR, insist on the new Transcriptor First Strand cDNA Synthesis Kit.

For more information, visit www.roche-applied-science.com/pcr or contact your local Roche representative.

Roche Diagnostics

Roche Diagnostics GmbH
Roche Applied Science
68298 Mannheim
Germany

[†] This product is optimized for use in the Polymerase Chain Reaction ("PCR") process covered by patents owned by Roche Molecular Systems, Inc. and F. Hoffmann-La Roche Ltd. ("Roche"). No license under these patents to use the PCR process is conveyed expressly or by implication to the purchaser by the purchase of this product.

[‡] Purchase of this product includes a limited non-transferable end-user license to the purchaser under the SYBR Green I Technology owned by Idaho Technology under U.S. Patents 6,569,627 and foreign counterparts to use this product for any purpose.

[§] Purchase of this product is accompanied by a limited license to use it in the Polymerase Chain Reaction (PCR) process, including homogeneous PCR methods described in U.S. Patent Nos. 5,994,056 and 6,171,785 and their foreign counterparts, for life science research in conjunction with a thermal cycler whose use in the automated performance of the PCR process is covered by the up-front license fee, *i.e.*, an authorized thermal cycler. No rights for any other application, including any *in vitro* diagnostic application, are conveyed expressly, by implication or by estoppel under U.S. Patents 5,210,015, 5,487,972 and 5,804,375 or their foreign counterparts, or any other patents owned by Roche Molecular Systems, Inc. and F. Hoffmann-La Roche Ltd claiming real-time amplification and detection methods.

(p. 473) present a proteomic analysis of the life-cycle stages of *T. cruzi*. The parasite appears to use histidine as an energy source during its development in insect vectors, but uses fatty acids when it resides in mammalian cells. Knowledge of stage-specific pathways may aid in selection of targets for drug intervention.

Aging and Death

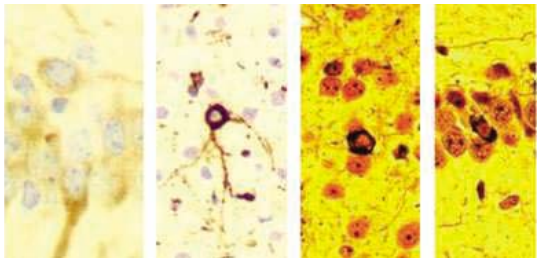

Mutations in mitochondrial DNA (mtDNA) are thought to play a central role in mammalian aging, but the underlying cellular mechanisms have remained elusive. **Kujoth *et al.*** (p. 481) examined mice genetically manipulated to accumulate high levels of mtDNA mutations. The mutant mice had a significantly reduced life span compared with wild-type littermates and showed features of premature aging such as hearing loss, a decline in muscle mass, and dysfunction of tissues that normally undergo rapid cellular turnover. Surprisingly, the aging phenotype did not appear to arise from increased oxidative stress, as predicted by current working hypotheses, but rather from an increase in cell death (apoptosis). Mutations in mtDNA may drive the aging of certain tissues by triggering the loss of irreplaceable cells.

Reversing Neurodegenerative Change

Neurofibrillary tangles are the most common intraneuronal inclusion in the brains of patients with neurodegenerative diseases and are composed, at least in part, of deposits of the protein tau. **SantaCruz *et al.*** (p. 476) describe the remarkable effects of suppressing transgenic tau overexpression in mice: the recovery of memory loss after significant neuron loss and brain atrophy despite continued accumulation of neurofibrillary tangles. This dissociation of cognitive deficits from tangle pathology suggests that recovery of cognitive function is possible even after considerable neurodegeneration has occurred during the development of tauopathies such as Alzheimer's disease.

Distorted Body Awareness

A strange and disturbing neurological condition, anosognosia, can cause obviously intelligent, awake, and talking individuals to be unaware of paralysis on one side of their body. **Berti *et al.*** (p. 488) investigated patients with spatial neglect and found that about half of them were also anosognosic for their left hemiplegia because of lesions in the right brain hemisphere. Comparison of the two groups with and without anosognosia revealed that damage to frontal areas (particularly brain areas 6 and 44, motor cortex BA 4, and the somatosensory cortex) underpins the loss of awareness of motor impairment in these patients.

Three Toxins Are Better Than One

Understanding molecular mechanisms of neurotransmitter release and short-term synaptic plasticity is one of the central questions in neuroscience. **Sakaba *et al.*** (p. 491) studied the roles of SNARE proteins in neurotransmitter release using clostridial neurotoxins. A detailed kinetic analysis of the action of several toxins revealed that the kinetics of transmitter release differs, depending on which SNARE proteins were cleaved. Toxins cleaving synaptobrevin and syntaxin reduced the number of fusion-competent vesicles without changing Ca^{2+}-sensitivity of the release apparatus of remaining vesicles. In contrast, toxins cleaving the C terminal of SNAP-25 reduced intracellular Ca^{2+}-sensitivity of vesicle fusion, suggesting that the C terminal is important for driving rapid fusion. Furthermore, toxins cleaving synaptobrevin led to a modification of the coupling between Ca^{2+}-channels and release-competent vesicles.

CREDIT: SANTACRUZ *ET AL.*

Announcing the

McNEIL RESEARCH GRANT AWARDS

From the makers of Tylenol®
ACETAMINOPHEN

The McNeil Research Grant Awards are designed to sponsor original research on the use of acetaminophen in the following investigative areas:

Cardioprotection • Anticarcinogenicity • Neuroprotection • Complications of Diabetes

A maximum of $75,000 per grant per year will be made available. Extensions of one additional year (maximum grant $150,000) will be considered. Selected applicants must be willing to publish results in a peer-reviewed journal or present findings at a national scientific meeting.

Investigators will be required to submit interim reports on the project's progress. *Proposals must be post-marked by September 30, 2005. All applicants will be notified of their status by November 30, 2005.*

For details of the procedures and conditions of the program, please call:
1-800-962-5357

McNeil Consumer & Specialty Pharmaceuticals

TYLENOL® ACETAMINOPHEN

Trypanosomes at the Gates

Like many colleagues, I sometimes thought I'd never see the day when three small parasites would be so celebrated. After all, why should people outside of the small cohort of dedicated scientists and sponsors pay any attention to these "Tritryps"—*Trypanosoma brucei*, *Trypanosoma cruzi*, and *Leishmania major*—whose genomes appear in this issue of *Science*?

These three motile, unicellular, nucleated (eukaryotic) protozoa belong to a family of ubiquitous parasites of insects, plants, fish, amphibians, reptiles, birds, and mammals. Notably, the family contains species—represented by these genomes—that are responsible for major region-specific human diseases. All three organisms and their diseases have been studied for more than 100 years. Surprisingly, some of the highly toxic and inadequate drugs that are used to combat them today—based on arsenic or antimony—have their origins almost as long ago. Why is this? The answer is simple: These are primarily geographically restricted diseases of the ultra-poor in underdeveloped countries.

Trypanosoma brucei and its relatives are responsible for devastating diseases of humans ("sleeping sickness") and livestock in equatorial Africa, and have also spread to South America and Asia. Although its relative importance has paled in comparison with the impact of HIV, the parasite presents a continual threat of sleeping sickness epidemics because of the ubiquity of its animal reservoirs (and of the tsetse fly that transmits it), combined with the breakdown of social and economic infrastructure.

Trypanosoma cruzi is responsible for Chagas' disease. It primarily affects rural South America but also constitutes a potential hazard in Mexico and the United States, primarily through blood and organ donations. How many Americans have pondered the question "Have you EVER had Chagas' disease?" on a blood donor questionnaire?

Leishmania major is responsible for one variety of leishmaniasis. Other species contribute to a broad spectrum of invasive diseases throughout South and Central America, across the Mediterranean, and throughout Asia. In Europe and the United States, outbreaks of leishmaniasis and Chagas' disease have occurred in dogs, but there have been few cases in humans, save for those contracted by expeditionary military personnel.

The human devastation dealt by these parasites continues, but is this what has kept them alive in the minds of scientists? Not entirely. The Tritryps happen to be amenable to laboratory investigation, making them the best-studied examples of ancient eukaryotes. These organisms have followed an evolutionary track distinct from those that are extolled for their conservation of key features, from yeast to human. Some universal cellular pathways operate in Tritryps in interestingly different ways, and some of the things Tritryps do are striking because they represent unique mechanisms of pathogenicity, yet reflect genetic mechanisms that occur elsewhere. RNA editing and the anchoring of proteins to membranes with a lipid moiety were famously discovered in trypanosomes.

The Tritryp genomes are thus intrinsically interesting—but what will they contribute to the amelioration of disease? Because of their distinct evolution, trypanosomes present a plethora of potential drug targets, and potential drugs are almost certainly languishing in the chemical libraries of pharmaceutical companies. There have been several initiatives to tackle diseases of neglected people: The Drugs for Neglected Diseases Initiative exists entirely for the purpose of Tritryps drug development; the World Health Organization fosters drug research on neglected diseases; the Bill and Melinda Gates Foundation provides major funds; Medicines for Malaria Venture is a key organization. But we need resources and commitment on a far larger scale to transform drug targets into clinical successes. It is clear that the traditional pharmaceutical industry will not become effectively involved in this area, and the current promotion-and-reward system in academia does not attract or sustain the necessary human and financial resources. Consortia move slowly and are frequently restrained by similar problems, compounded by the egos of scientists and sponsors.

What are the solutions, then? Perhaps we need research institutes that are solely dedicated to drug development for "diseases of the poor." Governments of the wealthier nations need to place such diseases higher on their priority lists, but we shouldn't hold our breath on that, even as these diseases continue to expand their geographical reach. What about other donors? There is an ominous call at the gates—can anyone hear it?

George A. M. Cross

George A. M. Cross heads the Laboratory of Molecular Parasitology, Rockefeller University, New York, NY 10021, USA.

10.1126/science.1116055

Genetic Engineering that is Right on Target!

The TargeTron™ Gene Knockout System is a revolutionary method for rapid and specific disruption of genes in prokaryotic organisms. Utility of the technology has been demonstrated for prokaryotic genetic engineering, systems biology and functional genomics approaches.

The method exploits the retrohoming ability of group II introns and utilizes a simple PCR step to "re-target" the TargeTron group II intron for specific insertion into the host genome. Gene knockout using the TargeTron system has been validated in a broad range of bacterial strains such as *Escherichia coli, Staphylococcus aureus, Lactococcus lactis, Clostridium perfringens, Shigella flexneri* and *Salmonella typhimurium.*

- Targeted and permanent gene disruption
- Simple, streamlined protocol; Knockouts in 3 days or less
- Minimal screening to isolate mutants.
- No cell conjugation or specific host factor requirements
- >90% successful targeted insertion

Product	Description	Unit
TA0100	TargeTron™ Gene Knockout System	3EA 10EA

For additional details and product availability, please visit www.sigma-aldrich.com/s1target

EDITORS' CHOICE

edited by Gilbert Chin

BIOMEDICINE

Tracking the Origins of Lung Cancer

Lung cancer is the leading cause of cancer deaths in the United States. Most patients are diagnosed at an advanced stage of the disease, which has hampered research into its molecular and cellular origins. Consequently, only 15% of patients who are diagnosed today with the most common subtype of lung cancer will survive for 5 years—a bleak statistic that has not changed over the past 15 years.

Two reports illustrate that there may be reasons for optimism, due largely to recent advances in how the disease is approached methodologically and conceptually. To identify genes that play a role in the pathogenesis of the distinct subtypes of lung cancer, Tonon *et al*. studied human tumors by comparative genomic hybridization and expression profiling, two methods that, when integrated, provide a comprehensive picture of the critical genomic alterations that characterize each subtype. Interestingly, adenocarcinomas and squamous cell carcinomas (SCCs), two subtypes previously thought to have diverse etiologies because of their distinct histopathological features, were found to have nearly identical genomic signatures, suggesting that they may in fact arise from a common stem/progenitor cell.

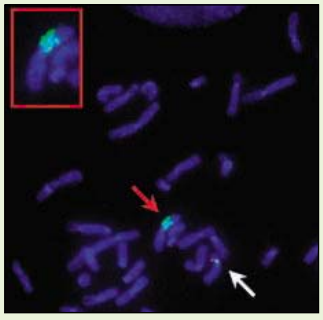

Both adenocarcinomas and SCCs exhibit amplification (green dots) of a region on chromosome 8.

The possible stem cell origin of lung cancer was the focus of independent work by Kim *et al*. Using a mouse model, they identified a population of cells, termed BASCs (bronchioalveolar stem cells), whose anatomical location and ability to self-renew and differentiate into multiple lung cell types are features consistent with those predicted for a lung stem/progenitor cell. Remarkably, BASCs were enriched in early-stage lung tumors in mice, and they expanded in response to oncogenic stimuli in cell culture, suggesting that they might play a role in tumorigenesis. Should future studies identify BASC counterparts with a causal role in human lung cancer, this could lead to new therapies that target the earliest stage of disease, a development that is desperately needed. — PAK

Proc. Natl. Acad. Sci. U.S.A. **102**, 9625 (2005); *Cell* **121**, 823 (2005).

APPLIED PHYSICS

Holographic Sensors

Chemical sensors generally depend on the response of an absorbing or adsorbing material when it is exposed to the chemical of interest. Optimum performance is usually a trade-off between sensitivity and response time. Ye *et al*. describe a chemical sensor, based on holographic interferometry, in which the presence of a chemical on a suitably sensitive material results in a detectable shift in the optical path length through that material. The use of holography allows a large area to be scanned at one time, which offers the potential of storing a two-dimensional odor image in the hologram. They demonstrate the ability to sense ethyl alcohol down to the level of 40 parts per billion, with a relatively fast measurement window of 5 s—a response time that may allow dynamical sensing to be achieved. — ISO

Opt. Lett. **30**, 1467 (2005).

ECOLOGY/EVOLUTION

Second Banana

The mountain gorilla is one of our closest living relatives, surviving in the wild as a population of perhaps no more than a few hundred individuals. Despite the gorillas' extreme rarity, their wariness of humans, and the remoteness of their habitat, an understanding of their ecology and behavior is slowly emerging through decades of patient observation.

In the latest example of such work, Bradley *et al*. investigated patterns of dominance and reproduction in wild populations of the mountain gorilla in Rwanda over a 15-year period, with a particular focus on how reproduction is apportioned between the adult males. In groups with two adult silverback males, genotypic analyses revealed that the dominant male was responsible for 85% of paternity. The subordinate male is typically unrelated to the dominant, having joined the group after migrating from another. When combined with the genetic data, behavioral observations suggested that the most likely explanation for the dominant male's lack of a reproductive monopoly is that he is unable to prevent the subordinate from having access to the females. This is an example of the "tug-of-war" model of reproductive skew in animal societies, as opposed to the "concessions" model, where the dominant male permits limited matings by subordinates—a situation that is more likely when the males are related to one another. — AMS

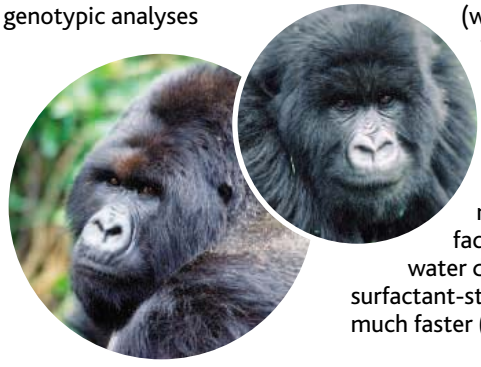

Mountain gorillas.

Proc. Natl. Acad. Sci. U.S.A. **102**, 9418 (2005).

MATERIALS SCIENCE

Silanized Bubbles

Foams (for example, the head on a pint of beer) are mixtures of fluid and millimeter-sized gas bubbles. To retard collapse of the foam due to leakage of the fluid component, organic molecules such as surfactants or proteins are usually added.

Binks and Horozov describe a different approach to the stabilization of foams by showing that silica nanoparticles can serve as stabilizers. The foam volume depends on how hydrophobic (water-repelling) the nanoparticles are. Comparison of the foam stability to that of a foam made with a commonly used surfactant shows that water drains out of the surfactant-stabilized foam much faster (within minutes)

CONTINUED ON PAGE 359

CREDITS: (TOP) TONON *ET AL., PROC. NATL. ACAD. SCI. U.S.A.* **102**, 9625 (2005); (BOTTOM) LINDA VIGILANT

“THE FASTEST GROWING CROP IN IOWA IS NOT WHAT YOU EXPECT.”

MORE AND MORE BIOSCIENCE COMPANIES PLANNING TO EXPAND ARE TAKING A LOOK AT IOWA. And for good reason. Iowa leads the nation in the production of raw biomass at roughly 2.75 billion bushels. The state is home to three public universities that are world-renowned for their research in plant, animal and human bioscience. And to date there are more than 1,800 Iowa establishments already involved in the bioscience industry. To learn more about expanding your business in Iowa, visit iowalifechanging.com. Because the closer you look, the more Iowa grows on you.

www.iowalifechanging.com

IOWA

life | changing™

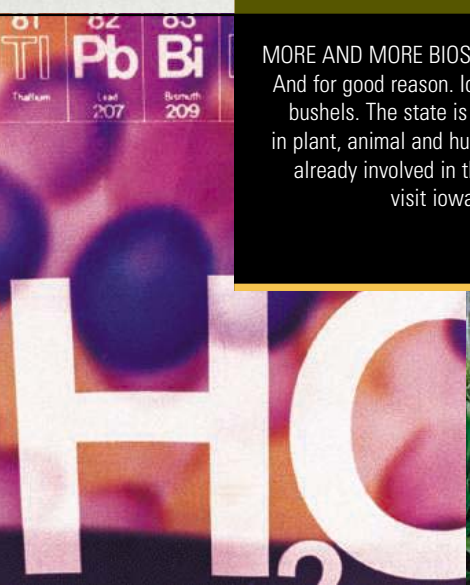

than out of the nanoparticle-stabilized foam (within hours). Addition of a small amount of salt (à la Stan Murch) further improves foam longevity. Nanoparticle-stabilized foams of this kind may find application in the food, detergent, and cosmetics industries. — JFU

Angew. Chem. Int. Ed. **44**, 3722 (2005).

NEUROSCIENCE

Preserving Memories

Long-term potentiation (LTP), one of the most widely studied forms of neuronal plasticity, has been amply documented in excitatory synapses on pyramidal neurons. However, there is scant evidence for this phenomenon in inhibitory interneurons.

Using perforated-patch recordings, Lamsa *et al.* elicited robust Hebbian-type LTP in hippocampal stratum radiatum interneurons. This pathway-specific LTP does not require dendritic spines and depends on disynaptic feedforward inhibition of pyramidal cells. If memory encoding mediated by LTP were to enhance only monosynaptic excitation and not disynaptic inhibition of pyramidal neurons, this would degrade the fidelity of information processing. However, the temporal fidelity of synaptic integration and action potential generation can be preserved if LTP also occurs in feedforward interneurons. — PRS

Nat. Neurosci. **8**, 916 (2005).

CHEMISTRY

Signal When You Get There

Quantitating how readily DNA can pass through a thin film is important for designing a gene therapy or drug release system. Measuring permeability accurately requires a method for detecting small amounts of nucleic acid, preferably without the added complication of having to rely on derivatizing the DNA with bulky fluorophores.

Johnston and Caruso have used a molecular beacon approach to monitor the passage of unaltered DNA segments through an organic film that was applied to a mesoporous silica particle with layer-by-layer assembly. Their detector is an encapsulated single-stranded DNA that forms a stem-loop structure and whose ends are labeled with a fluorophore and a quencher. When a complementary DNA molecule passes through the film, it disrupts the stem-loop, freeing the fluorophore to emit a signal. Using this arrangement, they were able to observe the slowing of permeation as the length of the target DNA molecules was increased from 15 to 60 bases. — PDS

J. Am. Chem. Soc. 10.1021/ja0527166 (2005).

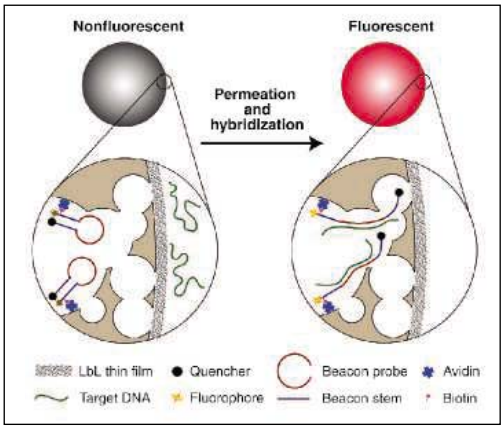

Schematic of DNA detection.

CREDITS: JOHNSTON *ET AL.*, *J. AM. CHEM. SOC.* 10.1021/JA0527166 (2005)

EVOLUTION

Lianas for Phylogenetic Trees

Patterns of evolutionary descent are traditionally depicted as phylogenetic trees. This concept has become too constraining for microbial taxonomists whose subjects appear to swap chunks of DNA promiscuously, gratuitously obscuring clean lines of descent.

Kunin *et al.* have developed a model, assuming that the main tracks of inheritance in microorganisms do follow vertical, treelike routes. Nevertheless, swapping events (lateral gene transfer, or LGT) between genomes can be traced and mapped as many, thin vines swinging through the branches of the tree of life to link phylogenetically distant organisms. The two types of inheritance mapping can be separated, allowing the consistency of the vine network to be tested. The vines tend to arise from definable nodes or network hubs, so LGT is not random or universal, although it is scale-free, and can occur at any time and very rapidly. One benefit of this approach is being able to locate sources of LGT. Whichever tree was used, some species, including *Erwinia carotovora* and *Bradyrhizobium japonicum*, were consistently revealed as hubs for LGT, and it appears that these species may act like bacterial gene banks for a particular environment. — CA

Genome Res. **15**, 954 (2005).

www.sciencemag.org

Science

1200 New York Avenue, NW
Washington, DC 20005
Editorial: 202-326-6550, FAX 202-289-7562
News: 202-326-6500, FAX 202-371-9227

Bateman House, 82-88 Hills Road
Cambridge, UK CB2 1LQ
+44 (0) 1223 326500, FAX +44 (0) 1223 326501

SUBSCRIPTION SERVICES For change of address, missing issues, new orders and renewals, and payment questions: 800-731-4939 or 202-326-6417, FAX 202-842-1065. Mailing addresses: AAAS, P.O. Box 1811, Danbury, CT 06813 or AAAS Member Services, 1200 New York Avenue, NW, Washington, DC 20005

INSTITUTIONAL SITE LICENCES please call 202-326-6755 for any questions or information

REPRINTS Ordering/Billing/Status 800-635-7171; Corrections 202-326-6501

PERMISSIONS 202-326-7074, FAX 202-682-0816

MEMBER BENEFITS Bookstore: AAAS/BarnesandNoble.com bookstore www.aaas.org/bn; Car purchase discount: Subaru VIP Program 202-326-6417; Credit Card: MBNA 800-847-7378; Car Rentals: Hertz 800-654-2200 CDP#343457, Dollar 800-800-4000 #AA1115; AAAS Travels: Betchart Expeditions 800-252-4910; Life Insurance: Seabury & Smith 800-424-9883; Other Benefits: AAAS Member Services 202-326-6417 or www.aaasmember.org.

science_editors@aaas.org (for general editorial queries)
science_letters@aaas.org (for queries about letters)
science_reviews@aaas.org (for returning manuscript reviews)
science_bookrevs@aaas.org (for book review queries)

Published by the American Association for the Advancement of Science (AAAS), *Science* serves its readers as a forum for the presentation and discussion of important issues related to the advancement of science, including the presentation of minority or conflicting points of view, rather than by publishing only material on which a consensus has been reached. Accordingly, all articles published in *Science*—including editorials, news and comment, and book reviews—are signed and reflect the individual views of the authors and not official points of view adopted by the AAAS or the institutions with which the authors are affiliated.

AAAS was founded in 1848 and incorporated in 1874. Its mission is to advance science and innovation throughout the world for the benefit of all people. The goals of the association are to: foster communication among scientists, engineers and the public; enhance international cooperation in science and its applications; promote the responsible conduct and use of science and technology; foster education in science and technology for everyone; enhance the science and technology workforce and infrastructure; increase public understanding and appreciation of science and technology; and strengthen support for the science and technology enterprise.

INFORMATION FOR CONTRIBUTORS

See pages 135 and 136 of the 7 January 2005 issue or access www.sciencemag.org/feature/contribinfo/home.shtml

EDITOR-IN-CHIEF **Donald Kennedy**
EXECUTIVE EDITOR **Monica M. Bradford**
DEPUTY EDITORS **R. Brooks Hanson, Katrina L. Kelner**
NEWS EDITOR **Colin Norman**

EDITORIAL SUPERVISORY SENIOR EDITORS Barbara Jasny, Phillip D. Szuromi; SENIOR EDITORS Gilbert J. Chin, Lisa D. Chong, Pamela J. Hines, Paula A. Kiberstis (Boston), Beverly A. Purnell, L. Bryan Ray, Guy Riddihough (Manila), H. Jesse Smith, Valda Vinson, David Voss; ASSOCIATE EDITORS Marc S. Lavine, Jake S. Yeston; ONLINE EDITOR Stewart Wills; CONTRIBUTING EDITOR Ivan Amato; ASSOCIATE ONLINE EDITOR Tara S. Marathe; BOOK REVIEW EDITOR Sherman J. Suter; ASSOCIATE LETTERS EDITOR Etta Kavanagh; INFORMATION SPECIALIST Janet Kegg; EDITORIAL MANAGER Cara Tate; SENIOR COPY EDITORS Jeffrey E. Cook, Harry Jach, Barbara P. Ordway; COPY EDITORS Cynthia Howe, Alexis Wynne Mogul, Sabrah M. n'haRaven, Jennifer Sills, Trista Wagoner; EDITORIAL COORDINATORS Carolyn Kyle, Beverly Shields; PUBLICATION ASSISTANTS Chris Filiatreau, Joi S. Granger, Jeffrey Hearn, Lisa Johnson, Scott Miller, Jerry Richardson, Brian White, Anita Wynn; EDITORIAL ASSISTANTS Ramatoulaye Diop, E. Annie Hall, Patricia M. Moore, Brendan Nardozzi, Michael Rodewald; EXECUTIVE ASSISTANT Sylvia S. Kihara; ADMINISTRATIVE SUPPORT Patricia F. Fisher

NEWS SENIOR CORRESPONDENT Jean Marx; DEPUTY NEWS EDITORS Robert Coontz, Jeffrey Mervis, Leslie Roberts, John Travis; CONTRIBUTING EDITORS Elizabeth Culotta, Polly Shulman; NEWS WRITERS Yudhijit Bhattacharjee, Jennifer Couzin, David Grimm, Constance Holden, Jocelyn Kaiser, Richard A. Kerr, Eli Kintisch, Andrew Lawler (New England), Greg Miller, Elizabeth Pennisi, Charles Seife, Robert F. Service (Pacific NW), Erik Stokstad; Carolyn Gramling, Genevra Ornelas, Cathy Tran (interns); CONTRIBUTING CORRESPONDENTS Marcia Barinaga (Berkeley, CA), Barry A. Cipra, Adrian Cho, Jon Cohen (San Diego, CA), Daniel Ferber, Ann Gibbons, Robert Irion, Mitch Leslie (NetWatch), Charles C. Mann, Evelyn Strauss, Gary Taubes, Ingrid Wickelgren; COPY EDITORS Linda B. Felaco, Rachel Curran, Sean Richardson; ADMINISTRATIVE SUPPORT Scherraine Mack, Fannie Groom BUREAUS: Berkeley, CA: 510-652-0302, FAX 510-652-1867, New England: 207-549-7755, San Diego, CA: 760-942-3252, FAX 760-942-4979, Pacific Northwest: 503-963-1940

PRODUCTION DIRECTOR James Landry; SENIOR MANAGER Wendy K. Shank; ASSISTANT MANAGER Rebecca Doshi; SENIOR SPECIALISTS Vicki J. Jorgensen, Jessica K. Moshell; SPECIALISTS Jay R. Covert, Stacey Ferebee; **PREFLIGHT** DIRECTOR David M. Tompkins; MANAGER Marcus Spiegler; SPECIALIST Jessie Mudjitaba;

ART DIRECTOR Joshua Moglia; ASSOCIATE ART DIRECTOR Kelly Buckheit; ILLUSTRATOR Katharine Sutliff; SENIOR ART ASSOCIATES Holly Bishop, Laura Creveling, Preston Huey, Julie White; ASSOCIATE Nayomi Kevitiyagala; PHOTO RESEARCHER Leslie Blizard

***SCIENCE* INTERNATIONAL**

EUROPE (science@science-int.co.uk) EDITORIAL: INTERNATIONAL MANAGING EDITOR Andrew M. Sugden; SENIOR EDITOR/PERSPECTIVES Julia Fahrenkamp-Uppenbrink; SENIOR EDITORS Caroline Ash (Geneva: +41 (0) 222 346 3106), Stella M. Hurtley, Ian S. Osborne, Peter Stern; ASSOCIATE EDITOR Stephen J. Simpson; EDITORIAL SUPPORT Emma Westgate; Deborah Dennison ADMINISTRATIVE SUPPORT Janet Clements, Phil Marlow, Jill White; NEWS: INTERNATIONAL NEWS EDITOR Eliot Marshall DEPUTY NEWS EDITOR Daniel Clery; CORRESPONDENT Gretchen Vogel (Berlin: +49 (0) 30 2809 3902, FAX +49 (0) 30 2809 8365); CONTRIBUTING CORRESPONDENTS Michael Balter (Paris), Martin Enserink (Amsterdam and Paris); INTERN Mason Inman

ASIA Japan Office: Asca Corporation, Eiko Ishioka, Fusako Tamura, 1-8-13, Hirano-cho, Chuo-ku, Osaka-shi, Osaka, 541-0046 Japan; +81 (0) 6 6202 6272, FAX +81 (0) 6 6202 6271; asca@os.gulf.or.jp JAPAN NEWS BUREAU: Dennis Normile (contributing correspondent, +81 (0) 3 3391 0630, FAX 81 (0) 3 5936 3531; dnormile@gol.com); CHINA REPRESENTATIVE Hao Xin, + 86 (0) 10 6307 4439 or 6307 3676, FAX +86 (0) 10 6307 4358; haoxin@earthlink.net; SOUTH ASIA Pallava Bagla (contributing correspondent +91 (0) 11 2271 2896; pbagla@vsnl.com); CENTRAL ASIA Richard Stone (+7 3272 6413 35, rstone@aaas.org)

EXECUTIVE PUBLISHER **Alan I. Leshner**
PUBLISHER **Beth Rosner**

FULFILLMENT & MEMBERSHIP SERVICES (membership@aaas.org) DIRECTOR Marlene Zendell; MANAGER Waylon Butler; SYSTEMS SPECIALIST Andrew Vargo SENIOR SPECIALIST Pat Butler; SPECIALISTS Laurie Baker, Tamara Alfson, Karena Smith

BUSINESS OPERATIONS AND ADMINISTRATION DIRECTOR Deborah Rivera-Wienhold; BUSINESS MANAGER Randy Yi; SENIOR BUSINESS ANALYST Lisa Donovan; BUSINESS ANALYST Jessica Tierney; FINANCIAL ANALYST Michael LoBue, Farida Yeasmin; RIGHTS AND PERMISSIONS: ADMINISTRATOR Emilie David; ASSOCIATE Elizabeth Sandler; MARKETING: DIRECTOR John Meyers; MEMBERSHIP MARKETING MANAGER Darryl Walter; MARKETING ASSOCIATE Julianne Wielga; RECRUITMENT MARKETING MANAGER Allison Pritchard; ASSOCIATES Mary Ellen Crowley, Amanda Donathen, Catherine Featherston; DIRECTOR OF INTERNATIONAL MARKETING AND RECRUITMENT ADVERTISING Deborah Harris; INTERNATIONAL MARKETING MANAGER Wendy Sturley; MARKETING/MEMBER SERVICES EXECUTIVE: Linda Rusk; JAPAN SALES AND MARKETING MANAGER Jason Hannaford; SITE LICENSE SALES: DIRECTOR Tom Ryan; SALES AND CUSTOMER SERVICE Mehan Dossani, Catherine Holland, Adam Banner, Yaniv Snir; ELECTRONIC MEDIA: INTERNET PRODUCTION MANAGER Lizabeth Harman; ASSISTANT PRODUCTION MANAGER Wendy Stengel; SENIOR PRODUCTION ASSOCIATES Sheila Mackall, Amanda K. Skelton, Lisa Stanford; PRODUCTION ASSOCIATE Nichele Johnston; LEAD APPLICATIONS DEVELOPER Carl Saffell

PRODUCT ADVERTISING (science_advertising@aaas.org); MIDWEST Rick Bongiovanni: 330-405-7080, FAX 330-405-7081 • WEST COAST/W. CANADA B. Neil Boylan (Associate Director): 650-964-2266, FAX 650-964-2267 • EAST COAST/E. CANADA Christopher Breslin: 443-512-0330, FAX 443-512-0331 • UK/SCANDINAVIA/FRANCE/ITALY/BELGIUM/NETHERLANDS Andrew Davies (Associate Director): +44 (0)1782 750111, FAX +44 (0) 1782 751999 • GERMANY/SWITZERLAND/AUSTRIA Tracey Peers (Associate Director): +44 (0) 1782 752530, FAX +44 (0) 1782 752531 JAPAN Mashy Yoshikawa: +81 (0) 33235 5961, FAX +81 (0) 33235 5852 ISRAEL Jessica Nachlas +9723 5449123 • TRAFFIC MANAGER Carol Maddox; SALES COORDINATOR Deiandra Simms

CLASSIFIED ADVERTISING (advertise@sciencecareers.org); U.S.: SALES DIRECTOR Gabrielle Boguslawski: 718-491-1607, FAX 202-289-6742; INTERNET SALES MANAGER Beth Dwyer: 202-326-6534; INSIDE SALES MANAGER Daryl Anderson: 202-326-6543; WEST COAST/MIDWEST Kristine von Zedlitz: 415-956-2531; EAST COAST Jill Downing: 631-580-2445; LINE AD SALES Emnet Tesfaye: 202-326-6740; SENIOR SALES COORDINATOR Erika Bryant; SALES COORDINATORS Rohan Edmonson, Christopher Normile, Joyce Scott, Shirley Young; INTERNATIONAL: SALES MANAGER Tracy Holmes: +44 (0) 1223 326525, FAX +44 (0) 1223 326532; SALES Christina Harrison, Suitlana Barnes; SALES ASSISTANT Helen Moroney; JAPAN: Jason Hannaford: +81 (0) 52 789 1860, FAX +81 (0) 52 789 1861; PRODUCTION: MANAGER Jennifer Rankin; ASSISTANT MANAGER Deborah Tompkins; ASSOCIATE Amy Hardcastle; SENIOR TRAFFICKING ASSOCIATE Christine Hall; SENIOR PUBLICATIONS ASSISTANT Robert Buck; PUBLICATIONS ASSISTANT Natasha Pinol

AAAS BOARD OF DIRECTORS RETIRING PRESIDENT, CHAIR Shirley Ann Jackson; PRESIDENT Gilbert S. Omenn; PRESIDENT-ELECT John P. Holdren; TREASURER David E. Shaw; CHIEF EXECUTIVE OFFICER Alan I. Leshner; BOARD Rosina M. Bierbaum; John E. Burris; John E. Dowling; Lynn W. Enquist; Susan M. Fitzpatrick; Richard A. Meserve; Norine E. Noonan; Peter J. Stang; Kathryn D. Sullivan

AAAS
ADVANCING SCIENCE, SERVING SOCIETY

NetWatch

edited by Mitch Leslie

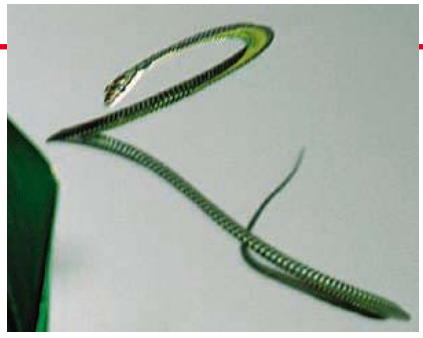

IMAGES

Snakes Aloft

Most snakes get around by crawling, but a few species, such as the paradise tree snake (*Chrysopelea paradisi*; above), take to the air. Learn more about these adventurous serpents at an image-packed site created by postdoc Jake Socha of Argonne National Laboratory in Illinois. Native to southern Asia, the five species of flying snakes can't gain altitude like a bird or bat. Instead, they launch themselves into the air and parachute, flattening their bodies to slow their descent. Herpetologists aren't sure why the snakes adopted the aerial habit—perhaps to avoid predators or pursue prey. The site showcases photos and videos of the reptiles flinging themselves from high perches.

www.flyingsnake.org

TOOLS

Choose Your Rat

Whether you're probing the genetics of diabetes or dissecting the neural basis of learning, you'll find guidance on picking the best rat strain for your work at this site from Kyoto University in Japan. Users can compare more than 100 inbred lines on dozens of anatomical, physiological, and behavioral characteristics, from forelimb grip strength to blood cholesterol to memory retention time. Another tool lets visitors chart the genetic differences among strains based on 357 markers known as simple sequence length polymorphisms. The figure at left contrasts many of the lines.

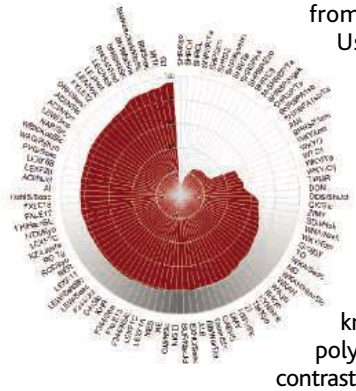

www.anim.med.kyoto-u.ac.jp/nbr/home.htm

DATABASE

Visualizing Eye Diseases

Students and researchers studying eye diseases might want to focus on this new pathology collection from the U.S. National Eye Institute (NEI). The database presents 1040 case descriptions of eye illnesses, injuries, and disorders gathered by the late David Cogan, an ophthalmologist at Harvard Medical School and NEI. Examples range from cataracts to a parasitic worm infestation of the retina. Featuring more than 3000 photos, the collection is particularly strong on certain topics such as the retinal degeneration spurred by diabetes. You can search the cases by location in the eye, diagnosis, and type of tissue abnormality.

vision4.nei.nih.gov/Cogan/index.jsp

EDUCATION

Meeting of the Molecules

From crystallization to protein folding, basic biological and chemical processes depend on interactions among atoms and molecules. High school and beginning college students can study and manipulate these liaisons at Molecular Logic from the Concord Consortium, an educational nonprofit based in Massachusetts. A database furnishes scores of interactive activities that run with free software available from the site. For example, by moving a virtual protein from water to oil, users can observe how the type of solution modifies the molecule's folding. In water, hydrophobic amino acids jostle to reach the molecule's interior, but in oil the hydrophilic amino acids seek the center. Students can also explore the basis for techniques such as electrophoresis and Southern blotting.

molo.concord.org

EDUCATION

Earth, the Early Years

It's hard enough to remember what you did last Wednesday afternoon, let alone what happened during the Jurassic period. Geologic Time, a new interactive timeline from the Smithsonian Institution, offers a handy reference on the different stages of Earth's past. The site spotlights the geological and biological events of the different eons, eras, periods, and epochs. For example, you can leap back to the Archean Eon, which lasted from 4 billion to 2.5 billion years ago, when life originated and today's continents formed. Photo albums display representative rocks and fossils from each time. While *Allosaurus* and other dinosaurs stalked the land during the Jurassic, these ammonites (below), relatives of today's squid, plied the seas. The site also includes backgrounders on concepts such as radioactive dating and plate tectonics.

www.nmnh.si.edu/paleo/geotime

Send site suggestions to netwatch@aaas.org. Archive: www.sciencemag.org/netwatch

CREDITS (TOP TO BOTTOM): JAKE SOCHA/ARGONNE NATIONAL LABORATORY; INSTITUTE OF LABORATORY ANIMALS/KYOTO UNIVERSITY; STEVE JABO/NATIONAL MUSEUM OF NATURAL HISTORY

NEWS

This Week

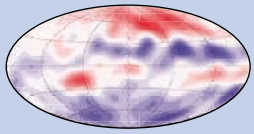

PAGE 364
Flipping over a new Earth model

366
Shake lightly

ENVIRONMENTAL HEALTH

Lead Paint Experts Face a Barrage of Subpoenas

A high-stakes legal battle involving the health hazards of lead paint has turned ugly. A paint company sued by the state of Rhode Island has demanded raw and even unpublished data sets from several researchers so that the court can review scientific claims. Although a lawyer for the company calls the probe routine, one target says it feels like harassment.

Many states and legal experts are watching this trial because a victory by Rhode Island could spur lawsuits by other cities and states seeking compensation for cleaning up lead paint. In the meantime, some scientists whose research is involved say the dueling over data has become unreasonable. "I didn't realize what I was getting into," says epidemiologist Kim Dietrich of the University of Cincinnati in Ohio, who has been asked to turn over 25 years' worth of data even though he is no longer an expert witness.

The company, Sherwin-Williams, is one of seven firms named in the lawsuit that once made or sold lead-based paint. Rhode Island claims that the companies knew of its risks and should pay to clean up a "public nuisance" they helped create. At issue is a long-established link between lead exposure and a drop in IQ, as well as recent studies suggesting that very low blood levels of lead pose a risk and that lead exposure can increase criminal behavior. Before a 2002 trial, Superior Court Judge Michael Silverstein denied the companies' request for raw data from the state's three expert witnesses. The trial ended with a hung jury.

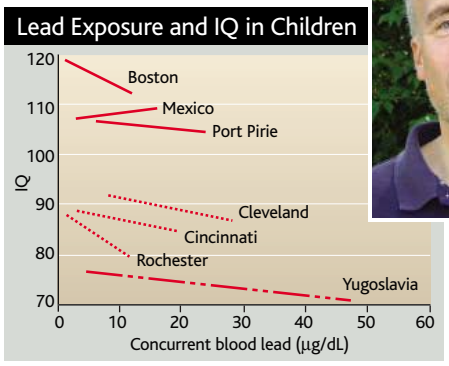

Data duel. Epidemiologist Kim Dietrich is battling company demands for raw data, including this pooled analysis of lead and IQ.

But Silverstein changed his mind in advance of a new trial. Lawyers for Sherwin-Williams asked for data sets from cohort studies in four cities. They demanded even unpublished data, arguing that peer-reviewed studies might have omitted information, such as a father's IQ, that could invalidate the apparent links between lead and adverse health effects. In allowing their request last September, Silverstein cited a 1993 Supreme Court case, *Daubert* v. *Merrell Dow*, which called for pretrial hearings to evaluate scientific experts' opinions. "One cannot … blindfold the defendants and preclude the raw data," he declared.

Two expert witnesses for the state have since turned over certain data sets from their published studies. They are psychiatrist Herbert Needleman of the University of Pittsburgh in Pennsylvania, who has battled data demands before, and environmental health researcher Bruce Lanphear of Cincinnati Children's Hospital Medical Center. In February and May, ▶

CREDITS (TOP TO BOTTOM): GRAPH ADAPTED FROM B. LANPHEAR *ET AL.*, *ENVIRON. HEALTH PERSPECT.* **113**, 894 (2005); (INSET) K. DIETRICH; FRED CHARTRAND/CANADIAN PRESS/AP PHOTO

CLIMATE CHANGE

G8 Leaders Make a Promise to Do More

The U.K. government, champion of a global campaign to control greenhouse gases, let it be known in advance that the G8 meeting it hosted in Scotland wasn't likely to produce any miracles. It didn't.

The G8 plan for mitigating global warming that came out on 8 July was heavy with proposals but light on commitments.* The heads of the eight leading industrial nations promised to boost energy-efficient technology; adopt low CO_2-emitting energy sources (including possibly even nuclear power and hydrogen fuels); and back research collaborations, such as a huge monitoring network called the Global Earth Observation System of Systems (*Science*, 25 February, p. 1182). They pledged to ask the International Energy Agency to work up efficiency standards and the World Bank to boost technology investment. But they endorsed no new targets for reducing greenhouse gases.

Tepid applause? Tony Blair didn't get all that he wanted on climate change from G8 leaders.

The plan's vagueness angered green groups that want action. "This is a very disappointing finale," said Tony Juniper, leader of Friends of the Earth International in London. "The text conveys no sense of the scale or urgency of the challenge." Others, such as the Natural Resources Defense Council in Washington, D.C., found a silver lining in the Bush Administration's failure to "block world action" on limits, "despite [its] intense lobbying."

U.K. Prime Minister Tony Blair acknowledged after the meeting that "we were never going to be able … to resolve the disagreement" over the Kyoto Protocol, the 1997 treaty that commits the 151 participants (the United States refused to sign on) to meet difficult goals for greenhouse-gas reduction by 2012. However, the G8 members should be "proud" of their solidarity, Blair insisted, because all attendees endorse the view "that climate change is a problem, that human activity is contributing to it, and that we have to tackle it." In November, Blair is planning to hold "a new dialogue" on climate change in Britain before a meeting of the Kyoto partners later that month in Montreal.

—ELIOT MARSHALL

With reporting by Eli Kintisch.

* www.fco.gov.uk/Files/kfile/PostG8_Gleneagles_Communique.pdf

368
Vietnam tracks an epidemic

376
A core usage for nanomaterials

two more researchers—neurologist David Bellinger of Children's Hospital in Boston and Dietrich—received subpoenas.

For Bellinger, the request amounted to providing attorneys with a Boston data set he had given to Lanphear for a pooled analysis on IQ and blood lead level appearing this month in *Environmental Health Perspectives*. He initially vowed to resist but relented last month after the judge ruled this could disqualify Lanphear as a witness.

Dietrich is still in limbo. He was an expert witness in the first trial and initially in the second trial, until Sherwin-Williams requested raw data from his study, started in 1979, of some 300 Cincinnati children followed from birth. He asked to be reimbursed for the cost of reconstructing old data tapes and providing other materials—and stripping out identifying information—at about $125,000. He also refused to provide sensitive data on behavior, such as self-reports of criminal arrests. After those conditions were rejected, Dietrich stepped down as a witness in mid-2004. "I thought I was out of the picture," he says.

Then early on 6 May, "a gentleman barged into my office" and demanded materials, Dietrich says. He refused, then was served a subpoena later that day. "As far as I'm concerned, they have no right to the data," he says.

Dietrich has not heard from Rhode Island's lawyers since he withdrew from the case. University of Cincinnati lawyers have offered legal help, but it is unclear whether they will try to quash the subpoena, Dietrich says. Spokesperson Richard Puff said the university cannot comment.

Whereas Dietrich sees it as an "extraordinary" case of harassment, Laura Ellsworth, a lawyer for Jones Day, which represents Sherwin-Williams, says "litigants are entitled to data on which the experts are relying," even if the owners of the data aren't expert witnesses in the case. Such requests are rare but have sometimes been granted, for example in tobacco lawsuits, notes Joe Cecil of the Federal Judicial Center in Washington, D.C. One case last year involved documents from peer reviewers of a book on industrial pollution.

The Rhode Island trial is set to begin on 7 September. For environmental health researchers, the case is a reminder of the risks that come with their work. "Regardless of what happens to me," says Dietrich, "it's something scientists should be aware of."

—JOCELYN KAISER

ASTRONOMY

Improved X-ray Telescope Takes Flight

TOKYO—Scientists hope that, as can happen with love, the Japanese-U.S. Astro-E2 x-ray satellite is better the second time around.

Successfully launched on 10 July, Astro-E2 carries the same six instruments as the original mission that failed on launch 5 years ago. But their performance has been improved. And recent findings from NASA's Chandra X-ray Observatory and the European XMM-Newton Observatory, both launched in 1999, have enabled scientists to hone their list of observational targets. "Although it was a big catastrophe 5 years ago, the mission now is more timely because we know much more about the x-ray sky and have greater [observational] capabilities," says Nicholas White, chief of the Laboratory for High Energy Astrophysics at NASA's Goddard Space Flight Center in Greenbelt, Maryland. The mission is a joint effort of NASA and the Japan Aerospace Exploration Agency (JAXA).

Astro-E2's crown jewel is the X-ray Spectrometer (XRS), which "allows investigations that have never been possible before," says Andrew Fabian, an astrophysicist at the University of Cambridge, U.K., and science adviser to the mission. Developed by JAXA's Institute for Space and Astronautical Science (ISAS) and NASA, XRS measures the energy of individual x-ray photons. The original XRS had higher spectral resolution, or a greater ability to distinguish energy levels, than any other x-ray instrument in space. By eliminating some sources of noise, scientists doubled that resolution. And improved cryogenics add half a year or more to the 2-year life of the instrument.

Second try. Astro-E2 blasts off from Japan's Uchinoura Space Center.

These improved capabilities will be put to good use. Richard Kelley, NASA's principal investigator for XRS, explains that Chandra has seen evidence of blobs of material in the accretion disks surrounding certain black holes. Astro-E2 should be able to determine if these blobs are real and then to use them "as probes to tell whether the general picture of matter spiraling [into a black hole] makes sense," he says. XRS should also be able to confirm previous glimpses of the telltale distortion of x-ray emissions expected when iron elements encounter a black hole's intense gravitational pull. XRS will also be looking at clusters of galaxies for clues to the role of dark matter in their evolution and dynamics.

Other instruments are expected to keep working for 5 to 7 years, says Hideyo Kunieda, an astrophysicist at Nagoya University who is the principal mission scientist for ISAS. These include the hard x-ray detector, developed by ISAS and a group at the University of Tokyo, that looks at very high energy x-rays emanating from the most violent astrophysical phenomena. There is also a set of four x-ray charge-coupled device cameras covering a wide range of energies. All instruments will be observing the same objects simultaneously for a broad picture of emissions over the x-ray spectrum.

The satellite was given a new name, "Suzaku," after the launch from the Uchinoura Space Center in southwestern Japan. But mission scientists caution that it will take a few weeks to make sure everything is operating properly. "We can't be completely at ease yet," says ISAS astrophysicist Noriko Yamasaki. If all goes well, scientific observations will start early next month.

—DENNIS NORMILE

CREDIT: GSFC/NASA

GEOPHYSICS

Threshold Crossed on the Way to a Geodynamo in a Computer

How do you tell whether you've got the right answer if you never get to look at the answer sheet? Geophysicists trying to conjure up the geodynamo that generates Earth's magnetic field have been grappling with that conundrum for years. Seemingly any computer model with the basic physics of the churning molten-iron core produces a reasonable-looking magnetic field as seen at Earth's surface. Yet the models produce those similar surface fields by creating entirely different geodynamos in their cores (*Science*, 10 January 1997, p. 160). Without access to the real core, how do you tell which one is right?

On page 459, Japanese modelers report that one of the world's fastest computers has pushed their geodynamo model into a new regime, in which for the first time a crucial aspect of core behavior matches theoretical expectations. "It's the closest yet to describing what happens with the real Earth," says planetary physicist David Stevenson of the California Institute of Technology in Pasadena. "This might actually be a realistic model." If so, it might reveal whether Earth's magnetic field is beginning one of its once-in-100,000-years flip-flops, as geophysicists have recently wondered.

Much as weather forecasting models use equations of motion to calculate the flow of the atmosphere, geodynamo models calculate the flow of the core's highly conductive molten iron. The models must also include calculations of the electric currents and magnetic forces generated when the conducting iron flows across magnetic fields.

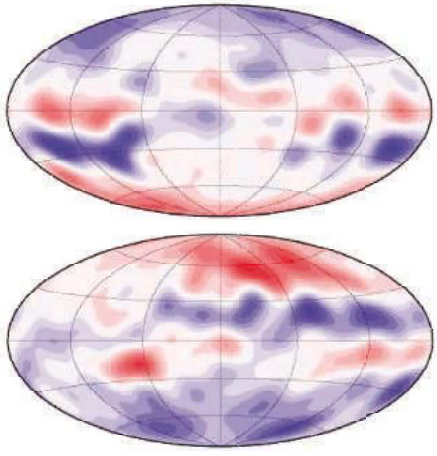

How to flip-flop. In simulation, patches of the emerging magnetic field (blue, *top*) appear at low latitudes and then head poleward (*bottom*).

What gave the Japanese group an edge over previous modelers was the Earth Simulator, once the world's most powerful computer and now the fourth most powerful (*Science*, 1 March 2002, p. 1631). Using just a tenth of the Earth Simulator's 5120 processors during 6500 hours of computation, Futoshi Takahashi of the Japan Aerospace Exploration Agency in Kanagawa and Masaki Matsushima and Yoshimori Honkura of the Tokyo Institute of Technology achieved an unprecedented level of realism in their simulations.

In particular, they were able to use the lowest-ever value of a key parameter, the Ekman number, which represents the relative importance of the fluid iron's viscosity to the rotation rate of the planet. In theory, a small enough Ekman number—approaching the real value in the core—would allow viscous drag forces to approach zero, but previous simulations couldn't calculate the flow of molten iron on a small enough scale to let that happen. The Earth Simulator run lowered the Ekman number by an order of magnitude.

Cranking up all that computer power produced "a lot of Earth-like qualities in their maps" of changing magnetic fields, says modeler Andrew Jackson of the University of Leeds, U.K. But what impresses geodynamo researchers most is the way the core in the new simulations behaves. In previous simulations, the viscous drag of the fluid iron was on a par with the forces induced by flowing currents. Here, however, viscous effects have become negligible, just as theory says they should be. Although not all the input parameters are realistic yet, the Japanese modelers "seem to have reached a regime like Earth's," says Stevenson. "It's a remarkable achievement."

A truly realistic simulation of geodynamo behavior could allow researchers to forecast the "weather" in Earth's core, with practical implications. Geophysicists have been worrying out loud lately that a 10% weakening of the magnetic field during the past 170 years may presage an overdue flipping of Earth's magnetic poles, a so-called magnetic reversal. It's been 780,000 years since the last reversal, although millennia-long reversals have occurred on average every 100,000 years or so. Aside from millennia of confused magnetic navigation, a reversal would ▶

CREDIT: F. TAKAHASHI *ET AL.*, *SCIENCE*

AVIAN INFLUENZA

Chinese Ministry Questions Bird Flu Findings

The Chinese Ministry of Agriculture sharply criticized a paper published online by *Nature* last week suggesting that an outbreak of H5N1 avian influenza among wild birds in northwest China originated from apparently unreported outbreaks among poultry in southern China. The researchers defend their results and worry that the ministry's reaction may lead to overly strict enforcement of new guidelines on handling the H5N1 virus.

The brief report by Honglin Chen of Shantou University Medical College and colleagues there and at the University of Hong Kong and other institutions, posted on 6 July, claims that the virus recovered from wild birds at Qinghai Lake is a genetic match to one found among poultry earlier this year at a live market in China's Guangdong Province. The following day, China's official Xinhua News Agency quoted Jia Youling, director general of the Agriculture Ministry's Veterinary Bureau, questioning the article's credibility because H5N1 has not been reported in Guangdong this year. He added that the Shantou lab doesn't have the proper biosafety features for handling the virus.

Chen says the report's conclusions will be supported by additional data on H5N1 circulating in southern China in an upcoming publication. He adds that the research conducted in the Shantou lab, a biosafety level 2-plus lab, conforms "entirely with … World Health Organization guidelines." And Chen denies news reports that the ministry is attempting to close their operations. "We are now establishing communications with the ministry to gain an understanding about our research," he says.

The Agriculture Ministry's guidelines for handling highly pathogenic viruses, adopted in late May, simply spell out in more detail previously established procedures, says George Gao, a virologist at the Chinese Academy of Sciences' Institute of Microbiology and the corresponding author of a paper on the Qinghai outbreak published online by *Science* on 7 July. (That paper focuses on the pathogenicity of the viral strain without tracing it to any previously reported outbreaks among poultry.) Roy Wadia, a spokesperson for the World Health Organization's Beijing office, says the agency hopes that the guidelines "will be interpreted in a way that will both ensure that research is carried out in a safe manner but also encourage, stimulate, and support research into this virus."

–DENNIS NORMILE

With reporting by Martin Enserink.

greatly weaken Earth's magnetic shield that fends off cosmic radiation.

In the Earth Simulator model runs, at least, reversals begin with distinctive pairs of magnetic flux patches, areas at the surface where magnetic fields of opposing polarity protrude from the interior. These patches first appear in the model at low to middle latitudes as a reversal begins and migrate poleward as the reversed field emerges from the outer parts of the core. Curiously, parts of the early stages of a simulated reversal "look a lot like the South Atlantic today," says paleomagnetist Bradford Clement of Florida International University in Miami.

Intriguing reversal simulations aside, "we've still got a ways to go," says Gary Glatzmaier of the University of California, Santa Cruz, one of the first to run simulations of the dynamo 10 years ago. "They're getting closer [to realistic conditions], but you're still not close enough to be confident you've got something Earth-like." Among other shortcomings, the model still doesn't have enough computing power to banish glitches such as too-frequent reversals. "It's going to take 5 to 10 years for computers to be fast enough," says Glatzmaier.

–RICHARD A. KERR

CLIMATE FORECASTING

India Chucks Monsoon Model

NEW DELHI—The Indian government has decided that its controversial, homegrown computer model to predict the all-important monsoon is all wet. Turned off by the model's poor track record, officials at the Department of Science and Technology (DST) have teamed up with modelers at the U.S. National Center for Atmospheric Research (NCAR) in Boulder, Colorado, to use the center's new software for weather prediction and forecasting.

The June-to-September monsoon is vital to Indian farmers and to the country's economy. But the complex atmospheric conditions make it extremely difficult to predict. A model developed in the 1980s by the India Meteorological Department (IMD) incorporated data from 16 factors in hopes of eliminating much of the uncertainty (*Science*, 23 August 2002, p. 1265). Instead, the model tended to predict normal levels of rainfall and missed extreme events like the massive flooding in 1994 and widespread droughts in 1987, 2002, and last year (see graph). IMD's poor performance goes back even further, say atmospheric scientists Sulochana Gadgil and Ravi Nanjundiah of the Indian Institute of Science in Bangalore and IMD's M. Rajeevan. Writing recently in India's *Current Science*, they argue that "the forecast skill has not improved over seven decades despite continued changes in the IMD operational models."

Although IMD officials continue to believe that the model has been a useful tool, DST Secretary Valangiman Subramanian Ramamurthy says he concluded late last month that it was time for a change. "If it's failing," he says, "we can't continue with it." Unfortunately, he says, India does not have the necessary skills or time to start from scratch.

Thanks to the new Weather Research and Forecasting (WRF) model, it doesn't have to. Greg Holland, director of NCAR's mesoscale and microscale meteorology division, calls the model "a very advanced system, usable down to very fine resolutions of less than 1 kilometer." Using globally available data as a starting point, scientists can plug in regional data to fine-tune the forecast. In addition to short-range weather prediction, the model is also capable of making the type of seasonal forecasts that Indian officials desire for the monsoon.

Both sides see important benefits from the collaboration, which was worked out earlier this month when Ramamurthy visited NCAR. NCAR gets to expand the WRF model, already used in China, Taiwan, and South Korea, to the Indian subcontinent.

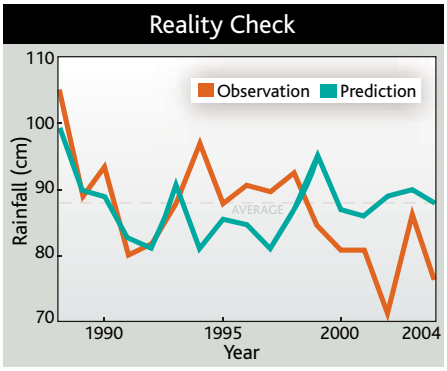

Dry runs? India's monsoon forecast has failed to predict recent droughts.

The two countries agree to conduct joint research not only on the monsoon but also on a 2-year demonstration project to predict deadly tropical cyclones in the Bay of Bengal. And India gets the promise of a more accurate monsoon prediction.

To make the most of the new software, Ramamurthy says DST is close to signing a $7 million deal to purchase a more powerful supercomputer. "A teraflop machine running WRF would definitely bring India to the leading edge of atmospheric modeling," says Holland, as well as "substantially improving local weather forecasts."

–PALLAVA BAGLA

SOURCE: S. GADGIL *ET AL.*, *CURRENT SCIENCE* (10 MAY 2005)

ScienceScope

WHO Strengthens Pandemic Team

The World Health Organization (WHO) is beefing up its efforts against influenza. Besides Margaret Chan, the new head of the Communicable Disease Surveillance and Response Department (*Science*, 8 July, p. 243), the agency is bringing on several new experts, including Keiji Fukuda, an epidemiologist at the Centers for Disease Control and Prevention in Atlanta, Georgia. Chan says she will seek more money from agencies such as the European Commission and the World Bank. Former flu program head Klaus Stöhr, long the public face of influenza, will continue to lead a group focusing on science but will no longer talk to the press, says Chan.

–MARTIN ENSERINK

Senate Jostling on Stem Cells

Stem cell supporters in the Senate are going all-out to prevent defections as a vote nears on a measure to expand the number of lines available to federally funded researchers. Senators Arlen Specter (R–PA) and Tom Harkin (D–IA) fear that some members will champion alternative ways to obtain stem cells to avoid taking a stand on their bill. Possible alternatives include cultivating a single cell from an early embryo without harming it or a cloning technique that creates a nonviable embryo.

This week, Specter and Harkin assembled scientists at a hearing to analyze means of deriving new human stem cell lines that don't destroy embryos. James Battey, the National Institutes of Health's stem cell point man, and stem cell researcher George Daley of Harvard agreed that the proposals that sound most promising are still far from being technically feasible and said some carry ethical problems of their own. Senate bill 471—identical to H.R. 810 passed by the House in May—is due for a vote before the August recess.

–CONSTANCE HOLDEN

ITER: India Wants In

This week, India expressed formal interest in joining the effort to build an energy-producing fusion reactor. The six current partners—China, the European Union (E.U.), Japan, Korea, Russia, and the United States—have just agreed on Cadarache, France, as the site of the International Thermonuclear Experimental Reactor (ITER). Now India's Atomic Energy Commission says in a letter to the E.U. that his country is considering "full partner" status.

–DANIEL CLERY

ENERGY SCIENCE

Tight Budgets Force Lab Layoffs

Shifting priorities and the expectation of worsening budgets have triggered layoffs at two U.S. synchrotron facilities in California. Officials at the Department of Energy's (DOE's) Advanced Light Source (ALS) at Lawrence Berkeley National Laboratory and the Stanford Synchrotron Radiation Laboratory (SSRL) say the cutbacks, which include shutting down one beamline at each facility, are necessary to free up money for new projects, such as brighter beams. The cuts may not be reversed, managers say, even if Congress beefs up the lean 2006 DOE budget proposed by the Bush Administration.

Beaming down. Stanford's synchrotron lab has dropped a beamline used by Michigan's John Bilello to study thin metallic films.

"I had to make some tough choices," says SSRL director Keith Hodgson, who in April let go eight scientists and technicians and stopped scheduling users on one beamline doing materials research. "I could have stopped advanced beamline development and saved jobs" in response to the president's proposal to cut the lab's 2006 budget by 8%. Instead, Hodgson says, he chose to protect his most promising programs in the face of uncertainty.

The two labs are funded by DOE's $1.1 billion Office of Basic Energy Sciences (BES), which received a $41 million boost in the president's request for 2006. But that 4% increase includes $151 million in new funds to expand nanoscale research facilities and begin work on the Linac Coherent Light Source at Stanford and a high-flux neutron beam under construction in Oak Ridge, Tennessee, the pair of which should benefit physicists, doctors, and chemists. Taking into account $52 million in construction costs that DOE will save in 2006, the result is a proposed $58 million belt tightening within existing BES programs, including 7% at ALS.

Pat Dehmer, DOE associate director of science for BES, says funds for new projects have led to similar tradeoffs elsewhere in the DOE budget. "As a result of those high priorities, cuts had to be made virtually across the Office of Science," she says.

Two other DOE-funded synchrotron sources, at the Argonne (Illinois) and Brookhaven (New York) national labs, have so far avoided layoffs. But there are hiring cutbacks at each facility that affect about a dozen positions now vacant.

In addition to financial pressures, the cutbacks also reflect shifting science trends on a local scale. This spring, ALS acting Director Janos Kirz shuttered an x-ray spectroscopy line used for diagnosing silicon wafers and removed from the Berkeley lab's payroll 16 scientists and support staff. New analysis methods have been shown to be "simpler or better," he said. At the same time, Stanford's Hodgson stopped scheduling users for an undersubscribed topography imaging beamline used to characterize ▶

NONLINEAR OPTICS

To Physicists' Surprise, a Light Touch Sets Tiny Objects Aquiver

Much as a child might make a soda bottle shake by blowing across its top and filling it with sound waves, physicists have set a tiny disk of glass vibrating by "whistling" light through it. The effect could lead to optically controlled micromachines but might also limit the sensitivity of giant gravitational-wave detectors.

"I'm deeply impressed," says Dirk Bouwmeester, a physicist at the University of California, Santa Barbara. "The findings add a completely new tool to the fields of optical interferometry and information processing."

The fat-rimmed disk of silica used by physicist Kerry Vahala and colleagues at the California Institute of Technology (Caltech) in Pasadena is an "optical microcavity" that "rings" with light of distinct frequencies, just as a soda bottle whistles at specific pitches. Optical microcavities control lasers in CD and DVD players, and higher-quality cavities that can hold more light might help shuttle photons through "photonic" circuits. This week, the Caltech researchers report online in the journal *Optics Express* that light coursing through a microcavity can set the thing in motion.

In the experiment, light from a nearby optical fiber bled into the disk and raced around its rim. Pressure from the circulating light set the disk vibrating. The vibrations stretched the disk and altered the frequency of the light in telltale ways, the researchers found.

Theorists had predicted that light pressure might cause an optical cavity to vibrate, but the rattling caught the researchers off-guard. "We were studying the nonlinear optical properties of these cavities," Vahala says. "This one really came out of the blue."

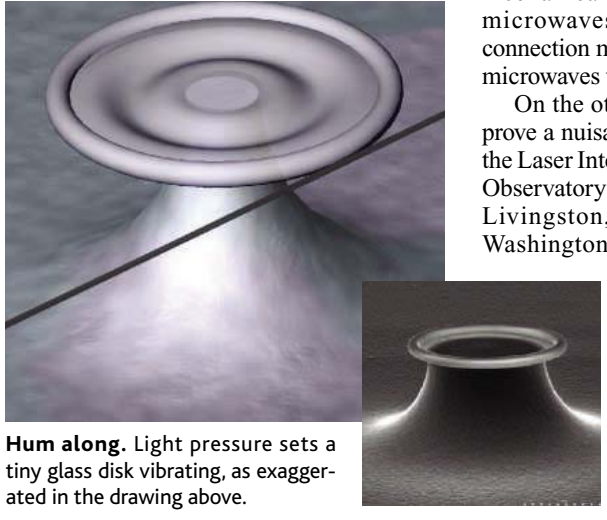

Hum along. Light pressure sets a tiny glass disk vibrating, as exaggerated in the drawing above.

The effect could prove useful, says Ming Wu, an electrical engineer at the University of California, Berkeley. For example, researchers are already developing micrometer-sized mechanical oscillators that interact with microwaves. So the light-to-vibrations connection might make it possible to control microwaves with light, Wu says.

On the other hand, the vibrations could prove a nuisance for researchers working on the Laser Interferometer Gravitational-Wave Observatory (LIGO). With installations near Livingston, Louisiana, and in Hanford, Washington, LIGO relies on high-power, 4-kilometer-long optical cavities to search for gravitational waves, which would stretch the cavities. Vibrations caused by light pressure might limit LIGO's ultimate sensitivity, Bouwmeester says, and that's no small shakes.

–ADRIAN CHO

CREDITS (TOP TO BOTTOM): UNIVERSITY OF MICHIGAN; DENIZ ARMANI/CALTECH; (INSET) TOBIAS KIPPENBERG/CALTECH

stress in metallic thin films.

Some users acknowledge the need for change, despite the disruption. "Given that nanotechnology is moving toward more biomaterials, I would support [Hodgson]," says materials scientist John Bilello of the University of Michigan, Ann Arbor, who used the SSRL beamline and now eyes the CERN high-energy physics lab near Geneva, Switzerland, as an alternative.

Congress seems eager to help. In separate bills that must be reconciled, the Senate and House have added back $95 million and $27 million, respectively, to the BES budget. "Existing capabilities cannot be sacrificed to purchase new facilities," Senate appropriators wrote in a committee report that observers see as a vote of confidence in current work. But even with a restored 2006 budget, Hodgson and Kirz say it may be difficult to rehire staff or reopen beamlines.

–ELI KINTISCH

RESEARCH MANAGEMENT

NSF Looks Inward for Geoscience Head

It's been 16 years since the National Science Foundation (NSF) has hired a senior research manager from within the ranks. But that streak seems about to end.

Unlike other federal science agencies, NSF has relied on so-called rotators—academic scientists chosen after a national search and on temporary leave from their institutions—to head each of its seven research directorates as assistant NSF directors (ADs). The theory is that the best people to allocate the agency's $5 billion research and education portfolio are those working at the frontiers of science—and who want to go back. Indeed, the succession of outsider appointments since Mary Clutter was promoted to lead the biology directorate in 1989 has created the impression that such a policy was carved in stone.

In the lead. NSF's Margaret Leinen seems to have the inside track for the geosciences post.

Apparently not. This month, NSF Director Arden Bement took a chisel to that philosophy by laying the groundwork for the incumbent, paleoceanographer Margaret Leinen, to remain as head of the geosciences directorate. A job notice posted 5 July says that candidates must be federal employees and that the successful applicant will be hired as a career appointment. They also have a scant 2 weeks to apply. That combination has raised eyebrows among those within the foundation who feel that NSF should conduct a national search before filling such an important job. But the rules reflect Bement's willingness to consider alternatives to the rotator model as well as his high regard for Leinen.

"She's eminently qualified, and we'd like to have her around for a long time," says Bement. "She's truly outstanding, and she has great experience." Bement also says he's "much more open" to the idea of having a career AD than some of his predecessors.

Like a typical rotator, Leinen, 58, took leave from her post as a top administrator at the University of Rhode Island (URI) to come to NSF in January 2000. Three years later, then–NSF Director Rita Colwell announced a national search for the geosciences post that culminated in extending Leinen's stay at NSF until January 2007, in a temporary category called a limited-term employee. If Leinen is hired under the new job posting, she would need to sever her ties to URI and become a career federal worker.

"I have not yet applied for the job," Leinen said last week, "and whether or not I do is my business." She declined further comment.

Scientists who have seen Leinen in action give her high marks. "She's good at articulating environmental issues and programs in ways that excite people and at getting the geosciences involved in interdisciplinary efforts," says Susan Brantley, head of the Earth and Environment Institute at Pennsylvania State University, University Park, and a member of NSF's geosciences advisory committee. Another advisory panelist, Robert Harriss of the National Center for Atmospheric Research in Boulder, Colorado, which receives more than $60 million a year from NSF, says approvingly that "she likes to think big."

Bement acknowledges that NSF's "routine approach" to finding an AD is through a national search. But Leinen rose to the top during two such previous searches, he notes, adding that he sees no reason "to stretch things out for 6 months" if there's a person "who's fully qualified."

–JEFFREY MERVIS

CREDIT: MICHAEL SALERNO/URI

ScienceScope

Solar Bill Advances in California

Two key California legislative committees approved an ambitious new solar energy initiative last week. The initiative, backed by California Governor Arnold Schwarzenegger, aims to raise power generation from solar cells from the current level of 100 megawatts to more than 3000 megawatts, enough to power more than 500,000 homes. The bill is expected to become law next month. It would require builders of new homes to offer solar power systems to buyers. The solar systems would likely cost about $15,000, but buyers would receive about $5000 in rebates from the state. The rebates are set to decline 7% per year before expiring in 2016, a progression that the state hopes will encourage innovation by forcing manufacturers to cut costs and boost efficiency.

–ROBERT F. SERVICE

Trial Awaits Growth Hormone Researchers

PARIS—The French Supreme Court has cleared the way for 12 French scientists and doctors to stand trial for their role in treating hundreds of children with contaminated human growth hormone (HGH). The 12 defendants include Fernand Dray, who was in charge of purifying the material at the Pasteur Institute. A total of 968 children were treated in France with high-risk batches of HGH between December 1983 and June 1985, and 103 so far have died from Creutzfeldt-Jakob disease, the human form of "mad cow disease" (*Science*, 18 March, p. 1711). If convicted, the scientists could each face up to 4 years in prison. The court last week ruled that a 3-year statute of limitations on bringing charges begins when symptoms first appear and not when the suspect material was administered. The criminal investigation, begun in 1991, is winding down, and the trial may start early next year, says the victims' lawyer.

–BARBARA CASASSUS

Finalists Vie to Be Pasteur Head

PARIS—The 117-year-old Pasteur Institute has never had a woman president. But that could change this fall after the board of directors announced two finalists to succeed Philippe Kourilsky. One is Alice Dautry-Varsat, a chlamydia researcher who heads Pasteur's Biology of Cell Interactions Unit. The other candidate is Pierre Legrain, a former Pasteur scientist who in 1997 co-founded Hybrigenics, a Paris-based biotech. A decision is expected during the board's 2 September meeting.

–MARTIN ENSERINK

While international experts warn of a potential human pandemic, scientists in Vietnam are striving to do their share to bring the H5N1 avian influenza virus under control

Vietnam Battles Bird Flu ... And Critics

HANOI AND HO CHI MINH CITY—Ever since the H5N1 avian influenza virus started its devastating sweep through Southeast Asia, international health experts and Western scientists have vacillated between praising and criticizing Vietnam's efforts and willingness to cooperate.

The World Health Organization (WHO) has repeatedly complained that Vietnamese authorities have been slow to report new human cases and relatively tight with epidemiological data. But the government's own epidemiologists did sound an alarm this spring, alerting international authorities after they had spotted apparent changes in the virus's behavior. Vietnam asked for help in interpreting data but also seems intent on going its own way in vaccine development, to the consternation of some public health experts. Research institutes here are looking for collaborations, but they have subtly let it be known they will pick and choose among proposals to ensure that they are mutually beneficial. This leaves some prominent virologists begging for samples and information. A particularly sore point among researchers trying to track the outbreak in poultry has been the paucity of relevant data from Vietnam. But Vietnamese animal health authorities readily admit that their surveillance system is rudimentary, and this is the area that's received the least international assistance.

Despite the system's shortcomings, scientists working with counterparts in Vietnam say that the country deserves praise for doing so much with so little. "We have been very impressed with the work that the Vietnamese are doing," says Tim Booth, director of the Viral Diseases Division at Canada's National Microbiology Laboratory in Winnipeg, which is collaborating with Vietnamese colleagues on serum surveys that might uncover subclinical cases. Adds Masato Tashiro, who has been on several missions to Vietnam as director of WHO's Collaborative Center for Influenza Surveillance and Research at Japan's National Institute of Infectious Diseases (NIID) in Tokyo: "The surveillance and research effort by Vietnam, I think, is highly respected in the community."

Building capacity. Pasteur Institute virologist Phan Van Tu says technology transfers would help Vietnam do more on its own.

Vietnamese scientists are both stung and genuinely puzzled by claims that they aren't cooperating. At the National Institute of Hygiene and Epidemiology (NIHE) in Hanoi, Vice Director Pham Ngoc Dinh lists the foreign labs the institute has worked with: NIID, the U.S. Centers for Disease Control and Prevention (CDC), Hong Kong's Department of Public Health, and Canada's National Microbiology Laboratory. At the Pasteur Institute in Ho Chi Minh City, virologist Phan Van Tu mentions many of the same partners and adds a group in Israel.

Still, Tu emphasizes that as long as the outbreak continues, there will be additional opportunities for international support. "We want to do more [to combat the outbreak] on our own," Tu says. "But we need collaborations with labs in developed countries for transfers of technology."

Starting from scratch

Vietnam has every incentive to take H5N1 seriously. Not only has it been hit with the largest number of human cases (87) and deaths (38), but losing 46 million chickens and ducks to disease and culling has also had a cruel economic impact. The government estimates that in the first half of 2004 alone, direct and indirect costs ran to $190 million and shaved 0.5% off the nation's gross domestic product.

But in confronting this challenge, Vietnam's public health system was starting almost from scratch. "Before the outbreak, few scientists in Vietnam were interested in influenza because very few people die of ordinary flu here," says Tu. Despite the country's experience with severe acute respiratory syndrome in 2003, its labs weren't equipped to deal with infectious pathogens. "We didn't even have personal protection equipment" such as masks and gloves, says Le Thi Quynh Mai, an NIHE virologist. (Both NIHE and the Pasteur Institute are now Vietnamese governmental institutions.)

Early in the outbreak, Tu recalls, Pasteur drew up a wish list of needed equipment; WHO arranged for roughly $60,000 worth of polymerase chain reaction (PCR) test gear, safety cabinets, centrifuges, incubators, and freezers. And NIHE got a similar package of goodies. One important item that didn't come through, however, was a biosafety level 3 (BSL-3) lab—ruling out local work on some important aspects of the contagious H5N1 virus.

Vietnamese epidemiologists and virologists have done well with the resources at

CREDITS (TOP TO BOTTOM): ASSOCIATED PRESS; D. NORMILE/*SCIENCE*

hand, says Jeremy Farrar, director of the Oxford University Clinical Research Unit at the Hospital for Tropical Diseases in Ho Chi Minh City, who points to two major achievements. The first was simply catching the few human H5N1 cases among the hundreds of patients with respiratory illnesses that turn up each week. As soon as H5N1 was reported among poultry in the region in late 2003, NIHE's Mai readied reverse transcription–PCR (RT-PCR) assays, which probe for the RNA of a replicating virus, as a precaution. And in January 2004, her lab detected the H5N1 virus in a flu victim, confirming the first human case of the outbreak in Southeast Asia. "It was one of the biggest achievements of our institute," NIHE's Dinh says.

NIHE and Pasteur immediately started collecting throat swabs and serum samples from family members and contacts of victims, as well as from random poultry workers. Through the first months of 2004, NIHE collected several hundred samples in northern Vietnam; Pasteur got several dozen more in the south. In addition to patients, their contacts and poultry workers were tested using the RT-PCR assay; the results were overwhelmingly negative. The two institutes were unable to check for antibodies to the virus in blood samples, a sign of past infection, because the most sensitive procedure, the microneutralization assay, requires a BSL-3 lab. Instead, they shipped the samples to CDC in Atlanta, Georgia, where tests confirmed the negative findings.

The second achievement was detecting a change in the behavior of the virus in early 2005, when epidemiologists traced contacts in northern Vietnam and turned up clusters of cases, including asymptomatic and mild cases. This raised fears that the virus was becoming less lethal but more infectious. At Vietnam's request, WHO sent in a fact-finding team of virologists and public health experts and organized expert meetings to review the data. (In late June, WHO issued a brief report concluding that the virus was not undergoing a major change.)

Vietnamese scientists seem miffed that even achievements such as these don't always earn credit. For instance, although scientists from both NIHE and Pasteur presented findings from their 2004 surveys at avian influenza meetings in Asia last year, as late as spring of 2005, members of the global influenza community were publicly urging Vietnam to undertake these kinds of surveys (*Science*, 25 March, p. 1865). And when the asymptomatic cases surfaced this spring, many Western scientists—instead of praising the subtle finding—openly worried that Vietnam's epidemiologists were missing a hidden iceberg. Yet later, WHO concluded it was unlikely that large numbers of cases were going undetected.

A missing part of the picture. Physician Nguyen Hong Ha understands the need for autopsies to better understand the H5N1 virus, but families in Vietnam rarely consent.

This gap in communication is due partly to the fact that Vietnamese researchers are only now forming ties to the tight-knit global influenza community, and partly to differing attitudes toward publishing. Peter Horby, an epidemiologist in WHO's Hanoi office, explains that Western researchers rush results into high-profile journals. But that tradition "is much less strong here," he says, adding that Vietnamese scientists feel their first responsibility is to provide scientific data to guide government policy.

International collaborators. Twin colonial-era buildings house the governmental National Institute of Hygiene and Epidemiology in Hanoi (shown) and the Pasteur Institute in Ho Chi Minh City.

Respect the dead

Although Vietnam's epidemiological work has earned respect, international health officials and scientists are frustrated with some aspects of the clinical research and are questioning the country's vaccine efforts.

In the 18 months since the outbreak hit Southeast Asia, only four or five autopsies have been performed on victims—all of them in Thailand. Nguyen Hong Ha, an infectious disease specialist at the Institute for Clinical Research in Tropical Medicine in Hanoi, says scientists there understand the importance of autopsies in elucidating how the virus attacks the body. "But by Vietnamese law, the consent of the family is required to conduct any postmortem research, and families have not given that consent," he says. Farrar adds that a national association of physicians has urged the Vietnamese government either to modify the law or to exercise the right to mandate autopsies under exceptional circumstances. But authorities hesitate to go against a deeply rooted cultural bias.

WHO is also concerned about—and very interested in—NIHE's effort to develop an H5N1 vaccine for humans. David Wood, coordinator of WHO's Quality Assurance and Safety of Biologicals Team, says the organization applauds Vietnam's initiative but worries that the development process used for one of its vaccines "goes into uncharted territory," raising questions about efficacy and contamination.

CREDITS (TOP TO BOTTOM): D. NORMILE/*SCIENCE*; MAP INSET: D. NORMILE/*SCIENCE*

ALMOST 40 YEARS AFTER THE LAST INFLUENZA PANDEMIC, an explosion of the H5N1 strain in Asia is fueling worries that a lethal new flu virus may soon sweep the world. H5N1 has devastated the Asian poultry industry and infected at least 100 people in roughly three successive waves; it has also been shown to infect several other mammal species. Because human-to-human transmission is still rare, the World Health Organization (WHO) categorizes the current outbreak as a "phase 3" pandemic threat.

Some 40 countries now have published plans to deal with a pandemic, varying from a few to many hundreds of pages. At least 18 countries have ordered stockpiles of oseltamivir, an anti-influenza drug, but the percentage of the population that would be covered varies widely by country. Roche, the drug's only supplier, is in negotiations with a dozen other countries; it may take years to fill all the orders.

Around the globe, other avian influenza strains—including H7N7 and H9N2—have occasionally infected humans in recent years, and they too could transform into the next pandemic virus.

–Martin Enserink (text); Kelly Buckheit (design)

WHO

SWITZERLAND

Roche oseltamivir factory in Basel

WHO headquarters in Geneva

H7N7
NETHERLANDS
89 cases, 1 death
2003

WHO

WHO

H5N1
ASIA (see detail)
2003–05

H5N1
HONG KONG
18 cases, 6 deaths, *1997*
2 cases, 1 death, *2003*

H9N2
HONG KONG
2 cases, *1999*
1 case, *2003*

WH

H5N1'S ANIMAL HOSTS

H5N1 infects an extraordinary variety of species. Its currently known animal hosts include:

WILD BIRDS
Believed to be H5N1's source. Migratory species may spread the virus far and wide.

DUCKS
Can be symptomless carriers of H5N1, making them a particularly dangerous reservoir.

HOUSE CATS
Dutch study showed they can be fatally infected and transmit virus to cagemates.

JUPITER IMAGES

BIG CATS
Tigers and leopards in two zoos in Thailand were infected and killed after eating infected poultry.

CHICKENS
Thousands of poultry farms affected throughout Asia, more than 60 million chickens culled.

JUPITER IMAGES

PIGS
Reported to be infected in China and Indonesia. Suspected mixing vessels for avian and human flu viruses.

HUMANS
More than 100 laboratory-confirmed cases, including more than 50 deaths. True spread may be much greater.

STAGES OF A PANDEMIC according to WHO

PHASE 1: No new influenza virus subtypes detected in humans. An influenza virus subtype that has caused human infection may be present in animals, but the risk for humans is considered low.

PHASE 2: No new influenza virus subtypes detected in humans. However, a circulating animal influenza virus subtype poses a substantial risk of human disease.

INTERPANDEMIC PERIOD

PHASE 3: Human infection(s) with a new subtype. No human-to-human spread, or at most rare instances of spread to a close contact.

PHASE 4: Small cluster(s) with limited human-to-human transmission but spread is highly localized, suggesting that the virus is not well adapted to humans.

PHASE 5: Larger cluster(s) but human-to-human spread still localized, suggesting that the virus is becoming increasingly better adapted to humans but may not yet be fully transmissible. Substantial risk of a pandemic.

PANDEMIC ALERT PERIOD

PHASE 6: Increased and sustained transmission in the general population.

PANDEMIC

Current level

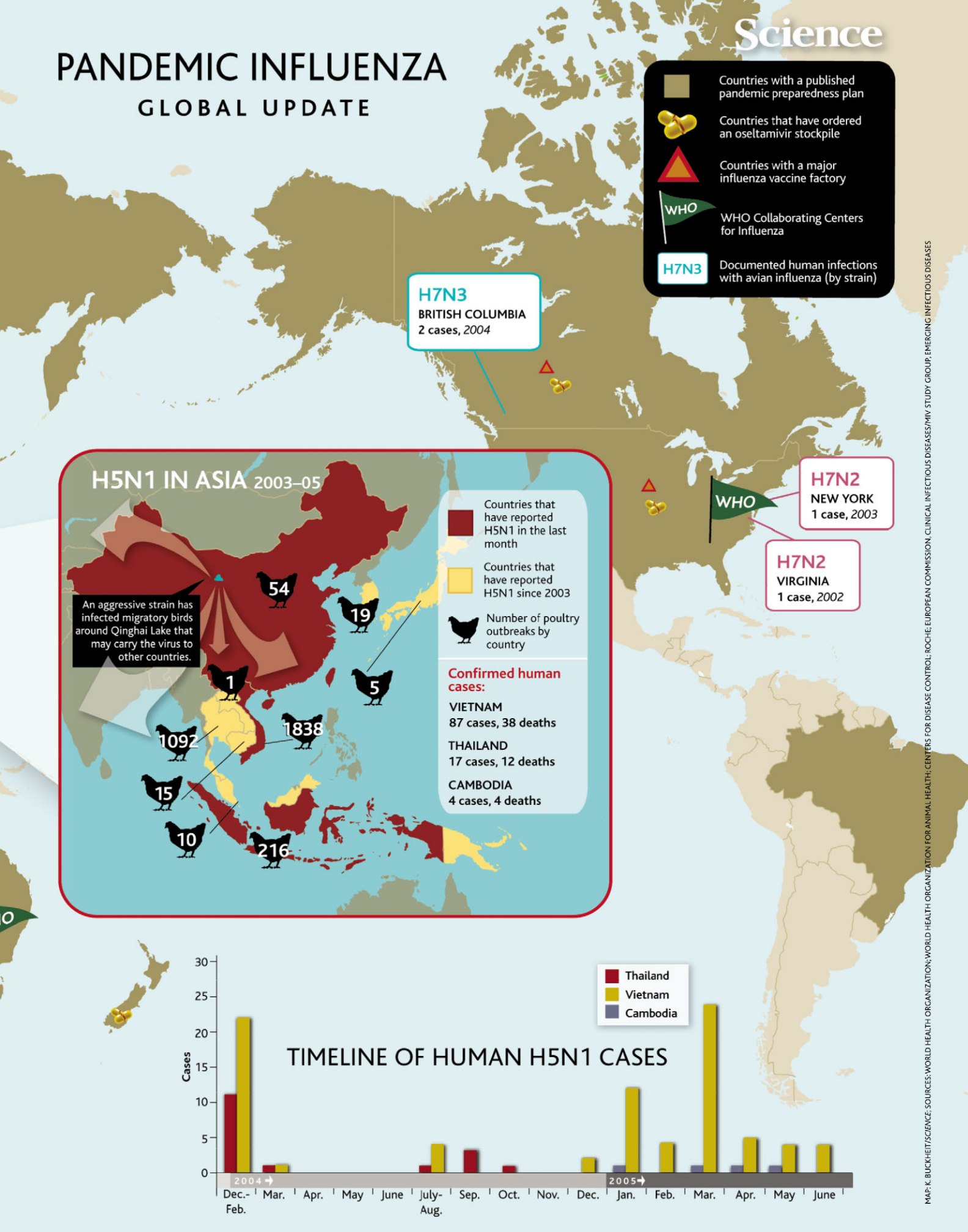

MAP: K. BUCKHEIT/*SCIENCE*; SOURCES: WORLD HEALTH ORGANIZATION; WORLD HEALTH ORGANIZATION FOR ANIMAL HEALTH; CENTERS FOR DISEASE CONTROL; ROCHE; EUROPEAN COMMISSION, CLINICAL INFECTIOUS DISEASES/MIV STUDY GROUP, EMERGING INFECTIOUS DISEASES

Who Controls the Samples?

In early 2004, University of Hong Kong virologist Guan Yi was tracking the evolution of the H5N1 virus that had infected poultry in Japan that winter when he found a source of samples. But he also ran into a Catch-22. Concerned about bioterrorism, both Japan and Hong Kong had put H5N1 on the list of infectious agents requiring special handling. Guan's lab needed an import permit, and Japan's National Institute of Infectious Diseases (NIID) needed an export permit. In theory, the transfer was doable, but Hong Kong's import permit was valid for only 1 week, and NIID couldn't get export approval that fast.

"We tried time after time, but we were never able to export the material," says NIID virologist Masato Tashiro.

At a time when averting a global influenza pandemic may depend on the rapid sharing of samples and information, researchers in developed and developing countries alike are running into roadblocks. The bioterror concerns are being added to the usual difficulties of sharing coveted samples that may have commercial value or may give researchers an advantage in scientific prestige and funding. The need for speed is imperative. Like all flu viruses, H5N1 is continually changing. Researchers want to track its genes to see if the virus is becoming more easily transmissible among humans, which could trigger a pandemic. This also means that vaccines and reagents used in diagnostic kits must be updated regularly to be effective.

"For this kind of pandemic preparedness, we need samples almost in real time," says Guan. The problem is finding the best way to share them.

Despite a consensus that samples of H5N1 strains should be sent to international reference labs as soon as they appear, no existing international agreement requires labs or countries to do so. "You have to ask" individual labs and governmental authorities for samples and information, says Astrid Tripodi, former avian influenza coordinator for the United Nations Food and Agriculture Organization (FAO) in Hanoi.

And those requests have to get to the right people. Although Vietnam was faulted for delays in sharing viral samples earlier this year (see main text), Phan Van Tu, head of the Department of Microbiology at the Pasteur Institute in Ho Chi Minh City, says no one requested the serum samples he collected over the

Dead end? Sharing samples is hindered by bioterrorism concerns.

CREDIT: ASSOCIATED PRESS

NIHE's researchers derived a live but modified H5N1 virus in so-called 293 cells and are culturing the virus in primary monkey kidney cells for use in vaccines. This process takes some unprecedented steps, the first being the use of 293 cells, which in some cases have produced tumors when injected into mice with deficient immune systems. Wood says that he's seen little data on the specific batch of 293 cells used by NIHE. "Consequently, we do not know the risks posed by any 293 cell residuals in the vaccine," he says. Wood also expresses concerns about potential contaminants in the primary monkey kidney cells: "There are tests to exclude such risks, but we do not know how they are being implemented for the flu vaccine production [in Vietnam]."

WHO has provided an alternative vaccine seed stock that meets international quality standards. But there is a catch. It was produced using a patented reverse-genetics process in which the viral genes are cloned individually and assembled into a "safe" strain. Hoping to avoid fees that could make the vaccine unaffordable for Vietnam and other developing countries, WHO is negotiating deals with MedImmune Inc. in Gaithersburg, Maryland, which holds the patent for the reverse-genetics process, and with those who hold patents covering other aspects of the seed stock. Meanwhile, NIHE's Dinh says the vaccine program is continuing, without confirming current plans. "Our institute has a lot of valuable experience producing vaccines, and we strongly believe we can reduce the number of human infections with our own H5N1 vaccine," he says.

It's about the birds

The biggest hole in Vietnam's effort to contain H5N1 may be its spread in poultry—which many experts believe must be controlled to keep it out of humans. Hoang Van Nam, deputy director of animal health for the Ministry of Agriculture and Rural Development, admits that the animal health infrastructure is woefully incomplete. Many local animal health officers aren't on the government payroll. "They earn money by treating sick animals, and they don't have any responsibility to report disease outbreaks," he says. Faced with the ongoing outbreak, many commercial poultry farms have adopted effective biosafety practices, so the brunt of the animal epidemic is now falling on rural households that keep small flocks for their own consumption. In such settings, sick birds are even harder to spot. When chickens die, Nam says, "they don't think to report it; they just discard or burn the dead chickens."

To reduce the threat, the Ministry of Agriculture is starting a pilot poultry vaccination program in two provinces this summer; it hopes to extend it to all affected provinces before the winter flu season. For now, says

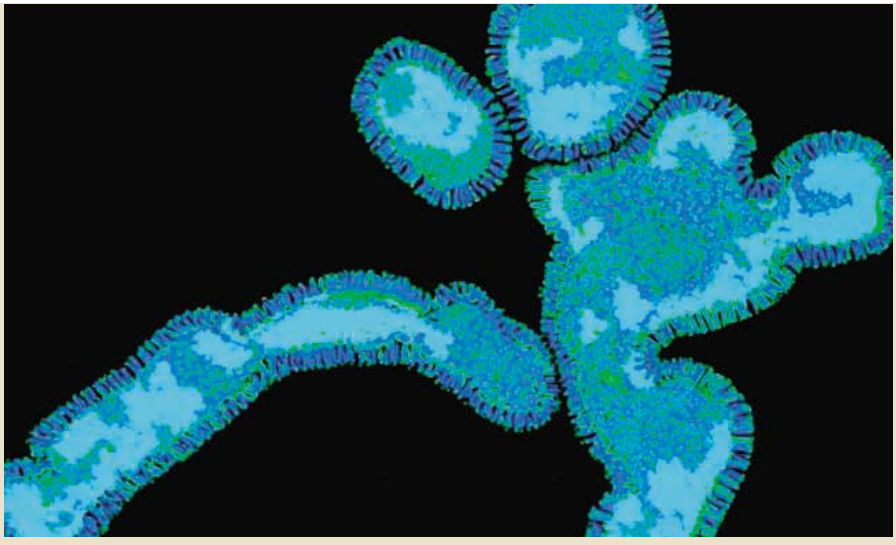

Changeable beast. Because the H5N1 virus is constantly changing, diagnostics and vaccines must be updated regularly to remain effective.

winter and spring. So he sent one bulk shipment of samples to the U.S. Centers for Disease Control and Prevention (CDC) in Atlanta, Georgia, in mid-June, just as he did last year.

Even sending samples to CDC and other World Health Organization (WHO) collaborating centers may not mean that samples and results get to all who want them. The collaborating centers must first report the results of any studies to the country or lab that supplied the samples; they also need the source's permission to pass samples on to third parties.

Bioterror precautions impede sharing, even with highly regarded labs. In early 2004, Canada's National Microbiology Laboratory (NML) in Winnipeg asked CDC for recent H5N1 samples to update diagnostic kits. "If an outbreak hit Canada, local hospitals would expect us to provide the proper reagents for diagnostics," says NML virologist Yan Li. Even so, he says, approval took 4 or 5 months.

David Daigle, a spokesperson for CDC's National Center for Infectious Diseases, confirms that an initial clearance for exporting a "select agent" can take several months, although the agency is trying to speed the process.

Approvals generally go more smoothly when the receiving lab is affiliated with WHO or FAO, says Tashiro, who heads WHO's Collaborative Center for Reference and Research on Influenza at Japan's NIID. But he would like to send samples more easily to nonnetwork labs. He would also like to see the WHO network database, which has extensive information on sequences and viral genetics, opened to outside researchers.

Margaret Chan, WHO's new director of Communicable Disease Surveillance and Response, agrees with the need to disseminate specimens and data more widely. She says expanding the WHO network is a possibility, but new labs "would have to satisfy biosafety requirements."

But that won't solve the problem for university researchers, who feel left out. Albert Osterhaus, a virologist at Erasmus University Medical Center in Rotterdam, the Netherlands, thinks WHO and FAO should assemble a permanent H5N1 task force, modeled on the one that tackled the severe acute respiratory syndrome virus. He would like to see government, university, and even private sector labs share samples and research results rapidly and freely. "This goes way beyond scientific cooperation," he admits, but should be done to safeguard public health.

Tim Booth, director of the Viral Diseases Division of Canada's NML, among others, remains unconvinced of the need to abandon traditional approaches to collaboration just yet. "I don't think rigid regulations on [sharing samples and information] would be useful," he says, adding, "it is better to build collaborations by developing a mutual understanding of the roles and responsibilities of all parties involved." The question is which model of cooperation will best suit the challenges posed by a potentially pandemic virus.

–D.N.

Nam, the ministry plans to mandate vaccination only at farms with 200 or more birds. Extending the campaign to small holders—those with one or two dozen birds—would require additional governmental or international support.

Indeed, there is no shortage of needs. Asked if her hospital could handle H5N1 patients turning up by the dozens instead of in ones and twos, Nguyen Thi Dung, a physician handling human avian flu cases at the Hospital for Tropical Diseases, just winces. For one, they don't have a proper isolation ward. "We have a plan to build one but no funding yet," she says.

Pasteur's Tu says that to extend the search for H5N1 cases, his institute and NIHE are setting up a network of six sentinel hospitals around the country; each week, each hospital will screen throat swabs and serum samples from 10 patients with respiratory problems to see if any cases of avian flu are going undetected. Again, Tu says Pasteur would like to expand the network to more regional hospitals—a move recommended by many epidemiologists—"but we'd need more [outside] support."

Help might just be on the way. At a conference on avian influenza in Kuala Lumpur last week, representatives of WHO, the U.N. Food and Agriculture Organization, and the World Organisation for Animal Health renewed appeals to the international community to support the fight against bird flu. On the animal side, the organizations emphasize the need to bring vaccination campaigns and biosafe farming practices to small-scale and backyard poultry operations. For public health, they want to strengthen the capabilities of affected countries in laboratory diagnosis, vaccine development, surveillance, and public education. They are seeking donations of $100 million for the poultry farming plans and $150 million for human health efforts.

For the birds. Animal epidemiologist Hoang Van Nam hopes poultry vaccination will reduce the amount of H5N1 in circulation.

Vietnam is ramping up its own funding for H5N1 efforts. The government, for instance, is providing $5 million each to Pasteur and NIHE for BSL-3 labs. But NIHE's Dinh says they will continue to request further support from developed countries. "Any pandemic would not only affect Vietnam but the world, and we have to share responsibility for averting it," he says. **–DENNIS NORMILE**

CREDITS (TOP TO BOTTOM): GETTY IMAGES; D. NORMILE/*SCIENCE*

FAIRBANKS, ALASKA—At Evolution 2005, from 10–14 June, evolutionary biologists, natural historians, and systematists shared results about fungi, mice, yeasts, and other organisms.

Fungal Trees Grow Faster With Computer Help

Researchers trying to determine the relatedness of organisms are finding it hard to keep up with the torrent of DNA sequence data gushing from biology's spigots. Now, two new computer programs are coming to the rescue, at least for biologists constructing the fungal family tree. One program, created by Frank Kauff of Duke University in Durham, North Carolina, and his colleagues, helps validate, assemble, and keep track of raw data from fungal DNA sequencing efforts. The other, developed by David Hibbett of Clark University in Worcester, Massachusetts, automatically retrieves fungal DNA sequences from the public archives and incorporates the data into an ever-improving phylogeny of this diverse group of microorganisms. Both efforts are part of the "Assembling the Fungal Tree of Life" project begun in 2003 and may be bellwethers of taxonomy's future. "It's great to have this all automated," says Michael Donoghue, a botanist at Yale University. "It means that progress can be made while we sleep."

Fast track. New computer programs are automating the classification of mushrooms and other fungi.

Molecular studies now dominate fungal systematics, but the plethora of data they provide has not necessarily brought clarity. There are hundreds of published family trees for the fungi or their various branches, and many conflict with one another. Yet no one has really tried to piece together where the discrepancies lie. That's where automated computer analyses will help, says Hibbett, a fungal systematist.

Among other fungal projects, Hibbett's lab focuses on mushroom-forming varieties, which make up an estimated 20,000 of the more than 70,000 known fungal species. To deal with the ever-growing number of DNA sequences for this group, Hibbett's program, which he dubbed mor, sifts through GenBank for newly deposited data on a single gene, called *nuc-lsu rDNA*, in mushrooms. If a researcher has deposited a new sequence of this gene for a species, the computer program compares it with other deposited copies of the gene for that species, weeding out any redundancies. It then compares the best version with the sequence of the gene in other species and uses the differences to adjust the branches of the fungal family tree. It even assigns names to new subgroups as needed. So far, mor has 2401 sequences representing 1899 mushroom species in 562 genera, Hibbett reported in Fairbanks, Alaska.

"It's one of the first attempts to automate large-scale phylogenetic analysis," says Roderic Page, a systematist at the University of Glasgow, United Kingdom.

Although fungal experts may need that help more than most—these organisms are among the most diverse and the most difficult to sort out—Hibbett's approach should also be portable. "It's easy to see how it could be expanded to fit other organisms," says David Baum, a botanist at the University of Wisconsin, Madison. Adds Donoghue, "I'd love to have something like this for plants."

Kauff's program, dubbed WASABI for Web Accessible Sequence Analysis for Biological Inference, comes into play before fungal family trees are created. In essence, it ensures that such trees sprout from good seeds. The consortium working on the fungal tree of life project is sequencing eight genes in 1500 different fungi, and WASABI rates the accuracy of each newly submitted DNA sequence. The program also pieces together short fungal DNA sequences into ever longer ones and compares these so-called contigs with existing sequence information. This all happens automatically, providing researchers with one place to find refined data that originated from various consortium members. Finally, WASABI archives its manipulations and analyses of the raw information. "WASABI considerably reduces the time users would otherwise have to spend," verifying and piecing together sequences, says Kauff. "The speedup is many orders of magnitude."

Together with other consortium members, Hibbett and Kauff have already published one 588-species fungal tree, with all the major branches, such as the mushrooms, represented. The goal is to have the 1500 under study linked up in the proper relationships by 2006. Says Baum, "Fungal systematists are really leading the pack in terms of their critical use of cutting-edge analytical tools."

Color Genes Help Mice and Lizards

The light-skinned deer mice (*Peromyscus polionotus*) found along Florida's shoreline didn't always have such a bleached-out look. It took the beach rodents less than 5000 years to go from brown to blond; the darker look may have provided camouflage in the dense fields in which they used to dwell, but on the white sand, it would have made the mice a conspicuous meal for predators. At the meet-

CREDIT: D. HIBBETT/CLARK UNIVERSITY

Beached and bleached. Interacting pigment genes helped whiten—and camouflage—mice migrating onto dunes.

ing, a research team described how a key gene aided the animal's colorful transformation. And another group reported that changes in the same gene helped lizards evolve a similar adaptation.

Researchers have studied the genetics of color in lab mice for decades, implicating more than 100 genes, half of which are now sequenced. But Hopi Hoekstra, an evolutionary biologist at the University of California, San Diego, says she "wanted to see what kinds of genes are involved" in shaping color patterns in nature.

In the southeastern United States, deer mice living in forests and dense fields have brown backs and light gray underbellies. But their cousins living on the vegetation-sparse white dunes on islands along the Gulf Coast have lost most of the brown on their backs, and their bellies look bleached. The beach mice have also dropped a characteristic dark stripe running down their face for a more muted look that helps camouflage the animals in their burrows.

To get at the genetics behind such adaptations, Hoekstra and her colleagues bred male beachcombers with female forest mice and vice versa. They now have 600 second-generation mice. "We see a lot of variation in pigmentation" among the animals, says Hoekstra, estimating that about a dozen genes control the pattern of colors distributed across the rodent's flanks, faces, tails, and other body parts. With these crossbred mice, she began testing whether various genes shown to have roles in coloration in lab mice are involved in the beach mouse's new look. "Hoekstra can ask where in the pathway natural selection is working," notes Johanna Schmitt, an evolutionary biologist at Brown University in Providence, Rhode Island. By happenstance, Hoekstra and her colleagues scored a hit with *Mc1R*, a gene involved in the switch between light and dark pigments. A single base change in the gene resulted in the Mc1R protein having abnormally low activity, causing less melanin to be made in the beach mice and resulting in whiter fur. In fact, the change in just this one gene accounts for 34% of the color variation in beach mice, Hoekstra reported. Hoekstra's postdoc Cynthia Steiner subsequently showed that a second gene called *agouti* is more significant for patterning than overall color.

Further analyses indicate that the two genes influence each other, a process called epistasis, in defining the overall patterns of body coloration. "It's the interaction that explains the variation" in color from body part to body part, Hoekstra notes.

Lizards from White Sands, New Mexico, also seem to have exploited changes in *Mc1R* to transform themselves from dark brown to light-colored, Erica Rosenblum of the University of California, Berkeley, reported. She studied three distantly related lizard species that have moved into the dunes in the past 600 years. Rosenblum found that all three had mutations in the gene, dramatically reducing their colors. "What is most striking is the repeating pattern as different species converge on the same phenotype," says Hoekstra.

Lizards and mice are far apart on the tree of life, and scales and fur bear little resemblance, but the metabolic pathways to produce melanin pigment in both animals are very similar. As a result, "it may be evolutionarily 'easy' to evolve color and color pattern differences" by means of the *Mc1R* gene, says Rosenblum.

Wine Yeast's Surprising Diversity

Since the days of the pharaohs, the yeast *Saccharomyces cerevisiae* has enabled us to make bread, as well as wine, beer, and other alcoholic beverages. More recently, it has become a model organism for cell and molecular biologists. Yet it has barely been studied outside the lab. Now, a research team has begun to trace the genetic diversity of this simple eukaryote in the wild.

Evolutionary biologist Jeffrey Townsend of the University of Connecticut, Storrs, and his colleagues have identified several distinct *S. cerevisiae* strains from forests and vineyards in Italy and the United States. Different strains found on grapes from different vineyards "may in part be responsible for the distinctive tastes of naturally fermented wines," Townsend speculates.

Until recently, yeast researchers paid little mind to grapes, thinking that any yeasts on the grapevines were escapees from the nearby vats, where the microbes are often added for the fermentation process. That thinking came into question, however, in 2004, when Paul Sniegowski of the University of Pennsylvania in Philadelphia discovered *S. cerevisiae* just below the bark of oak trees and in the soil around the base of these trees, establishing that this organism had a broader distribution beyond rotting fruit and vineyards. He "demonstrated that there are isolated, variant populations of *S. cerevisiae*," says Townsend.

Sniegowski's finding led researchers to wonder how many yeast strains there are in the wild, how the oak strains are related to those in vineyards, and whether one is derived from the other. While working in John Taylor's lab at the University of California, Berkeley, Townsend and graduate student Erlend Aa of the University of Tromsø in Norway compared DNA of 15 *S. cerevisiae* strains from Italian vineyards—primarily from grapes used in Chianti wine—with two lab samples and a strain from crushed grapes used to make wine. They also analyzed yeast strains provided by Sniegowski that were found on and near oak trees.

Aa sequenced four genes from each yeast and found 78 single-base differences

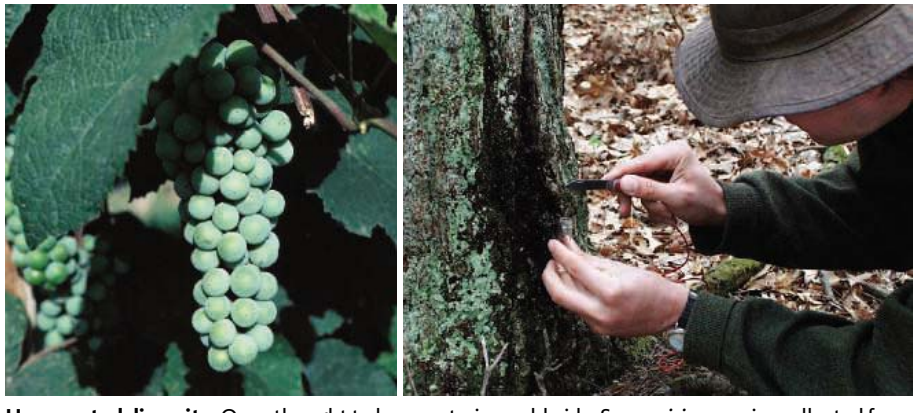

Unexpected diversity. Once thought to be one strain worldwide, *S. cerevisiae* species collected from oaks and vineyards are quite distinctive.

CREDITS (LEFT TO RIGHT): HOPI HOEKSTRA/UCSD; JUPITER IMAGES; M. LACHANCE/WESTERN ONTARIO UNIVERSITY

in these genes among the strains. Various combinations of these altered genes established distinguishable genotypes for each sample. Aa and Townsend demonstrated that the yeast found on grapes were not that similar to the yeast recovered from the wine must in fermentation vats. Instead, yeast from wine vineyards around the world include many wild strains and greater genetic diversity than that of yeast from the must. "The wine yeast does not represent a [global] population of domesticated strains as has been suggested," notes Christian Landry of Harvard University in Cambridge, Massachusetts. The vineyard yeast were also quite different than the yeast recovered from oaks.

Two samples from Italy's Elba Island also hinted that the yeast found on grapes may differ significantly from vineyard to vineyard within a region. Townsend discovered that yeast from the Elba samples resembled mainland strains but also contained genotypes unique to the island. He plans to expand the study to determine whether other places have distinctive yeast populations and, perhaps as a result, distinctive wines.

Two of the four yeast genes studied by Townsend and Aa had telling changes that may explain some of the vineyard-to-vineyard strain variation. One, the *SSU1* gene, is involved in transporting sulfite—a toxin—out of the yeast cell. The second is a gene whose protein regulates *SSU1*'s activity. The more active *SSU1* is, the more resistant the yeast is to this toxin. The *SSU1* regulatory gene showed the greatest number of differences from strain to strain, which translated into slightly different proteins and indicated that it had evolved the fastest of the four genes studied. Viniculture practices could explain this rapid change, says Townsend. In the vineyard, grapes are treated with sulfite and sulfite-containing compounds that destroy mold and other microbes, presumably killing all but those yeast with high *SSU1* activity. Also, winemakers add sulfite to sterilize fermentation vats, again presumably killing all but the most tolerant yeast.

Townsend notes that with such treatments, winemakers end up with ever more useful strains. The more resistant a *S. cerevisiae* strain is to sulfur-based chemicals, the longer the yeast cells will survive in vats treated with sulfite, and the more alcohol they make. "[Wild] wine yeast has inadvertently been domesticated," concludes Townsend. That's worth a celebratory drink.

—ELIZABETH PENNISI

Nanomaterials

'Smart Coatings' Research Shows The Virtues of Superficiality

Thin, shallow, and out to strike it rich—high-tech protective paints and varnishes look poised to become the first "killer apps" for nanotechnology

BERLIN—Clothing with computers woven into the fabric. Microscopic robots that make repairs with tools the size of a virus. No question about it: Nanotechnology, the applied science of the very small, has generated its share of megahype. For companies researching nanomaterials, however, profitability is the priority—and not in the dreamy future but now. Many are concluding that the beauty of the technology is literally skin deep.

Hot and heavy. This Fraunhofer Institute test furnace measures how much weight treated wood can bear after burning.

CREDIT: FRAUNHOFER INSTITUTE

At a recent meeting here,* researchers from around the world swapped news about efforts to spin nanotech into products based on surfaces with novel properties. "Coatings applications are among the first true everyday uses of nanotechnology," says Dirk Meine, a chemist who organized the conference for Vincentz Network, a coatings industry media group. Examples include nanoparticle-laden varnishes that combine the scratch resistance of an inorganic crystal with the versatility of an organic plastic. (Super–scratch-resistant coatings are already on the market.) Researchers offered a glimpse of what may be the next wave of nano applications to enter daily life.

Combating corrosion

The biggest task in the coatings industry is to slow down corrosion. Pipes rust, bricks crumble, and timbers rot, calling for repairs that add up to 4% of the gross national product of Western countries, according to Ubbo Gramberg, a corrosion chemist at Bayer in Leverkusen, Germany. "Not all these corrosion problems can be solved by coatings, but a considerable percentage can," says Michael Rohwerder, a physicist at the Max Planck Institute for Iron Research in Düsseldorf, Germany.

Top prize will go to a coating that prevents the corrosion of steel. Today, even the best protective coatings allow oxygen to diffuse slowly through to the metal surface. Corrosion kicks into overdrive when coatings begin to peel off, a process called delamination.

The trouble starts at microscopic nicks or pits on the surface introduced during manufacturing or through wear and tear. These defects form miniature circuits in which electrons flow through the metal in one direction while positive ions such as sodium flow back along the metal surface, leaving a degraded metal-coating interface in their wake. The coating becomes separated from the metal and flakes away, exposing fresh metal and accelerating the process.

That is where nanotechnology could come to the rescue. Rohwerder's group is working on coatings that allow a corroding metal surface to "self-heal." The oxidative attack at the site of a defect triggers nanoparticles to release corrosion-inhibiting ions—in this case, negatively charged molybdate ions—that stand in for the metal and form a protective oxide skin. Once the defect is sealed, the coating stops releasing ions until the next attack.

But there's a catch. Because these coatings sense corrosion with innately conductive polymers (ICPs)—carbon chains that allow charge to flow along their length like the semiconductors in microchips—they actually pro-

* Fourth Annual Smart Coatings Conference, 9–10 June.

mote corrosion except under controlled conditions. Designing "smart" ICP coatings that remain protective in unpredictable environments requires a "balancing act," says Sze Yang, a chemical engineer at the University of Rhode Island in Kingston. Another problem is that most ICPs are difficult to work into standard coating solutions, a drawback that could make them a commercial nonstarter despite their excellent anticorrosion properties.

Yang says he and colleagues have discovered an elegant solution to some of these problems. They found that synthesizing an ICP called polyaniline into a DNA-like double helix makes it far less corrosion-prone. The helix form is also easier to integrate into several coating mixtures. The researchers hope to find a replacement for chromates, the nearly universal additive to metal coatings that protects against corrosion but is a potent toxin, causing environmental havoc when it leeches out. It's too soon to say whether the badly needed successor to chromate will be Yang's double-helix ICP, but most coating experts agree that whatever it is, it will likely come from nanotechnology.

Fighting fire with nanoparticles

Nanomaterials may also help hold at bay rust's dramatic cousin, fire. Flame-retardant coatings have been widely used since the 1970s, but they have a serious drawback. According to Stefan Sepeur, a chemist at technology company Nano-X in Saarbrücken, Germany, more than 90% of fire-related deaths "are not caused by the flames but by the emission of toxic and corrosive gases"—many of which come from the fire-retardant coatings themselves. So finding alternatives for these formulas, which include toxic epoxy and acrylates, would save lives.

At Inomat, a coating research company in Bexbach, Germany, engineers have developed a way of coating surfaces with nanoparticles of flame-retardant oxides of aluminum or silicon. Because the particles are so small, they can be incorporated into a water-based solution, sidestepping the toxic organic compounds that make up standard formulas. One problem still to be overcome is that it requires a temperature of 100°C during application, limiting its use to steel and aluminum rather than the inside walls of houses where it is most needed.

In a very different approach, researchers at the Fraunhofer Institute for Wood Research in Braunschweig, Germany, are trying to endow surfaces with their own fire extinguishers. What looks and behaves like a normal paint or varnish at room temperature suddenly erupts in a layer of carbon foam in the presence of flame. The foam, composed of so-called ceramizing elastomers, was developed 35 years ago to insulate the combustion chambers of rockets, says Sebastian Simon, a chemical engineer on the project. The first challenge, he says, was to engineer the unexpanded polymers into a heat-sensitive coating that could pass muster as a household varnish. To test it, Simon and colleagues coated a wooden staircase and roasted it at 900°C for half an hour. Each stair could still bear a 100-kilogram weight after the ordeal.

Where there's smoke. Toxic fumes from fire-retardant coatings can be as deadly as flames.

War and peace

Other researchers are pitting smart coatings against even worse worst-case scenarios. At the University of Pittsburgh, Pennsylvania, molecular biologists Richard Koepsel and Alan Russell are working on a coating that protects against attacks with biological or chemical weapons. With funding from the U.S. military, they are developing a "bioreactive plastic" embedded with antibodies and enzymes that decontaminate surfaces as soon as pathogens or toxins arrive.

The biological principles are simple, Koepsel says. The coating contains enzymes for breaking down various poisons into harmless smaller molecules. And for each of the prime pathogenic suspects, such as anthrax or smallpox, a specific antibody lies in wait to grab it with enzymes such as cell-popping lysozymes nearby.

Handle with care. Nanomaterials may someday replace toxic rustproofing compounds.

One problem is that all these proteins evolved to function in the wet, salty environment within organisms, not outdoors. But after much tinkering, Koepsel and Russell found mixtures of water-retaining materials such as polyurethane in which enzymes remain 60% active after more than 20 weeks. Other chemical tricks helped keep the proteins at the outermost surface of the coating where the action is, instead of trapped and useless within the interior.

Koepsel says the coating has done well against simulated attacks of *E. coli* bacteria and harmless molecules, and the same principles should apply for the real deal. A self-decontaminating surface alone, he acknowledges, won't keep people inside a building or vehicle perfectly safe. But it should provide at least "a moderate level of protection for occupants of unsealed buildings and vehicles" and could make it easier to clean up after an attack. He says he is also pondering ways to equip the coating with an alarm system to alert people that an invisible attack is taking place.

Antimicrobial coatings could also soon find niches in operating rooms and in medical devices such as catheters that must remain inside the body for days at a time. When it comes to fighting infection, "nano is a natural given the size of bacteria," says Alexander Klibanov, a materials scientist at the Massachusetts Institute of Technology in Cambridge. The main obstacle right now, Klibanov says, is that antibacterial nanocoatings are expensive. He expects that the coatings won't make it onto the consumer market until they've been adopted by the "price-insensitive" hospital and homeland security areas. But once they have become cheap and proven effective, he predicts, they're bound to become as common as a coat of paint.

—JOHN BOHANNON

John Bohannon is a writer in Berlin, Germany.

CREDITS (TOP TO BOTTOM): ASSOCIATED PRESS; JUPITER IMAGES

Random Samples

Edited by Constance Holden

Ancient Human Footprints in Mexico?

Humans left their footprints on the shores of an ancient Mexican lake more than 25,000 years before people were thought to have colonized the Americas, according to a controversial new report.

Geochronologist Silvia Gonzalez of Liverpool John Moores University in the U.K. stumbled upon the prints in an abandoned quarry along what had once been a lake in the Valsequillo basin in central Mexico. "It felt like a thunderbolt," she says.

Apparent human footprint in Mexico.

Radiocarbon and electron spin resonance dating of nearby sediments place the prints—more than 150 apparently from humans, plus others from animals—at about 40,000 years old. Gonzalez believes the prints were made on a layer of fresh ash deposited by a nearby volcano, similar to the 3.5-million-year-old hominid prints in Laetoli, Tanzania. Some show clear outlines of toes, she says.

The findings have generally met with skepticism because there is little evidence that humans arrived in the Americas before 15,000 years ago. Although the dating may be accurate, "I have really serious reservations about whether these are footprints," says geoarchaeologist Michael Waters of Texas A&M University in College Station. The impressions are probably marks from quarrying and erosion; nonetheless, he says, they're "worthy of further investigation."

"I know we are in for a fight," says Gonzalez. Last week, her team got a $372,000 U.K. government grant to do excavations at the site.

Portrait of a Photon

It's darn hard to visualize a colorless particle of light, or any other subatomic particle, for that matter. Designer Jan-Henrik Andersen of the University of Michigan, Ann Arbor, has stepped in to help out. In consultation with physicists, he has developed a series of large-scale computer-generated images of subatomic particle energy and matter. The show, "Sized Matter—Perception of the Extreme Unseen," is on view at the Fermi National Accelerator Laboratory in Batavia, Illinois, through 26 August.

The Horse's Tale

DNA analysis has straightened out some of the tangled history of the North American horse and reduced its species from 50 to 2.

Because of rich fossil evidence and dramatic physical changes, horses are a textbook example of evolution. Equids originally arose in North America about 60 million years ago as small, five-toed animals. But their history on that continent is still being debated, especially for the period from about 3 million years ago to 10,000 years ago when they all went extinct. Some scientists have postulated that as many as 50 different horse species existed during that era.

To clarify the matter, Jaco Weinstock of the University of Oxford and colleagues examined mitochondrial DNA from the fossils of 53 horses from around the world ranging from 2000 to 50,000 years old. The evidence points to only two species, they report in *PLoS Biology*. One species spanned Eurasia and North America and continues today in the form of the modern horse.

The other species included the now-extinct stilt-legged horse, so-called because of its long, thin legs. The DNA analysis shows that despite its similarity to Asian asses, this species was a native product and not a transplant from Asia as some had thought.

R. Dale Guthrie, a paleontologist at the University of Alaska, Fairbanks, says the new study will help clear up the complicated and confusing history of horses. "It's taken something like mitochondrial DNA to answer the question," he says.

I'm a Physicist, Not a Gym Teacher

A rose by any other name would smell as sweet, but a scientific society might be easier to identify if it adopts a simpler moniker. At least that's what physicists in the United States are hoping. Tired of being mistaken for gym teachers and physicians, leaders of the American Physical Society (APS) have proposed changing the organization's name to the American Physics Society.

Few people equate the word "physical" with physicists, explains Marvin Cohen, president of the 106-year-old society. "Many of us have stories of being confused with physical therapists and people involved with athletics," he says. "The simple change to American Physics Society would suffice to show people what we do and that we're an organization of physicists." APS is currently polling its more than 43,000 members to see if they agree.

Early feedback shows that most members welcome the change, Cohen says. But some say it's unnecessary. "I don't quite see how anyone who's literate can misinterpret" the current name, says physicist and writer David Mermin of Cornell University. Mermin also notes that a "physic" is a purgative, so "American Physics Society could be interpreted as an organization for the promotion of laxatives."

CREDITS (TOP TO BOTTOM): J.-H. ANDERSEN; BOURNEMOUTH UNIVERSITY

Edited by Yudhijit Bhattacharjee

JOBS

AIDS chief. Europe's biggest HIV research organization—the $49 million French National Agency for Research on AIDS and Viral Hepatitis (ANRS)—has a new director. Jean-François Delfraissy, a clinician at the forefront of HIV research and treatment since the early 1980s and most recently director of internal medicine at the Bicêtre Hospital in Paris, has authored more than 200 papers and played a key role in many clinical trials, including the first one to show the effectiveness of AZT against mother-to-child transmission of HIV. He has also promoted ANRS's recent expansion into hepatitis B and C research.

"He's an amiable person who doesn't seek the limelight," says Joep Lange, past president of the International AIDS Society, who predicts that Delfraissy's accessible style will help foster international collaborations. Delfraissy succeeds Michel Kazatchkine, who in February became the French government's ambassador in the fight against AIDS.

DATA-POINT

Steady strides. The percentage of women earning U.S. mathematics Ph.D.s has nearly doubled in the past 25 years. The all-time high of 333 doctorates awarded to women in 2003–04 represents one-third of the U.S. total (including citizens and noncitizens), according to a study appearing in the August issue of the *Notices of the American Mathematical Society*. That's up from 18% in 1980.

An increased interest in graduate school seems to be the driving force behind the growth, given that the percentage of women undergraduate math majors has remained flat at 45% for nearly a decade. And it undermines any argument that women aren't up to the challenge. "We would not be seeing this increase if women did not have the ability or the stamina to pursue math degrees," says Ellen Kirkman, a professor at Wake Forest University in Winston-Salem, North Carolina, and lead author of the study.

More good news: Top-tier public universities are hiring more women with math Ph.D.s. Their slice of the job pie rose from 13% in 2000 to 23% in 2004.

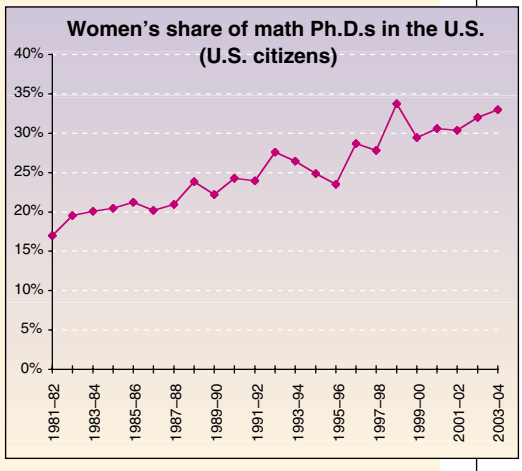

FOLLOW-UP

Sharing the blame. Urologist Rolf-Hermann Ringert of the University of Göttingen in Germany has been barred from applying for grants from the German research agency DFG after the agency said he shared responsibility for "misrepresentations" in a 2000 paper that he co-authored with a former departmental former colleague.

A previous investigation by a university committee had found only the first author of the paper, Alexander Kugler, guilty of misconduct based on sloppy work and other irregularities in a paper that reported glowing results from a trial of a kidney cancer vaccine (*Science*, 22 November 2002, p. 1531). The DFG panel, however, decided that Ringert was responsible as lead author of the study and head of the department in which the research took place. The study, published in *Nature Medicine*, was retracted in September 2003.

The decision to impose an 8-year ban is not open to appeal, but Ringert says he is exploring his legal options.

Delayed payment. Stefanie Dimmeler can finally receive a $2 million prize from DFG after being cleared of a misconduct allegation. Dimmeler, a cardiologist at Wolfgang Goethe University in Frankfurt am Main, did not accept the Leibniz Prize in March pending a university committee investigation into why she had published the same figure, with different captions, in two papers (*Science*, 11 March, p. 1559). Dimmeler said the mistake was an innocent one. Last week, DFG announced that the committee had concluded that the incident did not constitute misconduct. She will receive the money and prize citation immediately.

PIONEERS

Germ of an idea. Genomics entrepreneur J. Craig Venter has launched yet another ambitious pursuit: designing artificial bacteria. The leader of the corporate effort to sequence the human genome and captain of an around-the-world survey of marine microbes, Venter kicked off the enterprise last month by founding Synthetic Genomics Inc.

The Rockville, Maryland, company hopes to raise $30 million from private donors to build and commercialize organisms designed to make fuels such as hydrogen and ethanol. Other microbes would contain metabolic pathways useful for drug production and bioremediation. Part of the money will be used to support research at the nonprofit Venter Institute to develop the technology needed to make bacteria with humanmade genomes.

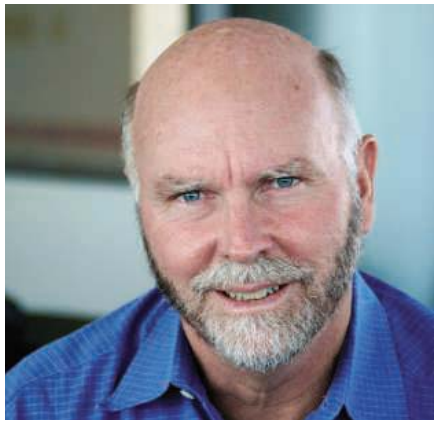

Got any tips for this page? E-mail people@aaas.org

CREDITS (TOP TO BOTTOM): ANRS; UNIVERSITY OF GÖTTINGEN; J. CRAIG VENTER INSTITUTE

LETTERS

Chronic Versus Acute Diseases

IN THEIR EDITORIAL "GLOBAL CHRONIC DISEASES" (21 Jan., p. 317), D. Yach *et al.* quote a World Bank analysis that states that more gains in life expectancy would accrue from the control of cardiovascular diseases (CVD) than from targets related to child and maternal mortality (*1*), and they question the Millennium Development Goals (MDG), which target infectious diseases and maternal/child health. We think it is unfortunate to base suggestions for global funding changes on what was essentially a regional report.

Although we share the view of the authors that obesity-related diseases and smoking are rapidly becoming pandemic, we strongly believe that infectious diseases still remain a major economic burden for low- and middle-income countries. Annually, malaria kills about 3 million, 3 million die from HIV/AIDS, and tuberculosis (TB) claims another 2 million lives. The total costs of malaria as a proportion of household income have been estimated to be between 4.9 and 18% for infected households in endemic countries, and this burden can be considerably higher for poorer households, reaching up to 32% (*2*). Economic growth has been estimated to be 1.3% lower in malaria-endemic countries (*2*).

Although the monetary value of economic losses due to TB is difficult to assess, estimates for India, where there are 2 million new cases and 500,000 deaths annually, indicate that the total cost of TB could reach as high as 40% of annual per capita household income (*3*).

It is projected that by 2010, there will be 25 to 50 million AIDS orphans, most of them in Africa and Asia. A World Bank document (*4*) reports that in the typical developing country, cost per adult death ranges from 8 to 400% of annual income per capita (average = 150% annual income/capita). The number of AIDS orphans stands at over 10 million, and destitute children may turn to violence and prostitution and drop out of school.

Effective prevention and treatment programs as envisioned under the MDG will go a long way to save lives, reduce poverty, and help economies to develop. We fear that the statements made by the authors could generate a climate of confusion, diverting allocation of resources from much-needed health interventions. We cannot afford to focus on chronic noncommunicable diseases at the expense of preventable killer infectious diseases.

ABIOLA C. SENOK[1] AND GIUSEPPE A. BOTTA[1,2]

[1]Department of Microbiology, Immunology and Infectious Diseases, College of Medicine and Medical Sciences, Arabian Gulf University, Post Office Box 22979, Manama, Kingdom of Bahrain. [2]Udine Medical School, Department of Morphological and Medical Sciences, Pzle Kolbe 1, 33100, Udine, Italy.

References

1. World Bank, "Millennium Development Goals for Health in Europe and Central Asia: Relevance and Policy Implications" (World Bank, Washington, DC, 2004).
2. S. Russell, "The economic burden of illness for households: A review of cost of illness and coping strategy studies focusing on malaria, tuberculosis and HIV/AIDS," Disease Control Priorities Project (DCPP) Working Paper 15 (DCPP, Bethesda, MD, 2003).
3. R. Rajeswari *et al.*, *Int. J. Tuberc. Lung Dis.* **3**, 869 (1999).
4. M. P. Over *et al.*, Impact of Adult Death on Household expenditures in Jagera, Tanzania (Policy Research Working Paper, World Bank, Washington DC, 2001).

Labnya Boro and her husband Ranjan Basumatary, both suffering from malaria, lie on a hospital bed in Nowkata village in the eastern state of Assam in India.

CREDIT: REUTERS/UTPAL BARUAH

Response

THE NEED FOR EFFECTIVE INVESTMENT IN global health is urgent. Senok and Botta balance our call for attention to noncommunicable diseases by arguing persuasively for continued investment in infectious disease control. Such investments will have their major impact among the poorest billion people.

But we cannot wait until these problems are solved before addressing concurrent chronic disease risks like tobacco, increasingly unhealthy diets, and increasing physical inactivity, which are prevalent in much of the developing world. In low- and middle-income countries that are home to over 4 billion people, tobacco use (already causing nearly 5 million deaths a year) (*1*) and diabetes rates are soaring (*2*). Waiting would accelerate both a health and an economic tragedy.

Heart attack and stroke, thought to be quintessential western diseases of affluence, are fast becoming major threats in developing countries. They now cause four times as many deaths in mothers in most developing countries as childbirth and HIV/AIDS combined (*3*). Worldwide, HIV/AIDS causes 3 million deaths a year; stroke and heart attacks cause 17 million (11 million deaths in developing countries) (*3*).

Yet heart disease, diabetes, and cancers receive only trivial interest from international agencies committed to improving global health. Heart disease and stroke are pushing families into poverty in developing countries as breadwinners and mothers die young. These breadwinners are also the most productive members of the workforce, and their efforts determine future prosperity and investment.

Billions of dollars have been committed to the Global Fund for AIDS, Malaria and TB, and the Global Alliances for Vaccine and Immunization (GAVI) and for Improved Nutrition (GAIN). But although it is true that chronic diseases are more prevalent among countries that are above desperate poverty, virtually no funds have been raised to reduce chronic diseases or their risks. Less than 5% of the World Health Organization budget, less than 3% World Bank loans for health, and few international donors support chronic disease research, policy development, or actions.

Is the case for investment in global health either/or? We think not.

An investment approach to global health that includes diseases on the basis of need rather than whim or fashion has much to commend it.

DEREK YACH,[1] STEVE LEEDER,[2] JOHN BELL[3]

[1]Division of Global Health, Yale University, New Haven, CT 06520, USA. [2]School of Public Health, University of Sydney, Sydney, NSW 2006, Australia. [3]Regius Professor of Medicine, Oxford University, Oxford OX3 9DU, UK.

References
1. *World Health Report 2002—Reducing Risks, Promoting Healthy Life* (World Health Organization, Geneva, 2002).
2. *Diabetes Atlas* (International Diabetes Federation, Brussels, ed. 2, 2003).
3. *World Health Report 2003—Shaping the Future* (World Health Organization, Geneva, 2003), chap. 6.

Domesticated Pigs in Eastern Indonesia

IN THEIR REPORT "WORLDWIDE PHYLOGEOG-raphy of wild boar reveals multiple centers of pig domestication" (11 Mar., p. 1618), G. Larson *et al.* note the potential significance of island Southeast Asia in the ancestry of pig mtDNA lineages in the Old World, but they fail to address archaeological data from this region. The authors report the possible existence of an indigenous clade of *Sus scrofa* in Wallacea and suggest that the island of Halmahera (the largest in Maluku Utara) might have been important in the genesis of their Pacific clade, which spread ultimately from New Guinea to Polynesia. Unfortunately, a substantial program of archaeology in Maluku Utara has revealed that pigs were completely absent here until after 3500 years B.P., when their bones appear in Neolithic contexts, with pottery and polished stone adzes, succeeding preceramic flake industries dating back into the late Pleistocene. Before 3500 years B.P., the islands of Maluku Utara contained only marsupial mammal faunas (wallabies, bandicoots, phalangers), some of which were translocated from New Guinea or Misool Island during the Early Holocene (~10,000 years B.P.). Samples of over 5000 identified animal bones, from five cave and rock shelter sites on Halmahera, Morotai, Kayoa, and Gebe islands, render this conclusion very well founded (*1*–*3*).

If pigs were taken initially to New Guinea from Halmahera, they must also postdate 3500 years B.P. there, as archaeological evidence now suggests (*4*). Where does the Pacific clade originate? This remains uncertain, but it cannot be Halmahera and must be some other region of island Southeast Asia, either Sundaland or Sulawesi, or perhaps the Philippines or Nusa Tenggara/Timor, island chains not included in the analysis by Larson *et al.*

PETER BELLWOOD[1] AND PETER WHITE[2]

[1]School of Archaeology and Anthropology, Australian National University, Canberra, ACT 0200, Australia. [2]School of Philosophical and Historical Inquiry, University of Sydney, Sydney, NSW 2006, Australia.

References
1. P. Bellwood *et al.*, *Mod. Quat. Res. SE Asia* **15**, 233 (1998).
2. T. Flannery *et al.*, *Austral. Mammalogy* **20**, 391 (1998).
3. J. P. White, in *Voyages of Discovery*, S. M. Fitzpatrick, Ed. (Praeger, Westport, CT, 2004), pp. 147–164.
4. J. Allen, *Mod. Quat. Res. SE Asia* **16**, 139 (2000).

Response

ALTHOUGH WE ACCEPT THE IMPORTANCE (and significance) of the archaeological evidence noted by Bellwood and White, in our Report, we do not single out Halmahera as the origin of the "Pacific clade" of pigs. Instead, we point out that the close genetic association of a pig from Halmahera with pigs from Papua New Guinea, Vanuatu, and Hawaii is analogous to the pattern found in rats (*1*) and in humans (*2*). Rather than arguing that all pigs found on Pacific islands trace their ancestry to Halmahera, we point out that Halmahera is currently the most westerly point represented by our "Pacific clade."

The current picture regarding the status of *Sus* specimens located on islands east of the Wallace line is far from clear. And although the fossil and archaeological record is important in this respect, it is by no means definitive (*3*). This uncertainty is further compounded by a lack of resolution on our phylogenetic tree, which obscures the relationships between distinct, well-supported clades, thus preventing us from drawing firm conclusions about both the geographic relatedness of the clades and the specific origin of the "Pacific Clade."

We agree with Bellwood and White that that there exist many possible points for origin of the "Pacific clade," including both areas we sampled in our Report and regions we have yet to sample.

GREGER LARSON,[1] KEITH DOBNEY,[2] UMBERTO ALBARELLA,[3] ELIZABETH MATISOO-SMITH,[4] JUDITH ROBINS,[4] STEWART LOWDEN,[5] PETER ROWLEY-CONWY,[2] LEIF ANDERSSON,[6] ALAN COOPER[7]

[1]Henry Wellcome Ancient Biomolecules Centre, Department of Zoology, University of Oxford, South Parks Road, Oxford OX1 3PS, UK. [2]Department of Archaeology, University of Durham, South Road, Durham DH1 3L, UK. [3]Department of Archaeology, University of Sheffield, West Street, Sheffield S1 4ET, UK. [4]Department of Anthropology and Allan Wilson Centre for Molecular Ecology and Evolution, University of Auckland, Private Bag 92019, Auckland, New Zealand. [5]Jurox Pty Limited, 85 Gardiners Road, Rutherford, NSW 2320, Australia. [6]Department of Animal Breeding and Genetics, Swedish University of Agricultural Sciences and Department of Medical Biochemistry and Microbiology, Uppsala University, Uppsala Biomedical Center, Box 597, SE-75124 Uppsala, Sweden. [7]School of Environmental Sciences, University of Adelaide, Adelaide, SA 5005, Australia.

References
1. E. Matisoo-Smith, J. H. Robins, *Proc. Natl. Acad. Sci. U.S.A.* **101**, 9167 (2004).
2. S. J. Oppenheimer, M. B. Richards, *Nature* **410**, 166 (2001).
3. P. V. Kirch, *On the Road of the Winds: An Archaeological History of the Pacific Islands before European Contact* (Univ. of California Press, Berkeley, CA, 2000).

Letters to the Editor

Letters (~300 words) discuss material published in *Science* in the previous 6 months or issues of general interest. They can be submitted through the Web (www.submit2science.org) or by regular mail (1200 New York Ave., NW, Washington, DC 20005, USA). Letters are not acknowledged upon receipt, nor are authors generally consulted before publication. Whether published in full or in part, letters are subject to editing for clarity and space.

Mechanism of JCV Entry into Oligodendrocytes

IN THEIR REPORT "THE HUMAN POLYOMA-virus, JCV, uses serotonin receptors to infect cells" (19 Nov. 2004, p. 1380), G. F. Elphick *et al.* report the dramatic finding that human polyomavirus (JCV) infection of SVG astroglial cells in culture can be mediated in part by serotonergic receptors, in particular 5HT2aR. This finding is potentially of great clinical importance, as it suggests that serotonin receptor antagonists may be useful in the treatment of progressive multifocal leukoencephalopathy (PML), a devastating demyelinating disease resulting from JCV infection and destruction of oligodendrocytes. Highly active antiretroviral therapy (HAART) remains the only partially effective treatment option.

We caution though, that in the midst of the growing enthusiasm for testing serotonin receptor antagonists clinically for the treatment of PML, that more should be done to explore the mechanism of JCV entry into oligodendrocytes. Our concern arises from two observations: (i) The cell line used in the authors' experiments, SVG-A cells, has been previously characterized as astrocyte-derived rather than oligodendrocyte-derived (*1*, *2*), and (ii) immunohistochemical analysis of human and animal central nervous system (CNS) tissue reported in the literature, and from our personal experience of analyzing serotonin receptor expression has shown that astrocytes express 5HT2aR (*3*, *4*); there is as of yet no clear report that oligodendrocytes also express 5HT2aR.

Although JCV can infect both astrocytes and oligodendroglia in human patients, productive infection is established in oligodendrocytes, and it is these cells that are predominantly destroyed by the virus. It clearly remains possible and even likely that JCV infection of astrocytes and other 5HT2aR-expressing cells such as vascular endothelial and choroid plexus cells play an important role in the pathogenesis of PML. We

believe, though, that whether JC virus enters oligodendrocytes by a serotonin receptor-mediated mechanism and whether entry can be blocked by serotonin receptor antagonists require further investigation.

SANDRO SANTAGATA[1] AND HANNAH C. KINNEY[2]*
[1]Department of Pathology, Brigham and Women's Hospital, [2]Department of Neuroscience, Children's Hospital and Harvard Medical School, Boston, MA 02115, USA.
*To whom correspondence should be addressed: Hannah.Kinney@childrens.harvard.edu

References

1. E. O. Major *et al.*, *Proc. Natl. Acad. Sci. U.S.A.* **82**, 1257 (1985).
2. B. Schweighardt, W. J. Atwood, *AIDS Res. Hum. Retroviruses* **17**, 1133 (2001).
3. M. Maxishima *et al.*, *Brain Res.* **889**, 270 (2001).
4. T. Xu, S.C. Pandey, *Brain Res. Bull.* **51**, 499 (2000).

Response

I AGREE WITH SANTAGATA AND KINNEY, BUT wish to point out that laboratory work with JCV is limited to cells and cell lines that permit viral infection. The only cell types permissive for JCV growth in culture are primary human fetal glial cells (predominantly astrocytes) and some cell lines such as SVG, SVG-A, and POJ that were derived from these primary cultures by transformation with either SV40 T antigen (SVG and SVG-A) or JCV T antigen (POJ). Primary cultures of oligodendrocytes isolated from adult brain are rare and difficult to obtain. A human oligodendrocyte cell line has not been established.

In our Report, we show that the 5HT2a receptor is required for infection of SVG-A cells by JCV. Expression of the 5HT2a receptor in receptor-negative HeLa cells restored their susceptibility to infection by JCV, indicating that the 5HT2a receptor is an important receptor for the virus on diverse cell types. We also agree with Santagata and Kinney that there are no clear reports demonstrating 5HT2aR expression on human oligodendroctes. Because of this, we are examining normal human brain and brain from HIV-infected patients with and without PML for the presence of 5HT2a receptors on oligodendrocytes. It is possible that 5HT2a receptor expression is low in normal brain but higher in the brains of patients infected with HIV, which might explain their increased susceptibility to PML. We suggest that 5HT2a receptor antagonists may be useful prophylactically by preventing the spread of JCV into the CNS and establishment of disease. Whether these compounds are useful in the treatment of an already established CNS infection is less clear, and more work clearly needs to be done to determine the potential efficacy of the latter approach.

WALTER J. ATWOOD
Department of Molecular Microbiology and Immunology, Brown University, Providence, RI 02903, USA.

HISTORY OF SCIENCE

Science as Comic Metaphysics

Susan Lindee

The Worlds of Herman Kahn
The Intuitive Science of Thermonuclear War
by Sharon Ghamari-Tabrizi

Harvard University Press, Cambridge, MA, 2005. 395 pp. $26.95, £17.95, €24.90. ISBN 0-674-01714-5.

Herman Kahn, the "*real* Dr. Strangelove," would be right at home with imaginary weapons of mass destruction, for imagination was his research tool. The "affable psychopath" and his times are vividly reconstructed in *The Worlds of Herman Kahn* by Sharon Ghamari-Tabrizi. Kahn dreamed up the doomsday machine and the "mineshaft gap," was a pioneer in the dubious discipline of "futurology," and was a disheveled, obese, would-be stand-up comic whose scientific briefings at the RAND Corporation were notorious for their black humor. Ghamari-Tabrizi, an independent scholar who specializes in the social studies of science and technology, tracks his uncanny ideas and public meanings and in the process excavates the Cold War in ways that resonate eerily with the present war on terror.

Kahn's basic perspective, well-elucidated in the book, was that nuclear war was both likely and survivable. To many observers, his program called for a deranged garrison state, a pathological world busily calculating how to efficiently destroy 40 million corpses. He imagined a post-attack world, anticipating what preparations would make that future world a continuation, more or less, of 1950s America. Kahn's winner would have fewer millions vaporized instantly and a more disciplined, better prepared population that was ready to move underground until the radiation cleared. Mineshafts, civil defense drills, bomb shelters, and militarized civilians were part of deterrence: unless the United States created a massive civil defense infrastructure, fortified its air defenses, and restructured its society, all threats to use nuclear weapons against the Soviets would be recognized as empty.

Kahn enthused about the economic boom that civil defense would facilitate—he cheerfully forecast growth industries in decontamination, blast engineering, excavating equipment, and food preservation technologies. And he joked about nuclear war, complaining that it was hard to do real experiments with nuclear weapons and proposing that "parents will learn to love two-headed children twice as much." Ghamari-Tabrizi quotes Kahn as once saying, "These issues are fun to study. There are qualities of paradox and absurdity that appeal to analysts and other non-serious people." Journalists' portraits of Kahn commonly used the adjective "jovial," and at the height of his celebrity, one critic asked "Is there really a Herman Kahn? It is hard to believe."

The middle son of Jewish Polish immigrants, Kahn was born in 1922. He was raised initially in the Bronx and then, after his parents divorced when he was 10, in Los Angeles by his mother. Pudgy as a child, he continued to gain weight throughout his life. Brilliant and easily bored, he earned a master's degree in physics at the California Institute of Technology. In December 1947, he joined RAND (the U.S. Air Force's nonprofit research institute) as a physicist, working while there with both Edward Teller, another improbable Cold War figure, and Hans Bethe. As Ghamari-Tabrizi relates, in 1952 Kahn submitted Monte Carlo studies he had carried out at RAND to Cal Tech as a dissertation. It was rejected because the work had been commercially sponsored. He then tried to find another California university that would allow him to use the work for a doctorate, but requirements that he enroll full time for a year or more led him to forgo the degree (*1*). Then, in 1961, after the publication of his first and best-known book, *On Thermonuclear War* (*2*), he left RAND to found his own research institute at Croton-on-Hudson, New York. (The Hudson Institute now has offices in Washington, D.C.) He was commonly called a futurologist, and in later years he went on to theorize about other futures—including Japan's economic potential, the oil crisis, and Vietnamization. As Ghamari-Tabrizi deftly shows, he was an important popular symbol of scientific rationality in the Cold War, and he both attracted and repelled observers from across the political spectrum.

This is the first scholarly study of Kahn, although in 2000 Kahn's sometime co-author Barry Bruce-Briggs self-published a fascinating (and more explicitly biographical and personal) book about his former boss, *Supergenius* (*3*)—a work that for some reason is not cited by Ghamari-Tabrizi. Bruce-Briggs's account includes many of the anecdotes about Kahn's public persona that Ghamari-Tabrizi offers, but his book is clearly an insider's view shaped by its author's immersion in Hudson Institute culture and his personal knowledge of so many of the players. Ghamari-Tabrizi's work instead places Kahn in a broader context, slyly drawing comparisons to the fine arts avant garde, to the beat poets and the abstract expressionists, to the gestalt social psychology of the 1950s, and even to Billy Graham's Christian crusade in New York City in the summer of 1957. Kahn in her text is a performance artist, a devotee of science as comic metaphysics, and a master of artful intuition and artificial experience. She writes, "Kahn mocked the military and the public with his scenarios and his burlesques, his gadgets and his predictions, and his unseemly dialogue between the earthly and the cerebral, the high and the low, the vomiter and the scientist." Ghamari-Tabrizi has produced an affecting and intelligent portrait of a Cold War figure who can still puzzle and amaze.

Was Kahn intellectually honest and rigorous, as Hubert Humphrey said he was when Humphrey had much of *On Thermonuclear War* entered into the Congressional Record as a Senate document? Or was he a proponent of mass murder, a madman whose ideas would legitimate an authoritarian society, as his many critics (including the historian Gabriel Kolko) suggested? Kahn freely used fiction throughout his work and was sometimes impatient with tedious empiricism, proposing that it did not matter what had actually happened, only what could have happened. His books were full of numbers, but the numbers and graphs measured nothing real, describing only hypothetical events and future possibilities. His ideas oscillated along the edge of reason and

The reviewer is in the Department of History and Sociology of Science, 303 Logan Hall, University of Pennsylvania, 249 South 36th Street, Philadelphia, PA 19104–6304, USA. E-mail: mlindee@sas.upenn.edu

unreason, fact and fiction. Ghamari-Tabrizi's compelling work illuminates the chilling potential of that edge, both for Kahn's time and for our own. *The Worlds of Herman Kahn* is a book that should be widely read.

References and Notes

1. Barry Bruce-Briggs proposes instead that in 1954 Kahn began a dissertation related to his work at Lawrence Livermore Laboratory, but "he soon learned that essentially the same research had been published previously" (*3*).
2. H. Kahn, *On Thermonuclear War* (Princeton Univ. Press, Princeton, NJ, 1960).
3. B. Bruce-Briggs, *Supergenius: The Mega-Worlds of Herman Kahn* (North American Policy Press, New York, 2000).

10.1126/science.1114032

SCIENCE AND SOCIETY

Deconstructing Biotechnology

Juan Enriquez

No species, except humans, deliberately transmits nonbiological data across hundreds, even thousands, of years. Memories of light, sounds, touch, and smells fade and disappear. For all other species, all that is left over time is instinct, a mother's quick lessons, and nature's harsh tests. Meanwhile, humans survive and thrive by becoming ever smarter at transmitting and absorbing ever-increasing amounts of data. We can recall what humans learned last month, last year, last century, and last millennium.

The way we record and transmit this knowledge keeps changing. In 1900, serious diplomacy without speaking French would have been laughable, and serious science without reading German would have been difficult indeed. By 1980, global business without some understanding of English would have been a hard slog. By 2000, launching a completely nondigital business would have taken a lot of work.

As the dominant language changes, those who adapt and adopt tend to become dominant. Cave wall paintings were enough to show how to light a fire or hunt a mammoth, but they were not enough to transition from tribe to empire. For that development, drawings had to become standardized into hieroglyphs or writing. They also had to be portable—on stone, clay, papyrus, velum, or paper. As a 20-odd–letter code permeated Europe, the printing press allowed rapid reproduction and dissemination of knowledge; Christianity increasingly lost its grasp, and information, books, and knowledge exploded.

Over the last three or four decades, the dominant alphabet shifted yet again because it became possible to collapse all words, written or spoken, in all alphabets and languages, into two-bit notation. And one could do the same with every piece of music and every image, moving or still. Societies and regions that went digital early enjoyed an explosive growth in wealth and power.

Now, as DNA, cDNA, RNA, proteins, tissues, brain scans, and a host of other data generate a language of life sciences, the dominant code is changing yet again. Life sciences last century was primarily about mapping and decoding; biotechnology relied primarily on relatively small alterations of existing genomes. But as we begin to decipher the world's most powerful and complex coding system, that of life, we begin to alter, directly and deliberately, the evolution of many species, including ourselves.

Once we map the DNA of an orange, we understand, on one level, how the source code works. Tweak that code a little and the orange becomes a grapefruit, a tangerine, or a lemon. Tweak it a little more, and it begins to generate vaccines against diarrhea. This ability to alter life forms increasingly permeates aspects of our daily life. Visits to the doctor's office are becoming data- and informatics-driven experiences. Our foods are very different from the foods of our great-grandparents, and increasingly engineered. We are finding many links between the types of questions we ask in biology and computing. Businesses that formerly worked far from the fields of biology are increasingly driven by genomics and other biological data.

The Global Genome
Biotechnology, Politics, and Culture
by Eugene Thacker
MIT Press, Cambridge, MA, 2005. 440 pp. $39.95, £25.95. ISBN 0-262-20155-0. Leonardo Books.

In *The Global Genome: Biotechnology, Politics, and Culture*, Eugene Thacker attempts to describe this transition in the dominant alphabet from various perspectives. The book ambitiously tries to follow the ever-expanding ripples the genetic code is propagating in the pond of civilization. The author (an assistant professor in the School of Literature, Communication, and Culture at the Georgia Institute of Technology) deconstructs the meaning of words and molecules. He asks us to think of DNA as wet (in the test tube), dry (coded on a computer), and commercial (patented). Considering how knowledge of DNA helps shape thought, society, wealth, and power, Thacker explores the question raised by Schrodinger: "What is life?" Biomaterials are often stored, represented, and exchanged through computers. As the molecule dematerializes, it becomes, in Thacker's mind, "inseparable from all philosophical, scientific, and economic mediations."

Thacker relies on vast streams of voices. The book runs though discourses based on how Marx, Foucault, von Neumann, Canguilhem, Shannon, Wallerstein, and other worthies would view bioinformatics and genomics. The author publishes in *Ars Electronica*, *Culture Machine*, *Postmodern Culture*, *Cultural Critique*, *Theory and Event*, and *Dialectical Anthropology*. Not surprisingly, the book has chapters on "a political economy of the genomic body," biocolonialism, bioinfowar, and "tactical media and bioart." Throw in a little blogging, experimental science fiction, and multimedia, and at times Thacker reads like a Jacques Derrida of biotechnology, deconstructing texts in a sometimes contradictory fashion. In Thacker's world, the "point cannot be stressed enough: bioinformatics is as material as it is immaterial, all the while constituted by an informatic approach to the biological domain."

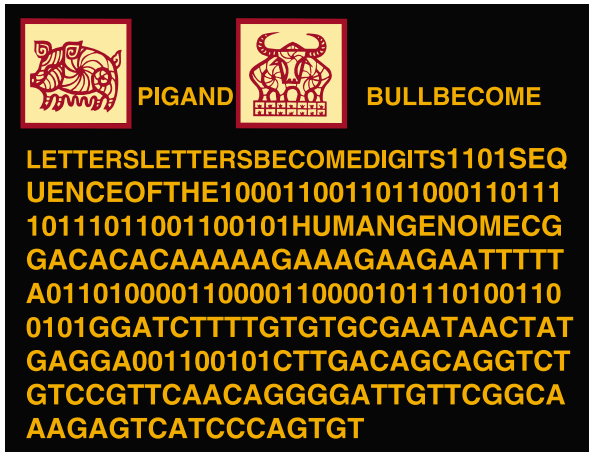

Thacker's is an interesting mind that wanders in and explores many directions. *The Global Genome* is a book likely to trigger very different thoughts, associations, and reactions from each reader. As he begins to rely more on his own voice and less on those of others and as he simplifies and clarifies what he has to say, Thacker's journey of discovery in future articles and books will probably be worth following. He is exploring a path taken by many art critics in the 1960s and 1970s, where the writing and critique of what was on the pedestal or on the wall meant as much as the artwork itself. But today, to quote Derrida, "a critique of what I do is indeed impossible."

10.1126/science.1114034

CREDIT: COURTESY JUAN ENRIQUEZ

The reviewer is at Biotechonomy LLC, Wellesley Hills, MA 02481, USA. E-mail: jenriquez@biotechonomy.com

ETHICS

Moral Issues of Human–Non-Human Primate Neural Grafting

Mark Greene,[1] Kathryn Schill,[2] Shoji Takahashi,[3] Alison Bateman-House,[4] Tom Beauchamp,[5] Hilary Bok,[6,7] Dorothy Cheney,[8] Joseph Coyle,[9] Terrence Deacon,[10] Daniel Dennett,[11] Peter Donovan,[3] Owen Flanagan,[12] Steven Goldman,[13] Henry Greely,[14] Lee Martin,[3] Earl Miller,[15] Dawn Mueller,[16] Andrew Siegel,[7] Davor Solter,[17] John Gearhart,[3] Guy McKhann,[6] Ruth Faden[7]*

If human neural stem cells were implanted into the brains of other primates what might this do to the mind of the recipient? Could such grafting teach us anything of value for treatment of neurological injury and disease? Could we change the capacities of the engrafted animal in a way that leads us to reexamine its moral status? These questions have gained significance since publication of research involving grafting human neural stem cells into the brains of fetal monkeys (*1*). In 2004, we formed a multidisciplinary working group; two plenary meetings over 12 months provide the basis for this Policy Forum.

Some group members have serious ethical concerns over *any* use of nonhuman primates in invasive research. However, we set aside broader controversies to focus on ethical challenges specific to human–to–nonhuman primate (H-NHP) neural grafting. We did not take votes or seek consensus on all the questions raised.

There is considerable controversy (reflected within our group) over the likely value of interspecies stem cell work for progress toward therapies (*2*). We cannot graft human neural stem cells into human beings solely for experimental purposes, even if they will lead to human therapies. Group members arguing for the value of research on human cells in NHPs pointed out that, because the aim is to learn about human neural stem cells, it makes most sense to use human lines. The fact that available NHP lines are few and poorly characterized (*3*) is an additional reason to use human lines. Another consideration is the need to assess candidate human cell lines for viability, potential to differentiate, and safety with regard to such possibilities as tumor formation. NHPs may be appropriate for in vivo screening.

Skeptics argued that differences between humans and NHPs could render results uninterpretable and that the preferred path for many questions is to study NHP neural stem cells in NHPs. Assessments of the scientific merit of the research must form and develop along with the field itself.

We unanimously rejected ethical objections grounded on unnaturalness or crossing species boundaries (*4*). Whether it is possible to draw a meaningful distinction between the natural and the unnatural is a matter of dispute. However, stipulating that research is "unnatural" says nothing about its ethics. Much of modern medical practice involves tools, materials, and behaviors that cannot be found in nature but are not unethical as a consequence

Another concern is that H-NHP neural grafting is wrong because it transgresses species boundaries (*5*). However, as the recent National Academy report notes (*6*), the notion that there are fixed species boundaries is not well supported in science or philosophy. Moreover, human–nonhuman chimerism has already occurred through xenografting. For example, the safety and efficacy of engrafting fetal pig cells has been studied in people with Parkinson's disease and Huntington's disease without moral objection. Indeed, some have suggested that porcine sources may be less morally contentious than the use of human fetal tissue (*7*). Merely because something has been done does not prove it right. However, we, like the National Academy, see "no new ethical or regulatory issues regarding chimeras themselves" [(*6*), p. 33].

The central challenge is whether introducing human cells into NHP brains raises questions about moral status. A variety of reasons have been given for according different moral standing to humans and NHPs. In the Abrahamic traditions, humans are set apart by God as morally special and are given stewardship over other forms of life (Genesis 1:26–28). For Kantians, human capacities for rationality and autonomy demand that we be treated as ends in ourselves (*8*). Mill finds, in the richness of human mental life, an especially fecund source of utility (*9*). Singer, although strongly defending equal consideration of nonhuman interests, argues that self-awareness affects the ethically allowable treatment of a creature by changing the kinds of interests it can have (*10*).

Many of the most plausible and widely accepted candidates for determining moral status involve mental capacities such as the ability to feel pleasure and pain, language, rationality, and richness of relationships. To the extent that a NHP attains those capacities, that creature must be held in correspondingly high moral standing. There are those, including Singer and some of our working group, who believe that we already overestimate differences in relevant mental capacities, and thus of moral status, between humans and NHPs. But the issue here is the extent to which human/NHP neural grafting might change capacities in a way that changes moral status.

Although we cannot assess altered capacities by experiencing an animal's mental life from within, we can assess its performance on cognitive tasks and observe its behavior. Establishing whether and in what ways engrafted animals undergo cognitive or behavioral changes requires an understanding of what the normal range is for a particular NHP species. Unfortunately, our understanding of NHP cognitive capacities is patchy, data are tricky to gather and difficult to interpret [(*11*); see supplementary material]. Thus, even if we observe what appear to be more humanlike capacities in an engrafted animal, we may be unable either to establish whether the capacities are outside of the normal range for that species, or to interpret the moral meaning of observed changes.

One conceivable result of H-NHP neural grafting is that the resulting creature will develop humanlike cognitive capacities relevant to moral status. H-NHP neural grafting may not be unique in having the potential to alter the capacities of NHPs. Chimps reared with humans behave in a more humanlike way than chimps reared by chimps (*12*). Transfer between species of predispositions

[1]University of Delaware; [2]Case Western Reserve University; [3]School of Medicine, Johns Hopkins University; [4]Columbia University; [5]Georgetown University; [6]Johns Hopkins University; [7]Phoebe R. Berman Bioethics Institute, Johns Hopkins University; [8]University of Pennsylvania; [9]Harvard University; [10]University of California at Berkeley; [11]Tufts University; [12]Duke University; [13]University of Rochester; [14]Stanford University; [15]Massachusetts Institute of Technology; [16]University of Maryland; [17]Max Planck Institute of Immunobiology. [For complete addresses, see SOM.]

*To whom correspondence should be addressed: rfaden@jhsph.edu

relating to auditory perception was found after transplantation of already formed portions of brain tissue (*13*). Introduction of human neural progenitor cells into developing mouse brains resulted in widespread incorporation of human neural progenitor cells; but behavioral alterations were not reported (*14*). Although such results are not reasons to think it likely, one unanimous conclusion of our group is that we are unable to rule out the possibility of effects on cognition of the sort that matter to moral status.

One option is to treat any development of more humanlike cognitive capacities as a risk to avoid. Alternatively, it might be argued that the challenge is less to avoid a direct ethical ill and more to understand the mental capacities of engrafted animals and to treat them in a manner appropriate to their moral status. Indeed, it might even be argued that such changes constitute a potential benefit to the engrafted animal, insofar as the changes are viewed as enhancements of the sort we value for ourselves. However, these more humanlike capacities might also confer greater capacity for suffering that would add to existing concerns about the harms caused by inadequate conditions for NHPs in research.

We propose six factors that research oversight committees and other review groups should use as a starting framework. They are (i) proportion of engrafted human cells, (ii) neural development, (iii) NHP species, (iv) brain size, (v) site of integration, and (vi) brain pathology.

Though even a few engrafted cells may affect neural activity, we expect that a higher proportion of engrafted human cells relative to host cells will increase the prospect of more humanlike neural function and, thus, of more humanlike cognitive capacities. High proportions of engrafted cells are more likely to be achieved by implantation early in neural development.

We also expect that the potential for engrafted cells to have significant functional influence will be markedly greater for engraftment at very early stages of development than for engraftment into the established architecture of adult brains. Although neural progenitor cells engrafted into the neonatal primate brain disseminate widely and integrate throughout the brain (*1*), the mature primate brain tends to resist incorporation of engrafted cells (*15*).

A graft recipient's degree of relatedness to our own species may matter for several reasons. Genetics contribute to brain structure by providing the protein building blocks that shape neurons and their interconnections. Factors such as cell surface markers and the mechanisms of cellular signaling are more similar in our closer relations (*2*, *3*). Also, although the picture is complicated by lifestyle similarities that cut across phylogenetic groups, our closest relatives among NHPs tend to show greater neuroanatomic similarities to human brain structures (*16*).

Also related to recipient species is brain size. It is unlikely that the structural complexity needed for any significant degree of humanlike mental capacity can be achieved under tight size limitations. However, brain size influences the size of the developing cranium, an effect seen naturally in hydrocephalus. Thus, a fetal marmoset engrafted with human neural cells might, to some extent, develop a larger brain than is typical for the species.

The specific sites into which the human neural cells become integrated within the recipient brain is also of potential significance. Functional integration into the cerebrum, which is associated with higher brain functions, seems more likely to affect cognitive capacities than does integration into the cerebellum; although engrafted neural cells may migrate and project to disparate brain areas.

Overall, we think it unlikely that the grafting of human cells into healthy adult NHPs will result in significant changes in morally relevant mental capacities. However, in the case of NHP models of human neurological disease and injury, adult recipients of human neural cells may have extensive disruption to their neural structures that might allow greater scope for engrafted human neural cells to affect cognitive capacities. We do not consider this a strong possibility, because diseased or injured brains will be starting from an impaired state from which even a return to species' normal functional levels is unlikely. However, the therapeutic point is to reinstate lost function, and we cannot be certain that this will be the only functional result of interspecies neural grafting. Furthermore, some of the disorders likely to be of interest (such as Alzheimer's) involve higher-level cognitive capacities.

There is no simple relation between these factors and, thus, no formula for making evaluative judgments. Considering issues of moral status that go beyond the ethical challenges attending any invasive NHP work, our framework suggests that experiments of greatest concern are those in which human neural stem cells are engrafted into the developing brains of great apes and constitute a large proportion of the engrafted brain. On the basis of this concern, and on doubts about scientific merit, some of us believe that engraftment of human neural cells into great apes should not be permitted, particularly early in neural development. Others argue against outright prohibition on grounds that scientific justifications might be forthcoming as the field progresses. For example, if a useful great ape model of a neurological disease is developed, and a promising human neural stem cell line is ready for use, there might be reason to proceed with human–great ape work, rather than waiting to develop great ape lines. Our framework suggests that experiments involving engraftment into healthy adult brains of our most distant monkey relations, especially when the proportion of engrafted cells is small relative to host cells, are the least likely to raise concerns about significant cognitive effects. However, especially as we consider experiments involving implantation of relatively large numbers of human cells early in development, there is no present empirical basis on which to rule out changes that might implicate moral status, whether the engrafted NHPs are great apes or monkeys.

In view of the challenges arising from moral status, we support the National Academy's recommendation that H-NHP neural grafting experiments be subject to special review. We agree that such review should complement, not replace, current review by animal-use panels and institutional review boards. We further recommend that experiments involving H-NHP neural grafting be required, wherever possible, to look for and report changes in cognitive function. Explicit data collection on cognition and behavior will help to ensure that ethical guidelines can be developed appropriately as the field advances.

References and Notes

1. V. Ourednik *et al.*, *Science* **293**, 1820 (2001).
2. J. S. Robert, *Bioessays* **26**, 1005 (2004).
3. K.-Y. F. Pau, D. Wolf, *Reprod. Biol. Endocrinol.* **2**, 41 (2004).
4. P. Karpowicz, C. B. Cohen, D. van der Kooy, *Nat. Med.* **10**, 331 (2004).
5. F. Fukuyama, *Washington Post*, 15 February 2004, p. B04.
6. Committee on Guidelines for Human Embryonic Stem Cell Research, "Guidelines for Human Embryonic Stem Cell Research" (National Research Council, National Academy of Science, Washington, DC, 2005).
7. J. S. Fink *et al.*, *Cell Transplant.* **9**, 273, (2000).
8. I. Kant, in *Groundwork of the Metaphysics of Morals,* K. Ameriks, D. M. Clarke, Eds. (Cambridge Texts in the History of Philosophy, Cambridge Univ. Press, Cambridge, UK, 1998), pp. 37–38.
9. J. S. Mill, *Utilitarianism* (Prometheus Books, Buffalo, NY, 1987), 83 pp.
10. P. Singer, *Inquiry* **22**, 145 (1979).
11. M. Tomasello, J. Call, B. Hare, *Trends Cognit. Sci.* **7**, 153 (2003).
12. M. Tomasello, S. Savage-Rumbaugh, A. C. Kruger, *Child Dev.* **64**, 1688 (1993).
13. K. D. Long, G. Kennedy, E. Balaban, *Proc. Natl. Acad. Sci. U.S.A.* **98**, 5862 (2001).
14. O. Brustle *et al.*, *Nat. Biotechnol.* **16**, 1040.
15. P. Rakic, *Nature* **427**, 685 (2004).
16. C. E. Oxnard, *Int. J. Primatol.* **25**, 1127 (2004).

17. We thank the Greenwall Foundation for support.

Supporting Online Material

www.sciencemag.org/cgi/content/full/309/5733/385/DC1

10.1126/science.1112207

NEUROSCIENCE

Monte Carlo Places Strong Odds on Ectopic Release

Vladan Lučić and Wolfgang Baumeister

Neurotransmitters are molecules that transmit chemical signals between neurons. In the classic direct transmission model, neurotransmitters are released from synaptic vesicles only at a specialized region of the presynaptic terminal known as the active zone. The neurotransmitters diffuse across the synaptic cleft and bind to receptors located at the postsynaptic density directly apposed to the active zone (see the figure). Alternatively, in a still-debated indirect model termed spillover, neurotransmitter released from a given synapse may diffuse extensively in the lateral direction (along membranes) and activate receptors in extrasynaptic regions or at neighboring synapses. A model that has features of both direct transmission and spillover is termed ectopic release. Here neurotransmitter is released from sites outside the active zone and is most likely to activate apposed extrasynaptic receptors (see the figure). Ectopic release has been directly measured between Purkinje cells and Bergmann glia in the cerebellum, and proposed to occur at central nervous synapses at the calyx of Held, retinal bipolar cell terminals, and hair cell synapses (*1*).

On page 446 in this issue, Coggan *et al.* (*2*) combine Monte Carlo computer simulations and the existing experimental data to make a strong case for ectopic release at cholinergic synapses in chick ciliary ganglions. Computer modeling is emerging as an important method for elucidating the molecular events underlying various cellular processes. Cellular signaling involves a bewildering array of molecules that show complex regulation and intricate localization properties. Thus it is not surprising that most modeling efforts in neuroscience, while aiming to describe phenomena at the whole-cell level, are based on simplified models of basic components such as dendrites or axons. In contrast, Coggan *et al.*, have simulated a single synaptic transmission event using a model that is based on the actual binding constants and realistic membrane morphology.

Models of cellular biochemical processes have as input relevant initial concentrations, and locations and binding constants of reactants. To simulate the rate of change in concentration and spatial distribution of reactants, the model must account for diffusion of reactants and biochemical reactions that transform reactants, including conformational changes like transitions between open and closed states of ion channels.

Modeling follows either a deterministic or a stochastic approach. In the deterministic approach, biochemical reactions are mathematically represented as a system of ordinary differential equations that can usually be solved using numerical algorithms. The solutions to these equations represent the average values of a particular quantity (usually concentration). Although the diffusion of reactants can be included in the deterministic formalism, the resulting partial differential equations can be solved only for simple geometries, such as spheres or cubes, making them unsuitable for many biological applications. The stochastic approach allows fluctuations, such as deviation from average concentrations. These fluctuations actually occur in nature and become important for low reactant concentrations such as in small chemically isolated compartments, transient microdomains, or in gene expression (*3*).

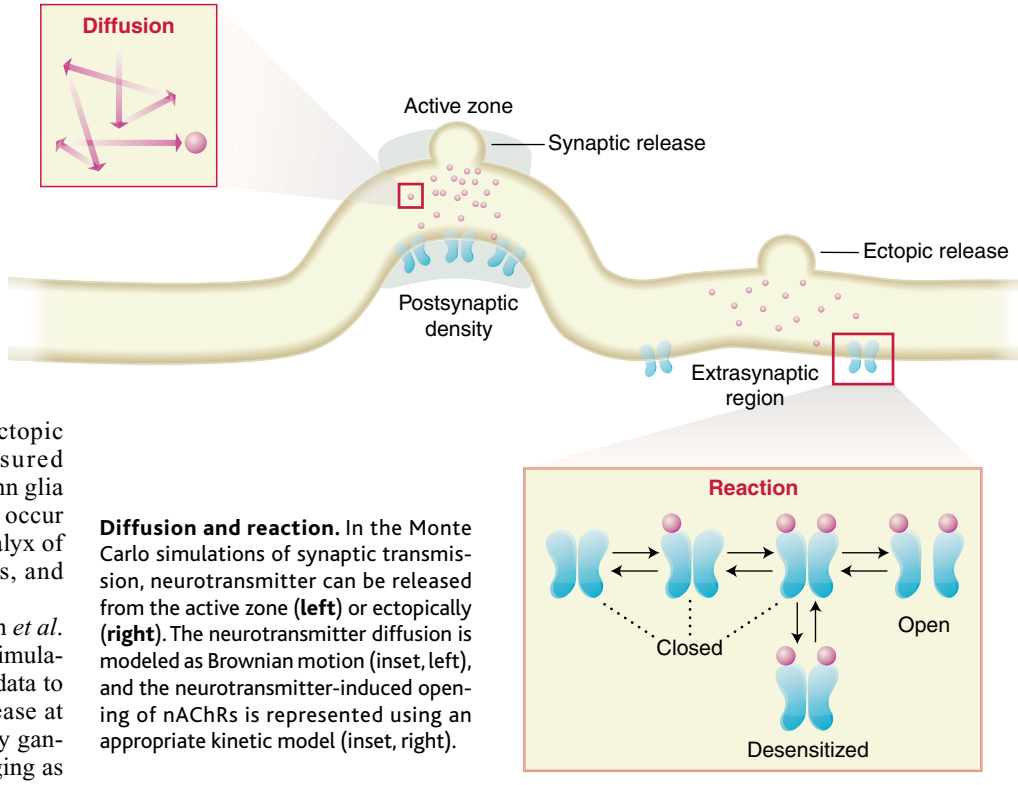

Diffusion and reaction. In the Monte Carlo simulations of synaptic transmission, neurotransmitter can be released from the active zone (**left**) or ectopically (**right**). The neurotransmitter diffusion is modeled as Brownian motion (inset, left), and the neurotransmitter-induced opening of nAChRs is represented using an appropriate kinetic model (inset, right).

Monte Carlo simulations are stochastic methods that rely heavily on random numbers (*4*). In order to model synaptic transmission at the ciliary ganglion, Coggan *et al.* used MCell, a software package that was originally developed for the simulation of synaptic transmission at the neuromuscular junction (*5*) and is therefore well suited to model dynamics at cellular membranes. Instead of tracking concentrations of reactants in a given volume, MCell tracks the position, and state, of every reactant particle (ion, molecule, channel) separately.

The authors are in the Department of Structural Biology, Max Planck Institute of Biochemistry, D-82152 Martinsried, Germany. E-mail: baumeist@biochem.mpg.de

Diffusion is implemented as random walk: At each time point, two random numbers are generated for each diffusible particle that define the direction and the magnitude of its movement. These random numbers are distributed so that they generate Brownian motion, thus simulating diffusion. Reactions are implemented in a similar way: For each reaction, a reaction probability is calculated on the basis of the binding constants and the local reactant concentrations (see the figure). At each time point a reaction event occurs if the random number generated for that particular reaction is greater than the reaction probability. Thus, one MCell run generates a realistic sequence of diffusion steps and reactions for each particle. Average concentration values are obtained by averaging results from many MCell runs.

Obtaining a realistic model is essential for this type of computer simulation. Coggan *et al*. used electron-tomographic reconstructions of ciliary ganglions containing clusters of somatic spines to extract and convert to digital form realistic surfaces of pre- and postsynaptic membranes and to identify synaptic and extrasynaptic regions. Two major classes of nicotinic acetylcholine receptors (nAChRs) are known to be present in postsynaptic neurons: α7-nAChRs, which are mostly extrasynaptic, and α3*-nAChRs, which are concentrated at the postsynaptic density. The authors populated the digitalized surfaces with both nAChR types, specified detailed kinetic models for neurotransmitter-induced opening, and included ACh hydrolysis by acetylcholinesterase. As is generally the case in modeling biochemical processes, not all parameters needed to make a realistic model of synaptic transmission are available in the literature. The authors used available experimental data, combined with their simulations when appropriate, to estimate the parameters needed for their model: the number of ACh molecules per vesicle, the distribution densities of both nAChR types and of acetylcholinesterase, the ACh binding constants, and the transition rates between the states of nAChR in each kinetic model.

Coggan *et al* used their model to simulate peak currents at the postsynaptic neuron after release of a single synaptic vesicle from different sites for a range of parameters. They show convincingly that their simulations are consistent with experimental data only if most, or even all, neurotransmitter release is ectopic. Ectopic release can explain some previously unresolved experimental observations, such as that the postsynaptic current arising from presynaptic stimulation is dominated by the contribution from α7-nAChRs, although these receptors are almost excluded from the postsynaptic density (*6*). Among the parameters used in the model, the uncertainty in the mean number of ACh molecules per vesicle had the strongest influence on the postsynaptic peak currents.

Models are rarely perfect, and here too there is of course room for improvement. For example, some parameters used by Coggan *et al*. were obtained from the neuromuscular junction, rather than the ciliary ganglion, and the binding of choline to α7-nAChRs was not taken into account. Further computational studies of synapses or other systems might benefit from the better structural models that can be obtained by using more recent methods for preserving samples for electron microscopy, such as rapid freezing followed by freeze substitution, or cryo preparation (*7, 8*). Although the simulation data presented by Coggan *et al*. fit experimental data well, there are still quantitative differences, probably due to uncertainties in the parameter values—the results of a modeling study are valid only for the conditions specified by the model. Nevertheless, Coggan *et al*. provide an example of how computer simulations based on carefully built, realistic models provide important insights that cannot be obtained by current experimental methods. We hope to see more such studies in the future.

References

1. K. Matsui, C. E. Jahr, *Neuron* **40**, 1173 (2003).
2. J. S. Coggan *et al*., *Science* **309**, 446 (2005).
3. H. H. McAdams, A. Arkin, *Trends Genet.* **15**, 65 (1999).
4. D. T. Gillespie, *J. Comput. Phys.* **22**, 403 (1976).
5. T. M. Bartol Jr., B. R. Land, E. E. Salpeter, M. M. Salpeter, *Biophys. J.* **59**, 1290 (1991).
6. Z. Zhang, J.S. Coggan, D.K. Berg, *Neuron* **17**, 1231 (1996).
7. A. Al-Amoudi, L. P. Norlen, J. Dubochet, *J. Struct. Biol.* **148**, 131 (2004).
8. V. Lučić, F. Förster, W. Baumeister, *Annu. Rev. Biochem.* **47**, 833 (2005).

10.1126/science.1115632

APPLIED PHYSICS

Where Do the Dopants Go?

Scott Roy and Asen Asenov

The rapid growth of the semiconductor industry in the past 40 years has largely been a result of the ever-decreasing size of CMOS (complementary metal-oxide semiconductor) switching elements, which form the underlying logic circuits in practically every modern digital system. As the size of CMOS switches—and of the field-effect transistors from which they are made—is reduced, integrated circuits constructed from these devices improve in speed, device density, and cost per function. The result is an intense industrial drive toward miniaturization, as predicted by Moore (*1*). Here, we consider key physical limitations to the miniaturization process and the evolution of modeling tools used to understand these limitations.

Each CMOS transistor consists of a source, a drain, a channel, and a gate (see the figure). The International Roadmap for Semiconductors (*2*) predicts that CMOS transistors with gate lengths of 7 nm will be mass-produced by 2018. Devices with channel lengths of 45 nm are already in production, and individual research devices with channel lengths of 4 nm have been demonstrated (*3*). CMOS devices will continue to shrink over the next two decades, but as they approach the scale of the silicon lattice, the precise atomic configuration of their structure will become critically important to their macroscopic properties.

Mead and Keyes recognized in the 1970s (*4*, *5*) that below a critical size, devices can no longer be described, designed, modeled, or understood as continuous semiconductors with smooth boundaries and interfaces. At nanometer-scale dimensions, the number and position of the dopant atoms, introduced to alter the electrical properties of regions of a field effect transistor, will vary between devices (see the figure); as a result, each transistor will be microscopically different. The variation in dopant position between devices leads to measurable differences in macroscopic parameters such as drive current, threshold voltage, and leakage. Further size reduction reduces the number of dopants, exacerbating the variations and hence the differences in device performance.

Furthermore, with decreasing device size, the interface roughness of typical gate oxides (one or two atomic layers) becomes comparable to the gate thickness itself. Thus, each device will have a unique gate thickness and a unique pattern of interface roughness. The use of high-permittivity (high-k) gate insulators as a replacement

The authors are in the Department of Electronics and Electrical Engineering, University of Glasgow, Glasgow G12 8QQ, UK. E-mail: s.roy@elec.gla.ac.uk

for present gate oxides will allow thicker gates, which may ease this source of variation for one or two technology generations (3 to 6 years). However, atomic-scale variation in the positions of impurity atoms, local variations in the silicon/silicon dioxide interface above the channel, and local variations of the thickness of the silicon dioxide introduce, between each transistor and its neighbor, fluctuations in device electrostatics, electron transport, and gate leakage, respectively. The granularity of the photoresist used to pattern the gate will introduce further local variations in the shape of the gate itself.

With existing technology, it is impractical to image the detailed atomic structure of individual nanometer-scale CMOS transistors and to link their structure to the corresponding device characteristics. Over the past decade, researchers aiming for an understanding of intrinsic parameter fluctuations in nanometer-scale CMOS transistors have therefore resorted to numerical simulation, using increasingly detailed mathematical models.

It was not until the mid-1990s that a body of experimental evidence confirmed fluctuations in device current-voltage characteristics due to atomic-scale structure variation, beyond that expected from variations in fabrication equipment, for devices with channel length below 1 μm (*6*, *7*). This gave the first serious impetus to model the problem, although initial theoretical analyses were qualitative in nature or used two-dimensional (2D) simulation techniques. It was realized early on that these 2D models could not capture all the relevant physics and that the results were inconsistent with experiment. A realistic dopant distribution is inherently 3D, defining a potential landscape under the gate. When the device is turned on, local variations in the potential landscape form chains of potential "valleys," allowing the formation of percolation paths between source and drain. However, a realistic potential landscape will rarely produce percolation paths that run parallel to the average electron flow in idealized devices, as assumed in the 2D model.

Wong and Taur were the first to report a full 3D simulation of field-effect transistors under the influence of random discrete doping (*8*). They used a drift-diffusion simulator, which models electron transport as incompressible fluid flow, considering the area under the gate as a checkerboard of smaller, interconnected devices, each with a different density of dopant atoms. The results showed the two classic fingerprints of randomly distributed, discrete dopants: a spread in the device threshold voltages, and a lowering of the mean threshold voltage relative to that of a continuously doped system (the formation of percolation paths will always allow current to flow at a lower gate potential than for an idealized device).

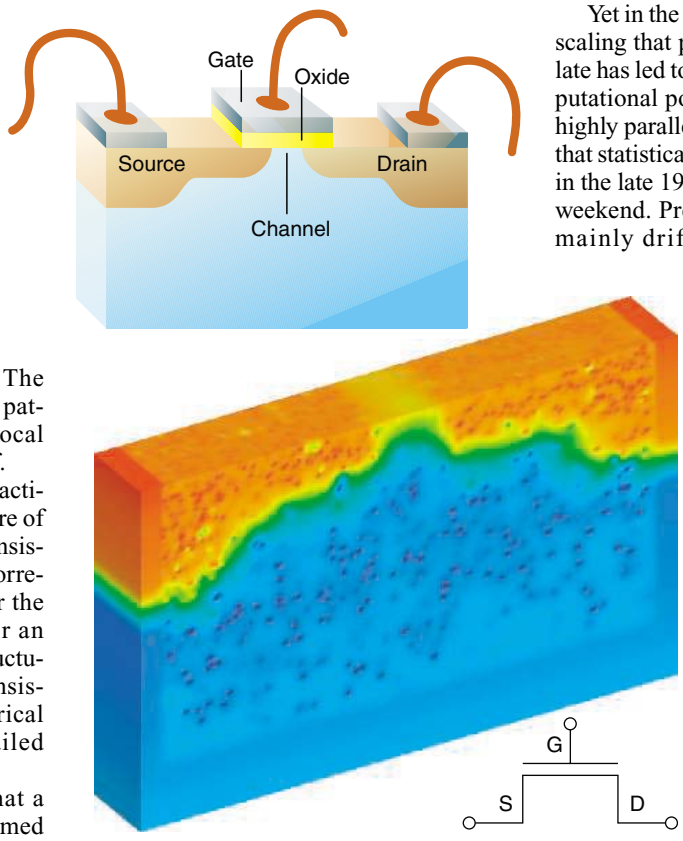

Dopants in a small transistor. 3D simulation of a 30 nm by 30 nm field-effect transistor domain that contains random discrete dopants in the source, drain, and substrate (bulk). The electrostatic potential is color-mapped from red (1 V) through the rainbow to blue (0 V). Potential fluctuations in the channel associated with the random distribution of dopants result in differing characteristics for each device. (**Top inset**) Schematic diagram of the basic interconnect wiring structure of a field-effect transistor. (**Bottom inset**) Circuit diagram symbol for a field-effect transistor.

These 3D simulations foreshadowed today's techniques and used a computationally efficient 3D device simulator, but they were not immediately adopted into commercial simulators. A 3D simulation requires substantial computational resources; the simulations are made even more demanding by the need to accurately model over atomic length scales. In addition, statistical information is required for each field effect transistor design, necessitating many 3D simulations for each design. Because of these formidable computational obstacles, 2D and analytical approximations remained popular, with researchers accepting substantial limitations in accuracy as a price for acceptable simulation times (*9*, *10*).

Yet in the past few years, the same device scaling that proves so problematic to simulate has led to radical improvements in computational power. Combined with modern, highly parallel simulation codes, this means that statistical simulations that ran for weeks in the late 1990s can now be completed in a weekend. Present simulation tools are still mainly drift diffusion–based and now include random distributions of dopants in the channel, source, drain, and gate of a field effect transistor (see the figure). In addition, variations in gate thickness and atomic-scale roughness in the pattern of the gate edges are accounted for, and the quantum nature of channel electrons is modeled through a density gradient adjustment to the device's potential profiles.

There is even a move to replace the drift-diffusion core of modern commercial and research device simulation codes with the computationally more expensive Monte Carlo approach (*11*) to correctly account for electron transport at the high lateral fields present in modern devices in the on-state. However, threshold voltage variations and the subthreshold operation of devices (which govern device leakage) remain the most important parameters for a circuit designer, and these can be adequately modeled with drift-diffusion simulators.

Now that rapid, robust, and accurate simulation tools have been developed, a wealth of applications present themselves in the fields of electronic devices, circuits, and systems. For instance, such simulations may help to develop devices that are resistant to fluctuation effects. Double-gate transistors (in which a 10-nm silicon channel is gated above and below) require no channel doping and are therefore immune to dopant fluctuation effects, but are subject to body thickness variations due to local roughness above and below the channel. The new simulation tools are being used to predict when industry should move to double-gate transistors, and when double-gate transistors themselves will become unviable.

In addition, methodologies have been developed to make use of the extracted data on fluctuations as an input to industrial circuit design tools (*12*, *13*). For the first time, circuit designers can quantitatively analyze how atomic-scale variations in field-effect

CREDIT: A. BROWN/UNIVERSITY OF GLASGOW

transistors will affect the yield and functionality of commercial digital logic and memory circuits.

References

1. G. E. Moore, *Electronics* **38**, 114 (1965).
2. *International Technology Roadmap for Semiconductors* (Semiconductor Industry Association, San Jose, CA, 2001).
3. H. Wakabayashi *et al.*, *Tech. Digest IEDM*, 989 (2003).
4. B. Hoeneisen, C. A. Mead, *Solid State Electron.* **15**, 819 (1972).
5. R. W. Keyes, *Appl. Phys.* **8**, 251 (1975).
6. T. Mizuno *et al.*, *IEEE Trans. Electron Dev.* **41**, 2216 (1994).
7. M. Steyaert *et al.*, *Electron. Lett.* **30**, 1546 (1994).
8. H.-S. Wong, Y. Taur, *Tech. Digest IEDM*, 705 (1993).
9. X. Tang *et al.*, *IEEE Trans. VLSI Syst.* **5**, 369 (1997).
10. P. A. Stolk *et al.*, *IEEE Trans. Electron Dev.* **45**, 1960 (1998).
11. J.-R. Zhou, D. K. Ferry, *Proceedings of the 3rd International Workshop on Computational Electronics* (Plenum, New York, 1994), pp. 74–77.
12. D. Burnett *et al.*, *1994 IEEE Symposium on VLSI Technology: Digest of Technical Papers* (IEEE, Piscataway, NJ, 1994), pp. 15–16.
13. B. Cheng *et al.*, *Solid State Electron.* **49**, 740 (2005).

10.1126/science.1111104

ASTRONOMY

The First Generations of Stars

Timothy C. Beers

The very first stars that formed after the Big Bang, some 13 to 14 billion years ago, are likely to have been quite massive and extremely short-lived; no examples are expected to remain in the universe today. However, they may have left behind their "calling cards" by producing a distinctive distribution of elements recorded in the atmospheres of long-lived stars that formed just after these massive progenitors. Stars that are extremely iron-poor (hyper metal-poor stars) are believed to be very old, and are thus possible candidates for second-generation stars.

On page 451 of this issue, Iwamoto *et al.* (*1*) describe a model that attempts to account for the elemental abundances in two hyper metal-poor stars. The stars, HE 0107-5240 (*2*) and HE 1327-2326 (*3*), contain less than 1/100,000 of the iron observed in the Sun. Furthermore, they are both greatly enhanced, relative to the Sun, in the light elements carbon, nitrogen, and oxygen (for HE 0107-5240; studies of the oxygen abundance in HE 1327-2326 are under way); these are the most important elements for the formation of life, at least of the form with which we are familiar.

Star formation in the Milky Way and throughout the present universe is poorly understood. This is because it takes place in a complex environment, where one has to account for the effects of the elements produced by previous generations of stars, the influence of magnetic fields, and star formation–triggering events such as shocks from nearby supernovae. In the very early universe, the physics of star formation is thought to have been much simpler, because only hydrogen, helium, and a small amount of lithium were present; stars most likely formed via radiative cooling by molecules involving these elements.

Modern computational models of early star formation predict that most stars that formed in the early universe were probably quite massive, on the order of several hundred times the mass of the Sun. Such stars burn their fuel extremely rapidly (within a few million years after their birth) and then explode. Astronomers are uncertain which elements might form in these very massive stars during their explosive death throes, but current calculations indicate that they should eject large amounts of iron and only small amounts of carbon (*4*, *5*).

This prediction is incompatible with the elements observed in the hyper metal-poor stars modeled by Iwamoto *et al.* (*1*). However, contemporary observations show that when stars form, they do so with a distribution of masses. The distribution of stellar masses in the early universe may have included first-generation stars with only 25 times the mass of the Sun. Iwamoto *et al.* suggest that these lower-mass first-generation stars are responsible for the elemental abundance patterns now observed in the second-generation stars HE 0107-5240 and HE 1327-2326.

These two stars—the most iron-poor stars known today—are inferred to have masses that are ~80% that of the Sun. Stars in this mass range have very long lifetimes, because they burn their fuel slowly—so slowly that, if they were born in the early universe, they could still be detected today. According to one popular model, the formation of such low-mass stars was triggered by shocks from the explosions of the massive first-generation stars (see the figure). These second-generation low-mass stars provide our only means to quantify the distribution of elements that were formed by their long-gone progenitors. Hence, stars like HE 0107-5240 and HE 1327-2326 are the "scribes" of the early universe. Their atmospheres retain the memory of the composition of the gas from which they formed.

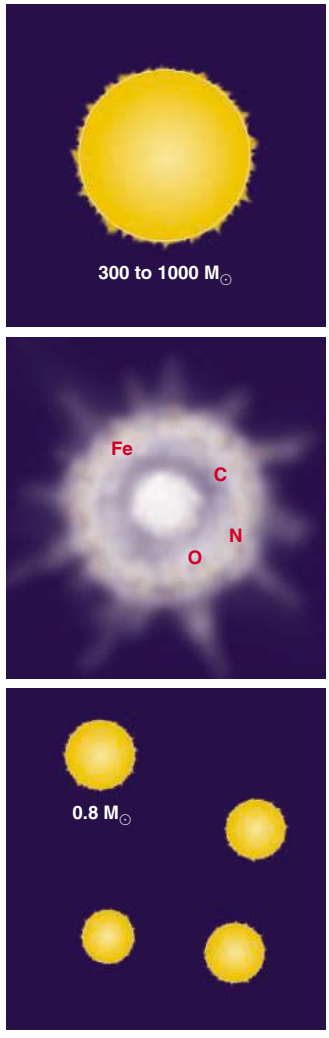

The story of element creation. The first generations of stars probably included objects that were extremely massive and short-lived. When they exploded at the end of their lives, the elements created within the first-generation stars were incorporated into lower-mass second-generation stars that may still be detectable in the universe today. $M_\odot$ is the solar mass.

CREDIT: PRESTON HUEY/*SCIENCE*

The search for stars with extremely low metallicity (astronomers refer to all elements heavier than hydrogen and helium as "metals") began 50 years ago, when it was recognized that stars with lower metallicity than the Sun exist in the Milky Way. In the past decade, several thousand stars with iron abundances less than 1% of the solar abundance have been identified. Many of the most extreme examples have been studied at high spectral resolution with the world's largest telescopes. These studies have shown that, of the 12 stars with the lowest iron abundance known to date, five exhibit highly enhanced light elements such as carbon, nitrogen, and, in some cases, oxygen (*6*). It seems inescapable that early element production favored the light elements. The early production of light elements is a crucial ingredient in models for early star formation, because these species pro-

The author is at Michigan State University and the Joint Institute for Nuclear Astrophysics, East Lansing, MI 48824, USA. E-mail: beers@pa.msu.edu

vide very efficient cooling pathways that enable the subsequent formation of additional low-mass stars.

Iwamoto *et al*. suggest that the iron-to-hydrogen ratio measured in the lowest-metallicity stars is set by the amount of iron produced by their progenitors and by the amount of interstellar hydrogen that this material mixed with before the stars formed. On the basis of their model, one might expect a continuous distribution of this ratio among low-metallicity stars. However, current data suggest that this may not be the case. The distribution of stellar metallicities from several large recent surveys exhibits a gap between stars with iron-to-hydrogen ratios of 0.01% of the solar value (ultra metal-poor stars) and the hyper metal-poor stars with ratios of <0.001% of the solar value. The precise shape of the metallicity distribution function at the lowest metallicity can only be obtained by discovering more low-metallicity stars; it will provide a sensitive test of the Iwamoto *et al*. model, as well as others.

Given the wealth of information that low-metallicity stars can reveal about the nature of the first generations of stars, astronomers have redoubled their efforts to identify and analyze many more examples of these objects. Among the most ambitious of these efforts is the SEGUE (Sloan Extension for Galactic Understanding and Evolution) survey, which will, over the next 3 years, obtain medium-resolution spectroscopy for 250,000 stars in the Milky Way. Based on tests of the subset of Milky Way stars that will be studied by SEGUE, I expect that some 20,000 SEGUE stars will have iron-to-hydrogen ratios less than 1% of the solar value. High-resolution spectroscopic studies of these stars will reveal the detailed patterns of elements created by the early generations of stars in the Milky Way, and form the basis for assembling the "story of creation" of the elements that were eventually incorporated into all of us.

References

1. N. Iwamoto, H. Umeda, N. Tominaga, K. Nomoto, K. Maeda, *Science* **309**, 451 (2005); published online 2 June 2005 (10.1126/science.1112997).
2. N. Christlieb *et al.*, *Nature* **419**, 904 (2005).
3. A. Frebel *et al.*, *Nature* **434**, 871 (2005).
4. H. Umeda, K. Nomoto, *Astrophys. J.* **565**, 385 (2002).
5. A. Heger, S. E. Woosley, *Astrophys. J.* **567**, 532 (2002).
6. T. C. Beers, N. Christlieb, *Annu. Rev. Astron. Astrophys.*, in press.

7. T.C.B acknowledges support from the U.S. National Science Foundaton and NASA.

10.1126/science.1114671

MATERIALS SCIENCE

The Renaissance of Magnetoelectric Multiferroics

Nicola A. Spaldin and Manfred Fiebig

Magnetic and electronic materials permeate every aspect of modern technology. For example, the vast amount of data generated by consumer electronic products is often stored as regions of opposite magnetic polarization in ferromagnets (materials with a spontaneous magnetic polarization that can be reversed by a magnetic field). The sensors industry relies heavily on a related class of materials known as ferroelectrics (materials with a spontaneous electric polarization that can be switched by an applied electric field). Many ferroelectrics are also ferroelastic—that is, a change in their electric polarization is accompanied by a change in shape. As a result, they are used to convert sound waves into electrical signals in sonar detectors, and to convert electrical impulses into motion in actuators. Such materials, which combine two or more "ferroic" properties (see the first figure) in the same phase, are known as multiferroics (*1*).

Trends toward device miniaturization have led to increased interest in combining electronic and magnetic properties into multifunctional materials, so that a single device component can perform more than one task. Ferromagnetic ferroelectric multiferroics are particularly appealing not only because they have the properties of both parent compounds, but also because interactions between the magnetic and electric polarizations lead to additional functionalities. For example, the magnetoelectric effect (the induction of a magnetization by an electric field, or of a polarization by a magnetic field) could yield entirely new device paradigms, such as electric field–controlled magnetic data storage. However, attempts to design multiferroics that combine ferromagnetism and ferroelectricity in the same phase have proved unexpectedly difficult.

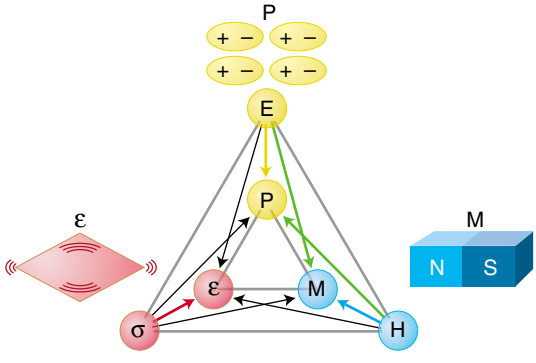

Phase control in ferroics and multiferroics. The electric field *E*, magnetic field *H*, and stress σ control the electric polarization *P*, magnetization *M*, and strain ε, respectively. In a ferroic material, *P*, *M*, or ε are spontaneously formed to produce ferromagnetism, ferroelectricity, or ferroelasticity, respectively. In a multiferroic, the coexistence of at least two ferroic forms of ordering leads to additional interactions. In a magnetoelectric multiferroic, a magnetic field may control *P* or an electric field may control *M* (green arrows).

Recent theoretical breakthroughs in understanding the coexistence of magnetic and electrical ordering, combined with advances in thin film growth techniques and experimental methods for observing magnetic and electric domains, have generated a flurry of research activity on such magnetoelectric multiferroics (*2*). Theoretical studies have shown that the usual atomic-level mechanisms driving ferromagnetism and ferroelectricity are mutually exclusive, because they require empty and partially filled transition metal orbitals, respectively (*3*). This recognition has prompted a search for alternative ferroelectric mechanisms that are compatible with the occurrence of magnetic ordering [for example, in $HoMnO_3$ (see the second figure)]. As a result, previously unknown multiferroic materials have been discovered.

These new multiferroics are in turn proving to be a rich source for exploring the fundamental science of phase control and magnetoelectric interactions. Huge magnetoelectric effects have been observed in the form of ferroelectric phase transitions induced by magnetic fields in perovskite manganites (*4*) and ferromagnetism induced by electric fields in hexagonal manganites (*5*). Magnetoelectric memory effects and magnetic switching of ferroelectric domains (and the converse process) have been demonstrated. An optical technique has been developed that

N. A. Spaldin is in the Materials Department, University of California, Santa Barbara, CA 93106, USA. E-mail: nicola@mrl.ucsb.edu M. Fiebig is at the Max-Born-Institut, Max-Born-Straße 2A, 12489 Berlin, Germany. E-mail: fiebig@mbi-berlin.de

allows separate access to both coexisting domain structures of a multiferroic in the same experimental setup; with this method, coupling between magnetic and electric domains has been observed (*2*). However, these single-phase multiferroics are not very attractive for applications in the short term, because none of the existing materials combine large and robust electric and magnetic polarizations at room temperature.

The difficulties associated with uniting electrical and magnetic ordering in a single phase have been circumvented by forming two-phase composite multiferroics that consist of a ferroelectric constituent [such as $PbZr_{1-x}Ti_xO_3$ (PZT)] and a ferromagnetic constituent [such as $Tb_{1-x}Dy_xFe_2$ (Terfenol-D)]. In such composites, the magnetoelectric effect arises from the interaction of the elastic components of the ferromagnetic and ferroelectric constituents. An electric field induces strain in the ferroelectric; this strain is passed on to the ferromagnet, where it causes magnetization. The magnetoelectric effect is large if the coupling at the interface is large; therefore, composites with large surface area (such as multilayered thin films) and strongly ferroelastic constituents are particularly effective.

This composite approach opens new avenues for tailoring the magnetoelectric response through the choice, ratio, and microstructure of the constituents; indeed, room-temperature magnetoelectric coupling coefficients have been achieved that exceed the low-temperature values found in single-phase compounds by three to five orders of magnitude (*2*). Composite magnetoelectric multiferroics are on the threshold of technological application, for example, as transducers converting between magnetic and electric fields. They may also find application as attenuators, filters, field probes, and data recording devices based on electric control of magnetization and vice versa.

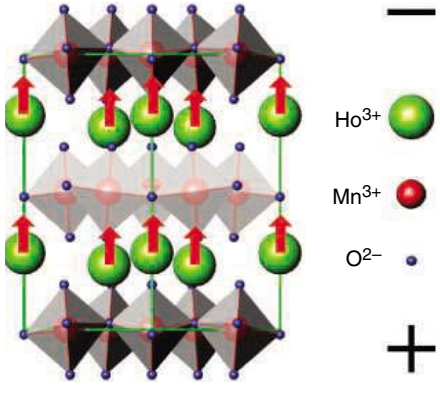

Structure of multiferroic $HoMnO_3$. Hexagonal $HoMnO_3$ is ferroelectric, because the oxygen bipyramids surrounding each Mn^{3+} ion are tilted and shifted relative to the Ho^{3+} ions. It is also magnetic, with ferromagnetic alignment of the Ho^{3+} magnetic moments combined with antiferromagnetic Mn^{3+} ordering. Therefore, hexagonal $HoMnO_3$ is multiferroic.

What are the major challenges for future research on magnetoelectric multiferroics? In composite materials, better understanding of the ferromagnetic-ferroelectric-ferroelastic coupling between the constituents is essential. New theoretical developments may be required, because linear elasticity models cannot be used to describe the responses on the atomic scale. Experimentally, the use of self-organized nanocomposites could offer particularly efficient coupling between the phases (*6*); these materials may even allow magnetoelectric switching of polarization and magnetization.

In the case of single-phase multiferroics, basic questions such as the origin of the ferroelectricity in some unusual multiferroics (*4*) remain to be answered. Furthermore, the quest for robust room-temperature ferromagnetic ferroelectrics that are sufficiently insulating to sustain a large macroscopic polarization is a major challenge. An increased effort to work with multiferroic thin films may expand the palette of accessible materials and may help to drive the single-phase compounds toward technological application.

Finally, advances in fundamental theoretical concepts—such as integration of the concept of ferrotoroidicity, characterized by a spontaneous magnetization vortex, into the group of primary ferroics (*7*)—should lead to a more concise picture of the different forms of ferroic ordering and the relations between them. This should result in a better understanding of the physics of multiferroics.

References

1. H. Schmid, *Ferroelectrics* **162**, 317 (1994).
2. M. Fiebig, *J. Phys. D* **38**, R123 (2005).
3. N. A. Hill, *J. Phys. Chem. B* **104**, 6694 (2000).
4. T. Kimura *et al.*, *Nature* **426**, 55 (2003).
5. T. Lottermoser *et al.*, *Nature* **430**, 541 (2004).
6. H. Zheng *et al.*, *Science* **303**, 661 (2004).
7. H. Schmid, *Ferroelectrics* **252**, 41 (2001).

10.1126/science.1113357

NEUROSCIENCE

Brain Under Surveillance: The Microglia Patrol

Luc Fetler and Sebastian Amigorena

Biophysicists and biologists have long worked together to develop tools to analyze the limits of the living world—molecules and cells at one end and whole organisms at the other. In contrast, important intermediate levels of organization, namely the organs and tissues, had received little attention until very recently. For instance, we understand very little about what controls the density, shape, and size of organs, or how cells direct their movements or communicate with each other within tissues. This has been due in part to technical limitations. The environment that cells encounter within tissues can include multiple three-dimensional chemotactic gradients and numerous physical constraints imposed by interactions with the extracellular matrix and with other cells. Such a complex milieu is virtually impossible to reconstitute in vitro.

The advent of two-photon microscopy (*1*) and its use on tissues of living animals is rapidly advancing our understanding of cell behavior and fate within tissues (*2*, *3*). Based on the simultaneous absorption of two photons, the technique allows greater imaging depth and minimal phototoxicity compared to conventional fluorescence microscopy. Whereas other imaging techniques require surgical dissection that can damage tissue, two-photon microscopy allows direct imaging of cells in the undisturbed physiological environment of an intact organ. Two recent studies by Nimmerjahn *et al.* (*4*) and Davalos *et al.* (*5*) used this powerful imaging approach to examine the activity of microglia, the most abundant immune cell in the brain, in live mice. Microglia comprise ~10% of the cells in the central nervous system. Under pathological conditions such as neurodegenerative disease, stroke, and tumor invasion, these cells become activated, surround damaged and dead cells, and clear cellular debris from the area, much like phagocytic macrophages of the immune system. In healthy mammalian brain tissue, microglia display characteristically elongated cell bodies with spine-like processes that often branch perpendicularly. Until Nimmerjahn and Davalos applied two-photon microscopy to a live

The authors are at the Curie Institute, 26 rue d'Ulm, 75245 Paris Cedex 05, France. L. Fetler is in the Laboratoire Physico-Chimie Curie, CNRS UMR 168, Institut Curie, Paris, France. E-mail: luc.fetler@curie.fr S. Amigorena is in the Immunité et Cancer, INSERM U365, Institut Curie, Paris, France. E-mail: sebastian.amigorena@curie.fr

CREDIT: MANFRED FIEBIG

and healthy mammalian brain, it was generally thought that microglia are essentially quiescent cells—dormant and nonmotile. But a static state is hardly what was observed.

The technique allowed the Nimmerjahn and Davalos groups to transcranially visualize microglia in live animals. Information was recorded from up to 200 μm below the brain's surface through a surgically thinned section of skull. Both groups generated transgenic mice whose microglia were fluorescently labeled. The easily detectable cells were observed for several hours in the brains of anesthesized mice. Whereas microglial cell bodies and main branches were stable for hours, their evenly distributed and highly ramified processes were remarkably motile, continuously and randomly undergoing cycles of formation, extension, and withdrawal on time scales of minutes (1.5 μm/min). These processes also displayed motile (4 μm/min), filopodia-like protrusions that typically formed bulbous tips with an average lifetime of 4 min. Although the function of these tips remains unclear, it is possible that they constitute specialized phagocytosis domains that clear accumulated metabolic products and deteriorated tissue. This high "resting" motility may serve a housekeeping function, enabling microglia to effectively sample and assess the status of the local surroundings and control their microenvironment. The restructuring activity of microglial processes is in sharp contrast to the apparent stability of dendritic processes of surrounding neurons. Microglial processes and protrusions were also observed to directly contact astrocytes, neuronal cell bodies, and blood vessels, suggesting that in healthy brain tissue, microglia communicate with other cortical cells to coordinately monitor the general health of the brain.

Both groups also performed laser-induced injury of individual capillaries in the brains of the transgenic mice. Within a few minutes, time-lapse imaging revealed rapid, targeted movements of nearby microglial processes toward the injured site (see the figure). The average velocity of microglial extensions radially impinging on the target site was similar to extension rates during the resting state. Within 30 min after laser ablation, processes of nearby microglia reached the damaged site and appeared to accumulate and fuse together, forming a spherical containment around the damaged area and establishing a potential barrier between healthy and injured tissue (*5*). Microglia responded to mechanical injury in a similar way. The shielding of injured sites suggests a neuroprotective role for microglia. Furthermore, the early formation of spherical inclusions within the microglial processes suggests immediate phagocytic engulfment and removal of damaged tissue or leaked blood components. Together, these findings confirm the idea that microglia represent the first line of defense against invading pathogens or other types of brain tissue injury.

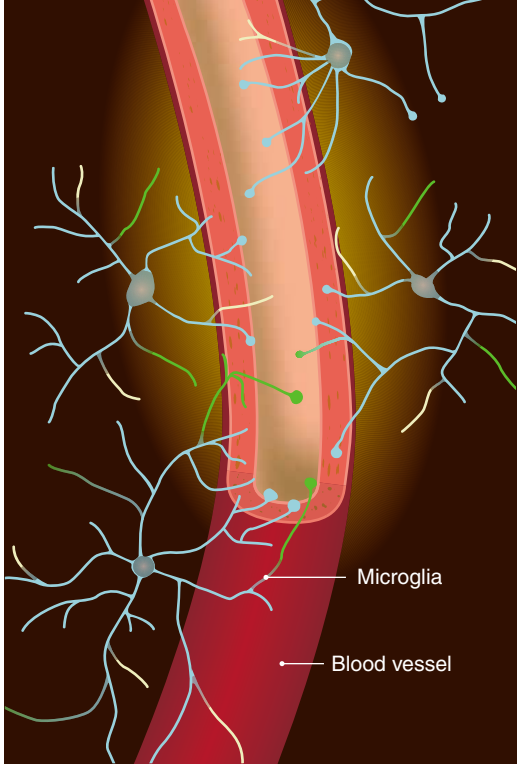

Microglia patrol the brain and shield it from injury. Microglia continually extend (green) and retract (yellow) processes, surveying their immediate environment within the brain. The processes move rapidly toward a site of injury, such as a damaged blood vessel in the brain, in response to the localized release of a chemoattractant (gradient of orange) from the injured sited. Once at the target site, the processes form a barrier to protect healthy tissue.

CREDIT: PRESTON HUEY/*SCIENCE*

To identify the molecular signals that mediate this targeted microglial response, Davalos *et al*. (*5*) made use of the observation that microglial migration can be induced in cell culture with nucleotides that signal through P2Y receptors expressed at the cell surface. They demonstrate that localized application of ATP to the mouse brain (through either a craniotomy or a small electrode; neither invasive technique itself elicited a response from microglia), which mimics nucleotide release from injured tissue, attracted microglial processes, similar to the microglial response to injury. Apyrase, an ATPase (adenosine triphosphatase) that hydrolyzes ATP and ADP, substantially reduced both the baseline motility of microglial processes as well as their response to laser-induced tissue injury. Furthermore, they showed that activation of P2Y receptors on microglia in the surrounding tissue is necessary for the rapid microglial response toward the injured site. Previous studies showed that extracellular ATP can induce ATP release from astrocytes. ATP also mediates communication between astrocytes and between astrocytes and microglia. This ATP-induced ATP release was essential for attracting microglial processes. Indeed, when the authors applied apyrase and then a nonhydrolyzable ATP analog from a microelectrode, they observed no such rapid microglial response. Applying connexin channel inhibitors, which inhibit ATP release from astrocytes, also blocked the microglial response toward the laser ablation site. Resting motility of microglial processes in the intact brain also seems to be modulated by the same ATP signaling mechanisms that mediate injury-induced responses, because apyrase and connexin channel inhibitors nearly abolished microglial baseline dynamics.

These two elegant studies provide direct evidence for the highly dynamic nature of microglia, indicating that the brain is under constant immune surveillance by these cells. In the adult mammalian brain, there is generally little movement of cellular processes, except perhaps for those associated with synaptic plasticity that underlie learning and memory. Microglia are apparently never at physical rest either.

Although the development of two-photon microscopy opens new perspectives for the analysis of intact organs, some major technical issues remain. Improvements in the resolution, depth penetration, image acquisition speed, and photon detector sensitivity of the microscopes will enhance our ability to follow intracellular signaling events and cellular traffic in living tissues. Likewise, the generation of mice expressing fluorescent proteins under the control of different cell type–specific promoters or inducible promoters should allow the study of multiple cell functions within intact organs using two-photon microscopy. Accurate methods to quantify image information are also needed. Despite these obstacles, the development of intact organ imaging should continue to have a major impact in biology over the coming years.

References

1. W. R. Zipfel, R. M. Williams, W. W. Webb, *Nat. Biotechnol.* **21**, 1369 (2003).
2. J. W. Wang, A. M. Wong, J. Flores, L. B. Vosshall, R. Axel, *Cell* **112**, 271 (2003).
3. B. J. Bacskai *et al.*, *Nat. Med.* **7**, 369 (2001).
4. A. Nimmerjahn, F. Kirchhoff, F. Helmchen, *Science* **308**, 1314 (2005).
5. D. Davalos *et al.*, *Nat. Neurosci.* **8**, 752 (2005).

10.1126/science.1114852

WIN A $250 GIFT CHEQUE!

Download the conference brochure by August 1 at www.drugdisc.com/us and you will automatically entered in the American Express Gift Cheque drawing.

Optimizing the Discovery & Development Interface to *Improve Productivity*

Enhance Safety & Efficacy

Develop New Business

Explore New Markets

10th Anniversary DRUG DISCOVERY TECHNOLOGY® & Development

Keynote Sessions

Lester M. Crawford, D.V.M., Ph.D.
Acting Commissioner, FDA

John L. LaMattina, Ph.D.
President, Pfizer Global R&D

Keynote Panel Discussion

Exploring the Industry and Regulatory Interface in Drug Development

Moderator:

Robert R. Ruffolo, Jr., Ph.D.
President, R&D, Wyeth

The Boston Convention & Exhibition Center, Boston, MA

Conference: **August 8-11, 2005**

Exhibition: **August 9-11, 2005**

Visit www.drugdisc.com/us

- ✔ Review the 150+ conference session options
- ✔ Create a customized schedule
- ✔ Participate in an industry survey & "quiz"
- ✔ Download the brochure & enter the drawing

Presidential Sponsors:

Executive Sponsor:

Supporting Publications:

Association Sponsor:

Organized by:

Putting research to work through international collaboration

Parasites are preventing many poor people in poor countries from working fully, from living healthy lives, and in many areas, are killing them too early in their short lives. Nowhere is this more evident than in three major diseases: **Chagas disease, Leishmaniasis**, and **African Trypanosomiasis** (sleeping sickness).

Because of the poverty in Africa, Asia and Latin America, there has been little incentive for industry to invest in research and development to create effective intervention tools. There have been significant advances (see next page), but no vaccines exist for any of these diseases and many of the drugs still in use are often toxic, lacking effectiveness, and there is a danger of parasites becoming resistant to them.

TDR, the special programme for tropical disease research and training, is proud to have been one of the early forces behind the global collaboration to sequence the genomes of the three trypanosomatids. At a meeting co-sponsored by TDR and the Oswaldo Cruz Foundation (FIOCRUZ) and held in Brazil in 1994 at the FIOCRUZ campus in Rio de Janeiro, the goals were laid out to provide a pump-priming scientific discovery effort in these areas, and create new opportunities for researchers from both the north and south to work together in a highly technological venture.

THERE IS AN URGENT NEED FOR RADICALLY NEW APPROACHES TO THE DEVELOPMENT OF DIAGNOSTICS, DRUGS, VACCINES AND VECTOR CONTROL TOOLS. THE SEQUENCING OF THESE PARASITES' GENOMES COMES AT A CRITICAL MOMENT.

Tritryp Genome support provided by:

- Burroughs Wellcome Fund (BWF)
- European Commission (EC)
- The Institute for Genomic Research (TIGR)
- Karolinska Institutet
- National Institute of Allergy and Infectious Diseases, National Institutes of Health (NIAID/NIH)
- Seattle Biomedical Research Institute (SBRI)
- TDR, the UNICEF/UNDP/ World Bank/WHO Special Programme for Research and Training in Tropical Diseases
- The Wellcome Trust
- The Wellcome Trust Sanger Institute

This early work motivated the support of regional networks of laboratories, particularly those funded by United States (NIAID, Burroughs Wellcome Fund), United Kingdom (Sanger), Spain (CYTED), France (CEPH and INSERM) and Sweden (SAREC). These were at the basis of the important investments in Brazil in the field of genomics that began with the activities related to the *Schistosoma* and *T. cruzi* regional genome projects. Several major research funding agencies and laboratories joined forces collectively to ensure the sequencing of the three trypanosomatid genomes became a reality (see the box on the left).

Parallel activities on vectors of diseases have also been successful. The *Anopheles gambiae* genome sequence was published in 2002 (Science, 2002, 298[5591]); another vector of dengue is currently being sequenced – *Aedes aegypti*; and preparations are being made for sequencing *Glossina*, the vector of African trypanosomiasis.

TDR will continue to promote genomics activities, because we believe it will transform analytical science into social impact by providing novel tools for treatments and disease control where it's needed most – among the poorest people in the poorest countries.

UNICEF/UNDP/World Bank/WHO
Special Programme for Research and Training in Tropical Diseases (TDR)

WHO/TDR
Avenue Appia 20
1211 Geneva 27 - Switzerland
Tel: (+41) 22-791-3725
Fax: (+41) 22-791-4854
E-mail: tdr@who.int
Web: www.who.int/tdr

Future directions

Genomics has great potential to create whole new interventions (drugs, diagnostics and vaccines) for people suffering from many tropical diseases. This work requires collaboration among scientists from many disciplines. Collective efforts are needed more than ever before.

TDR WILL CONTINUE TO BUILD AND FOSTER NETWORKS AND STRENGTHEN RESEARCH CAPACITY AMONG SCIENTISTS IN THE DEVELOPING COUNTRIES WHERE PEOPLE ARE SUFFERING FROM THESE DISEASES.

Through a cooperative agreement among TDR, Wellcome Trust and *Science*, a two-disc CD-ROM set has been created that contains the genome sequences of *T. brucei*, *T. cruzi* and *Leishmania major*, bioinformatics tools and related publications. We believe that the increasing genome availability will narrow the so-called genomics divide between industrialized and developing countries. The CD-ROM set is available free of charge and can be ordered online at: **http://www.who.int/tdr/media/multimedia.htm**

When new discoveries and innovations are identified, partnerships with industry and public sectors can deliver new tools of value for fighting diseases. Some TDR partnered successes in the control of these three diseases include:

- Development and donation of eflornithine (DFMO) for treatment of late stage African trypanosomiasis.
- Development of liposomal amphotericin B, miltefosine and rapid diagnostics for treatment of visceral leishmaniasis.
- Development of vector control tools that have enabled interruption of transmission of Chagas disease in some of the most infected countries in Latin America.

www.who.int/tdr

UNICEF/UNDP/World Bank/WHO
Special Programme for Research and Training in Tropical Diseases (TDR)

WHO/TDR
Avenue Appia 20
1211 Geneva 27 - Switzerland
Tel: (+41) 22-791-3725
Fax: (+41) 22-791-4854
E-mail: tdr@who.int
Web: www.who.int/tdr

Leishmaniasis

Distribution

Endemic in 88 countries on 4 continents. More than 90% of cutaneous leishmaniasis cases occur in Iran, Afghanistan, Syria, Saudi Arabia, Brazil and Peru. More than 90% of visceral leishmaniasis cases occur in Bangladesh, Brazil, India and Sudan.

Causative agent and vector

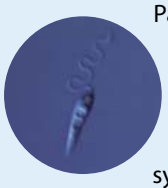

Parasitic protozoa of the genus *Leishmania*, transmitted to humans by sandflies. Over 20 species and subspecies infect humans, each causing a different spectrum of symptoms from simple, self-healing skin ulcers (e.g. due to infection with *Leishmania major*), to severe, life-threatening disease (e.g. visceral leishmaniasis caused by *L. donovani s.l.*).

Disease control and research challenges

- Long, difficult, expensive treatment
- Practical limitations of diagnostics
- Low priority, poor health systems

Chagas Disease

Distribution

Endemic in 18 countries in 2 ecological zones in the Americas:

- Southern Cone, where vector insects live inside human homes.
- Central America and Andean countries, where the vector lives both inside and outside dwellings.

Causative agent and vector

The protozoan parasite (*Trypanosoma cruzi*), which is transmitted by the *Triatominae* bugs and, to a lesser extent, through blood transfusion and congenital transmission.

The parasite invades most organs of the body, often causing heart, intestinal and oesophageal damage, killing up to a third of those with chronic infection.

Disease control and research challenges

- Control of non-domiciliated vectors
- Sustained vector control
- Millions infected at risk of disease

UNICEF/UNDP/World Bank/WHO
Special Programme for Research and Training in Tropical Diseases (TDR)

African trypanosomiasis (sleeping sickness)

Distribution

Occurs in 36 African countries. Many people are not diagnosed and treated early enough. Case fatality is very high and epidemics frequent.

Causative agent and vector

Protozoan parasites of the genus *Trypanosoma*, which enter the bloodstream via the bite of blood-

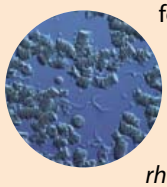

feeding tsetse flies (*Glossina spp.*), cause progressive illness, ultimately invading the central nervous system where the infection leads to death. *Trypanosoma brucei rhodesiense* occurs mainly in east and southern Africa.

T.b. gambiense mainly in west and central Africa. A third subspecies, *T.b. brucei* is responsible for the cattle disease but does not infect humans.

Disease control and research challenges

- Poor and toxic drugs
- Poor diagnostics
- Inadequate surveillance and poor health systems

The research pathway from genomics to health impact

Balancing field needs with scientific opportunities at every step

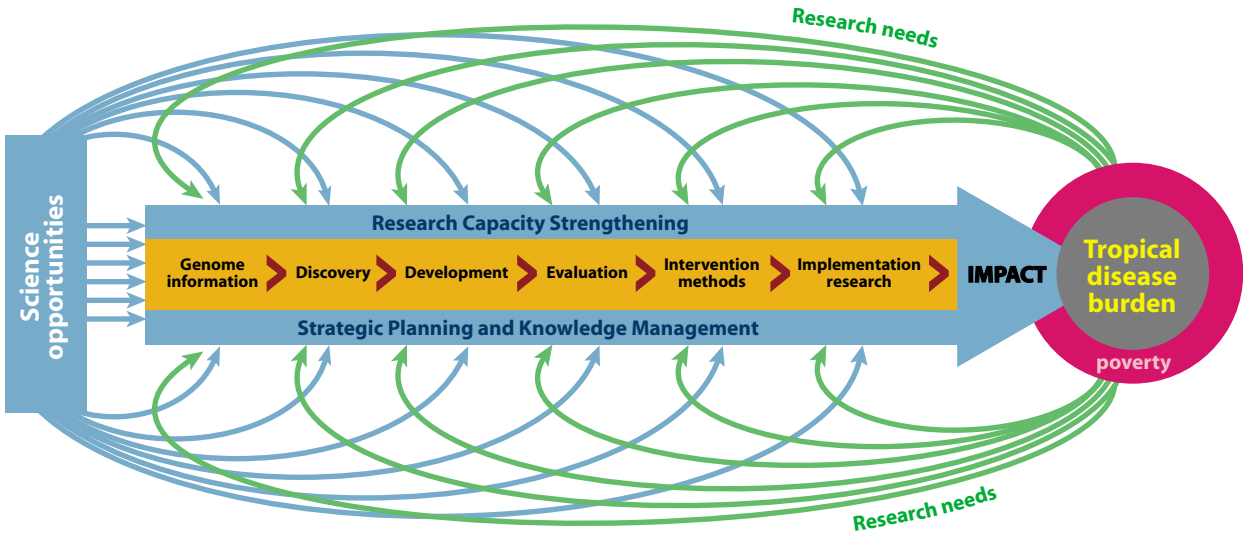

UNICEF/UNDP/World Bank/WHO
Special Programme for Research and Training in Tropical Diseases (TDR)

INTRODUCTION

Trypanosomatid Genomes

We have committed the pages of this issue to an exploration of three genomes of ancient organisms. Why? There are two important reasons. First, the body of work represented here is the culmination of more than a century of labor on parasites responsible for severe human diseases; many of those who have contributed have done so from deep-seated humanitarian motives. Second, this work symbolizes a huge intellectual triumph; these organisms have been recalcitrant to methodologies developed for the standard model organisms, not least in the difficulties encountered in the sequencing effort itself, yet the rewards for persistence have been remarkable: RNA editing and RNA trans-splicing, the T helper cell paradox, innate immunity, immune evasion, antigenic variation, glycophosphoinositol membrane anchoring, metabolic compartmentalization and the glycosome, the kinetoplast and chromosome evolution, vector biology, and epidemiological modeling.

This work also represents a triumph of international collaboration. After independent origins and discussions in the 1990s, it became clear that there was more to be gained by sharing experiences across the groups of researchers interested in these parasites. The three original international networks for trypanosomatid genome projects held the first "Tritryp" meeting in 2000 (http://tryp-pc1.path.cam.ac.uk/trypanosome/report2000.htm). It was jointly funded by the World Health Organization, Wellcome Trust, the National Institutes of Health, and the Burroughs Wellcome Fund, and also marked the beginning of closer collaboration among the sequencing centers at the Sanger Institute, The Institute for Genomic Research, the Seattle

CONTENTS

See also Editorial on page 355; Reports pages 469 and 473; STKE material on page 349

CREDIT: ELISBET CALER

Science

Biomedical Research Institutet, and the Karolinska Institute. Another triumph of this collaboration was the extent of international involvement: Most of the ESTs (expressed sequence tags) for all three organisms were sequenced at institutions in Africa and South America. The participation of endemic countries also included studies on strain diversity, construction of large-insert libraries, and early stages of physical mapping of the genomes.

Within the past 5 years, the sequencing of genomes per se has gone from being a revolutionary achievement to something commonplace. However, the sequences of *Trypanosoma cruzi*, *Trypanosoma brucei*, and *Leishmania major* (the so-called Tritryps) are revelatory. The desire to put the emphasis on biology led the authors of the Research Articles to adopt a somewhat unusual organization. Although there is nominally a comparative article and articles on each of the genomes, each article provides comparisons among the three organisms for different research themes. Hence, Berriman *et al*. (p. 416) emphasize metabolic and biochemical pathways of all three organisms within the article for *T. brucei*; Ivens and colleagues (p. 436) highlight fundamental aspects of molecular biology (such as transcription, translation, posttranslation modification, and proteolysis) while describing *L. major*; and El-Sayed *et al*. (p. 409) focus on repetitive elements, DNA replication and repair, and signaling pathways in *T. cruzi* and the other parasites. The comparative paper by El-Sayed *et al*. (p. 404) concentrates on gene content, genome architecture, composition, organization of protein domains, and rates of evolution. This special section also contains four fold-out plates (between pages 423 and 434), which are cross-referenced by all the Research Articles. Parasite invasion also depends on exploitation of host signaling pathways; an STKE Perspective by Burleigh discusses alternate models of *T. cruzi* invasion, highlighting the role of host phosphatidylinositol 3-kinases (PI3Ks) in this process.

Sequence information provides the launching pad for research into function which, in turn, can provide the forward thrust for the design of new therapeutics. We have included two examples here. From scrutinizing the proteome of *T. cruzi*, Atwood *et al*. (p. 473) have identified distinct energy sources used at different stages of its life cycle. Pérez-Morga *et al*. (p. 469) have resolved a long-standing conundrum, and present the mechanism by which apolipoprotein L-1, a factor in human serum, kills trypanosomes.

With so many unique tools and targets, why don't we have effective drugs? It is a terrible indictment that we have failed to support the translation of this work into cheap, safe products. Cross (p. 355) calls for something better than the standard modus operandi of the pharmaceutical companies and the academic promotions system. As Morel notes in his Viewpoint (p. 401), networks such as the one that led to the sequencing of these three organisms can enable developing countries to push forward in health innovation with their own energies and resources. Let's hope the genomes will fuel this process.

–CAROLINE ASH AND BARBARA R. JASNY

Health Innovation Networks to Help Developing Countries Address Neglected Diseases

Carlos M. Morel,[1]* Tara Acharya,[2] Denis Broun,[3] Ajit Dangi,[4] Christopher Elias,[5] N. K. Ganguly,[6] Charles A. Gardner,[7] R. K. Gupta,[8] Jane Haycock,[9] Anthony D. Heher,[10] Peter J. Hotez,[11] Hannah E. Kettler,[12] Gerald T. Keusch,[13] Anatole F. Krattiger,[14] Fernando T. Kreutz,[15] Sanjaya Lall,[16] Keun Lee,[17] Richard Mahoney,[14] Adolfo Martinez-Palomo,[18] R. A. Mashelkar,[19] Stephen A. Matlin,[20] Mandi Mzimba,[21] Joachim Oehler,[22] Robert G. Ridley,[23] Pramilla Senanayake,[24] Peter Singer,[25] Mikyung Yun[26]

Gross inequities in disease burden between developed and developing countries are now the subject of intense global attention. Public and private donors have marshaled resources and created organizational structures to accelerate the development of new health products and to procure and distribute drugs and vaccines for the poor. Despite these encouraging efforts directed primarily from and funded by industrialized countries, sufficiency and sustainability remain enormous challenges because of the sheer magnitude of the problem. Here we highlight a complementary and increasingly important means to improve health equity: the growing ability of some developing countries to undertake health innovation.

Improving the health of the poorest people in the developing world depends on the development and deployment of many varieties of health innovations, including new drugs, vaccines, devices, and diagnostics, as well as new techniques in process engineering and manufacturing, management approaches, software, and policies in health systems and services. In developed countries, philanthropic and government donors have created and invested more than $1 billion in global product development partnerships (PDPs) to develop and help to ensure access to new drugs, vaccines, and diagnostics for diseases of the poor (*1*). These PDPs have made major progress in a relatively short time period (*2*) but continue to face many challenges.

All developing countries can undertake health innovation to varying degrees. Some developing countries, however, are more scientifically advanced than others and are starting to reap benefits from decades of investments in education, health research infrastructure, and manufacturing capacity. We refer to these as innovative developing countries (IDCs) (*3*, *4*).

It is a challenge to get complete data on health research spending. According to the most recent available data, public spending on health research by developing countries totaled at least $2 billion (*5*). This number does not include China, for which data were not available. That investment, which has already led to important innovations, is projected to continue to grow (*3*, *5*–*7*). Furthermore, lower labor and other costs have the potential to magnify the impact of this investment. To put it in a different perspective, just 1/10th of these IDC public health research resources amounts to more than all that was spent in 2004 by the above-mentioned PDPs engaged in the development of drugs, vaccines, and diagnostics for diseases of the poor (*8*, *9*).

Patents and well-cited publications indicate the productivity of research investments, and in this light, IDCs have made major progress. The number of U.S. patents per capita is a common proxy used to measure the relative innovation efficiency of countries, but we believe that this computation underestimates the innovative capacity of developing countries, because it fails to detect the productivity of highly capable centers of excellence within countries with large populations. Adjusting for both relative economic status and population (U.S. patents per gross domestic product per capita) (*10*), the top 25 most productive countries in the world include India, China, Brazil, South Africa, Thailand, Argentina, Malaysia, Mexico, and Indonesia (*10*). For Brazil, China, India, and South Africa, the number of highly cited academic papers rose nearly two-fold from 1993–1997 to 1997–2001 (*11*), whereas the number of U.S. patents has increased 10-fold (*12*).

Academic research, publications, and patents do not help the poor (or anyone else) unless they are turned into tangible products or improved practices and policies. Detailed analyses and comparisons of countries' performance in turning ideas into innovations are limited (*13*), but there are case examples that imply growing capabilities. IDCs have a publication intensity that is much higher than the global average in health biotechnology fields that are relevant to the health needs of their own populations (*14*). As far as specific products now on the market, the list includes the following: (i) the first effective meningitis B vaccine, developed at the Cuban Finlay Institute and recently licensed to GlaxoSmithKline (*15*); (ii) new innovative processes for engineering local versions of the recombinant hepatitis B vaccine in Cuba, Korea, and India (*16*); and (iii) the antimalarial drug arteether (a semi-synthetic artemisinin derivative), developed at India's Central Drug Research Institute and transferred to Themis Chemicals for commercial development, now sold under the brand name E-mal in 48 countries (*17*). In terms of innovative health programs, Brazil's human immunodeficiency virus/acquired immunodeficiency syndrome (HIV/AIDS) program stands

[1]Center for Technological Development in Health, Oswaldo Cruz Foundation (FIOCRUZ), Avenida Brasil 4365, Rio de Janeiro, RJ 21040–900, Brazil. [2]300 East 93rd Street, Apartment 18A, New York, NY 10128, USA. [3]The Joint United Nations Programme on HIV/AIDS, 55 Lodi Estate, New Delhi, 110 003, India. [4]Organization of Pharmaceutical Producers of India, Peninsula Chambers, Peninsula Corporate Park, G. K. Marg, Lower Parel, Mumbai, 400 013, India. [5]Program for Appropriate Technology in Health, 1455 NW Leary Way, Seattle, WA 98107, USA. [6]Indian Council of Medical Research, V. Ramalingaswami Bhawan, Ansari Nagar, New Delhi, 110 029, India. [7]The Rockefeller Foundation, 420 Fifth Avenue, New York, NY 10018, USA. [8]Intellectual Property Management Division, Council for Scientific and Industrial Research, Third Floor, 14 Satsang Vihar Marg, Special Institutional Area, New Delhi, 110 067, India. [9]Mission of the United Kingdom to the United Nations, 1 Dag Hammarskjold Plaza, New York, NY 10017, USA. [10]University of Cape Town, Research and Innovation House, Lovers Walk, Lower Campus, Private Bag, Rodebosch 7701, Cape Town, South Africa. [11]Department of Microbiology and Tropical Medicine, George Washington University, Ross Hall Room 736, 2300 Eye Street N.W., Washington, DC 20037, USA. [12]Bill and Melinda Gates Foundation, Post Office Box 23350, Seattle, WA 98102, USA. [13]Boston University, 715 Albany Street, Talbot 443W, Boston, MA 02118, USA. [14]BioDesign Institute, Arizona State University, Tempe, AZ 85287–4501, USA. [15]FK Biotecnologia, Avenida Bento Gonçalves 9500, Building 43431, Campus do Vale, Federal University of Rio Grande do Sul, Porto Alegre, RS 91501–970, Brazil. [16]Oxford University, Queen Elizabeth House, 21 Saint Giles, Oxford OX1 3LA, UK. [17]Department of Economics, Seoul National University, Shillim-dong, Seoul, 151-742, Korea. [18]Ministry of Health, Periférico Sur 4118, Edifico Zafiro I, primero piso, Col. Jardine, DF 01900, Mexico. [19]Council for Scientific and Industrial Research, Anusandhan Bhawan, 2 Rafi Marg, New Delhi 110 001, India. [20]Global Forum for Health Research, 1-5 Route de Morillons, Post Office Box 2100, Geneva 2, CH-1211, Switzerland. [21]Department of Science and Technology, South African Embassy, 26 Rue de la Loi, Brussels 1040, Belgium. [22]The Concept Foundation, 111 Paholyothin Road, Thailand Science Park, Klongluang, Pathumthani 12120, Thailand. [23]Tropical Disease Research Program, World Health Organization, Geneva 27 GE, CH-1211 Switzerland. [24]Global Forum for Health Research, 79 Hyde Park Corner, Colombo 2, Sri Lanka. [25]University of Toronto, 88 College Street, Toronto, ON M5G-1L4, Canada. [26]Korea Institute for International Economic Policy, Seocho-gu, Yeomgokdong, 300-4 Seoul, 137-747 Korea.

*To whom correspondence should be addressed. E-mail: morel@fiocruz.br

out, because it has combined the local manufacturing of antiretrovirals and government financing to provide free access to all who need the drugs (*18*). A number of companies from IDCs are working on new products in collaboration with the global PDPs, including FIOCRUZ/Bio-Manguinhos and Butantan Institute of Brazil with the Human Hookworm Vaccine Initiative (*19*), Ranbaxy and Bharat Biotech in India with the Malaria Vaccine Initiative, and the Serum Institute of India with the Meningitis Vaccine Initiative.

Developing countries also play an increasingly important role in manufacturing health products to meet global health needs. China is the world's leading producer of penicillin. The Serum Institute of India is the world's leading manufacturer of diphtheria-pertussis-tetanus vaccine. Over 60% of the United Nations Children's Fund's vaccine requirements for the Expanded Programme on Immunization are met by Brazil, Cuba, India, and Indonesia (*20*, *21*). In dollar terms, 67% of India's drug exports and 74% of Brazil's drug exports go to other developing countries, whereas 63% of Uganda's drug imports and 54% of Tanzania's drug imports come from other developing countries (*22*). By volume, India is now the fourth largest producer of pharmaceuticals in the world (*23*).

Some observers have emphasized the need for developing countries to "build their own capacity to develop drugs, particularly in the case of neglected diseases … for which multinational pharmaceutical companies may have little interest in investing because the market is unlikely to provide adequate returns" (*24*). Yet there may be tensions between national health priorities and the desire for economic development (*25*). Although the Commission on Macroeconomics and Health has emphasized the direct link between health and economic development (*26*), others underscore the need to consciously align innovation policies and health priorities in a way that is consistent with the legitimate goals of wealth and job creation (*27*).

These perspectives help to highlight specific questions that require further study. For example: Under what conditions might a market that seems unattractive to a developed-country company be attractive to its developing-country counterpart? Under what circumstances might companies in the individual IDCs build a business based on national health needs, as opposed to global diseases with blockbuster profit potential? Are there opportunities for IDCs to help least-developed countries, either through the manufacture and export of low-cost products or through technical assistance and capacity building (*28*)? Is it in their economic interest to do so? In considering such questions, we raise the following points, each of which is based on observations that require further study

1) Public-sector infrastructure. Unlike in wealthier countries, most health research (and some manufacturing) in developing countries is funded by and conducted in the public sector and therefore may be driven more by public health goals (*5*, *29*, *30*).

2) Low-cost production. C. K. Prahalad points out (*31*) that some manufacturers in developing countries pursue a business model in which they specialize in high-volume, low-margin production, which leads to low-cost products, and they often explicitly develop products with the goal of distributing them to the poor in developing-country markets. Manufacturing cost advantages (*32*) mean that products produced in developing countries may be more affordable, an important factor in access to medicines.

3) Acceptability and social conscience. Those closest to the needs of the poor are the affected communities, scientists, policymakers, and institutions in developing countries. This proximity may motivate innovation for treating diseases of the poor. IDC products may also be more acceptable to governments and consumers in developing countries.

A recent study of innovation systems in health biotechnology in developing countries found that policies and practices affecting local public-private partnerships (PPPs), sustained government support for research, the retention and expansion of the scientific corps, the availability of venture capital, and manufacturing and regulatory approvals are particularly important factors in innovation to meet national health needs (*6*). Given that currently most of the infrastructure for health research in developing countries resides in the public sector (*5*, *29*, *30*), we believe that innovation through partnering of local public and private research organizations deserves particular attention. National innovation policies to encourage such partnerships, and capacity building in the management of intellectual property, among other competencies, can help make such partnerships more effective.

In 2002, the U.K. Commission on Intellectual Property Rights suggested the need for "a network of the public-private partnerships in developing countries, taking advantage of the concentration of research resources in public sector institutions but also the opportunity to build research capacity in the private sector" (*33*). Given the large and growing investments by IDCs in health research, we strongly advocate a network for health innovation in developing countries that promotes policy research, local innovation, South-to-South learning, and information sharing (Fig. 1).

Several networks have already formed, focusing on individual diseases, technologies, or components of health innovation systems. In April 1994, FIOCRUZ and the Special Programme for Research and Training in Tropical Diseases (TDR) organized in Rio de Janeiro the first Parasite Genome Network Planning Meeting (Fig. 2). The Developing Country Vaccine Manufacturers' Network, established in November 2000, includes both state-owned and private producers in Brazil, Cuba, China, India, Indonesia, and Mexico that are prequalified by the World Health Organization (WHO) for sale to United Nations (UN) agencies. The South-South Initiative (SSI) in tropical diseases research, a TDR initiative begun in 1991, is designed to facilitate sharing of resources among research groups in Latin America, Asia, and Africa in order to increase competitiveness and optimize scientific opportunities. The SSI currently in its full operation is managed by a coordinating committee representing African, Asian, and Latin American

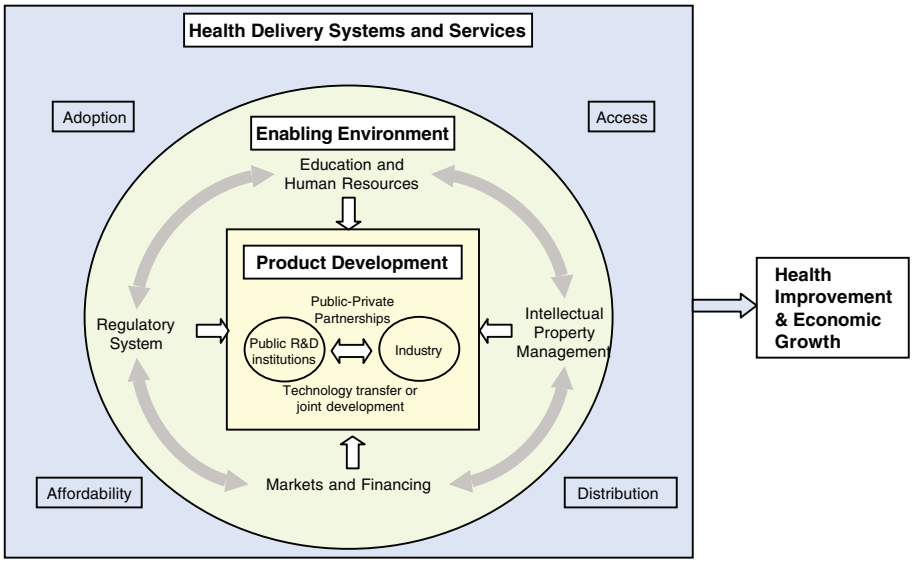

Fig. 1. Health innovation systems have multiple components, operating in both the public and private sectors, including the following: education, research, financing, manufacturing, technology management practices, intellectual property rules, regulatory rules, and domestic and export markets (including public procurement). The system refers not only to these components but also to the technical, commercial, legal, social, and financial interactions; the interlinkages among components; and the policies and practices that guide them. The function (or dysfunction) of and dynamic linkages among these components contribute to the production and delivery of health products and services to people—or lack thereof.

Fig. 2. Group photograph of the participants of the FIOCRUZ-TDR Parasite Genome Network Planning Meeting, held in Rio de Janeiro, Brazil, on 14 and 15 April 1994. This international meeting, attended by 40 scientists and 5 representatives from WHO, selected the three parasite strains whose genome sequences are published in this issue of *Science* by the Tritryp project.

investigators (*34*). The India–Brazil–South Africa Dialogue Forum, established in June 2003, includes a focus on intellectual property and access to medicine, traditional medicine, and R&D on vaccines and pharmaceutical products to address national health priorities. The Technological Network on HIV/AIDS, which was announced in Bangkok during the July 2004 International AIDS Conference, includes Brazil, China, Cuba, Nigeria, Russia, Thailand, and Ukraine (with perhaps India and South Africa joining in the near future). The Network supports research and South-South technology transfer to develop and manufacture antiretroviral drugs and new drug formulations, male and female condoms, microbicides, and HIV vaccines. Finally, the WHO Developing Countries' Vaccine Regulators Network, created in September 2004, involves Brazil, China, Cuba, India, Indonesia, Russia, South Africa, South Korea, and Thailand.

Broader networks could expand linkages to other like-minded organizations (*35*). We believe that more frequent robust exchanges of know-how among an expanding universe of public- and private-sector players would accelerate innovation and expedite the translation of knowledge about diseases of the poor while also reflecting national sensitivities, changing contexts, and the concomitant desire for economic growth. This goal will also require bringing together two communities whose communication has been, in our opinion, far from optimal. A growing body of scholarly economic studies has examined innovation systems in developing countries (*6*, *20*, *36*–*38*). This work tends to equate well-being with wealth creation, and it is built largely on case studies from the electronics, information technology, engineering, and other nonhealth manufacturing industries. At the same time, global health professionals concerned with the discovery, development, and introduction of new health technologies—who are, in fact, working to address challenges that are directly related to the components of health innovation systems—have not systematically applied concepts and methodologies from the field of innovation systems in their work. A network approach could help maximize substantial existing investments in health research made by IDCs and also complement global efforts to address health disparities and achieve the Millennium Development Goals.

We have sought to highlight two points: (i) A rapidly evolving phenomenon: IDCs are increasingly capable of health innovation to address their national health priorities and to help meet the needs of less advanced developing countries. (ii) A knowledge gap: Innovation systems theory has rarely been applied to global health problems, whereas the global health community has rarely focused on innovation systems (*39*). We believe that new insights may arise at the intersection of these two cultures and research communities (*40*).

References and Notes

1. R. Widdus, K. White, *Combating Diseases Associated with Poverty, Financing Strategies for Product Development and the Potential Role of Public-Private Partnerships*, (www.who.int/entity/intellectualproperty/topics/ppp/en/CombatingDiseases-Abridged.pdf).
2. M. Moran, submissions to the Commission on Intellectual Property Rights, Innovation and Public Health of the WHO: *New Approaches to Funding Drug R&D for Neglected Diseases* (www.who.int/entity/intellectualproperty/submissions/Mary.Moran.pdf) and *Fast Track Options as a Fundraising Mechanism to Support R&D into Neglected Diseases* (www.who.int/entity/intellectualproperty/submissions/Mary.Moran2.pdf).
3. C. Morel *et al.*, *Innovation Strategy Today* **1**, 1 (2005); available at www.biodevelopments.org/innovation/index.htm.
4. These concepts spring from the meeting "Accelerating Product Development and Ensuring Product Access for Diseases of Poverty: The Role of Public-Private Partnerships in Developing Countries" held in Bellagio, Italy, on 10 to 13 May 2004.
5. Global Forum for Health Research, *Monitoring Financial Flows for Health Research*, Vol. 2 (Global Forum for Health Research, Geneva, 2004), pp. 14–15.
6. *Nat. Biotechnol. Suppl.* **22** (125), (2004).
7. UN Millennium Project and UN Development Group, *Interim Report of Task Force 10 on Science, Technology and Innovation* (1 February 2004); available at www.unmillenniumproject.org.
8. This is an estimate by C. A. Gardner based on annual reports and grant applications from the product development PPPs and personal communications with individual PPP chief executive officers.
9. These PPPs include the International AIDS Vaccine Initiative, the International Partnership for Microbicides, the Medicines for Malaria Venture, the Malaria Vaccine Initiative, the Global Alliance for Tuberculosis (TB) Drug Development, and Aeras Global TB Vaccine Foundation.
10. Materials and methods are available as supporting material on *Science* Online.
11. D. A. King, *Nature* **430**, 311 (2004).
12. For more information, see www.uspto.gov.
13. Knowledge for Better Health, *Strengthening Health Systems*, The Mexico Statement on Health Research, from the Ministerial Summit on Health Research, Mexico City, 16 to 20 November 2004.
14. H. Thorsteinsdóttir, personal communication.
15. "YM Bio Springs a Cuban Surprise," *Financial Times*, 14 June 2002.
16. See www.who.int/csr/disease/hepatitis/whocdscsrlyo20022/en/index4.html.
17. R. A. Mashelkar, V. Tripathi, unpublished data.
18. G. C. Levi, M. A. Vitoria, *J. Acquir. Immune Defic. Syndr. Hum. Retrovirol.* **16**, 2373 (2002).
19. P. J. Hotez, J. Bethony, M. E. Bottazzi, S. Brooker, P. Buss, *PLoS Med.* **2**, e67 (2005).
20. C. Grace, *The Effect of Changing Intellectual Property on Pharmaceutical Industry Prospects in India and China: Considerations for Access to Medicine* (Issues Paper, Health Systems Resource Centre, Department for International Development, United Kingdom, June 2004).
21. According to the Developing Country Vaccine Manufacturers' Network, the number is 64%, excluding oral polio vaccine.
22. H. E. Bale, Commission on Macroeconomics and Health 2001. CMH Working Paper Series Paper No. WG 4:3 (WHO, Geneva, 2001).
23. See www.indiaoppi.com/keystat.htm.
24. House of Commons, *The Use of Science in UK International Development Policy* (Thirteenth Report of Session 2003 to 2004, October 2004, London).
25. H. Kettler, R. Modi, *Bull. World Health Organ.* **79**, 742 (2001).
26. WHO Commission on Macroeconomics and Health, *Macroeconomics and Health: Investing in Health for Economic Development. Report of the Commission on Macroeconomics and Health* (WHO, Geneva, 2001).
27. J. C. Pereira, V. T. Baltar, D. L. de Mello, *Rev. Saude Publica* **38**, 1 (2004).
28. In 2002, the Brazilian Ministry of Health created an International Cooperation Programme (ICP) for HIV and AIDS Prevention and Control Activities for Developing Countries "to provide funds for the establishment of ten pilot projects to the annual value of U.S. $100,000 each [for] technical assistance and antiretroviral drug supply" (*41*). Brazil has provided support and antiretroviral drugs to several African and Latin American countries, and both Brazil and Thailand have pledged to assist several African countries to develop antiretroviral manufacturing capacity. Brazil is also the largest producer of yellow fever vaccine in the world.
29. R. Saha *et al.*, *IP Strategy Today* **9**, 23 (2004).
30. The data in (*42*) support the observation that the public sector accounts for 40% of health R&D infrastructure in developed countries but 60% in developing countries. These data refer to R&D in general and are not specific to health.
31. C. K. Prahalad, *The Fortune at the Bottom of the Pyramid: Eradicating Poverty Through Profits* (Wharton School Publishing, Philadelphia, PA, 2004).
32. For example, the Organization of Pharmaceutical Producers of India and Monitor Company Group estimate that basic drug production costs in India are at least 50% less than in the United States, and in some cases the manufacturer's selling price in India is below production costs of the same product in the United States (*43*).
33. Commission on Intellectual Property Rights, "Integrating Intellectual Property Rights and Development Policy" (Commission on Intellectual Property Rights, London, 2002).
34. See www.ssi-tdr.net.
35. Examples of such organizations are the Global Forum for Health Research; the UN University Institute for New Technology; the Danish Research Unit for Industrial Dynamics; the Science and Technology Policy Research Unit of Sussex University; the Program for Appropriate Technology in Health; the Global Network for the Economics of Learning, Innovation, and Competence Building Systems; the World Bank Millennium Science Initiative; and a proposed Research Agency Collaborative on Health.
36. C. Dahlman, R. R. Nelson, in *Social Capability and Long Term Economic Growth*, B. Koo, D. Perkins, Eds. (MacMillan Press, London, 1995), pp. 82–122.
37. C. Edquist, *Systems of Innovation for Development*, background paper for United Nations Industrial Development Organization World Industrial Development Report 2001 (Vienna, 2001).
38. C. Juma *et al.*, *Int. J. Technol. Manage.* **22**, nos. 7/8 (2001).
39. The global health community, however, has recently embraced the application of systems theory to national health systems.
40. These issues were discussed in April 2005 during a meeting at the Rockefeller Foundation's Bellagio Conference Center, which brought together leading experts from these two fields to recommend a plan of action.
41. Ministry of Health of Brazil, *Scaling Up an International Response to AIDS–The Brazilian Initiative* (White Paper, National Program on Sexually Transmitted Diseases and AIDS), availiable at www.aids.gov.br.

42. World Development Report (World Bank, Washington DC, 2005), chap. 3.
43. Organization of Pharmaceutical Producers of India and Monitor Company Group, in *Outsourcing Opportunities in Indian Pharmaceutical Industry* (Mumbai, India, 2004); available at www.indiaoppi.com/puboutsourcing2003.htm., pp. 24–25.

44. The authors are grateful to all who contributed to this paper and to The Rockefeller Foundation for financial support. The views expressed in this paper are those of the authors in their individual capacities and do not necessarily reflect those of their respective institutions. We dedicate this work to Professor Sanjaya Lall, co-author, Friend, and colleague to us all, who passed away on 18 June 2005.

Supporting Online Material
www.sciencemag.org/cgi/content/full/309/5733/401/DC1
Materials and Methods
Fig. S1

10.1126/science.1115538

RESEARCH ARTICLE

Comparative Genomics of Trypanosomatid Parasitic Protozoa

Najib M. El-Sayed,[1,2*†] Peter J. Myler,[3,4,5*†] Gaëlle Blandin,[1] Matthew Berriman,[6] Jonathan Crabtree,[1] Gautam Aggarwal,[3] Elisabet Caler,[1] Hubert Renauld,[6] Elizabeth A. Worthey,[3] Christiane Hertz-Fowler,[6] Elodie Ghedin,[1,2] Christopher Peacock,[6] Daniella C. Bartholomeu,[1] Brian J. Haas,[1] Anh-Nhi Tran,[7] Jennifer R. Wortman,[1] U. Cecilia M. Alsmark,[8] Samuel Angiuoli,[1] Atashi Anupama,[3] Jonathan Badger,[1] Frederic Bringaud,[9] Eithon Cadag,[3] Jane M. Carlton,[1] Gustavo C. Cerqueira,[1,10] Todd Creasy,[1] Arthur L. Delcher,[1] Appolinaire Djikeng,[1] T. Martin Embley,[8] Christopher Hauser,[1] Alasdair C. Ivens,[6] Sarah K. Kummerfeld,[11] Jose B. Pereira-Leal,[11] Daniel Nilsson,[7] Jeremy Peterson,[1] Steven L. Salzberg,[1] Joshua Shallom,[1] Joana C. Silva,[1] Jaideep Sundaram,[1] Scott Westenberger,[1‡] Owen White,[1] Sara E. Melville,[12] John E. Donelson,[13] Björn Andersson,[7] Kenneth D. Stuart,[3,4] Neil Hall[6†§]

A comparison of gene content and genome architecture of *Trypanosoma brucei*, *Trypanosoma cruzi*, and *Leishmania major*, three related pathogens with different life cycles and disease pathology, revealed a conserved core proteome of about 6200 genes in large syntenic polycistronic gene clusters. Many species-specific genes, especially large surface antigen families, occur at nonsyntenic chromosome-internal and subtelomeric regions. Retroelements, structural RNAs, and gene family expansion are often associated with syntenic discontinuities that—along with gene divergence, acquisition and loss, and rearrangement within the syntenic regions—have shaped the genomes of each parasite. Contrary to recent reports, our analyses reveal no evidence that these species are descended from an ancestor that contained a photosynthetic endosymbiont.

The protozoan pathogens *Leishmania major*, *Trypanosoma cruzi*, and *Trypanosoma brucei* (family *Trypanosomatidae*, order *Kinetoplastida*) collectively cause disease and death in millions of humans and countless infections in other mammals, primarily in developing countries in tropical and subtropical regions (*1*). There are no vaccines for these diseases and only a few drugs, which are inadequate because of toxicity and resistance. Although the three pathogens (referred to here as the "Tritryps") share many general characteristics, including subcellular structures such as the kinetoplast and glycosomes, each is transmitted by a different insect and has its own life-cycle features, different target tissues, and distinct disease pathogenesis in their mammalian host [box 1 in (*2*) and fig. S1]. They also use different immune evasion strategies: *L. major* alters the function of the macrophages it infects, *T. cruzi* expresses a complex variety of surface antigens from within the cells it infects, and *T. brucei* remains extracellular but circumvents the host immune response by the periodic switching of its major surface protein (*3*).

The availability of the three draft genome sequences (*4*–*6*) allows better understanding of the genetic and evolutionary bases of the shared and distinct parasitic modes and lifestyles of these pathogens. In the accompanying Research Articles, the discussion of each species reflects the current state of knowledge for each organism. Thus, the Research Article by Berriman *et al*. (*4*) emphasizes metabolism and biochemical pathways of *T. brucei*; the Research Article by Ivens *et al*. (*5*) highlights fundamental aspects of molecular biology (transcription, translation, post-translational modification, and proteolysis) of *L. major*; and the Research Article by El-Sayed *et al*. (*6*) focuses on repeats and retroelements, DNA replication and repair, and signaling pathways of *T. cruzi*. Here, we compare gene content and genome architecture, composition, and organization of protein domains encoded by each genome and offer an analysis of the rates of gene evolution.

Core proteome. The *T. brucei*, *L. major*, and *T. cruzi* haploid genomes contain between 25 and 55 megabases (Mb) distributed over 11 to 36 (generally) diploid chromosomes, and encode about 8100, 8300, and 12,000 protein-coding genes, respectively (Table 1). An "all-versus-all" basic local alignment search tool (BlastP) comparison of the predicted protein sequences within each of the three genomes was made using a suite of algorithms designed to collapse closely related paralogous genes. In the case of *T. cruzi*, all alleles were included because of the hybrid nature of this genome (*2*, *6*). The mutual best BlastP hits between the three collapsed proteomes were grouped as clusters of orthologous genes (COGs). Iteration of this process with manual inspection and reannotation, especially of two-way COGs (i.e., those with members in only two of the Tritryps), resulted in 6158 three-way COGs, which defined the Tritryp core proteome, as well as 1014 two-way COGs (Table 1,

[1]The Institute for Genomic Research, 9712 Medical Center Drive, Rockville, MD 20850, USA. [2]Department of Microbiology and Tropical Medicine, George Washington University, Washington, DC 20052, USA. [3]Seattle Biomedical Research Institute, 307 Westlake Avenue North, Seattle, WA 98109–2591, USA. [4]Department of Pathobiology, University of Washington, Seattle, WA 98195, USA. [5]Division of Biomedical and Health Informatics, University of Washington, Seattle, WA 98195, USA. [6]Wellcome Trust Sanger Institute, Wellcome Trust Genome Campus, Hinxton, Cambridgeshire CB10 1SA, UK. [7]Center for Genomics and Bioinformatics, Karolinska Institutet, Berzelius väg 35, S-171 77 Stockholm, Sweden. [8]School of Biology, The Devonshire Building, University of Newcastle, Newcastle upon Tyne NE1 7RU, UK. [9]Laboratoire de Génomique Fonctionnelle des Trypanosomatides, UMR-CNRS 5162, Université Victor Segalen Bordeaux II, 33076 Bordeaux cedex, France. [10]Departamento de Bioquímica e Imunologia, Universidade Federal de Minas Gerais, CEP 31270-901, Belo Horizonte, MD, Brazil. [11]Medical Research Council Laboratory of Molecular Biology, Hills Road, Cambridge CB2 2QH, UK. [12]Department of Pathology, University of Cambridge, Tennis Court Road, Cambridge, CB2 1QP, UK. [13]Department of Biochemistry, University of Iowa, 4-403 Bowen Science Building, Newton Road, Iowa City, IA 52242, USA.

*These authors contributed equally to this work.
†To whom correspondence should be addressed. E-mail: nelsayed@tigr.org (N.M.E.-S.); peter.myler@sbri.org (P.J.M.); nhall@tigr.org (N.H.)
‡Present address: Department of Microbiology, Immunology, and Molecular Genetics, University of California, Los Angeles, CA 90095, USA.
§Present address: The Institute for Genomic Research, 9712 Medical Center Drive, Rockville, MD 20850, USA.

Fig. 1A, and table S1). Amino acid sequence alignment of a large sample of three-way COGs reveals an average of 57% identity between *T. brucei* and *T. cruzi*, and 44% identity between *L. major* and the two other trypanosomes, reflecting expected phylogenetic relationships (*7*–*10*). The intracellular parasites, *L. major* and *T. cruzi*, appear to share slightly more two-way COGs than do *T. brucei* and *T. cruzi* and considerably more than do *L. major* and *T. brucei*. The remainder of each proteome is composed of species-specific members (table S1), of which *T. cruzi* (32%) and *T. brucei* (26%) have a much greater proportion than *L. major* (12%). Because the majority of the species-specific proteins appear to be members of surface antigen families, the different numbers may relate to different strategies of survival and immune evasion used in each organism. Other species-specific proteins carry out distinct metabolic and physiological functions, some of which are discussed below [see also (*4*–*6*)].

Species-specific protein domains. A comparison of the Pfam and TIGRFAMs protein domains in the Tritryp genomes revealed very few that are unique to individual organisms (Fig. 1B). Of the 1617 protein domains identified in the Tritryp genomes, fewer than 5% are unique to a single species (table S2). For example, macrophage migration inhibitory factor (Pfam accession number PF01187) domain, restricted to *L. major*, may inhibit macrophage activation and consequent destruction of the parasites, as described in *Brugia malayi* (*5*, *11*). Another domain specific to *L. major* (PF04133) is involved in vacuolar transport, suggesting that the protein may act to divert proteases within the host phagolysosome. These domains are not seen in *T. cruzi*, which escapes from the lysosomal compartment into the cytoplasm soon after invasion, or in *T. brucei*, which is extracellular.

The variant surface glycoprotein (VSG) expression site–associated gene (ESAG) domains ESAG1 (PF03238) and ESAG6-7 (PF05446) are restricted to *T. brucei*. Likewise, the AOX domain (PF01786), which acts as an alternative terminal oxidase in mitochondria, and the LigB domain (PF02900), which is involved in aromatic compound metabolism, account for some of the few metabolic capabilities of *T. brucei* that are not found in *L. major* or *T. cruzi* (*4*–*6*).

T. cruzi has a serine carboxypeptidase S28 domain (PF05577) not found in *T. brucei* or *L. major*. Several lines of evidence indicate that *T. cruzi* secretes a small peptide processed by a serine peptidase, which interacts with a host-cell receptor in a wide variety of mammalian cells (*12*). This interaction leads to a calcium signaling reaction that triggers lysosome migration to the host-cell plasma membrane, enabling parasite entry (*13*). *T. cruzi* also contains a number of hormone-type domains such as PF00220 (neurohypophysial hormones, N-terminal domain) and the PF02044 (bombesin-like peptide), which are not found in *T. brucei* or *L. major*, but the functional significance of these domains is uncertain.

Specific domain expansion and loss. Several interesting examples of domain expansion or contraction (table S3) were revealed (fig. S2), similar to those seen in other parasites such as *Plasmodium* (*14*). Many of these proteins appear to be involved in host interactions and often are encoded in tandem arrays, typically at species-specific subtelomeric locations (*4*–*6*). For example, *T. brucei* has expanded ESAG4 proteins that contain adenylate and guanylate cyclase catalytic domains and proteins containing leucine-rich repeat domains. *T. cruzi* has expanded bacterial neuraminidase/Asp-box repeat, mucin-like glycoprotein, leishmanolysin, and trypanosome retrotransposon hot spot (RHS) domains in trans-sialidases, mucins, glycoprotein (gp) 63 proteases, and RHS proteins, respectively. *L. major* contains a large tandem array of amastin surface glycoproteins but also possesses expanded protein families containing mitochondrial carrier protein, adenosine 5′-triphosphate–binding cassette transporters, and heat shock protein (HSP) 90. Interestingly, compared with *T. brucei* and *T. cruzi*, *L. major* has a marked underrepresentation of domains involved in RNA binding (pumilio and zinc finger domains), protein-protein interaction (leucine-rich and tetratricopeptide repeats), and calcium signaling (calmodulin and EF hand), suggesting a reduced role or alternate pathways for these activities.

Large-scale synteny. Despite having diverged 200 to 500 million years ago (*15*–*18*) and thus predating the emergence of mammals (*19*), the genomes of the trypanosomatid species are highly syntenic (i.e., show conservation of gene order). Of all the genes in *T. brucei* and *L. major*, 68 and 75%, respectively, remain in the same genomic context. Moreover, almost all (94%) of the three-way COGs that form the core proteome fall within regions of conserved synteny. The *T. brucei* and *L. major* genomes (*2*) show 110 blocks of synteny spanning 19.9 and 30.7 Mb, respectively (Fig. 2). Detailed examination of the synteny breakpoints revealed that 40% were associated with expansions of multigene families, retroelements and/or structural RNAs (Plate 1, fig.

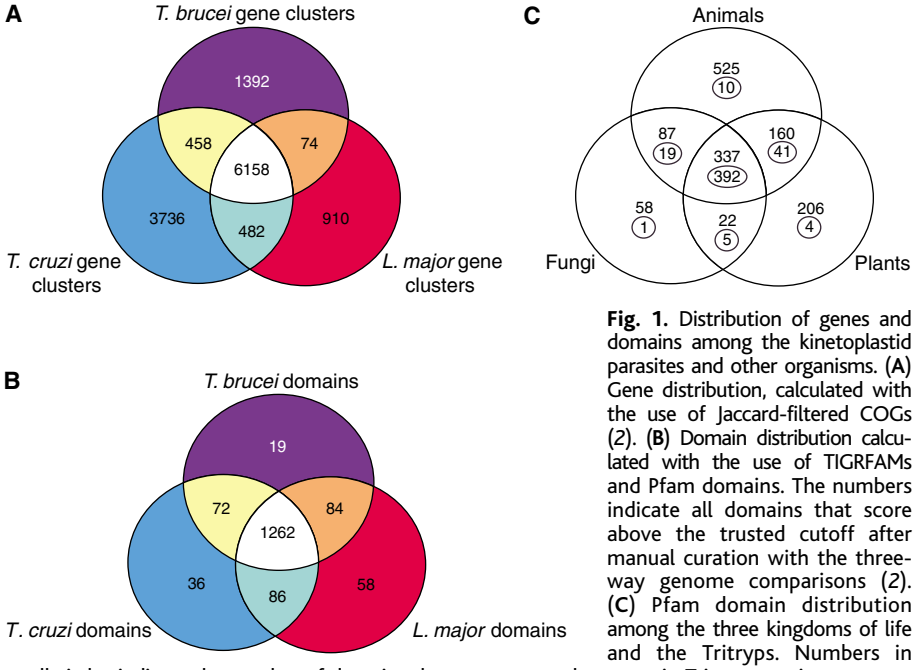

Fig. 1. Distribution of genes and domains among the kinetoplastid parasites and other organisms. (**A**) Gene distribution, calculated with the use of Jaccard-filtered COGs (*2*). (**B**) Domain distribution calculated with the use of TIGRFAMs and Pfam domains. The numbers indicate all domains that score above the trusted cutoff after manual curation with the three-way genome comparisons (*2*). (**C**) Pfam domain distribution among the three kingdoms of life and the Tritryps. Numbers in small circles indicate the number of domains that occur more than once in Tritryp parasite genomes. The numbers above the small circles indicate Pfam domains that are not present in the Tritryps.

Table 1. General features of the Tritryp genomes. We found 5812 syntenic three-way COGs and 346 nonsyntenic three-way COGs. Mbp, mega–base pairs; NC, not computed.

	T. brucei	*T. cruzi*	*L. major*
Haploid genome size (Mbp)	25*	55	33
No. of chromosomes (per haploid genome)	11*	~28†	36
No. of genes (per haploid genome)	9068‡	~12,000§	8311‖
Total regions with synteny blocks (Mbp)	19.9	NC	30.7
Mean CDS size (bp) in syntenic three-way COGs	1511	1457	1731
Mean inter-CDS size (bp) between syntenic three-way COGs	721	561	1431

*Excluding ~100 mini- and intermediate-sized chromosomes (totaling ~10 Mb). †The exact number is not known and homologs can differ substantially in size. ‡Includes 904 pseudogenes. §The exact number of haploid genes has not been determined in *T. cruzi*. ‖Includes 34 pseudogenes.

S3, and table S4). Enrichment of segmental duplication in regions of synteny breakpoints has also been observed in mammals (*20*, *21*), but the implications are unknown. Interestingly, 43% of the synteny breakpoints in *T. brucei* and *L. major* (excluding chromosome ends) occur at or very close to the strand-switch regions separating the directional gene clusters (DGCs), which are characteristic of and unique to trypanosomatid genomes (*5*). Thus, there appears to be strong selective pressure to maintain gene order and to keep the DGCs intact, despite the extensive sequence divergence between the genes themselves. This may also be related to the relatively low incidence of sexual recombination in these organisms (*22*), which would limit opportunities for rearrangement during meiosis.

Localized chromosomal rearrangements. Despite the marked overall conservation, many local insertions, deletions, or substitutions were seen within otherwise syntenic regions. Although evidence for all three processes was found in the Tritryp genomes, gene insertions or substitutions (which result in species-specific genes and nonsyntenic three-way COGs) were more common than gene loss (two-way COGs that include a *L. major* gene). Some of these events can result in substantial physiological and biochemical differences between these parasites.

One example of an insertion involves two genes in *T. brucei* encoding subunits (ESAG6 and ESAG7) of the heterodimeric transferrin receptor (*23*) in the syntenic block Tb7.3/Lm 22.1 (Plate 1, inset A). The two genes are more similar (97% amino acid identity) to one another than they are to any of the subtelomeric copies (73 to 77% identity), indicating they encode a different form of the receptor than the telomeric copies. The surrounding region in this synteny block contains other insertions specific to *L. major* and *T. cruzi* and several translocated genes in the three genomes. *T. cruzi* seems to have undergone four separate insertions of genes belonging to a metabolic pathway that converts L-histidine to L-glutamate (*5*). Intriguingly, the gene (*hutG*) for the final enzyme has been previously found only in bacteria, and this may mark a horizontal gene transfer from bacteria, where the genes occur in a single operon.

Interestingly, a component of the RNA interference (RNAi) pathway is present only in *T. brucei* (Tb10.406.0020/*TbAGO1*) (*24, 25*) and a gene (LmjF33.0290) encoding a glucose transporter (*26*) is present only in *L. major* within the same synteny block (Plate 1, inset B). This region is also associated with a cluster of tRNA

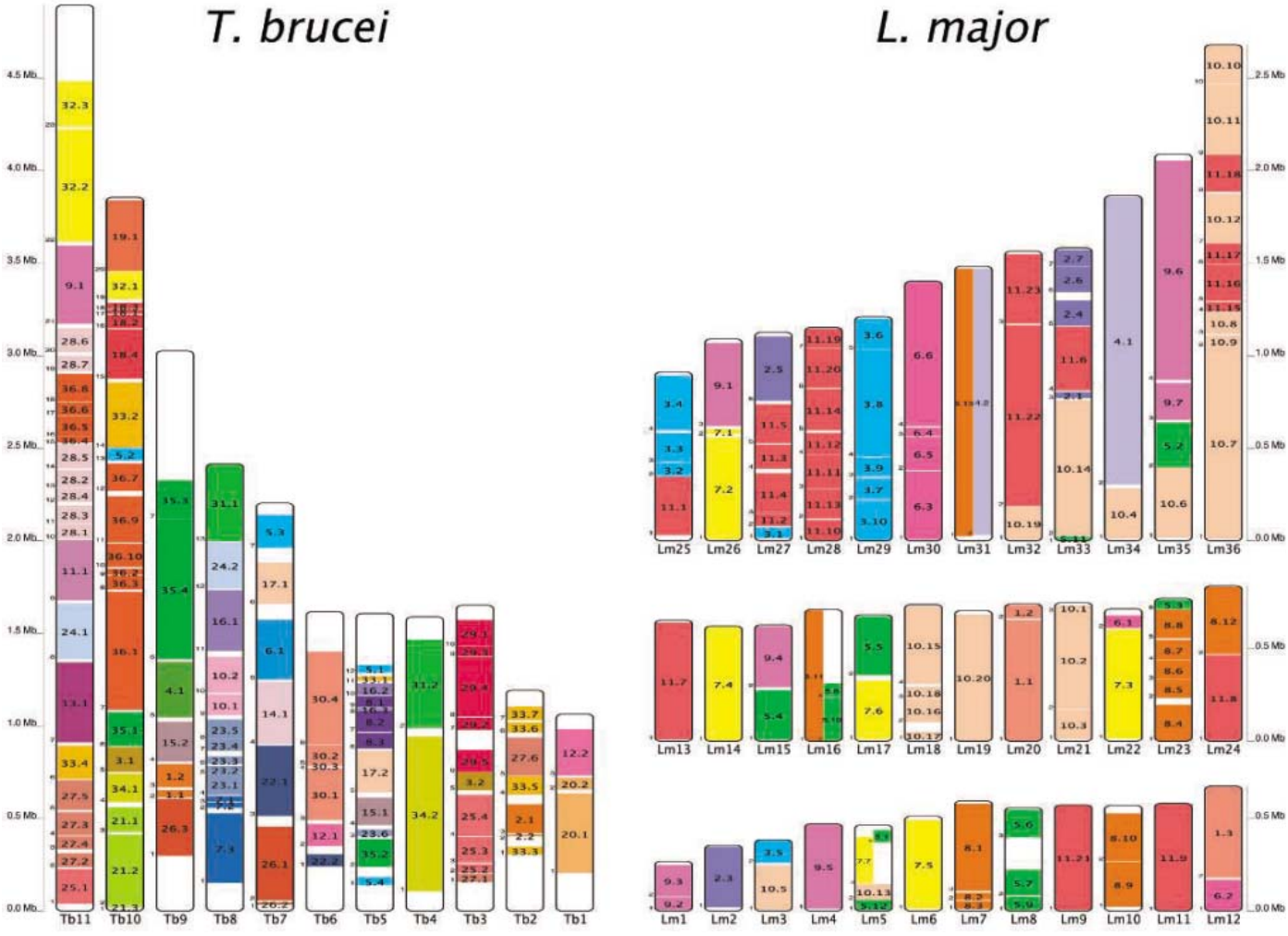

Fig. 2. Synteny maps. The 36 different colors in the *T. brucei* (left) panel represent the locations of the indicated synteny blocks in the 36 chromosomes of *L. major*, and the 11 colors in the *L. major* (right) panel depict the locations of the indicated synteny blocks in the 11 chromosomes of *T. brucei*. Each synteny block is named using a double nomenclature that refers to the chromosomal location of the block in both species. Labels on the left outside margin of the synteny blocks denote the block number in the reference genome. Labels within synteny blocks refer to their location on the other genome. For example, synteny block Tb1.1 of *T. brucei* chromosome 1 (Tb1; lower right of left panel) is synteny block Lm20.1 of *L. major* chromosome 20 (Lm20). As another example, all of the yellow synteny blocks in the *L. major* panel (blocks Tb7.1 to Tb7.7) are on *T. brucei* chromosome 7 (Tb7). Synteny blocks are defined as groups of five or more *T. brucei* genes that possess an ortholog on the same *L. major* chromosome (*2*). The entire map contains 7974 *T. brucei* and 7466 *L. major* protein-coding genes in 110 synteny blocks. Plate 1 and fig. S3, A to K, show more detailed views and table S4, A and B, has complete lists of genes and block coordinates.

genes and *HSP83* arrays (*27*, *28*) of variable lengths in the three genomes. In eukaryotes, RNAi maintains genome integrity and prevents invasion by nucleic acid, by means of double-stranded RNAs that induce the degradation of homologous mRNAs (*25*). None of the Tritryps possesses an obvious homolog of *Dicer*, an essential component of the RNAi pathway in other organisms, but two predicted proteins (named TbRN3A and TbRN3B; table S5) containing a single ribonuclease III domain are present in *T. brucei* (but are not seen in *L. major* or *T. cruzi*) and represent potential *Dicer* candidates. Thus, gene insertions are likely responsible for the RNAi activity seen in *T. brucei* but not *T. cruzi* or *L. major* (*28*), although the source(s) of the gene insertions remains unknown.

Both *L. major* and *T. cruzi* contain a gene encoding 5-oxoprolinase in synteny block Tb10.15/Lm18.4, which is absent from *T. brucei* (Plate 1, inset C) and thus appears to represent gene deletion. This enzyme catalyzes the formation of L-glutamate from 5-oxo-L-proline in the glutathione metabolism pathway. Further examples of small synteny breaks occur immediately upstream of this same region: *T. brucei* contains a receptor-type adenylate cyclase gene (GRESAG4) gene; *T. cruzi* contains one or two dispersed gene family 1 (DGF-1) pseudogenes, as well as a RHS pseudogene on one allele; and *L. major* contains a degenerate *Ingi*/L1*Tc*-related retroelement (DIRE). These sequences are often associated with frequent recombination in the Tritryps (*6*) and large synteny breaks.

Nonsyntenic and subtelomeric regions. Plotting the location of two-way and three-way COGs across the *L. major* and *T. brucei* genomes revealed that synteny extends over most of both genomes (Fig. 2 and fig. S4). *L. major* contains a few large chromosome-internal nonsyntenic regions, which mostly correspond to tandem arrays of both protein-coding and RNA genes. By contrast, *T. brucei* contains large blocks of nonsyntenic genes at the telomeres of all chromosomes (fig. S4), which can be several hundred kilobases (kb) in size and contain large arrays of species-specific VSG (pseudo)genes and ESAGs, as well as a large number of retroelements and RHS genes (*4*). The subtelomeric regions of *T. cruzi* are also large and nonsyntenic, consisting mostly of interspersed arrays of trans-sialidase superfamily, DGF-1 and RHS (pseudo)-genes, as well as vestigial interposed retroelements (VIPER), short interspersed repetitive elements (SIRE), *T. cruzi* L1*Tc* *T. cruzi* nonautonomous non-LTR retrotransposons (NAR*Tc*), and/or DIRE retroelements (*6*). Another intriguing feature of *T. cruzi* is the presence of large (up to 600 kb) nonsyntenic "islands" of genes coding for surface proteins such as trans-sialidase, mucin, mucin-associated surface protein (MASP), and gp63 peptidase, along with retrotransposons and RHS genes. Although the precise location of these "islands" is not certain, they appear often to lie between chromosome-internal synteny blocks. The *L. major* subtelomeric regions are quite short (<20 kb), with relatively few repetitive sequences, although there is evidence that there may be some recombination between telomeres (*5*). Nevertheless, the most telomere-proximal genes in *L. major* are often nonsyntenic, although usually not specific to *L. major*. Thus, the organization and gene content of the subtelomeric regions is quite different in each genome (Fig. 3).

Chromosome evolution. A comparison of the Tritryp genomes provides interesting insights into the karyotype of their common ancestor. *T. brucei* has only 11 large diploid chromosomes (plus numerous small chromosomes that contain largely repetitive sequence), and *T. cruzi* and *L. major* contain ~28 and 36 pairs of smaller chromosomes, respectively. Most rearrangements of synteny blocks represent inversions and/or translocations (Fig. 2 and fig. S3), but there appear to be several cases of chromosome fusions in *T. brucei*. Twenty of the 36 *L. major* chromosomes are almost entirely syntenic within a substantially larger *T. brucei* chromosome, except for a few instances of synteny block inversion or shuffling. In 10 further cases, there is only a single segmental translocation that has moved one end of the *L. major* chromosome to a different *T. brucei* chromosome. Although the *T. cruzi* genome contains gaps, many nearly chromosome-sized scaffolds were defined by virtue of arrays of telomeric repeats and characteristic subtelomeric genes at one end (*6*). Notably, many of the *L. major* chromosomes that are syntenic with these *T. cruzi* scaffolds also contain telomeric sequences at the corresponding end. In contrast, the syntenic *T. brucei* regions at the corresponding position generally represent internal chromosome regions with no typical telomeric structures. For example, the ends of the two *L. major* and *T. cruzi* chromosomes appear to have joined to form a single *T. brucei* chromosome at the junction between synteny blocks Tb11.7/Lm13.1 and Tb11.8/Lm24.1 (Plate 1). Interestingly, this synteny break region in *T. brucei* contains RHS, DIRE, and *Ingi* sequences, often associated with *T. brucei* subtelomeres, pointing to a telomeric origin for this region. Other examples of similar apparent chromosome fusions in *T. brucei* can be seen between synteny blocks Tb7.3/Lm22.1 and Tb7.4/Lm14.1, as well as Tb7.5/Lm6.1 and Tb7.6/Lm.1. Thus, the current chromosomal architecture of *T. brucei* seems to have derived from an ancestor with the more fragmented genomic organization of *L. major* and *T. cruzi*. This evolutionary topology supports the prevailing view of an early divergence of the *Leishmania* genus and the monophyly of the *Trypanosoma* genus (*7*–*10*).

The marked difference in the gene size and density between the Tritryp genomes is notable. The average *L. major* protein-coding sequence (CDS) is considerably longer than in *T. brucei* or *T. cruzi* (Table 1), often in regions specifying low-complexity amino acid insertions or expansions. The length differential is even more extreme in noncoding regions, with the average inter-CDS length in *L. major* being almost twice that in *T. brucei* and three times that in *T. cruzi* (Table 1). Consequently, gene density in *L. major* is considerably less than in *T. brucei* and *T. cruzi* (251 versus 319 and 385

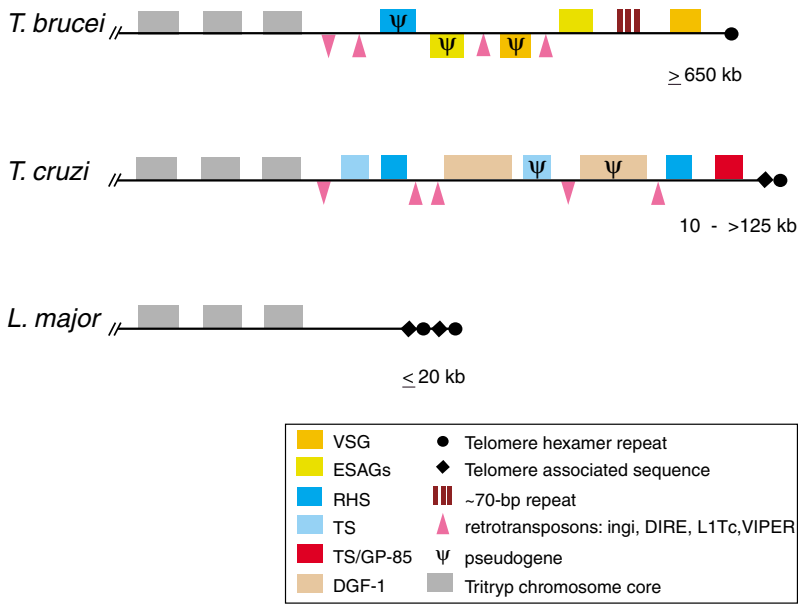

Fig. 3. Prototypes of Tritryp subtelomeric regions. Subtelomeric regions are defined here as the area that extends from the telomeric hexamer repeats to the first nonrepetitive sequence. Boxes indicate genes and/or gene arrays. Genes and/or gene arrays shown above the line are oriented toward the telomeres, whereas those shown below the line are oriented in the opposite direction. The size range of the subtelomeric regions in each genome is indicated on the right. The TS and TS/GP-85 boxes depict the trans-sialidase and GP-85 trans-sialidase superfamilies, respectively.

genes/Mb, respectively). Thus, genome compaction does not appear to be associated with an intracellular lifestyle in the Tritryps, in contrast to the suggestion for *Encephalitozoon cuniculi* (*29*, *30*).

The Tritryp chromosomes exhibited systematic purine excess, GC bias, and AT skew, correlated with the coding strand (*31*). This phenomenon is associated with replication in Eubacteria and Archaea (*32*), but local skews are linked to mutational bias arising from transcription in eukaryotes (*33*). Although this seems to be the case for *L. major*, GC skew has the opposite correlation with the coding strand in *T. brucei* and *T. cruzi* (*34*). The AT skew correlation is the same in all three species. Thus, there may be differences in DNA repair and/or transcriptional processes between *Leishmania* and *Trypanosoma*, which may account for their different GC contents (60% in *L. major*, 46 to 51% in *T. brucei* and *T. cruzi*).

No evidence for ancestral plastid endosymbiont. On the basis of recently reported evidence of plantlike traits associated with the metabolism of *Trypanosoma* parasites (*35*) and the close phylogenetic relatedness of kinetoplastids to *Euglena* (a photosynthetic protist), it has been suggested that the common ancestor of these protists harbored the same endosymbiotic green alga that gave rise to the secondary plastid in *Euglena*. Our data show that the protein domain content of the Tritryps is not consistent with large-scale horizontal transfer of genetic material from plants, given that we did not observe a large number of plant-specific domains in the Tritryps (Fig. 1C and table S6).

We used phylogenetic analyses to search for genes of cyanobacterial or green algal ancestry in the Tritryp genomes. Phylogenetic trees were made for all *L. major* genes (because this genome has the fewest protein-coding genes) with the use of alignments against proteins from all available completed genomes (*2*). Although some genes appeared to branch with plants or cyanobacteria in an initial screen, these relationships were not supported by more sophisticated Bayesian methods and a more comprehensive sampling of protein sequences (*2*). These analyses included the genes previously reported to have plantlike traits (*35*), as shown in fig. S5. We conclude from our analyses that the genome data provide no unambiguous support for the hypothesis that trypanosomatids have acquired genes from the endosymbiont that gave rise to the Euglena secondary plastid, suggesting that it was acquired subsequent to speciation with the kinetoplastida.

Gene evolution. Pathogen proteins involved in interaction with the host are often rapidly evolving, and can be identified by comparison of the number of synonymous mutations per synonymous site (d_S) and the number of nonsynonymous mutations per nonsynonymous site (d_N) (*36*). As the Tritryp genomes are too divergent to accurately estimate d_S, we calculated d_N using pairwise comparisons for every COG where there was a simple 1:1:1 orthologous relationship between genomes (or 1:1:2 in cases where both *T. cruzi* alleles were present), because this effectively gives a measure of how rapidly each protein sequence is diverging between species (*2*). Categorization of these genes by gene ontology (GO) term for biological processes (Fig. 4) showed that those with no functional annotation had the highest median d_N value, suggesting that they were subject to positive selection causing active accumulation of mutations or that they were under neutral evolution allowing the sequences to drift. Such genes of unknown function probably include trypanosomatid-specific genes involved in unique processes (including interaction with the host) or highly variable genes that elude annotation by homology.

Genes in the transport category also had a relatively high median d_N value for *L. major* versus *T. brucei* (Fig. 4). Rapid evolution of transport proteins may be due to their surface location (and consequent exposure to the host immune system) but may also reflect the different niches occupied by each parasite within their hosts and requirement for different nutrient uptake from their environment. Conversely, genes representing metabolism, cell growth, and maintenance have low d_N values, probably reflecting the core processes common to the Tritryps.

Concluding remarks. Although the majority of trypanosomatid genes in the same genomic context are conserved, there are substantial differences, which presumably reflect specific adaptations to distinct species-specific selection pressures and the distinct pathophysiologies and survival strategies of each organism. Antigenic variation and diversity are characteristic of *T. brucei* and *T. cruzi*, and the localization of large arrays of genes encoding surface proteins at or near telomeres and/or the presence of numerous retroelements within these regions may enhance recombination frequency and provide for rapid sequence variation. Thus, colocalization of previously uncharacterized genes (e.g., *T. cruzi* MASPs and DGF-1, as well as RHS in both *T. cruzi* and *T. brucei*) in these regions leads to the suspicion that they may also be involved with immune evasion or survival in different hosts. The frequent recombination in these regions results in large (up to 2 Mb) size polymorphisms between homologous chromosomes seen in *T. brucei* and *T. cruzi*.

The frequent correlation between conserved synteny blocks and the large DGCs characteristic of the Tritryps may also reflect their unique linkage of transcription with subsequent RNA processing by trans-splicing and polyadenylation. Transcription of protein-coding genes has been postulated to initiate at only a few sites on each chromosome (*37*–*39*), suggesting that there may be selective pressure against synteny breaks within the polycistronic gene clusters downstream of these sites. It is also possible (and not necessarily unrelated) that the synteny breaks associated with strand-switch regions may reflect higher rates of recombination at these sites, possibly as a result of linkage with replication processes.

The identification of numerous Tritryp-conserved and species-specific genes provides the opportunity for development of previously unexplored chemotherapeutic approaches against these parasites. Drugs designed against conserved core processes hold the advantage of being potentially useful against all three organisms, provided that they are sufficiently divergent from mammalian host proteins.

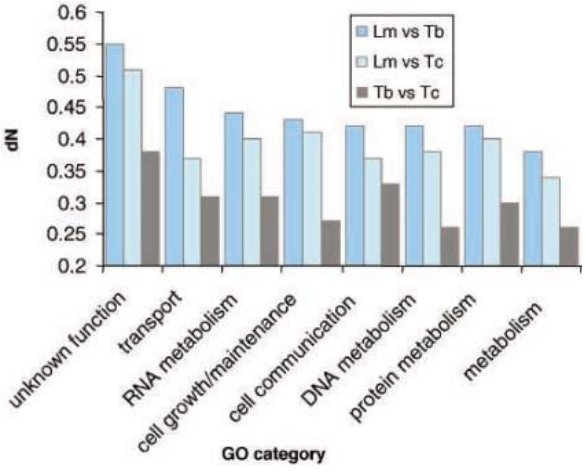

Fig. 4. Median *d*N values for genes categorized by GO process annotation. Each bar corresponds to a pairwise comparison of sets of orthologous genes from two species. Amino acid sequences were aligned for each gene and converted to nucleotide sequences to calculate nonsynonymous substitutions (*40*). Genes were annotated with GO process terms in *T. brucei* and then transferred to the other species with the use of orthology. Results from the selective constraint analyses are in table S7, A to C.

References and Notes

1. M. P. Barrett *et al.*, *Lancet* **362**, 1469 (2003).
2. Materials and methods are available as supporting material on *Science* Online.
3. E. Pays, L. Vanhamme, D. Perez-Morga, *Curr. Opin. Microbiol.* **7**, 369 (2004).
4. M. Berriman *et al.*, *Science* **309**, 416 (2005).
5. A. C. Ivens *et al.*, *Science* **309**, 436 (2005).
6. N. M. El-Sayed *et al.*, *Science* **309**, 409 (2005).
7. J. Haag, C. O'hUigin, P. Overath, *Mol. Biochem. Parasitol.* **91**, 37 (1998).
8. J. Lukes *et al.*, *J. Mol. Evol.* **44**, 521 (1997).
9. A. D. Wright, S. Li, S. Feng, D. S. Martin, D. H. Lynn, *Mol. Biochem. Parasitol.* **99**, 69 (1999).
10. J. R. Stevens, H. A. Noyes, G. A. Dover, W. C. Gibson, *Parasitology* **118**, 107 (1999).
11. F. H. Falcone *et al.*, *J. Immunol.* **167**, 5348 (2001).
12. B. A. Burleigh, N. W. Andrews, *Curr. Opin. Microbiol.* **1**, 461 (1998).

13. E. V. Caler, S. Vaena de Avalos, P. A. Haynes, N. W. Andrews, B. A. Burleigh, *EMBO J.* **17**, 4975 (1998).
14. J. Carlton, J. Silva, N. Hall, *Curr. Issues Mol. Biol.* **7**, 23 (2005).
15. P. Overath, J. Haag, A. Lischke, C. O'hUigin, *Int. J. Parasitol.* **31**, 468 (2001).
16. J. R. Stevens, H. A. Noyes, C. J. Schofield, W. Gibson, *Adv. Parasitol.* **48**, 1 (2001).
17. J. R. Stevens, W. C. Gibson, *Cad. Saude Publica* **15**, 673 (1999).
18. E. J. Douzery, E. A. Snell, E. Bapteste, F. Delsuc, H. Philippe, *Proc. Natl. Acad. Sci. U.S.A.* **101**, 15386 (2004).
19. S. J. O'Brien *et al.*, *Science* **286**, 458 (1999).
20. J. A. Bailey, R. Baertsch, W. J. Kent, D. Haussler, E. E. Eichler, *Genome Biol.* **5**, R23 (2004).
21. L. Armengol, M. A. Pujana, J. Cheung, S. W. Scherer, X. Estivill, *Hum. Mol. Genet.* **12**, 2201 (2003).
22. W. Gibson, J. Stevens, *Adv. Parasitol.* **43**, 1 (1999).
23. D. Salmon *et al.*, *Cell* **78**, 75 (1994).
24. H. Shi, A. Djikeng, C. Tschudi, E. Ullu, *Mol. Cell. Biol.* **24**, 420 (2004).
25. E. Ullu, C. Tschudi, T. Chakraborty, *Cell. Microbiol.* **6**, 509 (2004).
26. C. K. Langford, S. A. Ewbank, S. S. Hanson, B. Ullman, S. M. Landfear, *Mol. Biochem. Parasitol.* **55**, 51 (1992).
27. E. A. Dragon, S. R. Sias, E. A. Kato, J. D. Gabe, *Mol. Cell. Biol.* **7**, 1271 (1987).
28. J. C. Mottram, W. J. Murphy, N. Agabian, *Mol. Biochem. Parasitol.* **37**, 115 (1989).
29. M. D. Katinka *et al.*, *Nature* **414**, 450 (2001).
30. J. Zhang, *Trends Genet.* **16**, 107 (2000).
31. P. D. McDonagh, P. J. Myler, K. Stuart, *Nucleic Acids Res.* **28**, 2800 (2000).
32. J. R. Lobry, *Mol. Biol. Evol.* **13**, 660 (1996).
33. S. Aerts, G. Thijs, M. Dabrowski, Y. Moreau, B. De Moor, *BMC Genomics* **5**, 34 (2004).
34. D. Nilsson, B. Andersson, *Exp. Parasitol.* **109**, 143 (2005).
35. V. Hannaert *et al.*, *Proc. Natl. Acad. Sci. U.S.A.* **100**, 1067 (2003).
36. N. Hall *et al.*, *Science* **307**, 82 (2005).
37. E. A. Worthey *et al.*, *Nucleic Acids Res.* **31**, 4201 (2003).
38. S. Martinez-Calvillo *et al.*, *Mol. Cell* **11**, 1291 (2003).
39. C. E. Clayton, *EMBO J.* **21**, 1881 (2002).
40. H. Higo *et al.*, *Int. J. Parasitol.* **27**, 1369 (1997).

41. Funding for this project was provided by grants from National Institute for Allergy and Infectious Disease (NIAID) to N.M.E.-S. (AI45038), K.S. and P.J.M. (AI045039), and B.A. (AI45061) and the Wellcome Trust (WT) to the Sanger Institute. We also thank NIAID, the Burroughs Wellcome Fund (BWF), WT, and the World Health Organization Special Programme for Research and Training in Tropical Diseases (WHO TDR) for providing funds for several Tritryp meetings. G.C.C. is the recipient of a fellowship from the Conselho Nacional de Desenvolvimento Científico e Tecnológico (CNPq-Brazil). *L. major* genome accession numbers: AE001274, CP000078 to CP000081, NC_004916, AL389894, AL139794, and consecutive accession numbers CT005244 to CT005272. *T. brucei* genome accession numbers: Sequence data have been deposited at DDBJ/EMBL/GenBank with consecutive accession numbers CP000066 to CP000071 for chromosomes 3 to 8 and project accession numbers AAGZ00000000, AAHA00000000, AAHB00000000 for the whole-chromosome shotgun projects of chromosomes 9 to 11. The versions of chromosomes 9 to 11 described in this paper are the first versions, AAGZ01000000, AAHA01000000, and AAHB01000000, and unassembled contigs have accession number CR940345. *T. cruzi* genome accession numbers: This Whole-Genome Shotgun project has been deposited at DDBJ/EMBL/GenBank under the project accession AAHK00000000. The version described in this paper is the first version, AAHK01000000. All data sets and genome annotations are also available through GeneDB at www.genedb.org.

Supporting Online Material
www.sciencemag.org/cgi/content/full/309/5733/404/DC1
Materials and Methods
Figs. S1 to S5
Tables S1 to S7
References

14 March 2005; accepted 21 June 2005
10.1126/science.1112181

RESEARCH ARTICLE

The Genome Sequence of *Trypanosoma cruzi*, Etiologic Agent of Chagas Disease

Najib M. El-Sayed,[1,2]*† Peter J. Myler,[3,4,5]*† Daniella C. Bartholomeu,[1] Daniel Nilsson,[6] Gautam Aggarwal,[3] Anh-Nhi Tran,[6] Elodie Ghedin,[1,2] Elizabeth A. Worthey,[3] Arthur L. Delcher,[1] Gaëlle Blandin,[1] Scott J. Westenberger,[1,7] Elisabet Caler,[1] Gustavo C. Cerqueira,[1,8] Carole Branche,[6] Brian Haas,[1] Atashi Anupama,[3] Erik Arner,[6] Lena Åslund,[9] Philip Attipoe,[3] Esteban Bontempi,[6,10] Frédéric Bringaud,[11] Peter Burton,[12] Eithon Cadag,[3] David A. Campbell,[7] Mark Carrington,[13] Jonathan Crabtree,[1] Hamid Darban,[6] Jose Franco da Silveira,[14] Pieter de Jong,[15] Kimberly Edwards,[6] Paul T. Englund,[16] Gholam Fazelina,[3] Tamara Feldblyum,[1] Marcela Ferella,[6] Alberto Carlos Frasch,[17] Keith Gull,[18] David Horn,[19] Lihua Hou,[1] Yiting Huang,[3] Ellen Kindlund,[6] Michele Klingbeil,[20] Sindy Kluge,[6] Hean Koo,[1] Daniela Lacerda,[1,21] Mariano J. Levin,[22] Hernan Lorenzi,[22] Tin Louie,[3] Carlos Renato Machado,[8] Richard McCulloch,[12] Alan McKenna,[6] Yumi Mizuno,[6] Jeremy C. Mottram,[12] Siri Nelson,[3] Stephen Ochaya,[6] Kazutoyo Osoegawa,[15] Grace Pai,[1] Marilyn Parsons,[3,4] Martin Pentony,[3] Ulf Pettersson,[9] Mihai Pop,[1] Jose Luis Ramirez,[23] Joel Rinta,[3] Laura Robertson,[3] Steven L. Salzberg,[1] Daniel O. Sanchez,[17] Amber Seyler,[3] Reuben Sharma,[13] Jyoti Shetty,[1] Anjana J. Simpson,[1] Ellen Sisk,[3] Martti T. Tammi,[6,24] Rick Tarleton,[25] Santuza Teixeira,[8] Susan Van Aken,[1] Christy Vogt,[3] Pauline N. Ward,[12] Bill Wickstead,[18] Jennifer Wortman,[1] Owen White,[1] Claire M. Fraser,[1] Kenneth D. Stuart,[3,4] Björn Andersson[6]†

Whole-genome sequencing of the protozoan pathogen *Trypanosoma cruzi* revealed that the diploid genome contains a predicted 22,570 proteins encoded by genes, of which 12,570 represent allelic pairs. Over 50% of the genome consists of repeated sequences, such as retrotransposons and genes for large families of surface molecules, which include trans-sialidases, mucins, gp63s, and a large novel family (>1300 copies) of mucin-associated surface protein (MASP) genes. Analyses of the *T. cruzi*, *T. brucei*, and *Leishmania major* (Tritryp) genomes imply differences from other eukaryotes in DNA repair and initiation of replication and reflect their unusual mitochondrial DNA. Although the Tritryp lack several classes of signaling molecules, their kinomes contain a large and diverse set of protein kinases and phosphatases; their size and diversity imply previously unknown interactions and regulatory processes, which may be targets for intervention.

Trypanosoma cruzi causes Chagas disease in humans. Acute infection can be lethal, but the disease usually evolves into a chronic stage, accompanied in 25 to 30% of cases by severe debilitation and ultimately death. It is estimated that 16 to 18 million people are infected, primarily in Central and South America, with 21,000 deaths reported each year (*1*). *T. cruzi* is normally transmitted by reduviid bugs via the vector feces after a bug bite and also after blood transfusion. Attempts to develop vaccines for parasitic diseases have been futile, and there is a critical lack of methods for diagnosis and treatment.

The taxon *T. cruzi* contains two defined groups, *T. cruzi* I and *T. cruzi* II, as well as additional groups yet to receive a designation (*2*). *T. cruzi* I is associated with the silvatic transmission cycle and infection of marsupials (*3*). *T. cruzi* II consists of five related subgroups, termed IIa, IIb, IIc, IId, and IIe (*4*), and is associated with the domestic transmission cycle and infection of placental mammals

(*5*). *T. cruzi* strain CL Brener is a member of subgroup IIe and was chosen for genome sequencing because it is well characterized experimentally (*6*). *T. cruzi* is heterozygous at many loci (*7*), with different-sized homologous chromosome pairs (*8*). Data from several laboratories (*9*–*13*) are consistent with its being a hybrid between subgroup IIb and subgroup IIc [which itself is also apparently a hybrid derived from *T. cruzi* I (*12*)]. The finding of *T. cruzi* I sequences in the CL Brener strain (*14*) further supports the role of multiple progenitors in the evolution of *T. cruzi* hybrid strains.

[1]Department of Parasite Genomics, The Institute for Genomic Research, Rockville, MD 20850, USA. [2]Department of Microbiology and Tropical Medicine, George Washington University, Washington, DC 20052, USA. [3]Seattle Biomedical Research Institute, Seattle, WA 98109, USA. [4]Department of Pathobiology, School of Public Health and Community Medicine, [5]Department of Medical Education and Biomedical Informatics, University of Washington, Seattle, WA 98195, USA. [6]Center for Genomics and Bioinformatics, Karolinska Institutet, Berzelius väg 35, S-171 77 Stockholm, Sweden. [7]Department of Microbiology, Immunology and Molecular Genetics, University of California, Los Angeles, CA 90095, USA. [8]Departamento de Bioquímica e Imunologia, Universidade Federal de Minas Gerais, CEP 31270-901, Belo Horizonte, MG, Brazil. [9]Department of Genetics and Pathology, Uppsala University, SE-751 85 Uppsala, Sweden. [10]Instituto Nacional de Parasitología Dr. M. Fatala Chabén, Administración Nacional de Laboratories e Insitutos de Salud (ANLIS), 1063, Buenos Aires, Argentina. [11]Laboratoire de Génomique Fonctionnelle des Trypanosomatides, UMR-CNRS 5162, Université Victor Segalen Bordeaux II, 33076 Bordeaux Cedex, France. [12]Wellcome Centre for Molecular Parasitology, University of Glasgow, Glasgow G11 6NU, Scotland, UK. [13]Department of Biochemistry, University of Cambridge, Cambridge CB2 1GA, UK. [14]Departamento de Microbiologia, Imunologia e Parasitologia, Universidade Federal de São Paulo, CEP 04023–062, São Paulo, SP, Brazil. [15]BACPAC Resources, Children's Hospital Oakland Research Institute, Oakland, CA 94609, USA. [16]Department of Biological Chemistry, Johns Hopkins University School of Medicine, Baltimore, MD 21205, USA. [17]Instituto de Investigaciones Biotecnológicas–Instituto Tecnológico de Chascómús, National University of San Martin and National Research Council, 1650 Buenos Aires, Argentina. [18]Sir William Dunn School of Pathology, University of Oxford, South Parks Road, Oxford, OX1 3RE, UK. [19]London School of Hygiene and Tropical Medicine, Keppel Street, London, WC1E 7HT, UK. [20]Department of Microbiology, University of Massachusetts, Amherst, MA 01003, USA. [21]René Rachou Research Center/CPqRR, Oswaldo Cruz Foundation, Belo Horizonte, MG, Brazil. [22]Laboratory of Molecular Biology of Chagas Disease, Instituto de Investigaciones en Ingeniería Genética y Biología Molecular, National Research Council (CONICET-CYTED project), School of Sciences, Centro de Genomica Aplicada-CeGA-University of Buenos Aires, 1428 Buenos Aires, Argentina. [23]Instituto de Biología Experimental, Universidad Central de Venezuela and ADEA-MCT, 1041-A Caracas, Venezuela. [24]Departments of Biological Sciences and Biochemistry, National University of Singapore, Singapore. [25]Center for Tropical and Emerging Global Diseases, Department of Cellular Biology, University of Georgia, Athens, GA 30602, USA.

*These authors contributed equally to this work.
†To whom correspondence should be addressed. E-mail: nelsayed@tigr.org (N.M.E.-S.); peter.myler@sbri.org (P.J.M.); bjorn.andersson@cgb.ki.se (B.A.)

In this research article, we report on the sequencing of the *T. cruzi* genome, with an emphasis on our analysis of the Tritryp kinome, DNA replication and repair machinery, and organization of retroelements, as well as surface proteins, in *T. cruzi*. Other aspects of trypanosomatid biology and new insights gained from sequencing the Tritryp genomes are discussed in the accompanying papers (*15*–*17*).

Genome sequencing, assembly, and annotation. The sequence was obtained by using the whole-genome shotgun (WGS) technique (table S1), because the high repeat content (>50%) and hybrid nature of the genome limited the initial ''map-as-you-go'' bacterial artificial chromosome (BAC) clone–based approach. Assembly parameters were modified to contend with the high allelic variation, and postassembly generation of 2.5× genome sequence coverage of the Esmeraldo strain from the progenitor subgroup IIb allowed us to distinguish the two haplotypes (*18*).

The current *T. cruzi* genome assembly consists of 5489 scaffolds (containing 8740 contigs) totaling 67 Mb. On the basis of the assembly results, the *T. cruzi* diploid genome size was estimated to be between 106.4 and 110.7 Mb, which is larger than the previous estimate of 87 Mb, based on densitometric analysis of pulse-field gel-separated chromosomal DNA (*19*). Analysis of the 60.4-Mb annotated dataset (Table 1 and table S3) revealed that 30.5 Mb contain sequence found at least twice in the assembly, which suggests that they likely represent the two different haplotypes in the *T. cruzi* CL Brener genome. Comparison of the contigs with reads from the Esmeraldo genome, which is a member of one of the progenitor subgroups (IIb), allowed us to distinguish the two haplotypes (*18*). The two haplotypes display high levels of gene synteny, with most differences because of insertion/deletions in intergenic and subtelomeric regions and/or amplification of repetitive sequences (Plate 1). The average sequence divergence between the two haplotypes is 5.4%, and the protein-coding regions are considerably more conserved (2.2% difference) than intergenic regions.

On the basis of our haplotype analyses, we estimate that the haploid *T. cruzi* genome contains about 12,000 genes (see table S2 for details). Automated analysis of the 4008 *T. cruzi* contigs using AUTOMAGI (*18*) initially predicted 25,013 protein-coding genes in the diploid genome, which was manually refined to a total of 22,570 genes, of which 6159 represent alleles present in the IIb haplotype, 6043 represent alleles from the other haplotype, and 10,368 represent sequences that could not be assigned to a particular haplotype (table S2). A total of 594 RNA genes were also identified from this same sequence dataset (Table 1 and table S3), although another 1400 were identified in the unannotated contigs, which contained many tandemly repeated ribosomal RNA (rRNA), spliced leader (sl) RNA, and small nucleolar RNA (snoRNA) genes. As seen in the other trypanosomatids, the protein-coding genes are generally arranged in long clusters of tens-to-hundreds of genes on the same DNA strand. Putative function could be assigned to 50.8% of the predicted protein-coding genes on the basis of significant similarity to previously characterized proteins or known functional domains (table S3).

Repeats, retrotransposons, and telomeres. At least 50% of the *T. cruzi* genome is repetitive sequence, consisting mostly of large gene families of surface proteins, retrotransposons, and subtelomeric repeats. TRIBE-MCL analysis [which uses the Markov cluster (MCL) algorithm] (*18*) revealed 1052 paralogous clusters (of more than two genes) encompassing 8419 genes, of which 46 clusters (3836 genes) contained 20 or more paralogues (table S5). The largest gene families (which often fall into several TRIBE-MCL clusters) encode surface proteins such as mucin-associated surface proteins (MASPs), members of the trans-sialidase (TS) superfamily, mucins, and the surface glycoprotein gp63 protease (Table 2) that are often *T. cruzi*–specific and account for ~18% of the total of protein-coding genes.

Table 1. Summary of the *T. cruzi* annotated genome. For RNA genes, see details in table S3. tRNA, transfer RNA; snRNA, small nuclear RNA; srpRNA, signal recognition particle RNA.

Parameter	Number
The genome	
Size* (bp)	60,372,297
G+C content (%)	51
Sequence scaffolds†	838
Sequence contigs	4,008
Percent coding	58.9
Protein-coding genes	
No. of gene models	23,216
No. of genes‡	22,570
Estimated no. of genes per haploid genome§	~12,000
Pseudogenes	3,590
Mean CDS length‖ (bp)	1,513
Median CDS length‖ (bp)	1,152
G+C content (%)	53.4
Gene density (genes per Mb)	385
Intergenic regions¶	
Mean length (bp)	1,024
G+C content (%)	47
RNA genes	
tRNA	115
rRNA	219
slRNA	192
snRNA	19
snoRNA	1,447
srpRNA	2

*Includes all scaffolds and contigs >5 kb, from both haplotypes. †784 scaffolds + 54 contigs. ‡Genes split across contig boundaries were counted once. §See details in table S2. ‖Excluding partial genes and pseudogenes. ¶Regions between protein-coding CDSs.

These genes occur in dispersed clusters of tandem and interspersed repeats, often at subtelomeric locations (see below). There is also a large family of β-galactofuranosyltransferases, which likely reflects the extensive use of glycoconjugates on the parasite cell surface, similar to that seen in *L. major* (*17*), but in contrast to *T. brucei*, which has many fewer genes encoding enzymes in the glycosylation pathway. In addition, a relatively large number of mostly housekeeping genes occur in highly conserved tandem clusters throughout the genome. Because similar gene organization is seen in *L. major* and *T. brucei*, one possible function of these repeats may be to increase the expression level of these proteins. The copy number of these genes is likely underestimated because of the collapse of multiple tandem repeats into fewer copies during assembly, as evidenced by regions of locally high sequence coverage (table S4). Interestingly, the degree of sequence conservation between repeat copies is generally higher within the same haplotype than between haplotypes, which suggests that the expansions are recent, or that specific mechanisms are in place to conserve the gene copies.

One example of gene family expansion has occurred in the kinetoplastid myosin genes. Analysis of the Tritryp genomes reveals two classes of myosin: conventional MyoI proteins and a novel family of kinetoplastid myosins. *T. brucei* and *L. major* have a single member of both families, but *T. cruzi* has expanded the kinetoplastid myosin family to seven (haploid) members (at dispersed loci) with a considerable diversity of sequence (Fig. 1). Moreover, *T. cruzi* has retained the CapZ F-actin capping complex that is absent in both *T. brucei* and *L. major* [see (*16*)], which suggests a difference in myosin function between the trypanosomatid species. It is possible that this may be associated with the cytostome-cytopharynx complex, the major cytoskeletal feature (a funnel-shaped invagination in the plasma membrane that is the site of endocytosis for macromolecules such as low density lipoprotein) found only in the Stercorarian trypanosomes (including *T. cruzi*) (*20*).

Long terminal repeat (LTR) and non-LTR retroelements account for ~5% of the haploid *T. cruzi* genome and 2% of the haploid *T. brucei* genome. Several copies of the site-specific non-LTR retrotransposons CZAR (*21*) and SLACS (*22*) are present in the SL RNA loci of *T. cruzi* and *T. brucei*, but absent from *L. major*. Although the autonomous *T. brucei ingi* (*23*) and *T. cruzi* L1*Tc* (*24*) non-LTR retroelements have been reported as randomly distributed in the host genome, analysis of their genomic context in the complete *T. brucei* and *T. cruzi* genomes indicates that they are preferentially inserted downstream of conserved **A**xxxxxxx**TtgxGT**x**GG**x**T**xxx↑**t**x**T**x**T**xx**T**xxxxxx↑ and **GA**xx**A**x**Ga**xxxxx**t**x**TATG**↑**A**xxxxxxxxxxx↑ motifs, respectively, where the arrows indicate the single-strand cleavage sites (*25*). The nonautonomous RIME (*26*) and NARTc (*27*) elements, respectively, are preceded by the same conserved motifs, which indicates that they likely use the *ingi* and L1*Tc* retrotransposition machinery. It is interesting that both retroelement pairs share their 5′ extremities, and the *ingi*/RIME pair also share their 3′ sequences. To our knowledge, this sequence conservation has never been reported for other LINE-/SINE-like couples. A similar situation was seen with the *T. brucei* and *T. cruzi* LTR-retrotransposon pairs (autonomous VIPER and nonautonomous SIRE).

In contrast to *T. brucei* and *T. cruzi* (which contain three potentially active *ingi* and 15 L1*Tc* elements, respectively), no active retrotransposons have been described in *Leishmania* species, but the *L. major* genome does contain 52 copies of a degenerate retroelement called "DIRE" (*28*) (Table 3). Phylogenetic analysis conducted on the reverse transcriptase domain of non-LTR retrotransposons from different eukaryotes indicates that *ingi*, L1*Tc*, and DIRE form a monophyletic group, which suggests that the common ancestor of trypanosomatids contained active retrotransposons that evolved into the presently active elements in *T. brucei*. The last active *L. major* retroelements were probably lost in the ancient past, and only their vestiges (DIREs) still reside in the present genome. In nematodes, the RNA interference (RNAi) machinery down-regulates retroelement mobilization, which prevents the negative effects of rampant expansion (*29*). It is noteworthy that RNAi is operational in *T. brucei*, whereas *T. cruzi* and *L. major* do not seem to have the full RNAi machinery (*15*, *30*, *31*). This suggests that *T. cruzi*, and perhaps other trypanosomatids, uses an alternative strategy for retroelement silencing.

In several protozoan parasites, the subtelomeric regions are often associated with large gene families encoding surface proteins. Analysis of the *T. cruzi* genome assembly reported here reveals 49 scaffolds that contain the terminal THR sequence, which indicates that they are likely telomeric (table S6). In most cases, the THR sequences are immediately adjacent to a 0.4- to 1.8-kb telomere-associated sequence (TAS), similar to the *T. cruzi*–specific 189–base pair (bp) junction described previously (*32*). The subtelomeric region between TAS and the first upstream nonrepetitive gene is characterized by a polymorphic assembly of RHS (retrotransposon hotspot) (*33*), TS superfamily (*34*), DGF-1 (dispersed gene family–1) (*35*) genes or pseudogenes, as well as VIPER/SIRE, L1*Tc*/NAR*Tc*, and/or DIRE retroelements. These genes are all on the same strand, such that they would be transcribed toward the telomere.

Telomerase activity has been reported in the Tritryps (*36*), and we have now identified the gene encoding the protein component

Table 2. Large gene families in *T. cruzi*. Members are listed as total genes (pseudogenes in parentheses).

Gene product	Members	Tritryp orthologs
trans-Sialidase (TS)	1430 (693)	*Tb*
MASP	1377 (433)	No
Mucin	863 (201)	No
Retrotransposon hot spot (RHS) protein	752 (557)	*Tb*
Dispersed gene family protein 1 (DGF-1)	565 (136)	No
Surface protease (gp63)	425 (251)	*Tb* + *Lm*
Mucinlike protein	123	No
Hypothetical	117	*Lm*+*Tb*
Hypothetical	93	*Lm*+*Tb*
Kinesin, putative	79	*Lm*+*Tb*
Protein kinase (CMGC group)	77	*Lm*+*Tb*
Protein kinase (several groups)	79	*Lm*+*Tb*
Hypothetical protein	42	No
Glycosyltransferase	52	*Lm*+*Tb*
RNA helicase (eIF-4a)	47	*Lm*+*Tb*
Protein kinase (NEK group)	39	*Lm*+*Tb*
MASP-related	38	No
Glycosyltransferase	36	*Lm*+*Tb*
Hypothetical	35	*Lm*+*Tb*
Amino acid permease	28	*Lm*+*Tb*
AAA ATPase	33	*Lm*+*Tb*
Protein phosphatase	30	*Lm*+*Tb*
Heat shock protein HSP70	21	*Lm*+*Tb*
Protein kinase (STE group)	25	*Lm*+*Tb*
RNA helicase	23	*Lm*+*Tb*
Phosphatidylinositol phosphate kinase–related	23	*Lm*+*Tb*
Hypothetical	24	*Lm*+*Tb*
Elongation factor 1-γ (EF-1-γ)	22	*Lm*+*Tb*
DNA helicase (DNA repair)	21	*Lm*+*Tb*
Actin-related	20	*Lm*+*Tb*
Cysteine peptidase	20	*Lm*+*Tb*

(TERT) of this enzyme in all three trypanosomatids (table S7), along with a putative homolog of telomerase-associated protein TEP1, which has been shown to interact with telomerase in other cell types (*37*). We were unable to identify other putative capping or telomere repeat–binding proteins, but all three trypanosomatids contain genes encoding two proteins (JBP1 and JBP2) that bind the β-D-glucosyl(hydroxymethyl)uracil DNA base modification (also known as J) enriched at telomeres in the bloodstream from *T. brucei* and in other trypanosomatids (*38*). JBP2 also has a snf2-like helicase domain, which suggests a possible role in gene regulation.

DNA repair, recombination, replication, and meiosis. The genes that encode many of the enzymatic components of DNA repair were identified in the *T. cruzi* (and Tritryp) genomes (table S8), and thus, these organisms appear able to catalyze most repair pathways. Three pathways of direct repair are apparent. Single homologs of *O*-6 methylguanine alkyltransferase, for alkylation reversal, and the AlkB dioxygenase, for oxidative damage repair, are present in all three genomes. However, *T. cruzi* does not contain a clear photolyase homolog, although *T. brucei* and *L. major* do, presumably for photoreactivation.

Most components of the base-excision repair pathway are conserved in the Tritryps. In contrast, genes implicated in mechanisms that prevent the effects of oxidative stress, such as catalase and the Mut T homolog 8-oxoguanine hydrolase, were not detected in any of the three parasites. About half of the DNA glycosylases described in other organisms are identifiable, but only one has been experimentally characterized (*39*). Trypanosomatids contain most components of the eukaryotic nucleotide excision repair pathway but may share some biochemical novelties with the less-characterized systems of plants and *Plasmodium falciparum*. For example, although the core XPB/RAD25 and XPD/RAD3 helicases, as well as the XPG/RAD2, XPF/RAD1, and ERCC1 endonucleases, are discernible, many other genes (including XPA/RAD14) are not. The possible consequences of these differences are unknown. All three genomes appear to contain a complete complement of genes for base mismatch repair.

Homologous recombination has been well documented in the trypanosomatids, because it is exploited for experimental genome manipulation (*40*) and is a key mechanism for antigenic variation that *T. brucei* uses for immune evasion (*41*). However, some genes for homologous recombination are notably absent, including RAD52, which is critical for homologous recombination in *Saccharomyces cerevisiae* (*42*). Surprisingly, the enzymatic machinery for nonhomologous end-joining is not readily detectable in the trypanosomatids, although homologs of KU70 and KU80, the components of the Ku heterodimer, were found and are known to function in *T. brucei* telomere length regulation (*43*). Thus, this enzymatic pathway may have been lost or altered in the trypanosomatids during evolution, as in *P. falciparum* (*44*). Multigene families encoding DNA polymerase κ were discovered in the three trypanosomatids. This enzyme is a low-fidelity, exonuclease-deficient DNA polymerase involved in translesion DNA synthesis.

The replication fork synthetic machinery of kinetoplastid nuclear chromosomes appears to resemble that in higher eukaryotes (table S9), although the machinery for initiation of replication may differ significantly. Most strikingly, Tritryps have a candidate gene for only one of the six subunits of the origin recognition complex, ORC1, which is also homologous to CDC6. Also, there are no clear orthologs for the MCM10, CDT1, DBF4, and possibly CDC7, proteins that play key roles in initiation of replication in *S. cerevisiae* and other eukaryotes (*45*). On the basis of the proteins encoded in the kinetoplastid genomes, replication initiation may resemble that in the Archaea, which also have only a single ORC subunit, ORC1/CDC6 (*46*), and lack the collection of initiation factors utilized by eukaryotes.

The Tritryp mitochondrial DNA is a unique network structure, known as kinetoplast DNA (kDNA), composed of thousands of minicircles and dozens of maxicircles topologically interlocked and replicated at a specific time in the cell cycle (*47*). The complexity of this structure dictates an unusual replication mechanism and accounts for the substantial differences from higher eukaryotes we observe. The Tritryp nuclear genomes encode six DNA polymerases that have been localized to the mitochondria in *T. brucei* (*48*, *49*), whereas yeast and mammalian mitochondria have only one, DNA polymerase γ. There also appear to be multiple DNA ligases (*50*) and helicases. The Tritryp genomes reveal no candidate genes for mitochondrial primase, single-strand binding protein, or DNA polymerase processivity factors, which suggests that these genes may have diverged from their prokaryotic or eukaryotic counterparts. In contrast, the gene for mitochondrial RNA polymerase, which apparently plays a role in maxicircle replication (*51*), resembles those from yeast and human. Finally, the Tritryp genomes provide no clues to the mechanisms triggering the initiation of kinetoplast DNA replication in a cell cycle–dependent manner.

Table 3. Retrotransposon copy numbers in the Tritryp genomes. The copy number per haploid genome is indicated, with the number of intact copies in parentheses.

Retrotransposons	Tb	Tc	Lm
LTR retrotransposons			
VIPER (4.5 kb)	26 (0)	275 (0)	0
SIRE (0.43 kb)	10 (0)	480 (0)	0
Non-LTR retrotransposons			
SLACS (6.3 kb)	4 (1)	0	0
CZAR (7.25 kb)	0	8 (*)	0
ingi (5.2 kb)	115 (3)	0	0
RIME (0.5 kb)	86 (0)	0	0
L1*Tc* (4.9 kb)	0	320 (15)	0
NAR*Tc* (0.25 kb)	0	133 (0)	0
DIRE(4 to 5 kb)	73 (0)	257 (0)	52 (0)

*The number of intact copies was not determined.

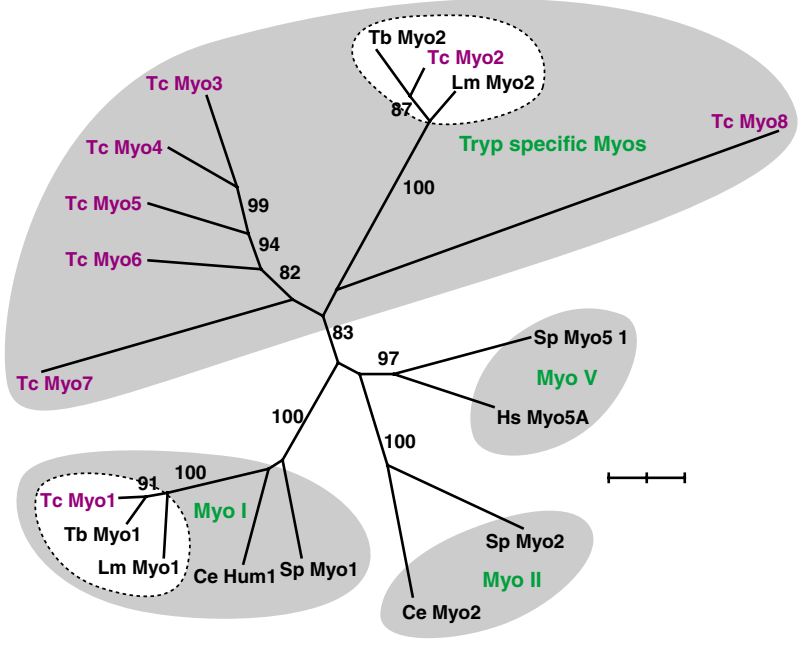

Fig. 1. Evolutionary analysis of trypanosomatid myosins, in comparison with myosins from *Schizosaccharomyces pombe* (Sp), *C. elegans* (Ce), and *Homo sapiens* (Hs). See supporting online material (*18*) for details.

The Tritryps are essentially diploid, but sexual reproduction is not an obligatory part of their life cycles. Genetic exchange occurs in both *T. brucei* (*52*) and *T. cruzi* (*11*), and there is Mendelian inheritance in *T. brucei* (*53*), but the molecular processes involved in genetic exchange are poorly characterized. Of the genes uniquely expressed during meiosis, six were identified as being sufficiently conserved to be readily identifiable in the genomes of most eukaryotes with an obligatory meiosis. Homologs for SPO11, DMC1, MND1, MSH4 (except for *L. major*), and MSH5, which are involved in homologous recombination, and HOP1, which is a component of the lateral elements of the synaptonemal complex, were identified in the Tritryp genomes. Thus, the Tritryps have the potential to undergo meiotic homologous exchange, but it is not possible to determine whether the potential for reductive divisions is present.

Signaling pathways. Several classes of important signaling molecules are absent in trypanosomatids, including serpentine receptors, heterotrimeric G proteins, most classes of catalytic receptors, SH2 and SH3 interaction domains, and regulatory transcription factors. Some catalytic receptors have been found, and all are adenylate cyclases (47 genes in *T. brucei*, 11 in *L. major*, and 25 in *T. cruzi*). The Tritryps, however, have a large and complex set of protein kinases (PKs), as well as a diversity of protein phosphatases (tables S10 and S11). They also have multiple enzymes involved in phosphoinositide metabolism, as well as modular domains that interact with those small molecules, although little is known concerning their functions (table S12).

Table 4. Comparison of Tritryp, yeast, and human kinome. The comparison is based on catalytic domains. Data for human (Hs) and yeast (Sc) were derived from Manning *et al.* (*68*).

PKs	Tb	Tc	Lm	Sc	Hs
		Eukaryotic PKs			
AGC	12	12	11	17	63
CAMK	13	13	16	21	74
CK1	5	6	7	4	12
CMGC	42	41*	47	21	61
NEK	20	23	22	1	15
STE	24	28	32	14	47
TK	0	0	0	0	90
TKL	0	0	0	0	43
Unique	21	25	27	4	7
Other†	19	19	18	33	61
Total	156	167	180	115	478
		Atypical PKs			
ABC	5	5	5	3	5
Alpha	2	1	5	0	6
Bud32	1	1	1	1	1
Cofilin	1	1	1	1	2
PDHK	3	3	3	2	5
PIKK	6	6	6	5	6
RIO	2	2	2	2	3
Other	0	0	0	1	12
Total	20	19	23	15	40

*Multiple copies of CDK8 in Tc were counted as one gene. †Other trypanosomatid eukaryotic PKs include Aurora, CAMKK, CK2, PEK, PLK, TLK, ULK, VPS15, and WEE1 kinases.

The Tritryp genomes encode 180, 156, and 167 distinct eukaryotic PKs in *L. major*, *T. brucei*, and *T. cruzi*, respectively, that are likely to be catalytically active, as well as 23, 20, and 19 atypical PKs, respectively. The trypanosomatid kinome is more than twice that of *P. falciparum* (*54*) and one-third larger than that of *S. cerevisiae*, although the overall representation of PK groups is similar (Table 4). Almost all receptor PKs in mammals are tyrosine kinases, but no such group is present in the parasites, and only a handful of trypanosomatid PKs have predicted transmembrane domains. Indeed, catalytic domains that map to the tyrosine kinase group are entirely missing, but dual-specificity kinases are present. Also missing is the TKL group, which shows features of both tyrosine and serine-threonine kinases, and the RGC (receptor guanylate cyclase) group, which is structurally related to PKs. The expansion of a few groups of PKs hints at a regulatory complexity focused on stress and the cell cycle (*55*). For example, *T. brucei* has many CMGC PKs, including 11 cyclin-dependent kinases (CDKs) (plus 10 cyclins) and 11 mitogen-activated protein kinases (MAP kinases). The STE kinases, which function in the MAP kinase activation cascade, are also very numerous in trypanosomatids. Their roles in trypanosomatids are relatively unexplored, although the importance of signaling pathways in flagellar length control (*56*), differentiation (*57*), and cellular proliferation (*58*) is apparent. A further example of expansion is the large NEK family of trypanosomatids. More than 20 PKs could not be classified into any established group. Their low similarity to human PKs raises the possibility of targeted intervention.

A key finding is the relative lack of identifiable accessory domains on the trypanosomatid PKs. Although ~50% of human PKs bear an additional PFAM domain, only 14% of Tritryp predicted PKs do. The diversity of such domains is also more restricted, with 83 domains represented on human PKs but only 21 represented on Tritryp PKs. Most striking in their absence are the domains most frequently found on human PKs: SH2, SH3, FN-III, and immunoglobulin-like domains. Most well represented in trypanosomatid PKs are PH domains (with six or seven in each species), again pointing to a role of phosphoinositide metabolism in regulatory networks in the parasite. Despite the paucity of recognizable domains, the vast majority of Tritryp PKs are much larger than a simple catalytic domain.

Surface molecules. Many trypanosomatid surface proteins are heavily glycosylated. Although the Tritryps have biosynthetic pathways for some sugars and have several glycosyltransferases (*17*), they are unable to synthesize sialic acid, which is present in several parasite surface glycoconjugates. However, in *T. cruzi* and *T. brucei*, incorporation of host sialic acid is possible because of a surface-bound TS (*34*, *59*), which can transfer sialidase from sialoglycoconjugates in the host to the terminal β-galactose on the highly *O*-glycosylated mucins in *T. cruzi* (*34*), and the glycosylphosphatidylinositol (GPI) anchor of procyclin in the insect stage of *T. brucei* (*60*).

Intriguingly, in comparison with *L. major* and *T. brucei*, *T. cruzi* shows a dramatic expansion of several families of surface molecules, including the TS, mucin, MASP, and gp63 protease families, which are each encoded by several hundred genes in the *T. cruzi* genome (Table 2). The *T. cruzi* assembly contains 1430 gene members of the TS superfamily, including 693 pseudogenes, which have previously been classified into two major subfamilies (*34*) (table S13). One subfamily includes 12 genes that share more than 90% identity with genes encoding enzymatically active TSs. This number may represent an underestimate because of collapsed assembly of near-identical repeats. Most, but not all, active TSs contain a variable number of 12–amino acid SAPA (shed acute-phase antigen) repeats and are GPI-anchored (*61*, *62*). The remaining TS superfamily members consist of more than 725 genes encoding enzymatically inactive TS-like proteins with variable degrees of homology to the active TSs. Only 371 genes have the conserved sialidase superfamily motif (VTVxNVxLYNR). The significant sequence variability suggests a strong selective pressure on the TS gene family to diversify. This pressure may be in part provided by the mammalian immune response, because TSs are targets of both humoral and cell-mediated immune responses (*34*). The TS family is much smaller in *T. brucei* and is absent from *L. major*.

The mucins represent another large (863 members) family of surface molecules in *T. cruzi*, which can be divided into two subfamilies (table S14). The 19-member TcSMUG family is relatively homogeneous, and members are expressed in the epimastigote stage in the insect vector (*63*). The much larger TcMUC subfamily is expressed in the mammalian stages (*64*) and contains 844 members. No mucin-related genes are found in *T. brucei*, but eight members of the large PSA-2 family (*17*) in *L. major* have a structure (including T_7KP_2 repeats) similar to those of TcMUC group I.

As indicated above, the TS genes can be found in subtelomeric repetitive regions, although they also occur in intrachromosomal arrays, often at Tritryp synteny breaks [see (*15*)]. We have identified another large *T. cruzi*–specific gene family within large (up to 600 kb) clusters of TS and mucin genes,

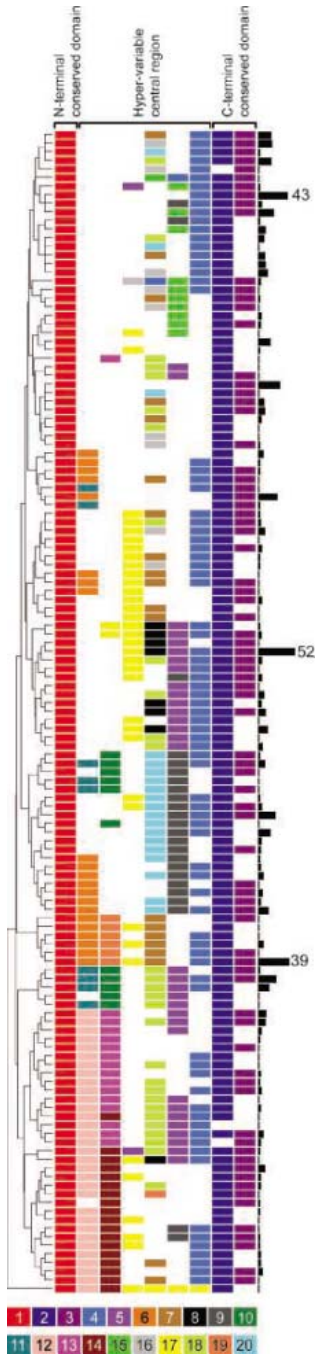

Fig. 2. Schematic representation of MASP protein structure and variability. The MEME algorithm (version 3.0) was used to identify motifs shared by members of the MASP family. The relative numbers in each of the defined subgroups are represented as a histogram on the right. The N- and C-terminal conserved domains and the central variable region are indicated on the top. Because patterns of variable length cause gaps and are split by MEME into two or more separate motifs, the C-terminal conserved domain of MASP is represented by two motifs separated by variably repeated leucine and valine residues. The motif consensus sequences are numbered in decreasing order of statistical significance and color coded. The MEME parameters, grouping methods, and amino acid sequence corresponding to each of the motifs are listed in the supporting online material (*18*).

members of which are characterized by conserved N- and C-terminal domains that encode a signal peptide and a GPI anchor addition site, respectively, which suggests a surface location in the parasite. The central region of these proteins is highly variable (Fig. 2) and often contains repeated sequence. Because most members of this family are located downstream of TcMUC II mucins (which they resemble structurally, if not at the sequence level), we have named the family mucin-associated surface proteins (MASPs). Of the 1377 *masp* genes identified, 771 appear to be intact and encode both N- and C-terminal conserved regions; 433 are pseudogenes. An interesting observation is the existence of chimeras (*26*) that contain the N- or C-terminal conserved domain of MASP combined with the N- or C-terminal domain of mucin or the C-terminal domain from the TS superfamily. The mechanism for the generation of such chimeric *masp* genes is unknown, although previous studies have described mosaic genes formed by group II and III members of the TS superfamily (*65*). Proteomic data from four different *T. cruzi* developmental stages revealed at least four distinct *masp* genes in trypomastigotes and another in epimastigotes (*66*). The low number of MASP peptides detected by proteomic approaches suggests that MASPs may contain extensive posttranslational modifications. Alternatively, *masp* genes may be expressed in intermediate stages not represented in the proteome data or may be expressed in a mutually exclusive fashion, similar to the *T. brucei* variant surface glycoproteins (VSGs).

The gp63 family of surface metalloproteases is found in the three trypanosomatids and has been implicated in virulence, host cell infection, and release of parasite surface proteins (*67*). Although *L. major* has only four gp63 genes and two gp63-like genes, and *T. brucei* has only 13, *T. cruzi* contains more than 420 genes and pseudogenes. These appear to be dispersed throughout the genome, although they sometimes occur in tandem clusters. The reason for this massive expansion of the gp63 gene family in *T. cruzi* is not yet apparent.

Several common themes emerge from genomic examination of Tritryp surface proteins: Many are highly glycosylated, and the proteins are members of large families containing highly variable central domains. The genes in *T. cruzi* and *T. brucei* are often located in large haploid arrays. It is likely that they have evolved to evade the host immune response, and the presence of pseudogenes may contribute to the diversity of the sequence repertoire through recombination. Nevertheless, species-specific differences do occur, because *T. brucei* expresses only one VSG at a time and has evolved a sophisticated system to constantly change the expressed copy, whereas *T. cruzi* simultaneously expresses numerous copies of the TSs, mucins, and probably MASPs and gp63s.

Implications for novel therapies. The elucidation of critical pathways in DNA repair, DNA replication, and meiosis and the identification of numerous protein kinases and phosphatases afforded by analysis of the Tritryp genomes promise to provide novel drug targets. Differences from the typical eukaryotic machinery for nucleotide excision/repair, initiation of DNA replication, and the presence of additional bacteria-like DNA polymerases used in replication of the mitochondrial genome all provide potential points of attack against the parasites. In addition, the presence of several PKs with little similarity to those in other eukaryotes present new possibilities for targeted drug development. The surface TS activity, which is, in *T. cruzi* at least, essential for incorporation of host sialic acid into parasite glycoconjugates, is another target for chemotherapeutic intervention, and work is already well advanced in this area (*58*). The elucidation of the complete repertoire of active *T. cruzi* TSs should help in this endeavor.

References and Notes

1. WHO, *The World Health Report, 2002* (World Health Organization, Geneva, 2002).
2. Anonymous, *Mem. Inst. Oswaldo Cruz* **94**, 429 (1999).
3. C. G. Clark, O. J. Pung, *Mol. Biochem. Parasitol.* **66**, 175 (1994).
4. S. Brisse, C. Barnabé, M. Tibayrenc, *Int. J. Parasitol.* **30**, 35 (2000).
5. M. R. Briones, R. P. Souto, B. S. Stolf, B. Zingales, *Mol. Biochem. Parasitol.* **104**, 219 (1999).
6. B. Zingales *et al.*, *Acta Trop.* **68**, 159 (1997).
7. N. R. Sturm, N. S. Vargas, S. J. Westenberger, B. Zingales, D. A. Campbell, *Int. J. Parasitol.* **33**, 269 (2003).
8. A. Pedroso, E. Cupolillo, B. Zingales, *Mol. Biochem. Parasitol.* **129**, 79 (2003).
9. S. Brisse *et al.*, *Mol. Biochem. Parasitol.* **92**, 253 (1998).
10. C. A. Machado, F. J. Ayala, *Proc. Natl. Acad. Sci. U.S.A.* **98**, 7396 (2001).
11. M. W. Gaunt *et al.*, *Nature* **421**, 936 (2003).
12. S. J. Westenberger, C. Barnabé, D. A. Campbell, N. R. Sturm, *Genetics*, in press.
13. S. Brisse *et al.*, *Infect. Genet. Evol.* **2**, 173 (2003).
14. M. C. Elias *et al.*, *Mol. Biochem. Parasitol.* **140**, 221 (2005).
15. N. M. El-Sayed *et al.*, *Science* **309**, 404 (2005).
16. M. Berriman *et al.*, *Science* **309**, 416 (2005).
17. A. C. Ivens *et al.*, *Science* **309**, 436 (2005).
18. Materials and methods are available as supporting material on *Science* Online.
19. M. I. Cano *et al.*, *Mol. Biochem. Parasitol.* **71**, 273 (1995).
20. W. De Souza, *Curr. Pharm. Des.* **8**, 269 (2002).
21. M. S. Villanueva, S. P. Williams, C. B. Beard, F. F. Richards, S. Aksoy, *Mol. Cell. Biol.* **11**, 6139 (1991).
22. S. Aksoy, T. M. Lalor, J. Martin, L. H. Van der Ploeg, F. F. Richards, *EMBO J.* **6**, 3819 (1987).
23. B. E. Kimmel, O. K. ole-MoiYoi, J. R. Young, *Mol. Cell. Biol.* **7**, 1465 (1987).
24. M. Olivares *et al.*, *Electrophoresis* **21**, 2973 (2000).
25. F. Bringaud *et al.*, *Mol. Biol. Evol.* **21**, 520 (2004).
26. G. Hasan, M. J. Turner, J. S. Cordingley, *Cell* **37**, 333 (1984).
27. F. Bringaud *et al.*, *Mol. Biochem. Parasitol.* **124**, 73 (2002).
28. E. Ghedin *et al.*, *Mol. Biochem. Parasitol.* **134**, 183 (2004).

29. N. L. Vastenhouw *et al.*, *Curr. Biol.* **13**, 1311 (2003).
30. W. D. DaRocha, K. Otsu, S. M. Teixeira, J. E. Donelson, *Mol. Biochem. Parasitol.* **133**, 175 (2004).
31. K. A. Robinson, S. M. Beverley, *Mol. Biochem. Parasitol.* **128**, 217 (2003).
32. M. A. Chiurillo, I. Cano, J. F. Da Silveira, J. L. Ramirez, *Mol. Biochem. Parasitol.* **100**, 173 (1999).
33. F. Bringaud *et al.*, *Eukaryot. Cell* **1**, 137 (2002).
34. A. C. Frasch, *Parasitol. Today* **16**, 282 (2000).
35. P. Wincker, A. C. Murto-Dovales, S. Goldenberg, *Mol. Biochem. Parasitol.* **55**, 217 (1992).
36. M. I. Cano, J. M. Dungan, N. Agabian, E. H. Blackburn, *Proc. Natl. Acad. Sci. U.S.A.* **96**, 3616 (1999).
37. Y. Liu *et al.*, *Mol. Cell. Biol.* **20**, 8178 (2000).
38. M. Cross *et al.*, *Mol. Microbiol.* **46**, 37 (2002).
39. J. Pena-Diaz *et al.*, *J. Mol. Biol.* **342**, 787 (2004).
40. S. M. Beverley, *Nat. Rev. Genet.* **4**, 11 (2003).
41. E. Pays, L. Vanhamme, D. Perez-Morga, *Curr. Opin. Microbiol.* **7**, 369 (2004).
42. L. S. Symington, *Microbiol. Mol. Biol. Rev.* **66**, 630 (2002).
43. C. Conway *et al.*, *J. Biol. Chem.* **277**, 21269 (2002).
44. M. J. Gardner *et al.*, *Nature* **419**, 498 (2002).
45. S. P. Bell, A. Dutta, *Annu. Rev. Biochem.* **71**, 333 (2002).
46. L. M. Kelman, Z. Kelman, *Mol. Microbiol.* **48**, 605 (2003).
47. R. Woodward, K. Gull, *J. Cell Sci.* **95**, 49 (1990).
48. M. M. Klingbeil, S. A. Motyka, P. T. Englund, *Mol. Cell* **10**, 175 (2002).
49. T. T. Saxowsky, G. Choudhary, M. M. Klingbeil, P. T. Englund, *J. Biol. Chem.* **278**, 49095 (2003).
50. K. M. Sinha, J. C. Hines, N. Downey, D. S. Ray, *Proc. Natl. Acad. Sci. U.S.A.* **101**, 4361 (2004).
51. J. Grams *et al.*, *J. Biol. Chem.* **277**, 16952 (2002).
52. L. Jenni *et al.*, *Nature* **322**, 173 (1986).
53. C. M. Turner *et al.*, *Parasitology* **129**, 445 (2004).
54. P. Ward, L. Equinet, J. Packer, C. Doerig, *BMC Genomics* **5**, 79 (2004).
55. T. C. Hammarton, J. C. Mottram, C. Doerig, *Prog. Cell Cycle Res.* **5**, 91 (2003).
56. M. Wiese, D. Kuhn, C. G. Grunfelder, *Eukaryot. Cell* **2**, 769 (2003).
57. I. B. Muller, D. Domenicali-Pfister, I. Roditi, E. Vassella, *Mol. Biol. Cell* **13**, 3787 (2002).
58. A. E. Fujimura, S. S. Kinoshita, V. L. Pereira-Chioccola, M. M. Rodrigues, *Infect. Immun.* **69**, 5477 (2001).
59. G. Montagna *et al.*, *Eur. J. Biochem.* **269**, 2941 (2002).
60. M. A. Ferguson, *Philos. Trans. R. Soc. Lond. B Biol. Sci.* **352**, 1295 (1997).
61. G. D. Pollevick, J. L. Affranchino, A. C. Frasch, D. O. Sanchez, *Mol. Biochem. Parasitol.* **47**, 247 (1991).
62. R. Agusti, A. S. Couto, O. Campetella, A. C. Frasch, R. M. de Lederkremer, *Mol. Biochem. Parasitol.* **97**, 123 (1998).
63. V. Campo *et al.*, *Mol. Biochem. Parasitol.* **133**, 81 (2004).
64. C. A. Buscaglia *et al.*, *J. Biol. Chem.* **279**, 15860 (2004).
65. C. L. Allen, J. M. Kelly, *Exp. Parasitol.* **97**, 173 (2001).
66. J. A. I. Atwood III *et al.*, *Science* **309**, 473 (2005).
67. C. Yao, J. E. Donelson, M. E. Wilson, *Mol. Biochem. Parasitol.* **132**, 1 (2003).
68. G. Manning, D. B. Whyte, R. Martinez, T. Hunter, S. Sudarsanam, *Science* **298**, 1912 (2002).

69. We thank our colleagues in the *T. cruzi* Genome Network (TcGN) and the trypanosomatid research community for their continued support and encouragement. In particular, we thank the members of the Tritryp Sequencing Consortium for their help with comparative genome annotation; J. Donelson and S. Melville for a critical review of this manuscript; A. Kerhornou for his help with GPI anchor predictions; as well as O. Campetella, I. Dórso, V. Campo, G. Montagna, and F. Aguero for their help with the surface protein analyses. Funding for this project was provided by grants from the National Institute for Allergy and Infectious Diseases (NIAID) to N.M.E.-S. (AI45038), K.D.S. and P.J.M. (AI045039), and B.A. (AI45061); the M. J. Murdoch Charitable Trust to the Seattle Biomedical Research Institute; the Beijer Foundation to B.A. M.J.L. and A.C.F. are Howard Hughes Medical Institute International Research Scholars. G.C.C. is supported in part by CNPq, Brazil. We also express our gratitude to NIAID, Burroughs Wellcome Fund (BWF), the Wellcome Trust, and WHO (Tropical Disease Research) for providing funds for several TcGN and Tritryp meetings. Special thanks to C. Hertz-Fowler and P. Mooney at the Wellcome Trust Sanger Institute (WTSI) for coordinating data exchange with The Institute for Genomic Research (TIGR), and to A. Tivey and M. Aslett for loading and updating the *T. cruzi* data in GeneDB at WTSI. This Whole-Genome Shotgun project has been deposited at the DNA Databank of Japan (DDBJ), the European Molecular Biology Laboratory (EMBL), and GenBank under the project accession AAHK00000000. The version described in this paper is the first version, AAHK01000000. All data sets and genome annotations are also available through GeneDB at www.genedb.org.

Supporting Online Material

www.sciencemag.org/cgi/content/full/309/5733/409/DC1
Materials and Methods
Tables S1 to S14
References and Notes

23 March 2005; accepted 17 June 2005
10.1126/science.1112631

RESEARCH ARTICLE

The Genome of the African Trypanosome *Trypanosoma brucei*

Matthew Berriman,[1]* Elodie Ghedin,[2,3] Christiane Hertz-Fowler,[1] Gaëlle Blandin,[2] Hubert Renauld,[1] Daniella C. Bartholomeu,[2] Nicola J. Lennard,[1] Elisabet Caler,[2] Nancy E. Hamlin,[1] Brian Haas,[2] Ulrike Böhme,[1] Linda Hannick,[2] Martin A. Aslett,[1] Joshua Shallom,[2] Lucio Marcello,[4] Lihua Hou,[2] Bill Wickstead,[5] U. Cecilia M. Alsmark,[6] Claire Arrowsmith,[1] Rebecca J. Atkin,[1] Andrew J. Barron,[1] Frederic Bringaud,[7] Karen Brooks,[1] Mark Carrington,[8] Inna Cherevach,[1] Tracey-Jane Chillingworth,[1] Carol Churcher,[1] Louise N. Clark,[1] Craig H. Corton,[1] Ann Cronin,[1] Rob M. Davies,[1] Jonathon Doggett,[1] Appolinaire Djikeng,[2] Tamara Feldblyum,[2] Mark C. Field,[9] Audrey Fraser,[1] Ian Goodhead,[1] Zahra Hance,[1] David Harper,[1] Barbara R. Harris,[1] Heidi Hauser,[1] Jessica Hostetler,[2] Al Ivens,[1] Kay Jagels,[1] David Johnson,[1] Justin Johnson,[2] Kristine Jones,[2] Arnaud X. Kerhornou,[1] Hean Koo,[2] Natasha Larke,[1] Scott Landfear,[10] Christopher Larkin,[2] Vanessa Leech,[9] Alexandra Line,[1] Angela Lord,[1] Annette MacLeod,[4] Paul J. Mooney,[1] Sharon Moule,[1] David M. A. Martin,[11] Gareth W. Morgan,[12] Karen Mungall,[1] Halina Norbertczak,[1] Doug Ormond,[1] Grace Pai,[2] Chris S. Peacock,[1] Jeremy Peterson,[2] Michael A. Quail,[1] Ester Rabbinowitsch,[1] Marie-Adele Rajandream,[1] Chris Reitter,[9] Steven L. Salzberg,[2] Mandy Sanders,[1] Seth Schobel,[2] Sarah Sharp,[1] Mark Simmonds,[1] Anjana J. Simpson,[2] Luke Tallon,[2] C. Michael R. Turner,[13] Andrew Tait,[4] Adrian R. Tivey,[1] Susan Van Aken,[2] Danielle Walker,[1] David Wanless,[2] Shiliang Wang,[2] Brian White,[1] Owen White,[2] Sally Whitehead,[1] John Woodward,[1] Jennifer Wortman,[2] Mark D. Adams,[14] T. Martin Embley,[6] Keith Gull,[5] Elisabetta Ullu,[15] J. David Barry,[4] Alan H. Fairlamb,[11] Fred Opperdoes,[16] Barclay G. Barrell,[1] John E. Donelson,[17] Neil Hall,[1]† Claire M. Fraser,[2] Sara E. Melville,[9] Najib M. El-Sayed[2,3]*

African trypanosomes cause human sleeping sickness and livestock trypanosomiasis in sub-Saharan Africa. We present the sequence and analysis of the 11 megabase-sized chromosomes of *Trypanosoma brucei*. The 26-megabase genome contains 9068 predicted genes, including ~900 pseudogenes and ~1700 *T. brucei*–specific genes. Large subtelomeric arrays contain an archive of 806 variant surface glycoprotein (VSG) genes used by the parasite to evade the mammalian immune system. Most *VSG* genes are pseudogenes, which may be used to generate expressed mosaic genes by ectopic recombination. Comparisons of the cytoskeleton and endocytic trafficking systems with those of humans and other eukaryotic organisms reveal major differences. A comparison of metabolic pathways encoded by the genomes of *T. brucei*, *T. cruzi*, and *Leishmania major* reveals the least overall metabolic capability in *T. brucei* and the greatest in *L. major*. Horizontal transfer of genes of bacterial origin has contributed to some of the metabolic differences in these parasites, and a number of novel potential drug targets have been identified.

Human African trypanosomiasis, or sleeping sickness, primarily affects the poorest rural populations in some of the least developed countries of Central Africa (*1*). The incidence may approach 300,000 to 500,000 cases per year, and it is invariably fatal if untreated. The disease is caused by *Trypanosoma brucei*, an extracellular eukaryotic flagellate parasite, and current treatments are inadequate: Drugs for late-stage disease are highly toxic; there is no prophylactic chemotherapy and little or no prospect of a vaccine.

Livestock trypanosomiasis is caused by closely related *Trypanosoma* species. It has the greatest impact in sub-Saharan Africa, where the tsetse fly vector is common, and also occurs in Asia and South America.

We present the sequence and analysis of the 11 megabase-sized chromosomes of the *T. brucei* genome (Table 1). The nuclear genome also contains an unspecified number of small and intermediate-sized chromosomes (30 to 700 kb) (*2*, *3*) known to encode sequences similar to subtelomeric regions of megabase-sized chromosomes (*4*).

Genome structure and content. The genome data herein represent a haploid mosaic (*5*) of the diploid chromosomes and were determined by both whole chromosome shotgun (chromosomes 1 and 9 to 11) and bacterial artificial chromosome walking strategies (chromosomes 2 to 8). Most of the assembled chromosome sequences extend into the subtelomeric regions (the sequence between the telomere and the first housekeeping gene) (Plate 3 and table S1).

As previously observed on a smaller scale (*6*, *7*), both strands of the megabase chromosomes contain long, nonoverlapping gene clusters (Plate 3) that are probably transcribed as polycistrons and subsequently trans-spliced and polyadenylated. The unusual mechanisms of transcription and their implications for the parasite are discussed elsewhere (*8*). Just over 20% of the genome encodes subtelomeric genes

[1]Wellcome Trust Sanger Institute, Wellcome Trust Genome Campus, Hinxton CB10 1SA, UK. [2]The Institute for Genomic Research, Rockville, MD 20850, USA. [3]Department of Microbiology and Tropical Medicine, George Washington University, Washington, DC 20052, USA. [4]Wellcome Centre for Molecular Parasitology, University of Glasgow, 56 Dumbarton Road, Glasgow G11 6NU, UK. [5]Sir William Dunn School of Pathology, University of Oxford, South Parks Road, Oxford OX1 3RE, UK. [6]School of Biology, Devonshire Building, University of Newcastle upon Tyne, Newcastle NE1 7RU, UK. [7]Laboratoire de Génomique Fonctionnelle des Trypanosomatides, Université Victor Segalen Bordeaux II, UMR-5162 CNRS, 33076 Bordeaux cedex, France. [8]Department of Biochemistry, University of Cambridge, Cambridge CB2 1GA, UK. [9]Department of Pathology, University of Cambridge, Cambridge CB2 1QP, UK. [10]Oregon Health and Science University, 3181 SW Sam Jackson Park Road, Mail Code L474, Portland, OR 97239–3098, USA. [11]School of Life Sciences, Wellcome Trust Biocentre, University of Dundee, Dundee DD1 5EH, UK. [12]Department of Biological Sciences, Imperial College, London SW7 2AY, UK. [13]Institute of Biomedical and Life Sciences, Joseph Black Building, University of Glasgow, Glasgow G12 8QQ, UK. [14]Department of Genetics, Case Western Reserve University, 10900 Euclid Avenue, Cleveland, OH 44106, USA. [15]Department of Internal Medicine, Yale University School of Medicine, 333 Cedar Street, Post Office Box 208022, New Haven, CT 06520–8022, USA. [16]Christian de Duve Institute of Cellular Pathology and Catholic University of Louvain, Avenue Hippocrate 74-75, B-1200 Brussels, Belgium. [17]Department of Biochemistry, University of Iowa, Iowa City, IA 52242, USA.

*To whom correspondence should be addressed. E-mail: mb4@sanger.ac.uk (M.B.); nelsayed@tigr.org (N.M.E.-S.)

†Present address: Institute for Genomic Research, Rockville, MD 20850, USA.

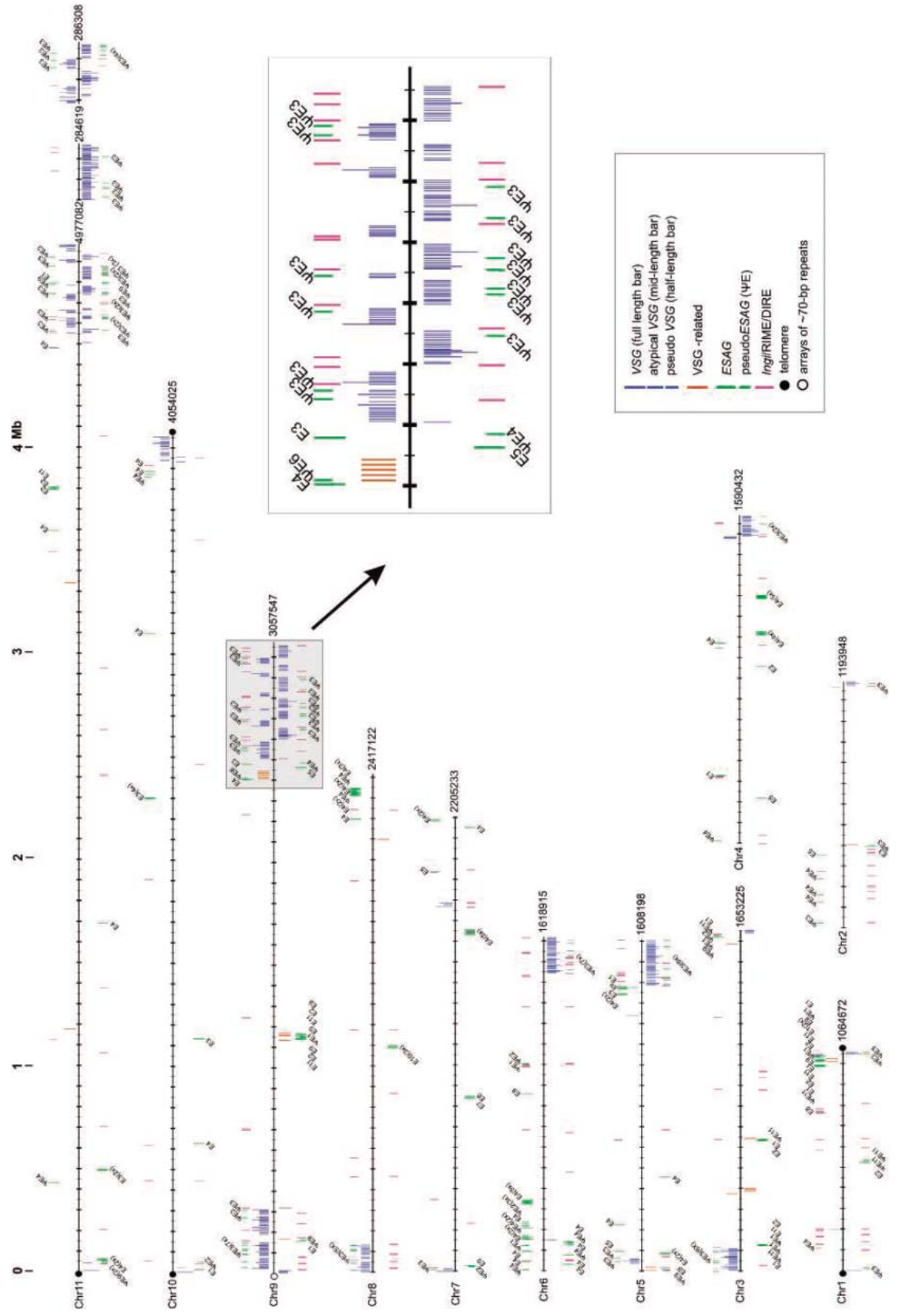

Fig. 1. Distribution of *VSG*s and *ESAG*s on chromosomes 1 to 11 of *T. brucei*. The four different *VSG* categories are defined in the text: *VSG*, atypical *VSG*, *VSG* pseudogene (gene fragments and full-length pseudogenes), and *VSG*-related. *ESAG* family members are identified (e.g., E1 is *ESAG1*), and degenerate, frameshifted, and truncated *ESAG*s are represented by ψ. Solid circles indicate arrays of telomeric-repeat hexamers and/or known terminal subtelomeric repeats, whereas open circles depict arrays of ~70-bp repeats. The *VSG* and *ESAG* array at the right-hand end of chromosome 9 is highlighted as an example.

(Plate 3) (*9*), the majority of which are *T. brucei*–specific and relate to the parasite's capacity to undergo antigenic variation in the bloodstream of its mammalian host. Expansion of gene families by tandem duplication is a mechanism by which the parasites can increase expression levels to compensate for a general lack of transcriptional control (*8*). Analysis of protein families (table S2) gives a measure of the resources that the parasite commits to key cellular processes. Kinesins and kinesin-like proteins, protein kinases (*8*), and adenylate cyclases are among the largest families, and two as-yet uncharacterized families of more than 10 members each appear to be expanded in the *T. brucei* genome relative to *L. major* and *T. cruzi* genomes.

Antigenic variation. Antigenic variation enables evasion of acquired immunity during infection or in immune host populations. Invariant antigens on the surface of *T. brucei* are shielded by a dense coat of 10^7 copies of a single variant surface glycoprotein (VSG) that must be replaced as antibodies against it arise (*10*, *11*). VSGs differ significantly in the hypervariable N-terminal domain, which is exposed to the immune system, whereas the C-terminal domain is more conserved and is buried in the coat. The genome was previously known to contain a large archive of an estimated 1000 nonexpressed *VSG* genes (*VSG*s) that are activated clonally during infection at a rate of up to one activation event per 100 cell doublings (*12*, *13*). These *VSG*s have a basic cassette organization, with one or more ~70–base pair (bp) repeats at their 5′ flank and sequence homology at their 3′ flank that includes parts of the coding sequence and the 3′ untranslated region (*14*). *VSG* activation relies on residence in specific transcription units known as bloodstream-form expression sites (BESs), which are immediately subtelomeric on megabase and intermediate chromosomes and possess additional co-transcribed expression site–associated genes (*ESAG*s). *VSG* switching normally involves duplication of *VSG* cassettes into BESs.

The first new insight of the genome analysis is that most sequenced silent *VSG*s are defective. It is not known what proportion of *VSG*s are intact among the intermediate chromosomes, minichromosomes, or the yet-to-be-sequenced subtelomeric regions. Of 806 analyzed (Fig. 1 and table S3), only 57 (7%) are fully functional (that is, encode all recognizable features of known functional VSGs), whereas 9% are atypical (complete genes possibly encoding proteins with inconsistent VSG folding or post-translational modification), 66% are full-length pseudogenes (with frameshifts and/or in-frame stop codons), and 18% are gene fragments, most of which encode C-terminal domains. This *VSG* archive could be a repository of defunct material, but it might also be an information pool of an unprecedented size among parasites. Antigen pseudogenes are known to exist in several bacterial and other protozoan pathogens and to contribute to immune evasion by partial gene conversions to become expressed mosaic genes (*15*). This combinatorial use of information economizes on the genome and, theoretically, can greatly increase the potential for variation. In African trypanosomes, it has long been known that VSGs of antigenic variants can be encoded by mosaics of pseudogenes and also by hybrids, where the N- and C-terminal domains are derived from separate genes (*16*, *17*). It now appears that more than one-third of the N-terminal domains encoded by full-length VSG are intact, whereas C-terminal domains are more degenerate, further indicating the likely importance of hybrid gene formation. It is also possible that a trypanosome may be able to reinfect a reservoir host previously exposed to trypanosomes by using the *VSG* archive to embark stochastically on a different pathway of mosaic formation.

The second new insight is that almost all *VSG*s form arrays, numbering 3 to ~250 (pseudo)genes, and that most of these are subtelomeric (Fig. 1). In contrast to genes in telomeric BESs, the majority of *VSG*s are oriented away from the telomere. This is consistent with other protozoa [except *Giardia* (*18*)], where antigen gene archives are at least partly subtelomeric, probably due to the ability of these chromosome domains to recombine with each other ectopically rather than merely between chromosome homologs (*19*). More than 90% of the *VSG*s have one or more ~70-bp repeats upstream. In addition, the non–long terminal repeat retransposons *ingi* and RIME are associated with the *VSG* arrays, in particular where coding strand switches occur, in keeping with the role of such elements in genome restructuring (*20*). We found no obvious organization of the most similar *VSG*s into subfamilies within arrays; *VSG*s are scattered apparently at random within and among arrays (fig. S1) or between homologous chromosomes (fig. S2).

VSGs can be subdivided into N- and C-terminal domains as defined by cysteine distribution and sequence homology (*21*). Two previously unknown types of C-terminal domain are encoded in the genome, and diversification among the three known N-terminal domains has occurred. Also, we identified a previously unknown set of 29 VSG-related genes that cluster distinctly from other VSGs in a multiple alignment and lack upstream ~70-bp repeats. The majority of these putative proteins do not contain cysteine residues in their C-terminal regions. They could have evolved novel functions, as has happened with the serum resistance-associated protein (*22*). This arrangement of genes resembles that of the VAR family in the malaria parasite *Plasmodium falciparum*; VARs encode variant erythrocyte surface proteins and most are subtelomeric, but some are internally located and differ from their subtelomeric counterparts (*23*).

Members of up to 11 families of *ESAG*s are normally associated with *VSG*s in the polycistronic BESs. All BESs appear to harbour an *ESAG6* and *ESAG7*, and most have a total of five to 10 ESAGs and pseudo-ESAGs (*24*). Of the 11 known ESAG families (Fig. 1 and table S4), *ESAG3* and *ESAG4* are remarkably abundant, but *ESAG3*s are preferentially associated with *VSG* arrays, where it is present exclusively as pseudogenes. A single copy of the tandem *ESAG6* and *ESAG7* (normally found at the BESs) resides outside BESs but not in the *VSG* arrays; it appears in tandem on chromosome 7 at an interruption in the conservation of synteny found between the Tritryps (*9*).

Intracellular protein vesicle trafficking. Membrane transport functions are critically important for the Tritryps, both in terms of their interactions with insect vectors and mammalian hosts as well as the recycling of surface membrane components, such as VSGs. The Tritryps have a polarized endomembrane system and restrict both exocytosis and endocytosis, which occur exclusively via a clathrin-dependent mechanism, to the flagellar pocket (*25*, *26*).

T. brucei has served as a paradigm for the study of transport processes in kinetoplastids, elucidating the role of cytoplasmic coat proteins (tables S5 and S6) and suggesting a fundamental difference in the mechanisms of

Table 1. Summary of the *T. brucei* genome. Genome size and chromosome numbers exclude intermediate and mini-chromosomes. Details of contig coverage for each chromosome are described in table S1. Intergenic regions are regions between protein-coding sequences (CDSs). The exact number of spliced leader (sl) RNA copies cannot be resolved in the assembly.

Parameter	Number
The genome	
Size (bp)	26,075,396
G+C content (%)	46.4
Chromosomes	11
Sequence contigs	30
Percent coding	50.5
Protein-coding genes	
Genes	9068
Pseudogenes	904
Mean CDS length (bp)	1592
Median CDS length (bp)	1242
G+C content (%)	50.9
Gene density (genes per Mb)	317
Intergenic regions	
Mean length (bp)	1279
G+C content (%)	41
RNA genes	
transfer RNA	65
ribosomal RNA	56
slRNA	>28
small nuclear RNA	5
small nucleolar RNA	353

endocytosis between the Tritryps (*26*). Analysis of the *T. brucei* Rab guanine triphosphatases (GTPases), regulators of membrane transport, indicates a complex, highly regulated vesicular transport system (*27*). This complexity now appears to be mirrored in the *L. major* and *T. cruzi* genomes (tables S5 and S7). A second GTPase family includes adenosine diphosphate ribosylation factors (ARFs), ARF-like proteins (ARLs), and Sar1, regulators of membrane traffic and the cytoskeleton (table S5). Phylogenetic reconstruction of the divergent Tritryp ARF and ARL family indicated previously unknown isoforms, some of which are not found in metazoan organisms (fig. S3) (*28*). This likely acquisition of a large family of trypanosomatid-specific GTPases may reflect the extreme emphasis of the trypanosomatid cytoskeleton on tubulin- rather than actin-mediated mechanisms.

Cytoskeleton. Generally, the eukaryotic cytoskeleton is divided into three filament classes: microtubules, intermediate filaments, and actin microfilaments. Proteins of the intermediate filament network are very diverse and poorly conserved in evolution. It appears that no homologs to known intermediate filament genes (table S8) are encoded in the Tritryp genome sequences. Homologs of components of actin- and tubulin-based cytoskeleton, however, are readily identifiable (Fig. 2 and table S8). Compared to other eukaryotic organisms, the Tritryps appear to have a reduced dependence on the acto-myosin network balanced by an elaboration of the tubulin-based cytoskeleton.

Six members of the tubulin superfamily are present in the Tritryps: α-, β,- γ-, δ-, ε-, and ζ-tubulin. The presence of δ- and ε-tubulin is characteristic of organisms with basal bodies and flagella. Five putative genes encoding centrins, elongation factor (EF)–hand proteins functioning at microtubule-organizing centers (MTOCs), occur in each genome. Yeasts, in contrast, have a single MTOC and a single centrin gene. The existence of a family of centrins in the Tritryps may reflect the diversity of dispersed MTOCs involved in cytoskeleton organization in these parasites. Outside of the centrins, few homologs to the components of the mammalian centrosome or yeast spindle-pole body were identified in the three genomes (Fig. 2).

The Tritryp dependence on diverse microtubule function is best exemplified by the kinesin superfamily. Each genome encodes >40 putative kinesins (excluding near-identical copies) compared with only 31 in humans. Furthermore, these kinesins have a huge diversity of primary sequences (unlike, for example, the numerous kinesins of *Arabidopsis*). Some of these kinesins fall into previously identified functional clades, but many belong to novel clades. There are no homologs for the kinetochore motor, CENP-E, or the spindle motor, BimC. However, there has been an expansion and diversification of the mitotic centromere-associated kinesin family. Characteristic trilaminar kinetochore-like plaques are seen in kinetoplastid mitotic nuclei attached to the spindle (*29*). Generally, the proteins of the mitotic kinetochore are only poorly conserved despite the near-ubiquity of the structure itself (Fig. 3). However, this appears to be particularly pronounced in the case of the Tritryps, where there are no homologs of CENP-C/Mif2,

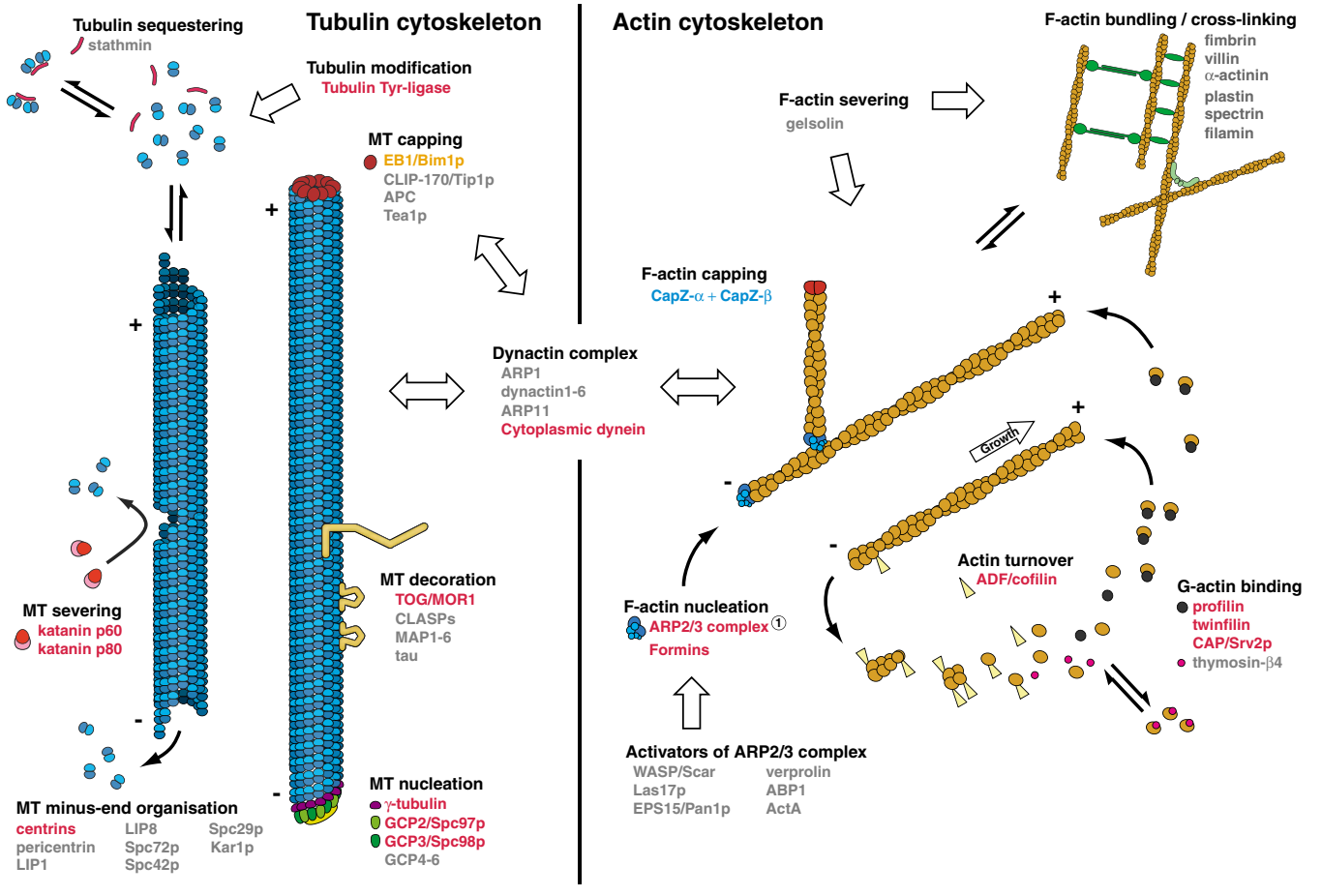

Fig. 2. Core cytoskeletal components in *T. brucei*, *T. cruzi*, and *L. major*. A schematic representation of the tubulin- and actin-based cytoskeleton. **(Left)** α- and β-tubulin subunits are depicted as light and dark blue circles, either assembled into the microtubule lattice or as dimers. **(Right)** Actin filaments composed of actin momomers (yellow circles). Black text indicates processes involved in cytoskeleton organization. Components for which the Tritryp genomes encode one or more homologs are shown in red text. Those that do not appear to be encoded by the three genomes are indicated in gray text. The CapZ proteins only present in *T. cruzi* are highlighted in blue text, whereas orange text points to homologs only encoded by the *T. brucei* and *T. cruzi* genomes. The Arp2/3 complex is divergent in *L. major*.

HEC1/Ndc80, or the centromeric checkpoint protein BUB1, each of which is highly conserved among yeast, plants, and mammals (Fig. 3). Indeed, it appears that the sole variant histone H3 in these genomes does not even function at the centromere (*30*).

The proteins of the flagellar axoneme appeared to be extremely well conserved. With the exception of tektin, there are homologs in the three genomes for all previously identified structural components as well as a full complement of flagellar motors and both complex A and complex B of the intraflagellar transport system (Fig. 4). Thus, the 9+2 axoneme, which arose very early in eukaryotic evolution, appears to be constructed around a core set of proteins that are conserved in organisms possessing flagella and cilia. The major divergence apparent in flagellar organization in Kinetoplastida is the augmentation of the axoneme by a paracrystalline extra-axonemal structure, the paraflagellar rod, that is unique to the Kinetoplastida and Euglenida.

No actin-based motility has been described in trypanosomatids; they do not exhibit the ruffles or pseudopodia seen in amoebae and metazoa or the myosin-based gliding motility of the Apicomplexa. Acto-myosin may not even be necessary for cytokinesis in these organisms. Actin is, however, involved in endocytosis (*31*). The genome sequences revealed putative homologs for proteins involved in monomeric-actin binding and actin filament nucleation (Fig. 2 and table S8) and for two myosin families (*32*). Surprisingly, the cohort of highly conserved proteins involved in severing, bundling, cross-linking, and capping of filamentous actin are missing [the latter is not the case for *T. cruzi* (*32*)]. Moreover, the dynactin complex is absent, indicating a major loss in the ability for cross-talk between the actin- and tubulin-filament networks (Fig. 2).

Metabolism and transport. Understanding the parasite's metabolism will underpin new drug discovery. To date, biochemical studies of trypanosomatids have been restricted to specific life-cycle stages that can be readily cultured in vitro or in vivo. In contrast, genome analysis provides a global view of the parasite's metabolic potential (Plate 2). In terms of overall capabilities, *T. brucei* has the most restrictive metabolic repertoire, followed by *T. cruzi*. This may reflect that, unlike *T. cruzi* or *L. major*, the parasite does not have an intracellular life cycle stage and therefore has greater access to nutrients in the plasma. Horizontal gene transfer may have provided additional metabolic versatility for the parasites. In almost 50 cases, there was strong evidence of putative horizontal transfer from bacteria into the Tritryp lineage (*5*) (table S11). Moreover, these provide us with candidate enzymes for new drug intervention points.

Across the three species, 633 genes (table S9) are annotated as transporters or channels, and 8113 are annotated as enzymes. Of the latter, more than 2000 have been classified with Enzyme Commission (EC) numbers (table S10).

Carbohydrate metabolism. The Tritryps possess a full complement of candidate genes necessary for uptake and degradation of glucose via glycolysis or the pentose phosphate shunt and the tricarboxylic acid (TCA) cycle (Plate 2). A limited number of hexose transporters are present in all species, but only *T. cruzi* possesses hexose phosphate transporters as seen in bacteria. This may reflect the fact that only *T. cruzi* amastigotes reside in the cytosol of the host cell with ready access to sugar phosphates. In contrast, only *L. major* appears capable of hydrolyzing disaccharides. This is consistent with the biology of the insect vectors: Tsetse and triatomines are obligate blood feeders, whereas sandflies also feed on nectar and aphid honeydew. *T. brucei* lacks several sugar kinases present in *L. major* or *T. cruzi*, possibly an adaptation to the restricted range of sugars available in plasma and in tsetse blood meals.

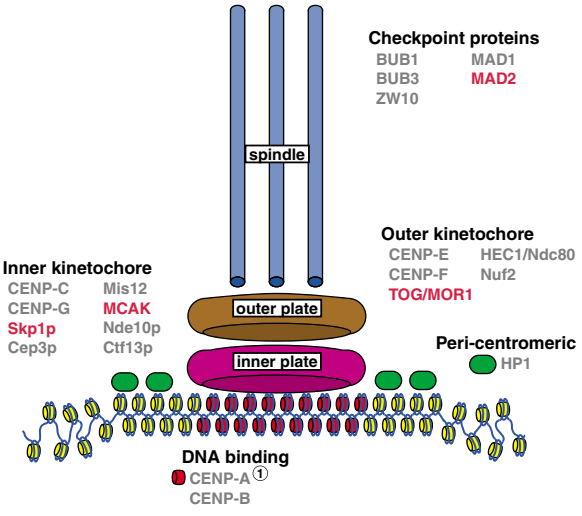

Fig. 3. Conservation of proteins of the kinetochore in *T. brucei*, *T. cruzi*, and *L. major*. A schematic representation of conserved components of a typical kinetochore is shown. The pair of plate-like kinetochores are present on the surface of the chromosome in the centromeric region, with the outer plate acting as microtubule attachment points radiating from spindle pole bodies. Kinetochore components for which the Tritryps encode one or more homologs are indicated in red text. Those that do not appear to be encoded by the three genomes are indicated in gray text. The kinetoplastid histone H3 variant does not appear to be centromeric (*30*).

Despite having potential pathways for complete oxidation, the Tritryps partially degrade glucose to succinate, ethanol, acetate, alanine, pyruvate, and glycerol (*33*) (Plate 2). L-lactate is not an end product because lactate dehydrogenase is absent from all three species, although D-lactate can be formed from methylglyoxal in *L. major*. A major route for formation of succinate from glucose in the insect stages is via an unusual nicotinamide adenine dinucleotide (NADH)–dependent fumarate reductase (*34*). In mitochondria, pyruvate is principally converted to acetate via an acetate:succinate coenzyme A (CoA)–transferase (*35*).

In many insects, including tsetse and sandflies, proline is a highly abundant energy source used in flight muscles. Proline is also a preferred energy source for the insect stages of the parasites. However, proline is only partially degraded to succinate (procyclic stage, *T. brucei*) or alanine, succinate, and other TCA intermediates (promastigote stage, *L. major*). In the Tritryps, neither an isocitrate lyase nor malate synthase could be identified, making a glyoxalate bypass in the TCA cycle unlikely.

Electron transport and oxidative phosphorylation. A fully functional mitochondrial electron transport system and adenosine triphosphate (ATP) synthase is present in the Tritryps. Several ubiquinone-linked dehydrogenases are present, including a flavin adenine dinucleotide (FAD)–dependent glycerol-3-phosphate dehydrogenase, which in *T. brucei* alone is linked to an alternative oxidase that represents a potential drug target (*36*).

In many organisms, heme is synthesized from glycine and succinyl-CoA and incorporated into hemoproteins, such as cytochromes. However, all trypanosomatids (except those with bacterial endosymbionts such as *Crithidia oncopelti*) are heme auxotrophs. Thus, the absence of the first two enzymes in heme biosynthesis (aminolevulinate synthase and aminolevulinate dehydratase) is not unexpected. It was surprising, however, to discover that genes for the last three enzymes (coproporphyrinogen III oxidase, protoporphyrinogen IX oxidase, and ferrochelatase) of heme biosynthesis are apparently present in *L. major*. Moreover, there is strong evidence (table S11 and fig. S4, A to C) that these genes may have been horizontally acquired from bacteria.

Glycosylphosphatidylinositol anchor biosynthesis. The surface of trypanosomatid plasma membranes contains a variety of glycoproteins (e.g., VSGs), phosphosaccharides (e.g., lipophosphoglycan), and glycolipids that are involved in immune evasion, attachment, or invasion. The most abundant of these are attached via glycosylphosphatidylinositol (GPI) anchors. GPI anchors are essential for parasite survival and are therefore a potential drug target (*37*). The GPI backbone contains mannose, glucosamine, and *myo*-inositol-phospholipid,

plus additional sugar modifications such as galactose (Plate 2). Pathways to the appropriate sugar nucleotide precursors are complete except for phosphoglucomutase, which was not identified in *T. brucei* despite ample biochemical evidence for its presence. Moreover, uridine diphosphate (UDP)–galactose can only be formed from glucose-6-phosphate via UDP-glucose (*38*), consistent with the absence of genes for conversion of galactose to this sugar in *T. brucei*. The *T. brucei* genome encodes a large family of UDP-galactose– or UDP-*N*-acetylglucosomine–dependent glycosyltransferases (table S2), nine of which appear to be pseudogenes associated with arrays of *VSG* pseudogenes. *Myo*-inositol can either be synthesized de novo from glucose-6-phosphate or salvaged via an inositol transporter (*39*) for the synthesis of phosphatidyl inositol, the first step in the GPI biosynthetic pathway.

Surface glycoproteins are attached to their GPI anchors via ethanolamine phosphate. In *T. cruzi* mucins, this linkage can optionally be replaced by aminoethylphosphonate (AEP). Enzymes for the complete synthesis of AEP from phosphoenol pyruvate are present only in *T. cruzi* (Plate 2) and could represent novel drug targets because they are absent from humans. The third (and last) step of the pathway (AEP transaminase) is also found in *L. major* and *T. cruzi*, and strong tree-based evidence supports its presence via horizontal acquisition from bacteria (table S11 and fig. S5). The second step of the pathway (phosphonopyruvate decarboxylase) is found in all three parasites, and homologs in other eukaryotes could not be found.

Amino acid metabolism. The Tritryps have some striking differences in amino acid metabolism (Plate 2, boxed). Amino acid transporters constitute one of the largest families of permeases in these parasites, with 29 predicted members in *L. major*, 38 in *T. brucei*, and 42 in *T. cruzi* (table S9). This is consistent with the Tritryps lacking biosynthetic pathways for the essential amino acids of humans and requiring exogenous proline as an energy source (except bloodstream *T. brucei*), glutamine for several biosynthetic pathways, cysteine as an additional sulfur source, and tyrosine for protein synthesis.

Most of the enzymes of the classical pathways for aromatic amino acid oxidation are missing. A putative biopterin-dependent phenylalanine-4-hydroxylase capable of converting phenylalanine to tyrosine could only be identified in *L. major*. However, *Leishmania* spp. are auxotrophic for tyrosine (*40*), so this gene (LmjF28.1280) may have another function. Candidate genes for transamination and reduction to the corresponding aromatic lactate derivative have been identified in all species. The role of this pathway is unclear, although secretion of these aromatic acids is found in *T. brucei* infections (*41*) and their presence in the central nervous system may result in the neurobehavioral disturbances (*42*) typically associated with human sleeping sickness.

The branched-chain amino acids can be converted to acyl-CoA derivatives in mitochondrion. However, no branched chain aminotransferase catalyzing the first step could be identified in *T. cruzi*. Leucine is converted to hydroxymethylglutaryl-CoA (HMG-CoA), which then can be incorporated directly into sterols via the isoprenoid synthetic pathway (*43*). Alternatively, HMG-CoA can be cleaved into acetyl-CoA and acetoacetate in *T. brucei* and *T. cruzi*, but the lyase is apparently absent from *L. major*. Isoleucine and valine use a similar pathway to form propionyl-CoA. However, the mitochondrial enzymes for further metabolism of propionyl-CoA to succinyl-CoA seem to be absent from both *T. brucei* and *T. cruzi*. Similarly, methionine can be converted to oxobutyrate, the precursor to propionyl-CoA, but no further. This could explain why threonine is not oxidized via the 2-oxobutyrate pathway in *T. brucei*: because the necessary threonine hydratase is missing. Instead, threonine is degraded to acetyl-CoA and glycine via the aminoacetone pathway by using a mitochondrial threonine dehydrogenase (*44*) and an aminoacetone synthase. The latter two genes are present in *T. brucei* and *T. cruzi* but absent from *L. major*.

Histidine catabolism appears to be absent from *T. brucei*. However, *T. cruzi* does have a pathway that looks typically eukaryotic, except for the last enzyme (glutamate formimino aminotransferase, Tc00.1047053507963.20), which only appears to be present in *T. cruzi* and *Tetrahymena*. Histidine is the precursor for ovothiol A, an antioxidant (*45*), which is in *L. major* and may help to protect the invading parasite from macrophage-derived hydrogen peroxide and nitric oxide. The biosynthetic pathway is thought to involve two intermediate steps requiring cysteine and adenosylmethionine. However, the sequences of these enzymes are not known in any organism and therefore cannot be identified.

A functional urea cycle (Plate 2) is missing from all three organisms. Although carbamoylphosphate synthetase is present in all three, this enzyme is also essential for pyrimidine biosynthesis. Argininosuccinate synthase and a bona fide glycosomal arginase were only identified in *L. major*. A second member of the arginase/agmatinase/formiminoglutamase gene family was found in all three parasites. However, deletion of the former gene in *L. major* renders it auxotrophic for ornithine, indicating that this second gene is probably not an arginase (*46*). Arginine kinase, present only in *T. brucei* and *T. cruzi*, has been proposed as a possible chemotherapeutic target (*47*). Phosphoarginine may play a role as a transient source of energy for renewal of ATP, similar to phosphocreatine in vertebrates.

Trypanothione metabolism. Arginine and ornithine are precursors for polyamine biosynthesis, essential for cell growth and differentiation and for the synthesis of the drug target, trypanothione (*48*). The first step in polyamine biosynthesis (ornithine decarboxylase) is the target for the human sleeping sickness drug difluoromethylornithine (Plate 2 boxed) (*48*) and was found in *T. brucei* and *L. major* but not *T. cruzi*. Arginine decarboxylase, catalyzing the proposed target for difluoromethylarginine in *T. cruzi* and an alternative route for putrescine synthesis, could not be identified either. Two candidate aminopropyltransferases were found in *T. cruzi*, in contrast to one in *L. major* and in *T. brucei*. The mammalian retroconversion pathway of polyamines appears to be absent.

Cysteine can be produced from homocysteine by the trans-sulfuration pathway present in all three organisms. De novo synthesis from serine appears possible only in *L. major* and *T. cruzi*. These parasites can also interconvert glycine and serine via serine hydroxymethyl transferase, which is apparently absent from *T. brucei*. Cysteine, glutamate, glycine, and methionine (as decarboxylated AdoMet) are the precursor amino acids for glutathione (GSH).

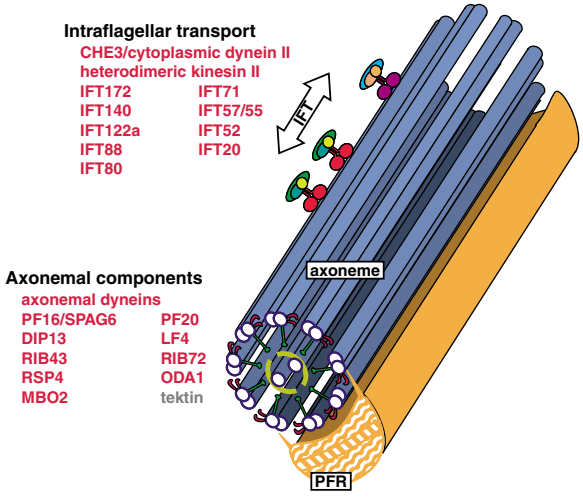

Fig. 4. Conservation of proteins of the flagellum in *T. brucei*, *T. cruzi*, and *L. major*. The figure shows the kinetoplastid flagellum with the axoneme (blue) and the lattice-like paraflagellar rod (PFR), unique to Kinetoplastida and Euglenida (yellow). Flagellar motors are seen attached to the axoneme. Components for which the Tritryps encode one or more homologs are indicated in red text. Those that do not appear to be encoded by the three genomes are indicated in gray text. (IFT, intraflagellar transport).

Trypanothione is synthesized from spermidine and glutathione and subsumes many of the roles of the latter in defending against chemical and oxidant stress. *T. cruzi* can also synthesize or salvage spermine to form the spermine-containing analog of trypanothione. Trivalent arsenical and antimonial drugs form conjugates with trypanothione and/or glutathione (*48*, *49*), and the synthesis of GSH, polyamines, and trypanothione are essential for survival in *T. brucei* (*50*–*52*).

The reactive by-product of metabolism, methylglyoxal, can be converted via the trypanothione-dependent glyoxalase pathway (*53*) to D-lactate. Homologs of glyoxalase I and II were found in *T. cruzi*, whereas *T. brucei* apparently lacks glyoxalase I but does have glyoxalase II (*54*). Unlike many bacteria, none of the parasites contain methylglyoxal synthase.

Trypanosomatids lack catalase and selenium-dependent peroxidases and are unusually dependent on trypanothione-dependent peroxidases for removal of peroxides. Tryparedoxins are homologs of thioredoxins, and all species contain both redox proteins. Thioredoxin reductase is absent, and all Tritryp peroxidases are coupled to trypanothione and trypanothione reductase, a validated drug target.

Purine salvage and pyrimidine synthesis. Several studies have shown that the trypanosomatids are incapable of de novo purine synthesis. This is now confirmed by the absence of 9 of the 10 genes required to make inosine monophosphate (IMP) from phosphoribosyl pyrophosphate (PRPP). Adenylosuccinate lyase is present, but this plays a role in purine salvage converting IMP to AMP. Present also are a large number of nucleobase and nucleoside transporters (*55*), (table S9) numerous enzymes for the interconversion of purine bases, and nucleosides and enzymes to synthesize pyrimidines de novo.

Lipid and sterol metabolism. Sterol metabolism has attracted considerable interest as a drug target in *T. cruzi* and *L. major* (*56*). Except for bloodstream *T. brucei*, which obtains cholesterol from the host, these parasites synthesize ergosterol and are susceptible to antifungal agents that inhibit this pathway. Candidate genes for most of ergosterol biosynthesis are present in all three parasites. Intermediates of this pathway, namely farnesyl- and geranyl-pyrophoshosphate, are also precursors for dolichols and the side chain of ubiquinone. *L. major* is capable of synthesizing the aromatic ring of ubiquinone from acetate, parahydroxybenzoate being an important intermediate. In this behavior it resembles prokaryotes.

The Tritryps seem to be capable of oxidizing fatty acids via β-oxidation in two separate celular compartments: glycosomes and mitochondria. This contrasts with yeasts and plants, where β-oxidation of fatty acids takes place exclusively in peroxisomes. In addition, the three trypanosomatids are capable of fatty acid biosynthesis.

Summary and concluding remarks. After more than a century of research aimed at understanding, controlling, and treating African trypanosomiasis, the genome sequence represents a major step in this process. It will not provide immediate relief to those suffering from trypanosomiasis. Instead, it will accelerate trypanosomiasis research throughout the scientific community. Through early data release before completion of the sequencing, the Tritryp genome projects have already allowed scientists to identify many new drug targets and pathways (e.g., GPI biosynthesis and isoprenoid metabolism) and have provided a framework for functional studies. Because about 50% of the genes of all three parasites have no known function, many more biochemical pathways and structural functions await discovery.

References and Notes

1. *The World Health Report 2004: Changing History* (World Health Organisation, Geneva, 2004).
2. B. Wickstead, K. Ersfeld, K. Gull, *Genome Res.* **14**, 1014 (2004).
3. S. E. Melville, V. Leech, C. S. Gerrard, A. Tait, J. M. Blackwell, *Mol. Biochem. Parasitol.* **94**, 155 (1998).
4. F. Bringaud *et al.*, *Eukaryot. Cell* **1**, 137 (2002).
5. Materials and methods are available as supporting material on *Science* Online.
6. N. Hall *et al.*, *Nucleic Acids Res.* **31**, 4864 (2003).
7. N. M. El-Sayed *et al.*, *Nucleic Acids Res.* **31**, 4856 (2003).
8. A. C. Ivens *et al.*, *Science* **309**, 436 (2005).
9. N. M. El-Sayed *et al.*, *Science* **309**, 404 (2005).
10. P. Borst, *Cell* **109**, 5 (2002).
11. E. Pays, L. Vanhamme, D. Perez-Morga, *Curr. Opin. Microbiol.* **7**, 369 (2004).
12. L. H. Van der Ploeg *et al.*, *Nucleic Acids Res.* **10**, 5905 (1982).
13. C. M. Turner, J. D. Barry, *Parasitology* **99**, 67 (1989).
14. A. Y. Liu, L. H. Van der Ploeg, F. A. Rijsewijk, P. Borst, *J. Mol. Biol.* **167**, 57 (1983).
15. A. Craig, A. Scherf, Eds., *Antigenic Variation* (Academic Press, Amsterdam, 2003), pp. 464.
16. C. Roth, F. Bringaud, R. E. Layden, T. Baltz, H. Eisen, *Proc. Natl. Acad. Sci. U.S.A.* **86**, 9375 (1989).
17. S. M. Kamper, A. F. Barbet, *Mol. Biochem. Parasitol.* **53**, 33 (1992).
18. I. R. Arkhipova, H. G. Morrison, *Proc. Natl. Acad. Sci. U.S.A.* **98**, 14497 (2001).
19. J. D. Barry, M. L. Ginger, P. Burton, R. McCulloch, *Int. J. Parasitol.* **33**, 29 (2003).
20. H. H. Kazazian Jr., *Science* **303**, 1626 (2004).
21. M. Carrington *et al.*, *J. Mol. Biol.* **221**, 823 (1991).
22. L. Vanhamme *et al.*, *Nature* **422**, 83 (2003).
23. M. J. Gardner *et al.*, *Nature* **419**, 498 (2002).
24. M. Becker *et al.*, *Genome Res.* **14**, 2319 (2004).
25. P. Overath, M. Engstler, *Mol. Microbiol.* **53**, 735 (2004).
26. M. C. Field, M. Carrington, *Traffic* **5**, 905 (2004).
27. J. P. Ackers, V. Dhir, M. C. Field, *Mol. Biochem. Parasitol.* **141**, 89 (2005).
28. H. P. Price, C. Panethymitaki, D. Goulding, D. F. Smith, *J. Cell Sci.* **118**, 831 (2005).
29. E. Ogbadoyi, K. Ersfeld, D. Robinson, T. Sherwin, K. Gull, *Chromosoma* **108**, 501 (2000).
30. J. E. Lowell, G. A. Cross, *J. Cell Sci.* **117**, 5937 (2004).
31. J. A. Garcia-Salcedo *et al.*, *EMBO J.* **23**, 780 (2004).
32. J. A. Atwood III *et al.*, *Science* **309**, 473 (2005).
33. J. J. Cazzulo, *FASEB J.* **6**, 3153 (1992).
34. S. Besteiro *et al.*, *J. Biol. Chem.* **277**, 38001 (2002).
35. J. J. Van Hellemond, F. R. Opperdoes, A. G. Tielens, *Proc. Natl. Acad. Sci. U.S.A.* **95**, 3036 (1998).
36. C. Nihei, Y. Fukai, K. Kita, *Biochim. Biophys. Acta* **1587**, 234 (2002).
37. M. A. Ferguson, *Proc. Natl. Acad. Sci. U.S.A.* **97**, 10673 (2000).
38. J. R. Roper, M. L. Guther, K. G. Milne, M. A. Ferguson, *Proc. Natl. Acad. Sci. U.S.A.* **99**, 5884 (2002).
39. M. E. Drew *et al.*, *Mol. Cell. Biol.* **15**, 5508 (1995).
40. R. F. Steiger, E. Steiger, *J. Protozool.* **24**, 437 (1977).
41. A. El Sawalhy, J. R. Seed, J. E. Hall, H. El Attar, *J. Parasitol.* **84**, 469 (1998).
42. V. Gazit, R. Ben-Abraham, C. G. Pick, Y. Katz, *Behav. Brain Res.* **143**, 1 (2003).
43. M. L. Ginger, M. L. Chance, I. H. Sadler, L. J. Goad, *J. Biol. Chem.* **276**, 11674 (2001).
44. D. J. Linstead, R. A. Klein, G. A. Cross, *J. Gen. Microbiol.* **101**, 243 (1977).
45. D. J. Steenkamp, *Antioxid. Redox Signal.* **4**, 105 (2002).
46. S. C. Roberts *et al.*, *J. Biol. Chem.* **279**, 23668 (2004).
47. C. A. Pereira, G. D. Alonso, H. N. Torres, M. M. Flawia, *J. Eukaryot. Microbiol.* **49**, 82 (2002).
48. A. H. Fairlamb, *Trends Parasitol.* **19**, 488 (2003).
49. S. Wyllie, M. L. Cunningham, A. H. Fairlamb, *J. Biol. Chem.* **279**, 39925 (2004).
50. T. T. Huynh, V. T. Huynh, M. A. Harmon, M. A. Phillips, *J. Biol. Chem.* **278**, 39794 (2003).
51. F. Li, S. B. Hua, C. C. Wang, K. M. Gottesdiener, *Exp. Parasitol.* **88**, 255 (1998).
52. M. A. Comini *et al.*, *Free Radic. Biol. Med.* **36**, 1289 (2004).
53. T. J. Vickers, N. Greig, A. H. Fairlamb, *Proc. Natl. Acad. Sci. U.S.A.* **101**, 13186 (2004).
54. T. Irsch, R. L. Krauth-Siegel, *J. Biol. Chem.* **279**, 22209 (2004).
55. S. M. Landfear, B. Ullman, N. S. Carter, M. A. Sanchez, *Eukaryot. Cell* **3**, 245 (2004).
56. J. A. Urbina, R. Docampo, *Trends Parasitol.* **19**, 495 (2003).
57. We thank our colleagues at the Wellcome Trust Sanger Institute and the Institute for Genomic Research, colleagues in the *T. brucei* and Tritryp genome networks, and the Trypanosomatid research community for their support. We also thank K. Stuart, P. Myler, E. Worthey [Seattle Biomedical Research Institute (SBRI)], and B. Andersson (Karolinska Institutet) for helpful discussions of the manuscript and P. Myler and G. Aggarwal (SBRI) for preparation of Plate 3. Funding for this work was provided by the Wellcome Trust and a grant from the National Institute for Allergy and Infectious Diseases (NIAID) to N.M.E.-S. (AI43062). Funding for provision of DNA resources was provided by Wellcome Trust grants to S.E.M. (062513) and C.M.R.T. (062513). Funding for several *T. brucei* genome network and Tritryp genome meetings over the past decade was provided by the Burroughs Wellcome Fund, NIAID, the Wellcome Trust, and the World Health Organisation Special Programme for Research and Training in Tropical Diseases. Correspondence and requests for sequence data should be addressed to M.B. (mb4@sanger.ac.uk) or N.M.E.-S. (nelsayed@tigr.org). Requests for DNA resources should be addressed to S.E.M. (sm160@cam.ac.uk), and requests for updates or amendments to genome annotation should be directed to C.H.-F. (chf@sanger.ac.uk). All data sets and the genome sequence and annotation are available through GeneDB at www.genedb.org. Sequence data have been deposited at DNA Data Bank of Japan/European Molecular Biology Laboratory/GenBank with consecutive accession numbers CP000066 to CP000071 for chromosomes 3 to 8 and project accession numbers AAGZ00000000, AAHA00000000, and AAHB0000000 for the whole-chromosome shotgun projects of chromosomes 9 to 11. The versions of chromosomes 9 to 11 described in this paper are the first versions, AAGZ01000000, AAHA01000000, and AAHB01000000, and unassembled contigs (overlapping contiguous sequences) have accession number CR940345.

Supporting Online Material

www.sciencemag.org/cgi/content/full/309/5733/416/DC1
Materials and Methods
Figs. S1 to S5
Tables S1 to S11
References and Notes

23 March 2005; accepted 22 June 2005
10.1126/science.1112642

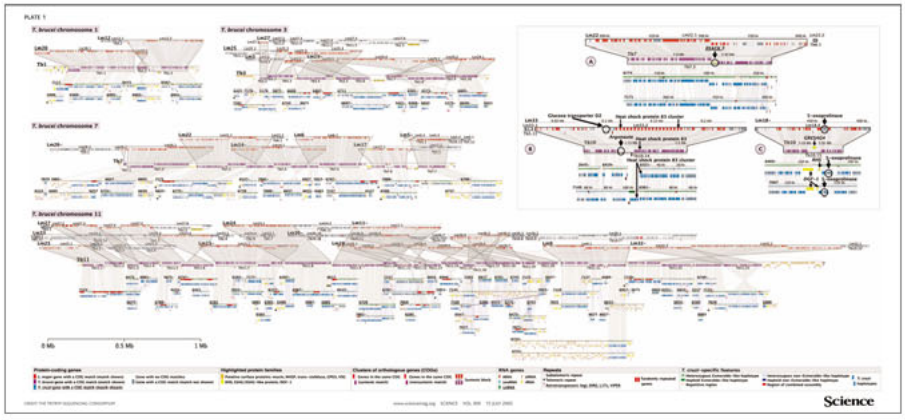
PLATE 1
T. brucei chromosome 1
T. brucei chromosome 3
T. brucei chromosome 7
T. brucei chromosome 11
0 Mb
0.5 Mb
1 Mb
Science

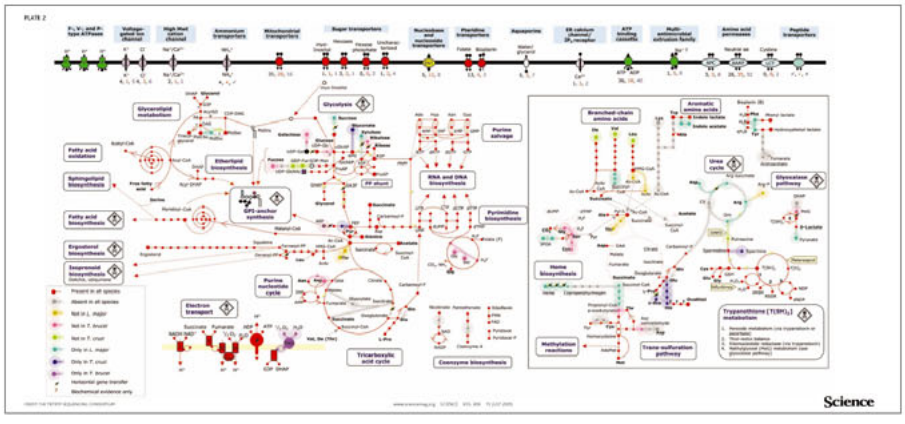
PLATE 2
Glycolysis
Glycerolipid metabolism
Fatty acid oxidation
Sphingolipid biosynthesis
Fatty acid biosynthesis
Ergosterol biosynthesis
Isoprenoid biosynthesis
Etherlipid biosynthesis
GPI-anchor synthesis
Purine salvage
RNA and DNA biosynthesis
Pyrimidine biosynthesis
Purine nucleotide cycle
Electron transport
Tricarboxylic acid cycle
Coenzyme biosynthesis
Branched-chain amino acids
Aromatic amino acids
Urea cycle
Glyoxalase pathway
Heme biosynthesis
Methylation reactions
Trans-sulfuration pathway
Trypanothione (T(SH)2) metabolism
Science

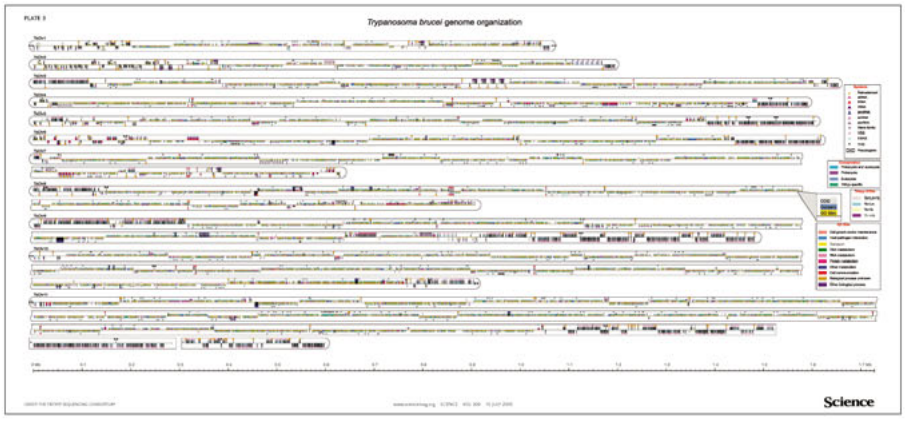
PLATE 3
Trypanosoma brucei genome organization
Science

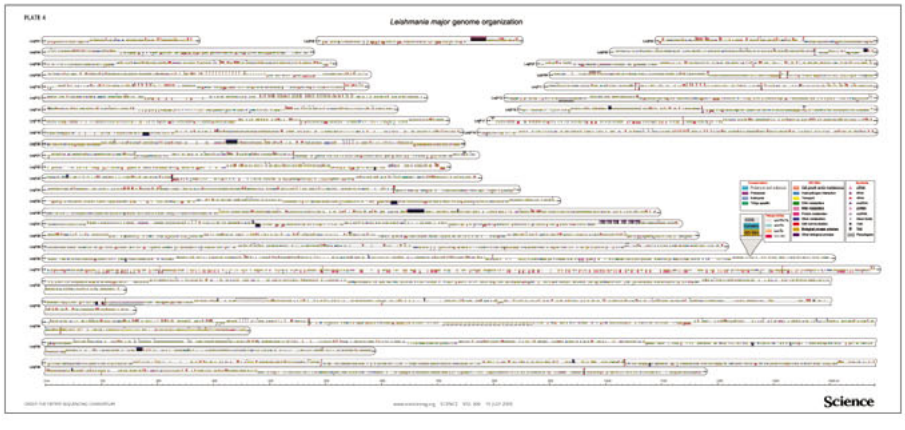
PLATE 4
Leishmania major genome organization
Science

PLATE 1

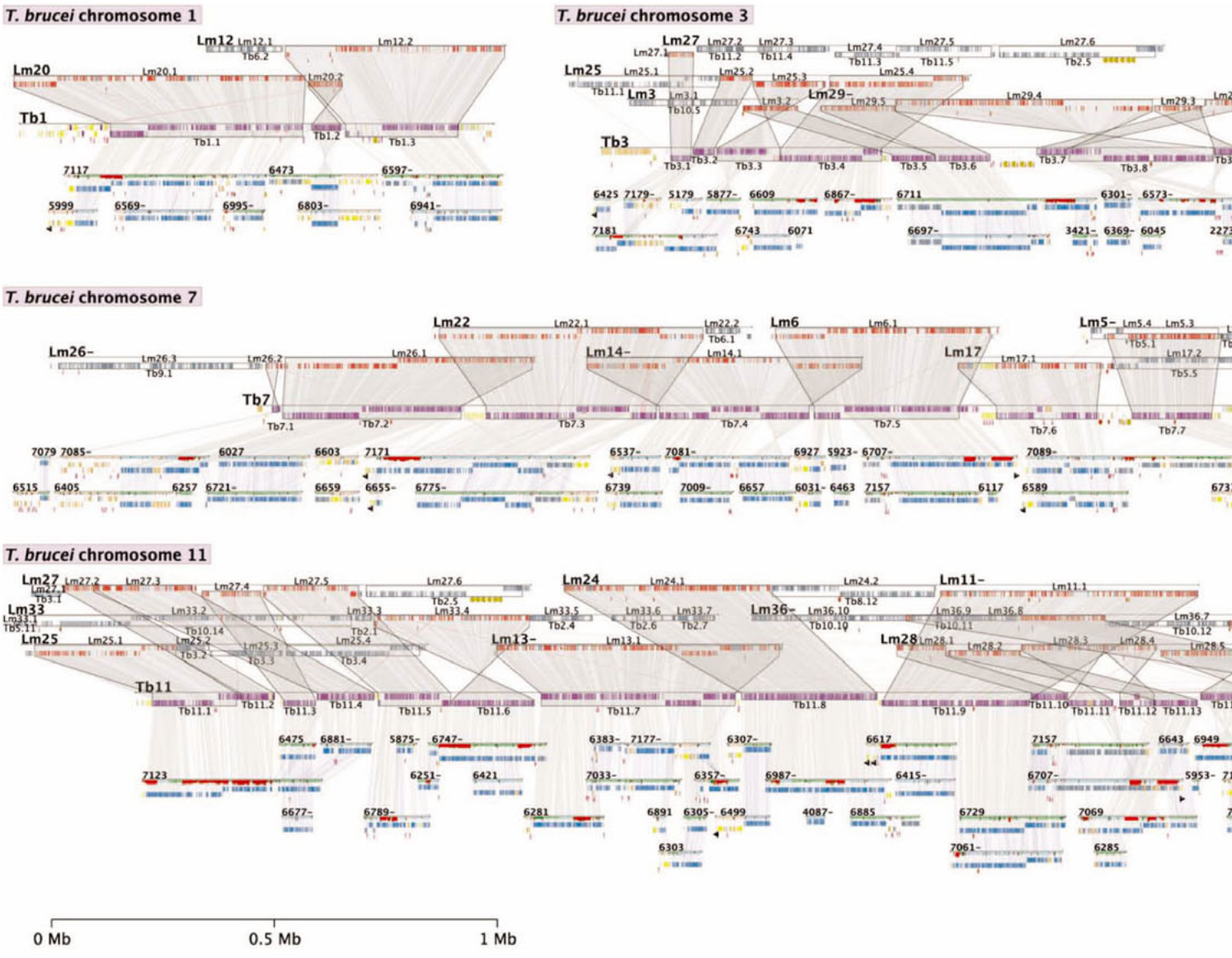

Protein-coding genes	Highlighted protein families	Clusters of orthologous genes (COGs)
L. major gene with a COG match (match shown)	Putative surface proteins: mucin, MASP, trans-sialidase, GP63, VSG	Genes in the same COG (syntenic match)
T. brucei gene with a COG match (match shown)	RHS, ESAG/ESAG-like protein, DGF-1	Genes in the same COG (nonsyntenic match)
T. cruzi gene with a COG match (match shown)		
Gene with no COG matches		
Gene with a COG match (match not shown)		

CREDIT: THE TRITRYP SEQUENCING CONSORTIUM

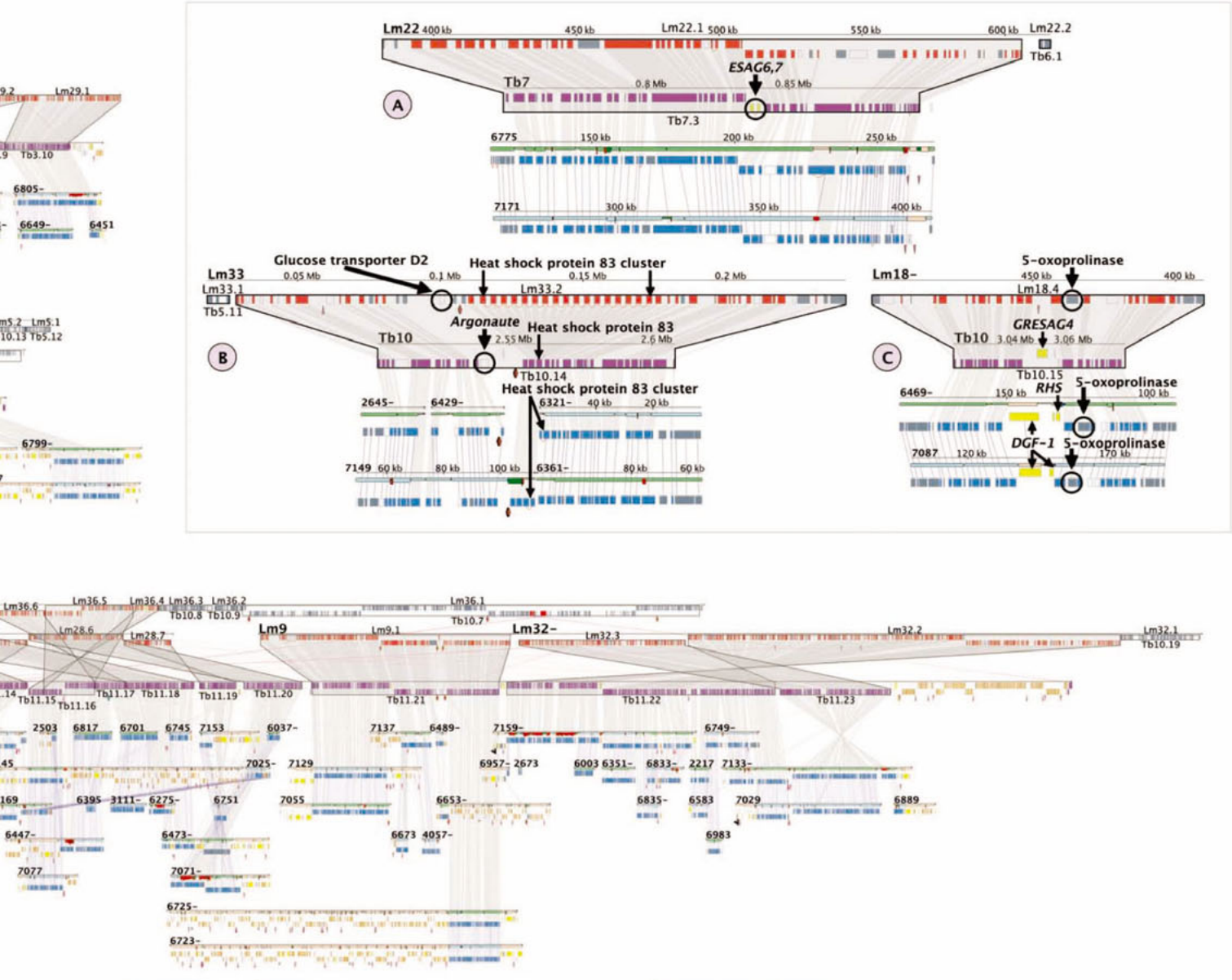
Lm22
Lm22.1
Lm22.2
Tb6.1
ESAG6,7
Tb7
Tb7.3
A
6775
7171
Lm33
Lm33.1
Lm33.2
Tb5.11
Glucose transporter D2
Heat shock protein 83 cluster
Argonaute
Heat shock protein 83
Tb10
Tb10.14
B
Lm18-
Lm18.4
5-oxoprolinase
GRESAG4
C
Tb10.15
RHS
DGF-1
6469-
7087
Lm9
Lm9.1
Lm32-
Lm32.1
Lm32.2
Lm32.3
Tb10.19
Tb11.21
Tb11.22
Tb11.23
RNA genes
tRNA
snoRNA
snRNA
sIRNA
rRNA
Repeats
Subtelomeric repeat
Telomeric repeat
Retrotransposons: ingi, DIRE, L1Tc, VIPER
Tandemly repeated genes
Syntenic block
T. cruzi-specific features
Heterozygous Esmeraldo-like haplotype
Haploid Esmeraldo-like haplotype
Repetitive region
Heterozygous non-Esmeraldo-like haplotype
Haploid non-Esmeraldo-like haplotype
Region of combined assembly
T. cruzi haplotypes

PLATE 2

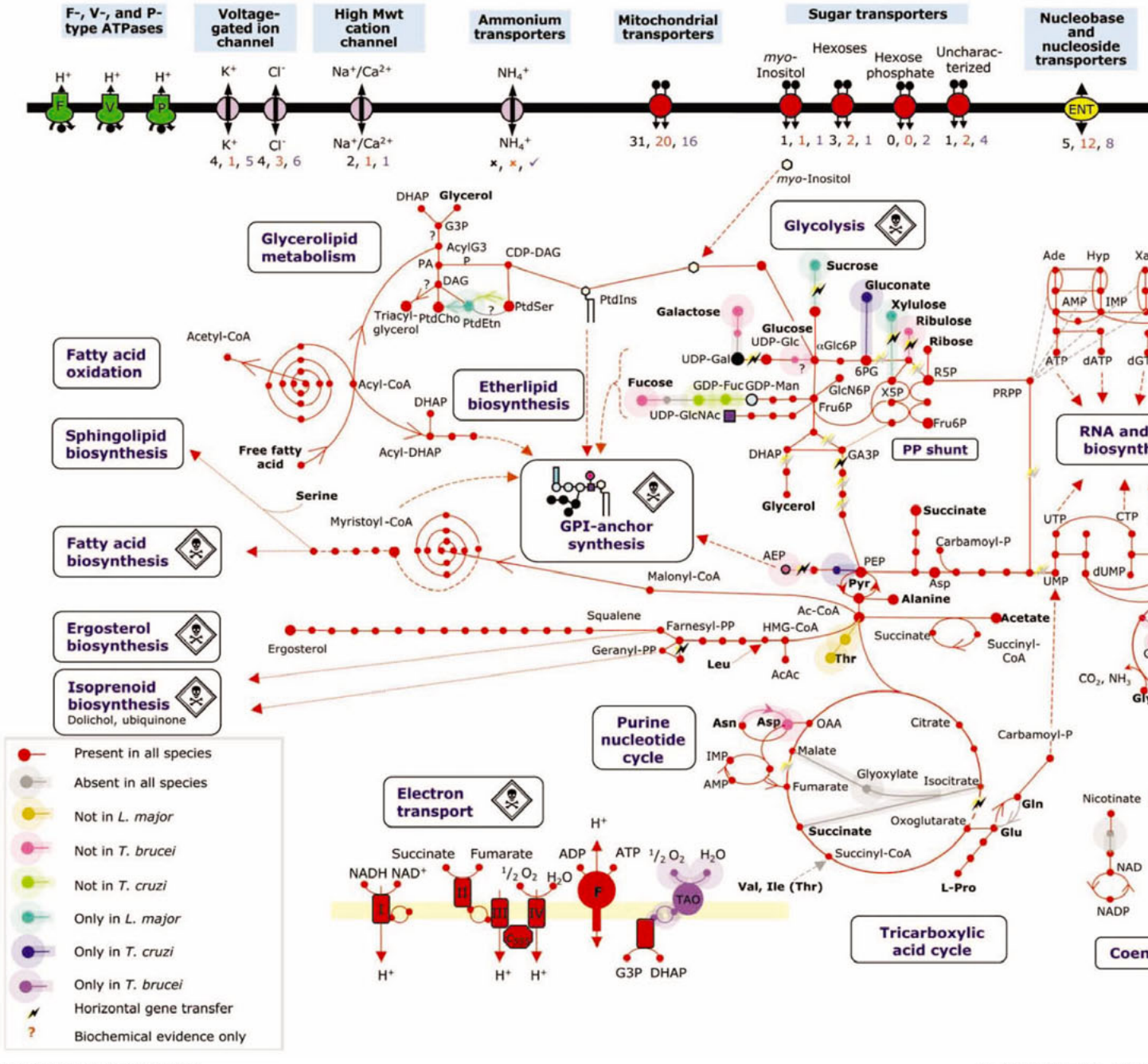

CREDIT: THE TRITRYP SEQUENCING CONSORTIUM

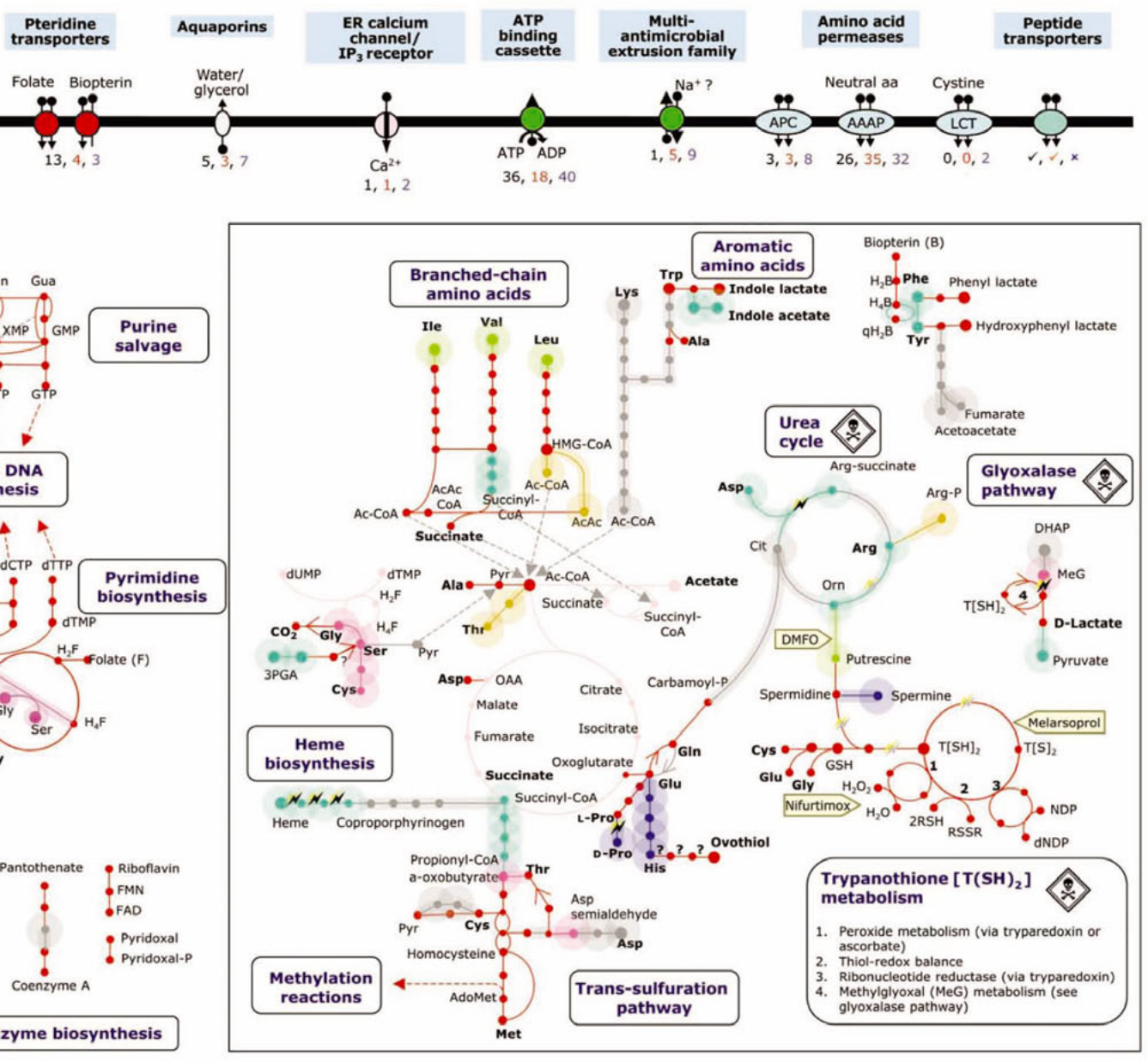
Pteridine transporters
Aquaporins
ER calcium channel/ IP3 receptor
ATP binding cassette
Multi-antimicrobial extrusion family
Amino acid permeases
Peptide transporters
Folate
Biopterin
Water/ glycerol
Na+ ?
Neutral aa
Cystine
APC
AAAP
LCT
13, 4, 3
5, 3, 7
Ca2+
1, 1, 2
ATP ADP
36, 18, 40
1, 5, 9
3, 3, 8
26, 35, 32
0, 0, 2
✓, ✓, ×
Purine salvage
Gua
XMP
GMP
GTP
DNA
esis
Pyrimidine biosynthesis
dCTP
dTTP
dTMP
Folate (F)
Ser
Pantothenate
Riboflavin
FMN
FAD
Pyridoxal
Pyridoxal-P
Coenzyme A
zyme biosynthesis
Branched-chain amino acids
Ile
Val
Leu
HMG-CoA
AcAc CoA
Ac-CoA
Succinyl-CoA
AcAc
Succinate
Aromatic amino acids
Trp
Indole lactate
Indole acetate
Lys
Ala
Biopterin (B)
Phe
Phenyl lactate
Tyr
Hydroxyphenyl lactate
Fumarate
Acetoacetate
Urea cycle
Arg-succinate
Asp
Arg-P
Cit
Arg
Orn
Glyoxalase pathway
DHAP
MeG
T[SH]2
D-Lactate
Pyruvate
DMFO
Putrescine
Spermidine
Spermine
Melarsoprol
T[S]2
Cys
GSH
Glu
Gly
H2O2
H2O
Nifurtimox
2RSH
RSSR
NDP
dNDP
dUMP
dTMP
H2F
Ala
Pyr
Ac-CoA
Acetate
Succinate
Succinyl-CoA
CO2
Gly
H4F
Ser
Thr
3PGA
Cys
Asp
OAA
Citrate
Carbamoyl-P
Malate
Fumarate
Isocitrate
Heme biosynthesis
Oxoglutarate
Gln
Glu
Succinate
Succinyl-CoA
Heme
Coproporphyrinogen
L-Pro
D-Pro
His
Ovothiol
Propionyl-CoA
a-oxobutyrate
Thr
Asp semialdehyde
Pyr
Cys
Asp
Homocysteine
Methylation reactions
AdoMet
Met
Trans-sulfuration pathway
Trypanothione [T(SH)2] metabolism
1. Peroxide metabolism (via tryparedoxin or ascorbate)
2. Thiol-redox balance
3. Ribonucleotide reductase (via tryparedoxin)
4. Methylglyoxal (MeG) metabolism (see glyoxalase pathway)

PLATE 3

Trypanosoma brucei ge

CREDIT: THE TRITRYP SEQUENCING CONSORTIUM

enome organization

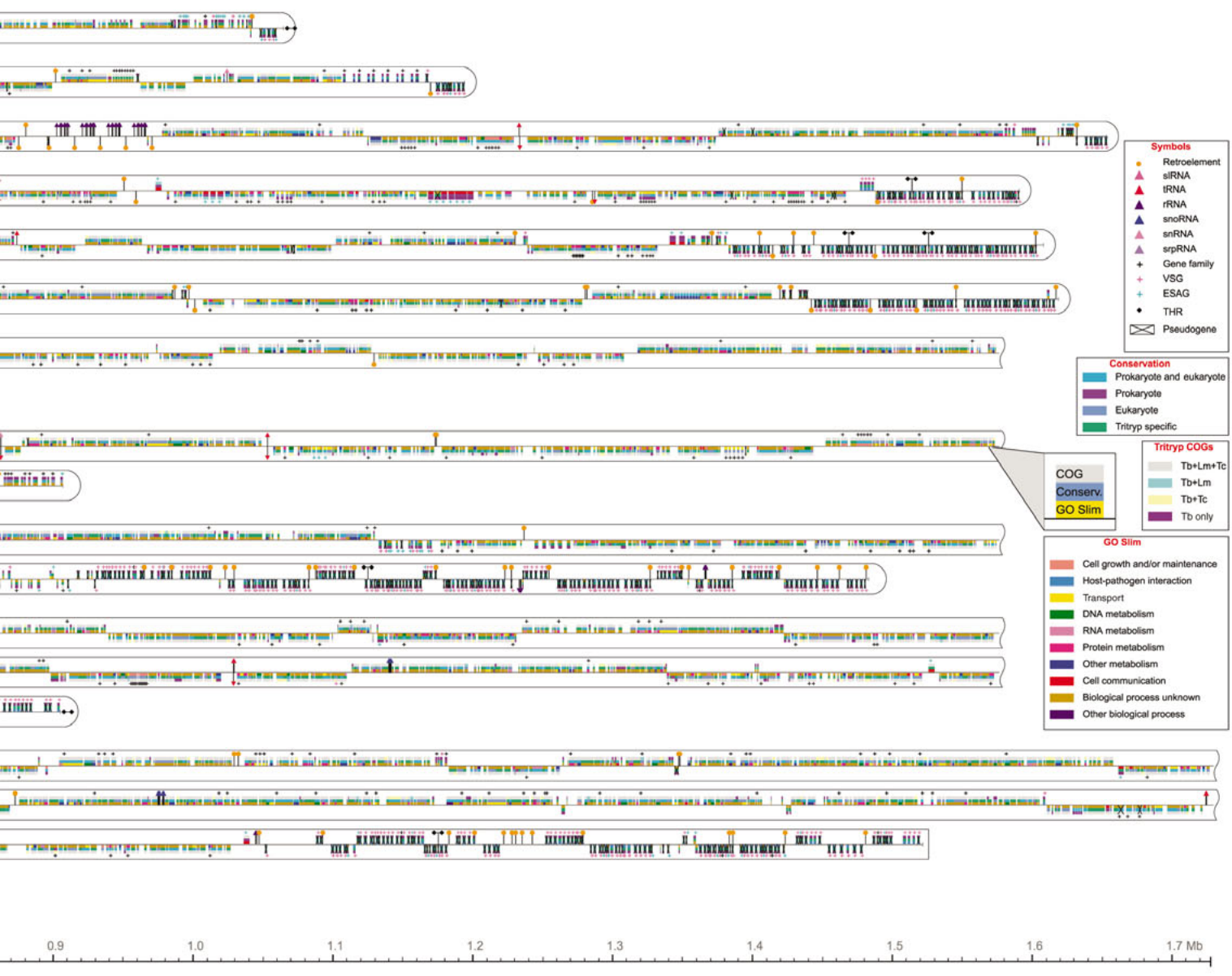

PLATE 4

Leishmania major

CREDIT: THE TRITRYP SEQUENCING CONSORTIUM

genome organization

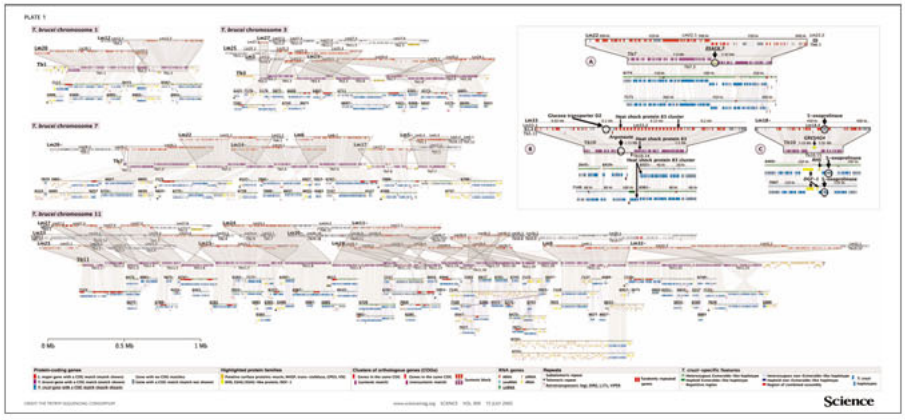
PLATE 1
T. brucei chromosome 1
T. brucei chromosome 3
T. brucei chromosome 7
T. brucei chromosome 11
0 Mb
0.5 Mb
1 Mb
Science

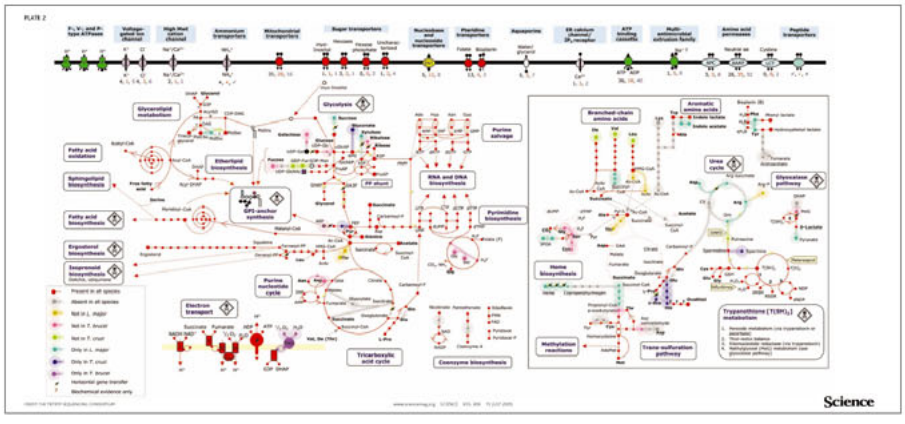
PLATE 2
Glycolysis
Glycerolipid metabolism
Fatty acid oxidation
Sphingolipid biosynthesis
Fatty acid biosynthesis
Ergosterol biosynthesis
Isoprenoid biosynthesis
Etherlipid biosynthesis
GPI-anchor synthesis
Purine salvage
RNA and DNA biosynthesis
Pyrimidine biosynthesis
Purine nucleotide cycle
Electron transport
Tricarboxylic acid cycle
Coenzyme biosynthesis
Branched-chain amino acids
Aromatic amino acids
Urea cycle
Glyoxalase pathway
Heme biosynthesis
Methylation reactions
Trans-sulfuration pathway
Trypanothione (T(SH)2) metabolism
Science

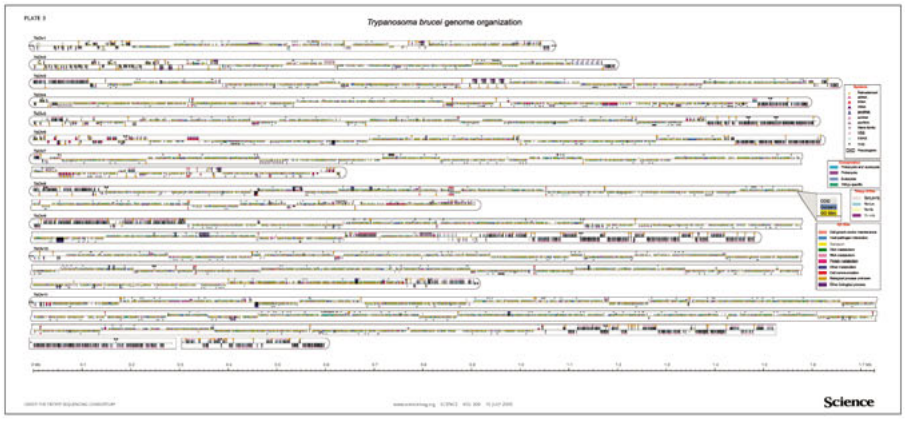
PLATE 3
Trypanosoma brucei genome organization
Science

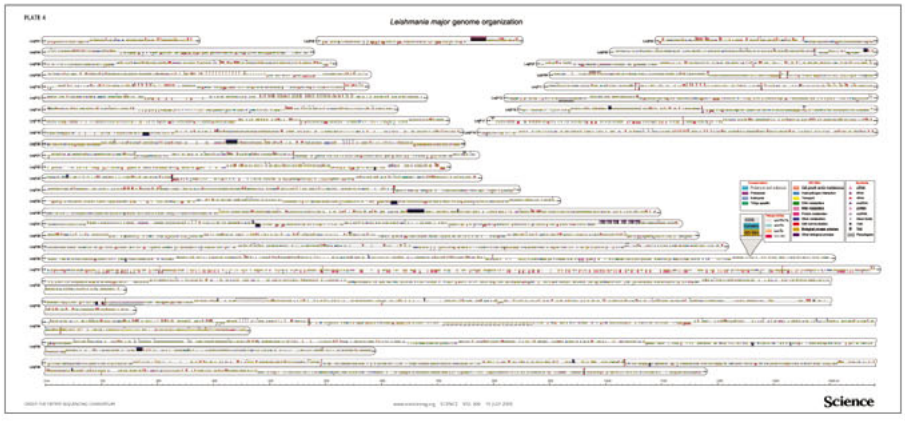
PLATE 4
Leishmania major genome organization
Science

Plate 1. Comparative architecture of Tritryp chromosomes. Clusters of orthologous genes (COGs) were computed between *T. brucei* (Tb), *T. cruzi* (Tc), and *L. major* (Lm) proteomes and used to define blocks of conserved synteny between Tb and Lm genomes. Tb chromosomes 1, 3, 7, and 11 were selected to illustrate the general organization of each of the three genomes and their notable degree of synteny. El-Sayed *et al*. (page 404) show a complete set of comparative maps in fig. S3, A to K. Lm chromosomes and Tc scaffolds that share at least five COGs with an individual Tb chromosome are displayed above and below the selected Tb chromosome, respectively. They are represented in their forward or reverse (minus sign) orientation. Each genome presents a comprehensive set of annotated genetic elements, which includes protein-coding genes with their pseudogenes, structural RNA genes, and retrotransposons. Gray and pink lines link genes that belong to the same COG, with the exception of Lm- and Tc-specific two-way COGs that are not shown. Corresponding Lm, Tb, and Tc genes are colored in red, purple, and blue, respectively. Genes colored in gray belong to COGs that are not shown. (Other COG members are not on the scaffolds presented on the figure and/or the genes belong to Lm- and Tc-specific COGs.) Genes colored in white represent singletons. Synteny block nomenclature is the same as in Fig. 2 of El-Sayed *et al*. (page 404). The inset (**top**, **right**) shows three close-ups (**A** to **C**) of localized chromosome rearrangements discussed in El-Sayed *et al*. (page 404). Tc CL-Brener contiguous regions were classified by haplotype as discussed in El-Sayed *et al*. (page 409). Tc scaffolds are labeled with the last four digits of a unique identifier (10470535xxxx).

Plate 2. An overview of metabolism and transport in *T. brucei*, *T. cruzi*, and *L. major*. Pathways of central metabolism are shown with differences between species highlighted. Possible cases of horizontal transfer from prokaryotes into the Tritryp lineage are indicated with lightning-bolt symbols; cases (listed in Berriman *et al*., table S11) supported by the strongest phylogenetic tree-based evidence (Berriman *et al*., supporting online material) are distinguished by darker symbols. Shown below each transporter symbol are the numbers of genes encoding them in each of the Tritryp genomes (*L. major*, black text; *T. brucei*, red; *T. cruzi*, blue). Amino acid metabolism is shown in the inset box. A question mark indicates where biochemical evidence for a pathway exists, but a candidate gene was not identified. The tricarboxylic acid cycle is included in the inset diagram as a common reference pathway for orientation purposes. The skull-and-bones symbol represents drug targets. Abbreviations used in the figure: 3PGA, 3-phosphoglycerate; AcAc, acetoacetate; Ac-CoA, acetyl coenzyme A; Ade, adenine; AEP, aminoethyl phosphonate; DAG, diacylglycerol; DHAP, dihydroxyacetone phosphate; Fuc, fucose; Fru6P, fructose 6-phosphate; G3P, glycerol 3-phosphate; GA3P, glyceraldehyde 3-phosphate; Gal, galactose; Glc, glucose; GlcN6P, glucosamine 6-phosphate; GlcNAc, *N*-acetyl D-glucosamine; GSH, reduced glutathione; Gua, guanine; HMG-CoA, 3-hydroxy-3-methylglutaryl CoA; Hyp, hypoxanthine; IMP, inosine monophosphate; Man, mannose; MeG, methylglyoxal; OAA, oxaloacetic acid; PA, phosphatidate; PEP, phosphoenol pyruvate; PP, pyrophosphate; PRPP, phosphoribosyl pyrophosphate; PtdCho, phosphatidylcholine; PtdEtn, phosphatidylethanolamine; PtdIns, phosphatidylinositol; PtdSer, phosphatidylserine; Pyr, pyruvate; R5P, ribose 5-phosphate; TAO, trypanosome alternative oxidase; X5P, xylulose 5-phosphate; and Xan, xanthine.

Plates 3 and 4. Gene organization of *T. brucei* and *L. major*. The schematic representations of the 11 *T. brucei* megabase chromosomes (TbChr1 to TbChr11) and 36 *L. major* chromosomes (LmjF01 to LmjF36) show protein-coding genes depicted as rectangles drawn proportional to their length (pseudogenes have an "x" through the rectangle), and their coding strand is indicated by their position above (top strand) or below (bottom strand) the central line. The three rows of colored rectangles represent (from outermost to innermost) orthology between the three trypanosomatid genomes (Tritryp COGs), sequence similarity based on BlastP analysis of the *T. brucei* and *L. major* predicted proteins with those in prokaryotes and/or eukaryotes (Conservation), and high-level gene ontology biological process assignment (GO Slim). RNA-coding genes and retroelements (*T. brucei* only) are depicted by symbols as detailed. Genes that are members of large (>10) families are indicated by a "+" above or below the respective rectangles, with variant surface glycoprotein genes (VSGs) and expression site–associated genes (ESAGs) shown in different colors in *T. brucei*. Locations with three or more tandem copies of the telomeric hexamer repeats (THR) are indicated in both genomes, and telomere-associated sequences (TAS) are indicated in *L. major* only. A scale in megabases (Mb) (*T. brucei*) or kilobases (kb) (*L. major*) is shown at the bottom of each plate. For more information, see http://apps.sbri.org/genemap/.

RESEARCH ARTICLE

The Genome of the Kinetoplastid Parasite, *Leishmania major*

Alasdair C. Ivens,[1]* Christopher S. Peacock,[1] Elizabeth A. Worthey,[2] Lee Murphy,[1] Gautam Aggarwal,[2] Matthew Berriman,[1] Ellen Sisk,[2] Marie-Adele Rajandream,[1] Ellen Adlem,[1] Rita Aert,[3] Atashi Anupama,[2] Zina Apostolou,[4] Philip Attipoe,[2] Nathalie Bason,[1] Christopher Bauser,[5] Alfred Beck,[6] Stephen M. Beverley,[7] Gabriella Bianchettin,[8] Katja Borzym,[6] Gordana Bothe,[5] Carlo V. Bruschi,[8,9] Matt Collins,[1] Eithon Cadag,[2] Laura Ciarloni,[8] Christine Clayton,[10] Richard M. R. Coulson,[11] Ann Cronin,[1] Angela K. Cruz,[12] Robert M. Davies,[1] Javier De Gaudenzi,[13] Deborah E. Dobson,[7] Andreas Duesterhoeft,[14] Gholam Fazelina,[2] Nigel Fosker,[1] Alberto Carlos Frasch,[13] Audrey Fraser,[1] Monika Fuchs,[4] Claudia Gabel,[4] Arlette Goble,[1] André Goffeau,[15] David Harris,[1] Christiane Hertz-Fowler,[1] Helmut Hilbert,[14] David Horn,[16] Yiting Huang,[2] Sven Klages,[6] Andrew Knights,[1] Michael Kube,[6] Natasha Larke,[1] Lyudmila Litvin,[2] Angela Lord,[1] Tin Louie,[2] Marco Marra,[17] David Masuy,[15] Keith Matthews,[18] Shulamit Michaeli,[19] Jeremy C. Mottram,[20] Silke Müller-Auer,[4] Heather Munden,[2] Siri Nelson,[2] Halina Norbertczak,[1] Karen Oliver,[1] Susan O'Neil,[1] Martin Pentony,[2] Thomas M. Pohl,[5] Claire Price,[1] Bénédicte Purnelle,[15] Michael A. Quail,[1] Ester Rabbinowitsch,[1] Richard Reinhardt,[6] Michael Rieger,[4] Joel Rinta,[2] Johan Robben,[3] Laura Robertson,[2] Jeronimo C. Ruiz,[12] Simon Rutter,[1] David Saunders,[1] Melanie Schäfer,[4] Jacquie Schein,[17] David C. Schwartz,[21] Kathy Seeger,[1] Amber Seyler,[2] Sarah Sharp,[1] Heesun Shin,[17] Dhileep Sivam,[2] Rob Squares,[1] Steve Squares,[1] Valentina Tosato,[8] Christy Vogt,[2] Guido Volckaert,[3] Rolf Wambutt,[22] Tim Warren,[1] Holger Wedler,[14] John Woodward,[1] Shiguo Zhou,[21] Wolfgang Zimmermann,[22] Deborah F. Smith,[23] Jenefer M. Blackwell,[24] Kenneth D. Stuart,[2,25] Bart Barrell,[1] Peter J. Myler[2,25,26]*

Leishmania species cause a spectrum of human diseases in tropical and subtropical regions of the world. We have sequenced the 36 chromosomes of the 32.8-megabase haploid genome of *Leishmania major* (Friedlin strain) and predict 911 RNA genes, 39 pseudogenes, and 8272 protein-coding genes, of which 36% can be ascribed a putative function. These include genes involved in host-pathogen interactions, such as proteolytic enzymes, and extensive machinery for synthesis of complex surface glycoconjugates. The organization of protein-coding genes into long, strand-specific, polycistronic clusters and lack of general transcription factors in the *L. major*, *Trypanosoma brucei*, and *Trypanosoma cruzi* (Tritryp) genomes suggest that the mechanisms regulating RNA polymerase II–directed transcription are distinct from those operating in other eukaryotes, although the trypanosomatids appear capable of chromatin remodeling. Abundant RNA-binding proteins are encoded in the Tritryp genomes, consistent with active posttranscriptional regulation of gene expression.

Infection with pathogenic *Leishmania* results in a spectrum of human diseases, termed the leishmaniases, with an annual incidence of 2 million cases in 88 countries (*1*). *Leishmania* parasites are transmitted by sand flies as proliferative promastigotes, which differentiate into nondividing metacyclic forms before inoculation into the vertebrate host and phagocytosis by macrophages. The metacyclics subsequently differentiate into amastigotes, which proliferate in the phagolysosome, leading to macrophage lysis and serial infection of other macrophages (*2*). The outcome of infection is determined by the infecting species, host genetic factors, and the immune response.

Old World *Leishmania* (*L. donovani* and *L. major* groups) have 36 chromosome pairs (0.28 to 2.8 Mb) (*3*), whereas New World species have 34 or 35, with chromosomes 8+29 and 20+36 fused in the *L. mexicana* group and 20+34 in the *L. braziliensis* group (*4*). Gene order and sequence are highly conserved among the ~30 *Leishmania* species (*5*). The genome sequence of *L. major* MHOM/IL/81/Friedlin was determined on a chromosome-by-chromosome basis. Here we present the structure and content of the *L. major* genome, with an emphasis on fundamental molecular processes such as chromatin remodeling, transcription, RNA processing, translation, posttranslational modification, and protein turnover. We also discuss the synthesis of complex surface glycoconjugates that are characteristic of *Leishmania* species and essential at the host-parasite interface. Discussion of cytoskeleton, metabolism, and transport can be found in the accompanying description of the *Trypanosoma brucei* genome (*6*), while signaling pathways, DNA repair, recombination, and replication are discussed in the *Trypanosoma cruzi* article (*7*).

Genome structure and content. The 32,816,678–base pairs (bp) in the current assembly (version 5.2) were obtained by shotgun sequencing large-insert clones and purified chromosomal DNA. A single contiguous sequence was generated for each of the 36 chromosomes (Table 1, Plate 4, and table S1), although the "right" end of chromosome 8 lacks a small amount of subtelomeric sequence and telomeric hexamer repeats. The accuracy of sequence assemblies was assessed by comparison to an optical map (*8*), with only a few discrepancies occurring in regions of repetitive sequence. Although the genome is partially aneuploid (*9*) and there are three large-scale allelic differences (table S1), there are very few (<0.1%) sequence polymorphisms, contrasting notably with the genomes of *T. brucei* (*6*) and *T. cruzi* (*7*).

Analysis of the *L. major* sequence using several algorithms (*10*) predicts 911 RNA genes, 39 pseudogenes, and 8272 protein-coding genes (Table 1), of which 3083 cluster into 662 putative families of related genes (table S2). Most of the smaller (<10 members) gene families appear to have arisen from tandem gene duplication, whereas most members of larger (>10 members) families have multiple loci containing single genes and/or tandem arrays (Table 2); many of the latter contain *Leishmania*-specific genes.

L. major telomeres are heterogeneous in structure and quite distinct from those in *T. brucei* and *T. cruzi* (*11*). The extremity of each *L. major* chromosome contains the tripartite "repeated-repeat" structure previously reported (*12*). Six telomeres contain 0.7 to 25 kb of the *Leishmania* subtelomeric repeat (LST-R) sequences (*9*) between the TAS region and the first gene. Five additional groups of telomeres share varying amounts of sequence, including two cases (chromosome 17 and chromosome 10) in which the ends of a single

chromosome contain the same subtelomeric sequence.

Most *L. major* genes have orthologs in the *T. brucei* and *T. cruzi* genomes (*11*); however, 910 *L. major* genes have no orthologs in the other two Tritryp genomes, 74 orthologous groups contain only *L. major* and *T. brucei* genes, and 482 orthologous groups contain genes from only *L. major* and *T. cruzi*. These "*Leishmania*-restricted" genes are randomly distributed in the genome with respect to relative chromosomal position or distance from the telomere, although some are adjacent to strand-switch regions (see below) and synteny break points (*11*). Although some *Leishmania*-restricted genes are responsible for key metabolic differences between *Leishmania* and *T. brucei* and *T. cruzi* (e.g., certain peptidases, transporters, and glycoconjugate biosynthesis components), most (68%) have unknown functions. Of particular interest, however, are two closely related genes (*LmjF33.1740* and *LmjF33.1750*), whose predicted proteins both contain a macrophage migration inhibition factor (MIF) domain and show 30 to 40% identity to MIF homologs from several other organisms (including other *Leishmania* species). The *L. major* MIFs are predicted to retain the tautomerase activity found in other species, but lack the thiol oxidoreductase activity found in higher eukaryotes. Phylogenetic analysis places the *Leishmania* MIF genes into a bacterial clade (fig. S1). Human MIF has been shown to activate macrophages to kill *Leishmania* parasites via a T helper cell 1 (T_H1)–type pathway (*13*); the MIF homolog in the filarial worm, *Brugia malayi*, directs macrophages to a T_H2 pathway (*14*). Thus, it is tempting to speculate that *Leishmania* MIF may similarly modulate the host macrophage response and promote parasite survival.

RNA genes. RNAs participate directly in several cellular processes, including DNA replication (lagging-strand primers and telomerase RNA), splicing [spliced leader RNA (slRNA) and small nuclear RNAs (snRNAs)], RNA processing and modification [small nucleolar RNAs (snoRNAs) and ribonuclease P (RNaseP)], translation [ribosomal RNAs (rRNAs) and transfer RNAs (tRNAs)], translation regulation (microRNA and antisense RNA), and protein translocation across membranes [signal recognition particle (SRP) or 7slRNA]. Although all three genomes encode very similar repertoires of RNA genes, their organization differs between *L. major* and the two *Trypanosoma* species. For example, the 28*S*, 18*S*, and 5.8*S* rRNA genes occur as a single large tandem array in *L. major*, but in dispersed loci in several different chromosomes in *T. brucei* and *T. cruzi*. The 5*S* rRNA genes are found at 11 different loci on several chromosomes in *L. major*, but in a single tandem array in *T. brucei* and *T. cruzi*.

All three Tritryp genomes encode tRNAs with 45 of the 61 possible anticodons, but the number of genes and their locations (in numerous loci of up to five genes) differ between species (table S3). Eight of the 16 unrepresented anticodons can be covered by third-position wobble, whereas the others require modification of cognate anticodons. Six snRNAs (U1 to U6) for RNA splicing were found in the three genomes, generally associated with tRNA clusters. SnoRNAs function in 2′-*O*-methylation (C/D snoRNAs) and pseudouridylation (H/ACA snoRNAs) of rRNA, slRNA, and snRNA by formation of guide RNA-target duplexes. In the Tritryp genomes, the snoRNAs are encoded by several hundred genes organized in clusters of tandem repeats of one to five different genes in several loci on a number of different chromosomes (table S3); most occur on the same strand as the adjacent protein-coding genes. All three trypanosomatid genomes have a single gene encoding 7slRNA, located in a 5*S* rRNA/tRNA cluster in *L. major*, and a tRNA/snRNA cluster in *T. brucei* and *T. cruzi*. It has been suggested that a tRNA-like molecule found in the trypanosomatid SRP complex (*15*) provides (in trans) the translation elongation arrest function normally associated with the 7SL RNA Alu domain, which is absent in the Tritryp molecule.

Chromatin remodeling. Trypanosomatids contain multiple copies of the four core (H2A, H2B, H3, and H4) and linker (H1) histone genes, which package chromosomal DNA into nucleosomes in eukaryotes and regulate access by the RNA polymerase transcription complexes. Most of these genes are clustered in discrete single tandem arrays in *T. brucei* and *T. cruzi*, but each of the gene types occurs in two or more separate loci in *L. major*; dispersed single-copy variants are found in all three genomes (table S4). The H2A variant is a homolog of the highly conserved H2A.Z, which protects "active" chromatin from silencing in yeast (*16*). The H2B, H3, and H4 variants appear to be novel, but may have roles in gene silencing, gene expression, DNA repair, and centromere function. Centromeres have been reported in *T. cruzi* (*17*), but no homologs were found in the Tritryps for CenH3, which is required for kinetochore assembly during mitosis. The Tritryp genomes encode a number of enzymes involved in histone modification (table S4) that may influence transcription, replication, repair, and recombination. These include two families of acetyltransferases, at

Table 1. Summary of the *L. major* genome.

Parameter	Number
The genome	
Size (bp)	32,816,678
G+C content (%)	59.7
Chromosomes	36
Sequence contigs	36
Percent coding	47.9
Protein-coding genes	
Genes	8272
Pseudogenes	39
Mean CDS length (bp)	1901
Median CDS length (bp)	1407
G+C content (%)	62.5
Gene density (genes per Mb)	252
*Intergenic regions**	
Mean length (bp)	2045
G+C content (%)	57.3
RNA genes	
tRNA	83
rRNA†	63
slRNA†	63
snRNA	6
snoRNA	695
srpRNA	1

*Region between protein-coding CDS. †The exact number cannot be determined because of misassembly.

[1]Wellcome Trust Sanger Institute, Wellcome Trust Genome Campus, Hinxton, Cambridgeshire CB10 1SA, UK. [2]Seattle Biomedical Research Institute (SBRI), 307 Westlake Avenue North, Seattle, WA 98109–2591, USA. [3]Laboratory of Gene Technology, Katholieke Universiteit Leuven, Kasteelpark Arenberg 21, B-3001 Leuven, Belgium. [4]GENOTYPE GmbH, Angelhofweg 39, D-69259 Wilhelmsfeld, Germany. [5]GATC Biotech AG, Jakob-Stadler-Platz 7, 78467 Konstanz, Germany. [6]Max-Planck-Institut für Molekulare Genetik, Ihnestrasse 73, D-14195, Berlin (Dahlem), Germany. [7]Department of Molecular Microbiology, Washington University School of Medicine, 660 South Euclid Avenue, St. Louis, MO 63110–1093, USA. [8]Genomics Group–Genetics Laboratory, Department of Biology, University of Trieste, P. le Valmaura, 9, I-34148 Trieste, Italy. [9]International Centre for Genetic Engineering and Biotechnology, AREA Science Park–W, Padriciano 99, I-34012 Trieste, Italy. [10]Zentrum für Molekulare Biologie, Im Neueheimer Feld 282, D69120 Heidelberg, Germany. [11]European Molecular Biology Laboratory–European Bioinformatics Institute (EMBL-EBI), Wellcome Trust Genome Campus, Cambridge CB10 1SD, UK. [12]Departamento de Biologia Celular e Molecular e Bioagentes Patogenicos, Faculdade de Medicina de Ribeirao Preto, Universidade de Sao Paulo, Av. Bandeirantes, 3900, CEP 14049–900 Ribeirao Preto, Sao Paulo, Brazil. [13]Instituto de Investigaciones Biotecnologicas (IIB-INTECH), University of San Martin and National Research Council (CONICET), Av. Gral Paz 5445, 1650 Buenos Aires, Argentina. [14]QIAGEN GmbH, QIAGEN Strasse 1, 40724 Hilden, Germany. [15]Unité de Biochimie Physiologique, Institut des Sciences de la Vie, Université Catholique de Louvain, place Croix du Sud, 2/20, 1348 Louvain-la-Neuve, Belgium. [16]London School of Hygiene and Tropical Medicine, Keppel Street, London WC1E 7HT, UK. [17]Genome Sequence Centre, British Columbia Cancer Agency Genome Sciences Centre, 600 West 10th Avenue, Vancouver, BC V5Z-4E6, Canada. [18]Institute for Immunology and Infection Research, University of Edinburgh, The King's Buildings, West Mains Road, Edinburgh EH9 3JT, UK. [19]Faculty of Life Sciences, Bar-Ilan University, Ramat-Gan, 52900 Israel. [20]Wellcome Centre for Molecular Parasitology, University of Glasgow, 56 Dumbarton Road, Glasgow G11 6NU, UK. [21]UW Biotechnology Center, Laboratory for Molecular and Computational Genomics, University of Wisconsin-Madison, 425 Henry Mall, Madison, WI 53706, USA. [22]Agowa GmbH, Glienicker Weg 185, D-12489 Berlin, Germany. [23]Immunology and Infection Unit, Department of Biology, University of York, York YO10 5YW, UK. [24]Cambridge Institute for Medical Research, Wellcome Trust/MRC Building, Hills Road, Cambridge CB2 2XY, UK. [25]Department of Pathobiology, University of Washington, Seattle, WA 98195, USA. [26]Division of Biomedical and Health Informatics, University of Washington, Seattle, WA 98195, USA.

*To whom correspondence should be addressed. E-mail: alicat@sanger.ac.uk (A.C.I.), peter.myler@sbri.org (P.J.M.)

least three families of methyltransferases, and all three known classes of histone deacetylases, at least two of which are essential in *T. brucei* (*18*). Two of the acetyltransferases have putative methyl-lysine–binding chromodomains, implying an association with chromatin methylation. The genomes also encode at least four putative acetyl-lysine–binding bromodomain proteins, one (in *L. major* and *T. cruzi*) with a chromatin-associated CW-type zinc finger. The Tritryp parasites thus possess a range of chromatin-remodeling activities typical of eukaryotes, although there are some notable differences.

Transcription. Little is known about the mechanism of transcription initiation in trypanosomatids, and only a few promoters have been functionally analyzed (*19*). The chromosomes are characterized by their unique arrangement of directional gene clusters (DGCs), previously described in *L. major* (*20*, *21*) and *T. brucei* (*22*, *23*). The full extent of this organization is now evident. The *L. major* genome is organized into 133 clusters of tens to hundreds of protein-coding genes, with unrelated predicted functions, on the same DNA strand (Plate 4). The clusters can span up to 1259 kb and are separated by 0.9- to 14-kb divergent or convergent strand-switch regions, which show an unusual base composition (*24*). Experimental evidence suggests that polycistronic transcription by RNA polymerase II (RNAP II) initiates bidirectionally within the divergent strand-switch regions (*21*, *25*, *26*) and terminates within the convergent strand-switch regions, which often contain tRNA, rRNA, and/or snRNA genes (*26*). Several long DGCs contain intervening tRNA or snRNA genes (which are transcribed by RNAP III), suggesting that they may represent more than one polycistron. At most chromosome ends (55 of 72 for *L. major*), transcription proceeds toward the telomere, and in 12 cases, the DGC closest to the telomere is very short (one to three genes).

Eukaryotic RNAP I, II, and III contain 14, 12, and 17 protein subunits, respectively; in yeast, five shared and six conserved polypeptides are present in all three polymerases, with all other components specific to each complex (*27*, *28*). Tritryps have all the shared and conserved subunits except for ABC10α and A43, but many homologs for RNAP-specific subunits are absent (table S5 and Fig. 1). The Tritryp genomes contain two or three different genes encoding both ABC27 and ABC23, suggesting that these subunits may not be shared by the different RNAP complexes as they are in yeast. Tritryp RPB1 lacks the heptad repeats found in the higher eukaryotic C-terminal domain (*29*). Thus, the Tritryp RNAP I, II, and III components differ appreciably from those in other eukaryotes.

Few potential homologs of RNAP II basal transcription factors found in other eukaryotes could be identified (table S6 and Fig. 1); the three subunits of TFIIH present also function in DNA repair and cell cycle control (*30*). TRF4 (which is related to TATA-box binding protein component of TFIID and TFIIIB) is essential for transcription by all three RNAPs (*31*). Potential homologs of BTF3b, BRF, La antigen, SNAP50, and a trypanosomatid-specific SL RNA promoter-binding factor were identified, along with four genes encoding proteins similar to TFIIS (Fig. 1B), and a SNF2-like DNA helicase (table S6). A systematic search for Pfam domains relevant to gene expression revealed substantially fewer potential transcriptional regulators in the Tritryps than in most other eukaryotes (Fig. 2). By contrast, the Tritryp genomes contain a disproportionately higher number of proteins with CCCH-type zinc finger domains, which are found in RNA-binding proteins (see below). These findings, along with the polycistronic gene organization and paucity of RNAP II initiation sites, are consistent with posttranscriptional control mechanisms being the primary determinants of Tritryp gene expression (*19*).

RNA processing. Trypanosomatid mRNA processing is distinctive: In addition to the trans-splicing of a spliced-leader RNA to the 5′ end of almost all mRNAs, the site of polyadenylation is determined by trans-splicing of the downstream mRNA, rather than by an AAUAAA and downstream G/U-rich tract (*32*). Only four cases of cis-splicing could be identified (table S7). Two have been previously described (*33*, *34*); the two novel examples are both hypothetical proteins that are predicted to be capable of RNA binding. Both cis- and trans-splicing appear to be catalyzed by the Tritryp spliceosome (*35*). All snRNAs (table S4) and most spliceosomal proteins (table S8) were identified, but not all snRNP particle protein components were found. It was possible to identify many putative Tritryp splicing regulatory proteins, including those containing domains for 3′ splice site and branch point recognition factors, as well as several heterogeneous nuclear RNP (hnRNP) and sarcoplasmic reticulum (SR) proteins implicated in splicing and alternative splicing. Thus, it appears that regulation of splicing may have arisen early in eukaryotic evolution.

There are two dissimilar Tritryp poly(A) polymerases, which may have distinct functional roles. Homologs of the cleavage and polyadenylation specificity factor (CPF/CPSF) complexes, conserved between yeast and mammals, are also found in the Tritryps (table S9). However, no homologs of the CstF complex are evident, except for a possible CstF50 homolog. In mammalian cells, CstF50 interacts with the

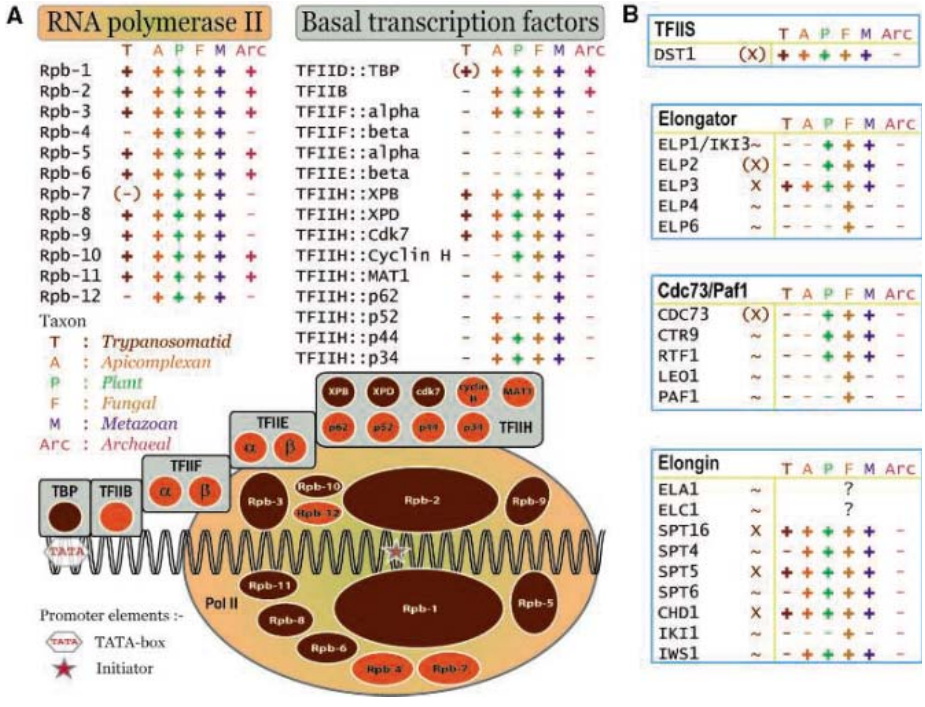

Fig. 1. Trypanosomatid RNA polymerase subunits and transcription factors. (**A**) The TRIBE-MCL (table S2) protein families containing subunits of human RNA polymerase II (Rpb-1 to -12) and basal transcription factors (TBP and TFII-B, -E, -F, -H) are shown as ovals and circles respectively. Families containing Tritryp sequences are colored sepia and indicated by "+" or "(+)" (when the Tritryp gene is not a direct ortholog), whereas families lacking Tritryp sequences are indicated by "−" or "(−)" (when a Tritryp ortholog was detected only by BlastP analysis). Orthologs present in other taxa are indicated by "+". The genomes queried for each taxon are detailed in (*10*). (**B**) Subunits of the yeast TFIIS, Elongator, Cdc73/Paf1, and Elongin complexes are displayed in blue boxes, with the first column of the row indicating whether Tritryp sequences with high "X", weak "(X)", or no "~" similarity were detected. The remaining columns of the row are marked as in (A); "?" indicates that the *S. cerevisiae* sequence is not present in the TAP reference set.

C-terminal domain of RNAP II and provides a link between polyadenylation and transcription initiation/termination. The absence of an RNAP II C-terminal domain may reflect the polycistronic transcription and resultant uncoupling of transcription termination and polyadenylation in the Tritryps.

Degradation of mRNAs is important in regulating trypanosomatid gene expression, and appears to resemble the situation in mammals, in which the exosome plays a dominant role. Tritryps have homologs of the deadenylation complexes, in addition to two poly(A) binding proteins. Although homologs of decapping proteins themselves were not found, a helicase involved in the process, and the exonucleases required to degrade decapped mRNAs, were (table S10). The six pleckstrin homology (PH)-domain exonucleases and three S1-domain proteins of the exosome "core" are conserved in these organisms and are essential in *T. brucei* (*36*). However, exosome-associated proteins that confer RNA processing and degradation specificity have not been found. The existence of nonsense-mediated mRNA decay in trypanosomatids is uncertain, because most of the genes required in yeast have not been identified in the Tritryp genome.

The paucity of Tritryp genes for transcriptional regulation (see above) implies a reliance on posttranscriptional control of gene expression (*19*) and is consistent with the presence of numerous genes for proteins with RNA-binding motifs. The total number of RNA recognition motifs (RRMs) is similar in yeast and Tritryps proteins (e.g., 103 in *T. brucei* versus 70 in *Schizosaccharomyces pombe*), but Tritryps have more small proteins with single RRMs (table S11), which may reflect unique Tritryp functions or cooperation between proteins. The Tritryp genomes encode ~40 proteins with canonical CCCH-type zinc finger RNA-binding domains (Fig. 2 and table S11C), compared to only seven in *Saccharomyces cerevisiae* and 12 in *S. pombe*. Nearly all ~40 Tritryp proteins have only a single CCCH domain, whereas two domains are typically required for RNA binding in other systems. We have identified a novel CCCH domain variant ($Cx_{10}Cx_5CxH$) that is occasionally found in association with a $Cx_8Cx_5Cx_3H$ finger. The roles of many of these proteins, beyond RNA binding, remain to be determined.

Translation and co-/posttranslational modification. Most major components of the translation machinery are found in the Tritryps (table S12), with similar copy numbers (one to seven) as observed in other lower eukaryotes. However, there appears to be paralogous expansion of the *eIF-4A* gene, with 15 copies showing 30 to 57% amino acid identity to that from *S. cerevisiae*, and ~100 with <30% identity. Most contain adenosine 5′-triphosphate (ATP)–dependent DEAD-box RNA helicase domains, implying nucleic acid binding, perhaps for transcriptional or translational processes. There are also numerous copies of eEF-1α, which complexes with guanosine 5′-triphosphate (GTP) and aminoacyl-tRNAs for

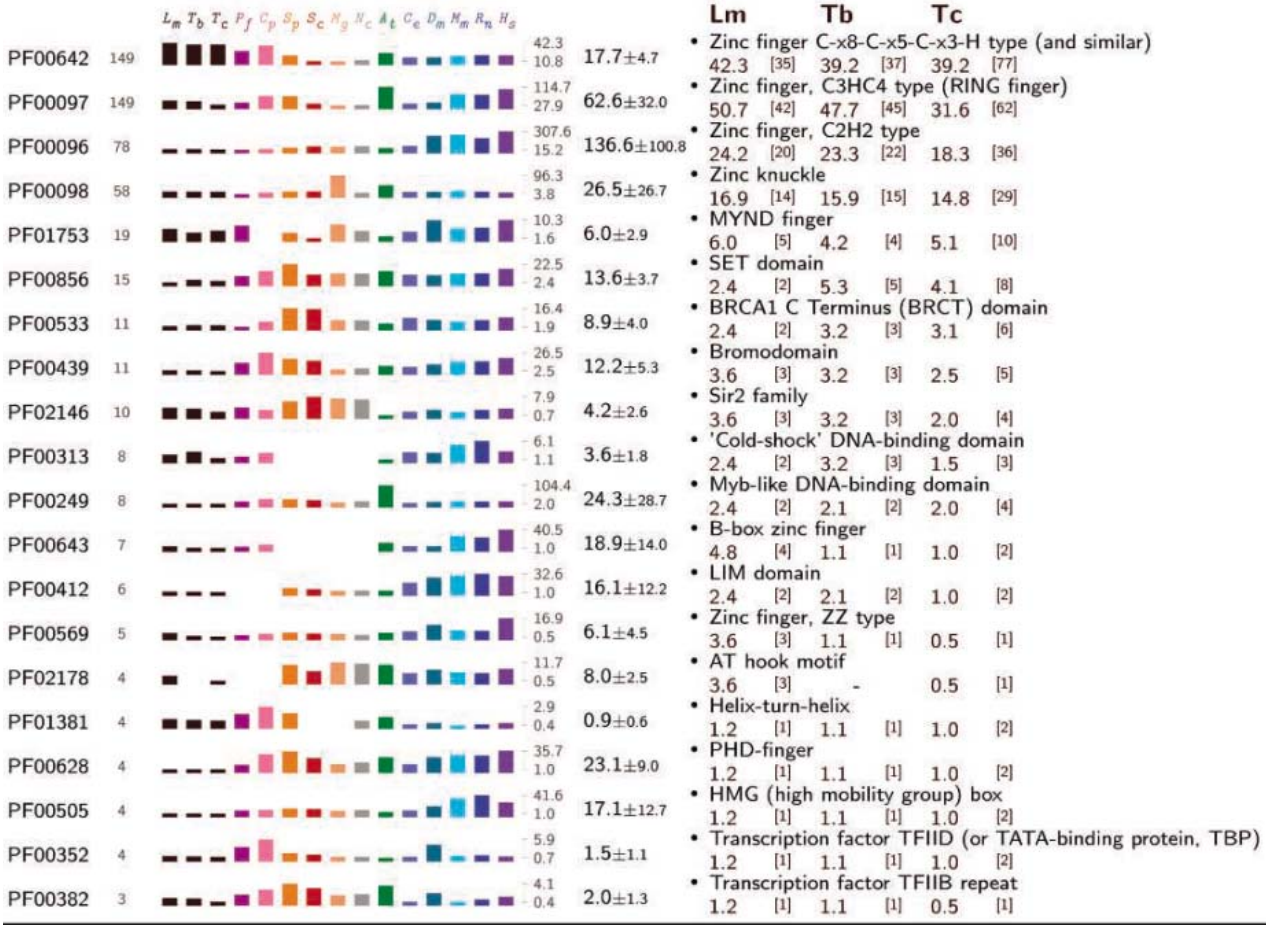

Fig. 2. Protein domains associated with regulation of gene expression in trypanosomatids. The Pfam accession numbers for HMMs that match Tritryp predicted proteins are shown at the left, with the next column indicating the total number of sequences matched in the Tritryp genomes. The matches in individual genomes (normalized by genome size) are shown by the bar graphs, expressed per 10,000 genes. Abbreviations: *L. major* (L_m); *T. brucei* (T_b); *T. cruzi* (T_c); *P. falciparum* (P_f); *Cryptosporidium parvum* (C_p); *S. pombe* (S_p); *S. cerevisiae* (S_c); *Magnaporthe grisea* (M_g); *N. crassa* (N_c); *A. thaliana* (A_t); *C. elegans* (C_e); *D. melanogaster* (D_m); *Mus musculus* (M_m); *Rattus norvegicus* (R_n); *H. sapiens* (H_s). The two numbers immediately to the right of the bar graphs show the maximum and minimum matches observed for all genomes, and the next column shows the mean ± SD for the 10 free-living eukaryotes. The Pfam description of the HMM is shown at the right, with the normalized and actual (in square brackets) number of matches in the *L. major*, *T. brucei*, and *T. cruzi* genomes shown beneath.

ribosomal A site binding during translation, but also functions in processes such as actin binding/bundling in cytokinesis in *Tetrahymena* (*37*). Functionally, *L. major* eIF-2B is predicted to also have mannose-1-phosphate guanyltransferase activity (*LmjF23.0110*) (*38*), whereas the eEF-1B complex has trypanothione *S*-transferase and peroxidase activity (*39*). Thus, the expanded number of potential translation factors in the Tritryps suggests a high degree of specialization.

Protein modification within the Tritryps involves typical eukaryotic processes, including phosphorylation, glycosylation, and lipidation for stabilization and/or activation. Several major modifications have been well characterized and shown to be essential, namely, glycosylphosphatidylinositol (GPI)–anchor addition, acylation (including *N*-myristoylation and palmitoylation), and prenylation, all of which facilitate membrane attachment and/or protein-protein interactions. The Tritryp genomes include a substantial number of proteins containing motifs for putative *N*-myristoylation (table S13) or prenylation (table S14), suggesting that the enzymes that catalyze these modifications may be promising drug targets, given their large number of possible substrates.

Table 2. *L. major* Friedlin protein-coding gene families.

Family size*	Gene product(s)	*L. major*–specific	Organization†	Chromosome(s)
491	Hypothetical proteins (several annotations)	Some	D	Multiple
189	Kinesins/hypothetical proteins	Some	T+D	Multiple
60	Protein kinases (several groups)	Some	T+D	Multiple
46	Amastins	Most	T+TI+D	8, 31, 34, 36
32	Protein kinases (CMGC group)	One	D	Multiple
32	PSA-2 (GP46)	All	T+D	12, 21, 31, 35
29	RNA helicases/eIF-4a	None	T+D	Multiple
27	ATPase/serine peptidases	None	D	Multiple
29	Hypothetical proteins (kinesin-like)	One	D	Multiple
25	Protein phosphatases	None	T+D	Multiple
25	Tuzins	Some	TI+D	8, 34, 36
24	Protein kinases (STE group)	Some	D	Multiple
23	Amino acid permeases	Some	T+D	Multiple
19	HSP83	None	T+D	29, 33
18	DNA helicases	Some	D	Multiple
18	β-tubulins	None	T+D	8, 21, 33
17	Hypothetical proteins (LACK)	One	D	Multiple
17	Hypothetical proteins	Some	T+D	11, 13, 21, 29, 31, 36
15	Calpain-like cysteine peptidases	Some	T+D	4, 20, 25, 31, 36
14	HSP70 and related proteins	None	T+D	1, 18, 26, 28, 30, 35
14	Phosphoglycan β 1,3 galactosyltransferases	Some	T+D	2, 7, 14, 21, 25, 31, 35, 36
14	Dynein heavy chain	One	D	Multiple
14	RNA helicases	None	D	Multiple
14	α,γ,ε-tubulins	Bone	T+D	13, 21, 25
13	Hypothetical proteins (PIPK-like protein)	One	D	Multiple
13	Pteridine transporters	Some	T+D	4, 6, 10, 19, 35
13	Microtubule-associated proteins	All	T	9
13	ABC transporters/P-glycoproteins	Some	T+D	23, 25, 26, 31, 32, 33, 34
12	Protein kinases (NEK group)	One	D	Multiple
12	DNAJ chaperones	Some	D	Multiple
12	Hypothetical proteins	None	T+D	12
11	Long-chain fatty acid CoA ligases	Some	T+D	1, 13, 19, 28
11	Protein kinases (DYRK and CLK families)	One	D	Multiple
11	Translation elongation factors	None	T+D	11, 17, 18, 34, 35
10	Cyclophilins	None	D	Multiple
10	ABC transporters	Some	T+D	2, 11, 15, 27, 29
10	ATPases	None	T+D	4, 7, 17, 18, 33, 35
10	Clan CA, family C1 cysteine peptidases	Some	T+D	8, 19, 29
10	Hypothetical proteins (possible peptidases)	None	T+D	15, 16, 27

*Families correspond to Tribe-MCL clusters (table S2) obtained using inflation value 4, and BlastP cut-off of e^{-15}. Under these conditions, more divergent, but nonetheless functionally related proteins, may not get classified into a given gene family. †Tandem (T), tandem interspersed (TI), distributed (D).

Surface molecules. The surface of the *Leishmania* parasite is distinguished by the presence of a variety of novel glycoconjugates implicated in various aspects of the infectious cycle in the sand fly and mammalian host. These include lipophosphoglycan (LPG), glycoinositolphospholipids (GIPLs), and membrane proteophosphoglycan (PPG), as well as glycosylated GPI-anchored proteins (e.g., GP63, PSA-2/GP46). The secreted acid phosphatase and other PPGs also contain similar posttranslational modifications and vary in structure, expression, and function among *Leishmania* species, as well as between the Tritryps. Although genes of the ether phospholipid synthetic pathway have been identified (*6*), mapping the entire LPG synthetic pathway remains incomplete (table S15), because many of the currently identified genes appear to be novel (*40*).

LPG is assembled in the lumen of the Golgi and requires the provision of activated sugars by nucleotide sugar transporters. The *LPG2* gene product transports GDP-mannose, as well as GDP-arabinose and GDP-fucose, for LPG and phosphoglycan (PG) synthesis; and several potential UDP-Gal transporters can be found in *L. major*. Other nucleotide sugar transporters are present, but their specificity is unknown. Genes for several glycosyltransferases with likely roles in LPG and PG synthesis have been identified, as have genes with roles in synthesis of the LPG glycan core, PG repeating units, and species- and stage-specific PG repeat unit modification. Many, but not all, of these genes appear to be *L. major*–specific, although *T. brucei* and *T. cruzi* both contain a number of genes encoding glycosyltransferases with different specificities (table S15). Seven genes (*SCG1* to *SCG7*) encoding PG-galactosyltransferases and three copies of a gene (*LPG1G*) encoding a possible GIPL β-galactofuranosyltransferase have telomeric locations. Six *SCG*-related (*SCGR*) genes are found in a cluster on chromosome 2, where they are interspersed with the *SCA1* and *SCA2* genes, which mediate the arabinosyl capping of the Gal-[PG] repeat necessary for parasite midgut release during metacyclogenesis (*41*). The functional significance of these nonrandom genomic locations is not yet apparent.

Sphingolipids are essential membrane components in all eukaryotic cells, and their metabolites also function in intracellular signaling. The primary sphingolipid species in the Tritryps is inositol phosphorylceramide (IPC), a target for drug development in pathogenic fungi, because it is not made in mammals. Genes for most of the sphingolipid biosynthetic pathway are present in the Tritryps, with the important exception of IPC synthase (table S16). However, this pathway is not essential for intracellular survival, because *L. major* scavenges lipid precursors from the host and remodels them to generate parasite-specific IPCs (*42*, *43*).

The zinc metallopeptidase GP63 (leishmanolysin, MSP, or PSP) is the major insect-

stage surface protein of *Leishmania*. It facilitates resistance to complement-mediated lysis on host cell entry and is also implicated in receptor-mediated uptake of *Leishmania* (*44*). In *L. major*, there is a tandem array of *GP63* genes on chromosome 10 (some of which encode proteins with predicted GPI-anchors), a single *GP63* gene on chromosome 28, and a related gene on chromosome 31 (table S17). *T. brucei* and *T. cruzi* both contain a tandem cluster of *GP63* genes orthologous to the *L. major* chromosome 10 locus, as well as five genes in two other loci in *T. brucei*, and >350 (including pseudogenes) *GP63*-like genes in *T. cruzi*. Amastin was first described as an abundant amastigote surface protein in *T. cruzi*, where it occurs in tandem clusters, alternating with another putative surface protein, tuzin (*45*). *L. major* has 57 *amastin* genes, most of which are also located in tandem clusters on several chromosomes (table 2), but *tuzin* genes are found in only three of the loci (chromosomes 8, 34, and 36). *T. brucei* has only single, separate, orthologs of *amastin* and *tuzin*. All *L. major* amastins have transmembrane domains; 38 have predicted signal peptides, and some also have predicted GPI-anchors. Expression analyses in *L. major* and *L. infantum* demonstrate that some amastins are lifecycle stage–specific, and that the expression profiles of the various orthologs are dissimilar between these two species (*46*). Another large gene family that encodes GPI-anchored glycoproteins, alternatively known as PSA-2 or GP46 (depending on the *Leishmania* species), is found on chromosome 12, with five divergent copies at other loci (Table 2). The PSA-2 proteins function in macrophage binding and show structural similarity (but not sequence identity) with the *T. cruzi* mucins (*7*); there are no closely related orthologs in *T. brucei*.

Proteolysis. As found in most eukaryotes, peptidases represent ~2% of the protein-coding genes in the Tritryps, and some have already been identified as virulence factors, vaccine candidates, and drug targets. Peptidases are structurally and functionally diverse and are grouped according to intrinsic evolutionary relationships (*47*). Only two aspartic peptidase homologs were identified in the Tritryps: presenilin 1 and signal peptide peptidase that cleave type I and II membrane proteins, respectively (table S18). Tritryps lack the pepsin-like aspartic peptidases (e.g., plasmepsins) that abound in apicomplexan parasites, but have many papain family (including the abundant and well-studied CPB/cruzipain lysosomal enzymes and CPA, which is unique to *L. major*) and calpain cysteine peptidases, as well as ubiquitin C-terminal hydrolases. Trypanosomatids, which are the only known eukaryotes with both a proteasome (*48*) and a eubacterial HslVU complex (*49*), also have numerous ubiquitin-conjugating enzymes, indicative of an active nonlysosomal cytosolic protein degradation system. In addition, the presence of two ATG4 cysteine peptidases, their potential substrate ATG8, and other ATG genes suggests that autophagy operates in organelle and protein turnover. The Tritryps lack caspases but contain several metacaspases, consistent with a caspase-independent cell death mechanism (*50*).

No trypsin/chymotrypsin family serine peptidases were found in Tritryps. Other serine peptidase families are present, however, including a subtilisin-like serine peptidase with a signal peptide and thus likely involved in the processing of secreted proteins. Other serine peptidases identified include six putative prolyl oligopeptidase family proteins [which have been shown to be important for cell invasion in *T. cruzi* (*51*) and are potential drug targets], a type I signal peptidase, a 26*S* regulatory proteasome subunit, a nucleoporin homolog, and several orthologs of rhomboidlike intramembrane serine peptidases, which might have signaling functions. Although GP63 is the most abundant metallopeptidase family, especially in *T. cruzi* (see above), there are 14 other families of metallopeptidases. Seven metallopeptidases, belonging to three paralogous families, show evidence of lateral gene transfer from prokaryotes (*6*), as do a putative peptidase T and a serine peptidase.

No representatives of the almost 200 mammalian peptidase inhibitors (e.g. serpins and cystatins) were found. However, Tritryps encode inhibitors of cysteine peptidases (ICP) that mammals seem to lack; one of these is chagasin, a potent inhibitor of cruzipain and mammalian cathepsin-L. Recent data suggest that *Leishmania* ICP play an important role in host-parasite interaction (*52*), whereas *T. cruzi* chagasin has a role in modulating parasite differentiation and invasion of mammalian cells (*53*). Curiously, the Tritryps also encode inhibitors of serine peptidases (ISPs) that are similar to ecotins, which are normally found in only a few bacterial species, including *Escherichia coli*. Ecotins are inhibitors of trypsin/chymotrypsin-like serine peptidases, which are notably absent in the Tritryps. However, because these peptidases are abundant in both mammals and insects, ISPs very likely play an important role in host-parasite interactions.

Implications and concluding remarks. The Tritryp genome sequences provide insights not only into the unique aspects of the biology of these parasites, but also eukaryote evolution, given their early divergence. Key differences from other eukaryotes include the manner in which the genome is organized into polycistronic gene clusters, a simplified transcriptional machinery, and mRNA trans-splicing coupled with polyadenylation. Although trypanosomatids can dynamically modify histones, implying an early origin of chromatin regulatory pathways, they primarily rely on posttranscriptional mechanisms for regulating gene expression. The lack of transcriptional control mechanisms is further manifested in the use of gene duplication/amplification as a means of increasing expression levels. Gene duplication and divergence are also exploited for the generation of antigenic diversity, particularly in *T. brucei* and *T. cruzi*. Trypanosomatids exhibit extensive posttranslational protein modification, especially for surface and secreted proteins, and have substantial species-specific arrays of glycoconjugate biosynthetic enzymes. The Tritryp genomes have much in common but display important differences (*11*), reflecting different survival requirements and pathogenesis in the specific niches they exploit.

The availability of the entire genetic content of one *Leishmania* species provides the foundation for the identification and in-depth functional analysis of virulence factors, critical enzymes in key metabolic pathways, and potential vaccine candidates. All provide crucial information for the development of new therapies for the leishmaniases. Genome sequence comparisons to additional *Leishmania* strains and species, projects that are ongoing, may elucidate the contribution of parasite factors to tropism and disease pathology.

References and Notes

1. WHO/TDR (World Health Organization–The Special Programme for Research and Training in Tropical Diseases) Web site on leishmaniasis, www.who.int/tdr/diseases/leish
2. J. Alexander, D. G. Russell, *Adv. Parasitol.* **31**, 175 (1992).
3. P. Wincker *et al.*, *Nucleic Acids Res.* **24**, 1688 (1996).
4. C. Britto *et al.*, *Gene* **222**, 107 (1998).
5. C. Ravel *et al.*, *Nucleic Acids Res.* **27**, 2473 (1999).
6. M. Berriman *et al.*, *Science* **309**, 416 (2005).
7. N. M. El-Sayed *et al.*, *Science* **309**, 409 (2005).
8. S. Zhou *et al.*, *Mol. Biochem. Parasitol.* **138**, 97 (2004).
9. S. M. Sunkin, P. Kiser, P. J. Myler, K. D. Stuart, *Mol. Biochem. Parasitol.* **109**, 1 (2000).
10. Materials and methods are available as supporting material on *Science* Online.
11. N. M. El-Sayed *et al.*, *Science* **309**, 404 (2005).
12. M. A. Chiurillo *et al.*, *Exp. Parasitol.* **94**, 248 (2000).
13. S. Juttner *et al.*, *J. Immunol.* **161**, 2383 (1998).
14. F. H. Falcone *et al.*, *J. Immunol.* **167**, 5348 (2001).
15. L. Liu *et al.*, *J. Biol. Chem.* **278**, 18271 (2003).
16. F. Van Leeuwen, D. E. Gottschling, *Cell* **112**, 591 (2003).
17. S. O. Obado, M. C. Taylor, S. R. Wilkinson, E. V. Bromley, J. M. Kelly, *Genome Res.* **15**, 36 (2005).
18. A. K. Ingram, D. Horn, *Mol. Microbiol.* **45**, 89 (2002).
19. C. E. Clayton, *EMBO J.* **21**, 1881 (2002).
20. P. J. Myler *et al.*, *Proc. Natl. Acad. Sci. U.S.A.* **96**, 2902 (1999).
21. E. Worthey *et al.*, *Nucleic Acids Res.* **31**, 4201 (2003).
22. N. Hall *et al.*, *Nucleic Acids Res.* **31**, 4864 (2003).
23. N. M. El-Sayed *et al.*, *Nucleic Acids Res.* **31**, 4856 (2003).
24. V. Tosato *et al.*, *Curr. Genet.* **40**, 186 (2001).
25. S. Martinez-Calvillo *et al.*, *Mol. Cell* **11**, 1291 (2003).
26. S. Martinez-Calvillo, D. T. Nguyen, K. D. Stuart, P. J. Myler, *Eukaryot. Cell* **3**, 506 (2004).
27. E. P. Geiduschek, M. S. Bartlett, *Nat. Struct. Biol.* **7**, 437 (2000).
28. Y. Huang, R. J. Maraia, *Nucleic Acids Res.* **29**, 2675 (2001).
29. R. Evers *et al.*, *Cell* **56**, 585 (1989).
30. M. Zurita, C. Merino, *Trends Genet.* **19**, 578 (2003).
31. J. P. Ruan, G. K. Arhin, E. Ullu, C. Tschudi, *Mol. Cell. Biol.* **24**, 9610 (2004).
32. K. R. Matthews, C. Tschudi, E. Ullu, *Genes Dev.* **8**, 491 (1994).
33. G. Mair *et al.*, *RNA* **6**, 163 (2000).
34. E. Ullu, personal communication.
35. X. H. Liang, A. Haritan, S. Uliel, S. Michaeli, *Eukaryot. Cell* **2**, 830 (2003).
36. A. M. Estevez, T. Kempf, C. Clayton, *EMBO J.* **20**, 3831 (2001).

37. O. Numata, Y. Kurasawa, K. Gonda, Y. Watanabe, *J. Biochem. (Tokyo)* **127**, 51 (2000).
38. A. Garami, T. Ilg, *EMBO J.* **20**, 3657 (2001).
39. T. J. Vickers, S. H. Wyllie, A. H. Fairlamb, *J. Biol. Chem.* **279**, 49003 (2004).
40. D. E. Dobson *et al.*, *J. Biol. Chem.* **278**, 15523 (2003).
41. D. E. Dobson, L. D. Scholtes, P. J. Myler, S. J. Turco, S. M. Beverley, in preparation.
42. K. Zhang *et al.*, *Mol. Microbiol.* **55**, 1566 (2005).
43. P. W. Denny, D. Goulding, M. A. Ferguson, D. F. Smith, *Mol. Microbiol.* **52**, 313 (2004).
44. C. Yao, J. E. Donelson, M. E. Wilson, *Mol. Biochem. Parasitol.* **132**, 1 (2003).
45. S. M. Teixeira, D. G. Russell, L. V. Kirchhoff, J. E. Donelson, *J. Biol. Chem.* **269**, 20509 (1994).
46. A. Rochette *et al.*, *Mol. Biochem. Parasitol.* **140**, 205 (2005).
47. N. D. Rawlings, D. P. Tolle, A. J. Barrett, *Nucleic Acids Res.* **32 (Database issue)**, D160 (2004).
48. C. C. Wang *et al.*, *J. Biol. Chem.* **278**, 15800 (2003).
49. B. Couvreur *et al.*, *Mol. Biol. Evol.* **19**, 2110 (2002).
50. H. Zangger, J. C. Mottram, N. Fasel, *Cell Death Differ.* **9**, 1126 (2002).
51. B. A. Burleigh, A. M. Woolsey, *Cell. Microbiol.* **4**, 701 (2002).
52. S. Besteiro, G. H. Coombs, J. C. Mottram, *Mol. Microbiol.* **54**, 1224 (2004).
53. C. C. Santos *et al.*, *J. Cell Sci.* **118**, 901 (2005).
54. We thank our colleagues in the *Leishmania* Genome Network (LGN) for their support and encouragement. We thank the other members of the Tritryp Sequencing Consortium for their help with comparative genome annotation; special thanks to J. Donelson and S. Melville, who together have played a key driving role in the coordination, discussion, and collation of these manuscripts. Funding for this project was provided by grants from WHO TDR (T23/181/1 ID:940509), Burroughs Wellcome Fund (BWF) (APP#0500), and National Institute of Allergy and Infectious Diseases (NIAID) (RO1 AI040599) to SBRI; Wellcome Trust (WT) (054394/Z/98/Z, 060491/Z/00/Z, and 063272/Z/00/Z) to the Wellcome Trust Sanger Institute; the European Union (BIO4-CT98-0079) to the EULEISH consortium; NIAID (RO1 AI060645) to A.C.F.; and a Fundação de Amparo à Pesquisa do Estado de São Paulo fellowship (01/13461-9) to J.C.R. WHO TDR, WT, and NIAID also provided funds for several LGN meetings. Accession numbers: EMBL: CT005244 to CT005272, AL389894 and AL139794; GenBank: CP000078 to CP000081, AE001274, and NC_004916. All data are available in GeneDB (http://www.genedb.org).

Supporting Online Material
www.sciencemag.org/cgi/content/full/309/5733/436/DC1
Materials and Methods
Fig. S1
Tables S1 to S18
References and Notes

23 March 2005; accepted 21 June 2005
10.1126/science.1112680

Q AAAs

Who's making a splash with quality science reporting?

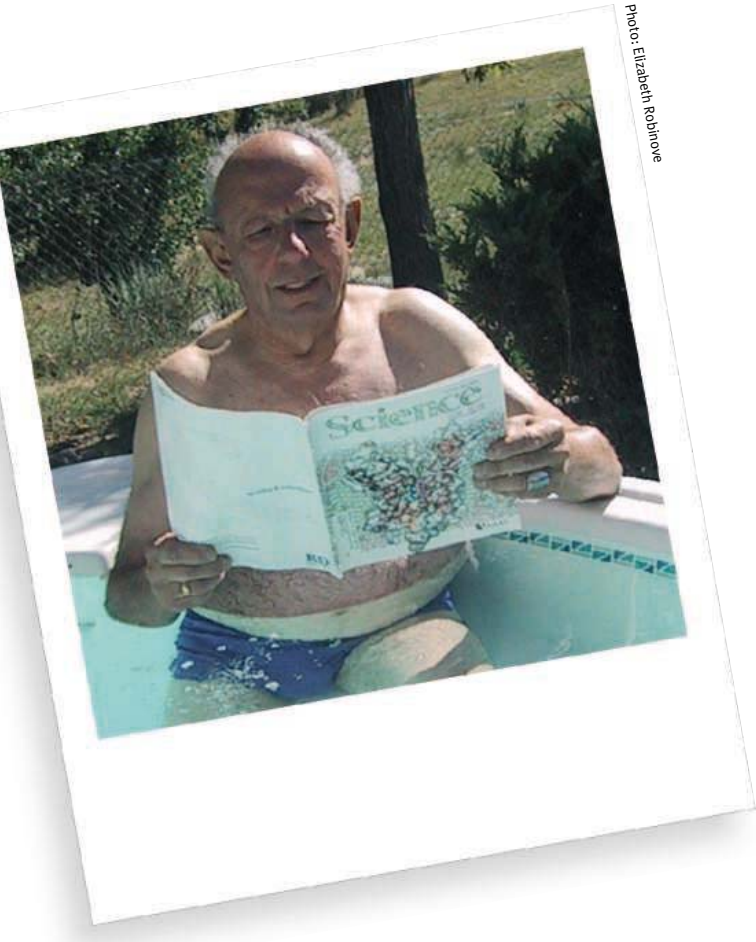

Photo: Elizabeth Robinove

"I dig reading my *Science* in the hot tub. Now that I'm retired, it makes a pleasant change from digging for samples in the field. I find reading *Science* the most relaxing way to stay on top of all the latest developments."

Chuck Robinove, retired USGS geologist and AAAS member

AAAS is committed to advancing science and giving a voice to scientists around the world. We work to improve science education, promote a sound science policy, and support human rights.

Helping our members stay abreast of their field is a key priority for AAAS. One way we do this is through *Science*, which features all the latest breakthroughs and groundbreaking research, and keeps scientists connected wherever they happen to be. Members like Chuck find it essential reading.

To join the international family of science, go to www.aaas.org/join.

To see other member photos, please visit:
http://promo.aaas.org/memberpics.shtml

Chuck Robinove

AAAS
ADVANCING SCIENCE, SERVING SOCIETY

www.aaas.org/join

CALL FOR PROPOSALS
Graduate Education Program

National Space Biomedical Research Institute

The National Space Biomedical Research Institute (NSBRI) is soliciting proposals for a Graduate Education Program to broaden students' academic and career skills in space life science. NSBRI encourages the leveraging of existing academic programs and infrastructure to develop cost-effective approaches that will prepare students for entry level careers at NASA, NSBRI consortium member institutions, private industry partners in the space initiative or other public or private organizations involved in NASA's space exploration endeavors.

NSBRI is a non-profit organization competitively selected by NASA in 1997 to lead a national effort for accomplishing the integrated biomedical research necessary to support long-term human presence, development, and exploration of space and to enhance life on Earth by applying the resultant advances in human knowledge and technology acquired through living and working in space.

Applicants must submit proposals with the demonstrated support and commitment of the home institution, and must represent accredited, degree-granting U.S. institutions offering the Doctor of Philosophy (Ph.D.) or equivalent degree in the biomedical sciences, engineering or other fields applicable to space life sciences. Proposals will be accepted only from U.S. citizens, permanent residents, or persons with pre-existing visas obtained through the sponsoring institution. All proposals will be evaluated by a peer-review panel.

Detailed program and application submission information is available at the NSBRI website: **http://www.nsbri.org/Announcements/rfp05-02.html**. Letters of intent, which are requested, but not required, and proposals must be submitted through the NSBRI's Internet-based Electronic Proposal Submission System. Letters of intent are due by **August 3, 2005**; the proposal deadline is **September 14, 2005**.

Questions may be directed to **Jeanne Becker, Ph.D., Associate Director, NSBRI**, email: **director@www.nsbri.org**; telephone: **713-798-7412**.

Arctic Seabirds Transport Marine-Derived Contaminants

Jules M. Blais,[1]* Lynda E. Kimpe,[1] Dominique McMahon,[1] Bronwyn E. Keatley,[2] Mark L. Mallory,[3] Marianne S. V. Douglas,[4] John P. Smol[2]

Transport of pollutants by migratory species, such as salmon, is known to affect contaminant distributions in Alaskan nursery lakes (*1*, *2*). Arctic seabirds may also be transporting industrial and agricultural contaminants from the ocean to land. Most of these seabirds are pelagic feeders with populations concentrated in very large breeding colonies of more than 20,000 individuals (*3*). Local nutrient enrichment from guano has been documented, but the possibility of contamination in areas near seabird nesting sites has been largely overlooked. In a recent study on Bear Island, the presence of seabird colonies adjacent to one lake coincided with elevated polychlorinated biphenyl concentrations in fish (*4*). Here we show that persistent organic pollutants and mercury concentrations in high arctic pond sediments are closely related to the varying influences of seabird populations in ponds on Devon Island, in the Canadian Arctic (Fig. 1A), and that the combined effects of biomagnification and biological transport of contaminants dwarf the amount transported from atmospheric pathways.

We studied contaminants in the surface sediments of high arctic ponds below the cliffs at Cape Vera (76°15′N, 89°15′W). The 245-m-high cliffs support a large colony (~10,000 breeding pairs) of northern fulmars (*Fulmarus glacialis*) (*3*), a medium-sized petrel that is found across the North Atlantic. During the breeding season, fulmars feed on zooplankton, squid, fish, and carrion (*5*). Fulmars from Cape Vera acquire most of their prey between Ellesmere Island and Greenland, 250 to 400 km from the colony.

We sampled 11 ponds; eight of these were located across a gradient of fulmar influence, and three ponds were outside the area influenced by seabird populations. The effect of birds on ponds was established by quantifying algal growth, water quality variables related to seabird guano inputs, and stable isotope ratios of nitrogen ($\delta^{15}N$) in pond sediment, which are enriched in guano relative to other N sources in the area. Because fulmars feed near the top of the marine food chain, $\delta^{15}N$ values in their tissues are elevated relative to atmospheric and terrestrial sources (*6*). $\delta^{15}N$ in sediment ranged from 0.74 to 18.4 per mil (‰), compared to 20.4‰ measured in guano (table S1).

Concentrations of dichlorodiphenyltrichloroethane (DDT), mercury, hexachlorobenzene (HCB), and other organochlorine compounds in the pond sediments showed strong correlations

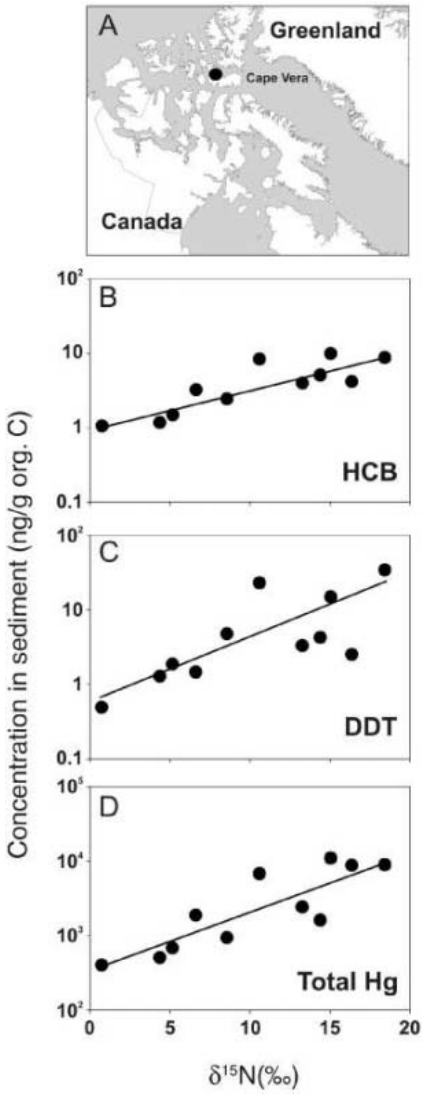

Fig. 1. (**A**) Sample sites. (**B** to **D**) Contaminant concentrations of (B) HCB, (C) DDT, and (D) total mercury (Hg) in surface sediments are plotted against $\delta^{15}N$. We use $\delta^{15}N$ as a proxy of seabird influence. However, when we expressed the contaminant data relative to other indicators of guano input [e.g., total P, total N, dissolved organic C (org. C), Cd], we found similar relationships. DDT values shown are the sum of DDT and its derivatives.

with both sedimentary $\delta^{15}N$ (Fig. 1) and nutrient concentrations in the water. Concentrations of HCB increased 10-fold over this impact range; mercury increased 25-fold; and DDT and its metabolites increased more than 60-fold, with the highest concentrations observed in the ponds that were most enriched by seabirds. Mercury concentrations in sediments of three ponds in the area most affected by seabirds approached or exceeded the Canadian environmental quality guidelines for protecting wildlife. Moreover, as animals convert DDT to its more persistent metabolite DDE, we might expect the relative proportions of DDT and its metabolites to be affected by the source of contamination. The ratio of DDE to DDT correlated significantly with $\delta^{15}N$; ratios in sediments reached 0.9, which are identical to values measured in guano. Thus, DDT in the more affected ponds was more "biologically processed," as we might expect of substances that have passed through the marine food web, which further corroborates their transport by biological vectors.

Contaminants in arctic wildlife are of particular concern both for ecosystem health and because traditional foods remain an important part of the diet of indigenous peoples. Although the biological pump mediated by seabirds provides a critical nutrient subsidy to terrestrial arctic ecosystems, seabirds are now also transporting and concentrating industrially produced contaminants to these remote environments.

References and Notes

1. G. Ewald, P. Larsson, H. Linge, L. Okla, N. Szarzi, *Arctic* **51**, 40 (1998).
2. E. Krümmel *et al.*, *Nature* **425**, 255 (2003).
3. M. L. Mallory, A. J. Fontaine, "Key marine habitat sites for migratory birds in Nunavut and the Northwest Territories" (Canadian Wildlife Service Occasional Paper No. 109, Ottawa, Ontario, 2004).
4. A. Evenset *et al.*, *Sci. Total Environ.* **318**, 125 (2004).
5. K. A. Hobson, *Mar. Ecol. Prog. Ser.* **95**, 7 (1993).
6. C. Kendall, in *Isotope Tracers in Catchment Hydrology*, C. Kendall, J. J. McDonnell, Eds. (Elsevier, New York, 1998), pp. 519–576.
7. Supported by the Natural Sciences and Engineering Research Council of Canada, the EJLB Foundation, the Polar Continental Shelf Project, and the Northern Scientific Training Program.

Supporting Online Material
www.sciencemag.org/cgi/content/full/309/5733/445/DC1
Table S1

23 March 2005; accepted 22 April 2005
10.1126/science.1112658

[1]Centre for Advanced Research in Environmental Genomics, Department of Biology, University of Ottawa, Ottawa, Ontario, K1N 6N5 Canada. [2]Paleoecological Environmental Assessment and Research Laboratory, Department of Biology, Queen's University, Kingston, Ontario, K7L 3N6 Canada. [3]Canadian Wildlife Service, Environment Canada, Iqaluit, Nunavut, X0A 0H0 Canada. [4]Department of Geology, University of Toronto, Toronto, Ontario, M5S 3B1 Canada.

*To whom correspondence should be addressed. E-mail: jblais@science.uottawa.ca

Evidence for Ectopic Neurotransmission at a Neuronal Synapse

Jay S. Coggan,[1,3*] Thomas M. Bartol,[1,8*] Eduardo Esquenazi,[3,5] Joel R. Stiles,[6,7] Stephan Lamont,[3] Maryann E. Martone,[3,4] Darwin K. Berg,[5] Mark H. Ellisman,[3,4] Terrence J. Sejnowski[1,2,5,8,†]

Neurotransmitter release is well known to occur at specialized synaptic regions that include presynaptic active zones and postsynaptic densities. At cholinergic synapses in the chick ciliary ganglion, however, membrane formations and physiological measurements suggest that release distant from postsynaptic densities can activate the predominantly extrasynaptic α7 nicotinic receptor subtype. We explored such ectopic neurotransmission with a novel model synapse that combines Monte Carlo simulations with high-resolution serial electron microscopic tomography. Simulated synaptic activity is consistent with experimental recordings of miniature excitatory postsynaptic currents only when ectopic transmission is included in the model, broadening the possibilities for mechanisms of neuronal communication.

Throughout the nervous system, release of synaptic vesicles from presynaptic nerve terminals is thought to be associated with pre- and postsynaptic specializations, including active zones (AZs) and postsynaptic densities (PSDs). Release of neurotransmitter vesicles at extrasynaptic sites (ectopic release) has been suggested by the presence of morphologically docked vesicles distant from PSDs in electron micrographs from tissues, including the ribbon synapses of bipolar neurons (*1*) and saccular hair cells (*2*). Recently, direct measurements of quantal release have been made from climbing fibers in the cerebellar cortex onto the closely apposed Bergmann glia (*3*). Despite these findings, there has been no demonstration of the participation of ectopic release of neurotransmitter in the course of interneuronal synaptic transmission.

At the structurally complex and umbrella-like calyceal synapse of the ciliary ganglion (CG), the case for ectopic release has been growing. Two major classes of kinetically distinct nicotinic acetylcholine receptors (nAChRs) are spatially segregated in the CG (*4*–*6*). The α7-nAChRs are expressed on matted spines but are largely excluded from PSDs regardless of where they occur (*7*–*9*). The α3*-nAChRs (*6*) are primarily localized to PSDs (whether on spines or somatic membrane) but are present at lower density on non-PSD membrane (*4*, *9*, *10*). The α7-nAChRs exhibit profound desensitization, an order of magnitude faster decay time, and an open probability lower by a factor of 30 than that of α3*-nAChRs (*11*–*13*).

The segregation of the two nAChR subtypes, especially the exclusion of α7-nAChRs from PSDs, has made it difficult to interpret physiological measurements that show that the α7-nAChRs account for the majority of current in evoked EPSCs (*11*, *12*), are necessary to sustain higher frequency throughput (*11*, *14*), and produce distinct Ca signals localized to spines (*15*). Images of presynaptic vesicles within docking distance (ready to release), as well as Ω profiles (the image capture of fusing vesicles), are seen throughout the calyx, including at loci far from PSDs (*4*). These findings have challenged the assumption that synaptic transmission is limited to traditional PSD-associated AZs in the CG and suggest that neurotransmitter is released ectopically (*15*).

The characteristic geometry of the CG, combined with its specialized molecular properties, is well suited to exploring detailed properties of synaptic transmission. Here, we present an accurate three-dimensional (3D) model of synaptic topology with 9-nm resolution derived from electron tomography (*5*, *16*), combined with Monte Carlo reaction/diffusion algorithms (MCell, www.mcell.cnl.salk.edu) that use 3D random-walk diffusion steps while tracking the probabilistic interactions of individual molecules governed by kinetic rate constants (*17*–*25*). The model makes surprising predictions about the behavior of the two classes of nAChRs within functional microdomains and also provides evidence that synaptic transmission in the CG requires ectopic neurotransmitter release.

Model assembly. An MCell model is comprised of a description of the 3D geometry of the system along with molecule distributions and kinetics. Pre- and postsynaptic membrane surfaces were digitized from a 3D reconstruction of a CG spine mat derived from serial-section electron tomography (4.4 nm/voxel) as described in (*16*) and as applied to the CG (*4*, *5*, *26*). The pre- and postsynaptic membrane contours were first traced manually in each slice of the tomographic volume (Fig. 1A) and then transformed into triangle mesh surfaces (Fig. 1, B and C) using the well-established marching cubes method from the field of computational geometry (*27*) (fig. S1). The postsynaptic surface was segmented into PSD and non-PSD regions, populated with nAChRs and acetylcholinesterase (AChE), and associated with presynaptic vesicle release sites (Fig. 1D). A close-up of one release site (200 μs after ACh release) with many components is presented (Fig. 1E). Distribution densities are α3*-nAChRs at 3600/μm^2 in PSD membrane and 80/μm^2 elsewhere (*10*), and α7-nAChR at 3600/μm^2 on spine membrane only (*4*). The number of ACh molecules per vesicle is 5000 (*17*), and the density of AChE is 3000/μm^2 uniformly (*28*, *29*). Simulation with MCell requires that the structural model be annotated with reaction mechanisms, rate constants, and spatial information regarding release sites and molecular components. These values were determined from published information (*26*) (fig. S2).

MCell counts the number of each molecular species in every state after each Monte Carlo time step (1 μs here). Figure 2A shows examples for the reaction of ACh with α3*- and α7-nAChRs in their various states: single-bound (red), double-bound closed (green), double-bound open (referred to as O-state henceforth) (black), and desensitized (blue; α7-nAChRs only).

Site-dependent mEPSC variability. Several vesicular release sites were chosen as simulation cases encompassing a variety of receptor subtype configurations and spatial geometries (Fig. 2B). One hundred trials were performed at each site. A composite of the averaged O-state response illustrates the wide variety of mEPSCs predicted according to the relative contributions of α3*- and α7-nAChRs and their spatial locations (Fig. 2C). [It is curious that the amplitudes of responses at both PSD sites (1 and 2) differ by a factor of 2, the difference being that site 2 is surrounded by α7-nAChRs.]

[1]Computational Neurobiology Laboratory, The Salk Institute, La Jolla, CA 92037, USA. [2]Howard Hughes Medical Institute, 4000 Jones Bridge Road, Chevy Chase, MD, 20815, USA. [3]National Center for Microscopy and Imaging Research, [4]Department of Neurosciences, School of Medicine, [5]Division of Biological Sciences, University of California, San Diego, La Jolla, CA 92093, USA. [6]Pittsburgh Supercomputing Center, Carnegie Mellon University, Pittsburgh, PA 15213, USA. [7]Department of Neuroscience, University of Pittsburgh, Pittsburgh, PA 15260, USA. [8]Center for Theoretical Biological Physics, University of California, San Diego, La Jolla, CA, 92093–0374, USA.

*These authors contributed equally to this work.
†To whom correspondence should be addressed: terry@salk.edu

Model sensitivity. We determined the sensitivity of our CG model to individual parameters. On the basis of their predominant receptor environments, site 1 was selected for α3*-nAChR and site 5 for α7-nAChR simulations. There was no sign of response saturation up to the maximum of 20,000 ACh molecules per quantum, which suggests additional ligand capacity in the system (Fig. 3A). The α3*-nAChR response was more sensitive to ACh than that of α7-nAChRs. The manipulation of K_+ as an independent variable showed that the original α3-nAChR K_+ lies in the relatively insensitive, low part of the curve, whereas the original K_+ for α7-nAChRs is located in the steepest part of the curve (Fig. 3B). Responses to α3*-nAChRs are more sensitive to changes in their respective receptor density than are α7-nAChR responses (Fig. 3C), but both exhibit residual capacity. The original density value for AChE lies at an efficient point (more AChE would not greatly reduce cleft ACh) (Fig. 3D). Although the simulated transient mEPSC events were far from equilibrium, the data (Fig. 3, A to D) were fit with equations derived from the equilibrium reaction mechanisms for the α3*- and α7-nAChRs as a benchmark (*26*, *30*).

We quantified the effects of individual parameter changes on model output by taking the first derivative (f')—a measure of rate of change—of the curves from the sensitivity analysis at the point representing original conditions. To create a general measure of sensitivity suitable for cross comparison, we normalized the derivatives by multiplying by the ratio of the *x*- and *y*-axis values corresponding to the same point [f'-norm = $(f')(x_o/y_o)$]. The unitless f'-norm values for α3*-nAChRs (with respect to ACh, AChR, AChE, and K^+) were 1.88, 0.91, –0.42, and 1.48; and for α7-nAChRs were 1.34, 0.69, –0.38, and 0.85, which suggests that the model was most sensitive to changes in number of ACh molecules per quantum.

Population mEPSC responses. To simulate population mEPSC responses, we programmed our model for 100 releases at each of 550 sites that represented vesicles within 5 nm (docking distance) of the presynaptic membrane in tomographic reconstructions of our CG volume (*5*). The peak mean open channel response for α3*-nAChR responses was 1.3 channels (Fig. 4A) and that for α7-nAChR responses was 2.13 channels, including 45 failures (Fig. 4E). Frequency histograms showing the distributions for the peak open channels, as well as the rise (20% to 80%) and fall times (τ), were also constructed for α3*- nAChRs (Fig. 4, B to D) and α7-nAChRs (Fig. 4, F to H). Differences in the distributions, including skew, median, and tightness, reflect variations in, and the importance of, spatial domain (Figs. 2 and 5) and kinetic properties.

If one assumes a single-channel conductance of 68 pS for α7- and 37 pS for α3*-nAChRs (*13*), then the corresponding mean

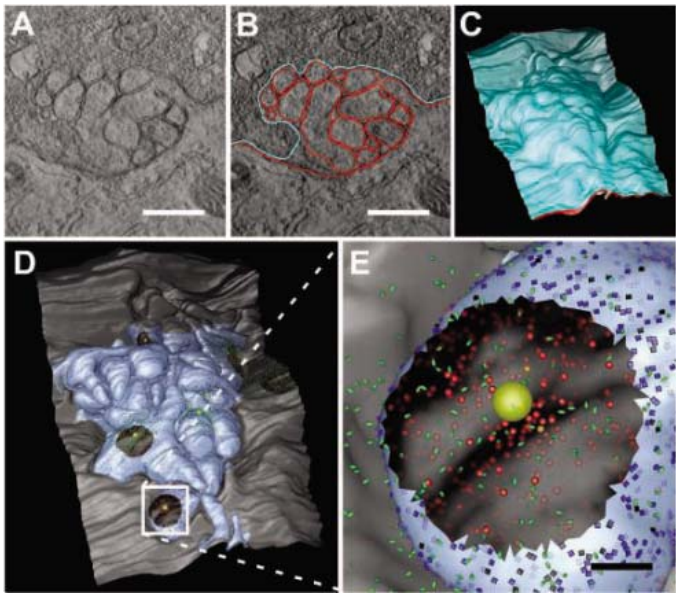

Fig. 1. 3D model reconstruction. (**A**) Cross-sectional view about halfway through the middle of an E15 chick CG acquired with serial EM tomography and visualization software AnalyzeAVW. Several somatic spine cross sections are seen, along with vesicles packed in the presynaptic calyx. (**B**) Same panel as in (A), with presynaptic and postsynaptic membranes traced in cyan and red, respectively, using Xvoxtrace. Scale bar, 0.5 μm. (**C**) Serial section reconstruction after the surface is reconstructed with the marching cubes algorithm. The presynaptic membrane (cyan) overlies the postsynaptic membrane (red). (**D**) Viewed with DReAMM, the MCell compatible model, complete with all previously reported PSDs (shown as black circular regions) (*4*). Postsynaptic spine mat membrane is light blue; somatic membrane is gray. Area within white box is enlarged in next panel. (**E**) Close-up view of MCell compatible model. Yellow sphere represents synaptic vesicle. Green ovoids represent ACh molecules. Translucent blue squares and red circles represent α7- and α3*-nAChRs, respectively. Opacity of nAChR color corresponds to level of receptor activation (fully opaque = open channel) 200 μs after ACh release. Scale bar, 0.1 μm.

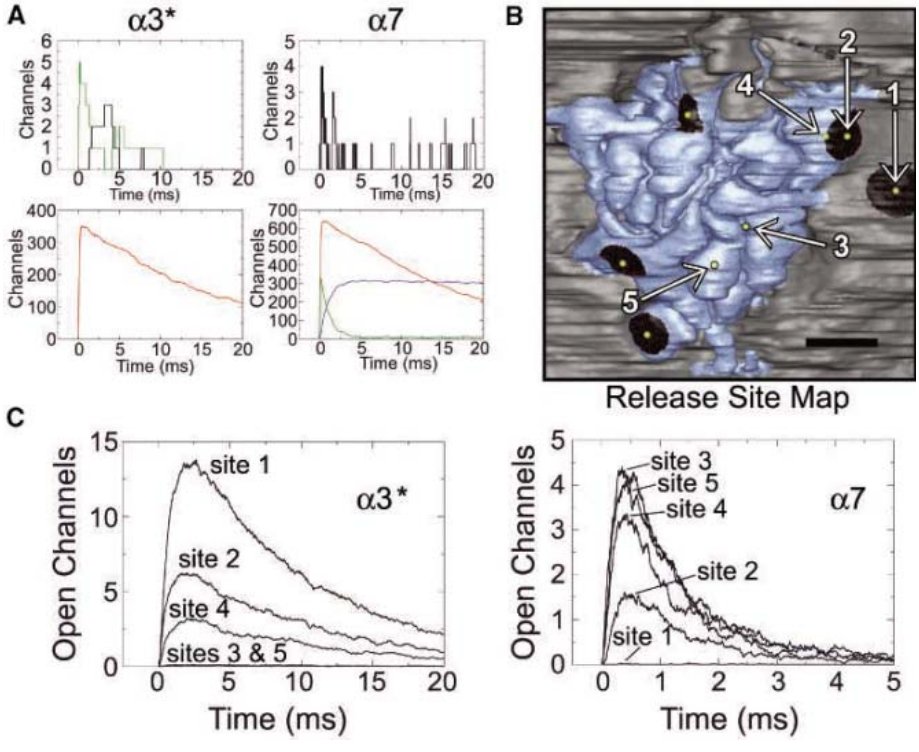

Fig. 2. MCell output and location effects. (**A**) Time course of α3*- and α7- nAChR channel states after release of a single quantum. Green, double-bound closed (C2); black, double-bound open (O); red, single-bound (C1); blue, desensitized (C3, α7-nAChRs only). See (*26*) and fig. S2 for mechanisms and states. Scaling differences require presentation in two panels per receptor type (top and bottom). (**B**) Site map of selected release sites representing the greatest range of nAChR distributions. Vesicles are released at numbered yellow spheres indicated with white arrows; PSDs indicated by black-shaded patches; spine membrane, blue; somatic membrane, gray. Scale bar, 0.5 μm. (**C**) O-state responses (mean of 100 trials) from five sites in (B).

mEPSC amplitudes at a holding potential of –60 mV would be 9.43 pA and 2.9 pA, respectively. The total mean mEPSC amplitude recorded in situ is 33 pA ± 0.7 at –60mV, with a range between 5 and 80 pA (*11*). When adjusted with a detection threshold of 3 pA, all α3*-nAChR responses in the histogram distribution below 1.36 open channels (201 out of 550, or 36.5%) would go undetected, and the new mean would rise by 50% from 1.3 to 1.95 open channels or 4.3 pA. Although this value is close to the 8.4-pA mean recorded in situ in the presence of the selective α7-nAChR antagonist α-Bgt (*11*), the difference might result from variations between specific model parameters (e.g., number of ACh molecules per quantum, α3*-nAChR densities) and real ganglionic recording conditions. Similarly, all α7-nAChR O-state responses below 0.73 (145 out of 550, or 26.4%) would not be measured with a 3-pA threshold, raising the mean by 34% from 2.13 to 2.85 open channels, or 11.7 pA. Assuming α3*-nAChRs contribute 8.4 pA in situ (the mean mEPSC amplitude in the presence of the α7-nAChR blocker α-bgt), α7-nAChRs should contribute about 24.6 pA in situ. On the basis of the difference between the simulated mEPSC amplitudes in the presence and absence of the 3-pA threshold, the true mean mEPSC amplitude, accounting for lost events, is predicted to be two-thirds to three-quarters the size of that measurable experimentally.

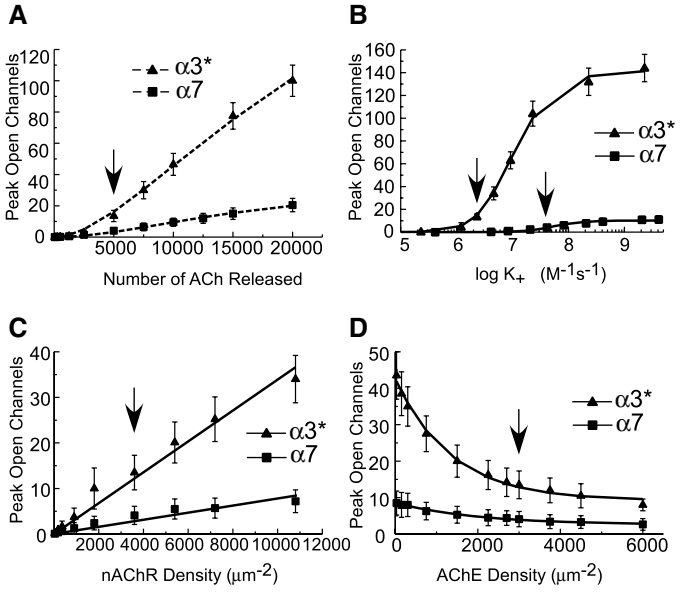

Fig. 3. Model sensitivity. The effects of modulating the levels of four model components on O-state. (**A**) Effect of number of ACh molecules per quantum. Original condition, n = 5000 on O-state for α3*- and α7-nAChRs (fit: α3*, r = 0.999; α7, r = 0.998). (**B**) Effect of varying the K_+ on O-state for α7- and α3*-nAChRs. Original values for α7-nAChR $K_+ = 4.1 \times 10^7$ $M^{-1}s^{-1}$; for α3*-nAChR $K_+ = 2.3 \times 10^6$ $M^{-1}s^{-1}$ (fit: α3*, r =0.999; α7, r = 0.987). (**C**) Effect of changing α3*- and α7-nAChR receptor density on O-state. Original value for both nAChRs was 3600/μm² (fit: α3*, r = 0.992; α7, r = 0.986). (**D**) Effect of AChE density on O-state. Original AChE density in model was 3000/μm² (fit: α3*, r = 0.997; α7, r = 0.995). All values in all panels are mean ± S.D., n = 100 per point. Arrows indicate original model values for each receptor type.

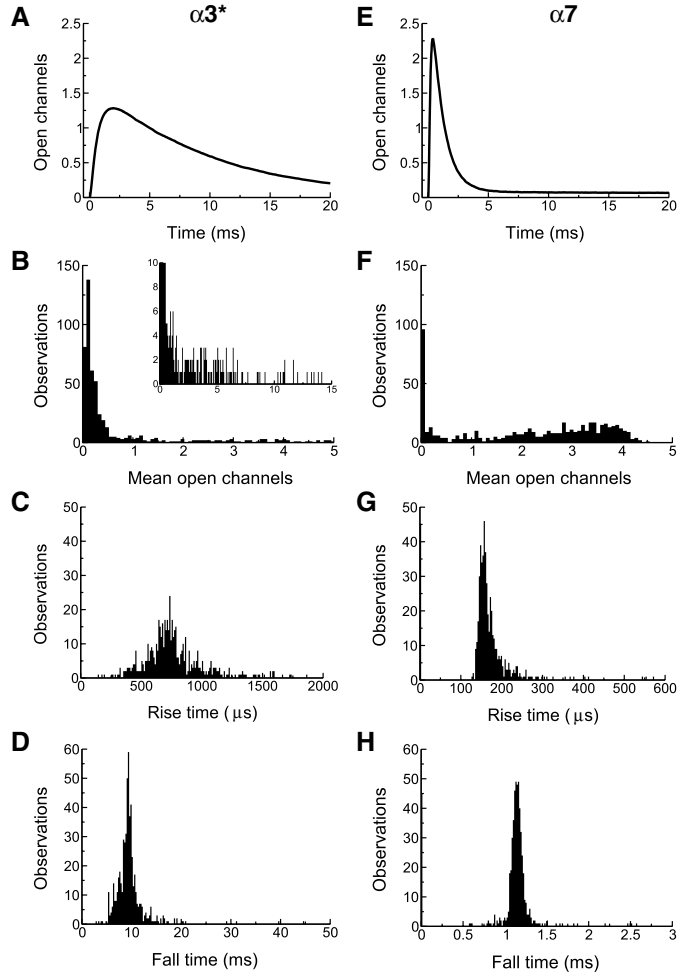

Fig. 4. Simulated population mEPSC analysis. (**A**) Cumulative mean O-state α3*-nAChR-mediated mEPSC. Histograms of (**B**) mean number of peak open channels [bin = 0.075; same x-axis scale as (**F**) for comparison] (inset is the expanded full x-axis scale), (**C**) rise times (bin = 10), and (**D**) fall times (bin = 0.25). (**E**) Cumulative mean α7-nAChR-mediated mEPSC (including 45 failures). Histograms of (**F**) open channels (bin = 0.076), (**G**) rise times (bin = 3), and (**H**) fall times (bin = 0.015).

Local Interactions between nAChR subtypes. To visualize the spatial distribution of the mEPSC population, the location of each release site was mapped onto the postsynaptic surface of our model volume, and the radius of a sphere marking each site was scaled in proportion to the corresponding mean O-state response amplitude (Fig. 5A). It was observed above that the α3*-nAChR O-state amplitude at site 2 was half that of site 1 (Fig. 2C), even if both were PSD release sites, suggesting an effect of α7-nAChRs on α3*-nAChR O-state around site 2. The population of 550 mEPSC simulations was reexamined with the α7-nAChRs turned off (blockade of α7-nAChRs), and the α3*-nAChR mEPSC amplitudes (number of open channels) were compared in the two conditions by subtraction (without α7-nAChRs minus with α7-nAChRs, Fig. 5B, left) and by percent increase (Fig. 5B, right). Positive changes are represented by yellow spheres and negative differences by cyan. The net effect of blocking α7-nAChR activity is an increase in the mean α3*-nAChR mEPSC amplitude from 1.27 to 1.36 open channels, a 7% rise (Fig. 5C, left). Responses gaining the most absolute amplitude were located on PSDs. The lack of cyan spheres over PSD areas that are surrounded by α7-nAChRs emphasizes the local interactions between the two nAChR subtypes (Fig. 5B, left). The locations of responses that exhibited the largest percentage increase in amplitude were regions where the smallest α3*-nAChR mEPSCs are normally produced (usually from non-PSD spine-regions, Fig. 5B, right). When we imposed a 3-pA detection threshold on the data, the mean α3*-nAChR mEPSC amplitude paradoxically declined 12% from 1.95 to 1.74 open channels (Fig. 5C, right). Under

this condition, the number of measurable α3*-nAChR mEPSCs increased (from 347 to 423), but most of these newly observable mEPSCs are low-amplitude events that reduce the mean.

Testing the prediction of ectopic release. The mechanism of activation of extrasynaptic receptors (primarily α7-nAChRs) that contribute significantly to the evoked synaptic response has been debated (*3*, *11*, *12*, *14*, *31*). In our population mEPSC simulations, we released vesicles at pan-calyceal sites (both PSD and ectopic), based on the observation that synaptic vesicles are widely distributed in the CG presynaptic terminal within 5 nm of the release face membrane (*5*). Thus far, we have kept the size of the vesicles uniform to better understand the effect of location and local geometry on synaptic response.

In addressing the issue of ectopic release, however, it was necessary to compare a mEPSC data set recorded from CG in situ (*11*) to a simulated data set based on a better estimate of vesicle size distribution. We measured synaptic vesicle lumen diameters from the reconstructed 3D tomographs (*26*) (mean = 49.0 nm ± 6.0) (Fig. 6A). This new distribution of vesicles (Fig. 6B) was adjusted volumetrically for the mean number of ACh molecules required to align our simulated mean mEPSC amplitudes with those from CG recordings (*11*). We cannot conclude, however, the actual number of molecules of ACh/vesicle without further experiments.

A new mEPSC population was created by sampling the distributed vesicle population 100 times for each of the 550 release sites (Fig. 6, C and D). These data are presented in histogram form along with mEPSC histograms from CG whole-cell recordings (blue bars) (*11*). A 6-pA detection threshold was applied to the simulated data for better comparison with recorded data (*11*) (Fig. 6, C to E). The mEPSC distributions from ectopic and PSD regions were considered separately and together (pan-calyx) when expressed as cumulative probability plots and compared with the results from whole-cell recordings. Additional simulations that included α7-nAChRs (with α3*-nAChRs) in the spine PSDs, at an equivalent density to non-PSD areas, were also included to determine the impact of the PSD exclusion of these receptors (Fig. 6E). Visual inspection of these data suggested a closer fit by either ectopic-only or pan-calyx events than by PSD-only events or mEPSC populations that include α7-nAChRs in the spine PSDs. The PSD-only population features a higher proportion of larger amplitude mEPSCs.

To quantitatively assess ectopic release contributions, distinct simulated mEPSC populations were generated by varying the fraction of vesicles released over PSDs (i.e., 1- ectopic fraction) and by varying the mean number of ACh molecules per quantum. The fraction of PSD vesicles was varied from 0 (i.e., 0% PSD vesicles and 100% ectopic) to 1 (i.e., 100% PSD and 0% ectopic). Simultaneously, the mean number of ACh molecules per quantum was varied from 5,000 to 15,000. The goodness-of-fit of each of these populations when compared with the population of experimentally recorded mEPSCs (*11*) was measured by the Kolmogorov-Smirnov test. The *P* value of the goodness-of-fit is shown in grayscale on the plot (Fig. 6F; darker gray indicates better fit). This analysis demonstrates that mEPSC distributions with a high fraction of ectopic-released vesicles best match the recorded data.

Extrasynaptic receptor activation. The impact of spatial-kinetic interactions on principal events in the course of synaptic transmission, including neurotransmitter spillover and the importance of extrasynaptic receptors, is unclear (e.g., *32*–*34*). We addressed the question of ectopic vesicle release in the CG by quantitative comparison of the distributions of our simulated population of mEPSCs with those previously recorded from intact CGs (*11*). We concluded that ectopic vesicle release is likely the dominant component of synaptic transmission in the CG. The best fit to nearly 0% PSD release is a likely result of variations with model parameter values; any uncertainties could change the quantitative outcome (percentage of allowable PSD release) but would not change the qualitative conclusion of a substantial ectopic release requirement.

Awareness of the important role of ectopic release at synapses is growing and challenging long-standing notions about synaptic structure and function (*3*). The function of non-PSD release in the CG specifically is probably closely linked to the specialized properties and function of α7-nAChRs, with their unique kinetics (*11*), calcium signals (*15*), and gene regulation (*35*). In future experiments, an analysis of the kinetic properties of the mEPSCs recorded from intact CG, as well as the effects of nonuniform release probabilities, will be incorporated into the model.

Sensitivity analysis. The source of mEPSC distribution variability has been attributed variously to the size of synaptic vesicles and the concentration of agonist in the cleft (*25*, *30*, *36*), the density of postsynaptic receptors (*37*), the release-site location or local environment (*36*), and the stochastics of receptor flickering (*18*). Our model CG is most sen-

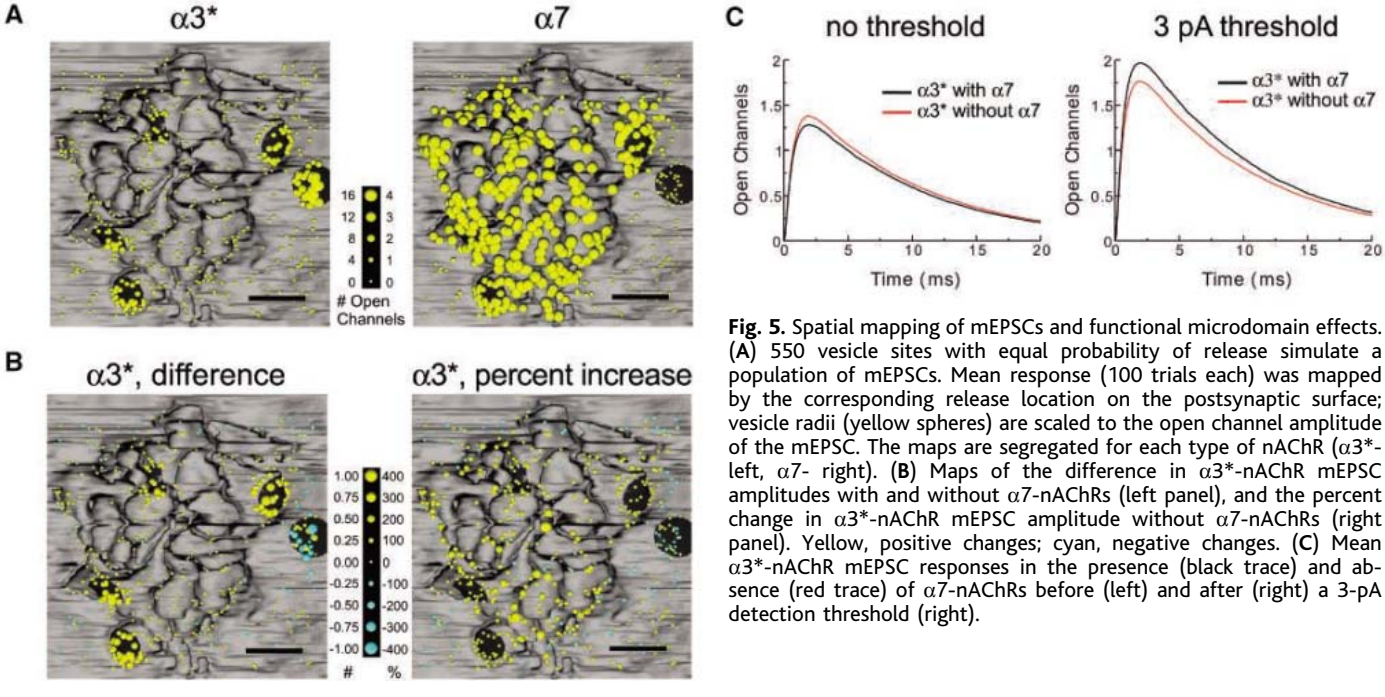

Fig. 5. Spatial mapping of mEPSCs and functional microdomain effects. (**A**) 550 vesicle sites with equal probability of release simulate a population of mEPSCs. Mean response (100 trials each) was mapped by the corresponding release location on the postsynaptic surface; vesicle radii (yellow spheres) are scaled to the open channel amplitude of the mEPSC. The maps are segregated for each type of nAChR (α3*-left, α7- right). (**B**) Maps of the difference in α3*-nAChR mEPSC amplitudes with and without α7-nAChRs (left panel), and the percent change in α3*-nAChR mEPSC amplitude without α7-nAChRs (right panel). Yellow, positive changes; cyan, negative changes. (**C**) Mean α3*-nAChR mEPSC responses in the presence (black trace) and absence (red trace) of α7-nAChRs before (left) and after (right) a 3-pA detection threshold (right).

sitive to the number of ACh molecules released into the cleft, implicating vesicle size as the primary source of variability (see normalized derivative sensitivity above; Fig. 3). The relative insensitivity of the O-state for nAChRs to variations in AChE densities in the vicinity of empirical measurements echoed those findings of previous Monte Carlo simulations in spatially synthetic conditions (*19*, *20*).

Functional microdomains. Our results indicate that a single quantum of ACh is able in most cases to reach some α7-nAChRs, consistent with reports indicating that both spontaneous and evoked synaptic responses are known to be mediated by both receptor types (*11*, *12*, *14*). In the case of site 1 (Fig. 2B), a somatic PSD release site, there was very little contribution of nearby spine-bound α7-nAChRs, suggesting a functional radius of ~0.2 μm for ACh in this CG model synapse. Population simulations similarly predict that the amplitude of mEPSCs generated by α3*-nAChRs at a PSD is greater when there are no surrounding α7-nAChRs; the magnitude of the ACh sequestering effect of α7-nAChRs thus depends on the location of ACh release relative to nAChR distributions (Fig. 5B).

Our finding that α7-nAChRs buffer the availability of ACh for binding to α3*-nAChRs suggests a role for spatial organization in determining intrinsic synaptic variability (*18*, *23*, *25*, *30*, *38*). A similar, cleft-limited diffusion buffering has been observed at snail synapses in culture where the extracellular glial-derived ACh binding protein modulates synaptic transmission by competing for released ACh (*39*, *40*). In contrast, receptor subtype interactions do not appear to affect channel openings in a recent Monte Carlo model of a glutamatergic synapse (*24*).

Conclusion. The computational model synapse strongly supports the ectopic release of synaptic vesicles as the predominant mechanism of activation of extrasynaptic α7-nAChRs at CG synapses. This conclusion makes sense given the limited effective ACh diffusion radius, the kinetic disparities between nAChR subtypes, and the principal contribution of the extrasynaptic, spine-bound α7-AChRs to many physiological measurements. The Kolmogorov-Smirnov analysis (Fig. 6F) verifies that in situ mEPSC distributions cannot be explained by traditional release patterns.

References and Notes

1. D. Zenisek, J. A. Steyer, W. Almers, *Nature* **406**, 849 (2000).
2. D. Lenzi, J. W. Runyeon, J. Crum, M. H. Ellisman, W. M. Roberts, *J. Neurosci.* **19**, 119 (1999).
3. K. Matsui, C. E. Jahr, *Neuron* **40**, 1173 (2003).
4. R. D. Shoop, M. E. Martone, N. Yamada, M. H. Ellisman, D. K. Berg, *J. Neurosci.* **19**, 692 (1999).
5. R. D. Shoop, E. Esquenazi, N. Yamada, M. H. Ellisman, D. K. Berg, *J. Neurosci.* **22**, 748 (2002).
6. W. G. Conroy, D. K. Berg, *J. Biol. Chem.* **270**, 4424 (1995).
7. M. H. Jacob, D. K. Berg, *J. Neurosci.* **3**, 260 (1983).
8. R. H. Loring, L. M. Dahm, R. E. Zigmond, *Neuroscience* **14**, 645 (1985).
9. H. L. Horch, P. B. Sargent, *J. Neurosci.* **15**, 7778 (1995).
10. J. F. Margiotta, D. K. Berg, V. E. Dionne, *J. Neurosci.* **7**, 3612 (1987).
11. Z. W. Zhang, J. S. Coggan, D. K. Berg, *Neuron* **17**, 1231 (1996).
12. E. M. Ullian, J. M. MacIntosh, P. B. Sargent, *J. Neurosci.* **17**, 7210 (1997).
13. M. E. McNerney, D. Pardi, P. C. Pugh, N. Qiang, J. F. Margiotta, *J. Neurophysiol.* **84**, 1314 (2000).
14. K. T. Chang, D. K. Berg, *J. Neurosci.* **19**, 3701 (1999).

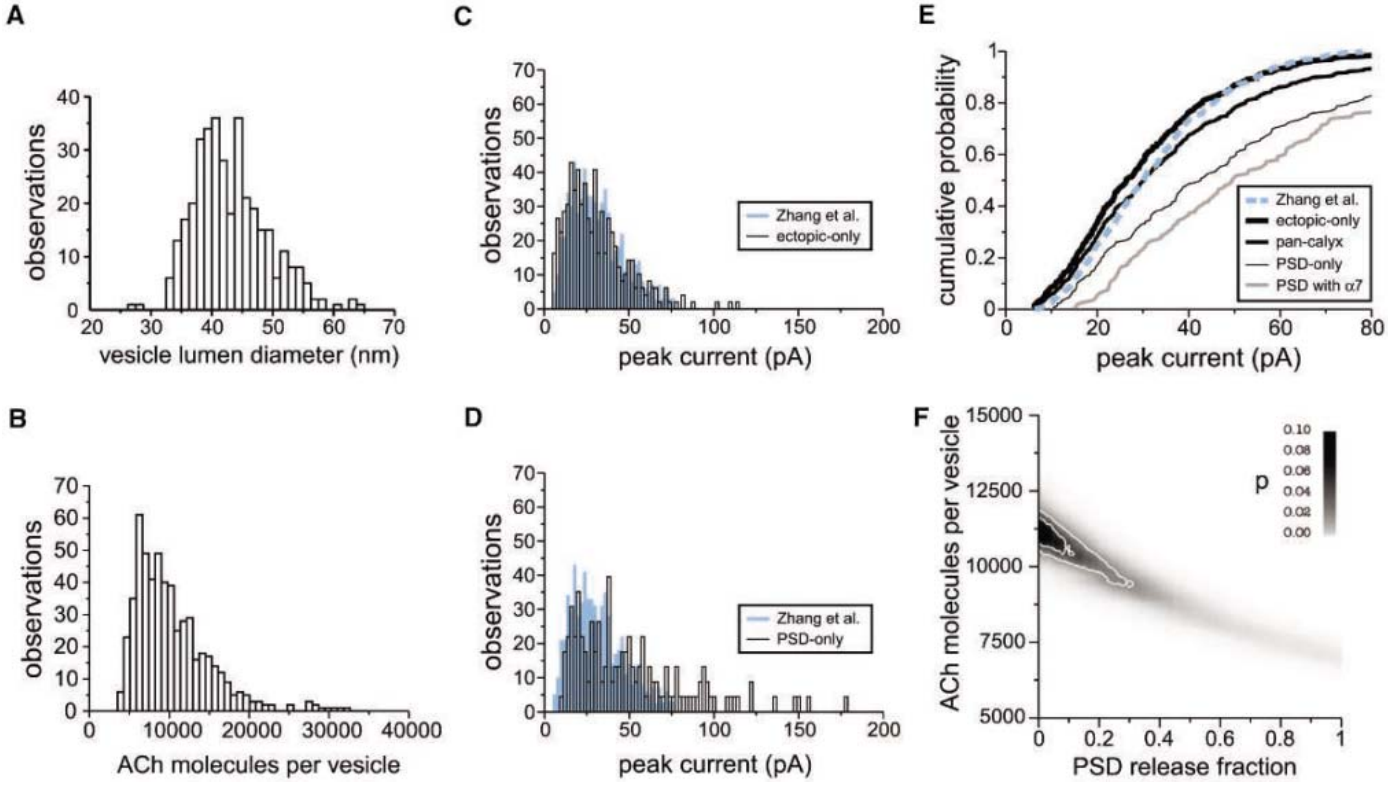

Fig. 6. Examination of ectopic release. (**A**) Frequency distribution of synaptic vesicle lumen diameters measured from tomographic reconstruction. (**B**) Vesicle size distribution adjusted volumetrically for ACh content. Mean number of ACh molecules (10,000) is that required to match the mean mEPSC amplitude from experimentally recorded events (*11*). (**C**) Population of mEPSCs from simulations with distributed vesicle sizes showing ectopic-only sites along with histogram of mEPSCs from CG whole-cell recordings (blue) (*11*). (**D**) Population of mEPSCs from simulations with distributed vesicle sizes showing PSD-only sites along with histogram of mEPSCs from CG whole-cell recordings (blue) (*11*). (**E**) Cumulative probability plots of mEPSCs from CG whole-cell recordings (dotted blue line) (*11*) and mEPSCs for simulated ectopic-only (thick black), pan-calyx (middle thickness black), PSD-only release (thin black), and PSD-only with α7-nAChRs (gray) populations. (**F**) Contour plot of goodness-of-fit between simulated and experimentally recorded mEPSCs. Distinct simulated mEPSC populations were generated by varying the fraction of vesicles released over PSD versus ectopic sites and by varying the mean number of ACh molecules per quantum. The fraction of PSD vesicles was varied from 0 (i.e., 0% PSD and 100% ectopic) to 1 (i.e., 100% PSD and 0% ectopic). The goodness-of-fit of each of these populations to the population of recorded mEPSCs (*11*) was measured by the Kolmogorov-Smirnov test. The P value of the goodness-of-fit is shown in grayscale. Darker gray indicates increasing similarity between the simulated and experimental populations. The outermost contour line indicates the $P = 0.02$ limit of confidence that the populations are dissimilar, and the inner line indicates the $P = 0.05$ limit.

15. R. D. Shoop, K. T. Chang, M. H. Ellisman, D. K. Berg, *J. Neurosci.* **21**, 771 (2001).
16. G. E. Soto *et al.*, *Neuroimage* **1**, 230 (1994).
17. T. M. Bartol Jr., B. R. Land, E. E. Salpeter, M. M. Salpeter, *Biophys. J.* **59**, 1290 (1991).
18. D. S. Faber, W. S. Young, P. Legendre, H. Horn, *Science* **258**, 1494 (1992).
19. L. Anglister, J. R. Stiles, M. M. Salpeter, *Neuron* **12**, 783 (1994).
20. M. R. Bennett, L. Farnell, W. G. Gibson, N. A. Lavidis, *Biophys. J.* **72**, 1595 (1997).
21. J. R. Stiles, T. M. Bartol, H. L. Fernandez, E. E. Salpeter, M. M. Salpeter, *Proc. Natl. Acad. Sci. U.S.A.* **93**, 5747 (1996).
22. J. R. Stiles, I. V. Kovyazina, E. E. Salpeter, M. M. Salpeter, *Biophys. J.* **77**, 1177 (1999).
23. J. R. Stiles, T. M. Bartol Jr., in *Computational Neuroscience: Realistic Modeling for Experimentalists*, E. de Schutter, Ed. (CRC Press, 2001), pp. 87–127.
24. K. M. Franks, T. M. Bartol, T. J. Sejnowski, *Biophys. J.* **83**, 2333 (2002).
25. K. M. Franks, C. F. Stevens, T. J. Sejnowski, *J. Neurosci.* **23**, 3186 (2003).
26. Materials and methods are available as supporting material on *Science* Online.
27. W. E. Lorensen, H. E. Cline, *Comput. Graph. (ACM)* **21**, 163 (1987).
28. J. Y. Couraud, H. L. Koenig, L. Di Giamberardino, *J. Neurochem.* **34**, 1209 (1980).
29. M. Vigny, S. Bon, J. Massoulie, F. Leterrier, *Eur. J. Biochem.* **85**, 317 (1978).
30. P. J. Kruk, H. Korn, D. S. Faber, *Biophys. J.* **73**, 2874 (1997).
31. D. Nguyen, P. B. Sargent, *J. Comp. Neurol.* **448**, 128 (2002).
32. J. S. Diamond, *J. Neurosci.* **21**, 8328 (2001).
33. D. A. DiGregorio, Z. Nusser, R. A. Silver, *Neuron* **35**, 521 (2002).
34. A. Momiyama *et al.*, *J. Physiol.* **549**, 75 (2003).
35. K. T. Chang, D. K. Berg, *Neuron* **32**, 855 (2001).
36. M. Frerking, S. Borges, M. Wilson, *Neuron* **15**, 885 (1995).
37. Z. Nusser, S. Cull-Candy, M. Farrant, *Neuron* **19**, 697 (1997).
38. H. Taschenberger, R. M. Leao, K. C. Rowland, G. A. Spirou, H. von Gersdorff, *Neuron* **36**, 1127 (2002).
39. A. B. Smit *et al.*, *Nature* **411**, 261 (2001).
40. K. Brejc *et al.*, *Nature* **411**, 269 (2001).
41. Supported by: State of California TRDRP (J.S.C.); NSF IBN-9985964, NIH P01-NS044306, and NIH GM068630 (T.J.S., T.M.B., J.R.S.); NSF PHY-0225630 (T.J.S., T.M.B.); HHMI (T.J.S.); NIH P41-RR06009 and NIH P20-GM065805 (J.R.S.); NPACI NSF-ASC 97-5249 (T.J.S., T.M.B., M.H.E., M.E.M.); NIH NCRR RR04050 (M.H.E., M.E.M.); Human Brain Project DC03192 (M.H.E., M.E.M.); and NIH NS12601 and NS35469 (D.K.B.). We thank P. B. Sargent, C. F. Stevens, and R. Kerr for advice. We dedicate this work to the vision of the late Dr. Miriam Salpeter.

Supporting Online Material
www.sciencemag.org/cgi/content/full/309/5733/446/DC1
Materials and Methods
Figs. S1 to S3
References and Notes

3 December 2004; accepted 17 May 2005
10.1126/science.1108239

REPORTS

The First Chemical Enrichment in the Universe and the Formation of Hyper Metal-Poor Stars

Nobuyuki Iwamoto,[1] Hideyuki Umeda,[2] Nozomu Tominaga,[2] Ken'ichi Nomoto,[2]* Keiichi Maeda[3]

The recent discovery of a hyper–metal-poor (HMP) star, with a metallicity Fe/H smaller than 1/100,000 of the solar ratio, together with one earlier HMP star, has raised a challenging question whether these HMP stars are the actual first-generation, low-mass stars of the universe. We argue that these HMP stars are second-generation stars formed from gases that were chemically enriched by the first-generation supernovae. The key to this solution is the very unusual abundance patterns of these HMP stars and the similarities and differences between them. We can reproduce these abundance features with core-collapse "faint" supernova models that include extensive matter mixing and fallback during explosions.

Identifying the first stars in the universe, i.e., metal-free Population III (Pop III) stars that were born in a primordial hydrogen-helium gas cloud, is one of the important challenges of current astronomy (*1*, *2*). Recently, two hyper–metal-poor (HMP) stars, HE0107-5240 (*3*) and HE1327-2326 (*4*), were discovered with metallicity Fe/H smaller than 1/100,000 of the metallicity of the Sun (i.e., with [Fe/H] < -5 in these two stars), more than a factor of 10 smaller than that of previously known extremely metal-poor (EMP) stars. (Here [A/B] = $\log_{10}(N_A/N_B) - \log_{10}(N_A/N_B)_\odot$, where the subscript $\odot$ refers to the solar value and N_A and N_B are the abundances of elements A and B, respectively.) This discovery raised an important question as to whether the observed low-mass ($\sim$0.8 $M_\odot$) HMP stars are actually Pop III stars or whether these HMP stars are second-generation stars being formed from gases that were chemically enriched by a single first-generation supernova (SN) (*5*). This is related to the question of how the initial mass function depends on metallicity (*6*). Identifying the origin of these HMP stars is thus indispensable to an understanding of the earliest star formation and the chemical enrichment history of the universe.

The elemental abundance patterns of these HMP stars provide a key to the answers to these questions. The abundance patterns of HE1327-2326 (*4*) and HE0107-5240 (*7*, *8*) are unusual (Fig. 1). The marked similarity of their [Fe/H] (-5.4 and -5.2 for HE1327-2326 and HE0107-5240, respectively) and their [C/Fe] ($\sim$4) suggests that similar chemical enrichment mechanisms operated in forming these HMP stars. However, the N/C and (Na, Mg, Al)/Fe ratios are more than a factor of 10 larger in HE1327-2326. In order for theoretical models to be viable, these similarities and differences should be explained self-consistently.

Here we report that the similarities and variations of the HMP stars can be well reproduced in a unified manner by nucleosynthesis in core-collapse "faint" supernovae (SNe) that undergo mixing and fallback (*5*). We thus argue that the HMP stars are second-generation low-mass stars, the formation of which was induced by first-generation (Pop III) SNe with efficient cooling of carbon-enriched gases.

The similarity of the [Fe/H] and [C/Fe] suggests that the progenitor's masses of Pop III SNe were similar for these HMP stars. We therefore chose the Pop III 25 $M_\odot$ models and calculated their evolution and explosion. The abundance distribution after explosive nucleosynthesis is shown in Fig. 2 for the kinetic energy E of the ejecta $E_{51} \equiv E/10^{51}$ erg = 0.74. The abundance distribution for $E_{51} = 0.71$ is similar. In the faint SN model, most of the materials that undergo explosive nucleosynthesis are decelerated by the influence of gravitational pull (*9*) and will eventually fall back onto the central compact object (Fig. 3). We did not calculate such "fallback" earlier (*5*) but found it to take place in our present models if $E_{51} < 0.71$. (For the 50 $M_\odot$ star, the fallback is found to occur for $E_{51} < 2$, because of deeper gravitational potential.) We obtained a relation between E and the mass cut M_{cut} (the mass of the materials that finally collapse to form a compact object); i.e., smaller E_{51} leads to a larger amount of fallback (a larger M_{cut}). The explosion energies of $E_{51} = 0.74$ and 0.71 lead to the mass cut $M_{cut} = 5.8\ M_\odot$ and 6.3 $M_\odot$, respectively, and we use the former and the latter models to explain the abun-

[1]Nuclear Data Center, Japan Atomic Energy Research Institute, Ibaraki 319-1195, Japan. [2]Department of Astronomy, School of Science, University of Tokyo, Tokyo 113-0033, Japan. [3]Department of Earth Science and Astronomy, College of Arts and Sciences, University of Tokyo, Tokyo 153-8902, Japan.

*To whom correspondence should be addressed. E-mail: nomoto@astron.s.u-tokyo.ac.jp

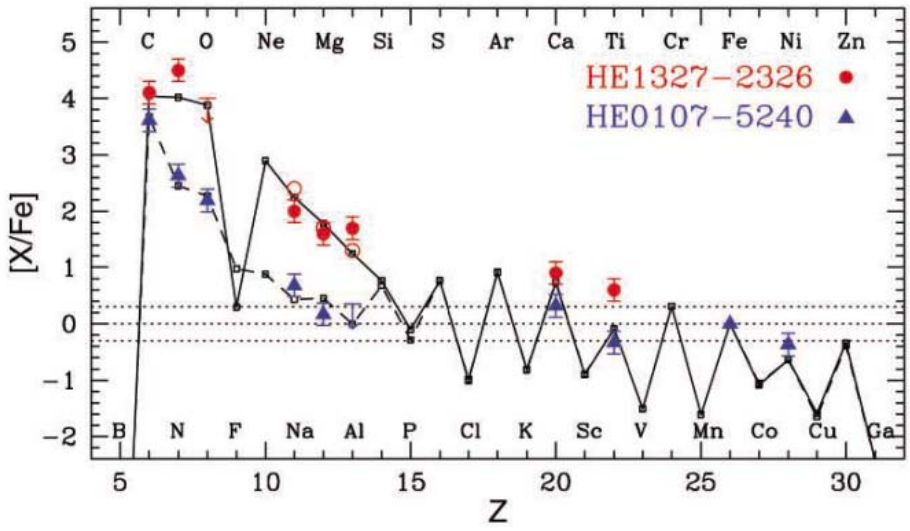

Fig. 1. Comparison of elemental abundance ratios observed in HE1327-2326 [solid circles, (*4*)] and HE0107-5240 [solid triangles, (*7*, *8*)] with those of our SN models (small open squares connected by the solid line for HE1327-2326 and by the dashed line for HE0107-5240), as a function of atomic number *Z*. The new solar abundances are used (*27*). For Na and Al, the importance of accurate nonlocal thermodynamic equilibrium (LTE) corrections are demonstrated from the comparison with the LTE values indicated by the open circles. The ejected yields are those from Pop III 25 $M_\odot$ SN models with the parameters described in Fig. 2. Dashed lines indicate the solar abundance ([X/Fe] = 0) and a typical uncertain range of observational and theoretical abundances ([X/Fe] = ±0.3 dex).

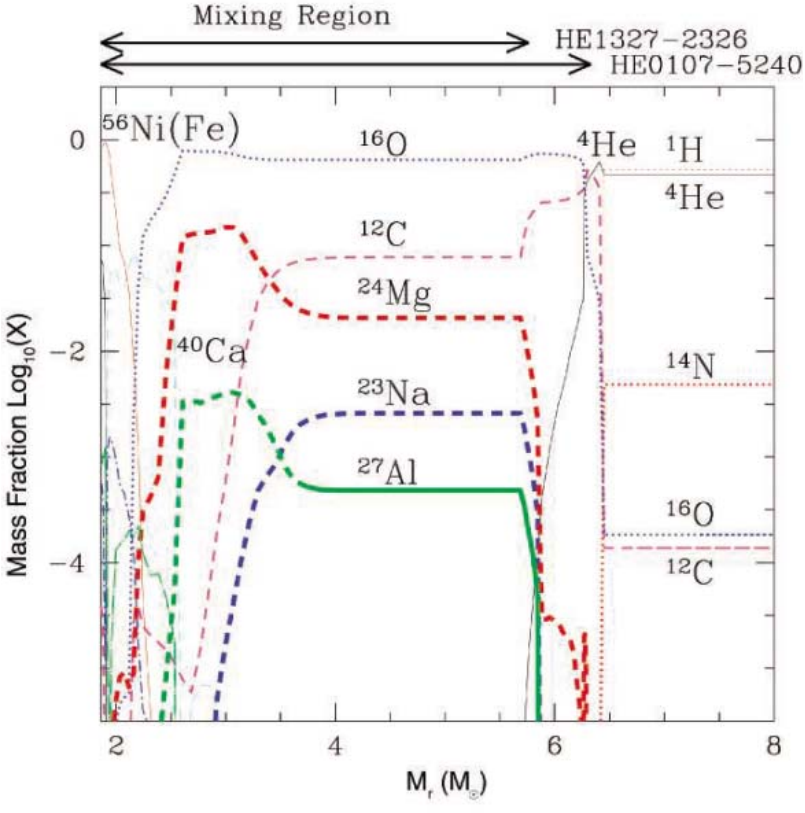

Fig. 2. Internal abundance distribution for nuclei (by mass fraction) in the Pop III 25 $M_\odot$ SN model for the explosion energy of E_{51} = 0.74 (for HE1327-2326). The distribution is similar for E_{51} = 0.71 (HE0107-5240). The mixing is assumed to take place in the region of M_r = 1.9 − 5.8 $M_\odot$ for HE1327-2326 and M_r = 1.9 − 6.3 $M_\odot$ for HE0107-5240. The mass fraction of the ejected materials with respect to the mixed fallback materials is $f = 8.7 \times 10^{-5}$ for HE1327-2326 and $f = 1.2 \times 10^{-4}$ for HE0107-5240. As a result, the ejecta contains 1.0×10^{-5} $M_\odot$ ^{56}Ni and 0.20 $M_\odot$ ^{12}C for HE1327-2326 and $1.4 \times 10^{-5} M_\odot$ ^{56}Ni and 0.12 $M_\odot$ ^{12}C for HE0107-5240.

dance patterns of HE1327-2326 and HE0107-5240, respectively.

During the explosion, we assume that the SN ejecta undergoes mixing. Materials are first uniformly mixed in the mixing region extending from M_r = 1.9 $M_\odot$ to the mass cut at $M_r = M_{cut}$ (where M_r is the mass coordinate and stands for the mass interior to the radius *r*) (Fig. 2). Only a tiny fraction *f* of the mixed material is ejected from the mixing region, together with all materials at $M_r > M_{cut}$; most materials interior to the mass cut fall back onto the central compact object. Such a mixing-fallback mechanism (which might mimic a jet-like explosion) is required to extract Fe group and other heavy elements from the deep fallback region into the ejecta (*5*, *10*).

Figure 1 shows the calculated abundance ratios in the SN ejecta models for a suitable choice of *f* (Fig. 2), which are respectively compared with the observed abundances of the two HMP stars. In order to reproduce [C/Fe] ~ 4 and other abundance ratios of HMP stars shown in Fig. 1, our models required an ejected Fe mass of only 1.0×10^{-5} $M_\odot$ for HE1327-2326 and 1.4×10^{-5} $M_\odot$ for HE0107-5240 (Fig. 2). These SNe are much fainter in the radioactive tail than the typical SNe and form massive black holes of ~6 $M_\odot$.

What causes the large difference in the amount of Na-Mg-Al between the SNe that produced HE0107-5240 and HE1327-2326? Because very little Na-Mg-Al is ejected from the mixed fallback materials (i.e., $f \sim 10^{-4}$) compared with the materials exterior to the mass cut, the ejected amount of Na-Mg-Al is very sensitive to the location of the mass cut. As indicated in Fig. 2, M_{cut} is smaller (i.e., the fallback mass is

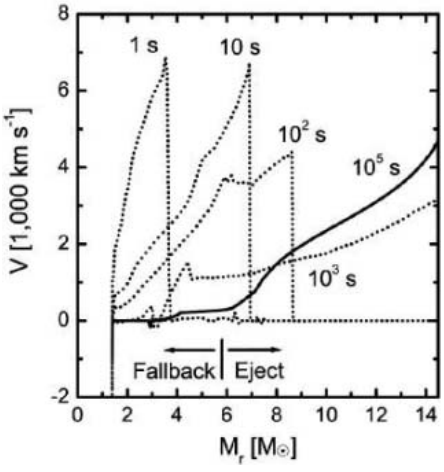

Fig. 3. Propagation of the shock wave and fallback for the HE1327-2326 model. The progenitor is the 25 $M_\odot$ star. As the shock propagates through the H envelope and breaks out of the surface, the materials in the inner region continue to decelerate and will eventually fall back onto the central remnant. The mass cut (that divides the materials fallen onto the central remnant and ejected outward) is determined by comparing the velocity (v) and the escape velocity at 10^5 seconds after the explosion.

smaller) in the model for HE1327-2326 (M_{cut} = 5.8 $M_{\odot}$) than for HE0107-5240 (M_{cut} = 6.3 $M_{\odot}$), so that a larger amount of Na-Mg-Al is ejected from the SN for HE1327-2326. Because M_{cut} is sensitively determined by the explosion energy, the (Na-Mg-Al)/Fe ratios among the HMP stars are predicted to show large variations and can be used to constrain E_{51}. The explosion energies of these SN models with fallback are not necessarily very small (i.e., $E_{51} \sim 0.7$). These explosion energies are also consistent with those observed in the actual faint SNe (*11*).

Our previous models (*5*) tended to underproduce Na compared with the abundances of HE0107-5240. This problem has been improved in our current presupernova models. Na and Al are mainly produced by C shell burning, and their production is very sensitive to the treatment of overshooting in the convective C burning shell as well as the ^{12}C abundance that remains after core He burning (*12*). By including overshooting with the overshooting length less than one-fifth of a pressure scale height for the entire presupernova evolution, our current supernova models contain large enough abundances of Na and Al (Fig. 2). Such an overshooting length has been estimated from the comparison with the Hertzsprung Russell diagrams of many young stellar clusters. After the mixing and fallback, the resultant abundance patterns with Na and Al are in reasonable agreement with HE1327-2326 and HE0107-5240 (Fig. 1). The enhancement of Na and Al attributable to overshooting in the progenitor evolution may better explain the small odd-even effect in the elemental abundance patterns observed in EMP stars (*13*).

The next question is why HE1327-2326 has a much larger N/C ratio than HE0107-5240. In our models, a large amount of N is produced by mixing between the He convective shell and the H-rich envelope during presupernova evolution (*14*), where C created by the triple-α reaction is burnt into N through the CNO cycle. For the HE1327-2326 model, we assume ~30 times larger diffusion coefficients (i.e., faster mixing) for the H and He convective shells to overcome an inhibiting effect of the mean molecular weight gradient (and also the entropy gradient) between the H and He layers. Thus, larger amounts of protons are carried into the He convective shell. [C/N] $\sim$ 0 is then realized as observed in HE1327-2326. Such an enhancement of mixing efficiency has been suggested to take place in the present-day massive stars known as fast rotators; these rotating stars show various degrees of N and He enrichments due to different rotation velocities (*15*).

If no large enhancement of N occurred in the SN ejecta, the following scenario can explain a high abundance of N (and also Na and Al) at the surface. If HE1327-2326 is in a binary system and its intermediate-mass companion star has experienced the asymptotic giant branch (AGB) phase, only the odd elements such as N, Na, and Al should be efficiently enriched. The observed C, Mg, and heavier elements should predominantly come from a faint SN as modeled above. The small accreted mass ($\sim 10^{-4}$ to 10^{-3} $M_{\odot}$) mixed with a shallow surface convective layer in HE1327-2326 would be enough to account for the observed abundance pattern. The smallness of the accreted mass requires that the observed star belong to a wide binary system and that accretion take place through mass loss from an AGB star. In contrast to an AGB scenario without pre-enrichment from the faint SN, this model can realize [C/N] $\sim$ 0 if the proper amount of N is transferred.

For HE0107-5240, an alternative scenario has been proposed (*16*), assuming that the HMP stars are actually Pop III stars. It is difficult for such a scenario to explain the differences between HE0107-5240 and HE1327-2326. This scenario assumes that the HMP star is in a binary system and that an AGB companion star has polluted the surface abundance of the HMP star. Even if Pop III AGB stars suffer surface pollution at an early phase of their evolution (*16*–*18*), the recurrent mixing process after He shell flashes will carry C-enriched materials (with no enrichment of N) from a deep He-rich layer to the surface. The surface C abundance of the low-mass companion progressively increases, but no N enhancement can be seen (i.e., [C/N] > 0). On the contrary, if a donor AGB star experiences hot bottom burning, dredged-up C is processed into N at the base of the convective envelope, and thus [C/N] = $-2 \sim -1$. Therefore, [C/N] $\approx$ 0 is difficult for Pop III AGB stars to reproduce, although the C/N ratio might be consistent with the observed value during a short period of the star's evolution.

What about stars with 130 to 300 $M_{\odot}$ (*19*, *20*)? Pair-instability SNe (PISNe) from this mass range have been widely considered to be the first source of chemical enrichment in the universe (*20*). However, PISNe provide abundance patterns that are incompatible with the observations of the HMP stars. Because PISNe undergo complete disruption and eject a large amount of Fe (*19*, *20*), the ejecta have [C/Fe] that is too low (< 0) to be compatible with the two HMP stars, and large [Fe/H] (> −4) is predicted.

What other elements are important to distinguish the different models? Oxygen is certainly important. For HE0107-5240, its large [C/O] ratio rules out the simple mass-cut models (without mixing and fallback) in the multiple SN model (*8*, *10*). For our faint SN models, [C/O] is sensitive to M_{cut} and thus to E.

Neutron-capture elements are important for constraining scenarios involving an AGB star. For HE1327-2326, the observed lower limit of [Sr/Ba] > −0.4 is inconsistent with stars enhanced by a slow neutron capture process (an s-process) (*21*, *22*) and with theoretical predictions of a low-metallicity AGB s-process (*23*), but it is very consistent with the values seen in the rapid (r-) process–enhanced stars (*24*, *25*). This may favor SN origins, because the r-process signature observed in EMP stars is thought to come from SNe. However, the s-process in AGB stars is still uncertain, and such Sr/Ba ratio might also be reproduced (*26*).

Our models offer several predictions for future observations of HMP stars. First, the metallicity Fe/H of an HMP star is determined by the mass ratios between the ejected Fe M_{Fe} and mixed interstellar hydrogen M_{Hmix}, and small M_{Fe} (i.e., small f) is responsible for the small [Fe/H]. Our spherical explosion models predict a continuous distribution of [Fe/H] in metal-poor stars. Thus, if the gap at [Fe/H] ~ -5 to -4 is real, jet-induced mixing might be responsible for constraining the distribution of the f value. Second, assuming that C/H needs to be higher than a certain value in order to form low-mass HMP stars, C/Fe would tend to be larger for smaller Fe/H. Third, the (Na-Mg-Al)/Fe ratios in HMP stars would show a continuous distribution, because their variations are the result of variation of E. Finally, if the large N/Fe is attributable to rotation and if rotation can contribute to enhanced E, N/Fe will show a positive correlation with (Na-Mg-Al)/Fe.

References and Notes

1. A. Weiss, T. G. Abel, V. Hill, Eds., *The First Stars* (Springer-Verlag, Berlin, 2000).
2. T. Abel, G. L. Bryan, M. L. Norman, *Science* **295**, 93 (2002).
3. N. Christlieb *et al.*, *Nature* **419**, 904 (2002).
4. A. Frebel *et al.*, *Nature* **434**, 871 (2005).
5. H. Umeda, K. Nomoto, *Nature* **422**, 871 (2003).
6. R. Schneider, A. Ferrara, R. Salvaterra, K. Omukai, V. Bromm, *Nature* **422**, 869 (2003).
7. N. Christlieb *et al.*, *Astrophys. J.* **603**, 708 (2004).
8. M. S. Bessell, N. Christlieb, B. Gustafsson, *Astrophys. J.* **612**, L61 (2004).
9. S. E. Woosley, T. A. Weaver, *Astrophys. J. Suppl. Ser.* **101**, 181 (1995).
10. H. Umeda, K. Nomoto, *Astrophys. J.* **619**, 427 (2005).
11. M. Turatto *et al.*, *Astrophys. J.* **498**, L129 (1998).
12. A. Chieffi, M. Limongi, *Astrophys. J.* **577**, 281 (2002).
13. R. Cayrel *et al.*, *Astron. Astrophys.* **416**, 1117 (2004).
14. H. Umeda, K. Nomoto, T. Nakamura, in (*1*), pp. 150–173.
15. A. Heger, N. Langer, S. E. Woosley, *Astrophys. J.* **528**, 368 (2000).
16. T. Suda, M. Aikawa, M. N. Machida, M. Y. Fujimoto, I. Iben Jr., *Astrophys. J.* **611**, 476 (2004).
17. A. Chieffi, I. Domínguez, M. Limongi, O. Straniero, *Astrophys. J.* **554**, 1159 (2001).
18. L. Siess, M. Livio, J. Lattanzio, *Astrophys. J.* **570**, 329 (2002).
19. H. Umeda, K. Nomoto, *Astrophys. J.* **565**, 385 (2002).
20. A. Heger, S. E. Woosley, *Astrophys. J.* **567**, 532 (2002).
21. W. Aoki *et al.*, *Astrophys. J.* **561**, 346 (2001).
22. S. Lucatello *et al.*, *Astron. J.* **125**, 875 (2003).
23. S. Goriely, N. Mowlavi, *Astron. Astrophys.* **362**, 599 (2000).
24. V. Hill *et al.*, *Astron. Astrophys.* **387**, 560 (2002).
25. C. Sneden *et al.*, *Astrophys. J.* **591**, 936 (2003).
26. L. Siess, S. Goriely, N. Langer, *Astron. Astrophys.* **415**, 1089 (2004).
27. M. Asplund, N. Grevesse, J. Sauval, in *Cosmic Abundances as Records of Stellar Evolution and Nucleosynthesis*, F. N. Bash, T. G. Barnes, Eds. (Astronomical Society of the Pacific Conference Series, San Francisco, 2004), in press (available at http://arxiv.org/abs/astro-ph/0410214).

28. Supported by the Japan Society for the Promotion of Science and the Ministry of Education, Culture, Sports, Science, and Technology in Japan.

31 March 2005; accepted 23 May 2005
Published online 02 June 2005;
10.1126/science.1112997
Include this information when citing this paper.

Controlled Single-Photon Emission from a Single Trapped Two-Level Atom

B. Darquié, M. P. A. Jones, J. Dingjan, J. Beugnon, S. Bergamini, Y. Sortais, G. Messin, A. Browaeys,* P. Grangier

By illuminating an individual rubidium atom stored in a tight optical tweezer with short resonant light pulses, we created an efficient triggered source of single photons with a well-defined polarization. The measured intensity correlation of the emitted light pulses exhibits almost perfect antibunching. Such a source of high-rate, fully controlled single-photon pulses has many potential applications for quantum information processing.

Implementing a deterministic or conditional two-qubit quantum gate is a key step toward quantum computation. Deterministic gates generally require a strong interaction between the particles that are used to carry the physical qubits (*1*). Recently, controlled-not gates have been realized with the use of trapped ions and incorporated in elaborate quantum algorithms (*2*–*4*). So far, individually addressed two-qubit gates have not been demonstrated with neutral atoms. Promising results have been obtained on entangling neutral atoms with the use of cold controlled collisions in an optical lattice (*5*), but the single-qubit operations are difficult to perform in such a system.

Another approach is to bypass the requirement for a direct interaction between the qubits and use instead an interference effect and a measurement-induced state projection to create the desired operation (*6*, *7*). An interesting recent development of this idea is the use of photon detection events to create entangled states of two atoms (*8*–*10*). This provides "conditional" quantum gates, where the success of the logical operation is heralded by appropriate detection events. These schemes can be extended to realize a full controlled-not gate, or a Bell-state measurement, or more generally to implement conditional unitary operations (*8*, *11*). They could be implemented by using, for instance, trapped ions (*12*) or atoms in microscopic dipole traps. These proposals require the controlled emission of indistinguishable single photons by at least two identical emitters.

Various single-photon sources have been implemented using solid-state systems as well as atoms or ions. Solid-state systems such as single molecules, nitrogen-vacancy centers in diamond, and quantum dots allow high single-photon rates (*13*). However, realizing truly identical sources is a major problem for such systems because of inhomogeneities in both the environment of the emitters and the emitters themselves. Another approach is provided by sources based on neutral atoms (*14*, *15*) or ions (*16*) strongly coupled to a mode of a high-finesse optical cavity. Such sources are spectrally narrow, and the photons are emitted into a well-defined spatial mode, thus opening the way to coherent coupling of the quantum state of single atoms and single photons. However, the rate at which the system can emit photons is limited by the cavity and is often low in practice. Moreover, the need to achieve the strong coupling regime of cavity quantum electrodynamics remains a demanding experimental requirement.

We present a triggered single-photon source based on a single rubidium atom trapped at the focal point of a lens with a high numerical aperture of 0.7. We also show that we have full control of the optical transition by observing Rabi oscillations. Under these conditions, our system is equivalent to the textbook model formed by a two-level atom driven by monochromatic light pulses. Previous work has shown that by using holographic techniques one can create arrays of dipole traps, each containing a single atom, which can be addressed individually (*17*). The work presented here can therefore be directly scaled to two or more identical emitters.

We trapped the single rubidium-87 atom at the focus of the lens using a far-detuned optical dipole trap (810 nm), loaded from an optical molasses. The same lens was used to collect the fluorescence emitted by the atom (Fig. 1). The experimental apparatus is described in more detail by Schlosser *et al.* (*18*, *19*). A crucial feature of our experiment is the existence of a "collisional blockade" mechanism (*19*) which allows only one atom at a time to be stored in the trap; if a second atom enters the trap, both are immediately ejected. In this regime, the atom statistics are sub-Poissonian and the trap contains either one or zero (and never two) atoms, with an average atom number of 0.5.

The trapped atom was excited with 4-ns pulses of laser light, resonant with the $S_{1/2}$, $F = 2 \rightarrow P_{3/2}$, $F' = 3$ transition at 780.2 nm. The laser pulses were generated by frequency doubling pulses at 1560 nm, generated by using an electrooptic modulator to chop the output of a continuous-wave diode laser. A fiber amplifier was used to boost the peak power of the pulses before the doubling crystal. The repetition rate of the source was 5 MHz.

Fluorescence photons were produced by spontaneous emission from the upper state, which has a lifetime of 26 ns. The pulsed laser beam was right-circularly polarized (σ^+-polarized) with respect to the quantization axis defined by a magnetic field applied during the excitation. The trapped atom was optically pumped into the $F = 2$, $m_F = +2$ ground state by the first few laser pulses. It then cycled on the $F = 2$, $m_F = +2 \rightarrow F' = 3$, $m_{F'} = +3$ transition, which forms a closed two-level system emitting σ^+-polarized photons. Impurities in the polarization of the pulsed laser beam with respect to the quantization axis, together with the large bandwidth of the exciting pulse (250 MHz), resulted in off-resonant excitation to the $F' = 2$ upper state, leading to possible de-excitation to the $F = 1$ ground state. To counteract this, we added a repumping laser resonant with the $F = 1 \rightarrow F' = 2$ transition. We checked that our two-level description was still valid in the presence of the repumper by analyzing the polarization of the emitted single photons (supporting online material text).

The overall detection and collection efficiency for the light emitted from the atom was measured to be 0.60 ± 0.04%. This was obtained by measuring the fluorescence rate of the atom for the same atomic transition driven by a continuous-wave probe beam and confirmed by a direct measurement of the transmission of our detection system (SOM text).

For a two-level atom and exactly resonant square light pulses of fixed duration T, the probability that an atom in the ground state

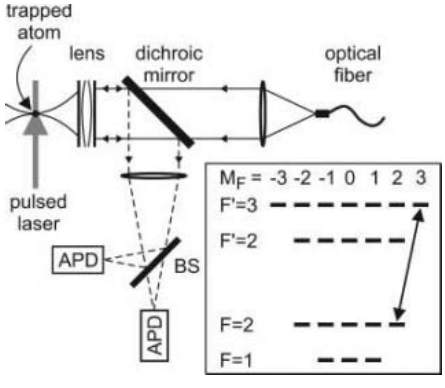

Fig. 1. Schematic of the experiment. The same lens is used to focus the dipole trap and collect the fluorescence light. The fluorescence is separated by a dichroic mirror and imaged onto two photon-counting avalanche photodiodes (APD), placed after a beam-splitter (BS). The insert shows the relevant hyperfine levels and Zeeman sublevels of rubidium-87. The cycling transition is shown by the arrow. Also shown is the nearby $F' = 2$ level responsible for the depumping.

Laboratoire Charles Fabry de l'Institut d'Optique (UMR 8501), Bâtiment 503, Centre Universitaire, 91403 Orsay, France.

*To whom correspondence should be addressed. E-mail: antoine.browaeys@iota.u-psud.fr

will be transferred to the excited state is $\sin^2(\Omega T/2)$, where the Rabi frequency Ω is proportional to the square root of the power. Therefore, the excited state population and hence the fluorescence rate oscillates as the intensity is increased. To observe these Rabi oscillations, we illuminated the trapped atom with the laser pulses during 1 ms. We kept the length of each laser pulse fixed at 4 ns, with a repetition rate of 5 MHz, and measured the total fluorescence rate as a function of the laser power. The Rabi oscillations are clearly visible on our results (Fig. 2). From the height of the first peak and the calibrated detection efficiency measured previously, we derived a maximum excitation efficiency per pulse of 95 ± 5%.

The reduction in the contrast of the oscillations at high laser power is mostly due to fluctuations of the pulsed laser peak power. This is shown by the theoretical curve in Fig. 2, based on a simple two-level model. This model shows that the 10% relative intensity fluctuations that we measured on the laser beam are enough to smear out the oscillations as observed.

The behavior of the atom in the time domain can be studied by using time-resolved photon-counting techniques to record the arrival times of the photons relative to the excitation pulses, thus constructing a time spectrum. By adjusting the laser pulse intensity, we observe an adjustable number of Rabi oscillations during the duration of the pulse, followed by the free decay of the atom once the laser has been turned off. The effects of pulses close to π, 2π, and 3π are displayed as inserts in Fig. 2 and show the quality of the coherent control achieved on a single atom.

To use this system as a single photon source, the laser power was set to realize a π pulse. To maximize the number of single photons emitted before the atom was heated out of the trap, we used the following sequence. First, we detected the presence of an atom in the dipole trap in real time using its fluorescence from the molasses light. Then, the magnetic field was switched on and we triggered an experimental sequence that alternated 115-μs periods of pulsed excitation with 885-μs periods of cooling by the molasses light (Fig. 3). The repumping laser remained on throughout, and the trap lifetime during the sequence was measured to be 34 ms. After 100 excitation/cooling cycles, the magnetic field was switched off and the molasses was turned back on until a new atom was recaptured and the process began again. On average, three atoms were captured per second under these conditions. The average count rate during the excitation was 9600 s^{-1}, with a peak rate of 29,000 s^{-1} (corresponding to twice the first peak in Fig. 3).

To characterize the statistics of the emitted light, we measured the second-order temporal correlation function, using a Hanbury Brown and Twiss type set-up. To do this, we used the beam splitter in the imaging system (Fig. 1), which sent the fluorescence light to two photon-counting avalanche photodiodes that were connected to a high-resolution time-to-digital conversion counting card in a start-stop configuration (resolution of about 1 ns). The card was gated so that only photons scattered during the 115 μs periods of pulsed excitation were counted, and the number of coincidence events was measured as a function of delay. The histogram obtained after 4 hours of continuous operation is displayed in Fig. 4 and shows a series of spikes separated by the period of the excitation pulses (200 ns). The $1/e$ half width of the peaks is 27 ± 3 ns, in agreement with the lifetime of the upper state. No background correction was done on the displayed data. The small flat background is attributed to coincidences between a fluorescence photon, and an event coming either from stray laser light (about 175 counts/s), or dark counts of the avalanche photodiodes (about 150 counts/s). When we correct for these events, the integrated residual area around zero delay is 3.4 ± 1.2% of the area of the other peaks.

We calculated (*20*) that under our experimental conditions, the probability to emit exactly one photon per pulse is 0.981, whereas the probability to emit two photons is 0.019. These two-photon events would show up in the correlation curve as coincidences close to zero delay (still with no coincidences at exactly zero delay). From our calculation, the value for the ratio of the area around zero delay to the area of the other peaks is 3.7%, in excellent agreement with the experimental results.

Finally, we discuss the coherence properties of the emitted photons, necessary for entanglement protocols based on the interference between two emitted photons, either from the same atom or from different atoms. As our collection optics are diffraction limited, the outgoing photons should be in a single spatial mode of the electromagnetic field. As far as temporal coherence is concerned, the main limiting factor appears to be the motion of the atom in the trap, which can be controlled by optimized cooling sequences. We then anticipate that our source should be Fourier limited by the lifetime of the excited state. We are now working to characterize the coherence of our single-photon source and to use it to observe multiple atom interference effects.

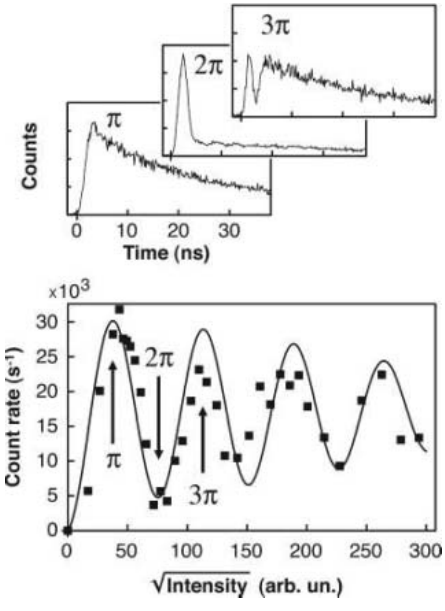

Fig. 2. Total count rate (squares) as a function of the average power of the pulsed beam, for a fixed pulse length of 4 ns and a repetition rate of 5 MHz. The solid line is a theoretical curve based on a simple two-level model that includes spontaneous emission and intensity fluctuations. The inserts show the time spectra for the laser intensities corresponding to π, 2π, and 3π pulses. arb. un., arbitrary units.

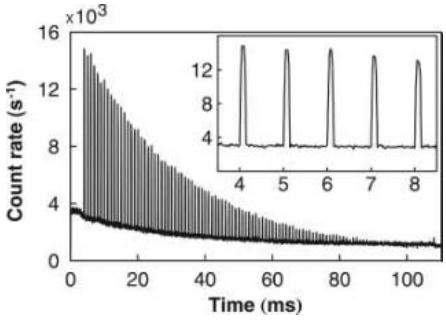

Fig. 3. Fluorescence signal measured by one of the two photodiodes during the experimental sequence, averaged over 22,958 cycles. Peaks are observed corresponding to the 115-μs periods of pulsed excitation, separated by periods of lower fluorescence induced by the molasses light during the 885 μs of cooling. The exponential decay of the signal is due to the lifetime of the atom in the trap, which is 34 ms under these conditions. (Insert) A close-up of the signal clearly shows the alternating excitation and cooling periods.

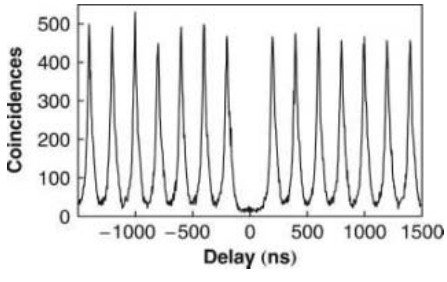

Fig. 4. Histogram of the time delays in the start-stop experiment. The histogram has been binned 4 times, leading to a 4.7-ns time resolution. No correction for background has been made. The absence of a peak at zero delay shows that the source is emitting single photons. During the 4-hour experimental run, 43,895 sequences were completed, which corresponds to a total of 505 s of excitation. A total of 4.83×10^6 photons were detected by the two photodiodes.

References and Notes

1. P. Zoller, J. I. Cirac, L. Duan, J. J. García-Ripoll, in *Les Houches 2003: Quantum Entanglement and Information Processing*, D. Estève, J.-M. Raimond, J. Dalibard, Eds. (Elsevier, Amsterdam, 2004), pp. 187–222.
2. M. Riebe *et al.*, *Nature* **429**, 734 (2004).
3. M. D. Barrett *et al.*, *Nature* **429**, 737 (2004).
4. J. Chiaverini *et al.*, *Nature* **432**, 602 (2004).
5. O. Mandel *et al.*, *Nature* **425**, 937 (2003).
6. E. Knill, R. Laflamme, G. J. Milburn, *Nature* **409**, 46 (2001).
7. J. P. Dowling, J. D. Franson, H. Lee, G. J. Milburn, *Quantum Inf. Process.* **3**, 205 (2004).
8. I. Protsenko, G. Reymond, N. Schlosser, P. Grangier, *Phys. Rev. A.* **66**, 062306 (2002).
9. C. Simon, W. T. M. Irvine, *Phys. Rev. Lett.* **91**, 110405 (2003).
10. L.-M. Duan, H. J. Kimble, *Phys. Rev. Lett.* **90**, 253601 (2003).
11. Y. L. Lim, A. Beige, L. C. Kwek, in press; preprint available at http://arXiv.org/abs/quant-ph/0408043.
12. B. B. Blinov, D. L. Moehring, L.-M. Duan, C. Monroe, *Nature* **428**, 153 (2004).
13. Single Photons on Demand, P. Grangier, B. Sanders, J. Vukovic, Eds. *New J. Phys.* **6**, 85–100, 129–163 (2004).
14. A. Kuhn, M. Hennrich, G. Rempe, *Phys. Rev. Lett.* **89**, 067901 (2002).
15. J. McKeever *et al.*, *Science* **303**, 1992 (2004).
16. M. Keller, B. Lange, K. Hayasaka, W. Lange, H. Walther, *Nature* **431**, 1075 (2004).
17. S. Bergamini *et al.*, *J. Opt. Soc. Am. B* **21**, 1889 (2004).
18. N. Schlosser, G. Reymond, I. Protsenko, P. Grangier, *Nature* **411**, 1024 (2001).
19. N. Schlosser, G. Reymond, P. Grangier, *Phys. Rev. Lett.* **89**, 023005 (2002).
20. We performed a full calculation of the second-order correlation function using the Heisenberg-Langevin equations, which gives the areas of the peaks. We also calculated the photon emission probabilities using density matrix and Monte Carlo methods, which lead to the same result.
21. We thank P. Georges for his assistance in designing the pulsed laser system. This work was supported by the European Union through the Information Society Technologies/Future and Emerging Technologies/Quantum Information Processing and Communications project "QGATES" and the Research Training Network "CONQUEST."

Supporting Online Material

www.sciencemag.org/cgi/content/full/309/5733/454/DC1
SOM Text

11 April 2005; accepted 25 May 2005
10.1126/science.1113394

Structural Relaxation of Polymer Glasses at Surfaces, Interfaces, and In Between

Rodney D. Priestley,[1] Christopher J. Ellison,[1] Linda J. Broadbelt,[1]* John M. Torkelson[1,2]*

We analyzed the glassy-state structural relaxation of polymers near surfaces and interfaces by monitoring fluorescence in multilayer films. Relative to that of bulk, the rate of structural relaxation of poly(methyl methacrylate) is reduced by a factor of 2 at a free surface and by a factor of 15 at a silica substrate interface; the latter exhibits a nearly complete arresting of relaxation. The distribution in relaxation rates extends more than 100 nanometers into the film interior, a distance greater than that over which surfaces and interfaces affect the glass transition temperature.

When cooled below the glass transition temperature (T_g), an amorphous material has higher specific volume, enthalpy, and entropy than in its equilibrium state at the same temperature. The resulting material is called a glass, which relaxes toward thermodynamic equilibrium in a process called structural relaxation (*1*–*3*). With polymers, glassy-state structural relaxation, often referred to as physical aging (*4*–*6*), can result in a time dependence of end-use properties of critical technological importance (*4*–*7*) such as increased modulus, increased brittleness, and reduced permeability. This glassy-state structural relaxation can be distinguished from the cooperative motion associated with T_g; the latter is associated with the α-relaxation [i.e., relaxation of cooperatively rearranging regions of some tens to hundreds of repeat units (*1*, *8*, *9*)], whereas the former has been commonly associated with the β-relaxation (*6*) (i.e., subsegmental relaxation such as the reorientation of an ester side group).

The glassy state and its associated phenomena, T_g and structural relaxation, are central challenges in condensed-matter physics (*10*–*14*) and are important in fields as varied as optical materials and the preservation of food and insect life (*11*, *12*). Numerous studies have established that confinement of amorphous materials between surfaces and interfaces at a length scale on the order of 100 nm can change T_g relative to its bulk value (*9*, *15*–*29*), whereas a limited number of studies have provided examples in which T_g is independent of confinement (*30*, *31*). Although many advanced technologies and materials (e.g., thin-film and asymmetric membranes and polymer nanocomposites) demand the long-time use of confined glasses (*4*, *28*, *29*), few studies have characterized the effect of nanoconfinement on structural relaxation in the glassy state.

Relative to bulk systems, enthalpy relaxation studies have indicated accelerated structural relaxation of a low molecular weight glass, *ortho*-terphenyl, confined to nanopores 11 to 12 nm in diameter (*32*). Physical aging in ultrathin polystyrene films was shown to be dependent on thickness and absent when the aging temperature was above the T_g of the confined film but below that of bulk polymer (*33*, *34*). In contrast, the presence of structural relaxation was observed above the bulk T_g for an ultrathin poly(methyl methacrylate) (PMMA) film supported on a silica substrate (*34*). The latter result was obtained because confinement leads to an increase in T_g due to attractive polymer-substrate interactions [hydrogen bond formation (*25*) between hydroxyl groups on the substrate surface and the polymer repeat unit]. Other investigations found little impact of confinement on structural relaxation of supported poly(isobutyl methacrylate) films (*18*) or superposed studies of structural relaxation with solvent evaporation in the case of supported PMMA films (*35*).

There is now substantial evidence that the origin of the T_g-nanoconfinement effect is related to surfaces and interfaces modifying relevant T_g dynamics in the interior regions of glass formers (*20*). Here, we report how surfaces and interfaces modify structural relaxation and to what extent these effects extend into the film interior. We use a fluorescence method in which dye-labeled polymer is inserted into known positions in a film in order to study the glassy-state relaxation dynamics. The dyes exhibit fluorescence intensities that increase substantially with minute increases in local density near the dye (*36*) and thereby provide an amplified sensitivity to structural relaxation. The method provides for highly sensitive, continuous monitoring of aging as well as the ability to measure aging rate distributions near surfaces, near interfaces, and in between. The distributions have been obtained with the use of 4-tricyanovinyl-[*N*-(2-hydroxyethyl)-*N*-ethyl]aniline (TC1)–labeled PMMA in single layers of multilayer PMMA films (*37*). We chose TC1 dye for the present study because its molecular structure allows for conformational mobility, which yields a high sensitivity of the dye fluorescence to the small densification that accompanies physical aging (*34*, *36*).

Figure 1 shows the increase in fluorescence intensity during relaxation at 305 K of a 400-nm-thick TC1-labeled PMMA film [T_g(bulk) = 393 K]. In agreement with specific volume and enthalpy relaxation measurements during physical aging of bulk polymer (*7*, *38*), the fluorescence intensity is roughly linear with logarithmic aging time. The intensity increases

[1]Department of Chemical and Biological Engineering, [2]Department of Materials Science and Engineering, Northwestern University, Evanston, IL 60208, USA.

*To whom correspondence should be addressed. E-mail: broadbelt@northwestern.edu; j-torkelson@northwestern.edu

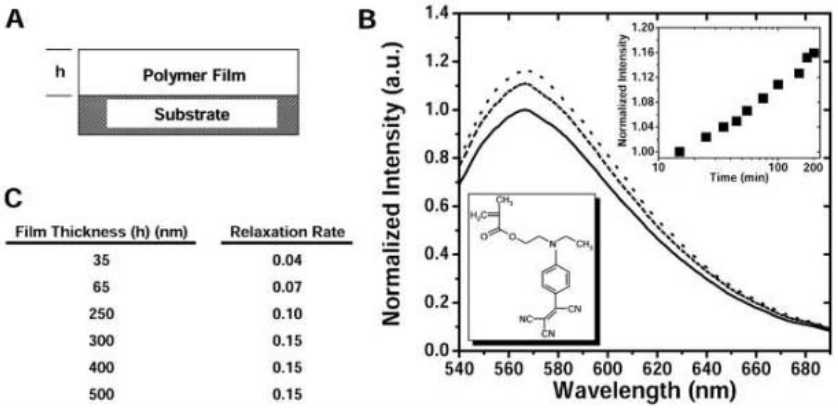

Fig. 1. Physical aging in single-layer PMMA films monitored via fluorescence. (**A**) Schematic of thin-film geometry. (**B**) Fluorescence emission spectrum of a 400-nm-thick TC1-labeled PMMA film after quenching from 418 K to 305 K taken after aging times of 15 min (solid curve), 100 min (dashed curve), and 200 min (dotted curve). Upper inset: Normalized fluorescence intensity at the maximum as a function of aging time. Lower inset: Molecular structure of TC1-labeled methacrylate monomer used in labeling PMMA. (**C**) Fluorescence aging/structural relaxation rate defined by Eq. 1 as a function of film thickness (h) for TC1-labeled PMMA at 305 K. Data are averages of two runs with SD of 0.01 or less.

16% (after a quench from 418 K to 305 K) as aging time increases from 15 min to 200 min. By analogy with physical aging rates based on volume relaxation (*7*, *38*), an aging rate based on fluorescence intensity, R_f, may be defined as

$$R_f = (1/F_o)[dF/d(\log t_a)] \qquad (1)$$

where F is fluorescence intensity at aging time t_a, and F_o is intensity at reference time t_o. Aging rates are a nonlinear function of temperature and typically exhibit a maximum. The maximum aging rate is a result of the competition between thermodynamic driving forces for aging, which is highest at temperatures well below T_g, and subsegmental mobility, which increases with temperature (*38*).

The results in Fig. 1C were obtained by fitting data similar to the upper inset of Fig. 1B to Eq. 1 for TC1-labeled single-layer PMMA films. The aging rate at 305 K increases by a factor of ~4 upon increasing film thickness from 35 nm to 300 nm (Fig. 1C). For film thicknesses ≥ 300 nm, R_f is independent of thickness and is equal to the relaxation rate of 0.15 obtained for a TC1-labeled PMMA film several μm thick, representative of bulk. [All values of the relaxation rate R_f, which is unitless, are determined via Eq. 1 with aging time t_a in units of minutes.] Although the sensitivity of TC1 fluorescence to aging is tied to volume relaxation [minute increases in local density near TC1 reduce the rate of nonradiative decay from the TC1 excited state, resulting in enhanced fluorescence (*34*, *36*)], the physical aging rate determined via TC1 fluorescence is amplified by orders of magnitude relative to that determined from volume relaxation. For example, the specific volume relaxation rate, R_v, of bulk PMMA is ~0.00055 during aging at 305 K (*38*). The specific volume relaxation rate is defined (*38*) as

$$R_v = -(1/V_o)[dV/d(\log t_a)] \qquad (2)$$

where V is specific volume at t_a, and V_o is specific volume at t_o. Over an aging time from 20 min to 200 min, this means that bulk PMMA at 305 K undergoes a 0.055% reduction in specific volume. Relative to R_v, R_f is greater by a factor of ~275 during physical aging at the same conditions.

We used multilayer films to explore the influence of confining substrate and free surfaces on glassy-state relaxation. Figure 2 shows structural relaxation data from a 25-nm-thick TC1-labeled PMMA middle layer sandwiched between two 1000-nm-thick PMMA layers (Fig. 2A), from a 25-nm-thick TC1-labeled free-surface layer sitting atop a 1000-nm-thick PMMA underlayer (Fig. 2B), and from a 25-nm-thick TC1-labeled substrate layer sandwiched between a 1000-nm-thick PMMA overlayer and the substrate (Fig. 2C). At 305 K, the relaxation rate is greatest in the middle layer, yielding $R_f = 0.14$, equal within error to that in bulk, and is reduced by a factor of 2 at the free surface. The substrate layer exhibits the slowest relaxation rate of 0.01 at 305 K, indicating that physical aging is almost totally suppressed next to the substrate.

At an aging temperature of 388 K, the free-surface layer exhibits almost no relaxation. This near-absence of aging is consistent with the notion that much of the 25-nm-thick free-surface layer has a T_g that is equal to or below 388 K and suggests that there is a rubbery equilibrium layer at the free surface. As the aging temperature is decreased, structural relaxation becomes more pronounced at the free surface but is always substantially less than that in the interior of the film. In

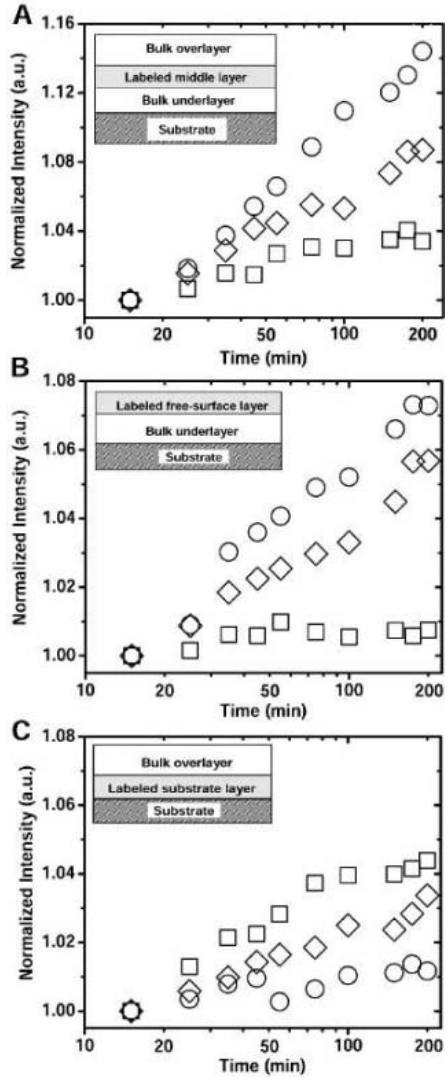

Fig. 2. Physical aging monitored by fluorescence in multilayer PMMA films with 25-nm-thick TC1-labeled layers and 1000-nm-thick unlabeled bulk overlayers/underlayers. Insets show schematics of the film arrangement. Normalized fluorescence intensity is shown as a function of aging time for a trilayer film (**A**) and two bilayer films (**B** and **C**) aged at 305 K (circles), 348 K (diamonds), and 388 K (squares). Data points are averages of two runs.

contrast, the substrate layer exhibits an increasing relaxation rate with increasing temperature and at 388 K has nearly the same rate as the middle layer. The additional thermal energy at higher temperatures approaching T_g likely reduces the ability of interfacial hydrogen bonds to suppress aging.

Further understanding of the impact of confinement on physical aging is obtained via buried-layer experiments, where 25-nm-thick TC1-labeled middle layers are placed a distance from the free surface or substrate interface. Figure 3 shows results from trilayer studies at 305 K. As a 25-nm-thick layer is moved from the free surface to a buried layer, there is a smooth increase in relaxation rate,

from 0.07 at the free surface to 0.08, 0.11, and 0.15 when buried 25 nm, 100 nm, and 250 nm, respectively, below the free surface (Fig. 3A). Within error (±0.01), the relaxation rate in the layer buried 250 nm below the free surface is identical to bulk. The rate of structural relaxation increases sharply from 0.01, when a 25-nm-thick layer is located next to the substrate, to 0.10, when located 25 nm from the substrate (Fig. 3B). Further displacement results in a smooth increase in relaxation rate, from 0.12 to 0.14 when the layer is located 100 nm and 250 nm, respectively, from the substrate. Thus, the substrate and free surface affect the structural relaxation rate in supported PMMA films over similar distances, but the substrate interactions perturb the structural relaxation to a greater extent.

Our results are consistent with a schematic (Fig. 4) of the surface- and interface-induced gradients in relaxation. At a distance of at least 100 nm but less than 250 nm from the free surface, there begins a smooth factor-of-2 reduction in structural relaxation rate between the bulk and the free surface. At a distance of at least 100 nm but less than 250 nm from the substrate interface, there begins a factor-of-15 reduction in relaxation rate from the bulk to the interface, the vast majority of which occurs within 25 nm of the interface. The origins of the perturbations near the free surface and substrate differ. Near the free surface, there is enhanced cooperative segmental mobility and a reduced T_g (*20*), resulting in a reduced thermodynamic driving force for structural relaxation. At the substrate interface, hydrogen bonds suppress cooperative segmental mobility and lead to an increased T_g (*25*). Hence, there is an enhanced thermodynamic driving force for structural relaxation. However, the interfacial hydrogen bonds also suppress smaller motions associated with structural relaxation; deep in the glassy state, this suppression can result in near-elimination of physical aging within 25 nm of the substrate and retardation of aging relative to bulk at a distance of at least 100 nm from the substrate. The manner in which retardation in aging occurs over distances of at least 100 nm from a substrate or free surface is not yet understood, but it may relate to the percolation of slowly relaxing dynamic heterogeneities that has been hypothesized as an explanation for the effect of confinement on T_g (*21*, *22*, *39*) and that is expected to result in long-range changes in dynamics induced by surfaces and interfaces (*39*). No current theory or model directly addresses the effect of confinement on glassy-state structural relaxation.

It is important to note that the distribution of glassy-state structural relaxation rates that we obtained is distinct from the distribution of T_g values in supported PMMA films. Although a determination of the full distribution of T_g values is beyond the scope of this study, selected measurements of T_g values have been obtained in experiments that equate T_g to the intersection of the rubbery- and glassy-state temperature dependences of fluorescence intensity (*20*). Relative to bulk T_g (393 K), a 25-nm-thick layer at the free surface of a 1000-nm-thick film exhibits a reduction in T_g of 5 to 6 K, whereas a 25-nm-thick layer at the substrate of a 1000-nm-thick film exhibits an increase in T_g of 12 K. However, the T_g of a 25-nm-thick layer that is located 100 nm from either the substrate interface or the free surface in an 800-nm-thick multilayer film is identical within error (±1 K per sample) to the T_g of bulk TC1-labeled PMMA. Thus, interfacial effects perturb glassy-state structural relaxation rates 100 nm from the substrate, but they do not perturb T_g values over the same length scale. This is possibly because T_g is associated with larger scale motions of cooperative segmental mobility (α-relaxation processes), whereas glassy-state structural relaxation may be associated with different, smaller-scale dynamics (β-relaxation processes) (*6*). Novel experiments need to be developed to characterize directly how α- and β-relaxation dynamics near T_g are separately affected by surfaces and interfaces. Our results suggest that surface and interface effects may potentially be tailored to control the structural relaxation of high-performance materials that have a large fraction of polymer near surfaces and interfaces, as with polymer nanocomposites.

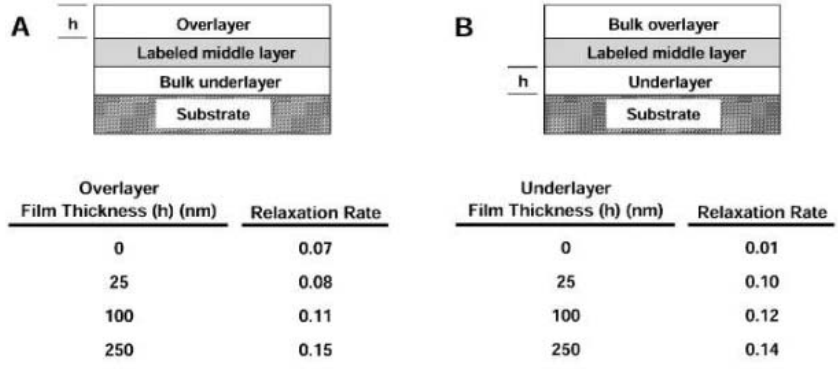

Overlayer Film Thickness (h) (nm)	Relaxation Rate
0	0.07
25	0.08
100	0.11
250	0.15

Underlayer Film Thickness (h) (nm)	Relaxation Rate
0	0.01
25	0.10
100	0.12
250	0.14

Fig. 3. Structural relaxation rates at 305 K for PMMA multilayer films with a 25-nm-thick TC1-labeled layer. The trilayer films characterize relaxation rates at known distances from free surfaces and substrate interfaces. Bulk overlayers and underlayers are 700 nm thick for trilayer films and 1000 nm thick for bilayer films. (**A** and **B**) Fluorescence relaxation rates of a TC1-labeled layer placed (A) at the free surface or at distances below the free surface (25, 100, and 250 nm) and (B) at the substrate or at distances from the substrate (25, 100, and 250 nm). Data are averages of two runs with SD of 0.01 or less.

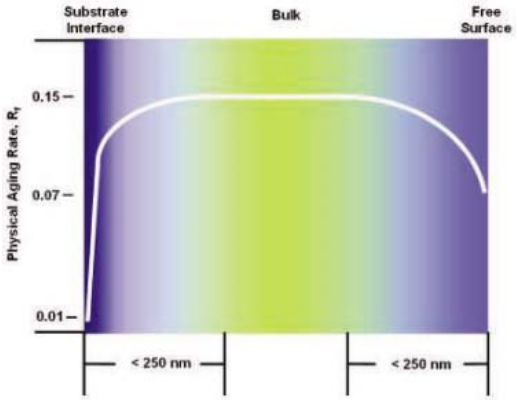

Fig. 4. Representation of the effect of the substrate interface and the free surface on the distribution of structural relaxation rates in PMMA at 305 K. Both the substrate interface and the free surface perturb the relaxation rate at least 100 nm but less than 250 nm into the film interior. Relative to bulk behavior, a 25-nm-thick layer at the free surface exhibits a factor-of-2 reduction in relaxation rate. In contrast, a 25-nm-thick layer at the substrate interface exhibits a factor-of-15 reduction in relaxation rate relative to bulk (i.e., almost a complete arresting of physical aging). Color gradations indicate continuous nature of change in aging rate (bright green, high rate; dark blue, low rate) in bulk.

References and Notes

1. C. A. Angell, K. L. Ngai, G. B. McKenna, P. F. McMillan, S. W. Martin, *J. Appl. Phys.* **88**, 3113 (2000).
2. E. R. Weeks, J. C. Crocker, A. C. Levitt, A. Schofield, D. A. Weitz, *Science* **287**, 627 (2000).
3. R. Torre, P. Bartolini, R. Righini, *Nature* **428**, 296 (2004).
4. Y. Huang, D. R. Paul, *Polymer* **45**, 8377 (2004).
5. J. Kurchan, *Nature* **433**, 222 (2005).
6. L. C. E. Struik, *Physical Aging in Amorphous Polymers and Other Materials* (Elsevier, New York, 1978).
7. J. M. Hutchinson, *Prog. Polym. Sci.* **20**, 703 (1995).
8. G. Adam, J. H. Gibbs, *J. Chem. Phys.* **43**, 139 (1965).
9. C. J. Ellison, M. K. Mundra, J. M. Torkelson, *Macromolecules* **38**, 1767 (2005).
10. J. I. Brauman, *Science* **267**, 1887 (1995).
11. P. G. Debenedetti, F. H. Stillinger, *Nature* **410**, 259 (2001).
12. C. A. Angell, *Science* **267**, 1924 (1995).
13. V. N. Novikov, A. P. Sokolov, *Nature* **431**, 961 (2004).
14. P. G. de Gennes, *Eur. Phys. J. E* **2**, 201 (2000).
15. C. L. Jackson, G. B. McKenna, *J. Non-Cryst. Solids* **131-133**, 221 (1991).
16. J. L. Keddie, R. A. L. Jones, R. A. Cory, *Europhys. Lett.* **27**, 59 (1994).
17. J. A. Forrest, K. Dalnoki-Veress, J. R. Stevens, J. R. Dutcher, *Phys. Rev. Lett.* **77**, 2002 (1996).
18. C. J. Ellison, S. D. Kim, D. B. Hall, J. M. Torkelson, *Eur. Phys. J. E* **8**, 155 (2002).
19. B. Jerome, J. Commandeur, *Nature* **386**, 589 (1997).

20. C. J. Ellison, J. M. Torkelson, *Nat. Mater.* **2**, 695 (2003).
21. S. Merabia, P. Sotta, D. Long, *Eur. Phys. J. E* **15**, 189 (2004).
22. A. R. C. Baljon, J. Billen, R. Khare, *Phys. Rev. Lett.* **93**, 255701 (2004).
23. F. Varnik, J. Baschnagel, K. Binder, *Phys. Rev. E* **65**, 021507 (2002).
24. T. S. Jain, J. J. de Pablo, *Phys. Rev. Lett.* **92**, 155505 (2004).
25. C. W. Frank *et al.*, *Science* **273**, 912 (1996).
26. C. B. Roth, J. R. Dutcher, in *Soft Materials: Structure and Dynamics*, J. R. Dutcher, A. G. Marangoni, Eds. (Dekker, New York, 2005).
27. M. Alcoutlabi, G. B. McKenna, *J. Phys. Condens. Matter* **17**, R467 (2005).
28. B. J. Ash, L. S. Schadler, R. W. Siegel, *Mater. Lett.* **55**, 83 (2002).
29. J. Berriot *et al.*, *Macromolecules* **35**, 9756 (2002).
30. P. A. O'Connell, G. B. McKenna, *Science* **307**, 1760 (2005).
31. C. J. Ellison, R. L. Ruszkowski, N. J. Fredin, J. M. Torkelson, *Phys. Rev. Lett.* **92**, 095702 (2004).
32. S. L. Simon, J. Y. Park, G. B. McKenna, *Eur. Phys. J. E* **8**, 209 (2002).
33. S. Kawana, R. A. L. Jones, *Eur. Phys. J. E* **10**, 223 (2003).
34. R. D. Priestley, L. J. Broadbelt, J. M. Torkelson, *Macromolecules* **38**, 654 (2005).
35. H. Richardson, I. Lopez-Garcia, M. Sferrazza, J. L. Keddie, *Phys. Rev. E* **70**, 051805 (2004).
36. J. S. Royal, J. M. Torkelson, *Macromolecules* **26**, 5331 (1993).
37. See supporting data on *Science* Online.
38. R. Greiner, F. R. Schwarzl, *Rheol. Acta* **23**, 378 (1984).
39. D. Long, F. Lequeux, *Eur. Phys. J. E* **4**, 371 (2001).
40. Supported by the NSF Materials Research Science and Engineering Center program at Northwestern University (grant DMR-0076097), a GEM Fellowship (R.D.P.), and a Henderson Dissertation Year Fellowship (C.J.E.).

Supporting Online Material
www.sciencemag.org/cgi/content/full/309/5733/456/DC1
Materials and Methods
References

14 March 2005; accepted 24 May 2005
10.1126/science.1112217

Simulations of a Quasi–Taylor State Geomagnetic Field Including Polarity Reversals on the Earth Simulator

Futoshi Takahashi,[1]* Masaki Matsushima,[2] Yoshimori Honkura[2]

High-resolution, low-viscosity geodynamo simulations have been carried out on the Earth Simulator, one of the fastest supercomputers, in a dynamic regime similar to that of Earth's core, that is, in a quasi–Taylor state. Our dynamo models exhibit features of the geodynamo not only in spatial and temporal characteristics but also in dynamics. Polarity reversals occurred when magnetic flux patches at high latitudes moved poleward and disappeared; patches with reversed field at low and mid-latitudes then moved poleward.

A dynamo process in Earth's fluid outer core, known as the geodynamo, is believed to generate Earth's intrinsic magnetic field. Numerical simulations of the geodynamo have been performed (*1*–*5*), and dynamo models have shown some similarity to the geomagnetic field (*6*, *7*), including polarity reversals (*1*, *2*, *5*, *8*). It is still unclear whether these models accurately reproduce the dynamics of Earth's outer core, because the simulations were performed at a dynamic regime much different from that of the core. The most essential parameter of the dynamic regime is the Ekman number, E, which represents the relative importance of viscosity to the rotation rate; its value is extremely small ($E \sim 10^{-9}$) for Earth's core. Previously, artificial treatments were needed to perform effective computations (*9*).

Taylor (*10*) showed that the magnetic field in the core varies such that the axial magnetic torque on cylindrical surfaces that are coaxial with the rotation axis is small, because it can be balanced only with the extremely small viscous and inertial torques. The limit of vanishing viscosity leads to the so-called Taylor's constraint that the axial magnetic torque must vanish. The dynamo satisfying Taylor's constraint is considered to be in a Taylor state. In reality, the geodynamo is in a quasi–Taylor state, in which the effect of viscosity plays a negligibly small role in core dynamics (*11*).

To obtain such a quasi–Taylor state dynamo, one must carry out high-resolution numerical simulations for lower viscosity, which are prohibitively time-consuming even on most supercomputers. The Earth Simulator alleviates this situation and is capable of reaching an Ekman number of 4×10^{-7}; our results are mostly based on computations for a slightly higher value, $E = 4 \times 10^{-6}$, in the definition of Kono and Roberts (*12*) using the core radius as a length scale. We used the spectral method to solve magnetohydrodynamic equations (*13*–*15*). The spatial resolution is ensured by including all the constituents of spherical harmonics up to degree and order 255.

We performed simulations for various values of the Rayleigh number Ra (*13*) and evaluated the resulting dynamo models with

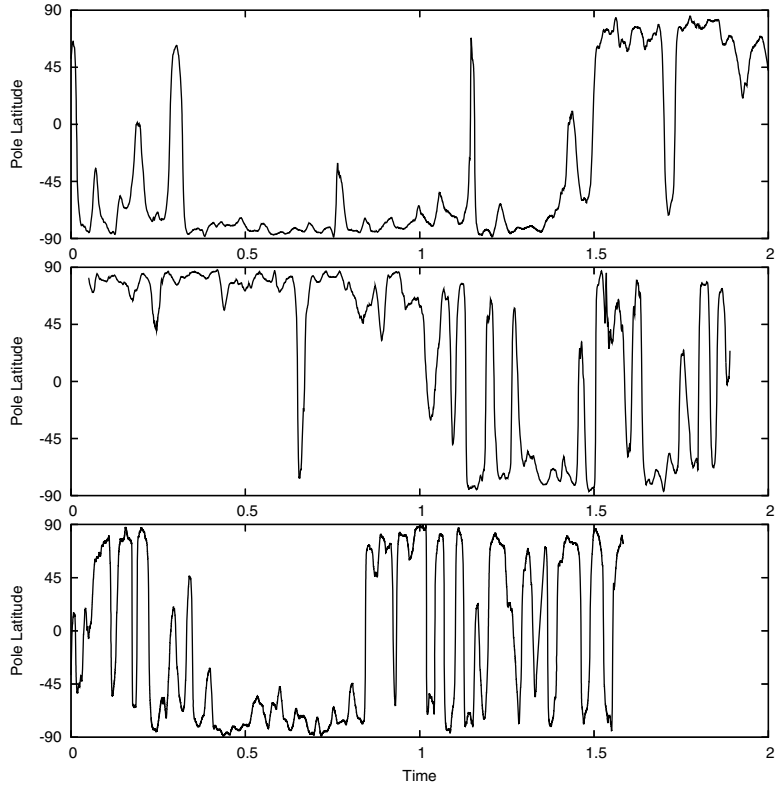

Fig. 1. Time evolutions of the north geomagnetic pole latitude for three Rayleigh numbers, $Ra = 1.57 \times 10^8$ (top), $Ra = 1.96 \times 10^8$ (middle), and $Ra = 2.35 \times 10^8$ (bottom). Time is scaled by the magnetic diffusion time t_m, corresponding to roughly 200,000 years.

[1]Institute of Space and Astronautical Science, Japan Aerospace Exploration Agency, 3-1-1 Yoshinodai, Sagamihara, Kanagawa, Japan. [2]Department of Earth and Planetary Sciences, Tokyo Institute of Technology, 2-12-1 Ookayama, Meguro-ku, Tokyo, Japan.

*To whom correspondence should be addressed. E-mail: futoshi@stp.isas.jaxa.jp

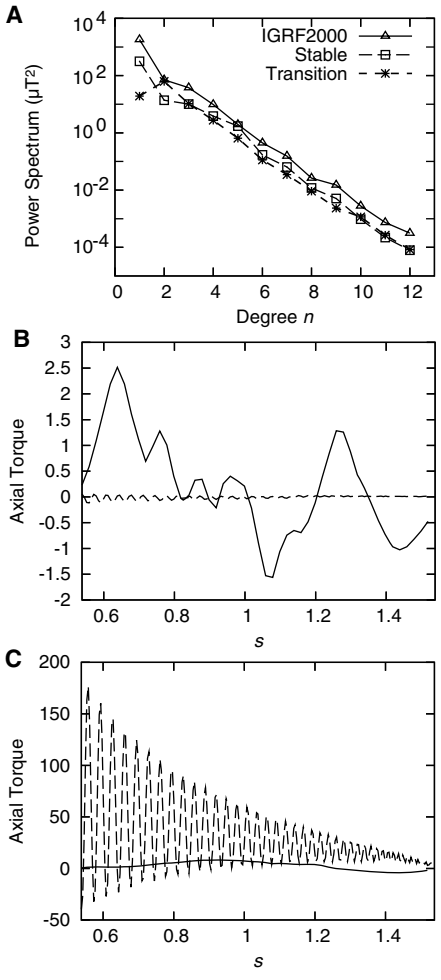

Fig. 2. Properties of the magnetic field at Earth's surface and within the core. (**A**) Magnetic power spectrum $W(n)$ at Earth's surface in terms of spherical harmonic degree n for $E = 4 \times 10^{-6}$ and $Ra = 2.35 \times 10^8$. $W(n)$ is given as

$$W(n) = (n + 1)\sum_{m=0}^{n}\left[(g_n^m)^2 + (h_n^m)^2\right]$$

where g_n^m and h_n^m are Gauss coefficients in the magnetic scalar potential Φ expanded into spherical harmonics in spherical polar coordinates (r,θ,ϕ) as

$$\Phi = a\sum_{n=1}^{\infty}\sum_{m=0}^{n}(a/r)^{n+1} \times (g_n^m \cos m\phi + h_n^m \sin m\phi)\, P_n^m(\cos\theta)$$

where a is Earth's radius, and P_n^m are Schmidt normalized associated Legendre polynomials. Symbols: squares, stable polarity period; stars, transitional period; triangles, present-day geomagnetic field (International Geomagnetic Reference Field IGRF 2000) (*19*). (**B**) For $E = 4 \times 10^{-6}$ and $Ra = 2.35 \times 10^8$, the surface-averaged axial magnetic (solid line) and viscous (dashed line) torques acting on a cylindrical surface at a distance s from the rotation axis ($r_i \le s \le r_o$), where r_i and r_o are the radii of the inner and outer cores, respectively. (**C**) Similar to (B) for a higher Ekman number, $E = 4 \times 10^{-5}$, and $Ra = 3.53 \times 10^7$.

respect to their similarity to the geodynamo, in terms of not only spatial and temporal features but also dynamic regime. Time evolutions of magnetic field in the models are consistent with secular variations in the historical and archaeomagnetic fields (*11*, *16*, *17*), and the magnetic field alternates its polarity at irregular intervals (Fig. 1). The frequency of polarity reversals is higher for larger *Ra*, but it is also controlled by other factors such as boundary conditions imposed at the core-mantle boundary (*5*) and input parameters (*8*). Hence, we do not intend to examine whether the reversal rate is similar to the geodynamo on a geological time scale (*18*).

The power spectrum of the magnetic field at the model-Earth's surface in terms of spherical harmonic degree during a stable period, corresponding to the state in which the magnetic pole exists near the geographic pole, is similar to that of the present geomagnetic field (*19*), although the strength is weaker; the dominant dipole component and modestly large octupole component are in contrast with the quadrupole component slightly below the trend (Fig. 2A). During a transitional period, corresponding to the state during which the magnetic pole deviates largely from the geographic pole as a result of a reversal or an excursion (*20*), the quadrupole component strengthens while the dipole component weakens (*21*).

Furthermore, our dynamo models are asymptotically in a dynamic regime similar to the regime in Earth's core. Axial torque balance clearly indicates that, relative to magnetic torque, viscous torque plays a negligible role in a low-E model (Fig. 2B). In short, our low-E models are in a quasi–Taylor state. In a high-E model ($E = 4 \times 10^{-5}$), however, the viscosity has a noticeable effect on dynamics (Fig. 2C), as in other dynamo models (*22*, *23*); that is, inertial and viscous torques are nearly balanced. The oscillatory behavior of the viscous torque is excited to counteract azimuthal acceleration due to the Reynolds stress, and is propagated outward with damping amplitude through viscous coupling between cylindrical surfaces. These features are negligible when a quasi–Taylor state is reached.

Examination of sequences of the magnetic field morphology at the core surface during transitional periods revealed a characteristic feature for every simulated polarity reversal and excursion (Fig. 3) (movie S1). Here, spatial resolution was reduced to the same level as that of real geomagnetic field observations to make comparison easier (spherical harmonics of degree and order $\le$12). Before the onset of any simulated reversal sequence, the magnetic field was characterized by two pairs of flux patches located at high latitudes, $(A) \cdot (A)'$ and $(B) \cdot (B)'$, as is the historical field (*24*). Also, there were five or six notable pairs of low- and mid-latitude flux patches drifting both eastward and westward with time. During a transitional period (after ~1000 years since onset), (A) and (B) shifted toward higher latitudes with reduced intensity while $(A)'$ and $(B)'$ remained stationary. A flux patch $(d)'$ moved poleward and a new flux patch (g) appeared. Near the end of the transition, some flux patches merged. In particular, negative flux patches (c) and (d) combined into $(c) + (d)$, shifted toward high latitudes, and replaced an original positive flux patch (B). A unified flux patch $(a) + (b)$ replaced (A) in the same manner. Then, (A) and (B) at high latitudes disappeared in accordance with the southward drift of flux patches with opposite polarity. At this stage, $(A)'$ and $(B)'$ remained near the north pole, but they were soon replaced and disappeared, which suggests a site dependence of the reversal duration (*25*). Once the polarity reversal terminated, strong flux patches formed again at high latitudes. In high-E models, however, a complicated structure arose from the dominance of nondipole fields because of a different dynamic regime influenced by the viscosity (Fig. 2C) (movie S2). This may be why no distinctive features have been found in sequences of polarity reversals for high E.

We also considered how polarity reversal starts (Fig. 4). A reversed field appeared deep in the core at low latitudes, grew toward the core surface, spread from low and mid-latitudes to high latitudes, and pushed out the magnetic field with original polarity, which was then extinguished. This corresponds to movement of flux patches from low to high latitudes (Fig. 3). Figures 3 and 4 suggest that the reversed magnetic field is generated at low latitudes outside the tangent cylinder (an imaginary cylinder aligned with the rotation axis and in contact with the inner core at the equator). We have never found a reversal or an excursion originating from the inside of the tangent cylinder, which thus seems to play a secondary role for the onset of a transitional period. This is contrary to the suggestion by Sarson and Jones (*26*) that a transitional period is triggered by the interior of the tangent cylinder and would not be affected by inner core conductivity (*27*). Our findings suggest that poleward movements of flux patches might be observed before or at the beginning of a transitional period, and that they are characteristic of various reversal processes (*28*).

References and Notes

1. G. A. Glatzmaier, P. H. Roberts, *Nature* **377**, 203 (1995).
2. G. A. Glatzmaier, P. H. Roberts, *Phys. Earth Planet. Inter.* **91**, 63 (1995).
3. G. A. Glatzmaier, P. H. Roberts, *Science* **274**, 1887 (1996).
4. W. Kuang, J. Bloxham, *Nature* **389**, 371 (1997).
5. G. A. Glatzmaier, R. Coe, L. Hongre, P. H. Roberts, *Nature* **401**, 885 (1999).
6. M. Kono, P. H. Roberts, *Rev. Geophys.* **40**, 10.1029/2000RG000102 (2002).
7. P. H. Roberts, G. A. Glatzmaier, *Rev. Mod. Phys.* **72**, 1081 (2000).
8. C. Kutzner, U. R. Christensen, *Phys. Earth Planet. Inter.* **131**, 29 (2002).
9. E. Grote, F. H. Busse, A. Tilgner, *Geophys. Res. Lett.* **27**, 2001 (2000).
10. J. B. Taylor, *Proc. R. Soc. London Ser. A* **274**, 274 (1963).
11. See supporting data on *Science* Online.
12. M. Kono, P. H. Roberts, *Phys. Earth Planet. Inter.* **128**, 13 (2001).

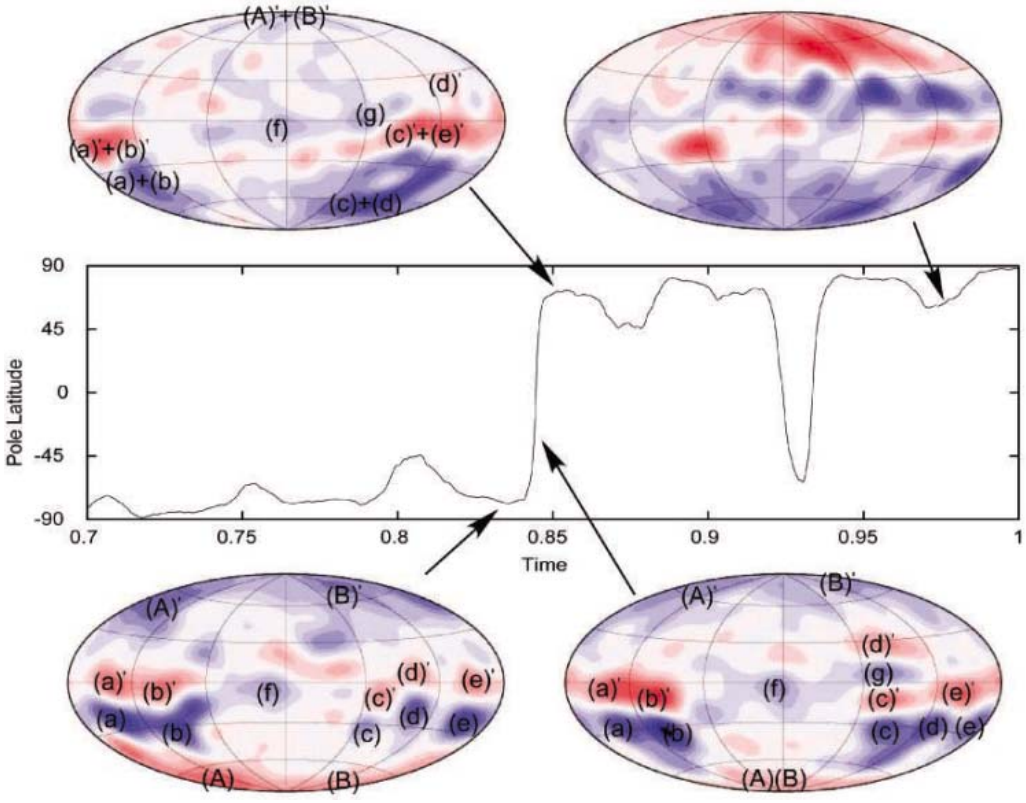

Fig. 3. Typical examples of morphology of the radial component of the magnetic field at the core surface during a sequence of polarity reversal in a model for $Ra = 2.35 \times 10^8$. Red regions represent outward fields from the core; blue regions represent inward fields to the core. The labels (*a*) to (*g*), (*a*)′ to (*e*)′, (*A*), (*B*), (*A*)′, and (*B*)′ in each plot define the notable magnetic flux patches. Capital letters denote flux patches at high latitudes. The maximum and minimum contour levels are 0.5 and –0.5 mT, respectively. Time is scaled as in Fig. 1.

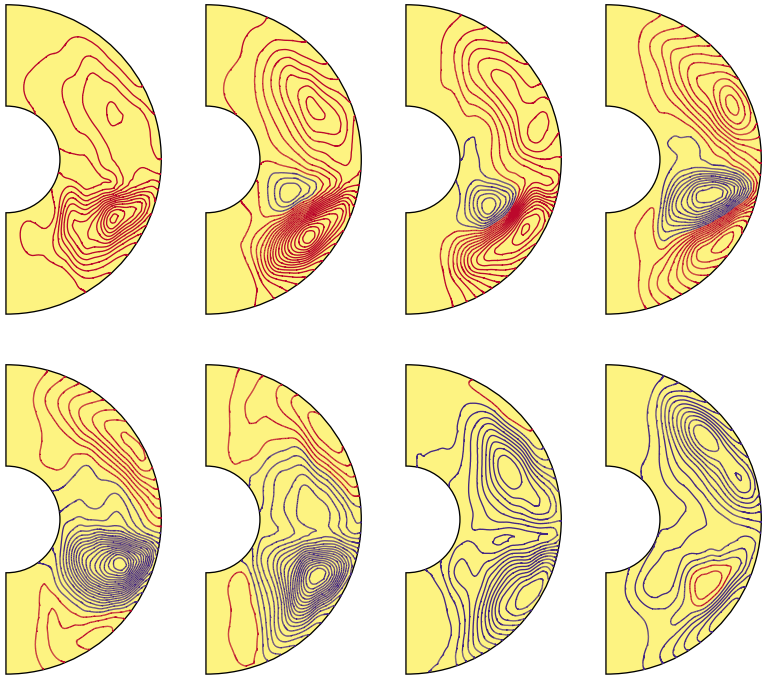

Fig. 4. Time evolution of the longitudinally averaged magnetic lines of force in a meridional plane during a polarity reversal for $Ra = 1.57 \times 10^8$. Time intervals are equal between panels, starting at top left and continuing to bottom right. The duration of the whole sequence is roughly 5200 years, consistent with the reversal time scale of the geomagnetic field. Red lines represent counterclockwise fields; blue lines represent clockwise fields.

13. Convection is driven by thermal buoyancy in the Boussinesq approximation. No-slip, electrically insulating, and isothermal boundary conditions at the inner and outer spherical surfaces are imposed. Nondimensional parameters in the governing equations are the Ekman number *E*, the Rayleigh number *Ra*, the magnetic Prandtl number *Pm*, and the Prandtl number *Pr*. Values of *Pm* and *Pr* are fixed at 0.5 and 1, respectively, whereas *Ra* varies. Applying a standard procedure of the spectral method (time-stepping the equations), we obtain time-dependent magnetohydrodynamic solutions of the magnetic field, the velocity field, and the temperature.
14. F. Takahashi, J. S. Katayama, M. Matsushima, Y. Honkura, *Phys. Earth Planet. Inter.* **128**, 149 (2001).
15. F. Takahashi, M. Matsushima, Y. Honkura, *Phys. Earth Planet. Inter.* **140**, 53 (2003).
16. G. Hulot, J. L. Le Mouël, *Phys. Earth Planet. Inter.* **82**, 167 (1994).
17. L. Hongre, G. Hulot, A. Khokhlov, *Phys. Earth Planet. Inter.* **106**, 311 (1998).
18. C. Constable, *Phys. Earth Planet. Inter.* **118**, 181 (2000).
19. N. Olsen *et al.*, *Geophys. Res. Lett.* **27**, 3607 (2000).
20. When deviation of the virtual geomagnetic pole from the geographic pole is larger than the usual secular variation, the term "transitional" is used in paleomagnetism. Because excursions are considered to be aborted reversals, they are also classified as transitional fields. Although some arbitrariness is inevitable in defining the duration of a transitional period, we term a sequence of large movement of the magnetic pole a transitional period.
21. J. Li, T. Sato, A. Kageyama, *Science* **295**, 1887 (2002).
22. G. R. Sarson, C. A. Jones, A. W. Longbottom, *Geophys. Astrophys. Fluid Dyn.* **88**, 225 (1998).
23. M. Dumberry, J. Bloxham, *Phys. Earth Planet. Inter.* **140**, 29 (2003).
24. A. Jackson, A. R. T. Jonkers, M. Walker, *Philos. Trans. R. Soc. London Ser. A* **358**, 957 (2000).
25. B. M. Clement, *Nature* **428**, 637 (2004).
26. G. R. Sarson, C. A. Jones, *Phys. Earth Planet. Inter.* **111**, 3 (1999).
27. J. Wicht, *Phys. Earth Planet. Inter.* **132**, 281 (2002).
28. R. S. Coe, L. Hongre, G. A. Glatzmaier, *Philos. Trans. R. Soc. London Ser. A* **358**, 1141 (2000).

29. Numerical simulations were performed on the Earth Simulator at the Earth Simulator Center, Yokohama, Japan. Supported by Research Fellowships of the Japan Society for the Promotion of Science for Young Scientists (F.T.).

Supporting Online Material

www.sciencemag.org/cgi/content/full/309/5733/459/DC1
Materials and Methods
Figs. S1 to S3
Movies S1 and S2

4 March 2005; accepted 7 June 2005
10.1126/science.1111831

Earthquake Source Fault Beneath Tokyo

Hiroshi Sato,[1] Naoshi Hirata,[1] Kazuki Koketsu,[1] David Okaya,[2] Susumu Abe,[3] Reiji Kobayashi,[1] Makoto Matsubara,[4] Takaya Iwasaki,[1] Tanio Ito,[5] Takeshi Ikawa,[3] Taku Kawanaka,[3] Keiji Kasahara,[4] Steven Harder[6]

Devastating earthquakes occur on a megathrust fault that underlies the Tokyo metropolitan region. We identify this fault with use of deep seismic reflection profiling to be the upper surface of the Philippine Sea plate. The depth to the top of this plate, 4 to 26 kilometers, is much shallower than previous estimates based on the distribution of seismicity. This shallower plate geometry changes the location of maximum finite slip of the 1923 Kanto earthquake and will affect estimations of strong ground motion for seismic hazards analysis within the Tokyo region.

In central Japan, the Philippine Sea plate (PSP) subducts beneath the Tokyo metropolitan region. This fault was the source of the Genroku earthquake of 1703 (magnitude M = 8.0) and the Kanto earthquake of 1923 (M = 7.9), which had 105,000 fatalities (*1*). The greater Tokyo urban region has a population of 33 million and is the center of about 40% of the nation's economic activities (*2*). A M = 7 or greater earthquake in this region has the potential to produce devastating loss of life and property with even greater global economic repercussions (*3*). The amount of shaking and ground motion in earthquakes depends on the magnitude and depth, among other factors. Here, we provide high-resolution images of this plate boundary and show that it is shallower than has been thought.

In the Kanto region, the PSP subducts northwestward under the Honshu arc at about 30 to 40 mm/year (*4*). The earthquakes of the subducting PSP identify a shallow and antiformally plunging surface from the Izu peninsula, southwest of Tokyo (Fig. 1) (*5*–*7*). High-resolution seismic velocity tomography (*8*) resolves both the high-velocity core of the slab and its associated overlying low-velocity lid and confirms that the PSP lies under Tokyo (fig. S1). The presence of the Izu-Bonin arc within the PSP creates two styles of forearc accretion and deformation. In eastern Kanto, an accretionary prism composed of late Cenozoic sediments overlies the downgoing PSP (Y to Y′ and AC in Fig. 1). In western Kanto, the Izu-Bonin arc has collided into the Honshu crust during the past 15 million years; remnant pieces such as the Tanzawa block were transferred to the Honshu crust (X to X′ and TZ in Fig. 1). A megathrust separates the downgoing PSP from the overlying forearc and Honshu crust [Mesozoic to early Cenozoic accretionary sediments and granitic intrusions (*9*)] (HpN in Fig. 1).

We collected four seismic profiles distributed across the greater Tokyo region to image the geometry of the PSP (P1 to P4 in Fig. 1) and the megathrust earthquake zones (*10*). Seismic reflections from the top of the PSP are visible in all four profiles (Fig. 2). The Neogene-Tertiary accretionary prism is identified in the eastern three profiles (AC in P2 to P4). A portion of the Izu-Bonin island arc (TZ in P1) is accreted into the Honshu middle crust via wedge-thrust tectonics. The large-scale forearc Kanto basin (KB) is present in P1, P3, and P4 and overlies the upper crustal Honshu pre-Neogene basement (HpN). These profiles image the primary structural features of the overall subduction and two forearc systems within the Kanto region (e.g., schematic cross sections in Fig. 1).

Seismic reflections of the upper surface of the subducted PSP (UPSP in Fig. 2) are observed on all of the seismic sections and are nearly concordant with slab geometry estimated from seismicity (*6*). These reflections are found at 5 to 24 km in P1, 4- to 11-km depths in P2, and 6 to 25 km in P3 (*10*). In the southern portion of P4, the megathrust dips at ~30° from 5- to 20-km depths but is flat

[1]Earthquake Research Institute (ERI), University of Tokyo, 1-1-1 Yayoi, Bunkyo-ku, Tokyo 113–0032, Japan. [2]Department of Earth Sciences, University of Southern California, Los Angeles, CA 90089–0740, USA. [3]JGI Incorporated, 1-5-21 Otsuka, Bunkyo-ku, Tokyo 112–0012, Japan. [4]National Research Institute for Earth Science and Disaster Prevention, 3-1 Tennodai, Tsukuba 305–0006, Japan. [5]Department of Earth Science, Chiba University, Chiba 263–8522, Japan. [6]Department of Geological Sciences, University of Texas El Paso, El Paso, TX 79968–0555, USA.

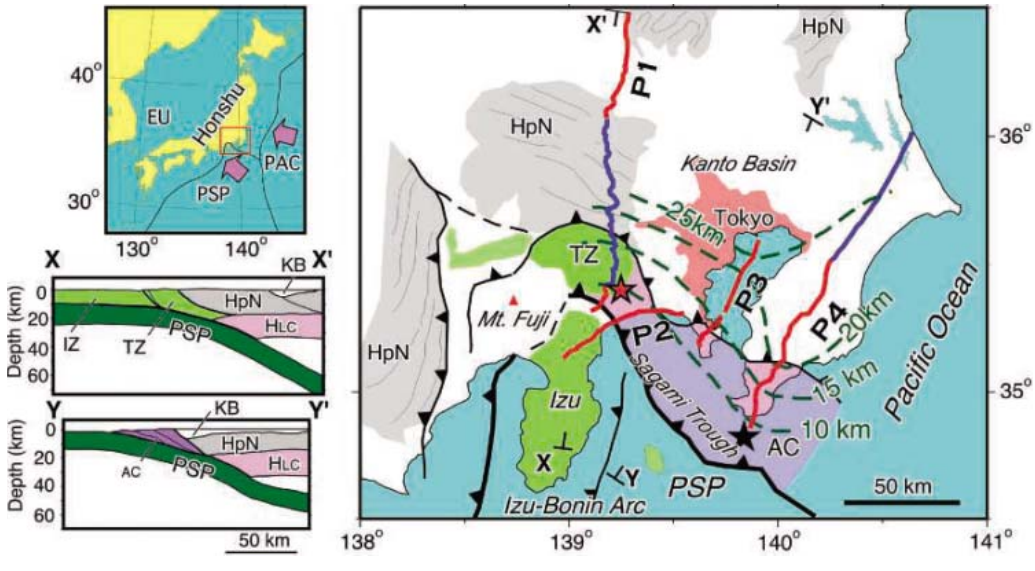

Fig. 1. Tectonic region of metropolitan Tokyo (Kanto) area. (**Top left**) Plate geometry of Honshu island. PAC denotes Pacific plate; EU, Eurasian plate; and PSP, Philippine Sea plate. Arrows denote plate convergence directions relative to Honshu. Red box is study area. (**Right**) Tectonic map of Kanto region and location of seismic profiles P1 to P4. Contours represent depth in km to upper surface of PSP based on our study. Tectonic elements include HpN, pre-Neogene rocks belonging to Honshu arc; HLC, lower crust of Honshu arc; KB, Neogene to Quarternary sediments of Kanto Basin; TZ, Tazawa block (arc fragment of Miocene Izu-Bonin arc); IZ, Izu block (volcanic Izu-Bonin arc crust); and AC, primarily Neogene accretionary complex. Stars are epicenters of 1703 Genroku (black) and 1923 Kanto earthquakes (red). Red and blue profile segments indicate multichannel vibroseis and explosion refraction and/or wide-angle reflection acquisition methods, respectively. X to X′ and Y to Y′ denote locations of schematic cross sections. (**Bottom left**) Lithospheric schematic cross sections across Kanto. X to X′ represents arc-arc forearc collision; Y to Y′ illustrates accumulation of a standard forearc accretionary complex.

toward the north; this flat dip is apparent because the profile is on a strike line to the locally westward dipping PSP (Fig. 1). These seismic profiles show that the top of the PSP is at depths of 4 to 26 km beneath the region, shallower than has been commonly assumed (Fig. 3A). Although there is good agreement in southern and eastern Kanto between our estimate and previous ones where the slab is shallow, there are large downdip differences in central and western Kanto of up to ~18 km of mismatch. Our shallower PSP geometry may lead to substantially larger estimates of strong ground motion simply because the region of megathrust earthquake rupture is closer to Earth's surface. In addition, this geometry serves as a new constraint for studies of Kanto seismotectonics and seismic imaging using earthquakes, such as high-resolution three-dimensional (3D) tomography and receiver function analysis.

The 1923 Kanto earthquake was the last major earthquake in this region. The source region of this earthquake was previously determined by finite-slip inversion (*11*, *12*) of coseismic geodetic and seismic waveform data (*13*); the 1923 Kanto earthquake produced two patches of large slip (Fig. 3B). Such zones, or asperities, may represent repeating ruptures in interplate earthquakes (*14*, *15*) and thus potential sources of strong ground motion. We recalculated the finite-slip inversion for this earthquake with the use of our revised PSP geometry. The location of the eastern patch moved about 40 km northward toward Tokyo (Fig. 3C). This new finite-slip solution (including modified slip rate distributions) can be used to calibrate the calculation of ground motions in the Tokyo metropolitan region with seismic wave simulation methods (*16*, *17*). This retuned procedure can then be used to make peak ground motion estimations for scenarios of potentially hazardous future earthquakes.

Surrounding these asperity patches are areas characterized by aseismic slip, slow earthquakes, repeating earthquakes, and/or greater rates of low-magnitude background seismicity (*18*, *19*). Several recent studies (*20*–*27*) have identified three basic asperity-nonasperity zones within megathrusts: an updip aseismic zone associated with the overlying accretionary prism, the locked seismogenic zone where large magnitude rupture will occur, and a downdip section with active seismogenic release (*28*). These zones have different physical states and properties, which can lead to the presence or absence of associated megathrust seismic reflections (*20*–*27*). In Kanto, the UPSP seismic reflections change laterally in the four profiles. In addition to the megathrust zonation, several nonstructural factors affect the presence and amplitudes of these reflections: the mix of acquisition styles (vibroseis, explosion, and air gun sources plus land cable, bay cable, and portable receiver sets); signal penetration (land versus marine near-surface conditions and the presence of basins); low versus high common-depth point stacking fold; and

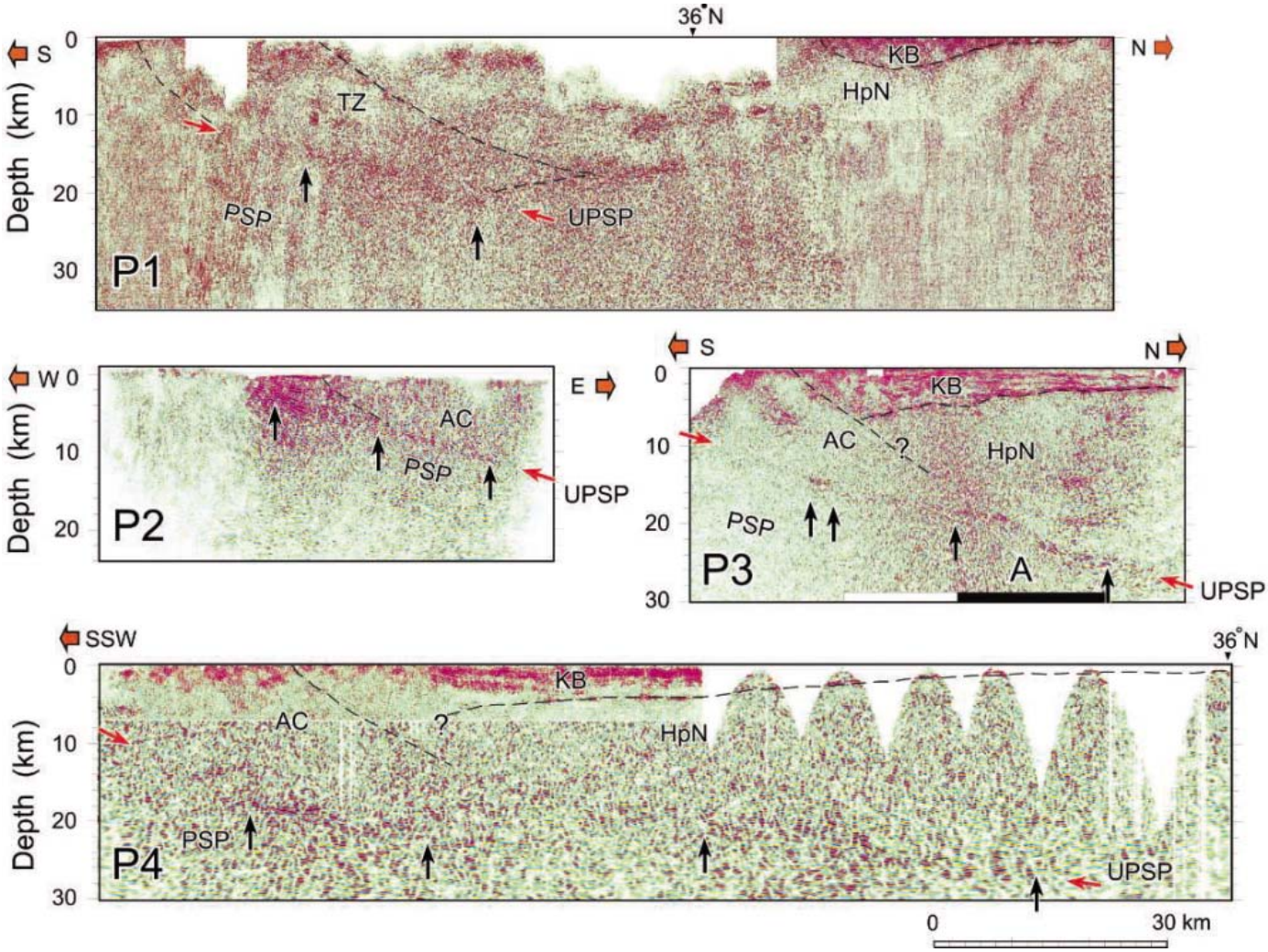

Fig. 2. Seismic reflection profiles P1 to P4 in the Tokyo metropolitan area. These profiles are post-stack migrated and depth converted. Symbols for tectonic elements are defined in Fig. 1. Red arrows denote positions of seismic reflections produced at the upper surface of the Philippine Sea plate (UPSP). Black arrows delineate clearly visible UPSP reflections. Bars at bottom of P3 indicate lateral presence of strong-amplitude (black and A) or weak-to-no-amplitude (white) reflections evaluated by relative amplitude processing (fig. S8).

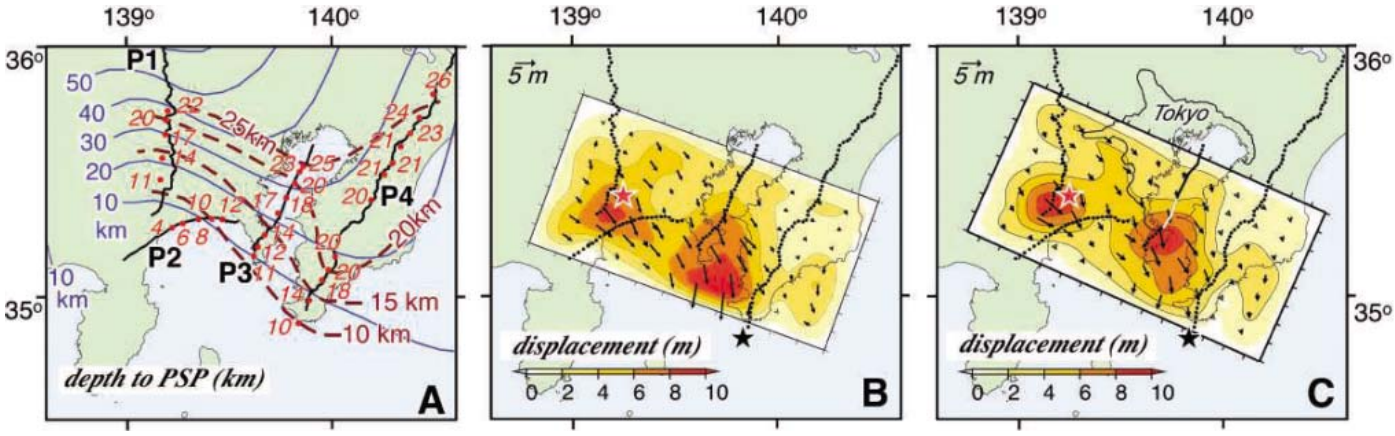

Fig. 3. PSP vertical and lateral characteristics derived from seismic profiles. (**A**) Depth to PSP in km. Blue contours are from a previously published study (*6*). Depths from seismic profiles are annotated (red) at marked locations (red dots); note substantial mismatch along P1 and northern P3. (**B**) 1923 Kanto earthquake finite-slip determination (*11*) based on previous fault model (*12*, *13*). Red zones of large displacement represent two asperity patches of 1923 Kanto earthquake rupture. (**C**) 1923 Kanto earthquake finite-slip determination recalculated with the use of our revised PSP geometry. Note the eastern red zone showing large coseismic slip is relocated northward toward the most densely populated area of greater Tokyo (solid outline). Stars are epicenters of 1703 Genroku (black) and 1923 Kanto earthquakes (red). Amplitude character color code along P3 defined in Fig. 2.

variable signal-to-noise recording conditions, particularly in the highly populated urban areas. The majority of P3 was acquired by using one marine seismic acquisition method and was amenable to relative amplitude seismic processing (*10*). The updip termination of UPSP reflection A in P3 (Fig. 2) correlates with the transition from low to high slip bounding the eastern asperity region (Fig. 3C). These revised geometries of the UPSP megathrust and its asperity regions as provided by our seismic profiles provide vertical and lateral constraints for improved estimations of seismic hazards within metropolitan Tokyo.

References and Notes

1. M. Takemura, *Great Kanto Earthquake* (Kajima, Tokyo, 2003).
2. The statistics were based on the 2003 annual report on the regional economy from the Cabinet Office of the Japanese government.
3. Y. Okada, *Earth Monthly* **34**, 94 (2001).
4. T. Seno *et al.*, *J. Geophys. Res.* **98**, 17941 (1993).
5. K. Kasahara, *Disaster Prev./Bosai* **35**, 33 (1985).
6. M. Ishida, *J. Geophys. Res.* **97**, 489 (1992).
7. S. Noguchi, *Bull. Earthquake Res. Inst. Univ. Tokyo* **73**, 73 (1998).
8. M. Matsubara *et al.*, *J. Geophys. Res.*, in preparation.
9. A. Taira *et al.*, in *The Evolution of the Pacific Ocean Margins*, Z. Ben-Abraham, Ed. (Oxford Univ. Press, New York, 1989), pp. 100.
10. See methods and data on *Science* Online.
11. R. Kobayashi, K. Koketsu, *Earth Planets Space* **57**, 261 (2005).
12. D. J. Wald, P. G. Somerville, *Bull. Seismol. Soc. Am.* **85**, 159 (1995).
13. M. Matsu'ura *et al.*, *J. Phys. Earth* **28**, 119 (1980).
14. T. Matsuzawa *et al.*, *Geophys. Res. Lett.* **29**, 11,1543 (2002).
15. Y. Yamanaka, M. Kikuchi, *J. Geophys. Res.* **109**, 1029/2003JB002683 (2004).
16. K. Koketsu, M. Kukuchi, *Science* **288**, 1237 (2000).
17. T. Furumura, K. Koketsu, *Pure Appl. Geophys.* **157**, 2047 (2000).
18. T. Sagiya, *Pure Appl. Geophys.* **161**, 2601 (2004).
19. S. Ozawa *et al.*, *Geophys. Res. Lett.* **30**, 1283 (2003).
20. S. Kodaira *et al.*, *J. Geophys. Res.* **105**, 5887 (2000).
21. S. Kodaira *et al.*, *Geophys. J. Int.* **149**, 815 (2002).
22. S. Kodaira *et al.*, *Science* **304**, 1295 (2004).
23. T. Hayakawa *et al.*, *Phys. Earth Planet. Inter.* **132**, 89 (2002).
24. A. Nakanishi *et al.*, *J. Geophys. Res.* **109**, 1029/2003JB002574 (2004).
25. M. Nedimovic *et al.*, *Nature* **424**, 416 (2003).
26. N. Bangs *et al.*, *J. Geophys. Res.* **104**, 20399 (1999).
27. T. Shipley *et al.*, *Geology* **22**, 411 (1994).
28. S. L. Bilek, T. Lay, *Science* **281**, 1175 (1998).
29. P. Wessel, W. H. F. Smith, *Eos* **72**, 445 (1991).

30. We thank K. Ito, K. Miller, J. Park, and F. Wu for discussions. Instruments used in the field program were provided by the seismic survey company JGI, Incorporated; ERI, the University of Tokyo; and the IRIS/PASSCAL instrument centers located at New Mexico Tech and University of Texas at El Paso (UTEP). We thank the JGI seismic crew and G. Kaip of UTEP for data acquisition. Figures were prepared with the use of the Generic Mapping Tool (*29*). This study was supported by the Special Project for Earthquake Disaster Mitigation in Urban Areas from the Ministry of Education, Culture, Sports, Science, and Technology of Japan.

Supporting Online Material
www.sciencemag.org/cgi/content/full/309/5733/462/DC1
Materials and Methods
Figs. S1 to S8

1 February 2005; accepted 27 May 2005
10.1126/science.1110489

Heat Flux Anomalies in Antarctica Revealed by Satellite Magnetic Data

Cathrine Fox Maule,[1]* Michael E. Purucker,[2] Nils Olsen,[1] Klaus Mosegaard[1]

The geothermal heat flux is an important factor in the dynamics of ice sheets; it affects the occurrence of subglacial lakes, the onset of ice streams, and mass losses from the ice sheet base. Because direct heat flux measurements in ice-covered regions are difficult to obtain, we developed a method that uses satellite magnetic data to estimate the heat flux underneath the Antarctic ice sheet. We found that the heat flux underneath the ice sheet varies from 40 to 185 megawatts per square meter and that areas of high heat flux coincide with known current volcanism and some areas known to have ice streams.

The geothermal heat flux depends on geologic conditions such as crustal heat production, mantle heat flux, and the tectonic history of the crust, which all vary spatially. Studies have shown that heat flux can vary much on scales less than 100 km (*1*, *2*). Underneath ice sheets, the geothermal heat flux influences the basal ice, which may cause varying amounts of basal melting in Greenland (*2*, *3*). Heat flux is thus an important boundary condition in ice sheet modeling. Little is known about the geologic setting of the crust underneath the

[1]Center for Planetary Science, Juliane Maries vej 30, 2100 Copenhagen Oe, Denmark. [2]Raytheon at Goddard Space Flight Center, NASA, Greenbelt, MD 20771, USA.

*To whom correspondence should be addressed. E-mail: foxmaule@gfy.ku.dk

Antarctic ice sheet from which the heat flux can be inferred, and direct measurements are hard to obtain because they require measurements at the bottom of ice boreholes reaching bedrock. So far, this has only been achieved at a few locations in Antarctica (*4*). The current available methods of (directly or indirectly) measuring the heat flux underneath the ice give only local results. Here, we present a method capable of providing a heat flux map covering Antarctica from satellite magnetic data. Using magnetic data to infer heat flux is possible because the magnetic properties of rocks are temperature dependent until they reach the Curie temperature (*5*). We use a magnetic field model based on satellite data to determine the depth to the Curie temperature, which is about 580°C for the low-Ti magnetite that is believed to be the dominant source of crustal magnetic anomalies (*6*). Combining this with a thermal model of the crust, we estimated the heat flux underneath the ice sheet.

On a global scale, Earth's magnetic field is dominated by contributions from the core, whereas only a few percent is of crustal origin. However, at wavelengths shorter than about 2600 km, the crustal part dominates the core field. The crustal field is caused by remanent magnetism and magnetism induced by the present core field. The latter depends on the magnetic susceptibility of the rocks, the ambient field strength, and the thickness of the magnetic crust, which is bounded above by bedrock surface and below by either Moho (*7*) or the Curie isotherm, whichever of the two is shallower. Thus, the magnetic crust can be thinner than the chemical crust in regions with high heat flux.

The measured magnetic field also includes time-varying contributions due to the interaction between the Earth's core field and the solar wind. The influence of the strong time-variable external field in polar regions is minimized by deriving spherical harmonic representations (field models) of the magnetic field with data from magnetically quiet times. Therefore, instead of using the satellite data directly, we based our analysis on the Magnetic Field Model 3 crustal field model (*8*), which is constructed from several years of data from the Challenging Minisatellite Payload and Oersted satellites and includes spherical harmonic terms up to degree and order 90. From this, we computed the vertical component at 300-km altitude (*9*). To remove the core field, we high-pass filtered by using only spherical harmonics above degree 14. However, this also eliminated the long-wavelength part of the crustal field. To isolate the induced part, we subtracted a model of the oceanic remanent field (*10*, *11*). Neither global nor regional models of remanent magnetism of continental areas exist, so we assumed that induced magnetism dominates here. The resulting induced field (Fig. 1A) is the data used in our modeling.

To infer the thickness of the magnetic crust from the induced field, we used the equivalent source magnetic dipole method (*12*), in which the crustal magnetization is represented by dipoles evenly distributed at the Earth's surface. We used 21,162 dipoles, each representing an area with a diameter of about 180 km. Because we used only the induced part of the field, the directions of the dipoles are given by the present core field; only their magnitudes (dipole moments) are determined from the magnetic data by forward modeling (*13*).

The average magnetization, inferred from the dipole moments, is proportional to the average magnetic susceptibility and the thickness of the magnetic crust. In general, the crustal field is stronger over the continents than over the oceans (*8*), and there is a relatively large difference between the continental (~40 km) and oceanic (~7 km) crustal thickness (*14*), whereas the difference in susceptibility between oceanic and continental rocks is not as large (*6*). It is therefore reasonable to assume that thickness variations dominate susceptibility variations. We used 0.035 (in the SI system, susceptibility has no unit) for the susceptibility of the continental crust and 0.040 for the oceanic crust (*15*). With this assumption, the magnetic crustal thickness can be determined from the magnetization. Only the short-wavelength variation of the magnetic crust is constrained by the magnetic field data (because of the high-pass filtering), so its long-wavelength part is taken from the 3SMAC crustal thickness model (*16*) (Fig. 1B), which is based on seismic and thermal data. Combining the long- and short-wavelength parts, we obtained the magnetic crustal thickness (Fig. 1C).

We found that the magnetic crustal thickness to some extent reflects the known crustal thickness difference between East and West Antarctica, with thicker crust in East than in West Antarctica (*16*, *17*). The magnetic crust is thicker in East Antarctica than in West Antarctica, and the thickest crust is in the central parts of East Antarctica. The area around Victoria Land, Oates Land, and George V Land in East Antarctica has a thin magnetic crust, as also found in a belt along the East-West Antarctica boundary and along the Siple Coast. Intermediate values of the magnetic crustal thickness are present in the coastal part of West Antarctica.

To estimate the geothermal heat flux, we constructed a thermal model for the continental crust, not including the ice [supporting online material (SOM) text]. We assumed that there was one-dimensional heat conduction, steady state, and constant thermal conductivity and that the lower boundary of the magnetic crust was the Curie isotherm. To account for radioactive heat production in the crust, we applied a model of exponentially decreasing heat production with depth (*18*), taking the heat production at the surface to be 2.5×10^{-6} W/m^3 and the scale depth to be 8 km [(*18*) and references therein]. The temperature difference over the magnetic crustal thickness is the difference between the Curie temperature and the temperature at the bedrock surface, which is close to 0°C underneath the ice sheet. With these boundary conditions, the heat conduction equation was solved to give the temperature-depth profile in the crust (SOM text). We obtained the heat flux at the bedrock surface from the temperature profile. We chose a thermal conductivity of 2.8 W/mK (*19*) and took the difference between the Curie temperature and the bedrock temperature to be 580 K. Choosing these values resulted in an average heat flux in Antarctica of 65 mW/m^2, which is the continental average (*20*). We validated our method using direct heat flux measurements in Australia; for error analysis we applied it to another geomagnetic field model, Comprehensive Model, Version 4 (*21*), and obtained similar results (<15 to 20% difference) to those presented here. Both indicate that magnetic anomalies are a robust proxy for geothermal heat flux (SOM text). Geothermal heat flux can vary on a scale of tens of kilometers as a result of local geologic settings (*1*, *2*). Satellite data limits our resolution to at least a few hundred kilometers, which causes a smoothing that should be kept in mind when comparing a heat flux map derived from satellite magnetic data with direct measurements.

The obtained heat flux map (Fig. 1D) reflects the variation in the magnetic crustal thickness. We found below average heat flux (50 to 60 mW/m^2) in the central part of East Antarctica and elevated heat flux along the East-West Antarctica boundary and around Siple Coast. Similarly high heat fluxes were found around Victoria Land, Oates Land, and George V Land. Our results are supported by geological evidence of high heat flux and may explain the occurrence of subglacial lakes and the Siple Coast ice streams. For example, around Victoria Land and in the coastal part of West Antarctica, areas of high heat flux coincide with current volcanic activity. At Siple Coast, where we found elevated heat flux, there are several ice streams, and it has previously been suggested that heat at the base of the ice could be one of the trigger mechanisms for their formation (*3*, *4*, *22*, *23*). Energy balance models (*24*) suggest that heat flux underneath one of the Siple Coast ice streams must exceed 80 mW/m^2 to maintain basal melting, which is the value we found for this area. Direct measurements at Siple Dome yield 69 mW/m^2 (*4*); the difference is within our error estimate (20 to 25 mW/m^2; SOM text). Subglacial lakes are widespread in Ant-

arctica (*25*). Studies on the thermal regime of the overlying ice sheet have shown that heat fluxes around 55 mW/m^2 are required to maintain the subglacial lakes in central parts of East Antarctica, whereas a substantially larger heat flux is necessary to maintain them in George V Land and Oates Land (*26*), in agreement with our results in these areas. In the Vostok area (78°S, 105°E), we found a heat flux of 54 mW/m^2, a value that exceeds the rate required to sustain a subglacial lake in this region [43 mW/m^2 in (*26*)]. On the basis of our results, one might speculate about volcanism in the area landward of Ronne Ice Shelf (*17*, *27*).

Errors in our estimate of geothermal heat flux (details in SOM text) beneath the Antarctic ice sheet arise through uncertainties in the magnetic field model (10 to 20 mW/m^2), unconsidered remanent magnetization (13 mW/m^2), our use of constant Curie and basal ice temperatures (5 mW/m^2), and lateral variations in thermal conductivity of the crustal rocks (10 mW/m^2). In addition, there are errors associated with uncertainties in the initial crustal model and lateral variations in magnetic susceptibility; although we are unable to quantify these contributions, we estimate that they are both less than 5 mW/m^2. The combined uncertainty of these independent, uncorrelated terms is 21 to 27 mW/m^2.

As an alternative to using satellite magnetic data, heat flux can be estimated from aeromagnetic data by, for example, power spectrum analysis (*28*). However, even with the creation of the Antarctic Digital Magnetic Anomaly Map (*29*), we believe that it currently would be difficult to make a Curie temperature depth map from aeromagnetic measurements covering Antarctica due to the sparsity of the data. The forte of power spectrum analysis of aeromagnetic data is that small-scale features can be resolved, but the method has difficulties at regional and global scales. Satellite data have the advantage of covering the entire Earth but can only see variations in excess of at least a few hundred kilometers (comparable to satellite altitude). Our results show that satellite magnetic data are a favorable way to estimate the regional scale of spatially varying

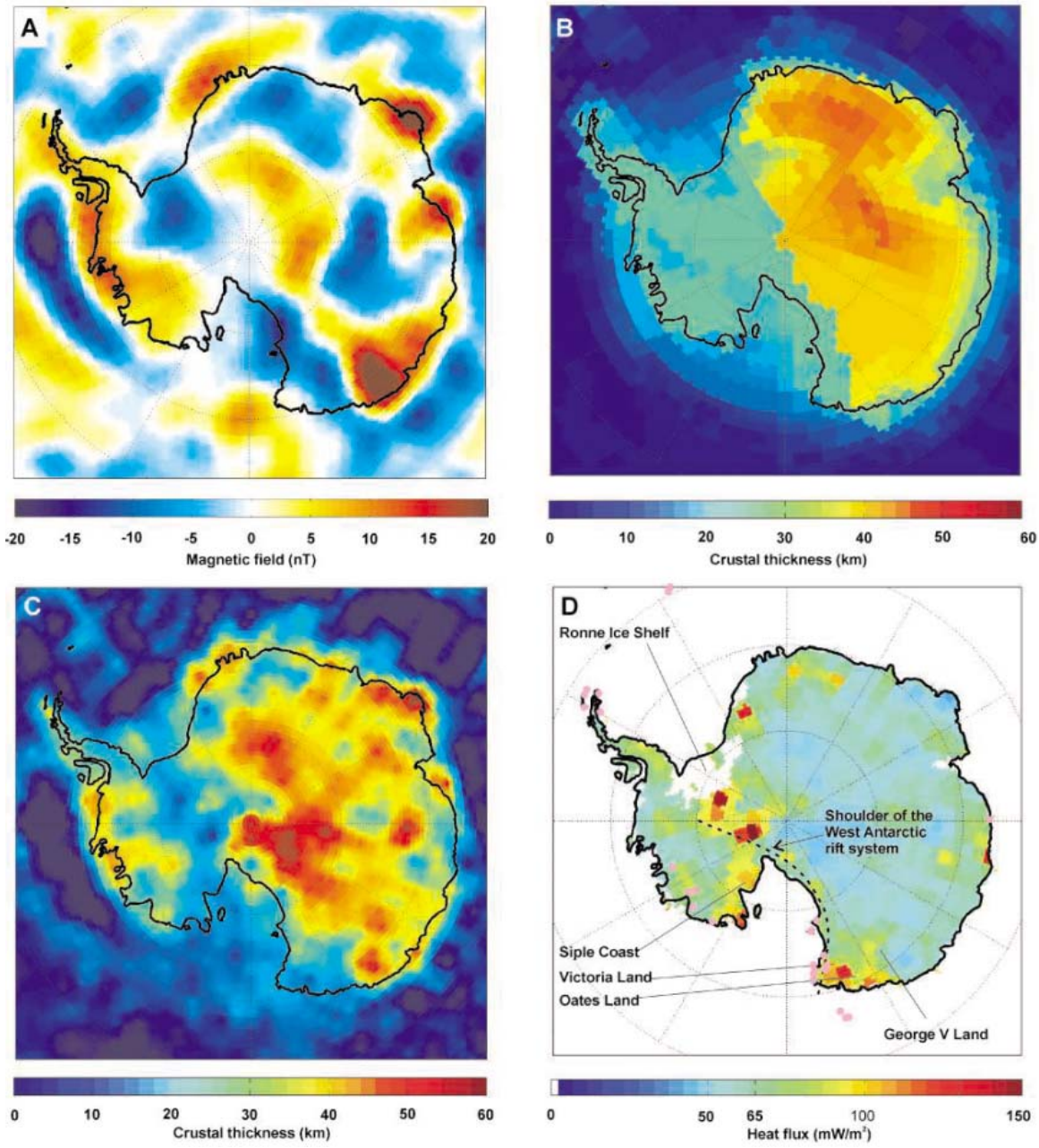

Fig. 1. (**A**) The radial component of the high-pass filtered observed magnetic field from MF3 at 300-km altitude, where a model of the remanent magnetism has been subtracted. Parallels are 10° apart, and meridians are 30° apart. (**B**) The initial model of crustal thickness from the 3SMAC model (*16*). (**C**) Obtained magnetic crustal thickness. The thickest magnetic crust is found in central parts of East Antarctica, and the thinnest crust is found around Victoria Land, Oates Land, and in the West Antarctic rift system. (**D**) Geothermal heat flux. The pink dots mark known volcanoes and coincide with areas of elevated heat flux, especially around Victoria Land. Areas of high heat flux are found close to the shoulder of the West Antarctic rift system (*17*). Because the heat flux model is valid only in continental areas, we have no results underneath Ronne Ice Shelf.

heat flux underneath large ice sheets. As the resolution of satellite magnetic field models improves in the future, this method will identify still finer features, and may eventually locate yet undiscovered volcanic areas (*27*) underneath the ice.

References and Notes

1. J.-O. Näslund, P. Jansson, J. L. Fastook, L. Andersson, J. Johnson, *Ann. Glaciol.*, in press.
2. D. Dahl-Jensen, N. Gundestrup, S. P. Gogineni, H. Miller, *Ann. Glaciol.* **37**, 207 (2003).
3. M. Fahnestock, W. Abdalati, I. Joughin, J. Brozena, P. Gogineni, *Science* **294**, 2338 (2001).
4. H. Engelhardt, *J. Glaciol.* **50**, 251 (2004).
5. The Curie temperature is the temperature above which materials lose their ability to sustain a (remanent or induced) magnetic field.
6. R. A. Langel, W. J. Hinze, *The Magnetic Field of the Earth's Lithosphere* (Cambridge Univ. Press, Cambridge, 1998).
7. Moho is the base of the chemical crust and is defined by seismic properties.
8. S. Maus, www.gfz-potsdam.de/pb2/pb23/SatMag/litmod3.html.
9. Although it is possible to calculate the field at any altitude from a spherical harmonic representation, downward continuation from satellite altitudes (400 to 800 km) amplifies shorter wavelengths. To avoid fitting artificial signatures due to amplified noise, we found that 300-km altitude was suitable for our parameter spacing.
10. J. Dyment, J. Arkani-Hamed, *J. Geophys. Res.* **103**, 15,423 (1998).
11. M. E. Purucker, J. Dyment, *Geophys. Res. Lett.* **27**, 2765 (2000).
12. J. Dyment, J. Arkani-Hamed, *Geophys. Res. Lett.* **25**, 2003 (1998).
13. C. Fox Maule, M. E. Purucker, N. Olsen, in *Earth Observation with CHAMP*, C. Reigber, H. Lühr, P. Schwintzer, J. Wickert, Eds. (Springer, Heidelberg, Germany, 2005).
14. W. Lowrie, *Fundamentals of Geophysics* (Cambridge Univ. Press, Cambridge, 1997).
15. M. E. Purucker, B. Langlais, N. Olsen, G. Hulot, M. Mandea, *Geophys. Res. Lett.* **29**, 10.1029/2001GL013645 (2002).
16. H.-C. Nataf, Y. Ricard, *Phys. Earth Planet. Inter.* **95**, 101 (1996).
17. J. C. Behrendt, *Global Planet. Change* **23**, 25 (1999).
18. M. Sandiford, S. McLaren, *Earth Planet. Sci. Lett.* **204**, 133 (2002).
19. G. R. Beardsmore, J. P. Cull, *Crustal Heat Flow* (Cambridge Univ. Press, Cambridge, 2001).
20. H. N. Pollack, S. J. Hurter, J. R. Johnson, *Rev. Geophys* **31**, 267 (1993).
21. T. J. Sabaka, N. Olsen, M. E. Purucker, *Geophys. J. Int.* **159**, 521 (2004).
22. D. D. Blankenship *et al.*, *Nature* **361**, 526 (1993).
23. M. R. Bennett, *Earth Sci. Rev.* **61**, 309 (2003).
24. C. F. Raymond, *J. Glaciol.* **46**, 665 (2000).
25. M. J. Siegert, *Earth Sci. Rev.* **50**, 29 (2000).
26. M. J. Siegert, J. A. Dowdeswell, *J. Glaciol* **42**, 501 (1996).
27. J. P. Winberry, S. Anandakrishnan, *Geophys. Res. Lett.* **30**, 10.1029/2003GL018001 (2003).
28. A. Stampolidis, G. N. Tsokas, *Pure Appl. Geophys.* **159**, 2659 (2002).
29. A. Golynsky *et al.*, *IX ISAES Proc.* (Springer, Heidelberg, in press).

30. We thank D. Dahl-Jensen and C. Hvidberg for comments on ice sheet stability and ice streams, and S. Maus for making MF3 available to us.

Supporting Online Material

www.sciencemag.org/cgi/content/full/1106888/DC1
SOM Text
Figs. S1 and S2
References

28 October 2004; accepted 1 June 2005
Published online 9 June 2005;
10.1126/science.1106888
Include this information when citing this paper.

RNA Polymerase II Is Required for RNAi-Dependent Heterochromatin Assembly

Hiroaki Kato,[1] Derek B. Goto,[2] Robert A. Martienssen,[2] Takeshi Urano,[3] Koichi Furukawa,[3] Yota Murakami[1]*

In *Schizosaccharomyces pombe*, the RNA interference (RNAi) machinery converts pericentromeric transcripts into small interfering RNAs (siRNAs) and is required for the assembly of pericentromeric heterochromatin. Here we describe a mutation in the second largest subunit of RNA polymerase II (RNAPII). Both wild-type and mutant RNAPII localized to the pericentromere. However, the mutation resulted in the loss of heterochromatic histone modifications and in the accumulation of pericentromeric transcripts, accompanied by the loss of siRNAs. This phenotype resembles mutants in RNAi and suggests that RNAPII couples pericentromeric transcription with siRNA processing and heterochromatin assembly.

Heterochromatin contributes to epigenetic regulation by inhibiting gene expression in specific chromosomal domains. RNAi-related factors play essential roles in heterochromatin formation (*1*–*3*). In the fission yeast *Schizosaccharomyces pombe*, transcripts from pericentromeric repeats generate siRNAs, which are responsible, at least in part, for targeting the RNAi-induced transcriptional silencing (RITS) complex. This targeting promotes histone H3–lysine 9 (H3-K9) dimethylation by the Clr4/Rik1 histone methyltransferase complex (*4*) that is required for the localization of Swi6, a heterochromatin protein 1 (HP1) homolog. These factors are conserved in higher eukaryotes, suggesting that siRNA-directed heterochromatin formation is an evolutionarily conserved mechanism (*5*). To further understand the mechanism of pericentromeric heterochromatin formation, we screened for mutations in fission yeast that affect pericentromeric heterochromatin. This led to the discovery of a previously undescribed mutation denoted as *m203* (*6*).

The *m203* mutation resulted in derepression of *ura4*$^+$ marker genes integrated into the outermost (*otr*) or innermost (*imr*) pericentromeric repeats of chromosome 1 (*otr1R::ura4*$^+$ and *imr1L::ura4*$^+$, respectively) (fig. S1). The extent of derepression was similar to that observed in RNAi-related ribonuclease III (RNase III) Dicer or histone H3K9 methyltransferase mutants (Δ*dcr1* and Δ*clr4*, respectively) (Fig. 1A). Like Δ*dcr1*, but unlike Δ*clr4*, the *m203* mutation did not affect silencing of the *ura4*$^+$ marker gene at the *mat* locus (*kint2::ura4*$^+$) (Fig. 1A). Thus, like mutants in RNAi, the *m203* mutation specifically disturbs pericentromeric silencing. We next demonstrated that the *m203* mutation alters the heterochromatic structure of the *ura4*$^+$ gene inserted at the *otr* locus by chromatin immunoprecipitation (ChIP) with antibodies specific for several modified histones or Swi6 (Fig. 1B). The *m203* mutation reduced H3-K9 methylation and Swi6 localization while increasing H3-K9 acetylation and H3-K4 methylation, both of which are euchromatic histone modifications (Fig. 1B). These changes are similar to those observed in Δ*dcr1* and Δ*clr4* mutants (Fig. 1B) (*3*, *7*). In addition, the *m203* mutation, like Δ*dcr1* and Δ*clr4*, impaired chromosome segregation (supporting online text, fig. S2), probably because of a defect in pericentromeric heterochromatin that resulted in improper sister chromatid cohesion (*8*, *9*).

Using genetic mapping and DNA sequencing (*6*), we identified an A-to-T base substitution within the *rpb2* gene, which encodes the second largest subunit (Rpb2) of RNA polymerase II (RNAPII), as the *m203* mutation. This allele is denoted as *rpb2-m203*, and the base substitution caused an alteration of asparagine-44 (Asn^{44}) to tyrosine (Tyr) (Fig. 2).

The *rpb2*$^+$ gene is essential for viability (*10*), but the *rpb2-m203* mutation did not impair growth at temperatures ranging from 23° to 36°C, indicating that its essential function was not affected by the mutation (fig. S4). In support of this, levels of constitutively expressed *act1* transcripts were not down-

[1]Department of Viral Oncology, Institute for Virus Research, Kyoto University, Kyoto 606–8507, Japan. [2]Cold Spring Harbor Laboratory, Cold Spring Harbor, NY 11724, USA. [3]Department of Biochemistry II, Nagoya University Graduate School of Medicine, Nagoya 466–8550, Japan.

*To whom correspondence should be addressed. Department of Viral Oncology, Institute for Virus Research, Kyoto University, Shogoinkawahara-cho, Sakyo-ku, Kyoto, Kyoto 606-8507, Japan. E-mail: yota@virus.kyoto-u.ac.jp

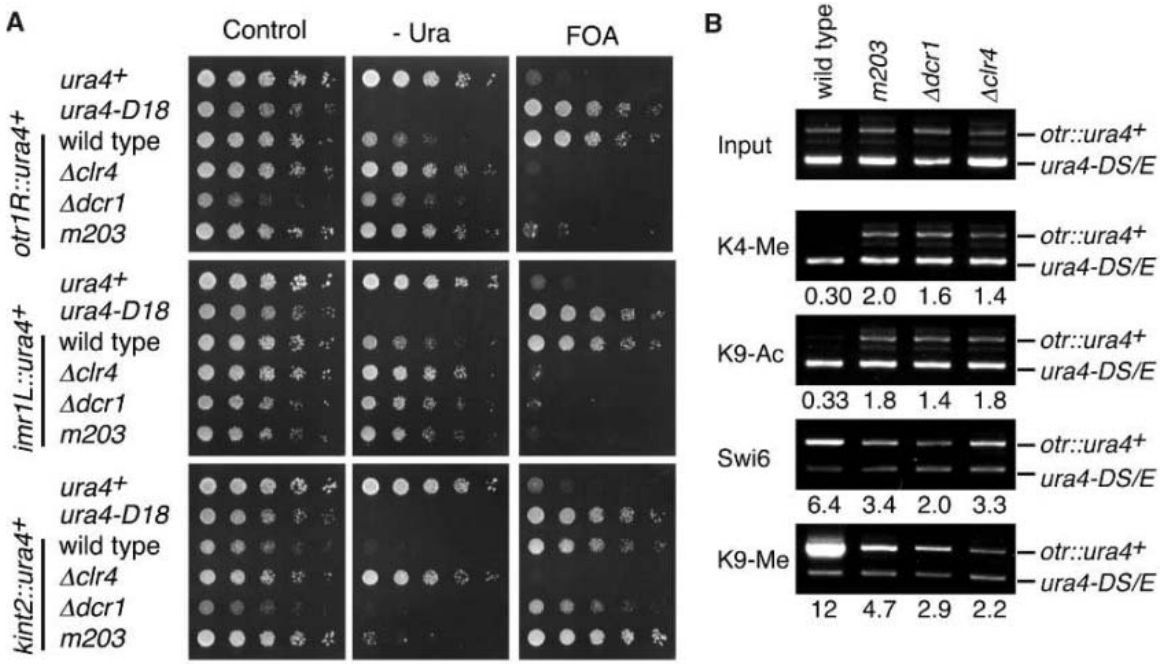

Fig. 1. The *m203* mutation abolishes gene silencing and heterochromatin structure at the centromere periphery. (**A**) *m203* cells and Δ*dcr1* cells show derepression of the *ura4*$^+$ gene at pericentromeric regions but not at the *mat* locus, whereas Δ*clr4* cells showed derepression at both loci. Strains harboring each reporter gene (*otr1R*::*ura4*$^+$, *imr1L*::*ura4*$^+$, or *kint2*::*ura4*$^+$) were serially diluted and spotted onto plates either lacking uracil or supplemented with 5-fluoroorotic acid (5-FOA), which is toxic to *ura4*$^+$-expressing cells. (**B**) The *m203* mutation, as well as Δ*clr4* and Δ*dcr1* mutations, abolishes heterochromatin modifications at the *otr1R*::*ura4*$^+$ locus. ChIP experiments were performed with the indicated antibodies. DNA from precipitates or the input cell extract (Input) were analyzed by competitive polymerase chain reaction (PCR), in which one primer amplifies two PCR products from *otr1R*::*ura4*$^+$ and the euchromatic *ura4-DS/E*. The relative fold enrichment shown below each lane was calculated by comparing the ratios of the *otr::ura4*$^+$ signal to the *ura4-DS/E* signal that had been amplified from the immunoprecipitated DNA and from the input cell extracts.

regulated in *rpb2-m203* cells (Fig. 3, B and C). In addition, microarray analysis of gene expression in *rpb2-m203* mutant cells revealed that genes involved in heterochromatin formation were not deregulated (table S3). RNAPII might instead specifically contribute to the transcription of the pericentromeric region that is presumably essential for siRNA generation. We hypothesized that RNAPII, rather than RNA polymerase III (RNAPIII), was likely to be the polymerase responsible for this transcription for the following reasons: The length of the transcripts is ~2.4 kb (*3*), much longer than the usual RNAPIII transcripts [~150 nucleotides (nt) (*11*)]; in the pericentromeric regions, there are several TATA-like sequences and stretches of more than five T's that act as transcription stop signals for RNAPIII (*12*); in higher eukaryotes, RNAPII transcribes noncoding primary microRNAs that are also cleaved into small RNAs (*13*). If this is the case, RNAPII should localize to the pericentromeric region. Indeed, ChIP analysis with an antibody specific for the C-terminal domain of the largest subunit of RNAP II (anti-CTD) indicated that RNAPII does localize to the pericentromeric region (Fig. 3A).

In wild-type cells, pericentromeric transcripts are quickly converted into siRNAs and are barely detectable, whereas the reverse is true in siRNA-processing mutants such as Δ*clr4* and Δ*dcr1* (Fig. 3, B to D). In *rpb2-m203* cells, pericentromeric transcript levels were clearly elevated (Fig. 3, B and C), whereas siRNAs could not be observed (Fig. 3D). Accumulated transcript levels in *rpb2-m203* cells were about one-half as much as those in Δ*dcr1* cells, in which RNA processing is likely to be completely blocked. Transcript levels in the *rpb2-m203* Δ*dcr1* double mutant were similar to those in the Δ*dcr1* single mutant. This indicates that the mutant RNAPII transcribes the pericentromeric region as efficiently as wild-type RNAPII, and mutant RNAPII localized to pericentromeric heterochromatin as in wild-type cells (Fig. 3A). We suggest that the lower level of pericentromeric transcripts in *rpb2-m203* compared with that in Δ*dcr1* reflects partial processing of the transcripts rather than reduced transcription. These data suggest that the *rpb2-m203* mutation affects siRNA-directed heterochromatin assembly not through a decrease in its transcriptional activity, but rather through a disturbance in downstream events that use pericentromeric transcripts to produce siRNAs.

One possible role that RNAPII may play is in coupling transcription with siRNA processing. In a manner analogous to mRNA processing (*14*), RNAPII may provide a site where the RNAi machinery can assemble and function coordinately to produce siRNA. A second possibility is that RNAPII may help "discriminate" noncoding pericentromeric repeat RNAs from general pre-mRNAs so that the former can be rapidly processed into siRNA. The basis for this selection may be the aberrant (double-stranded or hairpin) structure of the transcribed RNA (*15*). Alternatively, the chromatin structure of the transcribed region may somehow determine the fate of the transcripts.

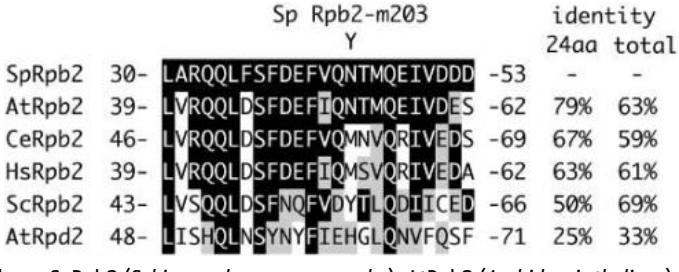

Fig. 2. *rpb2* is the gene in which the *m203* mutation is located. Multiple alignments show that the peptide sequence around the mutation site of the *rpb2-m203* allele in fission yeast is highly conserved among higher eukaryotes. The Rpb2 homologs are as follows; SpRpb2 (*Schizosaccharomyces pombe*); AtRpb2 (*Arabidopsis thaliana*); CeRpb2 (*Caenorhabditis elegans*); HsRpb2 (*Homo sapiens*); ScRpb2 (*Saccharomyces cerevisiae*). The second largest subunit of *A. thaliana* RNA polymerase IV is indicated as AtRpd2. Amino acid residues that are identical or similar to the corresponding residues in fission yeast Rpb2 are indicated by black highlighting and shadowing, respectively. The base substitution observed in *rpb2-m203* (Y) is shown above the SpRpb2 sequence. Identities between the homologs for the 24 residues around the *rpb2-m203* mutation in Rpb2 (24aa) or the whole protein (total) are indicated to the right.

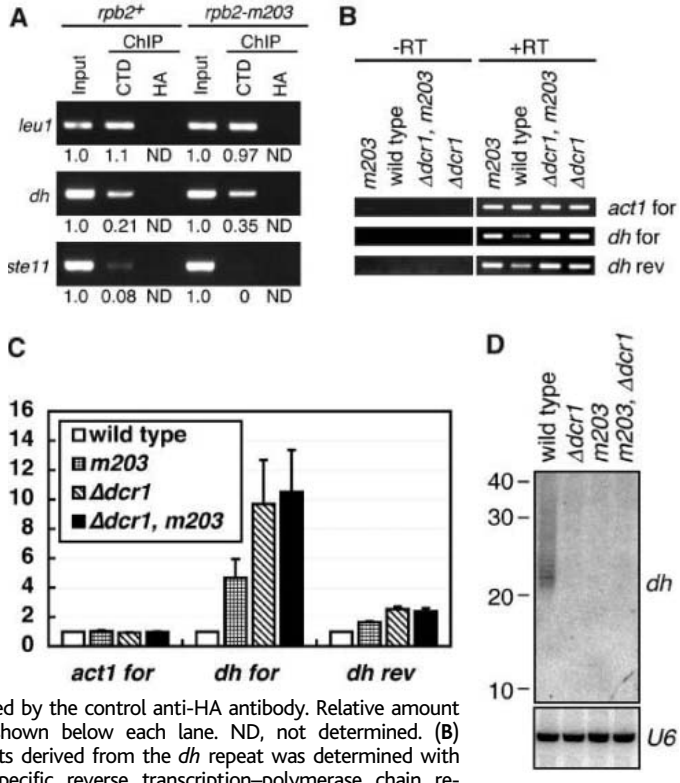

Fig. 3. The generation of siRNA requires RNAPII. (**A**) The wild-type and *m203* mutant RNAPII molecules both localize to the pericentromeric heterochromatin. ChIP analysis was performed with an antibody against the C-terminal domain of RNAPII (CTD) or an antibody to hemagglutinin (HA) as a negative control. The *dh* pericentromeric repeat, as well as the transcribed *leu1* gene, accumulated in immunoprecipitates obtained from both the wild-type and *rpb2-m203* extracts. In contrast, the gene-free upstream region of *ste11* gene, which is not transcribed in vegetative cells (*20*), did not accumulate. No signal was obtained from immunoprecipitates generated by the control anti-HA antibody. Relative amount of the PCR product is shown below each lane. ND, not determined. (**B**) Accumulation of transcripts derived from the *dh* repeat was determined with semiquantitative strand-specific reverse transcription–polymerase chain reaction (RT-PCR). Actin (*act1*) was used as a positive control. RNA samples subjected to first-strand cDNA synthesis without reverse transcriptase were used to discriminate genomic DNA contamination (−RT). for, forward strand; rev, reverse strand. (**C**) Mean signal intensities and standard deviation of three independent RT-PCR experiments as in (A) were plotted. Relative amounts of RT-PCR product from each mutant and the wild type are shown. *dh* transcripts are hardly detectable in the wild type, whereas both forward- and reverse-strand transcripts accumulated to high levels in the mutants. (**D**) Northern blot analysis of siRNA corresponding to the centromeric *dh* repeat. siRNAs spanning 22 to 26 nt are readily detected in the wild type. The siRNAs are lost in the Δ*dcr1* RNAi mutant, as well as *rpb2-m203* and the *rpb2-m203* Δ*dcr1* double mutant. Blots were reprobed for U6 snRNA as a loading control.

In *S. pombe* Rbp2, amino acid residue Asn[44] corresponds to Tyr[57] of *Saccharomyces cerevisiae* Rbp2 (Fig. 2). This residue is located on the surface of the protrusion domain of the RNAPII complex (*16*, *17*). We speculate that conversion of Asn[44] to Tyr in *rpb2-m203* may diminish possible interactions between RNAPII and unknown factors required for generating siRNA. *S. cerevisiae* Rbp2 already has Tyr at this site, and the surrounding region is less conserved than the protein as a whole (Fig. 2). This may reflect the absence of RNAi machinery in budding yeast (*3*).

It has recently been shown that the two largest subunits of RNA polymerase IV (RNAPIV) in *Arabidopsis* are required for siRNA production from pericentromeric 5*S* ribosomal RNA gene clusters and *AtSN1* retroelements and contribute to heterochromatic organization (*18*). However, homologs of these subunits are found only in the plant kingdom (*18*, *19*). Notably, the *rpb2-m203* mutation also has a highly specific effect on siRNA-directed heterochromatin formation in fission yeast, but unlike RNAPIV, Rbp2 is conserved in higher eukaryotes. It is likely that a role for RNAPII in RNAi is similarly conserved.

References and Notes
1. A. Verdel *et al.*, *Science* **303**, 672 (2004).
2. M. R. Motamedi *et al.*, *Cell* **119**, 789 (2004).
3. T. A. Volpe *et al.*, *Science* **297**, 1833 (2002).
4. M. Sadaie, T. Iida, T. Urano, J. Nakayama, *EMBO J.* **23**, 3825 (2004).
5. Z. Lippman *et al.*, *Nature* **430**, 471 (2004).
6. Materials and methods are available as supporting material on *Science* Online.
7. J. Nakayama, J. C. Rice, B. D. Strahl, C. D. Allis, S. I. Grewal, *Science* **292**, 110 (2001).
8. P. Bernard *et al.*, *Science* **294**, 2539 (2001).
9. N. Nonaka *et al.*, *Nat. Cell Biol.* **4**, 89 (2002).
10. M. Kawagishi-Kobayashi, M. Yamamoto, A. Ishihama, *Mol. Gen. Genet.* **250**, 1 (1996).
11. T. Tani, Y. Ohshima, *Nature* **337**, 87 (1989).
12. M. Hamada, A. L. Sakulich, S. B. Koduru, R. J. Maraia, *J. Biol. Chem.* **275**, 29076 (2000).
13. Y. Lee *et al.*, *EMBO J.* **23**, 4051 (2004).
14. D. A. Zorio, D. L. Bentley, *Exp. Cell Res.* **296**, 91 (2004).
15. R. A. Martienssen, *Nat. Genet.* **35**, 213 (2003).
16. J. Chen *et al.*, *Nucleic Acids Res.* **31**, 474 (2003).
17. K. J. Armache, S. Mitterweger, A. Meinhart, P. Cramer, *J. Biol. Chem.* **280**, 7131 (2005).
18. Y. Onodera *et al.*, *Cell* **120**, 613 (2005).
19. A. J. Herr, M. B. Jensen, T. Dalmay, B. Baulcombe, *Science* **308**, 118 (2005).
20. A. Sugimoto, Y. Iino, T. Maeda, Y. Watanabe, M. Yamamoto, *Genes Dev.* **5**, 1990 (1991).
21. We thank R. C. Allshire, S. I. S. Grewal, D. Q. Ding, and Y. Hiraoka for their gifts of strains and plasmids, and members of the Murakami laboratory and K. Tanaka for their support and discussions. D.B.G. is a U.S. Department of Energy–Energy Biosciences Research Fellow of the Life Sciences Research Foundation. This work is supported in part by a grant from NIH (R01-GM067014) to R.A.M., and by a Grant-in-aid for Scientific Research (B) to Y.M. from the Japan Society for the Promotion of Science.

Supporting Online Material
www.sciencemag.org/cgi/content/full/1114955/DC1
Materials and Methods
SOM Text
Figs. S1 to S5
Tables S1 to S3
References and Notes

17 May 2005; accepted 1 June 2005
Published online 9 June 2005;
10.1126/science.1114955
Include this information when citing this paper.

Apolipoprotein L-I Promotes Trypanosome Lysis by Forming Pores in Lysosomal Membranes

David Pérez-Morga,[1]* Benoit Vanhollebeke,[1]* Françoise Paturiaux-Hanocq,[1] Derek P. Nolan,[2] Laurence Lins,[3] Fabrice Homblé,[4] Luc Vanhamme,[1] Patricia Tebabi,[1] Annette Pays,[1] Philippe Poelvoorde,[1] Alain Jacquet,[5] Robert Brasseur,[3] Etienne Pays[1]†

Apolipoprotein L-I is the trypanolytic factor of human serum. Here we show that this protein contains a membrane pore-forming domain functionally similar to that of bacterial colicins, flanked by a membrane-addressing domain. In lipid bilayer membranes, apolipoprotein L-I formed anion channels. In *Trypanosoma brucei*, apolipoprotein L-I was targeted to the lysosomal membrane and triggered depolarization of this membrane, continuous influx of chloride, and subsequent osmotic swelling of the lysosome until the trypanosome lysed.

Apolipoprotein L-I (apoL-I) is a human-specific serum apolipoprotein bound to high-density lipoprotein (HDL) particles (*1*–*5*). This protein kills the African trypanosome *Trypanosoma brucei brucei*, except subspecies adapted to humans (*T. b. rhodesiense*, *T. b. gambiense*)

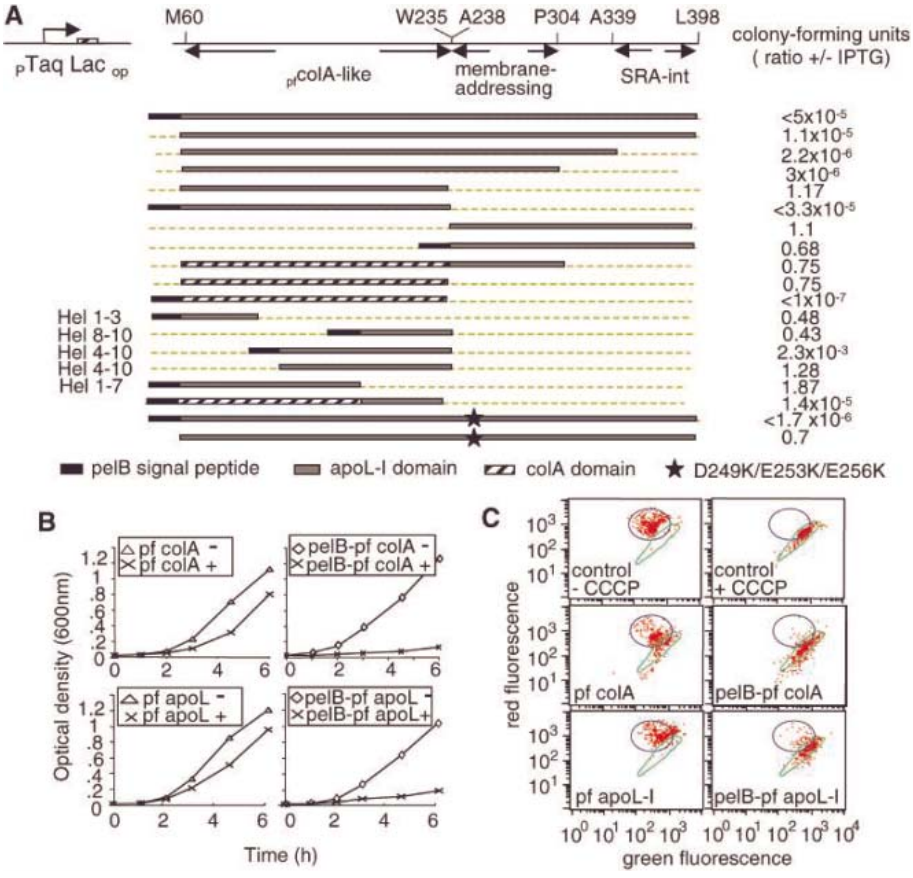

Fig. 1. Colicin-like activity of apoL-I. (**A**) Various pCT3-derived plasmids (*14*) were transfected into *E. coli C600*, and the bacterial plating efficiency was scored by comparing expression induction or not, after overnight incubation at 37°C. (**B**) Effect of the apoL-I and colA pf domains, flanked or not by pelB, on growth of *E. coli*. Expression of the two domains was induced (+) or not (−) by IPTG (isopropyl-β-D-thiogalactopyranoside). (**C**) Effect of the apoL-I and colA pf domains on the membrane potential of *E. coli*, as measured after 3 hours by flow cytometry with the $DiOC_2$ (*3*) probe. The ionophore CCCP (5 μM) was used to visualize the fluorescence shift linked to membrane depolarization.

(*5*–*7*). Trypanosome lysis results from uptake of apoL-I into the lysosome (*6*), and is thought to involve HDL receptor–mediated uptake of the lytic factor (*7*–*10*), which would lead to disruption of the lysosomal membrane following lipid peroxidation (*8*, *11*).

The C-terminal F342-L398 region of apoL-I, which interacts with the *T. b. rhodesiense* neutralizing protein SRA, is not required for trypanolytic activity (*6*). To define the lytic domain, we compared apoL-I with the database of protein family motifs (Pfam). A marginal Pfam match ($E = 0.95$) suggested a similarity between the E77–W235 region and the pore-forming (pf) domain of bacterial colicins (*12*–*14*), e.g., V389–H592 of colicin A (colA) (fig. S1). We investigated whether this region might possess bactericidal activity similar to that of the colA pf domain by assessing the activity of a plasmid encoding the colA pf domain fused to the membrane signal peptide pelB (*13*, *14*), in which the colA sequence was replaced by different regions of apoL-I (Fig. 1A). The M60-L398 region of apoL-I, which corresponds to the secreted 39-kD form of apoL-I (*1*), could replace the colA pf domain in the assay, irrespective of whether pelB was present. Deletion of the entire C-terminal region from P304 did not affect bactericidal activity. A further deletion from A238 resulted in complete loss of activity, which was rescued by the presence of pelB. The region deleted (A238–L398) was not in itself bactericidal even if pelB was added. Thus, the M60–W235 region was responsible for the bactericidal activity, and the C-terminal region P304–L398 was dispensable. The intervening region (A238–P304) was functionally analogous to pelB, although it did not act as a translocation signal peptide because it could not replace pelB in the colA pf domain assay. We will refer to this region as membrane-addressing (ma). Computational modeling of the ma sequence revealed two successive amphipatic α helices with a potential for hydrophobic interactions (fig. S2). Accordingly, the synthetic L248–A291 peptide exhibited affinity for lipids, as observed by measurement of the surface pressure of a DOPC (dioleoyl phosphatidyl choline) monolayer after injection of the peptide underneath the lipid phase. For an initial lipid pressure of ~8 mN/m, an increase of 23 mN/m ± 2 mN/m was observed ($n = 3$), which is close to the effect of known lipid-interacting peptides (*15*).

The role of the different helices of the apoL-I bactericidal domain was assessed in *Escherichia coli* (Fig. 1A). As also observed for the colA pf domain (*14*), helices 1 to 3, 1 to 7, or 8 to 10 were inactive even when provided with pelB; however, when flanked by pelB, the hel4-10 region was active, although much less so than the full domain. A pelB-containing chimera associating helices 1 to 7 from colA and 8 to 10 from apoL-I was active, which could be important given the primary role of helices 8 and 9 in membrane insertion of the colicin pf domain (*13*, *14*).

The bactericidal domain of apoL-I functionally mimicked the colA pf domain, because both domains similarly impaired growth of *E. coli* provided that the pelB module was present (Fig. 1B), and in both cases the effect on the bacterial proton electrochemical gradient was the same as that produced when adding CCCP (carbonyl cyanide *m*-chlorophenylhydrazone), demonstrating that, like colicins, apoL-I depolarizes the bacterial membrane (Fig. 1C).

Reconstitution of the putative pf domain of apoL-I in planar lipid bilayer membranes allowed passage of steady-state currents that displayed small fluctuations between discrete levels, consistent with the presence of ion channels (Fig. 2, A and B). The magnitude of the unitary channel conductance ranged between 2.5 and 10 pS, which is similar to the conductance of the isolated pf domain of colicins (*16*). At equal KCL concentration ([KCl]) (300 mM) on both sides of the membrane, the current-voltage curve was linear between ±50 mV, whereas in asymmetric solution (300/590 mM), the reversal potential shifted toward positive voltages (Fig. 2C). The relative permeability of anions over cations was 3.2 ± 0.1.

[1]Laboratory of Molecular Parasitology, IBMM, Université Libre de Bruxelles, 12, rue des Profs Jeener et Brachet, B6041 Gosselies, Belgium. [2]Department of Biochemistry, Trinity College, Dublin 2, Ireland. [3]Centre de Biophysique Moléculaire Numérique, Université de Gembloux, Belgium. [4]Structure et Fonction des Membranes Biologiques, Université Libre de Bruxelles, B1050 Brussels, Belgium. [5]Laboratory of Applied Genetics, IBMM, Université Libre de Bruxelles, B6041 Gosselies, Belgium.

*These authors contributed equally to this work.
†To whom correspondence should be addressed. E-mail: epays@ulb.ac.be

This selectivity is opposite to that reported for planar lipid bilayer membranes (*17*), indicating that apoL-I increases the anion permeability of the membrane. Reconstitution of recombinant apoL-I into liposomes clearly altered the Cl^- permeability of the bilayer, as indicated by the large influx of $^{36}Cl^-$ observed in the presence of apoL-I. This result was not observed with apoL-I lacking the putative pf domain (Fig. 2D). The influx of $^{36}Cl^-$ was higher at pH 5 than at pH 7, and it was insensitive to the anion-channel inhibitor DIDS (4,4-diisothiocyanatostilbene-2,2-disulfonic acid) (Fig. 2D).

Several apoL-I recombinant proteins were reconstituted into apoL-I–depleted normal human serum (NHS) (*6*) (fig. S3) and assayed for trypanolytic activity using NHS-sensitive (SRA^-) and NHS-resistant (SRA^+) *T. b. rhodesiense* clones. Recombinant apoL-I induced lysis of sensitive parasites only, with kinetics similar to that of NHS levels containing equivalent amounts of native apoL-I (Fig. 3A). The pf and ma domains of apoL-I were both required for trypanolysis, and the former domain could not be replaced by the colA pf domain in this assay (Fig. 3A). ApoL-I is normally associated with HDLs (*1*), and this association could allow rapid uptake of the toxin through receptor-mediated endocytosis of HDLs (*7–10*). Accordingly, the simple addition of recombinant apol-I to depleted serum without reconstitution delayed the lysis (Fig. 3A). Converting the negatively charged helix of the ma domain into a positive helix (D249K/E253K/E256K) (fig. S2) resulted in a total loss of trypanolytic activity equivalent to deletion of this domain (Fig. 3A). This mutant was also inactive in *E. coli* but recovered full activity when provided with the bacterial signal peptide (Fig. 1A). Thus, in trypanosomes, the ma domain probably targets apoL-I to a membrane, presumably the lysosomal membrane, because apoL-I localizes in this compartment (*6*).

Trypanosome lysis was analyzed in immobilized live cells. NHS or recombinant apoL-I, but not fetal calf serum (FCS) or the inactive D249K/E253K/E256K apoL-I mutant, caused swelling of the lysosome (Fig. 4A). The lysosome appeared empty and progressively occupied most of the cell body (Fig. 4B). These observations are consistent with osmotic swelling due to inward movement of an osmotically active species. Cl^- influx might be responsible because the cytoplasmic [Cl^-] is unusually high in trypanosomes (106 mM) (*18*) and the apoL-I pf domain is selective for anions. Lysosomal swelling and trypanolysis by NHS were both stopped when trypanosomes were transferred to a medium in which

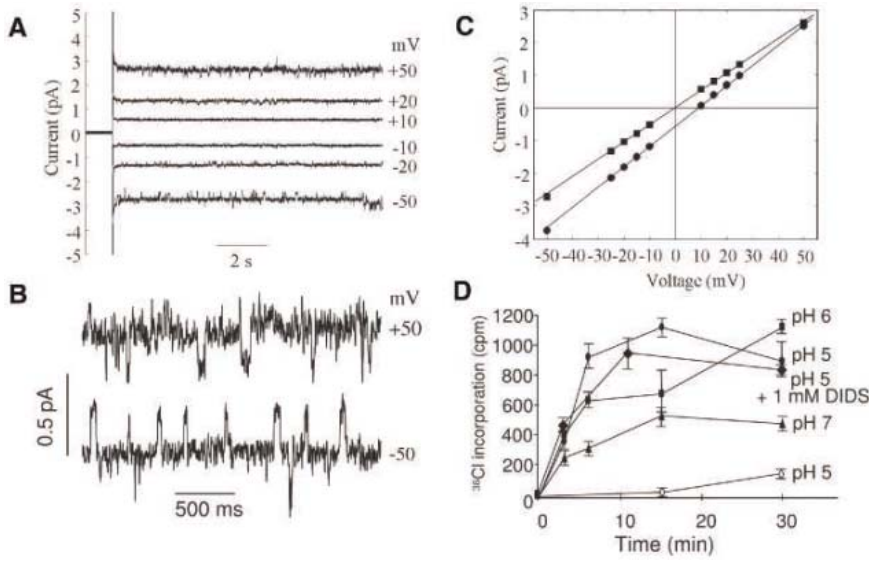

Fig. 2. Ion currents generated by apoL-I in lipid membranes. (**A** to **C**) Current traces recorded with planar lipid bilayer membranes containing the apoL-I pf domain. (A) Results at different voltages (mV) in 300 mM KCl. (B) Time scale–expanded current traces showing small current fluctuations between discrete levels, indicating channel gating. (C) Current-voltage curve in a symmetric 300 mM KCl (■) and in an asymmetric trans/cis 300/590 mM KCl (●). (**D**) ^{36}Cl flux into liposomes reconstituted with apol-I. The Cl^- incorporation was compared after insertion of the full apoL-I (filled symbols) or its version depleted of the pf domain (open symbols).

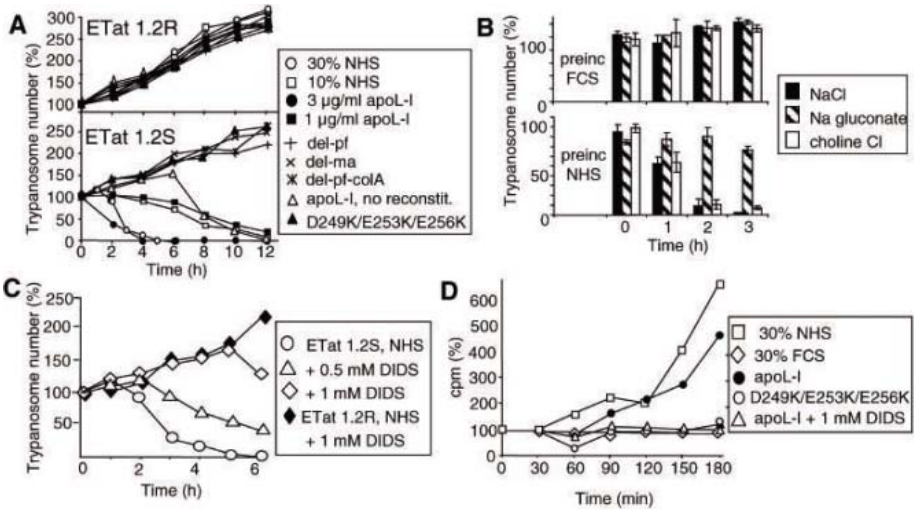

Fig. 3. Trypanosome lytic activity of apoL-I derivatives. (**A**) Effects on *T. b. rhodesiense* clones ETat 1.2S and ETat 1.2R (NHS-sensitive and NHS-resistant, respectively) of either NHS or serum reconstituted with the following recombinant proteins (3 μg/ml, unless stated otherwise): apoL-I, E28-L398; del-pf, deletion of the pf domain; del-ma, deletion of the membrane-addressing domain; del-pf-colA, replacement of the pf domain by that of colA; D249K/E253K/E256K, mutant of the ma domain. Assays were also conducted without proper serum reconstitution. 100%, 5×10^5 trypanosomes/ml. (**B**) Evidence for the involvement of Cl^- in trypanolysis by NHS. After incubation for 1 hour at 37°C in either 30% NHS or 30% FCS, the trypanosomes were centrifuged and then incubated at 37°C in 10 mM glucose, 1 mM hypoxanthine, catalase (50 μg/ml), 25 mM Hepes (pH 7.4) containing 10% FCS, and either 100 mM NaCl (■), 100 mM Na gluconate (■), or 100 mM choline Cl (□). (**C**) Effect of the Cl^- channel blocker DIDS on ETat 1.2S or ETat 1.2R trypanosomes incubated with 30% NHS. (**D**) Effect of recombinant apoL-I derivatives (3 μg/ml) and NHS or FCS (30%) on the amount of intracellular ^{36}Cl. About 50% of the cells were still alive, but swollen, after 180 min in either NHS or apoL-I. 100%, ~200 cpm.

Cl^- was replaced with gluconate (Fig. 3B). Lysis still occurred when the trypanosomes were transferred to a medium with Cl^- or to a medium with Na^+ replaced by choline, although after preincubation with FCS, none of these conditions affected the trypanosomes (Fig. 3B). Furthermore, the anion blocker DIDS, which inhibits Cl^-

channels of *T. brucei* (*19*), led to a substantial delay in lysis by NHS (Fig. 3C). At the same concentrations of DIDS, NHS-resistant parasites grew normally, indicating that the effect of DIDS on trypanolysis was specific (Fig. 3C). Finally, incubation of trypanosomes with NHS or recombinant apoL-I, but not FCS or the inactive D249K/E253K/E256K mutant, led to a DIDS-sensitive influx and accumulation of extracellular Cl^- in the cells (Fig. 3D). Thus, apoL-I triggered both the influx of Cl^- and the swelling of the lysosome. Because preventing the Cl^- flux by either removal of ions or blocking the ion channels inhibited the swelling, apoL-I must induce the ionic flux first.

The apoL-I–mediated effect was likely to involve the lysosomal membrane, because in trypanosomes apoL-I tightly colocalizes with the lysosomal membrane marker p67 (*6*). Indeed, in NHS-sensitive trypanosomes, apoL-I was concentrated at the periphery of the swollen lysosome (Fig. 4C). Moreover, the NHS-induced influx of Cl^- was linked to the specific loss of lysosomal fluorescence by the membrane-potential probe RH414 (*20*) (Fig. 4D). Imaging analysis indicated a rapid 200-fold decrease in lysosomal-associated fluorescence but no major change in mitochondrial-associated fluorescence (Fig. 4D). Despite its clear inhibitory effect on lysosome swelling by NHS, DIDS did not affect the NHS-induced change in lysosomal RH414 fluorescence (Fig. 4D). Moreover, DIDS did not affect the pf activity of apoL-I, but it clearly inhibited the NHS/apoL-I–mediated influx of extracellular $^{36}Cl^-$ (Fig. 3D). Thus, the inhibition by DIDS of trypanosome swelling and lysis by NHS was probably due to blocking of Cl^- entry into the cell. The most likely explanation is that the apoL-I–mediated influx of Cl^- from the cytoplasm to the lysosome causes a change in cytoplasmic [Cl^-] that in turn causes a compensatory movement of extracellular Cl^- across the plasma membrane through DIDS-sensitive channels (*19*) (fig. S4). The internal pressure resulting from the continuous enlargement of the lysosome presumably compromises the physical integrity of the plasma membrane, explaining the fraying of the surface coat and leakage of ions that precede lysis (*21*). These data contradict the model of lysis through disruption of the lysosomal membrane (*8*, *11*).

The Bcl-2 family is the only known example of eukaryotic proteins bearing a colicin-like pf domain (*22*), but the role of this domain is unclear (*23*). The pf domain is conserved within the human apoL family, most members of which encode intracellular proteins (*2*, *3*). Thus, the original function of apoLs might be the formation of pores in intracellular membranes. In humans, the appearance of an apoL version with a signal peptide created a new component of innate immunity endowed with antimicrobial activity.

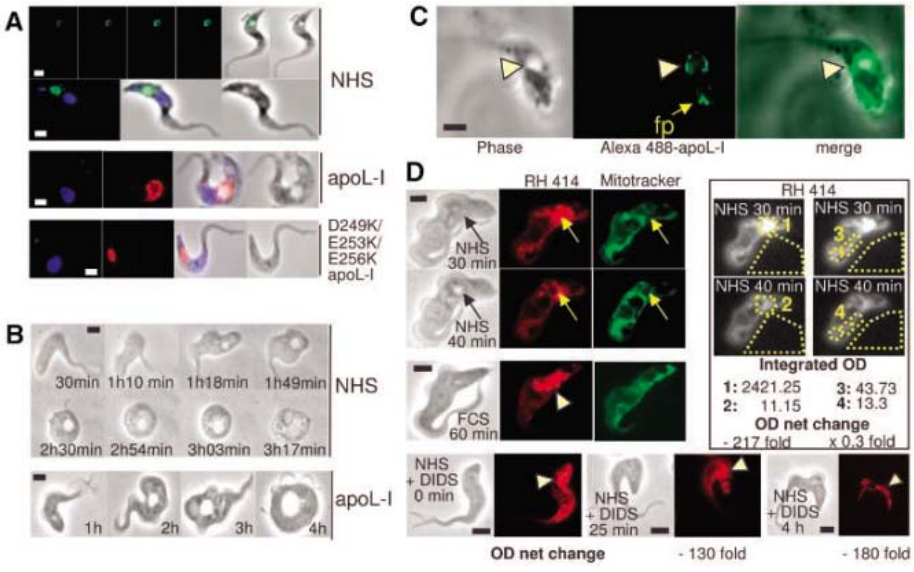

Fig. 4. Cellular effects of apoL-I. (**A**) Localization of the lysosomal membrane protein p67, detected by Alexa 488 (green)– or Alexa 594 (red)–coupled antibodies in trypanosomes incubated for 30 min at 33°C with 20% NHS (two upper rows) or with recombinant wild-type apoL-I (2 μg/ml) (third row) or D249K/E253K/E256K mutant apoL-I (bottom row). Top row: serial sections by confocal microscopy; other panels: epifluorescence microscopy [large and small blue dots, DAPI (4′,6′-diamidino-2-phenylindole)–stained nucleus and kinetoplast, respectively]. (**B**) Cellular changes induced in immobilized live trypanosomes at 33°C, by 10% NHS or serum reconstituted with recombinant apoL-I (1 μg/ml). Higher NHS concentrations and/or higher temperatures resulted in acceleration of the kinetics of lysis. (**C**) Localization of Alexa 488-apoL-I after incubation of ETat 1.2S parasites for 2 hours at 37°C (fp, flagellar pocket). (**D**) Effect of 30% NHS, 30% FCS, or 30% NHS + DIDS (1 mg/ml) on in vivo lysosomal fluorescence at 33°C by the membrane-potential probe RH414. Similar results were obtained with the RH414-like endolysosomal probe FM 4-64 (not shown). The arrows point to the lysosomal region, identified by the empty vacuole appearing between 30 and 40 min after addition of NHS. Arrowheads point to the corresponding region in trypanosomes where the lysosome does not swell. The mitotracker stains the mitochondrion. The panels at the right show the surfaces where the intensity of fluorescence was measured (1 to 4), using the respective control area. In all panels, the bar represents 2 μm.

References and Notes

1. P. N. Duchateau *et al.*, *J. Biol. Chem.* **272**, 25576 (1997).
2. N. M. Page *et al.*, *Genomics* **74**, 71 (2001).
3. P. N. Duchateau *et al.*, *J. Lipid Res.* **42**, 620 (2001).
4. H. Monajemi *et al.*, *Genomics* **79**, 539 (2002).
5. P. Poelvoorde *et al.*, *Mol. Biochem. Parasitol.* **134**, 155 (2004).
6. L. Vanhamme *et al.*, *Nature* **422**, 83 (2003).
7. L. Vanhamme, E. Pays, *Int. J. Parasitol.* **34**, 887 (2004).
8. K. M. Hager *et al.*, *J. Cell Biol.* **126**, 155 (1994).
9. M. R. Rifkin, *J. Lipid Res.* **32**, 639 (1991).
10. H. P. Green *et al.*, *J. Biol. Chem.* **278**, 422 (2003).
11. M. Shimamura, K. M. Hager, S. L. Hajduk, *Mol. Biochem. Parasitol.* **115**, 227 (2001).
12. J. Morlon *et al.*, *J. Mol. Biol.* **170**, 271 (1983).
13. D. Duché, *Biochimie* **84**, 455 (2002).
14. A. Nardi *et al.*, *J. Mol. Biol.* **307**, 1293 (2001).
15. R. Maget-Dana, *Biochim. Biophys. Acta* **1462**, 109 (1999).
16. P. K. Kienker *et al.*, *J. Gen. Physiol.* **122**, 161 (2003).
17. B. Fuks, F. Homblé, *Biophys. J.* **66**, 1404 (1994).
18. D. P. Nolan, H. P. Voorheis, *Eur. J. Biochem.* **267**, 4615 (2000).
19. N. Vanderheyden, J. Wong, R. Docampo, *Biochem. J.* **346**, 53 (2000).
20. A. Grinvald *et al.*, *Nature* **308**, 848 (1984).
21. M. R. Rifkin, *Exp. Parasitol.* **58**, 81 (1984).
22. S. W. Muchmore *et al.*, *Nature* **381**, 335 (1996).
23. Y. Lazebnik, *Curr. Biol.* **11**, R767 (2001).

24. We thank D. Duché (Marseille) for the gift of plasmids; K. Zouaoui Boudjeltia and M. Vanhaeverbeek (Vésale Charleroi) for help in collecting NHS; G. Vansanten, F. Delfosse, E. Dupont, C. Felu, and M. Magi for assistance; and G. Vandenbussche and C. Miller for advice. This work was supported by the Belgian National Fund for Scientific Research (FNRS, FRSM, and Crédit aux Chercheurs), the United Nations Development Program/World Bank/World Health Organization Special Programme for Research and Training in Tropical Diseases, and the Communauté Française de Belgique–Action de Recherches Concertées and the Interuniversity Attraction Poles Programme–Belgian Science Policy. F.H. and R.B. are Research Directors, L.V. and L.L. are Research Associates, and B.V. is a Research Fellow, all at the FNRS; D.P.N. is a senior fellow of the Wellcome Trust.

Supporting Online Material
www.sciencemag.org/cgi/content/full/309/5733/469/DC1
Material and Methods
Figs. S1 to S4
References

9 May 2005; accepted 14 June 2005
10.1126/science.1114566

The *Trypanosoma cruzi* Proteome

J. A. Atwood III,[1]* D. B. Weatherly,[2,3]* T. A. Minning,[2,3] B. Bundy,[2,3] C. Cavola,[1] F. R. Opperdoes,[4] R. Orlando,[1] R. L. Tarleton[2,3]†

To complement the sequencing of the three kinetoplastid genomes reported in this issue, we have undertaken a whole-organism, proteomic analysis of the four life-cycle stages of *Trypanosoma cruzi*. Peptides mapping to 2784 proteins in 1168 protein groups from the annotated *T. cruzi* genome were identified across the four life-cycle stages. Protein products were identified from >1000 genes annotated as "hypothetical" in the sequenced genome, including members of a newly defined gene family annotated as mucin-associated surface proteins. The four parasite stages appear to use distinct energy sources, including histidine for stages present in the insect vectors and fatty acids by intracellular amastigotes.

Trypanosoma cruzi exists in four morphologically and biologically distinct forms during its cycle of development in mammals and insects (Fig. 1). Metacyclic trypomastigotes develop in the hind gut of triatomine insect vectors and initiate infection in a wide variety of animal species, including humans. In host cells, trypomastigotes convert to replicative amastigote forms that reside in the host-cell cytoplasm. After multiple rounds of binary fission, the aflagellate amastigotes convert into flagellated trypomastigotes that burst from the host cell and circulate in the bloodstream. There, the trypomastigotes can invade other host cells and thus spread the infection throughout the body. Alternatively, trypomastigotes acquired during a blood meal convert to epimastigote forms, which replicate in the insect gut before eventually differentiating into infective metacyclic trypomastigote forms. Drugs for the treatment of *T. cruzi* infection are inadequate, and vaccines are lacking. Like other trypanosomatids, *T. cruzi* appears to regulate protein expression primarily posttranscriptionally through variations in mRNA stability or the translational efficiency of mRNAs (*1*). This limits the use of DNA microarrays (*2*–*5*) and makes proteomic analysis especially attractive for examining global changes in protein expression during development in *T. cruzi*.

Metacyclic trypomastigotes, amastigotes, trypomastigotes, and epimastigotes of *T. cruzi* were isolated, and proteins were extracted from whole-cell or subcellular lysates (fig. S1) (*6*). Peptides generated by digestion of the whole-cell or subcellular lysates were independently separated and analyzed at least in duplicate by offline multidimensional liquid chromatography, online reverse-phase liquid chromatography and tandem mass spectrometry (LC-MS/MS) (*6*, *7*). A total of 602 tryptic peptide samples were analyzed, generating 139,147 tandem mass spectra. Because of differences in protein recovery from the four life-cycle stages, trypomastigote and amastigote stages are undersampled relative to metacyclic trypomastigotes and epimastigotes (table S1). A total of 5,720 unique peptides were matched with high confidence to 1168 protein groups containing 2784 total proteins using the Mascot search engine and PROVALT parsing and clustering tools (*7*), as described in (*6*) (table S2). The approach of grouping protein isoforms (*8*, *9*) is particularly important in *T. cruzi* because the genome contains multiple, nonidentical copies of many genes, including a number of large gene families with hundreds of distinct members (*10*). In addition, the *T. cruzi* CL Brener strain used for the sequencing project is a hybrid of two genotypes and thus has multiple distinct alleles for most genes. Table 1 summarizes the proteins assigned to each life-cycle stage. Nearly 30% (838 of 2784) of the identified proteins, including most of the proteins previously documented or expected to be produced in the greatest abundance, were detected in all life-cycle stages.

Although there are limitations in the ability of shotgun proteome LC-MS/MS analysis to detect precise changes in protein levels, it is possible to track the relative abundance of proteins in the four *T. cruzi* stages using measures of protein coverage (*11*). Among the top-scoring proteins in all four *T. cruzi* proteomes are many housekeeping proteins that are also among the highest ranking proteins in yeast (*12*). However, many other highly abundant proteins in the *T. cruzi* proteome are either absent in the yeast genome or are expressed at very different relative levels in these two eukaryotes (see specific examples in supporting online text). Table 2 summarizes some of the major protein groups and families identified in the *T. cruzi* proteome. These data reflect a combination of the relative abundance of the proteins comprising each group, the size of gene families, and the ease with which certain proteins can be detected by LC-MS/MS analysis (supporting online text). Of the 2784 total proteins identified in this analysis, 1008 are from genes annotated as

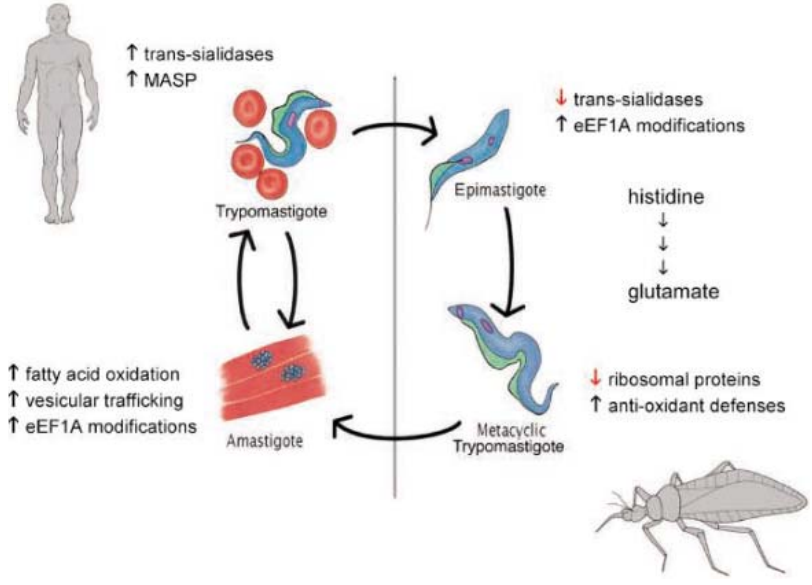

Fig. 1. Life cycle and summary of the major findings of proteome analysis in *T. cruzi*. *T. cruzi* trypomastigotes circulate in the blood of infected hosts, including humans, but must enter host cells (oftentimes muscle cells) and convert to amastigote forms to replicate. Triatomine bug vectors become infected by ingesting trypomastigotes during the course of a blood meal on infected mammalian hosts. Conversion of the trypomastigotes into epimastigotes, replication of these epimastigotes, and their eventual transformation into metacyclic trypomastigotes, occurs in the insect gut. Metacyclic trypomastigotes initiate new infection in mammals when infected insects are ingested or by deposition of parasites in the feces, usually during a blood meal.

[1]Complex Carbohydrate Research Center, [2]Center for Tropical and Emerging Global Diseases, [3]Department of Cellular Biology, University of Georgia, Athens, GA 30602, USA. [4]Research Unit for Tropical Diseases and Laboratory of Biochemistry, Christian de Duve Institute of Cellular Pathology, and Catholic University of Louvain, Brussels, Belgium.

*These authors contributed equally to this work.
†To whom correspondence should be addressed. E-mail: tarleton@cb.uga.edu

hypothetical," validating these as bona fide genes in *T. cruzi*. More than half of these hypothetical genes have orthologs in the *Leishmania major* and/or *T. brucei* genomes.

T. cruzi trypomastigotes circulate in the blood, where they are exposed to host immune effector molecules, including specific antibodies. Unlike the related African trypanosomes, *T. cruzi* trypomastigotes do not undergo antigenic variation but instead express on their surface multiple members of several large families of molecules; the best characterized of these are the mucin and trans-sialidase (ts) families (*13*). Thirty of the 50 top-scoring proteins detected exclusively in trypomastigotes are ts family members. Likewise, the amastigote and metacyclic stages appear to express subsets of ts molecules unique to each stage, whereas no ts expression was detected in the epimastigote proteome (Fig. 2 and table S2). Trans-sialidase enzymatic activity is reportedly present in only a small subset of the >1000 ts proteins encoded in the *T. cruzi* genome, and it has been linked to the presence of Tyr342 in the catalytic N-terminal region and SAPA repeats in the C terminus (*13*). Among the 223 ts proteins detected in the proteome are the products of all 15 genes predicted to encode enzyme-active ts. The production of a large number of non-enzymatic ts family members coincident with these ts enzymes may deflect immune responses away from the enzymatically active targets or may provide a pool of altered peptides that could antagonize T cell responses (*14*).

In addition to the ts and mucin families, the *T. cruzi* genome contains several other high-copy multigene families (Table 2 and supporting online text). We detected expression of several mucin-associated surface proteins (MASPs), a gene family first discovered as part of the sequencing and annotation effort (*10*), predominantly in the trypomastigote proteome. Like proteins from the other multigene families in *T. cruzi*, many MASP family members have predicted signal sequences and glycosylphosphatidylinositol anchor addition sites and thus are likely to be surface expressed. Nine MASP gene family proteins were identified in our analysis, each by only a single peptide match. This result suggests either that MASPs are not as abundantly expressed as the trans-sialidase proteins or that, like the mucins, MASPs have extensive posttranslational modifications that complicate their detection by shotgun proteomics. However, detection of the MASPs in the relatively undersampled trypomastigote stage suggests that they are not minor constituents of the *T. cruzi* proteome.

The transition from trypomastigote to amastigote can be stimulated extracellularly by simulating the low pH environment of the phagosomal/lysosomal compartment that *T. cruzi* initially encounters upon cell entry (*15*), making early time points in the transformation process to the amastigote stage amenable to transcriptome and proteome analysis. The results from this proteome analysis of amastigotes are in agreement (with one exception) with the restricted data set generated by comparison of trypomastigotes and early-stage amastigotes using DNA microarray analysis (*3*) (table S4), further supporting the quality of this analysis. In addition to the expression of a distinct subset of trans-sialidase–family genes, many of which are related to the amastigote surface protein 2 molecule previously reported to be preferentially expressed in amastigotes (*16*) (Fig. 2), the transition of trypomastigotes to amastigotes also appears to be accompanied by a dramatic shift from carbohydrate- to lipid-dependent energy metabolism (table S3). This is demonstrated by the virtual absence of glucose transporters and the detection of enzymes that oxidize fatty acids to give acetylcoenzyme A. Enzymes of the citric acid cycle, which oxidize acetyl coenzyme A to carbon dioxide and water, are also abundant in amastigotes. Amastigotes are likely to be dependent on gluconeogenesis for the synthesis of glycoproteins and glycoinositolphospholipids (GIPLs), and aspartate aminotransferases (4698.t00001, 4779.t00007) specific to amastigotes may be important in this process. These proteins lack the mitochondrial targeting signal present on the aspartate aminotransferase expressed in all stages (6015.t00007) and thus likely reside in the cytoplasm. Mitochondrially produced oxaloacetate, after transamination, may be transported to the cytosol by a malate/aspartate shuttle and then converted by the cytosolic aspartate aminotransferase and a phosphoenol pyruvate carboxykinase into phosphoenol pyruvate, the substrate for gluconeogenesis.

In addition to several heat-shock proteins and kinases, among the other proteins detected preferentially or exclusively in amastigotes are a group involved in endoplasmic reticulum (ER) to Golgi trafficking, including rab1 (4703.t00005), sec23 (8726.t00010), and sec31 (6890.t00029). The detection of this set of proteins involved in vesicular trafficking in amastigotes but not in the more highly sampled metacyclic and epimastigote stages suggests a more active trafficking process or the preferential use of selected rab and sec proteins in

Table 1. Protein group and protein identifications for each developmental stage.

Protein groups (proteins)		Amastigote	Trypomastigote	Metacyclic trypomastigote	Epimastigote
29	(49)	X			
21	(41)	X	X		
44	(161)	X	X	X	
335	(838)	X	X	X	X
27	(84)	X	X		X
65	(110)	X		X	
146	(538)	X		X	X
24	(50)	X			X
43	(125)		X		
47	(122)		X	X	
53	(93)		X	X	X
12	(22)		X		X
187	(315)		X	X	
92	(162)			X	X
43	(74)				X
1168	(2784)	691 (1871)	582 (1486)	969 (2339)	732 (1861)

Table 2. Major protein families and functional classes.

	Number of identified proteins
Protein functional classes	
Ribosomal	212
Proteasome/Ubiquitin	67
Heat shock/Chaperonins	61
Translation/Transcription	49
Histones	36
Gene families	
Trans-sialidase	223
RHS	399
GP63	29
Cysteine protease	30
MASP	9
Mucins	0
Hypothetical genes	
Hypothetical	155
Hypothetical conserved	505
Hypothetical to be annotated	348

amastigotes (table S3). We also extend the data on the selective expression in amastigotes and epimastigotes of several ABC transporters (7164.t00003, 8319.t00008) that are hypothesized to have a role in cargo selection and/or vesicular transport in trypanosomes (*17*). A putative lectin (6865.t00003) with homology to ERGIC (ER Golgi intermediate compartment), a protein involved in cargo selection in coat protein complex II vesicles, is also detected in trypomastigotes and amastigotes but not in metacyclic or epimastigote forms.

In contrast to both *T. brucei* and *L. major*, the *T. cruzi* genome encodes enzymes capable of catalyzing the conversion of histidine to glutamate. The first two enzymes in this pathway, histidine ammonia-lyase (6869.t00022) and urocanate hydratase (4881.t00011), are abundant in the insect stages but nearly undetectable in the mammalian stages (only a single spectrum matching histidine ammonia-lyase in amastigotes), consistent with the functioning of this pathway primarily in epimastigotes and metacyclic trypomastigotes. This expression pattern is notable, given that histidine is the dominant free amino acid in both the excreta and the hemolymph of *Rhodnius prolixus* (*18*, *19*), a well-studied vector for *T. cruzi*. The abundance of histidine in this and other blood-feeding insects likely reflects the high histidine content of hemoglobin (*20*). Thus, *T. cruzi* epimastigotes seem particularly adapted among the kinetoplastids to take advantage of this plentiful energy source in the gut of its insect vector. This is analogous to the use of proline as an energy source by *T. brucei* (*21*).

The transformation of epimastigotes to metacyclic trypomastigotes is accompanied by the production of a number of key enzymes and substrates important in antioxidant defense in *T. cruzi*. The H_2O_2 and peroxynitrite detoxifying enzymes ascorbate peroxidase (6846.t00006, 4731.t00003) (*22*) and the mitochondria-localized tryparedoxin peroxidase (8115.t00003) are both elevated after epimastigote to metacyclic conversion, as are tryparedoxin (5824.t00003), the substrate for tryparedoxin peroxidase, and the enzymes trypanothione synthase (8070.t00009, 7998.t00005) and iron superoxide dismutase (5781.t00004), responsible for synthesis of trypanothione and for the conversion of superoxide anion to hydrogen peroxides, respectively. These changes are consistent with a preadaptation of metacyclic forms to withstand the potential respiratory burst of phagocytic cells in the mammalian host. Enzymes of the pentose-phosphate shunt aid this process through the production of the nicotinamide adenine dinucleotide phosphate required for the reduction of trypanothione. Also noticeable in the transition of epimastigotes into metacyclic trypomastigotes is a substantial decrease in the representation of ribosomal proteins in the metacyclic proteome; 37 of the 50 highest scoring proteins in the epimastigote proteome that are not detected in the metacyclic trypomastigote proteome are ribosomal proteins. A reduction in the capacity for protein production would be consistent with the stationary, nonreplicating status of metacyclic trypomastigotes. DNA microarray analysis has also documented a substantial down-regulation of ribosomal protein expression in metacyclic forms in *L. major* (*23*).

A search for peptides with modifications (e.g., acetylations, methylations, or phosphorylations) resulted in 8 additional protein identifications and the detection of modifications on 81 previously identified proteins (supporting online text and table S5). To identify additional genes potentially missed in the annotations provided by the *T. cruzi* sequencing consortium, a database of approximately 817,000 open reading frames (ORFs) of >50 amino acids was constructed and screened using spectra that failed to match proteins predicted by the annotated genome (*6*). This analysis yielded 79 new genes, new alleles, or modifications to existing gene annotations (table S6). Sixty-six of these ORFans are new alleles of annotated genes or corrections to existing annotations, which suggests that the prediction models and annotations of The Institute for Genomic Research–Seattle Biomedical Research Institute–Karolinska Institutet *Trypanosoma cruzi* Sequencing Consortium (TSK-TSC) have been extremely efficient in accurately predicting genes. In all cases, these new annotations map to the "coding" strand of DNA among genes that are part of polycistronic units. This result is consistent with the model of kinetoplastid genes being clustered in large transcriptional units on the coding strand of DNA (*24*). Strand-switch regions separate these clusters and allow for changing of the coding strand at sites of transcription initiation. Thus, although transcriptional activity on the "noncoding" DNA strand has been documented (*25*), the proteome does not provide evidence for translation of those alternative strand transcripts.

High-throughput proteome analyses are inherently incomplete, because the available methodologies do not have sufficient dynamic range to identify and quantify all proteins expressed in an organism. In this analysis, nearly 50% of all the spectra matching to proteins mapped to the 67 most abundant protein groups. A higher number of lower abundance proteins can likely be revealed by depleting these highly abundant proteins before whole proteome analysis. Analysis of the proteomes of *T. cruzi* reveals the operation of several previously undocumented stage-specific pathways that could be appropriate targets for drug intervention. Among the most interesting of these are the proposed pathways for energy generation in amastigotes and epimastigotes. Additionally, the identification of the proteins expressed in abundance in trypomastigotes and amastigotes of *T. cruzi* provides a substantial new resource of candidates for vaccine development. This proteome analysis of *T. cruzi* also validates the high quality of the gene predictions generated by the TSK-TSC by confirming the expression of >1000 hypothetical genes and at the same time revealing <15 genes missed in the initial annotation.

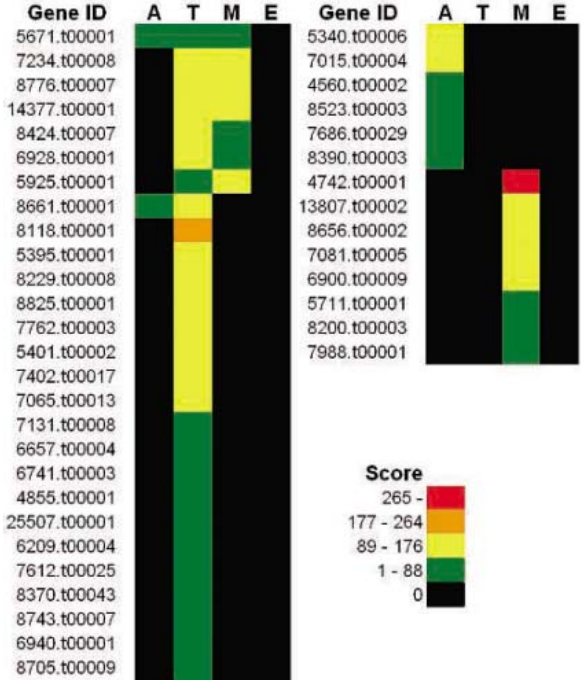

Fig. 2. Stage-specific detection of ts proteins. Cumulative protein scores based on summing the Mascot scores for all high-confidence peptides are used to display the stage-regulated expression of ts proteins detected in the proteomes. Peptides matching to 223 members of the ts family clustered into 47 protein groups; only the top-scoring protein for each protein group is shown. Most ts proteins are detected exclusively in one stage. A, amastigote; T, trypomastigote; M, metacyclic trypomastigote; E, epimastigote.

References and Notes

1. C. E. Clayton, *EMBO J.* **21**, 1881 (2002).
2. N. S. Akopyants *et al.*, *Mol. Biochem. Parasitol.* **113**, 337 (2001).
3. T. A. Minning, J. Bua, G. A. Garcia, R. A. McGraw, R. L. Tarleton, *Mol. Biochem. Parasitol.* **131**, 55 (2003).

4. S. Diehl, F. Diehl, N. M. El-Sayed, C. Clayton, J. D. Hoheisel, *Mol. Biochem. Parasitol.* **123**, 115 (2002).
5. R. Duncan, *Trends Parasitol.* **20**, 211 (2004).
6. Materials and methods are available as supporting material on *Science* Online.
7. D. B. Weatherly *et al.*, *Mol. Cell. Proteomics* **4**, 762 (2005).
8. A. I. Nesvizhskii, A. Keller, E. Kolker, R. Aebersold, *Anal. Chem.* **75**, 4646 (2003).
9. K. A. Resing *et al.*, *Anal. Chem.* **76**, 3556 (2004).
10. N. M. A. El-Sayed *et al.*, *Science* **309**, xxxx (2005).
11. L. Florens *et al.*, *Nature* **419**, 520 (2002).
12. S. Ghaemmaghami *et al.*, *Nature* **425**, 737 (2003).
13. A. C. Frasch, *Parasitol. Today* **16**, 282 (2000).
14. D. Martin, R. Tarleton, *Immunol. Rev.* **201**, 304 (2004).
15. S. Tomlinson, F. Vandekerckhove, U. Frevert, V. Nussenzweig, *Parasitology* **110**, 547 (1995).
16. H. P. Low, R. L. Tarleton, *Mol. Biochem. Parasitol.* **160**, 1817 (1997).
17. C. Torres, F. J. Perez-Victoria, A. Parodi-Talice, S. Castanys, F. Gamarro, *Mol. Microbiol.* **54**, 632 (2004).
18. J. S. Harington, *Parasitology* **51**, 309 (1961).
19. J. S. Harington, *Nature* **178**, 268 (1956).
20. H. B. Vickery, *J. Biol. Chem.* **144**, 719 (1942).
21. D. A. Evans, R. C. Brown, *J. Protozool.* **19**, 686 (1972).
22. S. R. Wilkinson, S. O. Obado, I. L. Mauricio, J. M. Kelly, *Proc. Natl. Acad. Sci. U.S.A.* **99**, 13453 (2002).
23. R. Almeida *et al.*, *Mol. Biochem. Parasitol.* **136**, 87 (2004).
24. S. Martinez-Calvillo *et al.*, *Mol. Cell* **11**, 1291 (2003).
25. E. A. Worthey *et al.*, *Nucleic Acids Res.* **31**, 4201 (2003).
26. The authors thank the TSK-TSC for providing access to genome sequence data before and after assembly and public release of an annotated genome, K. Tyler and D. Hoft for assistance in the production of metacyclic stages, L. Cheng for technical assistance, C. Reese for artwork, B. Striepen for comments on the manuscript, and S. Kring Sullivan for early work on mass spectrometric analysis of *T. cruzi*. This work is supported by NIH grant PO1 AI044979 to R.L.T. Data on all peptides mapping to annotated genes is available on TcruziDB (http://tcruzidb.org). Raw data in either the original peak-list (.PKL) format or in mzData XML format (Minimum Information About a Proteomics Experiment standard) can be downloaded from http://kiwi.rcr.uga.edu/tcprot/downloads.html. Complete lists of all peptides identified, prerun queries identifying proteins expressed in specific life-cycle stages, and tools to query and view these data are also available on http://tcruzidb.org and/or http://kiwi.rcr.uga.edu/tcprot.

Supporting Online Material
www.sciencemag.org/cgi/content/full/309/5733/473/DC1
Materials and Methods
SOM Text
Figs. S1 and S2
Tables S1 to S6
References

26 January 2005; accepted 13 June 2005
10.1126/science.1110289

Tau Suppression in a Neurodegenerative Mouse Model Improves Memory Function

K. SantaCruz,[1]* J. Lewis,[5]* T. Spires,[6]* J. Paulson,[2] L. Kotilinek,[2] M. Ingelsson,[6] A. Guimaraes,[2] M. DeTure,[5] M. Ramsden,[2] E. McGowan,[5] C. Forster,[1] M. Yue,[5] J. Orne,[6] C. Janus,[5] A. Mariash,[2] M. Kuskowski,[7] B. Hyman,[6] M. Hutton,[5] K. H. Ashe[2,3,4,7]†

Neurofibrillary tangles (NFTs) are the most common intraneuronal inclusion in the brains of patients with neurodegenerative diseases and have been implicated in mediating neuronal death and cognitive deficits. Here, we found that mice expressing a repressible human tau variant developed progressive age-related NFTs, neuronal loss, and behavioral impairments. After the suppression of transgenic tau, memory function recovered, and neuron numbers stabilized, but to our surprise, NFTs continued to accumulate. Thus, NFTs are not sufficient to cause cognitive decline or neuronal death in this model of tauopathy.

Neurofibrillary tangles are composed of filaments of hyperphosphorylated tau (*1–4*), a microtubule-associated protein (*5*). They correlate well with cognitive deficits (*6–8*) and neuron loss (*9*), and they have been implicated in mediating neurodegeneration and dementia in Alzheimer's disease (AD) (*10–13*) and other tauopathies (*14*). Transgenic mice expressing human tau have consistently demonstrated neurological deficits and neuron loss appearing with NFTs (*15–19*). The association between NFTs, neuron loss, and brain dysfunction in humans and mice has led to the belief that NFTs invariably cause brain dysfunction and neurodegeneration. However, this idea has never been rigorously tested. We hypothesized that examining the effects of suppressing the tau transgene would elucidate the dependence of functional changes on the structural and biochemical abnormalities related to abnormal tau expression for two reasons: It would provide an opportunity to evaluate the dependence of specific structural and functional abnormalities on the continuous expression of the tau transgene, and it would distinguish reversible from irreversible lesions.

We created transgenic mice expressing mutant tau that could be suppressed with doxycycline (fig. S1A). A responder transgene was generated consisting of a tetracycline-operon–responsive element (TRE) placed upstream of a cDNA encoding human four-repeat tau with the P301L mutation (4R0N tau_{P301L}) that is linked to hereditary tauopathy (*20*). An activator transgene in a second mouse line consisted of the tet-off open reading frame (*21*) placed downstream of Ca^{2+}–calmodulin kinase II promoter elements, which resulted in expression from the TRE that was restricted to forebrain structures (*22*). Mice harboring responder or activator transgenes were bred to generate bigenic progeny containing both transgenes. As expected, transgenic tau mRNA expression in bigenic mice was largely restricted to structures in the forebrain (Fig. 1A).

To ascertain the relation between tau_{P301L} dosage and the development of neurofibrillary pathology, we examined two lines of mice expressing ~7 and ~13 units of tau_{P301L} (one unit is equivalent to the level of endogenous murine tau) (Fig. 1B). The rate at which mice developed neurofibrillary pathology was directly related to the amount of tau_{P301L} expression. Mice with ~7 units of tau_{P301L} showed accumulation of hyperphosphorylated tau in cortical neurons (pretangles) by 14.5 months of age, but did not develop argyrophilic tangle-like inclusions until 20 months of age. Mice with ~13 units of tau_{P301L}, rTg(tau_{P301L})4510 (r for regulatable), developed pretangles, which we detected using immunohistochemistry with multiple antibodies to human phospho-tau epitopes, as early as 2.5 months of age. Pathology progressed rapidly in these mice (Fig. 1C). Argyrophilic tanglelike inclusions appeared in the cortex by 4 months and in the hippocampal formation by 5.5 months. The neuronal inclusions in this line were composed of a mass of straight tau filaments and are henceforward referred to as NFTs (Fig. 1D). A significant loss in brain weight was evident by 5.5 months (Fig. 2A), as well as significant decreases (~60%) in total numbers of CA1 hippocampal neurons (Fig. 2B). The loss in brain weight and neurons progressed in 7- and 8.5-month-old mice, with ~23% of CA1 pyramidal cells remaining at 8.5 months. Gross atrophy of the forebrain was evident in a 10-month-old mouse (Fig. 1E). Thus, the expression of tau_{P301L} was sufficient to produce an age-related loss of neurons and generalized forebrain atrophy, with concomitant abnormal accumulation of hyperphosphorylated tau lesions.

[1]Department of Laboratory Medicine and Pathology, [2]Department of Neurology, [3]Department of Neuroscience, and [4]Graduate Program in Neuroscience, University of Minnesota Medical School, Minneapolis, MN 55455, USA. [5]Department of Neuroscience, Mayo Clinic Jacksonville, Jacksonville, FL 32224, USA. [6]Department of Neurology, Massachusetts General Hospital, Charlestown, MA 02129, USA. [7]Geriatric Research, Education, and Clinical Center (GRECC), Minneapolis VA Hospital, Minneapolis, MN 55417, USA.

*These authors contributed equally to this work.
†To whom correspondence should be addressed. E-mail: hsiao005@umn.edu

To test the effects of tau_{P301L} expression in rTg(tau_{P301L})4510 mice on spatial reference memory, we examined performance using a version of the Morris water maze tailored to mice (*23*). There were no significant abnormalities during the probe trials in the water maze in 1.3-month-old rTg(tau_{P301L})4510 mice, the youngest mice we were able to test, indicating no major deficits in the retention of spatial memory at this age (fig. S2C). However, the retention of spatial memory became dramatically impaired as the mice aged (Fig. 3D and fig. S6B). Indeed, from 2.5 to 4 months of age and older, target quadrant occupancies fell in the probe trials from ~45% to random swimming (25%). Motor function assessed during the cued phase of the water maze (fig. S3D) and by a panel of motor function tests (fig. S4) revealed no significant deficits in mice up to 6 months of age. Thus, the retention of spatial reference memory declined dramatically in rTg(tau_{P301L})4510 mice in an age-dependent manner.

However, we observed significantly longer path lengths in the hidden platform phase of the Morris water maze in 1.3-month-old rTg(tau_{P301L})4510 mice (fig. S2B), revealing a deficit in spatial navigation. This behavioral deficit was accompanied by a subtle, but significant, reduction in brain weights (~9%) in mice <5 months of age, compared with age-matched littermates lacking tau_{P301L} (Fig. 2A). Thus, overexpression of tau_{P301L} during brain development may cause subtle anatomical and cognitive, but not motor, abnormalities in rTg(tau_{P301L})4510 mice. It has been important in the study of behavioral deficits in transgenic mice overexpressing amyloid precursor proteins (APPs) to distinguish between age-independent and age-dependent abnormalities (*23*, *24*): the former appear to result from the overexpression of APPs during brain development; the latter are related to biochemical or structural changes that occur as the mice age. Similarly, age-independent and age-dependent behavioral and pathological changes are found in rTg(tau_{P301L})4510 mice. We observed developmental, age-independent behavioral (spatial navigation deficit during the acquisition phase) and pathological (smaller brain size) abnormalities in rTg(tau_{P301L})4510 mice that are subtle when compared with the age-dependent functional (impaired retention of spatial reference memory) and structural (neurofibrillary pathology, neuron death, and gross atrophy) changes.

To investigate the potential differences in the plasticity and recovery of brain structure and function during the various stages of neurofibrillary pathology, we suppressed transgenic tau by feeding doxycycline to rTg(tau_{P301L})4510 mice. At ages ranging from 2.5 to 10 months (fig. S1B), doxycycline was administered for either a brief (6- to 8-week) or a long (4- to 4.5-month) period. We then performed extensive behavioral, biochemical, and histological analyses on the treated mice in comparison with animals that had not received doxycycline. Brief doxycycline treatment of rTg(tau_{P301L})4510 mice (for 6 to 8 weeks) at different ages reduced the total levels of tau_{P301L} mRNA to ~15% of the maximum level, which decreased the amount of tau_{P301L} mRNA relative to endogenous murine tau mRNA from ~15 units to ~2.5 units (Fig. 2C) and the amount of soluble tau_{P301L} to ~27% of the maximum level (Fig. 2D). The levels of tau_{P301L} mRNA and sarkosyl-soluble protein decreased with age, even without doxycycline (Fig. 2, C and D), which probably reflects a progressive, preferential loss of tau_{P301L}-expressing neurons. The levels of tau_{P301L} mRNA in the brain were uniformly suppressed by doxycycline (Fig. 2E).

After brief or long doxycycline treatment of the mice was complete, we investigated whether the progression of tau pathology was dependent on transgenic tau expression. The progression of tau pathology was dependent on transgenic tau expression at 2.5 months of age; when tau_{P301L} was suppressed at 2.5 months of age, the pathological abnormalities ceased to

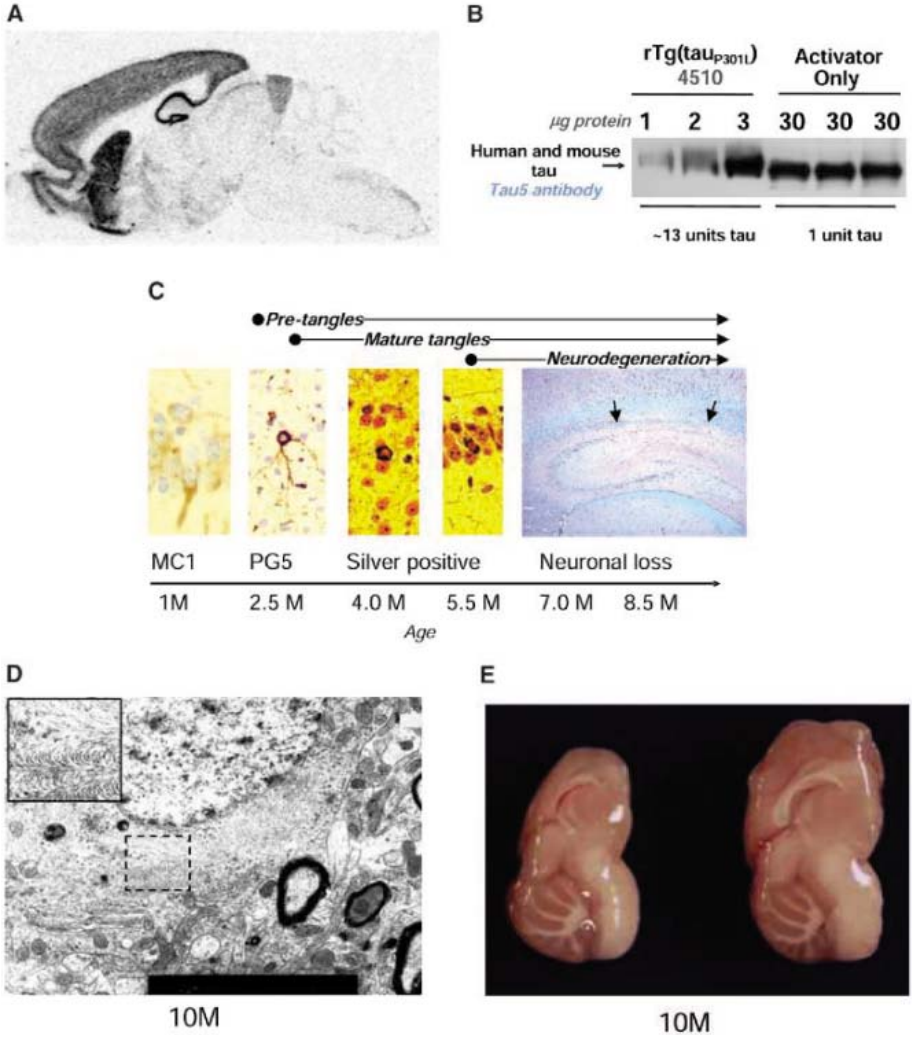

Fig. 1. Molecular and neuropathological characterization of rTg(tau_{P301L})4510 mice. (**A**) The location of tau_{P301L} mRNA was analyzed by in situ hybridization and found to be largely restricted to the hippocampus, cortex, olfactory bulb, and striatum. (**B**) The amount of tau_{P301L} protein in total forebrain homogenates of a 2.5-month-old rTg(tau_{P301L})4510 mouse was ~13 times the endogenous tau in a littermate expressing the activator only, assessed by immunoblotting. (**C**) Tau pathology was evaluated by using a panel of antibodies, including tau conformation–specific MC1 and tau phosphoserine 409 PG5, and histological methods, including modified Bielschowsky and Nissl with periodic acid Schiff stains. These analyses revealed conformational changes, followed by nonargyrophilic, hyperphosphorylated pretangles and culminating in abundant argyrophilic tangles and neuronal loss (CA1 hippocampal subfield is between the arrows). (**D**) Tangle pathology in a 10-month-old mouse, examined by electron microscopy, consists of straight filaments, which sometimes formed a herringbone pattern (inset) identical to that previously reported in the JNPL3 mouse (*10*). Scale bar, 2 μm. (**E**) Gross forebrain atrophy, with preservation of hindbrain structures, in a 10-month-old tau_{P301L}-positive transgenic mouse (left) compared with a nontransgenic littermate (right).

progress in comparison with 4-month-old mice untreated during the same period (Fig. 4A). Although tau_{P301L} suppression caused cessation of the progression of tau pathology, pretangle lesions (accumulations of nonargyrophilic hyperphosphorylated tau in the neuronal cell body) in 4-month-old mice treated with doxycycline begun at 2.5 months ($4M^{2.5OFF}$) appeared to be stable, as their numbers were not reduced by transgene suppression even at this stage. The progression of the tau pathology became independent of transgenic tau expression at 4 months of age; when tau_{P301L} was suppressed at ≥4 months NFT levels continued to increase until neuronal loss became extreme in old (8.5-month-old) mice. This was the case whether the amount of neurofibrillary pathology was assessed semiquantitatively by histopathology (Fig. 4A and fig. S5A), quantitatively using statistically unbiased stereological estimates of PHF-1–positive cells (Fig. 4B), biochemically by measuring a 64-kD sarkosyl-insoluble hyperphosphorylated tau species by immunoblot (Fig. 4C and fig. S5B), or biophysically by examining the number and length of sarkosyl-insoluble fibrils with electron microscopy (Fig. 4D). Indeed, once lesions were present in ≥4-month-old mice, the amounts of NFTs were similar whether transgenic tau was expressed continuously or suppressed with doxycycline. The transition from transgenic tau–dependent progression of tau pathology at 2.5 months to transgenic tau–independent progression of neurofibrillary pathology at 4 months was linked to the appearance of an insoluble 64-kD tau species (Fig. 4C and fig. S5B). The continued accumulation of the insoluble 64-kD tau species, which was clearly associated with increasing NFT numbers, even when transgenic tau was substantially reduced, suggests that it represents a stable, favorable state that probably acts as a sink for remaining tau_{P301L} species. The 64-kD tau species is a hyperphosphorylated form of 4R0N tau, because the only tau species present after dephosphorylation comigrated with 4R0N recombinant tau (*25*). Importantly, the insoluble 64-kD tau species observed in this mouse model comigrates with a major hyperphosphorylated tau species observed in human NFTs in AD and other tauopathies.

We next determined the effects of transgenic tau suppression on neuronal loss and brain atrophy. To do this, we compared brain weights and numbers of CA1 neurons by unbiased stereological estimates in mice fed doxycycline or control feed. Doxycycline-treated mice were divided into groups according to brief treatment (6 to 8 weeks) and lengthy treatment (4 to 4.5 months) groups. Comparisons of brain weight between these two groups and the control group, adjusted for the possible confounding variables of gender and age-at-death, were obtained [ANCOVA, $F(2,64) = 4.81$, $P = 0.011$]. Although brief suppression of transgenic tau had no significant effect on loss of brain weight, longer suppression (from 5.5 to ~10 months) significantly protected against the loss of brain weight [$t(45) = 3.47$, $P = 0.003$] (Fig. 3A). Indeed, these $10M^{5.5OFF}$ mice had brain weights similar to those of 5.5-

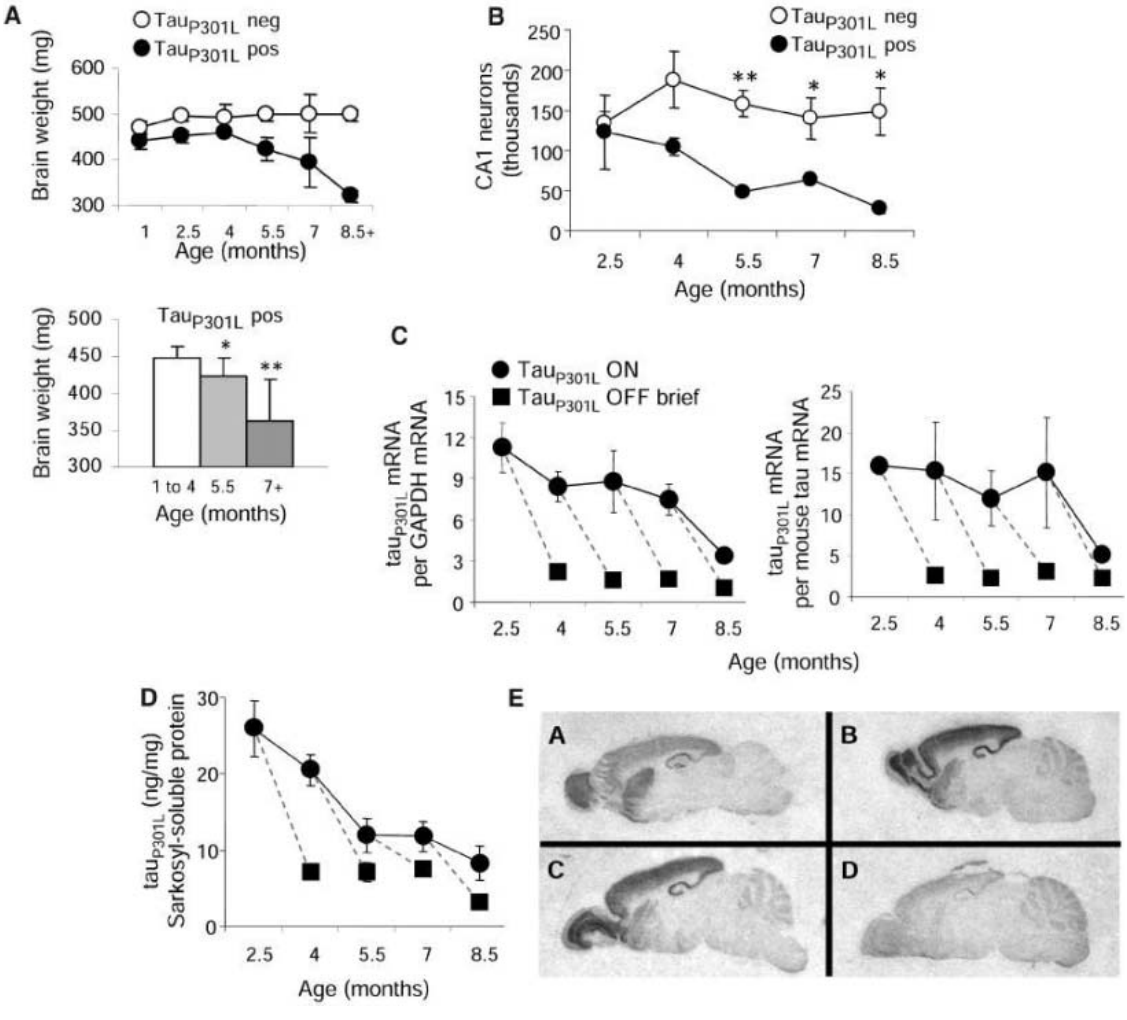

Fig. 2. Neurodegeneration and suppression of transgenic tau. (**A**) Brain weights of tau_{P301L}-positive mice <5 months were significantly lower than those of tau_{P301L}-negative littermates ($P < 0.001$) (upper). Brain weights were significantly lower in 5.5-month-old and ≥7-month-old tau_{P301L}-positive mice, relative to younger mice (lower). *$P < 0.05$; **$P < 0.001$. (**B**) CA1 neuron estimates in one hippocampal subfield ($n = 3$ per group) were significantly lower in tau_{P301L}-positive mice 5.5 months of age and older. [ANOVA for genotype, $F(1,16) = 23.97$, $P < 0.001$]. *$P < 0.05$, **$P < 0.01$. (**C**) Transgenic tau_{P301L} mRNA levels, whether normalized to GAPDH or to murine tau mRNA levels, declined with age and were dramatically suppressed after brief exposure (6 to 8 weeks) to doxycycline. (**D**) Sarkosyl-soluble tau_{P301L} levels, measured in extracts from forebrain homogenates by using immunoblots, declined with age and were substantially reduced in animals receiving doxycycline. (**E**) In situ hybridization: A (top left) 7-unit tau_{P301L}-expressing mouse; B (top right) 2-month-old 13-unit tau_{P301L}-expressing mouse; C (lower left) 4-month-old 13-unit tau_{P301L}-expressing mouse; D (lower right) 4-month-old 13-unit tau_{P301L}-expressing mouse treated with doxycycline for 6 weeks. In this and subsequent figures, data are presented as means and SEM, and dashed lines compare groups of animals at the beginning and the end of doxycycline administration.

month-old rTg(tau_{P301L})4510 mice. Moreover, CA1 neuron estimates were stabilized after even brief (6- to 8-week) tau_{P301L} suppression (Fig. 3B). In all age groups, there were significantly more neurons in mice receiving doxycycline than in untreated age-matched control mice [ANCOVA, $F(1,21) = 5.38$, $P = 0.03$]. Thus, there was a cessation in the loss of neuron number and brain weight when tau_{P301L} was suppressed, despite steady increases in NFTs.

To investigate the relation between NFT formation and memory function, we tested mice with transgenic tau–dependent (2.5-month) and transgenic tau–independent (≥4 months) progression of neurofibrillary pathology. First, we observed the cognitive effects of transgene suppression at 2.5 months, a model that halted tau pathology progression. In order to determine effects of transgene suppression specifically on impaired mice, doxycycline was fed to 2.5-month-old mice with established cognitive dysfunction. Thus, we administered doxycycline or control feed to 2.5-month-old mice that displayed deficits in the retention of spatial memory, with target quadrant occupancy <39.5%, made up of the lower half of a 2.5-month-old cohort. The performance of $4.5M^{2.5OFF}$ mice improved [paired $t(9) = 2.77$, $P = 0.02$], in contrast to mice receiving control diet (Fig. 3C and fig. S6A). Analysis of target quadrant occupancies of tau_{P301L}-expressing mice revealed a significant age-at-testing by treatment interaction [RMANOVA, $F(1,18) = 4.88$, $P = 0.04$], which was not observed among control littermates lacking tau_{P301L} that were in the bottom performing half of their 2.5-month-old cohort [RMANOVA, $F(1,42) = 0.25$, $P = 0.62$] (Fig. 3C). Similar results were obtained for path lengths in the hidden portion of the water maze (fig. S3A), whereas path lengths in the cued portion of the water maze were unaffected (fig. S3B), as predicted. Thus the ability to acquire and retain new spatial memories was restored when 2.5-month-old mice were treated with doxycycline, and the improvement in memory function was related to the suppression of tau_{P301L} and not to a nonspecific effect of doxycycline on improving neurological function.

We also examined the effects on memory function of transgenic tau suppression at an age when the progression of NFT pathology was independent of tau_{P301L} expression. We selected 15 high-performing mice with target quadrant occupancy >39.5% at 2.5 months, and examined them longitudinally at 4.5, 7, and 9.5 months of age. We observed a significant deterioration in the retention of spatial memory at 4.5 months [paired $t(14) = 9.83$, $P < 0.0001$] (Fig. 3D). We tested cognitive effects of transgene suppression at 5.5 months, a paradigm that had no effect on the progression of NFT pathology. Thus, doxycycline was administered to 10 mice starting at 5.5 months; the remaining five mice were maintained on control feed. Memory was tested in the water maze at 7 and 9.5 months. The ability to acquire and retain new spatial memories improved significantly in $7M^{5.5OFF}$ mice [paired $t(9) = 2.47$, $P = 0.04$] and in $9.5M^{5.5OFF}$ mice [paired $t(9) = 2.91$, $P = 0.02$] (Fig. 3D and fig. S6B). This was surprising because at 5.5 months, when transgenic tau was suppressed in these mice, there are already abundant NFTs and significant losses in both brain weight and hippocampal neurons in rTg(tau_{P301L})4510 mice (Fig. 1C; Fig. 2, A

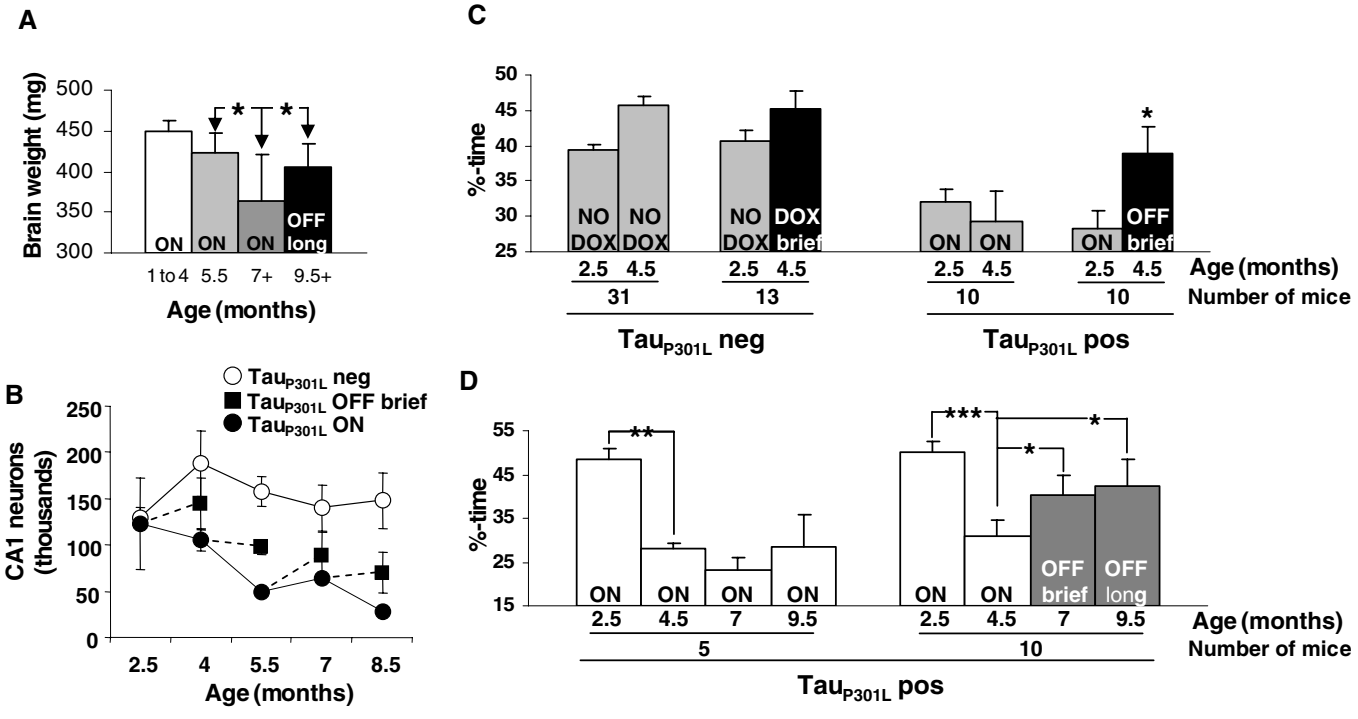

Fig. 3. Neuron death ceases and memory recovers when transgenic tau expression is suppressed. (**A**) Brain weights in 9.5- to 10-month-old tau_{P301L}-positive mice exposed to doxycycline for 4.5 months were significantly higher than brain weights in 7-month-old tau_{P301L}-positive mice but were not higher than those of tau_{P301L}-positive mice at 5.5 months, the age at which doxycycline was initiated. *$P < 0.01$. (**B**) CA1 neuron numbers in one hemisphere were estimated and found to stabilize after doxycycline treatment. (**C**) Twenty mice with target quadrant occupancies <39.5%, making up the half of a 2.5-month-old cohort having lower performance ratings, were tested in the water maze a second time at 4.5 months in the presence ($n = 10$) or absence of doxycycline ($n = 10$), which was initiated at 2.5 months. In tau_{P301L}-positive mice, memory recovered significantly when transgenic tau was suppressed. In tau_{P301L}-negative mice with target quadrant occupancies in the half of a cohort at 2.5 months of age having lower performance ratings in the presence ($n = 13$) or absence ($n = 31$) of doxycycline, a trend toward improved performance at 4.5 months was due to regression toward the mean (~48% in tau_{P301L}-negative mice), as the trend was not apparent when the complete cohort was examined. *$P < 0.05$. (**D**) Memory was tested longitudinally at four ages in 15 mice in the top performing half of their cohort at 2.5 months of age (target quadrant occupancies >39.5%). Doxycycline was administered at 5.5 months to 10 mice, and control feed was administered to 5 mice. Significant improvements were found in tau_{P301L}-positive mice treated with doxycycline, but not in tau_{P301L}-positive mice maintained on the control diet. *$P < 0.05$, **$P < 0.01$, ***$P < 0.0001$.

and B; Fig. 4, A and B). To confirm that the progression of tau pathology had become transgenic tau–independent in these mice, we showed that the amounts of the insoluble 64-kD tau species at the end of doxycycline treatment in 10-month-old mice were significantly higher (fig. S7A), that there was more extensive NFT pathology (fig. S7B), and that the numbers of PHF-1–positive CA1 neurons were greater (fig. S7C) than in 5.5-month-old mice. Any degree of neurodegeneration present at the start of doxycycline treatment in these mice may account for the incomplete recovery of the retention of spatial memory, but also makes the improvement in memory all the more remarkable. There was no significant change in path lengths in the hidden platform phase of testing in $7M^{5.5OFF}$ or $9.5M^{5.5OFF}$ mice, nor in $7M^{ON}$ or $9.5M^{ON}$ mice, compared with their own previous performance at 4.5 months (fig. S3C). No further deterioration in spatial navigation was observed in either group, despite the progressive accumulation of tangle pathology and the insoluble 64-kD tau species (Fig. 4 and figs. S5 and S7). Path lengths in the cued platform phase of testing remained intact (fig. S3D), and doxycycline had no effect on the acquisition or retention of new spatial memories in tau_{P301L}-negative mice (fig. S3E), which indicated that the improved ability of tau_{P301L}-positive mice to acquire and retain new memories was unrelated to nonspecific effects of doxycycline on cognitive or motor function.

That memory function improved in ≥4-month-old mice fed doxycycline despite ongoing accumulation of NFTs clearly implies dissociation between the processes that lead to memory loss and those that cause NFTs and that the NFTs remaining after tau suppression are not sufficient to disrupt cognitive function. The recovery of memory in this mouse model implies either that reversible neuronal dysfunction rather than irreversible structural degeneration is responsible for initial memory deficits or that neuronal remodeling of some form occurs after doxycycline treatment and allows recovery. Similarly, the cessation of neuron loss in ≥4-month-old mice fed doxycycline in the face of the persistent increase in NFTs suggests that NFTs do not invariably cause neuron death. Quantitative assessments show that neuronal loss far exceeds NFT number in human AD (*9*), which suggests that an NFT-independent method of neuronal death occurs both in the $rTg(tau_{P301L})4510$ line and in AD. However, whether NFTs are an incidental marker for the actual neurotoxic cascade in these mice and in human disease or represent a protective neuronal response, allowing sequestration of neurotoxic species into a less harmful stable form, as has been shown for the huntingtin protein (*26*), remains a crucial question. Finally, our results suggest that recovery of cognitive function may be possible in the early stages of the human tauopathies, including AD, although the clinical implications of our findings need to be interpreted with caution because of the limitations of modeling human disease in mice.

References and Notes

1. I. Grundke-Iqbal *et al.*, *Proc. Natl. Acad. Sci. U.S.A.* **83**, 4913 (1986).
2. K. S. Kosik, C. L. Joachim, D. J. Selkoe, *Proc. Natl. Acad. Sci. U.S.A.* **83**, 4044 (1986).
3. M. Goedert, C. M. Wischik, R. A. Crowther, J. E. Walker, A. Klug, *Proc. Natl. Acad. Sci. U.S.A.* **85**, 4051 (1988).
4. V. M. Lee, B. J. Balin, L. Otvos Jr., J. Q. Trojanowski, *Science* **251**, 675 (1991).
5. M. D. Weingarten, A. H. Lockwood, S. Y. Hwo, M. W. Kirschner, *Proc. Natl. Acad. Sci. U.S.A.* **72**, 1858 (1975).

A

Tau ON					
Age (M)	PG5 ctx	PG5 CA1	Biel ctx	Biel CA1	AT8 Neuro pil
1	0	0	0	0	+
2.5	+	+	+	0	++
4	++	++	+	+	++
5.5	++	++	++	++	++
7	+++	++	+++	++	+++
8.5	+++	++	+++	++	++

Tau OFF						
Age (M)	Age Dox begun	PG5 ctx	PG5 CA1	Biel ctx	Biel CA1	AT8 Neuro pil
nd	nd					
nd	nd					
4	2.5	+	+	+	0	+
5.5	4	+++	++	+++	++	++
7	5.5	+++	++	+++	++	+++
8.5	7	+++	++	+++	++	++

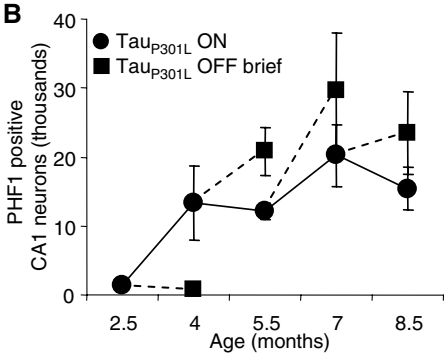

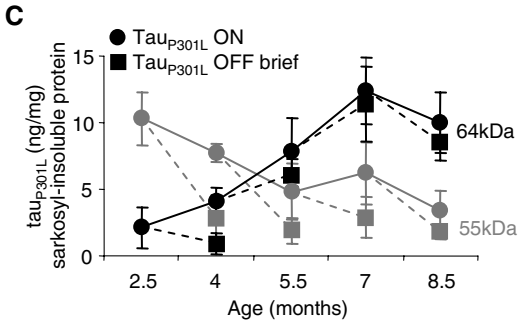

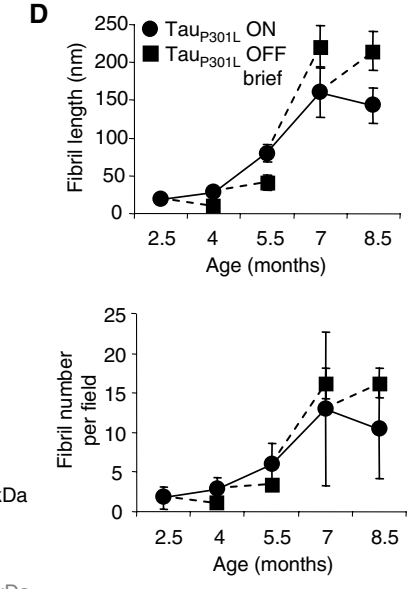

Fig. 4. Accumulation of NFTs after transgenic tau suppression. (**A**) Semiquantitative grading of neurofibrillary pathology in tau_{P301L}-positive mice. Tangles in three to five animals, at ages in months (M), evaluated with PG5, AT8, or Bielschowsky stain, in neocortical (ctx) and CA1 hippocampal (CA1) regions were graded using an adaptation of the CERAD (Consortium to Establish a Registry for AD) neuropsychological rating scales, by using area of most severe involvement, as follows: 0 (none), + (sparse, <5 NFTs/hpf), ++ (moderate, 5 to 25 NFTs/hpf), or +++ (severe, >25 NFTs/hpf). The neuropil scored 0 when AT8 staining was absent, + when only a mild granular background staining was noted, ++ when neuropil staining was moderate, and +++ when neuropil staining was severe and diffuse. (**B**) CA1 neurons staining with PHF1 antibody recognizing tau phosphoserines 396 and 404 did not diminish after transgene suppression for 6 weeks. (**C**) Concentrations of sarkosyl-insoluble tau_{P301L} proteins were measured in extracts of forebrain homogenates by using immunoblots. With age, the predominant tau species shifted from a doublet of ~55-kD proteins to a 64-kD protein. Suppression of tau_{P301L} reduced levels of the 55-kD species (gray symbols), but failed to halt the accumulation of the 64-kD species in mice ≥4 months of age (black symbols). (**D**) The number and length of fibrils in sarkosyl-insoluble fractions from extracts of forebrain homogenates increased with age. Suppressing transgenic tau in ≥4-month-old mice failed to prevent the increase in the amount or size of the fibrils.

6. P. V. Arriagada, J. H. Growdon, E. T. Hedley-Whyte, B. T. Hyman, *Neurology* **42**, 631 (1992).
7. C. Bancher, H. Braak, P. Fischer, K. A. Jellinger, *Neurosci. Lett.* **162**, 179 (1993).
8. A. L. Guillozet, S. Weintraub, D. C. Mash, M. M. Mesulam, *Arch. Neurol.* **60**, 729 (2003).
9. T. Gomez-Isla *et al.*, *Ann. Neurol.* **41**, 17 (1997).
10. J. Lewis *et al.*, *Science* **293**, 1487 (2001).
11. J. Gotz, F. Chen, J. van Dorpe, R. M. Nitsch, *Science* **293**, 1491 (2001).
12. S. Oddo, L. Billings, J. P. Kesslak, D. H. Cribbs, F. M. LaFerla, *Neuron* **43**, 321 (2004).
13. D. A. Bennett, J. A. Schneider, R. S. Wilson, J. L. Bienias, S. E. Arnold, *Arch. Neurol.* **61**, 378 (2004).
14. M. G. Spillantini, M. Goedert, *Trends Neurosci.* **21**, 428 (1998).
15. T. Ishihara *et al.*, *Neuron* **24**, 751 (1999).
16. J. Lewis *et al.*, *Nat. Genet.* **25**, 402 (2000).
17. J. Gotz, F. Chen, R. Barmettler, R. M. Nitsch, *J. Biol. Chem.* **276**, 529 (2001).
18. Y. Tatebayashi *et al.*, *Proc. Natl. Acad. Sci. U.S.A.* **99**, 13896 (2002).
19. C. Andorfer *et al.*, *J. Neurochem.* **86**, 582 (2003).
20. M. Hutton *et al.*, *Nature* **393**, 702 (1998).
21. M. Gossen, H. Bujard, *Proc. Natl. Acad. Sci. U.S.A.* **89**, 5547 (1992).
22. M. Mayford *et al.*, *Science* **274**, 1678 (1996).
23. M. A. Westerman *et al.*, *J. Neurosci.* **22**, 1858 (2002).
24. G. Chen *et al.*, *Nature* **408**, 975 (2000).
25. J. Lewis, M. Hutton, unpublished observations.
26. M. Arrasate, S. Mitra, E. S. Schweitzer, M. R. Segal, S. Finkbeiner, *Nature* **431**, 805 (2004).
27. We thank A. Michael for support; S. Iyadurai and G. Carlson for critical discussions; N. Nash, M. Sherman, A. Hanna, J. Knight, C. Zehr, S. Nelson, and D. Norton for technical help; and P. Sharpe for secretarial assistance. Supported by grants from the NIH (P01-AG15453, R01-026252 to K.H.A.; R01-AG26249, R01-AG08487 to B.H; T31-AG00277 to T.S.; R01-NS46355 to J.L.).

Supporting Online Material
www.sciencemag.org/cgi/content/full/309/5733/476/DC1
Materials and Methods
Figs. S1 to S8
References and Notes

18 April 2005; accepted 27 May 2005
10.1126/science.1113694

Mitochondrial DNA Mutations, Oxidative Stress, and Apoptosis in Mammalian Aging

G. C. Kujoth,[1] A. Hiona,[2] T. D. Pugh,[3] S. Someya,[4] K. Panzer,[1] S. E. Wohlgemuth,[2] T. Hofer,[2] A. Y. Seo,[2] R. Sullivan,[5] W. A. Jobling,[6] J. D. Morrow,[7] H. Van Remmen,[8] J. M. Sedivy,[6] T. Yamasoba,[9] M. Tanokura,[4] R. Weindruch,[3] C. Leeuwenburgh,[2] T. A. Prolla[1]*

Mutations in mitochondrial DNA (mtDNA) accumulate in tissues of mammalian species and have been hypothesized to contribute to aging. We show that mice expressing a proofreading-deficient version of the mitochondrial DNA polymerase γ (POLG) accumulate mtDNA mutations and display features of accelerated aging. Accumulation of mtDNA mutations was not associated with increased markers of oxidative stress or a defect in cellular proliferation, but was correlated with the induction of apoptotic markers, particularly in tissues characterized by rapid cellular turnover. The levels of apoptotic markers were also found to increase during aging in normal mice. Thus, accumulation of mtDNA mutations that promote apoptosis may be a central mechanism driving mammalian aging.

Mitochondria are the main source of cellular adenosine triphosphate and play a central role in a variety of cellular processes. These include fatty acid β-oxidation, phospholipid biosynthesis, calcium signaling, reactive oxygen species (ROS) generation, and apoptosis. Because the mitochondrion contains its own ~16-kilobase circular DNA, a central role for mtDNA mutations in aging has been postulated (*1*, *2*). Indeed, mtDNA mutations have been shown to accumulate with aging in several tissues of various species (*3*–*7*). The causal role of mtDNA mutations in mammalian aging is supported by a recent study demonstrating that mice with a mitochondrial mutator phenotype develop several aging phenotypes (*8*). Here, we used similar mice to investigate the cellular mechanisms by which mtDNA mutations contribute to aging.

We cloned the mouse POLG locus, *PolgA*, and used gene targeting in embryonic stem cells to introduce an AC → CT two-base substitution that corresponds to positions 1054 and 1055 of the *PolgA* cDNA (fig. S1) (*9*). This mutation results in a critical residue substitution in the conserved exonuclease domain of POLG, impairing its proofreading ability (*8*). Germline transmission of the mutation produced $PolgA^{D257A/+}$ mice, which were intercrossed to generate homozygous $PolgA^{D257A/D257A}$ mice, hereafter denoted D257A. Young D257A mice were indistinguishable from wild-type littermates, but long-term follow-up revealed a striking premature aging phenotype beginning at ~9 months of age, consisting of hair loss, graying, and kyphosis (Fig. 1, A and B). The mutant mice had a reduced life span (for

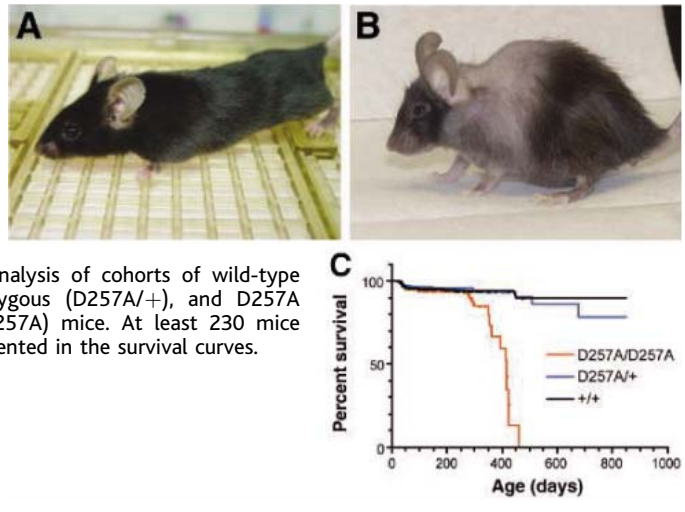

Fig. 1. D257A mice display a premature aging phenotype. Shown are wild-type (**A**) and D257A mice (**B**) at ~13 months of age. Progeroid features, including hair loss, graying, and kyphosis, become apparent at ~9 months of age. (**C**) Kaplan-Meier survival analysis of cohorts of wild-type (+/+), D257A heterozygous (D257A/+), and D257A homozygous (D257A/D257A) mice. At least 230 mice per genotype are represented in the survival curves.

[1]Departments of Genetics and Medical Genetics, University of Wisconsin, Madison, WI 53706, USA. [2]Department of Aging and Geriatric Research, College of Medicine, Institute on Aging, Biochemistry of Aging Laboratory, University of Florida, Gainesville, FL 32610-0107, USA. [3]Department of Medicine and Veterans Administration Hospital, University of Wisconsin, Madison, WI 53705-2286, USA. [4]Department of Applied Biological Chemistry, University of Tokyo, Bunkyo-ku, Tokyo 113-8657, Japan. [5]Waisman Center, University of Wisconsin, Madison, WI 53705-2280, USA. [6]Department of Molecular Biology, Cell Biology and Biochemistry and Center for Genomics and Proteomics, Brown University, Providence, RI 02912, USA. [7]Departments of Medicine and Pharmacology, Vanderbilt University School of Medicine, Nashville, TN 37232, USA. [8]Department of Cellular and Structural Biology and Barshop Institute on Longevity and Aging Studies, University of Texas Health Center at San Antonio, San Antonio, TX 78284, USA. [9]Department of Otolaryngology, University of Tokyo, Bunkyo-ku, Tokyo 113-8657, Japan.

*To whom correspondence should be addressed. E-mail: taprolla@wisc.edu

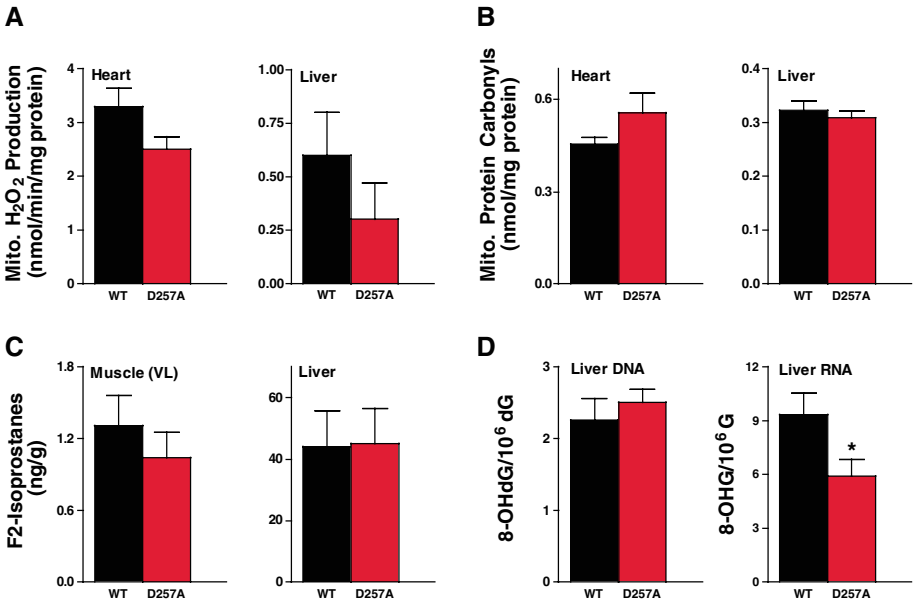

Fig. 2. Oxidative stress markers in isolated mitochondria and tissues from D257A mice. (**A**) Hydrogen peroxide production was measured by a sensitive fluorometric assay in mitochondria from wild-type (WT) and D257A mice at 9 months of age ($N \geq 8$). (**B**) Protein carbonyl levels, a marker of protein oxidation, were measured by an enzyme immunoassay in isolated mitochondria from WT and D257A mice at 9 months of age ($N \geq 7$). (**C**) F2-isoprostanes were measured by gas chromatography–negative ion chemical ionization mass spectrometry in liver and skeletal muscle (vastus lateralis) tissues from 6-month-old WT and D257A mice ($N = 6$). (**D**) Oxidative damage to DNA (8-OHdG) and RNA (8-OHG) was measured by high-performance liquid chromatography in liver tissue of 9-month-old WT and D257A mice ($N = 9$). *$P < 0.05$; error bars represent SEM.

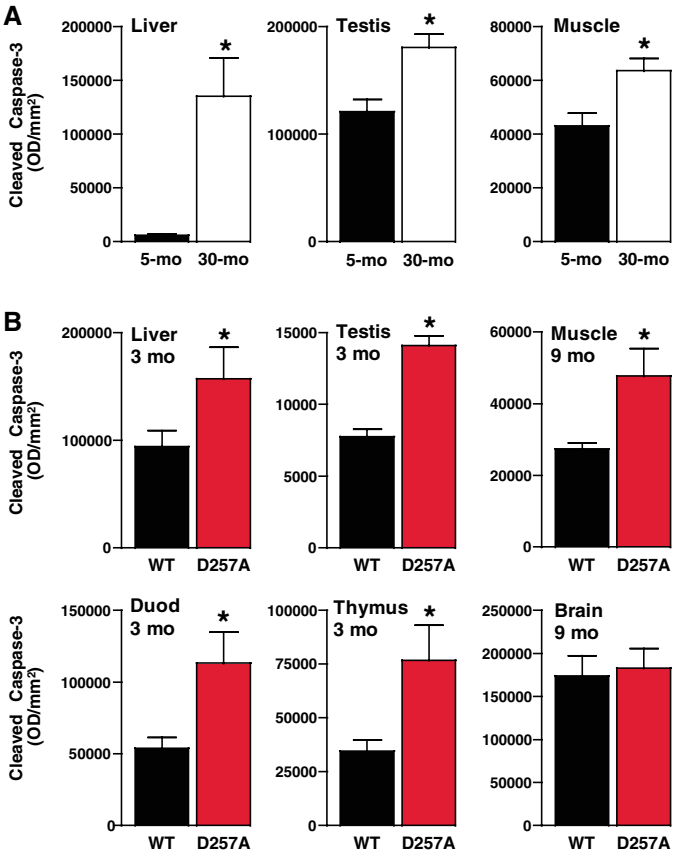

Fig. 3. Caspase activation in D257A mice and in normal aging. (**A**) Comparison of young (5 month) versus old (30 month) wild-type tissues. (**B**) Comparison of wild-type (WT) and D257A tissues at 3 months and 9 months of age. Activation of caspase-3 requires proteolytic processing of its inactive zymogen into activated fragments. The antibody used detects endogenous levels of the large fragment (17 to 19 kD) of activated caspase-3 resulting from cleavage adjacent to Asp^{175}. Extracts of tissues from WT and D257A mice of the indicated ages were subjected to SDS–polyacrylamide gel electrophoresis (PAGE) and probed with a rabbit monoclonal antibody to cleaved caspase-3 (5A1, Cell Signaling, Beverly, MA). Units are arbitrary OD units. For all tissues shown except brain, the difference between WT and D257A mice was significant ($N = 6$ to 8, *$P < 0.05$); error bars represent SEM. Duod, duodenum; Muscle, gastrocnemius.

D257A mice, maximum survival 460 days, median survival 416 days; for wild-type littermates, maximum and median survival >850 days; $P < 0.0001$; Fig. 1C) and displayed several overt phenotypes in tissues undergoing rapid cellular turnover. These phenotypes were age-related and included thymic involution, testicular atrophy associated with the depletion of spermatogonia, loss of bone mass, loss of intestinal crypts, progressive decrease in circulating red blood cells, and weight loss (figs. S2 to S4).

Age-related hearing loss (presbycusis) is a hallmark of aging in multiple species, including mice (*10*) and humans (*11*), and has been correlated with the age-related accumulation of mtDNA mutations in auditory tissue. Hearing loss can be monitored by an elevation in auditory-evoked brainstem response (ABR). We conducted ABR analysis and observed no difference in auditory function between wild-type and D257A mice at 2 months of age (fig. S5G), but we found marked elevation of ABR thresholds at 4, 8, and 16 kHz ($P < 0.0001$) in D257A mice by 9 months of age, indicating severe hearing loss (fig. S5H). Histological analysis revealed age-related loss of spiral ganglion neurons (fig. S5), a feature of presbycusis (*12*). Thus, accumulation of mtDNA mutations can have a causal role in presbycusis.

Aging in rodents (*13*) and humans (*14*) is also characterized by loss of muscle mass (sarcopenia). Consistent with a causal role for mtDNA mutations in sarcopenia, the D257A mice displayed age-related loss of skeletal muscle. At 3 months of age, muscle weight in the D257A mice was similar to that of wild-type mice (fig. S6A); at 9 months of age, however, the mutant mice showed a significant reduction in the weight of both gastrocnemius ($P < 0.002$, ~10% decrease) and quadriceps ($P < 0.005$, ~10% decrease) muscles (fig. S6B). Therefore, age-related accumulation of mtDNA mutations is likely to contribute to sarcopenia.

To determine whether mtDNA mutations accumulated to varying extents in different tissues of the D257A mice, we sequenced a 525–base pair (bp) region of mtDNA that spans the control region, as well as a 487-bp region of the *COX1* gene. Sequencing revealed that the frequency of mtDNA mutations in the mutant mice was ~3 to 8 times that in wild-type mice for most tissues examined (fig. S7). Surprisingly, the frequency of mtDNA mutations in 5-month-old wild-type mice was as high as 2.1×10^{-4} in the *COX1* gene and 5.9×10^{-4} in the control region. This corresponds to average mutation frequencies of ~4 and ~10 mutations per mitochondrial genome, respectively.

A fraction of the oxygen consumed by cells results in the production of superoxide ($O_2^{\bullet-}$) in mitochondria, which is dismutated to hydrogen peroxide (H_2O_2) by superoxide dismutase. The main tenet of the free radical theory

of aging (*15*) is that aging is due to the progressive accrual of ROS-inflicted damage, including mtDNA mutations, the accumulation of which has been postulated to lead to a "vicious cycle" of further mitochondrial ROS generation and mitochondrial dysfunction (*1*, *2*). To test this hypothesis, we measured H_2O_2 produced by mitochondria isolated from the heart and liver of young and old (3 months versus 9 months) D257A and wild-type mice. Levels of H_2O_2 were not significantly different between genotypes in either young or old heart or liver mitochondria (Fig. 2A) (fig. S8A). We also assayed protein carbonyls, a marker of oxidative damage to proteins, and found no significant differences between 9-month-old D257A and wild-type mice in mitochondrial (Fig. 2B) or cytosolic fractions (fig. S8B) of either heart or liver. Thus, despite increased mutational load, mitochondria from D257A mice do not show increased oxidative stress.

We next examined additional markers of ROS-induced damage in tissues of D257A and wild-type mice. We measured F2-isoprostanes, a marker of lipid peroxidation (*16*), in liver, skeletal muscle (Fig. 2C), and heart (fig. S8C), and observed no significant differences between 6-month-old D257A mice and wild-type controls. We also examined oxidative damage to RNA and DNA in 9-month-old D257A and wild-type mice. Liver DNA from wild-type and mutant mice had similar levels of 8-hydroxy-2′-deoxyguanosine (8-OHdG) (Fig. 2D). Interestingly, liver RNA from the D257A mice had lower steady-state levels of 8-hydroxyguanosine (8-OHG) relative to samples from wild-type mice (Fig. 2D, $P < 0.05$). Thus, our observations do not support the idea that mtDNA mutations contribute to increased ROS production and oxidative stress in mitochondria with age.

One possible mechanism for the phenotypes in mitotic tissues of D257A mice is a defect in cellular proliferation. We derived mouse embryonic fibroblast lines (MEFs) from D257A and wild-type littermates and measured the number of cell doublings before senescence. At 20% oxygen, both wild-type and D257A MEFs underwent rapid replicative senescence, whereas neither underwent senescence or reduced growth after 40 days of culture at 2% oxygen (fig. S9). Thus, accelerated aging in D257A mice is not likely to be due to an intrinsic defect in cellular proliferation, or to accelerated cellular senescence.

In the mitochondrial pathway of apoptosis, mitochondrial dysfunction can lead to mitochondrial outer membrane permeabilization, the release of cytochrome c into the cytosol, and the activation of a key effector protease, caspase-3, by proteolytic cleavage (*17*, *18*). To determine whether an increased level of cleaved caspase-3 is a feature of normal aging, we examined tissues of 5-month-old and 30-month-old wild-type mice by immunoblotting. Cleaved caspase-3 levels increased with aging in liver, skeletal muscle, testis (Fig. 3A), and heart (fig. S10A) of wild-type mice by ~50% or greater. We also monitored the extent of apoptosis in tissues of D257A and wild-type mice. Levels of cleaved caspase-3 were significantly elevated in the cytosolic fractions of duodenum, liver, testis, and thymus of 3-month-old D257A mice relative to wild-type controls (Fig. 3B), and this induction preceded phenotypes in most tissues. Levels of cleaved caspase-3 were not altered in 3-month-old D257A skeletal muscle and brain relative to wild-type samples (fig. S10B), which suggests that postmitotic tissues may be more resistant to the induction of apoptosis mediated by mtDNA mutations. Cleaved caspase-3 levels were increased, however, in D257A skeletal muscle at 9 months of age relative to controls (Fig. 3B), a time at which mutant animals displayed loss of muscle mass. Thus, normal aging is associated with the activation of a caspase-3–mediated apoptotic pathway in several tissues, and D257A mice display an early onset of this phenotype.

Apoptosis is also associated with nuclear DNA fragmentation. Because the intestinal epithelium, thymus, and testis were severely affected in D257A mice, we examined these tissues with the TUNEL (terminal deoxynucleotidyl transferase–mediated deoxyuridine triphosphate nick end labeling) assay, which detects apoptotic cells in situ. The 3-month-old D257A mice showed significantly more TUNEL positive cells relative to wild-type mice in all tissues examined (Fig. 4). Together, these findings strongly suggest that loss of critical, irreplaceable cells through apoptosis is a central mechanism of tissue dysfunction associated with the accumulation of mtDNA mutations.

We have demonstrated that accelerated development of aging phenotypes through mtDNA mutations can occur in the absence of increased ROS production or oxidative stress, and that tissue dysfunction is likely to arise through increased apoptosis. Moreover, we have shown that increased caspase-3 activation occurs in multiple tissues with normal aging. Tissues that are composed of mitotic cells display early caspase-3 activation in D257A mice, whereas skeletal muscle displays a later increase in cleaved caspase-3 and associated tissue degeneration. It is also clear that some cell types, such as spiral ganglion neurons, are exquisitely sensitive to the effects of age-related accumulation of mtDNA mutations. Because D257A mice display high levels of mtDNA mutations, it is possible that some of the phenotypes in these animals may be due to

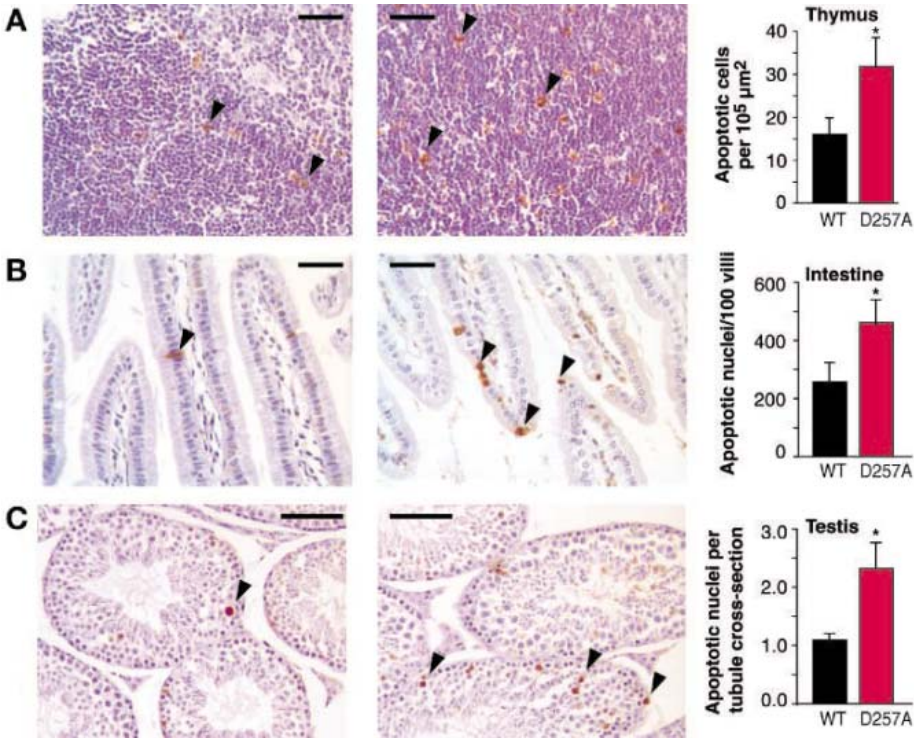

Fig. 4. Quantification of apoptosis by TUNEL in thymus (**A**), small intestine (**B**), and testis (**C**) of 3-month-old WT (left panels) and D257A (center panels) mice. Arrowheads indicate TUNEL-positive apoptotic nuclei. Numbers of apoptotic nuclei per 10^5 µm² section (thymus), per 100 villi (intestine), and per seminiferous tubule cross section (testis) were counted in hematoxylin-counterstained sections from the indicated genotypes. Each bar represents apoptotic nuclei from intestinal, thymus, and testis sections of at least four mice per genotype. *$P < 0.05$; error bars represent SEM. Scale bar, 100 µm.

complete exhaustion of tissue regenerative capacity, a process that may not be as severe in normal aging. However, the wide tissue distribution of phenotypes in D257A mice suggests that the age-related accumulation of mtDNA mutations reported in several species (*3*–*7*) contributes to physiological decline.

The concept that DNA damage contributes to aging is supported by the finding that humans and mice carrying mutations in several genes involved in DNA repair, including *Ercc2* (*Xpd*) (*19*), *Xrcc5* (*Ku86*) (*20*), and *Wrn* (*21*), display premature aging syndromes. It is likely that several types of DNA damage contribute to the aging process, and our findings suggest that apoptosis and subsequent loss of irreplaceable cells may be an important mechanism of aging in mammals. In agreement with this hypothesis, caloric restriction, the only nutritional intervention that retards aging, delays the accumulation of mtDNA mutations (*22*) and reduces mitochondria-mediated apoptotic pathways (*23*, *24*).

References and Notes

1. D. Harman, *J. Am. Geriatr. Soc.* **20**, 145 (1972).
2. J. E. Fleming, J. Miquel, S. F. Cottrell, L. S. Yengoyan, A. C. Economos, *Gerontology* **28**, 44 (1982).
3. Y. Wang *et al.*, *Proc. Natl. Acad. Sci. U.S.A.* **98**, 4022 (2001).
4. S. Melov, D. Hinerfeld, L. Esposito, D. C. Wallace, *Nucleic Acids Res.* **25**, 974 (1997).
5. M. Corral-Debrinski *et al.*, *Nat. Genet.* **2**, 324 (1992).
6. C. M. Lee, S. S. Chung, J. M. Kaczkowski, R. Weindruch, J. M. Aiken, *J. Gerontol.* **48**, B201 (1993).
7. M. Khaidakov, R. H. Heflich, M. G. Manjanatha, M. B. Myers, A. Aidoo, *Mutat. Res.* **526**, 1 (2003).
8. A. Trifunovic *et al.*, *Nature* **429**, 417 (2004).
9. See supporting data on *Science* Online.
10. Q. Y. Zheng, K. R. Johnson, L. C. Erway, *Hear. Res.* **130**, 94 (1999).
11. M. A. Gratton, A. E. Vazquez, *Curr. Opin. Otolaryngol. Head Neck Surg.* **11**, 367 (2003).
12. E. M. Keithley, C. Canto, Q. Y. Zheng, N. Fischel-Ghodsian, K. R. Johnson, *Hear. Res.* **188**, 21 (2004).
13. J. Wanagat, Z. Cao, P. Pathare, J. M. Aiken, *FASEB J.* **15**, 322 (2001).
14. J. Lexell, C. C. Taylor, M. Sjostrom, *J. Neurol. Sci.* **84**, 275 (1988).
15. D. Harman, *J. Gerontol.* **11**, 298 (1956).
16. L. J. Roberts 2nd, J. D. Morrow, *Cell. Mol. Life Sci.* **59**, 808 (2002).
17. D. R. Green, G. Kroemer, *Science* **305**, 626 (2004).
18. M. O. Hengartner, *Nature* **407**, 770 (2000).
19. J. de Boer *et al.*, *Science* **296**, 1276 (2002).
20. H. Vogel, D. S. Lim, G. Karsenty, M. Finegold, P. Hasty, *Proc. Natl. Acad. Sci. U.S.A.* **96**, 10770 (1999).
21. S. Chang *et al.*, *Nat. Genet.* **36**, 877 (2004).
22. L. E. Aspnes *et al.*, *FASEB J.* **11**, 573 (1997).
23. R. R. Shelke, C. Leeuwenburgh, *FASEB J.* **17**, 494 (2003).
24. H. Y. Cohen *et al.*, *Science* **305**, 390 (2004).

25. We thank J. Warren for stem cell injections, S. Kinoshita for histological processing, and D. Carlson for support in mouse colony management. Supported by NIH grants AG021905 (T.A.P.), AG18922 (R.W.), AG17994 (C.L.), AG21042 (C.L.), DK48831, GM15431, and RR00095 (J.D.M.), and AG16694 (J.M.S.); by NIH training grants T32 AG00213 (G.C.K.) and T32 GM07601 (W.A.J.); and by American Heart Association predoctoral fellowship 0415166B (A.H.). R.W. and T.A.P. are founders and members of the board of LifeGen Technologies, a company focused on nutritional genomics, including the impact of nutrients and caloric restriction on the aging process.

Supporting Online Material

www.sciencemag.org/cgi/content/full/309/5733/481/DC1
Materials and Methods
Figs. S1 to S10

11 March 2005; accepted 25 May 2005
10.1126/science.1112125

Chromatic Adaptation of Photosynthetic Membranes

Simon Scheuring[1]* and James N. Sturgis[2]

Many biological membranes adapt in response to environmental conditions. We investigated how the composition and architecture of photosynthetic membranes of a bacterium change in response to light, using atomic force microscopy. Despite large modifications in the membrane composition, the local environment of core complexes remained unaltered, whereas specialized paracrystalline light-harvesting antenna domains grew under low-light conditions. Thus, the protein mixture in the membrane shows eutectic behavior and can be mimicked by a simple model. Such structural adaptation ensures efficient photon capture under low-light conditions and prevents photodamage under high-light conditions.

The atomic force microscope (*1*) is a powerful tool for imaging membrane proteins (*2*). Recently, the first images at submolecular resolution of native membranes have shed light on the architecture of the photosynthetic apparatus in different photosynthetic bacteria, i.e., *Blastochloris* (*Blc.*) *viridis* (*3*), *Rhodospirillum* (*Rsp.*) *photometricum* (*4*, *5*), *Rhodobacter* (*Rb.*) *sphaeroides* (*6*), and *Rb. blasticus* (*7*). For photosynthesis to remain efficient, the composition of the photosynthetic apparatus alters under different light conditions. In many purple photosynthetic bacteria, this chromatic adaptation involves modulation of the quantity of peripheral and core light-harvesting (LH) complexes and, in some species, involves the expression of LH complexes with modified absorption (*8*).

How is the architecture of the photosynthetic membrane modulated during adaptation to different environmental conditions? Here we present a comparative study of native membranes from high- and low-light–adapted *Rsp. photometricum* cells. We used high-resolution atomic force microscopy (AFM) to investigate the structure, molecular interactions, and assembly of the membrane complexes. We imaged the cytoplasmic membrane surface of intact chromatophores (fig. S1), resorting neither to nanodissection (*4*) nor detergent treatment (*6*). The membrane components segregated into two distinct regions: (i) amorphous domains containing reaction centers (RCs) with defined molar ratios of LH1 and LH2, and (ii) paracrystalline peripheral antenna (LH2) domains. This two-phase structure could have an important functional role, as the antenna fields may exclude quinone/quinol (Q/QH_2). This will markedly reduce the membrane volume accessible to quinones and so accelerate transfer along preferential routes. As quinone diffusion is much slower than light capture, energy transfer, and the other electron transfer reactions (*9*), this effect will increase efficiency. Our analysis further suggests a model for understanding the interactions between the different components.

Qualitatively, we found the same photosynthetic complexes in high-light– and low-light–adapted membranes. Comparison with previous structural data for LH2 (*5*, *10*–*15*), LH1-RC core complexes (*3*, *7*, *16*–*18*), and RCs (*19*, *20*) allowed us to identify the small rings (~50 Å in diameter) as LH2 and the large elliptical complexes as core complexes. The LH1 assembly of the core complex forms a closed ellipse of 16 LH1 subunits surrounding an elongated RC (Fig. 1, A and B). The *Rsp. photometricum* core complex is reminiscent of that observed in *Blc. viridis* (*3*) and *Rsp. rubrum* (*16*), monomeric and without a gap in the LH1, unlike either the monomeric, W-containing core complex of *Rps. palustris* (*18*) or the PufX-containing dimeric complexes of *Rb. sphaeroides* (*21*–*23*) and *Rb. blasticus* (*7*). The functional consequences of the structural variability of core complexes remain unclear (*24*). The LH2 complexes were nonameric rings (Fig. 1D). Rarely, LH2 that either lack or have extra subunits are found (*5*). Such LH complexes with extra subunits (Fig. 1C) were found in both types of membranes and could consist of LH1 or LH2 subunits or mixtures

[1]Institut Curie, Unité Mixte de Recherche–CNRS 168, 11 rue Pierre et Marie Curie, 75231 Paris Cedex 05, France. [2]Unité Propre de Recherche–9027 Laboratoire d'Indenierie de Systemes Macromoleculaires, Institut de Biologie Structurale et Microbiologie, CNRS, 31 Chemin Joseph Aiguier, 13402 Marseille Cedex 20, France.

*To whom correspondence should be addressed. E-mail: simon.scheuring@curie.fr

of both. For crescent-shaped complexes (Fig. 1D), we cannot exclude a destructive influence of scanning. However, the missing subunits could not be detected beside the complex, and neighboring complexes were perfect nonameric rings—evidence that such complexes are imaged as synthesized.

High-light–adapted membranes were prepared from bacteria grown anaerobically and photoheterotrophically under high (~100 Wm^{-2}) light illumination (*25*). The ratio of LH2 to core complex depends on the light available during growth, because more antennae are required under low-light conditions than under high-light conditions (*26*). The ratio between absorptions at ~845 nm, due to LH2, and at ~880 nm, due to LH1, quantifies this. High-light–adapted membranes gave an absorption ratio A_{845}/A_{880} of 1.16 (Fig. 2B). Given extinction coefficients from *Rb. sphaeroides* (*27*) or values for purified *Rsp. photometricum* complexes, with stoichiometries of 18 Bchls per LH2 ring and 32 Bchls per LH1 ellipse in the core complex, this absorption ratio corresponds to an LH2 ring/core-complex ratio of 3.0, which agrees with the ratio of ~3.5 found in images (Fig. 2A). A high-resolution topograph of a high-light–adapted membrane shows the supramolecular assembly of complexes (Fig. 2A). The core complexes were homogeneously distributed over the membrane (Fig. 2A and fig. S1). Pair correlation function (PCF) analysis of core complexes in these membranes revealed distinct peaks (Fig. 2C). A PCF peak corresponding to distance r = 115 Å represents cores in contact. The most frequent distance corresponds to two core complexes separated by an intercalated LH2 (r = 175 Å). The distribution of core complexes with preferential short-range distances results in several long-range order peaks, corresponding to sums of short-range peaks. This distribution of cores in high-light–adapted membranes has two consequences. First, core complexes are sufficiently coupled that, should an exciton find an RC unable to accept energy, the exciton can frequently pass on to a neighboring RC. Second, no LH2 is separated from its closest core complex by more than one LH2 (Fig. 2A); thus no exciton can be further than ~10 nm from an RC, ensuring rapid energy trapping.

Low-light–adapted membranes were prepared from bacteria grown under low (10 to 20 Wm^{-2}) light illumination (*25*). Absorption spectra show an absorption ratio A_{845}/A_{880} of 2.6 (Fig. 3D), resulting in an LH2 ring/core-complex ratio of 6.7, again in good agreement with the observed ratio of ~7 (Fig. 3A). The dense packing of complexes resulted in ring patterns in calculated powder spectra (Fig. 3A, inset). The distribution of complexes was far less homogeneous than in high-light–adapted membranes. Domains of LH2 were found almost devoid of core complexes (*6*); however, these were paracrystalline (Fig. 3A, left box, and fig. S2), and other areas re-

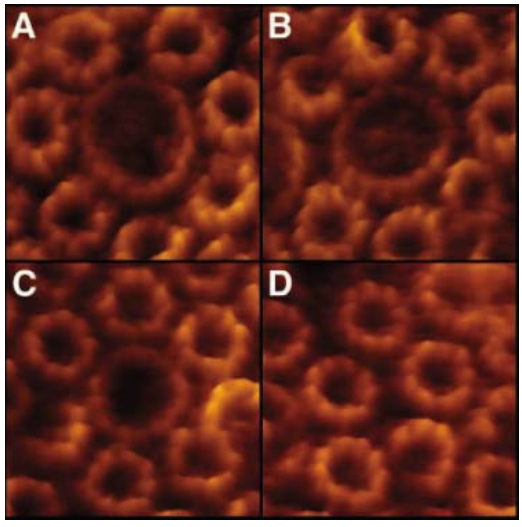

Fig. 1. Structure of photosynthetic complexes in high-light– and low-light–adapted chromatophores of *Rsp. photometricum*. (**A** and **B**) Individual core complexes imaged at high resolution. The LH1 assembly around the RC forms a closed ellipse (long axis, 99 ± 3 Å; short axis, 83 ± 3 Å; n = 12 measurements) protruding 15 ± 2 Å (n = 26 measurements) with 16 subunits. (**C**) An LH complex with a diameter of ~75 Å and a protrusion height of 15 Å. Some of the subunits are resolved, indicating a stoichiometry between 12 and 14 LH subunits. (**D**) A high-resolution topograph of nonameric LH2 complexes. LH2 have a top ring diameter of 50 Å and protrude 16 ± 2 Å (n = 32 measurements). A crescent-shaped molecule formed by 6 subunits is visible in the lower right (image edge lengths, 23 nm; color scales, 2 nm).

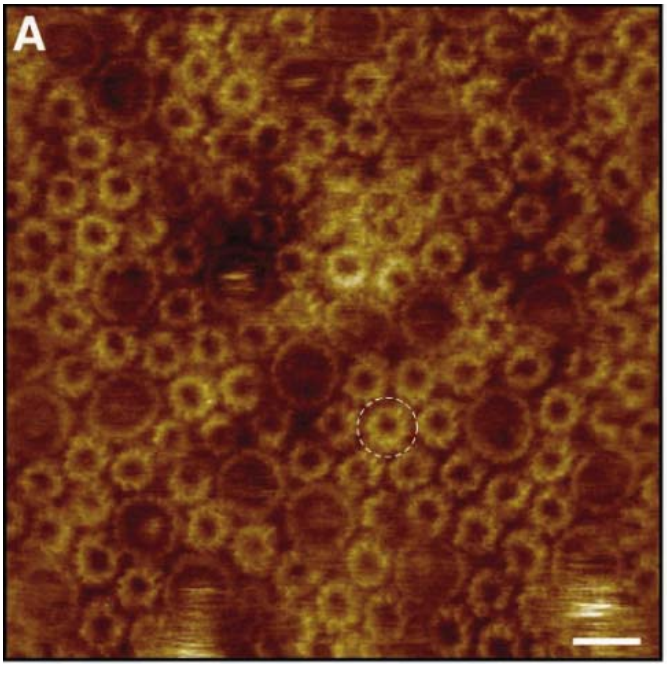

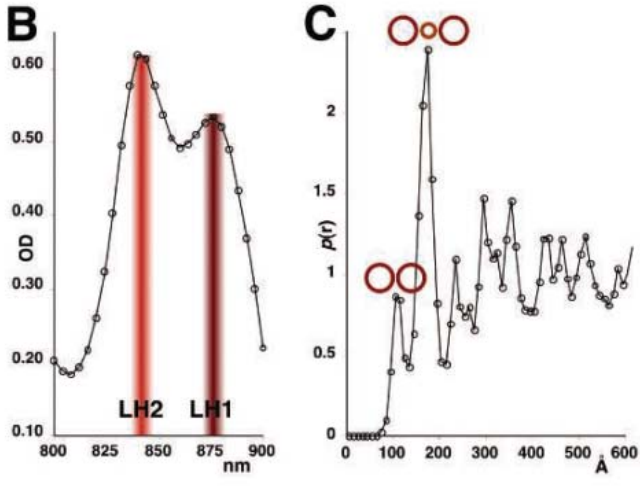

Fig. 2. High-light–adapted photosynthetic apparatus of *Rsp. photometricum*. (**A**) A high-resolution topograph of a native high-light–adapted photosynthetic membrane. The ratio of LH2 rings to core complex is ~3.5. The core complexes are homogeneously distributed within the membrane (scale bar, 10 nm; color scale, 3.1 nm). The dashed circle indicates an LH2 ring that does not touch a core complex. (**B**) The absorption spectrum (800 nm to 900 nm) of high-light–adapted photosynthetic membranes. The absorption ratio of LH2 (845 nm) to core complex (LH1, 880 nm) is 1.16. OD, optical density. (**C**) A PCF analysis graph calculated from 29,192 core-core distances. Discrete peaks at 115 Å, 175 Å, 235 Å, 295 Å, and 355 Å correspond to favored assembly interaction distances, as indicated by sketches above the peaks. $p(r)$, relative probability of finding a core at distance r.

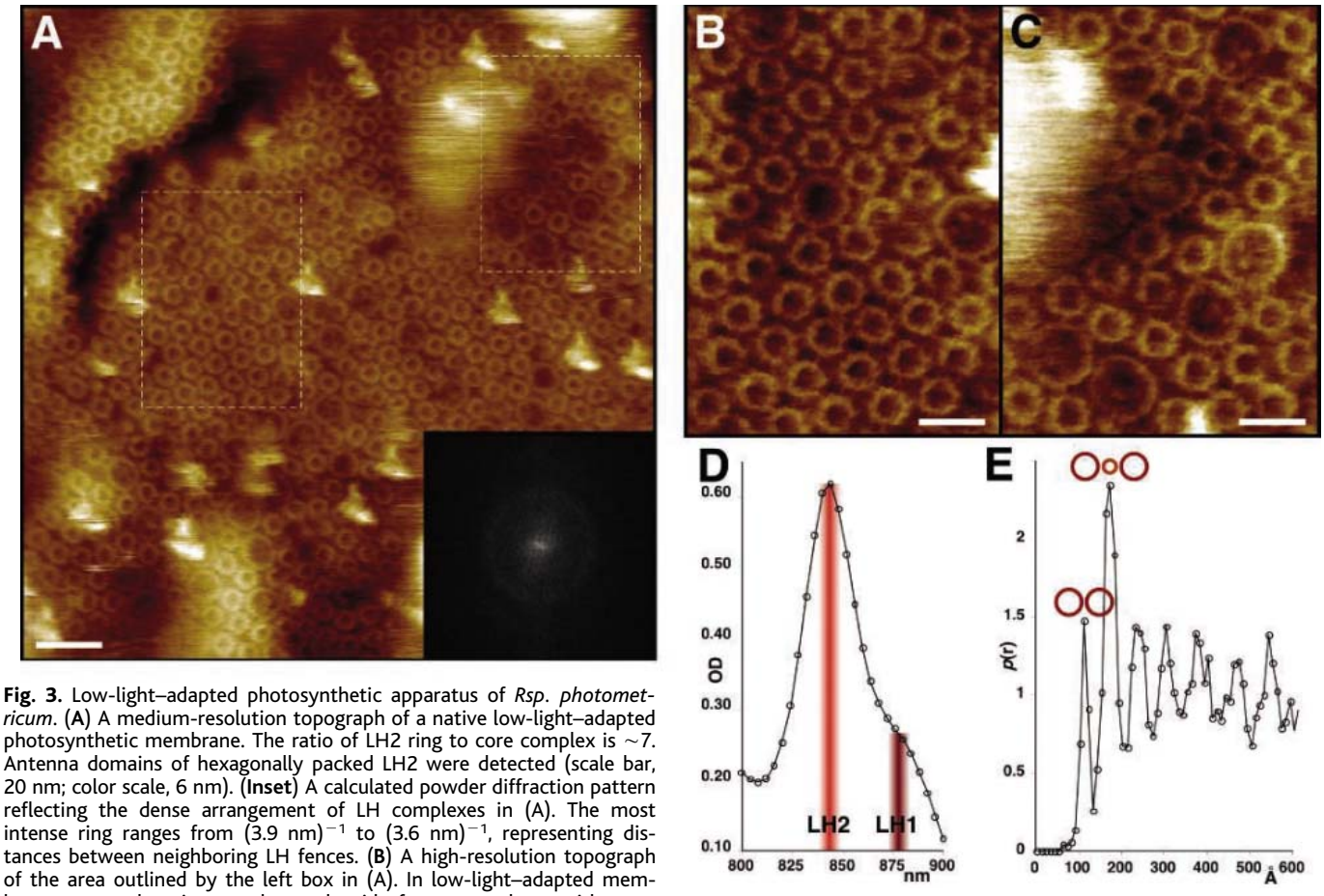

Fig. 3. Low-light–adapted photosynthetic apparatus of *Rsp. photometricum*. (**A**) A medium-resolution topograph of a native low-light–adapted photosynthetic membrane. The ratio of LH2 ring to core complex is ~7. Antenna domains of hexagonally packed LH2 were detected (scale bar, 20 nm; color scale, 6 nm). (**Inset**) A calculated powder diffraction pattern reflecting the dense arrangement of LH complexes in (A). The most intense ring ranges from $(3.9\ \text{nm})^{-1}$ to $(3.6\ \text{nm})^{-1}$, representing distances between neighboring LH fences. (**B**) A high-resolution topograph of the area outlined by the left box in (A). In low-light–adapted membranes, some domains are almost devoid of core complexes with paracrystalline LH2, $a = b = 75 \pm 1$ Å; $\gamma = 60 \pm 1°$ ($n = 20$ measurements; scale bar, 10 nm; color scale, 4 nm) (fig. S2). (**C**) A high-resolution topograph of the area outlined by the right box in (A). This area contains substantially more core complexes than the average. In these regions, core complexes are found in contact (scale bar, 10 nm; full color scale, 4 nm). (**D**) The absorption spectrum (800 nm to 900 nm) of low-light–adapted photosynthetic membranes. Because of the low photon flux available, large quantities of LH2 were synthesized. The absorption ratio of LH2 (845 nm) to core complex (LH1, 880 nm) was 2.6. (**E**) A PCF analysis graph calculated from 17,878 core-core distances. Discrete peaks at 115 Å, 175 Å, 235 Å, 305 Å, and 375 Å correspond to favored assembly interaction distances, as indicated by sketches above the peaks.

vealed high core-complex density (Fig. 3A, right box) that was better visible at high resolution (Fig. 3, B and C). In these extreme regions, the LH2 ring/core-complex ratio varied locally between >17 (Fig. 3B) and ~4 (Fig. 3C). Clustering of core complexes in certain membrane domains was reflected in the PCF analysis (Fig. 3E). This strongly resembled the analysis of high-light–adapted membranes (Fig. 2C), with similarly positioned short- and long-range peaks.

The strong resemblance of the core-core PCF analysis of high- and low-light–adapted membranes is noteworthy. The additional LH2 in low-light–adapted membranes (about twice as many LH2 rings as in high-light membranes) did not influence the preferred core-core assemblies. Cores were not diluted and spatially separated by additional LH2. Core clustering that reduces energy loss and radical formation from excess excitation energy was maintained. However, some LH2 are further from their nearest RC, separated by three or four LH2 rings; thus, an exciton must cross multiple LH2s to find a distant (~25 nm away) RC, making energy trapping for some excitons slower. In *Rsp. photometricum,* we found no specific core associations, such as the regular lines of dimeric core complexes observed in *Rb. sphaeroides* (*6*), but rather an irregular arrangement of cores and LH2 with certain statistically preferential associations.

To further survey the organization in these membranes, we analyzed the local environment of the different complexes. First, examination of core-complex neighbors in membranes with different LH2/core-complex ratios showed that the immediate environment of cores was independent of growth condition. Most core complexes were surrounded by six (44%) or seven (51%) neighbors and had no (52%), one (38%), or two (10%) neighboring cores. The distribution of nearest neighbors can be modeled by a binomial distribution with a fixed probability of a core complex neighboring a core of 0.105, or 1/9.5. Core-complex neighbors are thus much less frequent than expected given local core density, suggesting a preferential core-LH2 association.

We next analyzed the local environment of LH2, to distinguish LH2 in disordered areas or paracrystalline domains. Minimal crystal nuclei were identified as three triangularly arranged LH2 with interaction distances of 75.0 ± 5.5 Å, found in both low-light and high-light–adapted membranes (Figs. 2A and 3A), though more frequently and in larger arrays in low-light membranes (Fig. 3B and fig. S2). The ratio of noncrystalline LH2 per core complex was constant (~3.5), despite the varying total LH2/core-complex ratio. Thus, LH2 has a strong tendency to crystallize within the membrane. Interactions with core complexes break this crystallization to form disordered LH2-core domains of constant composition. Such separation of an amorphous phase of constant composition (LH2/core) and a crystalline component of variable size (depending on the total quantity of LH2) is typical for eutectic phase behavior of two-component systems. These observations were corroborated by PCF anal-

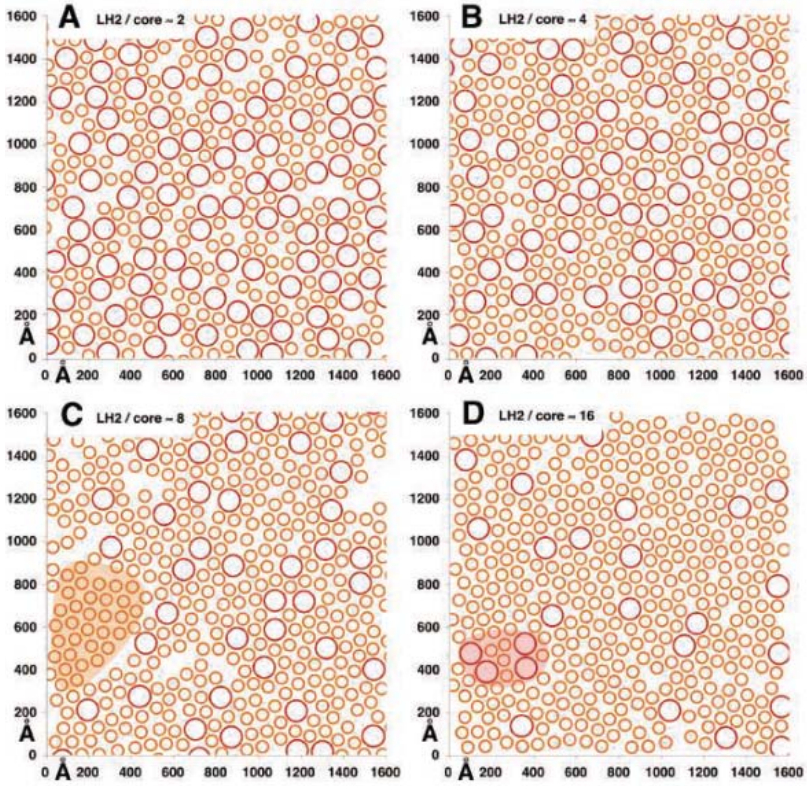

Fig. 4. Modeled architectures of the *Rsp. photometricum* photosynthetic apparatus at four different LH2/core-complex ratios. (**A**) LH2/core complex ≈ 2 (not observed experimentally). (**B**) LH2/core complex ≈ 4 (high-light–adapted membranes). (**C**) LH2/core complex ≈ 8 (low-light–adapted membranes). As in the experimental data, domains of paracrystalline LH2 are found (orange shading). (**D**) LH2/core complex ≈ 16 (not observed experimentally). In spite of the large amount of LH2, core-core contacts are preserved (red shading).

ysis of core-LH2 and LH2-LH2 distances in low-light– and high-light–adapted membranes, both indicating that a substantial fraction of the LH2 assembles in paracrystalline antenna phases in low-light–adapted membranes (fig. S3).

Combining the amorphous phase composition (3.5 LH2 per core complex) with the 9.5 times higher probability of a core complex having an LH2 neighbor rather than another core implies an LH2-core interaction 2.7 times favored over a core-core interaction. The formation of LH2 paracrystals implies strong LH2-LH2 interactions.

These data provide a basis for modeling assembly of the photosynthetic apparatus. A simple model presented to describe the phase behavior of a membrane protein has shown that the resulting architecture depends on the range and force of interactions (*28*). To mimic the structure and development of photosynthetic membranes with a minimum of parameters, we have examined, using a Gibbs Ensemble Monte-Carlo approach (*29*), potentials capable of driving the formation of membrane domains resembling those that we observed. Here we used potentials with long-range attractive forces and potential well depths for core-LH2 interactions [5 Boltzman constant times temperature (k_BT)] that are stronger than those for LH2-LH2 (3 k_BT) and core-core interactions (2 k_BT). The resulting structures (Fig. 4) resemble the photosynthetic membrane in several ways: (i) differentiation of protein-rich photosynthetic membranes from protein-poor membranes (*5*), (ii) an RC environment independent of the LH2/core-complex ratio, (iii) the formation of crystalline LH2 regions, and (iv) the positions of the short-range peaks in PCF analysis. However, although this model reproduces well the assembly of the photosynthetic apparatus, it is unclear how robust the different parameters are.

Despite the resolution and extent of our images, and in common with previous studies (*3*, *5*–*7*), we could neither detect a topography nor a topography gap of a size (~5 nm by ~10 nm) corresponding to the bc_1 complex (*30*). However, the cytoplasmic topography may be small. The obvious problem for electron transfer posed by the absence of the bc_1 complex remains enigmatic. Maintenance of core-core contacts must be of major importance, because it is preserved independently of the growth conditions. Core-core contacts reduce energy loss: If an RC is "closed" by photochemistry, an arriving exciton is lost as heat, fluorescence, or radical formation. Core-core contacts can reduce such effects, because cores with closed RCs can pass arriving excitons to nearby cores. Additionally, energy transfer from LH2 to LH2 is fast (~10 ps), so even an exciton coming from the middle of a large antenna domain will have the time to hop to an RC before energy loss. Here, we provide a detailed view and rationales of membrane protein assembly adaptation in response to environmental factors. Two different types of membrane protein assemblies are found in confined areas, with distinct architectures dividing functional tasks ensuring optimized photosynthetic activity under high-light and low-light conditions.

References and Notes

1. G. Binnig, C. F. Quate, C. Gerber, *Phys. Rev. Lett.* **56**, 930 (1986).
2. A. Engel, D. J. Müller, *Nat. Struct. Biol.* **7**, 715 (2000).
3. S. Scheuring *et al.*, *Proc. Natl. Acad. Sci. U.S.A.* **100**, 1690 (2003).
4. S. Scheuring *et al.*, *Proc. Natl. Acad. Sci. U.S.A.* **101**, 11293 (2004).
5. S. Scheuring, J.-L. Rigaud, J. N. Sturgis, *EMBO J.* **23**, 4127 (2004).
6. S. Bahatyrova *et al.*, *Nature* **430**, 1058 (2004).
7. S. Scheuring, J. Busselez, D. Levy, *J. Biol. Chem.* **180**, 1426 (2005).
8. N. Hartigan, H. A. Tharia, F. Sweeney, A. M. Lawless, M. Z. Papiz, *Biophys. J.* **82**, 963 (2002).
9. A. R. Crofts, S. W. Meinhardt, K. R. Jones, M. Snozzi, *Biochim. Biophys. Acta* **723**, 202 (1983).
10. T. Walz, S. J. Jamieson, C. M. Bowers, P. A. Bullough, C. N. Hunter, *J. Mol. Biol.* **282**, 833 (1998).
11. G. McDermott *et al.*, *Nature* **374**, 517 (1995).
12. J. Koepke, X. Hu, C. Muenke, K. Schulten, H. Michel, *Structure* **4**, 581 (1996).
13. M. Z. Papiz, S. M. Prince, T. D. Howard, R. J. Cogdell, N. W. Isaacs, *J. Mol. Biol.* **326**, 1523 (2003).
14. S. Scheuring *et al.*, *J. Mol. Biol.* **325**, 569 (2003).
15. S. Scheuring, F. Reiss-Husson, A. Engel, J.-L. Rigaud, J.-L. Ranck, *EMBO J.* **20**, 3029 (2001).
16. S. J. Jamieson *et al.*, *EMBO J.* **21**, 3927 (2002).
17. D. Fotiadis *et al.*, *J. Biol. Chem.* **279**, 2063 (2004).
18. A. W. Roszak *et al.*, *Science* **302**, 1969 (2003).
19. J. Deisenhofer, O. Epp, K. Miki, R. Huber, H. Michel, *J. Mol. Biol.* **180**, 385 (1984).
20. J. P. Allen, G. Feher, T. O. Yeates, H. Komiya, D. C. Rees, *Proc. Natl. Acad. Sci. U.S.A.* **84**, 6162 (1987).
21. C. Jungas, J.-L. Ranck, J.-L. Rigaud, P. Joliot, A. Vermeglio, *EMBO J.* **18**, 534 (1999).
22. C. A. Siebert *et al.*, *EMBO J.* **23**, 690 (2004).
23. S. Scheuring *et al.*, *J. Biol. Chem.* **279**, 3620 (2004).
24. P. Joliot, A. Joliot, A. Vermeglio, *Biochim. Biophys. Acta* **1706**, 204 (2005).
25. Materials and methods are available as supporting material on *Science* Online.
26. J. N. Sturgis, R. A. Niederman, *Arch. Microbiol.* **165**, 235 (1996).
27. J. N. Sturgis, C. N. Hunter, R. A. Niederman, *Photochem. Photobiol.* **48**, 243 (1988).
28. M. G. Noro, D. Frenkel, *J. Chem. Phys.* **114**, 2477 (2001).
29. A. Z. Panagiotopoulos, in *Observation, Prediction and Simulation of Phase Transitions in Complex Fluids*, M. Baus, L. R. Rull, J. P. Ryckaert, Eds. (Gibbs Ensemble Techniques, Kluwer, Dordrecht, 1995), vol. 460.
30. E. A. Berry *et al.*, *Photosynth. Res.* **81**, 251 (2004).

31. We thank J. L. Rigaud for constant support and V. Prima for technical assistance. Supported by INSERM (S.S.), CNRS (J.S.), and an Actions Concertées Incitatives Nanosciences 2004 grant (no. NR206).

Supporting Online Material

www.sciencemag.org/cgi/content/full/309/5733/484/DC1
Materials and Methods
Figs. S1 to S3

9 February 2005; accepted 31 May 2005
10.1126/science.1110879

Shared Cortical Anatomy for Motor Awareness and Motor Control

A. Berti,[1]* G. Bottini,[2] M. Gandola,[2] L. Pia,[1] N. Smania,[3] A. Stracciari,[4] I. Castiglioni,[5] G. Vallar,[6] E. Paulesu[6]

In everyday life, the successful monitoring of behavior requires continuous updating of the effectiveness of motor acts; one crucial step is becoming aware of the movements one is performing. We studied the anatomical distribution of lesions in right-brain–damaged hemiplegic patients, who obstinately denied their motor impairment, claiming that they could move their paralyzed limbs. Denial was associated with lesions in areas related to the programming of motor acts, particularly Brodmann's premotor areas 6 and 44, motor area 4, and the somatosensory cortex. This association suggests that monitoring systems may be implemented within the same cortical network that is responsible for the primary function that has to be monitored.

Although much of the functioning of the body's motor systems occurs without awareness, humans are aware that they are moving (or not moving) different parts of their body, even when performing automatic movements. They can also predict and be aware of the consequences of an intended motor act, with reference to their goals (*1*). There are, however, pathological states in which movement awareness is dramatically impaired (*2*, *3*). One instance of this phenomenon can be found in right-brain–damaged patients, affected by left-sided hemiplegia, who may deny their deficit and claim that their paralyzed limbs can still move. This disturbance has been termed anosognosia (*4*) or denial of motor deficit, and it has often been considered part of a multifaceted disorder of spatial representation and awareness, called unilateral neglect (*5*). However, because neglect and anosognosia may occur independently (*6*–*8*), their cognitive and possibly neuropathological bases might differ (*9*).

We compared the distributions of brain lesions in patients showing left spatial neglect, left hemiplegia, and anosognosia for motor deficit, with those of patients showing neglect, left hemiplegia, but not anosognosia. Any significant difference in brain damage between these groups of patients should correspond to the damage specific to anosognosia.

Thirty patients with a complete left motor deficit (hemiplegia) after unilateral right-

Table 1. Demographic and clinical data of the right-brain–damaged patients with and without anosognosia for hemiplegia. The ranges are reported in parentheses. The asterisk indicates the number of patients in whom tactile sensation was tested, with somatosensory deficit. n.t., not tested; A, anosognosia; N, neglect; + indicates present; – indicates absent.

Patient group	No.	Age	Education (years)	Somatosensory deficit of the contralesional side*	Line cancellation Albert test, mean no. of items crossed		Letter cancellation Diller test, percentage of items crossed		Bell test, mean no. of items crossed	
					Left	Right	Left	Right	Left	Right
A+N+	17	75.2 (36–89)	6.5 (0–13)	13/15 (86.7%)	4/18	12/18	0	14.8	0.6/17	3.2/17
A–N+	12	75.9 (62–85)	5.7 (4–13)	6/11 (54.5%)	8/18	15/18	8.6	65	1.8/17	7.7/17
A+N– (Patient RMA)	1	56	5	No somatosensory deficit	18/18	18/18	n.t.	n.t.	17/17	15/17

[1]Psychology Department and Center for Cognitive Science, University of Turin, Via Po 14, 10123 Turin, Italy. [2]Psychology Department, University of Pavia, Piazza Botta 6, 27100 Pavia, Italy. [3]Rehabilitation Unit, G.B. Rossi University Hospital, P. le L. A. Scuro, 37134 Verona, Italy. [4]Neurology Unit, S. Orsola-Malpighi Hospital, Via Massarenti 9, 40138 Bologna, Italy. [5]Bioimaging and Molecular Physiology Institute, Consiglio Nazionale delle Ricerche, Via Fratelli Cervi 93, 20090 Segrate, Milan, Italy. [6]Department of Psychology, Building U6, University of Milano-Bicocca, Piazza dell'Ateneo Nuovo 1, 20126 Milan, Italy.

*To whom correspondence should be addressed. E-mail: berti@psych.unito.it

Table 2. Brain lesion analysis. Results of anatomical statistical comparisons of patients with hemiplegia and anosognosia and patients with hemiplegia without anosognosia are shown. Stereotactic coordinates are distances, in millimeters, of the center of mass of a significant lesion, from the anterior commissure (*10*). The table also reports the results for the supramarginal gyrus [Broadmann's Area (BA) 40], the angular gyrus (BA 39), and the superior temporal gyrus (BA 22/42) associated with spatial neglect (*11*, *24*, *25*). These areas were not significantly more affected in either group of patients. DLPC, dorsolateral prefrontal cortex; dPMc, dorsal premotor cortex; IFGop, opercular inferior frontal gyrus; PostCG, post-central gyrus; PreCG, precentral gyrus; SMG, supramarginal gyrus; AG, angular gyrus; STG, superior temporal gyrus. n.a., not available, which indicated that it was technically not reliable to isolate the number of voxels damaged in the insula. ns, not significant.

Brain Region (Brodmann's area)	Patients with anosognosia	Patients without anosognosia	Overall regional chi-square *P* value	Mann-Whitney *P* value based on lesion voxel count	Stereotactic coordinates of voxels of maximal significance for each Brodmann's area			Voxel-wise chi-square *P* value
					X	*Y*	*Z*	
dPMc (6)	16/17	5/12	0.007	0.004	33	–2	43	0.025
IFGop (44)	15/17	4/12	0.007	0.0025	44	5	29	0.05
PostCG (3, 1, 2)	15/17	6/12	0.06	0.03	67	–18	37	0.01
PreCG (4)	14/17	4/12	0.021	0.012	43	–6	33	0.01
DLPC (46)	11/17	1/12	0.008	0.003	32	21	36	0.05
Insula	11/17	2/12	0.03	n.a.	49	4	11	0.05
SMG (40)	12/17	7/12	ns: 0.8	ns: 0.17	-	-	-	-
STG (22)	11/17	4/12	ns: 0.2	ns: 0.17	-	-	-	-
STG (42)	10/17	4/12	ns: 0.3	ns: 0.25	-	-	-	-
AG (39)	9/17	6/12	ns: >0.9	ns: 0.70	-	-	-	-
Deep centrum semiovale	0/17	7/12	0.001	n.a.	18	–20	21	0.05

sided brain lesions were investigated. Patients were grouped according to the presence or absence of anosognosia for left hemiplegia and left unilateral spatial neglect. Seventeen patients had anosognosia and neglect, and 12 had neglect without anosognosia (Table 1) (*10*). The superimposed lesion plots of the 17 hemiplegic patients with anosognosia (A+) and with neglect (N+) (Fig. 1A) were compared with the 12 hemiplegic patients without anosognosia (A–) and with neglect (N+) (Fig. 1B). Table 2 shows the areas that were most frequently involved in the anosognosic group and the statistical comparison between the two groups. The anatomical chi-square distribution of the comparison of A+N+ versus A–N+ patients is shown in Fig. 2. In anosognosic patients, the maximum overlap of brain lesion was centered on the dorsal premotor cortex (Brodmann's area 6; damaged in 94% of A+N+ patients), followed by area 44 and the somatosensory area (88% of the patients), and by the primary motor cortex (82% of the patients). Other neighboring structures that were differentially involved were area 46 and the insula. In both groups of patients, the inferior parietal lobule, which is traditionally associated with spatial neglect (*11*), was frequently involved. The reversed chi-square comparison of the distribution of the brain lesion in the A–N+ groups compared with the A+N+ group (Fig. 2 and Table 2) showed one single area of difference: the white matter, where axons of the corticospinal tract are located in the depth of the centrum semiovale. This suggest that A–N+ patients tend to have more subcortical lesions than do A+N+ patients, and less or no involvement of cortical areas, confirming that spared awareness of the motor deficit in patients A–N+ arises from the sparing of the premotor cerebral cortex, which is contrarily affected in A+N+ patients.

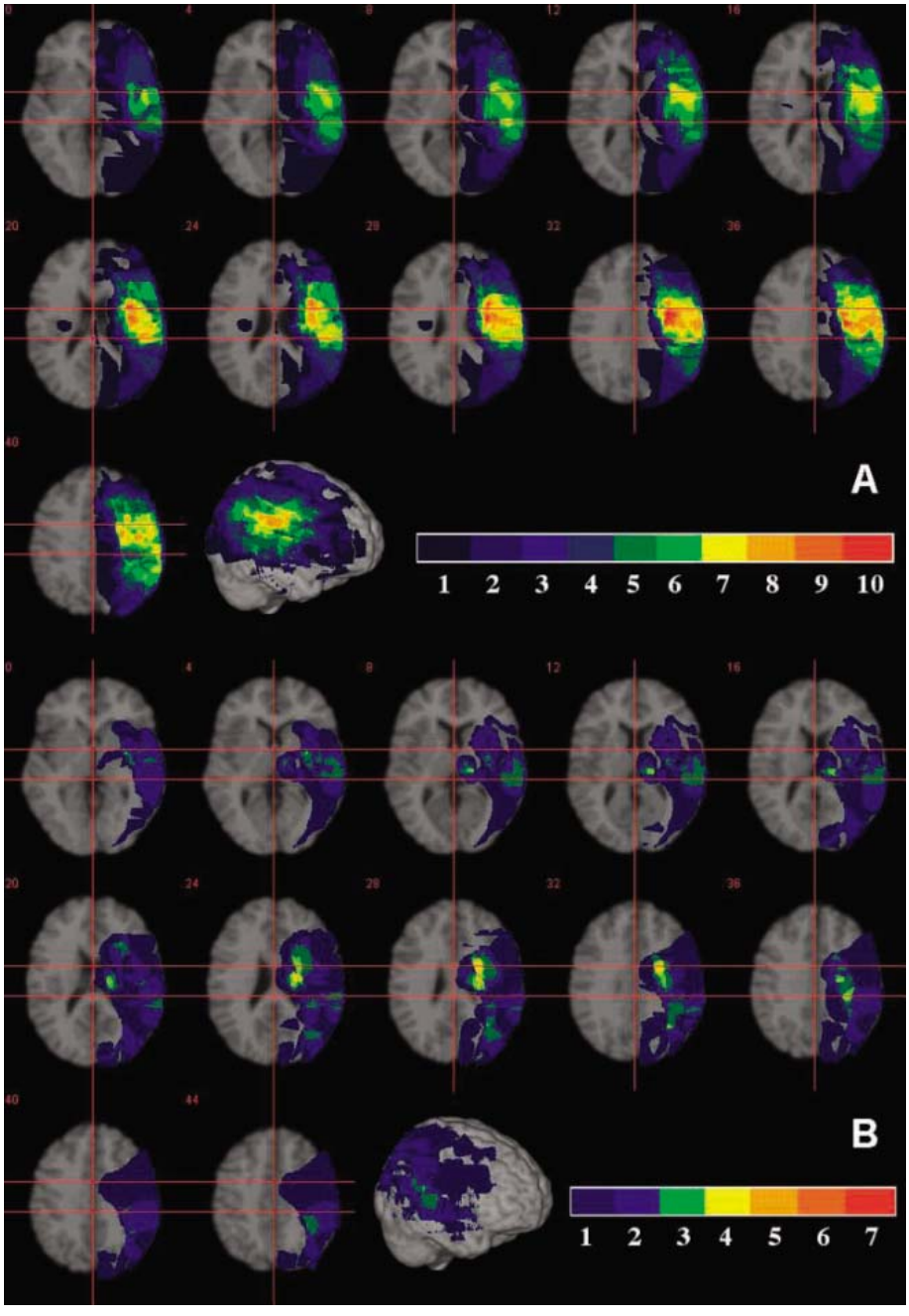

Fig. 1. (**A**) Regional lesion distribution in patients with hemiplegia, spatial neglect, and anosognosia. The regional frequency of brain lesions in each area of the right hemisphere is expressed according to the color scale (for example, areas in red show that a lesion is present in 10 patients). (**B**) Regional lesion distribution in patients with hemiplegia, spatial neglect, and no anosognosia. Each individual lesion has been superimposed onto a standard brain conforming to stereotactic space.

From the above statistical comparisons, having controlled for the factor "spatial neglect," we predicted that patients with pure anosognosia (i.e., patients showing the denial symptom without neglect) should present with a brain damage that largely overlaps with the areas that distinguish the A+N+ group from the A–N+ patients. We found such a patient (patient RMA in Table 1) who had a pure form of anosognosia without spatial neglect. Figure 3 shows the overlap between his brain damage and the areas that were significantly more affected in the A+N+ group, as compared with the A–N+ group. The predicted overlap is evident in areas 6, 4, 44, and 3 and in the insula.

These findings permit us to tease apart the neural correlates of denial of motor deficit from the parietotemporal network commonly associated with spatial neglect; anosognosia for hemiplegia is best explained by the involvement of motor and premotor areas (particularly area 6) and also, although less frequently, of prefrontal areas, such as area 46, and the insula. Observations in patient RMA, who has a pure form of anosognosia, also indicate that the frontal lesions did not affect prefrontal areas but mainly involved the frontal agranular cortex, including area 4, the dorsolateral portion of area 6, and area 44. These latter areas are fundamental components of circuits related to the programming of motor acts, both in humans and in monkeys (*12*, *13*). Premotor areas, and also the primary motor cortex, activate not only during motor preparation but also during motor imagery (*1*, *14*), and a large body of psychological and neuroimaging experiments have been interpreted as favoring a functional equivalence between action generation, action simulation, action verbalization, and perception of action (*15*). Moreover, even the interpretation of others' actions is related to the activity of neurons located in the premotor cortex (area 6) (*16*, *17*). Our data expand this

knowledge by providing evidence of an involvement of the premotor frontal regions in the conscious monitoring of motor acts. These findings are directly relevant for models of motor control and, more generally, for accounts of consciousness. Indeed, the involvement of premotor areas in self-monitoring of action implies that, at least for motor functions, monitoring is neither the prerogative of some kind of central executive system, hierarchically superimposed on sensory-motor and cognitive functions (*18*, *19*), nor a function that is physiologically and anatomically separated from the primary process that has to be monitored. Instead, the anatomical correlates of anosognosia show that monitoring can be implemented in the same neural network responsible for the process that has to be controlled. This is in keeping with other findings in the domain of altered self-monitoring (*20*).

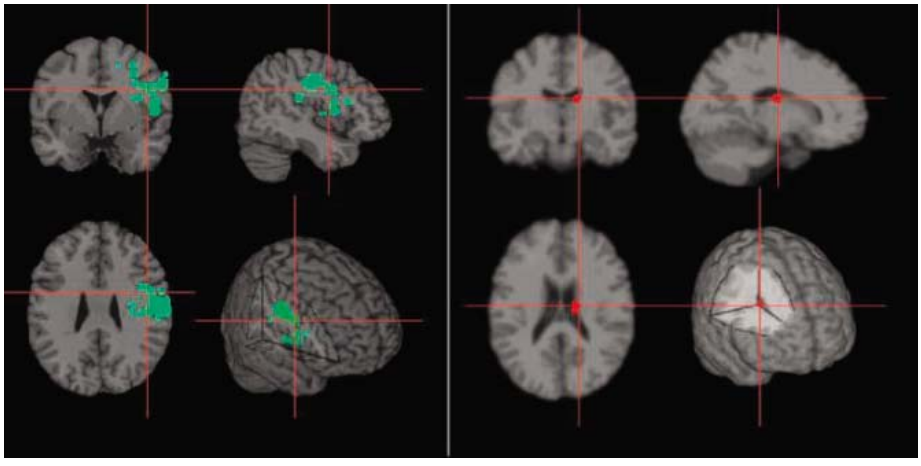

Fig. 2. Anatomical comparison between ansognosic and nonansognosic patients. On the left, brain areas more frequently damaged in patients with neglect, left hemiplegia, and anosognosia are shown as identified by a pixelwise chi-square analysis. On the right, brain areas more frequently damaged in patients with neglect, left hemiplegia, and without anosognosia are shown. Methods, stereotactic coordinates, and levels of significance are described in Table 2 (*10*).

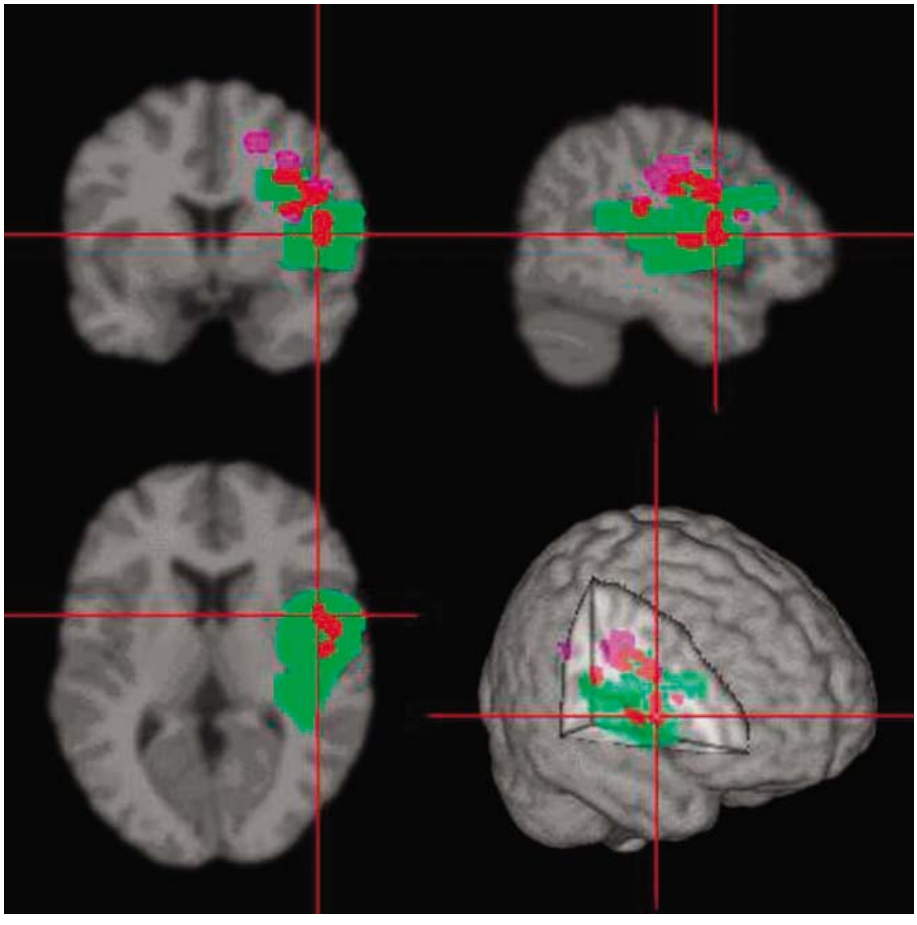

Fig. 3. Brain lesion in patient RMA, who has pure anosognosia for hemiplegia without spatial neglect. Areas in red are in common with the brain areas identified by the pixelwise chi-square comparison of patients with anosognosia, as opposed to those without anosognosia. Areas in green are brain areas damaged in patient RMA that are not identified by the chi-square analysis. Areas in purple are those identified by the chi-square analysis and not damaged in patient RMA.

Recently, it has been proposed that the denial behavior might be due to the fact that patients may experience the movement they intended to perform, but are not able to distinguish between a purely simulated (imaged) action and the actual status of the motor system (*3*, *21*). Our data show that some parts of the motor system can be spared in anosognosic patients. We may speculate that, although the damage to premotor areas impairs the motor-monitoring process, it is still possible, because of some spared premotor activity, to generate a distorted representation of the intended motor act, which is responsible for the false belief of being able to move. Also in this view, the experience of intention to move does not depend on the functioning of a single cortical region, but instead arises from a dynamic interaction between different premotor areas.

Finally, because movements occur in egocentric space, the close association often observed between left-sided anosognosia with left-sided neglect may reflect the damage to common components of a frontoparietal network, specifically related to spatiomotor integration. The lesion to a single component of this network gives rise to selective and spatially constrained disorders of awareness (*22*, *23*).

References and Notes

1. M. Jeannerod, *Behav. Brain Sci.* **17**, 187 (1994).
2. E. Bisiach, G. Geminiani, in *Awareness of Deficit After Brain Injury*, G. P. Prigatano, D. L. Schacter, Eds. (Oxford Univ. Press, New York, 1991), pp. 17–39.
3. C. D. Frith, S. J. Blakemore, D. M. Wolpert, *Philos. Trans. R. Soc. London Ser. B* **355**, 1771 (2000).
4. J. Babinski, *Rev. Neurol.* **27**, 845 (1914).
5. E. Bisiach, in *Handbook of Clinical and Experimental Neuropsychology*, G. Denes, L. Pizzamiglio, Eds. (Psychology Press, Hove, UK, 1999), pp. 479–493.
6. A. Berti, E. Ladavas, M. Della Corte, *J. Int. Neuropsychol. Soc.* **2**, 426 (1996).
7. E. Bisiach, G. Vallar, D. Perani, C. Papagno, A. Berti, *Neuropsychologia* **24**, 471 (1986).
8. V. Dauriac-Le Masson *et al.*, *Rev. Neurol.* **158**, 427 (2002).
9. M. Small, S. Ellis, *Eur. Neurol.* **36**, 353 (1996).
10. Materials and methods are available as supporting material on *Science* Online.
11. G. Vallar, D. Perani, *Neuropsychologia* **24**, 609 (1986).
12. G. Rizzolatti, G. Luppino, M. Matelli, *Electroencephalogr. Clin. Neurophysiol.* **106**, 283 (1998).
13. J. Tanji, *Curr. Opin. Neurobiol.* **6**, 782 (1996).
14. M. Roth *et al.*, *Neuroreport* **7**, 1280 (1996).
15. J. Grezes, J. Decety, *Hum. Brain Mapp.* **12**, 1 (2001).
16. P. L. Jackson, J. Decety, *Curr. Opin. Neurobiol.* **14**, 259 (2004).

17. G. Rizzolatti, L. Craighero, *Annu. Rev. Neurosci.* **27**, 169 (2004).
18. E. Bisiach, A. Berti, in *The Cognitive Neurosciences*, M. S. Gazzaniga, Ed. (MIT Press, Cambridge, MA, 1995), pp. 1131–1340.
19. G. Bottini *et al.*, *Nature* **376**, 778 (1995).
20. P. K. McGuire *et al.*, *Br. J. Psychiatry* **169**, 148 (1996).
21. A. Berti, E. Làdavas, A. Stracciari, C. Giannarelli, A. Ossola, *Cognit. Neuropsych.* **3**, 21 (1998).
22. A. Berti, G. Rizzolatti, *J. Cogn. Neurosci.* **4**, 345 (1992).
23. L. Pia, M. Neppi-Modona, R. Ricci, A. Berti, *Cortex* **40**, 367 (2004).
24. H. O. Karnath, S. Ferber, M. Himmelbach, *Nature* **411**, 950 (2001).
25. D. J. Mort *et al.*, *Brain* **126**, 1986 (2003).
26. This work was supported by Ministero dell'Istruzione, dell'Università e della Ricerca Prin grants to A.B., G.V., and E.P, and by a Bracco spa grant to G.B. and E.P.

Supporting Online Material
www.sciencemag.org/cgi/content/full/309/5733/488/DC1
Materials and Methods
References

3 February 2005; accepted 17 May 2005
10.1126/science.1110625

Distinct Kinetic Changes in Neurotransmitter Release After SNARE Protein Cleavage

Takeshi Sakaba,* Alexander Stein, Reinhard Jahn, Erwin Neher*

Neurotransmitter release is triggered by calcium ions and depends critically on the correct function of three types of SNARE [soluble *N*-ethylmaleimide–sensitive factor attachment protein (SNAP) receptor] proteins. With use of the large calyx of Held presynaptic terminal from rats, we found that cleavage of different SNARE proteins by clostridial neurotoxins caused distinct kinetic changes in neurotransmitter release. When elevating calcium ion concentration directly at the presynaptic terminal with the use of caged calcium, cleavage of SNAP-25 by botulinum toxin A (BoNT/A) produced a strong reduction in the calcium sensitivity for release, whereas cleavage of syntaxin using BoNT/C1 and synaptobrevin using tetanus toxin (TeNT) produced an all-or-nothing block without changing the kinetics of remaining vesicles. When stimulating release by calcium influx through channels, a difference between BoNT/C1 and TeNT emerged, which suggests that cleavage of synaptobrevin modifies the coupling between channels and release-competent vesicles.

Clostridial neurotoxins, which cleave SNARE [soluble *N*-ethylmaleimide–sensitive factor (NSF) attachment protein (SNAP) receptor] proteins (*1*), block Ca^{2+}-dependent neurotransmitter release (*2*). Distinct kinetic differences in their action (*3*, *4*) indicate that it matters which of the SNAREs is cleaved and at what particular site (Fig. 1A). However, studies disagree in their mechanistic interpretations regarding toxin action (*3*–*9*). Conventional synapses allow only limited manipulations at the presynaptic terminal, rendering it difficult to discern which steps between Ca^{2+} entry and transmitter release are impaired by a given toxin. The calyx of Held, a large glutamatergic nerve terminal in the auditory pathway, can be voltage-clamped (*10*, *11*); the intracellular Ca^{2+} concentration ($[Ca^{2+}]$) can be manipulated by caged Ca^{2+} as well as by controlled Ca^{2+} influx (*12*, *13*); and recombinantly produced light chains of the toxins can be introduced directly into the terminal. This allows for testing toxin action acutely, applying stimuli of graded strength, and monitoring Ca^{2+} influx. By using these possibilities, we uncovered remarkable differences in the action of toxins.

Presynaptic terminals were stimulated by voltage-clamp depolarization, and two toxins cleaving either syntaxin (BoNT/C1) (Fig. 1B) or SNAP-25 (BoNT/A) (Fig. 1C) were infused by a patch pipette (*14*). In each case, a pulse protocol consisting of 10 action potential–like (AP-like) depolarizations followed by a 50-ms depolarization was repeatedly applied to the presynaptic terminal. The presynaptic Ca^{2+} current did not change appreciably during the 10-min recording period (89 ± 7% and 91 ± 5%) (top traces, Fig. 1, B and C). The excitatory postsynaptic current (EPSC), however, changed strongly in this time interval (middle traces).

The earliest records (blue) were taken at a time when toxin action was still modest. Similar to control, the EPSCs evoked by AP-like pulses displayed facilitation during the first two to three stimuli, followed by depression. Subsequent long-lasting depolarizations elicited large EPSCs, which were sufficient to release all remaining vesicles of the releasable pool (RP) (*15*, *16*). The pattern of change during toxin action was simplest for the action of BoNT/C1 (Fig. 1B). About 10 min after the start of toxin infusion, only small postsynaptic currents were observed during both the initial 10 AP-like pulses and the long-lasting depolarization. At an intermediate time (red trace, Fig. 1B), EPSCs were substantially reduced both for AP-like and long depolarizations. The sequence of facilitation and depression was preserved throughout the time course of the experiment (Fig. 1B right). The pattern of change was strikingly different for BoNT/A (Fig. 1C): At about 10 min of toxin action, the responses to the AP-like pulses were completely blocked, whereas cumulative release elicited by the long depolarization was still almost intact (88 ± 9.0%, $n = 5$). Furthermore, at an intermediate time (7 min) responses during the AP-like pulses facilitated more strongly (Fig. 1C right).

The gradual and uniform decrease observed under BoNT/C1 is compatible with an all-or-nothing block of release sites, whereas the distinct kinetic changes induced by BoNT/A call for other mechanisms of action. Further characterization of the mechanisms is difficult to achieve by voltage-clamp experiments alone, because elevation of intracellular $[Ca^{2+}]$ through Ca^{2+} channels is spatially not homogenous, and different vesicles may be exposed to different $[Ca^{2+}]$ signals (*17*, *18*). Ca^{2+} uncaging circumvents this problem by elevating $[Ca^{2+}]$ uniformly within the presynaptic terminal. We infused a mixture of the caged-Ca^{2+} compound DM-Nitrophen (Calbiochem, Bad Soden, Germany) and the Ca^{2+} indicator dye Fura 2FF (TEFLABS, Austin, TX) into the cell together with toxins and rapidly elevated $[Ca^{2+}]$ by an ultraviolet flash to around 10 μM (Fig. 2). This $[Ca^{2+}]$ is within the range postulated to occur during nerve-evoked action potentials (*12*, *13*). Comparing control (Fig. 2A) with BoNT/C1 (Fig. 2B), BoNT/A (Fig. 2C), and a third toxin, tetanus toxin (TeNT) (Fig. 2D), which cleaves synaptobrevin. The absolute magnitudes of the EPSCs were found to be smaller under the influence of toxins. In all cases, the flash was followed after 60 ms by a long-lasting depolarization. At 8 min of toxin infusion, the total number of vesicles released shortly after the flash was 3120 ± 348 vesicles under control conditions and 1347 ± 258 vesicles and 995 ± 161 vesicles under BoNT/C1 and TeNT, respectively. However, the vesicles that escaped toxin action were released with a time course similar to that of control for both BoNT/C1 and TeNT (*14*). Subsequent depolarization evoked little further release. In contrast, the step-like elevation of $[Ca^{2+}]$ to 10 μM elicited only a

Department of Neurobiology and Department of Membrane Biophysics, Max Planck Institute for Biophysical Chemistry, Göttingen 37077, Germany.

*To whom correspondence should be addressed. E-mail: eneher@gwdg.de (E.N.); tsakaba@gwdg.de (T.S.)

trickle of release under BoNT/A (Fig. 2C right), whereas the depolarization, which further elevated [Ca^{2+}], led to a substantial EPSC. The amplitudes of [Ca^{2+}] and peak release rates (shown as rates per vesicle, i.e., measured peak rates during the flash response divided by the total number of vesicles released by flash and depolarization combined) indicate that the release rate of vesicles was reduced by almost two orders of magnitude under BoNT/A, whereas the remaining release-competent vesicles under BoNT/C1 and TeNT responded with about the same rate as that under control (Fig. 2E).

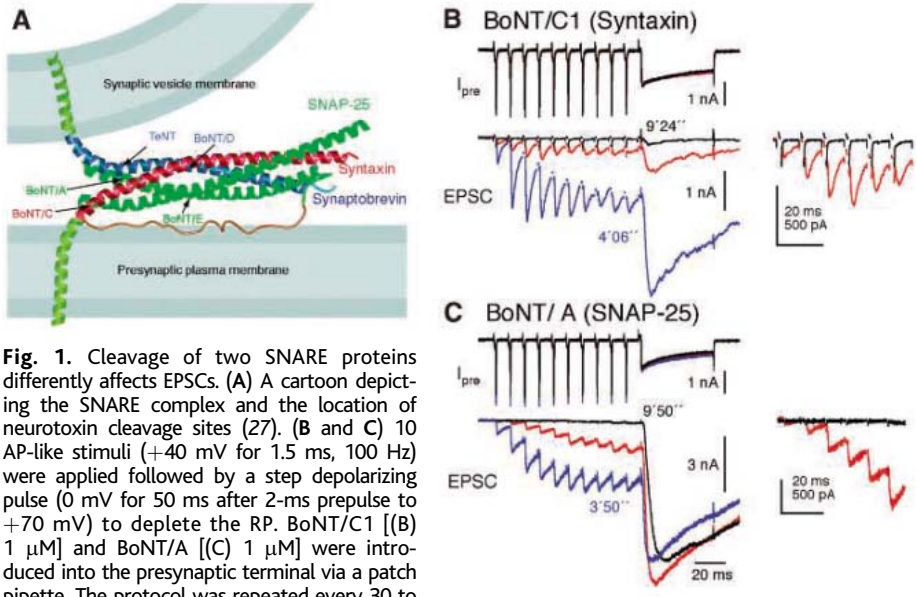

Fig. 1. Cleavage of two SNARE proteins differently affects EPSCs. (**A**) A cartoon depicting the SNARE complex and the location of neurotoxin cleavage sites (*27*). (**B** and **C**) 10 AP-like stimuli (+40 mV for 1.5 ms, 100 Hz) were applied followed by a step depolarizing pulse (0 mV for 50 ms after 2-ms prepulse to +70 mV) to deplete the RP. BoNT/C1 [(B) 1 μM] and BoNT/A [(C) 1 μM] were introduced into the presynaptic terminal via a patch pipette. The protocol was repeated every 30 to 45 s, and representative traces (presynaptic Ca^{2+} currents and EPSCs) at times early (blue), intermediate (red), and late (black) during dialysis of toxins were superimposed. Time of recording (after break-in) is indicated in minutes (′) and seconds (″). The first six EPSCs at intermediate and late during dialysis are shown on the right. In all experiments cyclthoazide and kynurenic acid were present (*14*).

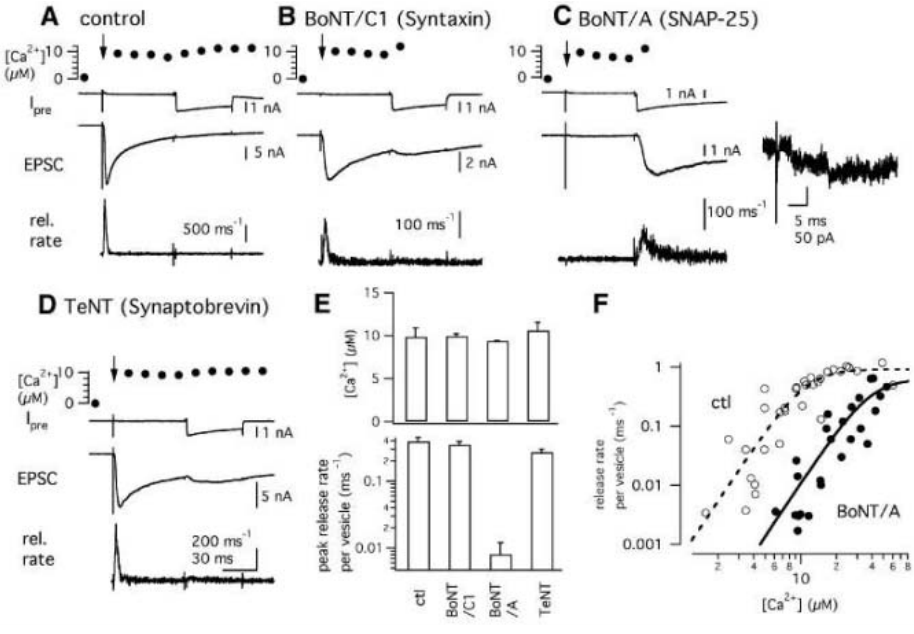

Fig. 2. The time course of transmitter release evoked by flash photolysis is altered only by BoNT/A. (**A** to **D**) A step-like [Ca^{2+}] increase from the basal concentration to 10 μM was obtained by flash photolysis of DM-Nitrophen (top). A depolarizing pulse was applied 60 ms after the flash to deplete the RP. Presynaptic Ca^{2+} currents, EPSCs, and release (rel.) rates are also shown. (A) to (D) are from control and in the presence of BoNT/C1 (2 μM), BoNT/A (1 μM), and TeNT (5 μM), respectively. Expanded EPSC trace under BoNT/A is shown on the right (C). (**E**) Average amplitudes of [Ca^{2+}] steps (top) and peak release rates per vesicle (bottom) during flash responses in control (ctl, six cells), BoNT/C1 (six cells), BoNT/A (six cells), and TeNT (five cells). (**F**) The relationship between [Ca^{2+}] and peak release rates per vesicle was plotted under control conditions (open circles, n = 14 cells) and in the presence of BoNT/A (solid circles, n = 13 cells). The data were fitted with a Hill coefficient of 3.

We further characterized the BoNT/A effect by performing Ca^{2+} uncaging with flashes of varying strengths, causing step-like Ca^{2+} increases to between 1 and 60 μM. Comparing peak release rates (per vesicle) for control cells and cells with BoNT/A indicated that BoNT/A decreased the Ca^{2+} sensitivity of vesicles about fourfold without a change in the slope of the Ca^{2+} dose-response curve (Fig. 2F). Release rates under BoNT/A reached values almost as high as those of control in the [Ca^{2+}] range of 50 to 60 μM (Fig. 2F). Further experiments using the Ca^{2+} ramp method (fig. S1) confirmed that BoNT/A strongly reduced the apparent Ca^{2+} sensitivity, whereas BoNT/C1 and TeNT only led to minimal kinetic changes (at most a factor of 2 in release rate) in the [Ca^{2+}] range of <10 μM. The results exclude the possibility that BoNT/A reduces maximal rate of secretion (*4*, *19*) or changes cooperativity for fusion (*20*, *21*). Rather, the shift of apparent Ca^{2+} affinity is best explained by an allosteric model of Ca^{2+} release coupling, as recently suggested to explain phorbol ester effects (*22*).

None of our Ca^{2+} uncaging experiments revealed any difference between cleavage of syntaxin and synaptobrevin, with all findings being readily interpretable as all-or-nothing blocks. However, when we studied TeNT (and BoNT/D, both cleaving synptobrevin) with the use of voltage-clamp depolarization, subtle but important differences in the action of two toxins became apparent. First, we observed that, in a pulse protocol as in Fig. 1, EPSCs after partial TeNT block showed different degrees of block for the responses to short and long depolarizations. At times when the cumulative amount of release during AP-like pulses was reduced to 37 ± 5% of control values, the release during a long depolarization was still 83 ± 13% (n = 5, fig. S2). Differences between TeNT and BoNT/C1 were most pronounced during long-lasting depolarizations. Thus, we analyzed release by using the deconvolution method (Fig. 3) (*14*, *23*) and applying 50-ms depolarizing pulses every 30 to 45 s with 0.5 mM EGTA in the presynaptic pipette. Such pulses deplete the RP almost completely, and two kinetic components of release can be separated under these conditions (time constants of 2 to 3 ms and 20 to 30 ms) (*16*). The amplitude of the fast component corresponds roughly to the cumulative amount of release by high-frequency trains (*15*). For control traces (Fig. 3A), cumulative release was fitted by a double exponential with an average RP size of 2901 ± 381 vesicles (n = 5), which remained constant at 98 ± 5.6% over 548 ± 17 s after the start of whole-cell recording (see Table 1 for kinetic

details). The amount of presynaptic Ca^{2+} influx during depolarizations stayed constant under control and also in the toxin experiments. Comparing the effect of BoNT/C1 to that of TeNT, in both cases EPSCs decreased strongly during 8 to 12 min of toxin action (Fig. 3, B and C). In the case of BoNT/C1, the decrease was uniform along the whole trace. Cumulative release decreased during toxin action without major changes in kinetics. This is best seen when traces were normalized to their values at 50 ms (Fig. 3B right). In contrast, under TeNT, cumulative release preferentially lost its fast component (Fig. 3 and Table 1). We then asked whether TeNT might also affect the rate at which new vesicles are recruited after depletion of the RP. Indeed, replenishment rates of the fast component under TeNT were slower than those of controls (fig. S4). In contrast, BoNT/C had no effects on the time course of recovery, showing once more that the two toxins act differently (fig. S4).

We postulate that the additional kinetic effects of TeNT most likely result from changes in the efficiency by which Ca^{2+} currents increase Ca^{2+} concentration at the Ca^{2+} sensor of the release apparatus (*17*, *18*), because differences between TeNT and BoNT/C1 were not observed when Ca^{2+} was directly applied to presynaptic terminals by caged Ca^{2+}. Furthermore, vesicles responded slowly to depolarizing stimuli after TeNT action, as if they were exposed to a reduced calcium concentration, in spite of the fact that Ca^{2+} currents were not reduced by any of the toxins (Figs. 1 and 3).

This effect of TeNT has interesting implications with respect to the general problem of Ca^{2+} channel–release coupling and the heterogeneity of release readiness of vesicles in the calyx of Held. The pool of release-ready vesicles can be divided into one subpool, which upon prolonged depolarization releases rapidly, and another one, which releases about 10-fold slower (*16*). The rapidly releasing pool recovers slowly upon depletion by strong stimulation, whereas the slowly releasing one recovers rapidly (*15*, *16*). The simplest explanation for these findings assumes that vesicles, after docking at the membrane, quickly reach a state in which their release apparatus is fully fusion-competent and only later become linked to regions of high Ca^{2+} channel density, which renders them more sensitive to Ca^{2+} influx. Such a sequence of events was suggested to explain the properties of different populations of vesicles visible by total internal reflection microscopy at terminals of retinal bipolar cells (*24*). In order to explain the special kinetic effect of TeNT, we only have to assume that after toxin action this maturation step cannot happen or happens slower (fig. S4), either because of the loss of the postulated interaction between vesicles and special release sites or because of a block of such sites by vesicles with compromised release machineries or with defective endocytosis (*25*). Asynchronous release during high-frequency stimulation persists under TeNT (*3*, *8*), and slowly releasing vesicles, which are less sensitive to TeNT (Fig. 2), contribute to asynchronous release during high-frequency stimulation at the calyx of Held (*26*). Asynchronous release, therefore, is likely to represent vesicles that have not yet reached their optimal position within the active zone.

References and Notes

1. Y. A. Chen, R. H. Scheller, *Nat. Rev. Mol. Cell Biol.* **2**, 98 (2001).
2. G. Schiavo, M. Matteoli, C. Montecucco, *Physiol. Rev.* **80**, 717 (2000).
3. Y. Humeau, F. Doussau, N. J. Grant, B. Poulain, *Biochimie* **82**, 427 (2000).
4. M. Capogna *et al.*, *J. Neurosci.* **17**, 7190 (1997).

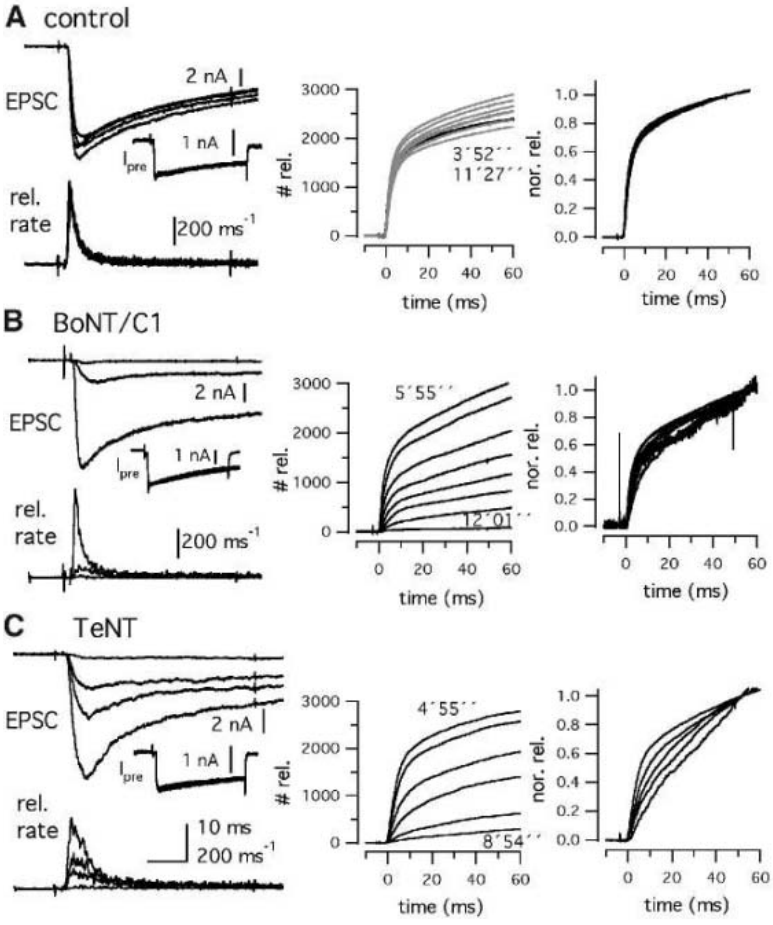

Fig. 3. Kinetic analysis of transmitter release using long-duration depolarizing steps. (**A** to **C**) Depolarizing pulses (to 0 mV for 50 ms after pre-depolarization to +70 mV for 2 ms) were applied every 30 to 45 s. This interstimulus interval is long enough such that responses recovered completely. Presynaptic patch pipettes contained 0.5 mM EGTA. Traces obtained at different times of whole-cell recording are superimposed. The left graphs show EPSCs, release rates, and presynaptic I_{Ca} as inset. The center and right graphs show cumulative release (number of vesicles) during depolarization and after normalization to the value at 50 ms, respectively.

Table 1. Effects of toxins on the time course of release during a depolarizing pulse. Dashed entries indicate not determined.

Condition	*N*	Early period (for control, initial 10 min)		Intermediate period		
		τ_1 (fraction)	τ_2	τ_1 (fraction)	τ_2	Inhibition of total release
Control	5	3.0 ± 0.4 ms (58 ± 4%)	41 ± 8 ms	—	—	—
BoNT/C1	5	3.8 ± 0.6 ms (53 ± 3%)	35 ± 5 ms	5.8 ± 0.7 ms (50 ± 7%)	55 ± 8 ms	34 ± 8%
TeNT	5	3.4 ± 0.7 ms (60 ± 2%)	34 ± 5 ms	21 ± 0.7 ms (100%)	—	32 ± 5%

5. S. M. Young, *Proc. Natl. Acad. Sci. U.S.A.* **102**, 2614 (2005).
6. T. Xu, T. Binz, H. Niemann, E. Neher, *Nat. Neurosci.* **1**, 192 (1998).
7. S. E. Jarvis, G. W. Zamponi, *Trends Pharmacol. Sci.* **22**, 519 (2001).
8. S. Schoch *et al.*, *Science* **294**, 1117 (2001).
9. P. Washbourne *et al.*, *Nat. Neurosci.* **5**, 19 (2002).
10. J. G. Borst, F. Helmchen, B. Sakmann, *J. Physiol.* **489**, 825 (1995).
11. T. Takahashi, I. D. Forsythe, T. Tsujimoto, M. Barnes-Davies, K. Onodera, *Science* **274**, 594 (1996).
12. J. H. Bollmann, B. Sakmann, J. G. G. Borst, *Science* **289**, 953 (2000).
13. R. Schneggenburger, E. Neher, *Nature* **406**, 889 (2000).
14. Materials and methods are available as supporting material on *Science* Online.
15. L. G. Wu, J. G. Borst, *Neuron* **23**, 821 (1999).
16. T. Sakaba, E. Neher, *Neuron* **32**, 1119 (2001).
17. R. S. Zucker, *Neuron* **17**, 1049 (1996).
18. E. Neher, *Neuron* **20**, 389 (1998).
19. M. F. Finley, S. J. Patel, D. V. Madison, R. H. Scheller, *J. Neurosci.* **22**, 1266 (2002).
20. B. A. Stewart, M. Mohatashimi, W. S. Trimble, G. L. Boulianne, *Proc. Natl. Acad. Sci. U.S.A.* **97**, 13955 (2000).
21. S. G. Cull-Candy, H. Lundh, S. Thesleff, *J. Physiol.* **260**, 177 (1976).
22. X. Lou, V. Scheuss, R. Schneggenburger, *Nature* **435**, 497 (2005).
23. E. Neher, T. Sakaba, *J. Neurosci.* **21**, 444 (2001).
24. D. Zenisek, J. A. Steyer, W. Almers, *Nature* **406**, 849 (2000).
25. F. Deak, S. Schoch, X. R. Liu, T. C. Südhof, E. T. Kavalali, *Nature Cell Biol.* **6**, 1102 (2004).
26. E. Neher, T. Sakaba, V. Scheuss, *Soc. Neurosci. Abstr.* **32**, 322.3 (2002).

27. R. B. Sutton, D. Fasshauer, R. Jahn, A. T. Brunger, *Nature* **395**, 347 (1998).
28. This study was supported by Deutsche Forschungsgeminschaft Center for Molecular Physiology of Brain. We thank R. Schneggenburger and S. Young for comments on the study.

Supporting Online Material
www.sciencemag.org/cgi/content/full/309/5733/491/DC1
Materials and Methods
Figs. S1 to S4
References

23 March 2005; accepted 1 June 2005
10.1126/science.1112645

New Products

http://science.labvelocity.com

Benchtop Proteomics System

The ClinProt Micro is an easy-to-use, compact system dedicated to peptide and protein profiling, biomarker discovery, and biomarker validation. It is based on a high-performance, benchtop matrix-assisted laser desorption ionization-time of flight mass spectrometer that provides excellent biomarker detection sensitivity and resolution, as well as the reliability and reproducibility needed for rigorous validation studies of putative biomarkers for cancer and other diseases. The system offers unique integrated sample preparation tools for biofluids and tissue extracts with comprehensive analysis, visualization, and model-building software. The system easily measures peptides and proteins that can be used to discover multi-marker panels or profile patterns indicative of specific diseases. These multi-marker panels or patterns potentially have better diagnostic specificity than single biomarkers. The system is suitable for research across a range of samples.

Bruker Daltronics For information 978-663-3660 www.bruker-biosciences.com

Biological Safety Cabinets

The Pass-Thru System Biological Safety Cabinets feature a unique differential pressure design that offers vivarium protection for animals and lab personnel. This through-the-wall animal transfer and receiving system makes use of standard SterilGARD III, Class II, Type A2 cabinets equipped with an integrated tunnel connection that allows passage of items into and out of the cabinets without compromising the integrity of the clean area. Baker's Class II vivarium pass-through connects to the user's heating and air conditioning system to provide a differential pressure between the receiving side and the clean side to ensure vivarium protection. Alarm systems can alert when the cabinet's flow rates are not within pre-determined parameters or if the room intake and exhaust systems are out of range.

Baker For information 800-992-2537 www.bakerco.com

High-Performance Centrifuges

The air-cooled Z 383 and refrigerated Z 383K are universal centrifuges with high-capacity and high-speed capabilities. These centrifuges now feature a total maximum capacity of 2000 ml (4 × 500 ml) in the swing-out rotor. Inserts for this rotor are available for a large number of tubes. Five high-speed angle rotors allow centrifugation of 0.2-ml to 85-ml tubes at g forces up to 26,810g. The Z 383 and Z 383-K feature a quiet, powerful, brushless induction drive that quickly accelerates rotors to their maximum speeds.

Labnet International For information 888-522-6381 www.labnetlink.com

For more information visit GetInfo, *Science*'s new online product index at http://science.labvelocity.com

From the pages of GetInfo, you can:

- Quickly find and request free information on products and services found in the pages of *Science*.
- Ask vendors to contact you with more information.
- Link directly to vendors' Web sites.

Platinum pH Electrodes

New Platinum pH electrodes are a novel solution to a long-standing problem faced by laboratories. When a conventional pH probe is suddenly exposed to a sample solution at a temperature different from past solutions, considerable time is lost before the pH measurement stabilizes at an accurate value. These new electrodes allow accurate readings to be registered within 30 seconds.

Mettler Toledo For information 614-438-4853 www.mt.com

Human Protein Arrays

The new version of the high-density, ProtoArray Human Protein Microarray nc v2.0 contains more than 3,000 purified human proteins. The functional protein arrays can be used to study protein–protein interactions, antibody specificity profiling, and sera autoimmune biomarker discovery.

Invitrogen For information 800-955-6288 www.invitrogen.com

Confocal Imager

The BD CARV II Confocal Imager delivers high-resolution charge-coupled device (CCD) confocal imaging in an easy-to-use and cost-effective optical package that can be attached to new or existing microscopes. High-speed multi-pinhole confocal scanning, combined with high quantum efficiency CCD cameras, allows recording of images at up to 100 frames per second. Instead of lasers, the BD CARV II Confocal Imager makes use of a long-life arc source that allows for full-spectrum (360 nm to 700 nm) confocal imaging. Automated filter selection allows the use of virtually any fluorescent probe on the market. The imager also offers automation of fluorescence recovery after photobleaching.

BD Biosciences For information 800-245-2614 www.atto.com

Cytokine Microarray Kits

FAST Macro membrane-based cytokine microarray kits are used to simultaneously evaluate the relative abundance of 20 different cytokines between different biological samples, such as disease state versus normal state. They are available with both human and mouse specificities. Detection is accomplished using streptavidin/horseradish peroxidase-based chemiluminescent detection, precluding the need for expensive scanners and software.

Whatman Schleicher & Schuell For information 800-245-4024 www.schleicher-schuell.com

Literature

Cell Culture Manual contains a comprehensive collection of products, protocols, and cutting-edge tools in a practical, easy-to-use format. The manual is a hybrid reference and product guide that contains extensive technical information and formulas, as well as popular cell culture products, equipment, supplies, and books. It features a number of general protocols, including cell freezing, subculture, buffer selection, cytokine selection, and contamination solutions.

Sigma-Aldrich For information 800-521-8956 www.sigma-aldrich.com/enzymeexplorer

Newly offered instrumentation, apparatus, and laboratory materials of interest to researchers in all disciplines in academic, industrial, and government organizations are featured in this space. Emphasis is given to purpose, chief characteristics, and availability of products and materials. Endorsement by *Science* or AAAS of any products or materials mentioned is not implied. Additional information may be obtained from the manufacturer or supplier by visiting www.science.labvelocity.com on the Web, where you can request that the information be sent to you by e-mail, fax, mail, or telephone.

ScienceCcareers.org

Classified Advertising

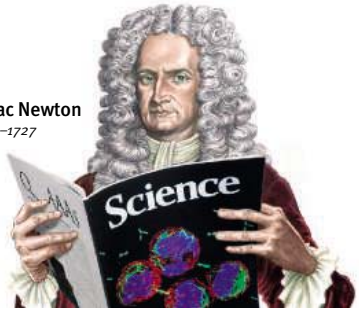

Isaac Newton
1642–1727

For full advertising details, go to **www.sciencecareers.org** and click on **How to Advertise,** or call one of our representatives.

United States & Canada

E-mail: advertise@sciencecareers.org
Fax: 202-289-6742

JILL DOWNING
(CT, DE, DC, FL, GA, MD, ME, MA, NH, NJ, NY, NC, PA, RI, SC, VT, VA)
Phone: 631-580-2445

KRISTINE VON ZEDLITZ
(AK, AZ, CA, CO, HI, ID, IA, KS, MT, NE, NV, NM, ND, OR, SD, TX, UT, WA, WY)
Phone: 415-956-2531

KATHLEEN CLARK
Employment: AR, IL, LA, MN, MO, OK, WI, Canada; Graduate Programs; Meetings & Announcements (U.S., Canada, Caribbean, Central and South America)
Phone: 510-271-8349

EMNET TESFAYE
(Display Ads: AL, IN, KY, MI, MS, OH, TN, WV; Line Ads)
Phone: 202-326-6740

BETH DWYER
(Internet Sales Manager)
Phone: 202-326-6534

Europe & International

E-mail: ads@science-int.co.uk
Fax: +44 (0) 1223-326-532

TRACY HOLMES
Phone: +44 (0) 1223-326-525

HELEN MORONEY
Phone: +44 (0) 1223-326-528

CHRISTINA HARRISON
Phone: +44 (0) 1223-326-510

JASON HANNAFORD
Phone: +81 (0) 52-789-1860

To subscribe to *Science*:
In U.S./Canada call 202-326-6417 or 1-800-731-4939
In the rest of the world call +44 (0) 1223-326-515

Science makes every effort to screen its ads for offensive and/or discriminatory language in accordance with U.S. and non-U.S. law. Since we are an international journal, you may see ads from non-U.S. countries that request applications from specific demographic groups. Since U.S. law does not apply to other countries we try to accommodate recruiting practices of other countries. However, we encourage our readers to alert us to any ads that they feel are discriminatory or offensive.

ScienceCareers.org
We know science AAAS

POSITIONS OPEN

WASHINGTON STATE UNIVERSITY

ASSISTANT/ASSOCIATE/FULL PROFESSOR
Neurobiology of Substance Abuse

The Department of Veterinary and Comparative Anatomy, Pharmacology, and Physiology (VCAPP) at Washington State University invites applications for a tenure-track position to begin July 1, 2006, or earlier. Required qualifications: Ph.D., Ph.D./D.V.M., Ph.D./M.D., or equivalent degree in an area related to neurobiology of substance abuse; at least two years postdoctoral training and a record of excellence in research. Applicants will be expected to establish an outstanding independent research program that will attract continued extramural funding and to participate in the teaching mission of the Department. He/she should have excellent communication skills and will be expected to teach undergraduate, graduate, and/or veterinary students. Willingness and ability to engage in collaborative research and graduate training within a vibrant local neuroscience community are also desired. Screening of application materials will begin August 15, 2005. The application must include a cover letter, curriculum vitae, description of teaching experience and philosophy, summary of research interests and goals, and the names, e-mail addresses, and contact information for three references. Indicate the rank sought. Send application materials to:

Neurobiology Search Committee
Department of VCAPP
Washington State University
Pullman, WA 99164-6520
E-mail: bmorton@vetmed.wsu.edu

Equal Employment Opportunity/Affirmative Action/ADA.

The University of Iowa Department of Internal Medicine is seeking faculty for a tenure-track position at the level of **ASSISTANT** or **ASSOCIATE PROFESSOR.** Qualifications include M.D. degree and/or Ph.D. M.D.s should have Board eligibility in internal medicine. The applicants should have documented broad interest in transplantation immunobiology such as T-, B-, and NK-cell immunology, signaling, or innate immunity. Applicants should have demonstrated outstanding ability in research, teaching, and, where relevant, in clinical medicine with evidence or clear potential for a funded research program. Salary is based on the academic level of entry and on the applicant's qualifications and responsibilities. A competitive startup package will be provided. Candidates should submit curriculum vitae to: **Nicholas Zavazava, M.D./Ph.D., Department of Internal Medicine, The University of Iowa, C51-F GH, Iowa City, IA 52242-1081. E-mail: nicholas-zavazava@uiowa.edu.** *The University of Iowa is an Equal Opportunity/Affirmative Action Employer. Women and minorities are strongly encouraged to apply.*

POSTDOCTORAL POSITION

Seeking candidates interested in biology of lung carcinogenesis with application of functional genomics to diagnosis and treatment of patients with lung cancer. Ph.D. in molecular genetics–related discipline required. Desired skills and experience include gene cloning, cytotoxicity, and animal cancer model studies. Please send curriculum vitae to **e-mail: cap6@columbia.edu.** Contact: **Charles A. Powell, M.D., Department of Medicine, Columbia University Medical Center.** *Columbia University is an Equal Opportunity/Affirmative Action Employer.*

POSITIONS OPEN

CASE WESTERN RESERVE UNIVERSITY

CHAIR
Department of Physiology
Case Western Reserve University
School of Medicine

Nominations or applications are invited from established, dynamic scientists with a creative vision for the position of Chair of the Department of Physiology at the Case Western Reserve University School of Medicine.

The Department has a fine tradition, excellent faculty, facilities, space, and a vigorous graduate program. The new leadership at the School of Medicine seeks a chairperson who will lead this strong department to greater national prominence and will provide resources to build on existing strengths or to develop a new area. New development and expansion of many programs at the School of Medicine provide exciting opportunities for interdisciplinary collaboration. The successful candidate will have an outstanding record of scholarly achievements with proven leadership, mentoring, and administrative abilities.

In addition to curriculum vitae and a list of publications, applicants should submit a letter describing their research, teaching, service, administrative experience, previous mentoring, and their legacy or vision in building interdisciplinary programs and resources.

Nominations and/or applications should be sent to **e-mail: chairphysiol@case.edu.**

For additional information, visit **website: http://physiology.case.edu.**

For questions or additional information you may call **Lynn Landmesser** at **telephone: 216-368-3996.**

Case Western Reserve University is an Equal Opportunity/Affirmative Action Employer.

ASSISTANT PROFESSOR
Evolutionary Biology

The University of Oregon Center for Ecology and Evolutionary Biology (CEEB) and The Department of Biology invite applications for a tenure-track position (Assistant Professor) in evolutionary biology. We are particularly interested in evolutionary biologists studying the evolution of gene function and other central biological processes at the molecular level, as well as those using molecular approaches to investigate fundamental evolutionary processes. The successful candidate will have an outstanding research program and a commitment to excellence in teaching. Applicants should submit curriculum vitae, statements of research interest and teaching philosophy, and three letters of recommendation to: **Evolution Search Committee, Department of Biology, University of Oregon, Eugene, OR 97403-1210 (website: http://evolution.uoregon.edu/).** To ensure full consideration, applications must be received by September 9, 2005.

The University of Oregon is an Equal Opportunity/Affirmative Action Institution committed to cultural diversity and compliance with the Americans with Disabilities Act. Women and minorities are encouraged to apply. We invite applications from qualified candidates who share our commitment to diversity.

The National Marine Fisheries Service of the National Oceanic and Atmospheric Administration provides stewardship of our nation's living marine resources. Incumbent is a senior research scientist; provides leadership to U.S. science delegation to the International Commission for the Conservation of Atlantic Tunas; develops and implements Highly Migratory Species research program. Search for "Supvy Res Fish Bio" at **website: http://jobsearch.usajobs.opm.gov/** for details. **E-mail: regina.d.james@noaa.gov. Telephone: 816-426-5016; fax: 301-562-8968.**

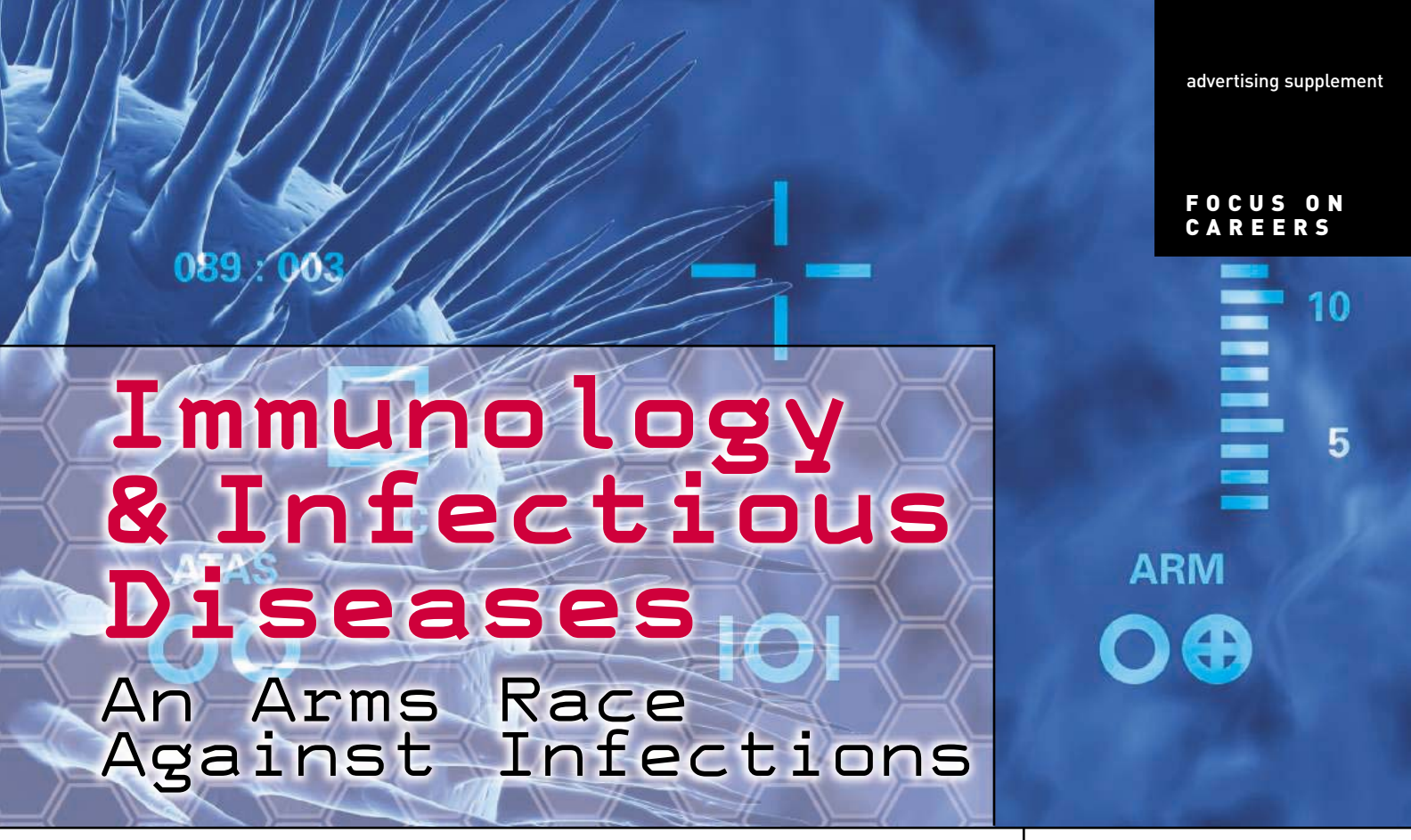

Immunology & Infectious Diseases

An Arms Race Against Infections

OLD AND NEW DISEASES—SUCH AS INFLUENZA AND TUBERCULOSIS, AIDS AND SARS—KEEP SCIENTISTS BUSY WORKING ON BOTH BASIC AND APPLIED RESEARCH. IN ADDITION, THIS RESEARCH HELPS SCIENTISTS FIGHT OTHER ILLNESSES, SUCH AS CANCER. TODAY, WORK ON INFECTIOUS DISEASES TAKES PLACE IN BASIC RESEARCH LABORATORIES AT ACADEMIC INSTITUTIONS, BIODEFENSE AND EPIDEMIOLOGICAL PROJECTS FOR THE GOVERNMENT, AND DIAGNOSTICS AND DRUG DISCOVERY IN INDUSTRY. **BY MIKE MAY**

- **Indiana University School of Medicine**
  http://www.medicine.iu.edu/
- **National Cancer Institute**
  http://www.nci.nih.gov/
- **Theravance**
  http://www.theravance.com/

In 1918-19, a Spanish flu pandemic killed 40-50 million people. Although the world has not experienced an influenza pandemic since then, the World Health Organization (WHO) says three or four are to be expected every century. In other words, a calamity is long overdue. As a result, many epidemiological eyes focus on H5N1, a strain of avian influenza that can infect humans. To study and treat such diseases, we need armies of researchers concentrating on infectious diseases.

As with much of medical science, battling infectious diseases begins with collecting information about how they work. For example, Janice Blum, professor of microbiology and immunology and codirector of the Center for Immunobiology at the Indiana University School of Medicine, says, "We are learning more about how pathogens work, how they exploit a host and evade the immune system." She points to an article in the 20 May 2005 issue of *Science* by Stéphane Méresse and colleagues in France, which revealed that *Salmonella* exploits the cellular system of its host to survive and spread. By learning the tricks of pathogens, scientists hope to defeat them.


JANICE BLUM

The Most Unwanted List

In a world seemingly overflowing with infectious diseases, it proved difficult to pick out the very worst one. Nonetheless, the experts interviewed here pointed out candidates for the most threatening infectious diseases for humans. John M. Coffin, director of the HIV Drug Resistance Program at the National Cancer Institute, says, "I still have to put HIV near the top of the list because it is so insidious." Much of the danger from HIV arises from the potentially long incubation period from infection to the appearance of symptoms. In addition, an untreated case of AIDS is nearly 100 percent lethal. Coffin adds, "We have no effective prevention strategy other than trying to encourage people to try to not get infected."

Blum picked smallpox—the disease that she studies—as the most dangerous. She says, "We have a vaccine, but it's not perfect and cannot be used for everyone." For instance, someone with a weakened immune system, say, from taking high levels of immunosuppressive drugs for arthritis cannot take the smallpox vaccine. Without the vaccine, there is a much higher probability of death particularly for those with diminished immunity. "It is very deadly," Blum says. "If CONTINUED »

Immunology & Infectious Diseases

you are infected by the smallpox virus, without therapeutics such as immunization, the disease symptoms progress rapidly from the hallmark rash and skin lesions to fever, generalized pain, and potentially death within a period of 2-3 weeks. It is a very painful and unpleasant death."

And the list goes on. In comparison to AIDS, Coffin says, "Ebola may be more scary but it always has been locally contained." Still, he knows that many people worry about an Ebola outbreak that spreads.


JOHN M. COFFIN

Research Interactions

Collecting information about one disease can also teach scientists about others. Blum says, "We've learned a lot about susceptibility to viruses through innovative work on HIV, including the development of new technologies to rapidly engineer small-molecule inhibitors to block viral proteins." In this case, drugs against HIV might also be used to treat other diseases. Blum continues: "Some of the anti-HIV drugs—protease inhibitors—are being tested for cancer therapy."

Likewise, expansion in one field can improve research in others related to infectious diseases. For example, "We are getting better tools to do really effective kinds of epidemiological studies," says Coffin. "We can see where diseases are coming from and how they spread." He adds, "Computational tools provide a good part of that improvement, in addition to ever-increasing methods for genetic analysis, such as looking at the genetics of hosts and infecting organisms and population genetics."

Sometimes, new research also focuses on older diseases, such as *Staphylococcus aureus*. This bacterium is especially easy to find in most healthcare facilities. In the past, it could be controlled with antibiotics, but it is growing resistant. So-called methicillin-resistant *Staphylococcus aureus* (MRSA) is resistant to amoxicillin, methicillin, oxacillin, and penicillin. Some strains are also growing resistant to vancomycin. This led scientists at Theravance in South San Francisco to look for new antibiotics.

Pat Humphrey, executive vice president of research at Theravance, says, "We are excited about telavancin, which works through multiple modes of action." Rick Winningham, chief executive officer of Theravance, adds, "Look at the development of HIV cocktails where the different drugs affect the virus in different ways to halt its replication. There are similarities between the two approaches—affecting *Staph aureus* by more than one mechanism but in one molecule."


PAT HUMPHREY

Get Involved

The ongoing evolution of existing infectious diseases and the development of new ones will make experts in this field employable in many ways. Every expert interviewed for this article indicates that jobs related to infectious disease exist in academics, industry, and the government.

More specifically, Blum says there are many job opportunities in research on HIV and hepatitis. She adds, "A lot of research focuses on viruses because of the potential for rapid disease transmission as well as improved capabilities for developing vaccines and therapeutics for worldwide distribution." She adds, "There is also lots of interest in manipulating the innate immune response that recognizes and reacts with bacteria and viruses. We can look at how pathogens interact with the immune system, and then use that information to fight the associated disease."

Work on infectious diseases, however, goes beyond fighting natural breakouts of illness. It also includes the battle against bioterrorism. For example many government institutions are working on detectors for pathogens, so that a bioterrorist's attack could be sensed as soon as possible. Blum adds, "The government has strongly promoted efforts for universities to develop programs and courses related to pathogenesis and biodefense to train more people."

Likewise, Winningham mentions that government organizations provide good training grounds. Specifically, he brings up the National Institutes of Health and the Centers for Disease Control and Prevention. For someone interested in epidemiology, Winningham says that the WHO provides broad opportunities.


RICK WINNINGHAM

Future Infection Fighters

For anyone interested in working in this field, the necessary background seems clear enough: expertise in cellular and molecular biology, knowledge in virology, familiarity with medicinal chemistry, and so on. In addition, the experts interviewed here encourage future infection-fighters to learn about teamwork, because projects in infectious diseases often come from the combination of various skills, often from groups of people. But no matter what background brings someone to this field, keep in mind Coffin's advice to each of his students: "You need to learn to think like a virus."

For those who accomplish Coffin's goal, the field of infectious diseases offers an exciting and rewarding career. As Winningham says, "We have one of the few livelihoods that let you do well while doing good."

Mike May (mikemay1@verizon.net) is a publishing consultant for science and technology based in Madison, Indiana, U.S.A.

Research Opportunities

VIRGINIA BIOINFORMATICS INSTITUTE AT VIRGINIA TECH VBI

Associate and full professorships in experimental, computational life science and biomedicine

The Virginia Bioinformatics Institute (VBI) invites applications for several faculty positions from established researchers in experimental and computational life sciences and biomedicine. Areas of strength among the 16 research groups at VBI include infectious diseases, ranging from the molecular to the population scale, systems biology approaches to study stress response in several organisms, modeling and simulation of biological networks, functional genomics, metabolomics, proteomics and bioinformatics/computational biology. Candidates are expected to have an established research program and a track record of extensive extramural research funding.

Established in 2000 by the Commonwealth of Virginia, the Institute is a part of Virginia Tech (VT) and has its own 130,000 sq ft research facility with state-of-the-art core laboratory and computational facilities. VBI strongly emphasizes synergistic interactions among faculty and is organized around the concept of team science. VBI places strong emphasis on systems biology and bioinformatics rather than organizing research according to academic disciplines. Instead, the research areas represented at VBI organize themselves around the specific needs of individual research projects. Extensive national and international collaborations complement the expertise of the faculty, including strong interactions with several biomedical research centers. Faculty entrepreneurial activities are strongly encouraged and the university provides support for the establishment of commercial ventures.

VBI is currently establishing a facility in the Washington, DC area, as part of Virginia Tech's expansion into that region. Faculty members whose programs will not require their own laboratory facilities will have the option of basing their primary research operation there. Faculty whose research programs require laboratory facilities will necessarily be primarily located at VBI's on-campus facility in Blacksburg, where state of the art laboratory facilities are available. The new faculty may also have the option of joint affiliations with other departments at Virginia Tech and prominent medical schools.

Along with a strong research environment, the Institute actively participates in "Genetics, Bioinformatics, and Computational Biology" an interdepartmental Ph.D. program, widely recognized for its strengths in computational and experimental sciences, which attracts outstanding students with an interdisciplinary research focus. posting 042478

Other professional research opportunities requiring advanced degrees:

- Biological Pathogen Curator, posting 041973
- Bioinformaticians, posting 041438
- Genomics Curator/Annotators, posting 041080
- Head Curator, posting 041595
- Proteomics Database Analyst, posting 042098
- Scientific Web Production Administrator, posting 041790
- Senior Metabolomics Specialist, posting 041981
- Senior Proteomics Specialist, posting 041525
- Software Developers, posting 041435
- Software Development and Quality Control Manager, posting 042039
- Software Evaluators, posting 041457

Postdoctoral appointments:

- Computational Biologist, posting 042479
- Metabolomics Specialist, posting 041979
- Microbiologist in Plant-Microbe Interactions, posting 030262
- Rickettsiae/Coxiella Bioinformatician, posting 041864

For more Information:

To Apply, visit www.jobs.vt.edu and search by posting number. To learn more about VBI and opportunities available, please visit us at www.vbi.vt.edu.

To learn more about the Interdisciplinary PhD program in Genetics, Bioinformatics, and Computational Biology, visit http://www.grads.vt.edu/gbcb/overview.htm.

Virginia Tech

THE UNIVERSITY OF TEXAS MD ANDERSON CANCER CENTER

The Center for Cancer Immunology Research
Department of Immunology and Department of Melanoma

The University of Texas M. D. Anderson Cancer Center in Houston has created a new Center for Basic and Cancer Immunology Research. The Center is housed in a 132,000 sq. ft. building, which provides state-of-the-art facilities to conduct basic research in molecular and cellular immunology and to develop cancer vaccines. We are offering ten postdoctoral positions. We invite applications for postdoctoral fellows in the following laboratories. Areas of expertise include:

Department of Immunology

(1) **Yong-Jun Liu's Lab:** Strong background in molecular biology and cell signaling to study T cell signaling and immunological synapes during T cell and dendritic cell interaction. *Nature Immunol* **3:**673-680, 2002; *Nature Immunol* **5:**426-434, 2004. (**yjliu@mdanderson.org**)

(2) **Steve Ullrich's Lab:** Experience in measuring apoptosis and *in vivo* models of carcinogenesis is required. PhD in Cancer Biology or Immunology required. *Mutation Research* **571:**185-205, 2005. (**sullrich@mdanderson.org**)

(3) **Steve Ullrich's Lab:** Experience with *in vivo* models of immunosuppression is required. Experience with immunohistochemistry is helpful. PhD in Toxicology required. *Toxicology and Applied Pharmacology* **195:**331-338, 2004. (**sullrich@mdanderson.org**)

(4) **Tomasz Zal's Lab:** Strong background in molecular immunology, advanced imaging methods, FRET, and/or multiphoton microscopy to study T cell receptor interactions and immunological synapse formation *in vivo*. *Immunity* **16:**521-534, 2002; *Nat Immunol Epub* June 2005. (**tzal@mdanderson.org**)

(5) **Xiao-Feng Qin's Lab:** Strong background in utilizing lentiviral delivery systems to modify gene expression in cancer cells, dendritic cells and T cells for anti-tumor immunotherapy. *PNAS* **100:**183-188, 2003. (**fqin@mdanderson.org**)

(6) **Kimberly Schluns' Lab:** Experience with *in vivo* T cell responses in mice and a strong interest in how CD8 T cell and dendritic cell interactions play a role in the generation and homeostasis of memory CD8 T cells. *Nature Reviews Immunology* **3(4):**269-279, 2003; *Blood.* **103:**755-756 2004; *PNAS* **101:**5616-5621, 2004. (**kschluns@mdanderson.org**)

(7) **Miles Wilkinson's Lab:** Projects involving RNAi, miRNAs, and RNA surveillance pathways that detect TCR and immunoglobulin mRNAs. Molecular biology experience required. *Science* **297:**108 2002; *Nature Cell Biology* **4:** E144 2002; *EMBO J.* **21:**125 2002; *Mol. Cell* **10:**951 2002; *Nature Genetics* **36:**361, 2002; *Mol. Cell* **12:**1059, 2003. (**mwilkins@mdanderson.org**)

(8) **Hector Martinez-Valdez's Lab:** A protein biochemist with extensive experience in protein purification, structure analyses and interactions to study a novel anti-apoptotic molecule. *J. Biol. Chem* **280:**17807-17814, 2005. (**hmartine@mdanderson.org**)

(9) **Jagan Sastry's Lab:** Innate and adaptive immunity against HIV and HPV. *Recent Res. Develop. Virol.* **3:**575-601, 2001; *Vaccine* **23:**2154-2159, 2005. (**jsastry@mdanderson.org**)

Department of Melanoma Medical Oncology

(1) **Patrick Hwu's Lab:** Experience with mouse tumor models and T cell and dendritic cell culture are required to study T-cell migration into tumors following adoptive T-cell transfer and anti-tumor vaccination. *Cancer Res.* 2004 Sep **15;64(18):**6783-90; *Hum Gene Ther.* 2002 Nov **1;13(16):**1971-80; *Nat Biotechnol.* 2002 Dec; **20(12):**1221-7. (**phwu@mdanderson.org**)

Interested individuals should contact: **The University of Texas M. D. Anderson Cancer Center, Department of Immunology or Department of Melanoma, SCRB, 7455 Fannin, Unit 901, Houston, TX 77030-1903.**

M.D. Anderson Cancer Center is an EOE Employer and does not discriminate on the basis of race, color, national origin, gender, sexual orientation, age, religion, disability or veteran status, except where such distinction is required by law. All positions at M.D. Anderson are considered security sensitive; drug screening and thorough background checks will be conducted. The University of Texas M.D. Anderson Cancer Center values diversity in its broadest sense. Diversity works at M.D. Anderson. Smoke-free environment.

INDIANA UNIVERSITY SCHOOL OF MEDICINE

Tenure-Track Faculty Position In Immunobiology

The Division of Rheumatology in conjunction with the Center for Immunobiology **(http://cimb.medicine.iu.edu/)** at the Indiana University School of Medicine is seeking candidates for a faculty position at the Assistant Professor or tenured Associate Professor level. We are searching for scientists or physician-scientists in areas of immunology that include autoimmunity and inflammation. Strong preference will be given to candidates whose research investigates mechanisms of disease, and involves translational studies. Candidates for the tenured Associate Professor position must have well established and funded research programs. Assistant Professor applicants should have demonstrated potential for independence and leadership in research. Indiana University and the Center for Immunobiology offers a highly collaborative environment that promotes interactions amongst all research and clinical faculty. Candidates must be eligible to work in the U.S.

Candidates with Ph.D. and/or M.D. should submit a curriculum vitae, a 2 – 3 page statement of research interests and future plans by e-mail to:

Rafael Grau, MD
Director, Division of Rheumatology
Department of Medicine
Indiana University School of Medicine
E-mail: rgrau@iupui.edu

Indiana University is an EEO/AA employer, M/F/D

TRUDEAU INSTITUTE, INC.

Postdoctoral Positions in Immunology and Infectious Disease at the Trudeau Institute

A postdoctoral position is open in the lab of **Dr. Troy Randall** to study the differentiation and responsiveness of influenza-specific memory T cells. References include *Nat. Med.* **10:**927-934, 2004 and *J. Exp. Med.* **198:**1759-1764, 2003.

Postdoctoral positions are open in the lab of **Dr. Frances Lund** to characterize regulatory roles of B cells in infection and autoimmune disease and to investigate the mechanisms controlling leukocyte trafficking. References include *Immunity* **20:**279-291, 2004 and *Nat Immunol.* **1:** 475-482, 2001.

Detailed descriptions of these projects, and other ongoing research in the laboratories offering postdoctoral positions, are available at **www.trudeauinstitute.org**.

Trudeau Institute, Inc. is a not-for-profit biomedical research institute with state-of-the-art facilities and an international reputation for excellence. Located in the heart of New York State's Adirondack Mountains overlooking beautiful Saranac Lake, Trudeau offers competitive salaries and benefits, including daycare, pension, and subsidized housing. **Trudeau fosters a highly collaborative research environment focused on basic immunology and infectious disease.**

Please send curriculum vitae, addresses of three references and a letter describing your research interests to:

Amy Richardson, Human Resource Manager
Trudeau Institute, Inc.
154 Algonquin Avenue
Saranac Lake, NY 12983
arichardson@trudeauinstitute.org

Health Research in a Changing World

Fighting Diseases and Improving Lives

DEPARTMENT OF HEALTH AND HUMAN SERVICES
NATIONAL INSTITUTES OF HEALTH
NATIONAL INSTITUTE OF ALLERGY AND INFECTIOUS DISEASES

With nationwide responsibility for improving the health and well-being of all Americans, the National Institutes of Health (NIH) and the National Institute of Allergy and Infectious Diseases (NIAID) conducts and supports a global program of research aimed at improving diagnosis, treatment and prevention of immunologic, allergic and infectious diseases. NIAID's mission is driven by a strong commitment to basic research, which incorporates the complementary fields of vaccine research, immunology, microbiology and infectious diseases.

Are you ready for an exciting career that could help improve millions of lives around the world? Then consider joining the scientific and medical forces at NIAID. The NIAID, NIH, DHHS offers competitive salaries and a comprehensive benefits package. NIAID has the following scientific opportunity available:

Scientific Review Administrator, Division of Extramural Activities

Come join a leading team of medical research administrators in the Division of Extramural Activities (DEA), NIAID, as a Scientific Review Administrator (SRA). Become an important resource for the implementation of policies related to research priorities, gaps in research, conflict of interest, human subject issues, and animal welfare. The SRA is responsible for managing peer reviews of biodefense and SARS initiatives, AIDS and infectious disease programs, national and international training activities. As a SRA you will make significant professional, scientific, clinical and administrative judgments based on specialized training and experience in basic, applied, pre-clinical or clinical research. We are seeking motivated individuals with strong backgrounds in microbiology, immunology, virology or related disciplines. Significant experience in basic, pre-clinical, and/or clinical biomedical research is also required. Highly developed written and verbal communication, analytical, interpersonal, and organizational skills are required. U.S. Citizenship (preferred) or Permanent Residence is required. All candidates must have a Ph.D./M.D. degree or equivalent training and extensive post doctoral training and experience in one of the following areas: infectious diseases, virology, immunology, tropical medicine, bacteriology and vaccines.

To apply for these vacancies, please visit
http://www.usajobs.opm.gov
Interdisciplinary GS-401/403-12/13/14
Salary: $62,886-114,882
Vacancy number: NIAID-05-71644 Open: 5/23-8/15/05

Health Scientist Administrator GS-601-12/13/14
Salary: $62,886-114,882
Vacancy number: NIAID-05-049 Open: 5/23-8/15/05

Applications must be submitted to Sherri Liggett, Human Resource Specialist, 301-402-0957
To have your resume reviewed and for other opportunities, please visit: http://healthresearch.niaid.nih.gov/science and click "submit your resume"

We are happy to respond to your questions, and you may contact us toll-free: 1-888-798 -4991.

Please reference "Science" on your resume

DHHS and NIH are Proud to be Equal Opportunity Employers

Department of Health and Human Services
National Institutes of Health
National Institute of Allergy and Infectious Diseases
Proud to be Equal Opportunity Employers

MedImmune

Advancing Science for Better Health

MedImmune, Inc. strives to provide better medicines to patients, new medical options for physicians, rewarding careers for employees, and increased value to shareholders. Dedicated to advancing science and medicine to help people live better lives, the company is focused on infectious diseases, cancer and inflammatory diseases.

With approximately 2,000 employees worldwide, MedImmune is headquartered in Maryland and has additional U.S. facilities in California and Pennsylvania.

We are currently seeking scientists with experience in B cell biology (oncology and autoimmunity), antibody engineering, cytokine signaling, and in vivo autoimmune and respiratory disease models in the following areas:

Molecular Biology • Cellular Immunology
In Vivo Disease Biology

We offer an outstanding compensation/benefits package and actively promote a work-life balance.

For immediate consideration, please forward your resume to Anthony J. Coyle, Senior Director, Immunology Research at: **jobopenings@medimmune.com**.

To learn more about us and to view all our open positions, please visit:

www.medimmune.com

MedImmune is proud to be an Equal Opportunity Employer.

TWO FACULTY POSITIONS IN IMMUNITY AND INFLAMMATION

DEPARTMENT OF PATHOLOGY AND LABORATORY MEDICINE
DAVID GEFFEN SCHOOL OF MEDICINE AT UCLA

The Department of Pathology and Laboratory Medicine at UCLA is seeking candidates for two faculty positions at the tenure-track Assistant Professor or tenured Associate/Full Professor level. We are searching for outstanding scientists in areas of immunology that include cell trafficking, autoimmunity, GI/mucosal immunology, inflammation, wound healing, and innate immunity. Strong preference will be given to applicants whose work addresses mechanisms of disease initiation and progression, identifies and rationalizes human biomarkers for those processes, or provides insights to manipulate and control abnormalities within or mediated by the immune system.

UCLA offers a highly collaborative research environment that promotes interactions between faculty in the School of Medicine, College of Letters and Science, the Jonsson Comprehensive Cancer Center, the California NanoSystems Institute, and the Crump Institute for Molecular Imaging. UCLA has also recently committed significant resources for the establishment of the Institute for Stem Cell Biology and Medicine (ISCBM), and faculty applying stem cell approaches to the above areas are particularly encouraged to apply.

Candidates for tenured Associate/Full Professor positions must have well established and funded research programs. Assistant Professor applicants should have demonstrated their potential for research leadership. In all cases, emphasis will be placed on the applicant's record of research accomplishment, creativity, and promise of continuing success.

Candidates with a Ph.D. and/or M.D. should forward 2 hard copies of (1) a description of their research background; (2) full curriculum vitae; and (3) a list of 3-5 references. Electronic submissions will not be considered.

Submit materials to:

Dr. Kenneth Dorshkind
c/o Ms. Dominica Salvatore
Department of Pathology and Laboratory Medicine 173216
David Geffen School of Medicine at UCLA
10833 Le Conte Avenue
Los Angeles, CA 90095-1732

UC is an Affirmative Action/Equal Opportunity Employer. All qualified candidates, including women and minorities, are encouraged to apply.

Eberhard Karls University Tübingen, Germany

In the context of SFB 685 Immune Therapy
***two PhD tenure track* positions are opened**

Candidates should have an excellent research record and interest in interdisciplinary research.

The laboratory focuses on the interactions between the immune system and somatic cells during inflammation, tissue regeneration and cancer development. Starting equipment, a sound background in immunology, excellent *in vivo* and *in vitro* imaging facilities and interdisciplinary exchanges are provided in a modern research environment. To complete the scope and performance, we are preferentially searching for scientists with profound experience in **developmental biology, cell signalling or cell-cell-interactions**.

Correspondence:
Prof. Dr. Martin Röcken
Chairman, Department of Dermatology
Eberhard Karls University Tübingen
Liebermeisterstr 25
D-72074 Tübingen, Germany

FACULTY POSITION IN MICROBIOLOGY/BACTERIOLOGY

The **Department of Veterinary and Biomedical Sciences, University of Minnesota**, invites applications for a full-time tenure-track faculty position in microbiology/bacteriology at the level of Assistant or Associate Professor. The selected candidate will join a Departmental program with demonstrated leadership in molecular biology, microbial and animal genome analysis, and infectious diseases. The successful candidate will receive a competitive salary and start-up package. Rank (Assistant or Associate Professor) will depend on qualifications and experience consistent with Collegiate and University policy. The successful candidate will become part of an expanding University commitment to cutting-edge research in infectious diseases, biomedical and agricultural genomics, and bioinformatics, and will have access to new facilities for high throughput screening, DNA sequencing, proteomics, microscopy and imaging.

Candidates must have a Ph.D. or foreign equivalent in a relevant field of biomedical, biological or agricultural sciences, and two or more years of postdoctoral experience. Demonstrated ability to publish in peer-reviewed journals, obtain extramural research support, and teaching experience are desired. The successful applicant is expected to develop or maintain an externally funded research program in an area of infectious diseases, participate in teaching of undergraduate microbiology and participate in graduate student programs. Start date is October 15, 2005, or when a suitable candidate is identified.

Applicants must provide an introductory letter, curriculum vitae, a statement of research and teaching goals, and should arrange to have three letters of reference sent to the Search Coordinator. Letters of reference should include assessment of the applicant's background and abilities in research and interpersonal skills. Send materials to: **Ms. Lea Schwartz, Search Coordinator, Department of Veterinary and Biomedical Sciences, University of Minnesota, 205 Veterinary Science, 1971 Commonwealth Avenue, St. Paul, MN 55108: Fax (612) 625-5203; email schwa142@umn.edu**. For inquiries, please contact **Dr. Randall Singer, Search Committee Chair, singe024@umn.edu**. Reviews of applications will begin **September 1, 2005** and continue until the position is filled.

The University of Minnesota is an Equal Opportunity Educator and Employer.

POSTDOCTORAL POSITIONS AVAILABLE

AMERICAN SOCIETY FOR MICROBIOLOGY AND NATIONAL CENTER FOR INFECTIOUS DISEASES

2006 POSTDOCTORAL RESEARCH PROGRAM

Up to ten positions will be awarded for full-time research on infectious diseases which cause significant public health problems. Fellows will perform research in residence at the National Center for Infectious Diseases (NCID) which is headquartered at the Centers for Disease Control and Prevention (CDC) in Atlanta, GA. In addition to Atlanta, NCID operates laboratories in Ft. Collins, CO, Anchorage, AK, and San Juan, Puerto Rico.

Eligible fields of study include:
- Bacterial and Mycotic Diseases
- Viral and Rickettsial Infections
- Nosocomial Infections
- HIV/AIDS
- Vector-borne Infectious Diseases
- Sexually Transmitted Diseases
- Parasitic Diseases

Positions are limited to individuals who either earned their doctorate degree (Ph.D., Sc.D., M.D., D.V.M., or D.D.S.) or have completed a primary residency within three years of their proposed start date. The program provides an annual stipend of $35,800, up to $500 relocation expenses, up to $3,000 health care benefits package and up to $2,000 for professional development. The fellowship is for 2 years.

The application deadline is **November 15, 2005**. For more information, visit **http://www.asm.org/Education/index.asp?bid=15497**. The brochure and application are available on line.

ASM
American Society for Microbiology

CDC/NCID
Centers for Disease Control and Prevention/National Center for Infectious Diseases

Postdoctoral Fellowship position available in the Department of Health and Human Services (DHHS), National Institutes of Health (NIH), National Cancer Institute (NCI), Center for Cancer Research (CCR), Laboratory of Molecular Immunoregulation (LMI), Cytokine Molecular Mechanisms Section (CMMS), Frederick, Maryland. Must have training in most aspects of molecular cloning with a working knowledge of transcription factors and protein phosphorylation. Candidate is expected to provide leadership and independence in a discovery-based project dealing with the genomic characterization of cancer stem cells. Excellent proficiency in English writing/speaking are required. Candidate must have a Ph.D. (within the past 5 years) and/or M.D. Salary is commensurate upon experience.

Send a statement of research interests/goals, curriculum vitae with publication record and 3 letters of recommendation to:

Dr. William Farrar
LMI, CCR, NCI
Bldg. 560, Rm. 31-68
1050 Boyles St
Frederick, MD 21702-1201

Applications are due by **August 31, 2005**.

DHHS , NIH, and NCI are Equal Opportunity Employers.

Choosing Roche

We all dream of doing big things.

Solving important problems.

Making a difference.

Improving lives.

As a result of our ongoing successes and expanding global efforts in inflammation, we are seeking talented Scientists to join our Respiratory-Inflammation/Autoimmunity Therapy Area to contribute to the discovery of innovative medicines for the treatment of inflammatory diseases such as asthma, COPD, multiple sclerosis and inflammatory bowel disease.

The following opportunities are available at our US Pharmaceuticals Headquarters in Nutley, NJ:

Senior Principal Scientist

Job Code 2597

As an integral member of the Immunopharmacology section, the successful candidate will interact directly with Project Team Leaders to identify and implement relevant animal models of respiratory and inflammatory diseases in support of target validation, lead optimization, and clinical candidate selection. Identify clinically relevant biomarkers and pharmacodynamic endpoints in support of early development and proof of concept studies in patients. This position requires a PhD in Pharmacology, Physiology, Immunology or related discipline with at least 4 years of industry experience, expertise in animal models of respiratory and inflammatory diseases, and the ability to work independently in a matrix environment. Supervisory experience a plus.

Principal Scientist

Job Code 2869

In addition to overseeing a Senior Scientist, the Principal Scientist will also be accountable for experimental design and results, participate in target discovery, identifying innovative technologies, and interacting with project teams and project leaders. The opportunity to propose new targets and lead projects are available, as well as the opportunity to present and publish findings. This position requires a PhD in Immunology, Pharmacology or a related discipline with at least three years of related industry experience in Inflammation/Autoimmune diseases. Demonstrated leadership, a strong publication record, and the ability to work in a flexible matrix environment are also required.

To apply, please visit our website at: **www.rocheusa.com** and reference the correct job code.

Roche is an Equal Opportunity Employer fully committed to workplace diversity.

We Innovate Healthcare
from research to real life

Roche

IMMUNOL. & INFECT. DISEASES

Composed of ten research Branches and four administrative offices, the **Ludwig Institute for Cancer Research** (LICR) is the largest international institute dedicated to cancer research. The uniqueness of LICR lies not only in its size and scale, but also in its philosophy and ability to drive its results from the laboratory into the clinic.

SCIENTIFIC ADMINISTRATIVE OFFICER

The LICR New York Office seeks a **Scientific Administrative Officer** to assist in identifying areas of LICR research suitable for patent protection. Working closely with scientists world-wide, members of the LICR's Intellectual Property Office and patent counsel, the successful candidate will be involved in the preparation and prosecution of patent applications.

Applicants should have at least three years post-graduate research experience, preferably in immunology or molecular biology. A wide ranging interest in science and an ability to rapidly assimilate new data are essential. Some knowledge of oncology and prior experience of technology transfer would be advantageous.

Salary depends on previous experience and is subject to negotiation. Interested candidates should apply in writing, enclosing a resume and the names of two references, before **July 31, 2005** to:

LUDWIG INSTITUTE FOR CANCER RESEARCH

Dr. Jonathan Skipper
Ludwig Institute for Cancer Research
605 Third Ave / 33rd Flr
New York, NY 10158 USA
Fax: +1 212 450-1555

The Children's Hospital at SCOTT & WHITE

College of Medicine
The Texas A&M University System Health Science Center

Endowed Chair
Pediatric Cardiovascular Research
Scott & White Health System
Texas A&M University System Health Science Center
College of Medicine

The **Children's Hospital at Scott & White** and **The Texas A&M University System Health Science Center College of Medicine** are seeking a nationally recognized research scientist as the first holder of the Josephine Ballard Endowed Chair in pediatric cardiovascular research. Applicants should be accomplished investigators (Ph.D., M.D. or M.D./Ph.D.) at the associate or professor level with current federal grants and a proven track record in cardiovascular basic, clinical, and/or translational research. The successful candidate will join an expanding faculty within a large academic healthcare system. The chair holder will play a critical role in directing and expanding research activities in pediatric cardiovascular disease, in close collaboration with investigators in the Cardiovascular Research Institute and other local, national and international experts in cell biology, genomics and proteomics.

The Children's Hospital at Scott & White serves a large clinical base throughout Central Texas. There are outstanding clinical practice and laboratory facilities on campus that perform state of the art molecular and cellular biology techniques, flow cytometry, proteomics and genomics as well as biostatistical support services. Animal laboratory facilities include areas to perform medical and surgical procedures. Laboratory space and an appropriate start-up package for the chair holder will be provided. The Scott & White Healthcare system is one of the largest multi-specialty integrated delivery systems in the nation. Scott & White is the primary clinical and hospital teaching campus for the College of Medicine. Academic appointments at the associate and professor level through the College of Medicine are commensurate with qualifications and experience.

Interested candidates should send a copy of their curriculum vitae, letter addressing their qualifications and a list of 3 individuals who can provide references to: **Don P. Wilson, M.D., Chair, Search Committee for Josephine Ballard Centennial Chair in Pediatric Cardiovascular Research; Chairman, Department of Pediatrics, 2401 South 31st Street, Temple, Texas 76508, 254-724-4363, fax 254-724-1938, email: dwilson@swmail.sw.org**

Scott & White is an equal opportunity employer. For more information regarding Scott & White and The Texas A&M University System Health Science Center College of Medicine, please log onto: www.tamu.edu and www.sw.org.

NATIONAL INSTITUTE OF ENVIRONMENTAL HEALTH SCIENCES
POSITION IN BIOSTATISTICS

The Biostatistics Branch of the National Institute of Environmental Health Sciences, National Institutes of Health, in Research Triangle Park, North Carolina, is seeking a senior-level biostatistician for a tenured position. The successful candidate will assume responsibility for directing the Statistical Consulting Service, which provides collaborative statistical support to some 80 scientists a year from the Division of Intramural Research. The work will involve collaboration in the design, analysis and interpretation of experiments, and also independent investigator-initiated statistical research related to methods required by new research initiatives. Such research could include, but not be limited to, analysis of the 2-year rodent carcinogenesis bioassay and shorter-term studies with transgenic rodents, methods of analysis for short-term in vitro tests, and methods related to new data-rich methods in genomics and bioinformatics, with applications to toxicogenomics. Applications are invited from persons with a Ph.D. in biostatistics or statistics. Excellent communication and computing skills are required, as is experience in consulting in toxicology. Documented research productivity is required and evidence of innovative work related to bioinformatics methods development is highly desirable.

For information about the Biostatistics Branch, visit website **http://dir.niehs.nih.gov/dirbb/.** Interested persons should send their curriculum vitae with a statement of research interests, and arrange for three letters of recommendation to be sent by **September 15, 2005**, to the following address. Applications received after that date will be considered on an as-needed basis until the position is filled. Interested candidates should send information to: **Ms. Cindy Garrard (DIR-05-08), National Institutes of Health, National Institute of Environmental Health Sciences, P.O. Box 12233, Maildrop A2-06, 111 Alexander Drive, Room A206, Research Triangle Park, NC 27709, E-mail: dir-appls@niehs.nih.gov**

Interview/Hire the World's Best Scientists

Reach innovative young scientists at the forefront of their fields

Attend the Job Fair for NIH Postdoctoral, Research, and Clinical Fellows

Date: October 20, 2005
Time: 10:30 am - 3:00 pm
Place: Natcher Conference Center
National Institutes of Health
Bethesda, Maryland

Access 3800 doctoral scientists and clinicians in training at the NIH

Register by September 15th at: **www.training.nih.gov/jobfair**

Office of Intramural Training and Education

WWW.NIH.GOV

STAFF CLINICIAN POSITION IN DIABETES

The Diabetes Unit in the Laboratory of Clinical Investigation at the National Center for Complementary and Alternative Medicine (NCCAM), National Institutes of Health (NIH) is seeking a staff clinician to conduct patient-oriented research in the intramural program at the Clinical Center of NIH. Applicants must possess an M.D. or D.O. degree, have a current U.S. medical license, be board certified in Internal Medicine, and board certified/eligible in Endocrinology and Metabolism. Prior experience in clinical research and a strong publication record are essential. The successful applicant will write clinical research protocols and conduct patient-oriented research exploring metabolic and vascular physiology and outcomes relevant to elucidating the mechanisms of action, safety, and potential efficacy of complementary and alternative medicine approaches for the treatment of diabetes, obesity, and cardiovascular diseases. Experience with glucose clamps and in vivo endothelial function studies is advantageous. Salary and benefits will be commensurate with experience.

NCCAM provides state-of-the-art research facilities in the intramural program at NIH in addition to a collegial and nurturing working environment. By **September 15**, please forward your CV, bibliography, list of three references, and a cover letter summarizing your scientific interests and experience to: **Michael J. Quon, M.D., Ph.D. Chief, Diabetes Unit, LCI, NCCAM, National Institutes of Health, Building 10, Room 6C-205, 10 Center Drive MSC 1632, Bethesda, Maryland 20892-1632, Fax (301) 402-1679, Email: quonm@nih.gov**

Postdoctoral Training Positions Translational Cancer Genomics

The Oncogenomics Section, at the National Cancer Institute, NIH, has two post-doctoral training positions available in translational genomics. Ongoing research efforts involve genomic and proteomic approaches to the investigation of Neuroblastoma. Using these approaches we have identified prognostic markers and potential new therapeutic targets in cancers. The candidate will work on combining molecular and genomic approaches to validate these targets both in vitro and animal models to bring these reagents to the clinic. The candidate should hold either a Ph.D. or M.D. degree and have an interest in oncology and significant experience in genomics and the microarray technology. Experience in mouse/animal models is preferred. Candidates should have less than five years post-doctoral experience.

Correspondence, names of references and CV should be sent to **Dr. Javed Khan, Advanced Technology Center, National Cancer Institute, Room 225B, 8717 Grovemont Circle, Gaithersburg, MD 20877, or via email at khanjav@mail.nih.gov**

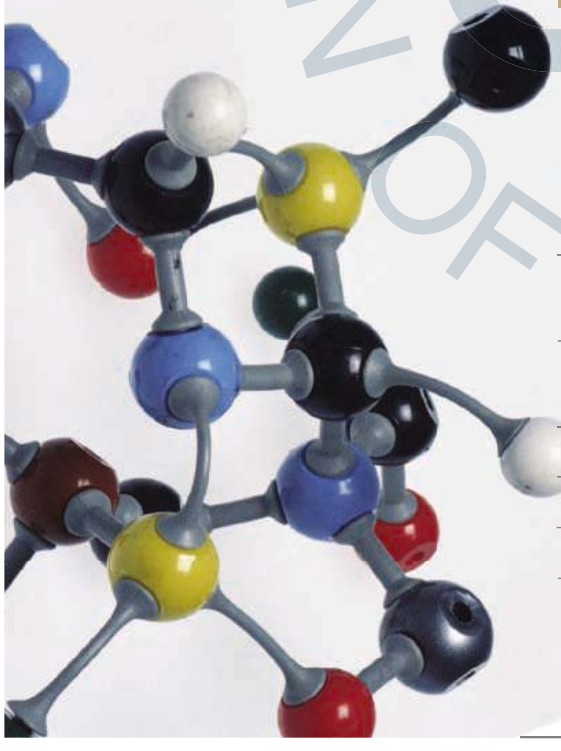

Postdoctoral Research Training at NIH

- Launch a career to improve human health
- Work in one of 1250 of the most innovative and well-equipped biomedical research laboratories in the world
- Explore new options in interdisciplinary and bench-to-bedside research
- Develop the professional skills essential for success
- Earn an excellent stipend and benefits
- Click on www.training.nih.gov

Office of Intramural Training and Education

Environmental Science and Policy Leader

CropLife America (**http://www.croplifeamerica.org/**) has an opening for an Environmental Science and Policy Leader. Incumbent provides leadership and organization for science and regulatory policy in the area of environmental issues on behalf of CropLife America. Responsible for monitoring, review and analysis of all relevant regulatory initiatives, including the identification of emerging environmental policy issues that impact the crop protection industry. Leads the development and implementation of effective strategies in support of CropLife America's strategic objectives, including preparation of public comments in response to regulatory proposals. Reports to the Vice President for Science and Regulatory Affairs.

Candidates must possess strong analytical and interpretive skills; a strong scientific background in environmental sciences; and demonstrate a strong grasp of ecological risk assessment principles and methodologies. Candidates must have excellent written and oral skills and experience in the submission of technical comments in response to federal regulatory proposals. Experience with the regulatory approval processes of the EPA is strongly preferred. An advanced degree in environmental science, environmental toxicology, or related discipline is required. We offer excellent paid benefits and competitive salaries.

Interested persons should submit resume and cover letter to:

Karen McEvoy
Human Resources Manager,
1156 15th St.,NW Suite 400,
Washington,DC 20005
Email :kmcevoy@croplifeamerica.org
FAX: 202.872.3890

Deadline to apply: **July 31, 2005**

CropLife America is an Equal Opportunity/Affirmative Action Employer.

Postdoctoral Fellowships for Research on Adult Stem Cells

Tulane Center for Gene Therapy

The Tulane Center for Gene Therapy offers a program of postdoctoral fellowships for research on adult stem/progenitor cells for non-hematopoietic tissues. The aim of the program is to prepare postdoctoral fellows for careers as independent academic scientists. Applicants can select from research projects that range from basic biology of stem cells to their application to animal models for genetic diseases of children, cancers, heart disease, lung disease, stroke, Alzheimer's disease, spinal cord injury and parkinsonism. The Center is a leader in isolation and characterization of adult stem cells, and conducts an NIH sponsored program to distribute fully characterized samples to other investigators. The Center includes a GMP level facility for preparing stem/progenitor cells for clinical trials. The Center is housed in a modern research building, it has a staff of over 70, and it is supported by ten core laboratories. Two members of the faculty also conduct research with stem/progenitor cells in non-human primates at the Tulane University National Primate Center.

Qualified applicants should have a Ph.D. degree or equivalent from a well-recognized college or university. For details, visit web site: **www.som.tulane.edu/gene_therapy/**.

Please send (1) curriculum vitae, (2) brief summary of research interests, and (3) two or more letters of recommendation to:

Dr. Darwin J. Prockop, Director
Tulane Center for Gene Therapy
Tulane University Health Sciences Center
1430 Tulane Avenue, SL-99
New Orleans, LA 70112

Fax: 504-988-7710
E-mail: dprocko@tulane.edu

Tulane is an Equal Opportunity Employer.

UNIVERSITY OF MICHIGAN

DEPT. OF DERMATOLOGY / COMPREHENSIVE CANCER CENTER

FACULTY POSITION

The University of Michigan Department of Dermatology and Comprehensive Cancer Center seek to recruit an investigator committed to a research program with direct relevance to tumors arising in skin. This individual will be a vital member of our Cutaneous Oncology Program, comprising an integrated team of investigators working at the basic, translational, and clinical levels. We expect the successful applicant to develop a robust research program to further our understanding of mechanisms underlying the development and progression of either melanoma or non-melanoma skin cancers. The University of Michigan provides an outstanding environment for biomedical research, with world-class core facilities and abundant clinical material from our Cutaneous Surgery and Oncology Unit, obtained through IRB-approved protocols. Candidates with MD, PhD, or MD/PhD degrees, and substantive post-doctoral training and publications, should send a CV, statement of research interests, and three letters of support to:

University of Michigan
Medical School

Andrzej Dlugosz, MD
U-M Dermatology /
Comprehensive Cancer Center
3310 CCGC, Box 0932
1500 E. Medical Center Drive
Ann Arbor, MI 48109-0932
dlugosza@umich.edu

The University of Michigan is an Affirmative Action/ Equal Opportunity Employer

Faculty Position
Department of Biochemistry
University of Toronto

The Department of Biochemistry in the Faculty of Medicine at the University of Toronto invites applications for a tenure-track position at the Assistant Professor level. The Department is part of an exciting and dynamic health research community, one of the largest in North America. Requirements include a Ph.D. in biochemistry or a related discipline, at least two years post-doctoral training and an excellent publication record. The Department is interested in building strength in key areas of structural, molecular and cellular biology, including molecular aspects of gene transcription, protein synthesis, signal transduction, cellular and cytoskeletal dynamics, functional biomolecular imaging, and the structure and function of membrane proteins, molecular complexes and molecular machines. The successful applicant will be expected to establish excellence in an independent research program, to compete effectively for external funding, and to contribute actively to the undergraduate and graduate teaching programs in the Department.

Applicants should arrange to have three letters of reference sent directly to the mailing address below. In addition, applicants should send their curriculum vitae, copies of significant publications, and a 2-3 page description of their research plans by either e.mail to: **chair.biochemistry@utoronto.ca** or by mail to: **Chair, Department of Biochemistry, Medical Sciences Building, University of Toronto, Toronto, Ontario, M5S 1A8, Canada**. Closing date for applications is **September 30, 2005**, or until the position is filled.

The University of Toronto offers the opportunity to teach, conduct research and live in one of the most diverse cities in the world and is strongly committed to diversity within its community. The University especially welcomes applications from women, visible minority group members, aboriginal persons, persons with disabilities, members of sexual minority groups, and others who may contribute to the further diversification of ideas. All qualified candidates are encouraged to apply; however, Canadians and permanent residents will be given priority.

www.biochemistry.utoronto.ca

OPEN TO

DISCOVER

With breakthrough science, we're exploring new frontiers of diabetes and metabolism research.

At our cutting-edge research facilities in Cambridge, MA, world-class scientists have the resources they need to carry out their mission. We invite you to join us in all areas of lifesaving drug discovery, including stem cell research and skeletal myogenesis.

Our openings include the following positions:

- Associate Scientist, Aging — BS/MS (5743BR)
- Associate Scientist, Cell Biology — BS/MS (6096BR)
- Associate Scientist, Enzymology — BS/MS (5724BR)
- Associate Scientist, In Vivo, Stem Cell — BS/MS (2246BR)
- Postdoctoral Fellow, Biochemistry and Kinetics (1517BR)
- Research Scientist, Bioinformatics — PhD (1389BR)
- Research Scientist, Enzymology — PhD (5306BR)
- Research Scientist, Enzymology, LC/MS — PhD (5737BR)
- Research Scientist, In Vivo, Stem Cell — PhD (4459BR)
- Scientific/Research Scientist, LC-MS/MS — BS/MS/PhD (3247BR)
- Visiting Postdoctoral Fellow, Novartis/Broad Collaboration (6336BR)
- Visiting Research Fellow, Novartis/Broad Collaboration — PhD (5479BR)

To view descriptions of all open positions and to apply, visit www.nibr.novartis.com and follow the links to Careers and Job Opportunities. Be sure to reference the corresponding Job ID number listed above.

Novartis is committed to embracing and leveraging diverse backgrounds, cultures, and talents to achieve competitive advantage.
Novartis is an equal opportunity employer. M/F/D/V

NOVARTIS
NOVARTIS INSTITUTES
FOR BIOMEDICAL RESEARCH

The New Pathway to Drug Discovery

www.nibr.novartis.com

NYCOM NYIT

New York College of Osteopathic Medicine
of New York Institute of Technology

The New York College of Osteopathic Medicine of New York Institute of Technology (NYCOM), the only osteopathic medical school in New York State, invites applications for the following position:

FACULTY POSITIONS – BIOMEDICAL SCIENCES

The New York College of Osteopathic Medicine of the New York Institute of Technology has academic positions available in Physiology, Pathology, Pharmacology/Toxicology, and Cellular/Molecular Biology at the Assistant/Associate Professor level. We are seeking individuals with the ability to establish and sustain vigorous and creative independent and/or collaborative research programs in their area of interest. Other responsibilities will include teaching first and second year medical students in an innovative medical school curriculum. Demonstrated excellence in teaching is highly desirable. Participating in select departmental and college committees will be required. Faculty rank and salary will be commensurate with experience. Minimal qualifications include a Ph.D. and/or D.O. or M.D. degree, plus 2-3 years of post-doctoral research experience or relevant clinical experience. Consideration of applicants will begin immediately and will continue until the positions are filled. Anticipated start date will be August/Sept. 2005 or soon thereafter. Interested candidates should send their CV, recent reprints, statement of research interests, and arrange to have 3 letters of reference sent to: Charles Pavia, Ph.D., Chairman, Search Committee, Dept. of Biomedical Sciences, NYCOM of NYIT, Northern Boulevard, P.O. Box 8000, Old Westbury, NY 11568. NYIT is an AA/EEO institution.

www.nyit.edu

MEDICAL COLLEGE OF GEORGIA
School of Dentistry
Augusta, Georgia
Director of Bioengineering and Regenerative Medicine
(Associate or Full Professor)

The Medical College of Georgia (MCG), a leading academic medical center and Georgia's health sciences university comprising the Schools of Dentistry, Allied Health Sciences, Graduate Studies, Medicine, and Nursing, and an affiliated health care system, is the only academic institution in the state of Georgia dedicated exclusively to the health sciences. MCG's School of Dentistry, ranked in the top tier of the nation's dental schools, has embarked on an ambitious effort to enhance and expand its research enterprise. The School has committed to investing significant resources to establish and pursue a bioengineering and regenerative medicine research program and now seeks an outstanding academic scientist (tenure track) to build and lead this strategic initiative.

The Director will be charged with catalyzing a world-class research program in basic mechanisms of tissue regeneration, especially related to craniofacial structures. A multidisciplinary, cross-campus research effort, the program will span fundamental, translational, and clinical research focusing on restoration of tissue function. This is an excellent opportunity for an innovative, entrepreneurial scientist to build on the School's strengths in biomaterials, biomaterials-tissue interactions, bone biology, oral disease, and orofacial disease and systemic conditions to leverage and expand scientific collaborations with the School of Medicine, Georgia Institute of Technology and others to advance the mission of MCG and the School of Dentistry.

The ideal candidate will be an academic leader (PhD, DDS/DMD or MD) with an outstanding record of grant support, scientific achievement, and peer-reviewed publications, and the capacity for faculty and student recruitment, development, and leadership. Competitive start-up package, research facilities, and staffing allocations will be offered to attract and build a critical mass of top-flight researchers.

Electronic submission of inquiries, referrals, and resumes with a cover letter preferred and should be sent in confidence to: Sarah Herman, Isaacson, Miller, 334 Boylston St., Boston, MA 02116; e-mail: 3041@imsearch.com; fax: 617-262-6509. Application deadline will be until this position is filled. MCG is an EOE/AA/ADA employer.

LCLS Instrument Scientists

The Linac Coherent Light Source Project (LCLS) at the Stanford Linear Accelerator Center (SLAC) will construct the world's first X-ray Free Electron Laser, providing a unique research tool for the study of ultra-fast phenomena within the fields of biology, chemistry, materials science, and physics. We currently have opportunities for four Instrument Scientists who will each have responsibility for preparing specifications and managing the design, construction and commissioning of one x-ray science instrument.

The four instruments will be designed for:

Atomic physics applications in the soft x-ray range (800-2000 eV)
Studies of laser-induced transient states using hard x-ray diffraction
X-ray imaging of non-periodic nanoscale samples including biological molecules
Studies of dynamics in materials using x-ray photon correlation spectroscopy

Applicants for these positions should have a PhD in physics, chemistry, or biology. Demonstrated experience with one of the areas of x-ray science listed above is preferred and experience with the development of complex scientific instruments is essential. Previous project management experience, as in the construction of a synchrotron beamline, is also desirable. Applicants must have the ability to work effectively within a large project environment.

For immediate consideration, please apply online at:
http://www-public.slac.stanford.edu/hr/jobs/. Please apply to one of the following requisition numbers: 029701, 029702, 029703 or 030240.

Stanford University is an Affirmative Action/Equal Opportunity Employer.

SLAC
STANFORD LINEAR ACCELERATOR CENTER

ASSISTANT PROFESSOR IN ECOLOGY

The Department of Biology at Washington University in St. Louis invites applications to a faculty position in **Ecology at the Assistant Professor level**. We are searching broadly, without regard to taxa, or system, for individuals who integrate theory with empirical studies across levels of biological organization. We are particularly interested in field ecologists who study organisms in their natural environments, as well as microbial ecologists. The individual must possess a Ph.D. and have strong commitments to developing an externally funded, internationally recognized, research program, and contribute significantly to both the undergraduate and graduate curricula through teaching and mentorship. Successful candidates will join a growing initiative at Washington University to enhance research and teaching in ecology, and will complement its strengths in other areas of biological and environmental sciences.

We particularly encourage applicants whose research would at least partially contribute to the design and execution of an integrative research program in Biology at Washington University. Resources include a ~810 hectare Tyson Research Center (**http://www.biology.wustl.edu/tyson/**) and the ~1000 ha Shaw Nature Reserve of the Missouri Botanical Garden (**http://www.shawnature.org/**). These facilities have a diverse flora and fauna in a mixture of natural and restored terrestrial and aquatic ecosystems.

For further information on the Department of Biology, see **www.biology.wustl.edu**, and on Environmental Studies, see **levee.wustl.edu/enst/**. To apply, please send a curriculum vitae, a statement of research interests, a statement of teaching experience and philosophy, copies of important publications, and arrange to have 3 letters of reference sent electronically to **ecology.search@biology2.wustl.edu**. If you are unable to submit electronically, you may mail your application and references to: **Ecology Assistant Professor Search, Washington University, Department of Biology, Campus Box 1137, One Brookings Drive, St. Louis, MO 63130-4899.** Review of applications will begin on **August 31, 2005**, and will continue until a suitable candidate is found.

Washington University is committed to excellence through diversity, and we particularly encourage applications from persons from underrepresented groups. Washington University is an Affirmative Action Employer.

Post Doctoral Positions
American Museum of Natural History

The Division of Invertebrates at the American Museum of Natural History in New York City has four Post Doctoral positions available and two Computer Programmers. Term positions for two years.

1. **Algorithm Scientist** will perform research and implementation of algorithms for full-genome phylogenetic and biogeographic analysis. **Required:** Ph.D. in computational science; exp in algorithm design, especially combinatorial optimization problems; programming skills for prototyping; exp in string/parallel algorithms and computational bio desired.
2. **System Scientist** will perform R&D of a computational system to integrate results of whole genome phylogenetic analysis with geographic and phenotypic data. **Required:** Ph.D. in computational science; exp in data modeling/development of middleware and user interfaces for larger-scale data management across diverse research sites; exp in geographical info systems; Java skills pfd.
3. **Virology Scientist** will develop sequencing and annotation strategies for sets of viral genomes. **Required:** Ph.D. in biology with significant exp in virology methods and high throughput technologies.
4. **GIS/Systematics Scientist** will perform analysis using Geographic Information Systems. **Required:** Ph.D.; skills in Java programming and application development; ability to travel occasionally.
5. **Computer Programmers** will be involved in the implementation of algorithms for full-genome phylogenetic and biogeographic analysis of the evolution of diverse genomic systems. **Required:** BS/MS in computer science or engineering; min 3 yrs' exp in scientific computation; exp in UNIX/LINUX environments and knowledge of at least one functional language (ML, Lisp, Haskell); Ocami or ML and C language pfd.

Please fax replies to **212-769-5277** indicating your position of interest and salary requirement.

EOE

OHSU | OGI SCHOOL OF SCIENCE & ENGINEERING

The Gordon and Betty Moore Chair
OGI School of Science and Engineering
Oregon Health and Science University

Distinguished applicants are encouraged to apply for the endowed **Gordon and Betty Moore Chair** at OHSU's OGI School of Science and Engineering. As an integrated part of the only academic health center in Oregon, OGI is uniquely positioned to bring advanced science, computational and engineering methodologies to bear on complex problems of human and environmental health. For more information about OGI and OHSU, please visit our website at www.ogi.edu.

We seek an investigator whose established research program(s) at the interface between advanced technology and human and environmental health will complement the existing strengths of our faculty. We are particularly interested in candidates whose research, interdisciplinary interests, vision, and leadership qualities will result in the creation of a world-class nanobiotechnology research and graduate education center that will leverage high-level collaborations with OHSU's research and patient care communities as well as with other institutions in Oregon.

Qualified applicants are encouraged to submit a letter of application, a curriculum vitae, and a summary of research and educational objectives to:

Dr. William H. Glaze, Associate Dean
Gordon and Betty Moore Chair Search Committee
OGI School of Science and Engineering
Oregon Health and Science University
20000 NW Walker Road, Mail Code OGI-801
Beaverton, OR 97006-8921

Electronic submissions may be sent to: **hendricc@ohsu.edu**

OHSU is an Affirmative Action, Equal Opportunity Institution.

International Max Planck Research School
PhD Program in Structure and Function of Biological Membranes

Max Planck Institute of Biophysics
Max Planck Institute of Brain Research
Goethe University
Frankfurt am Main, Germany

Several PhD fellowships are available in the International Max Planck Research School in Frankfurt. The two Max Planck Institutes and research groups at Frankfurt University offer a unique environment for the study of biological membranes and membrane proteins. PhD opportunities exist in internationally leading laboratories in the areas of membrane protein structure determination, membrane biochemistry, molecular biology and functional studies by electrophysiological and spectroscopic methods as well as studies of whole membranes, cells and organelles.

Highly qualified candidates with degrees in biochemistry, chemistry, physics, biology, medicine or related subjects are invited to apply for the next round of admission in November 2005. Application forms can be downloaded from the website of the Research School at *www.mpibp-frankfurt.mpg.de/research-school.* Completed application forms and two letters of reference should arrive not later than **31 August 2005**.

For further details please contact:
Dr. Janet Vonck , MPI of Biophysics, Max-von-Laue-Str. 3,
60438 Frankfurt am Main, Germany
Tel: +49+69-6303-3004/3001
Fax: +49+69-6303-3002
E-mail: Research.School@mpibp-frankfurt.mpg.de

NIST
National Institute of Standards and Technology
Technology Administration, U.S. Department of Commerce

PROTEIN CHEMIST

Applications are invited for candidates to establish a Protein Analysis and Characterization program with applications to proteomics measurements and standards in the Cell and Tissue Measurements Group, Biotechnology Division, at NIST in Gaithersburg, Maryland. The Cell & Tissue Measurements Group focuses on the development and validation of measurement methods for research in quantitative cell and systems biology. Protein science is a strategic priority of the Division.

The successful candidate will have a unique opportunity to develop a research program in advanced analytical methodologies related to measuring proteins which are expressed and/or secreted by cells (quantitative cell biology). This individual will be responsible for developing protein analysis, peptide mass fingerprinting, developing methods for the detection and quantitation of proteins in a complex matrix, and for developing procedures for protein extraction, isolation, and purification. More information on the Cell and Tissue Measurements Group can be found at **http://www.cstl.nist.gov/biotech/index.html**. Applicants must have demonstrated experience in leading and managing research, and a record of sustained scholarly accomplishments. Ideal candidates will have training and experience in protein and peptide analysis as well as in the analysis aspects of protein chemistry. A Ph.D. in the biological/chemical sciences is desired.

NIST is a non-regulatory federal agency within the U.S. Commerce Department's Technology Administration. NIST's mission is to develop and promote measurement, standards, and technology to enhance productivity, facilitate trade, and improve the quality of life.

The base salary ranges from $60,000 to $95,000, depending on qualifications. *U.S. citizenship is required.* Applicants should send a resume and three references (names and contact information only) by post or e-mail to: **Dr. Henry Rodriguez, Leader, Cell & Tissue Measurements Group, Biotechnology Division, NIST, 100 Bureau Drive, MS 8313, Gaithersburg, MD 20899**; **henry.rodriguez@nist.gov**. Applications should be received by **August 26, 2005**. At **www.usajobs.opm.gov** see **NIST-ASF-2005** for Biologist or Chemist.

Department of Commerce is an Equal Opportunity Employer.

Shanghai Genomics Inc.

Shanghai Genomics, a GNI Ltd. subsidiary, is a fast-growing global biopharmaceutical company. Located in the dynamic Zhangjiang Hi-Tech Park, Shanghai Genomics occupies a 30,000 square foot modern facility within China's biggest biotechnology cluster. Our mission is to develop novel therapeutic products for cancer and inflammation. To further our current research programs, we are looking for enthusiastic individuals to join our growing team.

Director/Project Leader - Cell and Molecular Biology

Responsibilities include participation in the overall research plan design and frequent communication with corporate partners. A Ph.D. and 2-5 years of postdoctoral experience are required. Must have excellent communication and organizational skills. Experience in biochemical kinase assays, cell cycle/apoptosis assays, and/or siRNA assays is highly preferred. Relocation to Shanghai, China or Fukuoka, Japan is required. For Fukuoka position, candidate must be fluent in Japanese.

Director - Animal Model Studies

Responsibilities include establishment of cancer and inflammation models in house. A Ph.D. and 2-5 years of postdoctoral experience are required. Industry experience is highly preferred. Must be able to work independently and to train and supervise junior level research associates. Experience with Xenogen's imaging system is a plus.

Director - Protein Biochemistry

Responsibilities include supervising a group of research associates to produce recombinant proteins. A Ph.D. with a strong background in protein biochemistry and a solid publication record are required. Must have strong problem-solving capabilities. Familiarity with E.coli, baculovirus, and mammalian protein expression systems is essential. Experience with various protein purification methods is highly preferred.

Project Leader - Nuclear Receptor Studies

Responsibilities include leading a group of research associates to set up biochemical and cell-based assays for nuclear receptors. The ideal candidate will have a Ph.D. degree and postdoctoral experience in nuclear receptor studies. Must be able to communicate fluently in English and interact well with corporate partners. Familiarity with protein-protein interaction assays is required.

We provide a stimulating working environment, a high level of professional and intellectual challenge, and a very competitive compensation package. Interested individuals may apply by specifying their job of interest and sending their resumes by e-mail to **bd@shanghaigenomics.com**. For additional information, please go to ***www.shanghaigenomics.com***. Address: 647 Song Tao Road, Building #1, Zhangjiang Hi-Tech Park, Pudong New Area, Shanghai 201203, P. R. China. Tel: 86-21-50802786, Fax: 86-21-50802783.

Job Announcement Position: Assistant/Associate/Full Professor Forage Breeding and Genetics/Genomics.

Description: The Department of Crop and Soil Sciences, University of Georgia, Athens GA, invites applications for a 12-month tenured/ tenure-track position, 70% research and 30% instruction. The successful candidate will combine traditional and genomic technology to develop improved cultivars and germplasms of forages, with emphasis in alfalfa, clover and tall fescue adapted to the Southeastern U.S. with flexibility to solve other agricultural problems based on industry needs and program direction. The successful candidate is expected to attract extramural funding, release improved cultivars and germplasms, and publish results from the program in peer reviewed journals.

The successful candidate must be committed to excellence in teaching and graduate student training. A contemporary plant breeding course will be taught biannually to undergraduate and graduate students. The successful candidate will also team teach a forage management course and develop a general interest undergraduate course related to agriculture and/or environmental sciences. The successful candidate will be expected to direct graduate student research projects and serve on graduate student advisory committees.

The position may be filled at the assistant, associate, or full professor level depending on the qualifications and experience of the selected individual. Qualifications include a Ph.D. degree in plant breeding, plant genetics, or closely related disciplines, and a demonstrated ability to work collaboratively, obtain extramural funding and publish results. Training or experience in forage or range management and molecular techniques is desirable. The successful candidate will have access to state-of-the-art laboratory and greenhouse facilities and field research stations.

Other Information: Athens, home of the University of Georgia, is located in Northeast Georgia at the foothills of the Appalachian Mountains, approximately 60 miles northeast of downtown Atlanta. UGA is a comprehensive university with approximately 35,000 students in14 schools and colleges: Agricultural and Environmental Sciences, Arts and Sciences, Business, Education, Environment and Design, Family and Consumer Sciences, Forest Resources, Graduate School, Journalism and Mass Communication, Law, Pharmacy, Public and International Affairs, Social Work, Veterinary Medicine. The Department of Crop and Soil Sciences resides in the College of Agricultural and Environmental Sciences along with the departments of Agricultural and Applied Economics, Agricultural Leadership, Education, and Communication, Animal and Dairy Science, Biological and Agricultural Engineering, Entomology, Environmental Health Science, Food Science and Technology, Horticulture, Plant Pathology, Poultry Science. The College operates at three campuses throughout the state - the main campus in Athens, GA, Coastal Plain Experiment Station in Tifton, GA and Georgia Experiment Station in Griffin, GA. The Department of Crop and Soil Sciences has teaching, research and extension faculty resident at all three locations which conduct basic and applied research that is important to clientele throughout the state of Georgia and that adds to the body of knowledge basic to agricultural production and environmental preservation throughout the world. Research in the department is classed into five general areas: 1. Crop Breeding and Genomics; 2. Crop Management and Physiology; 3. Weed Management; 4. Turfgrass Management; and 5. Environmental Sciences including Soil, Atmospheric Physics, Fertility, Water, and Waste Management.

Applicants should send their letter of application, CV, four letters of reference, and transcripts to: **Dr. Wayne Hanna, Search Committee Chair, 3111 Plant Sciences, University of Georgia, Athens, GA 30602-7272**. A review of applications will begin on **September 15, 2005** and continue until the position is filled or the search closed.

The University of Georgia is an Affirmative Action/Equal Opportunity Employer. Women and/or minorities are encouraged to apply.

POSITIONS OPEN

FACULTY POSITION
Pharmaceutical Chemistry
University of Kansas

The Department of Pharmaceutical Chemistry, University of Kansas (**website: http://www.pharm.ku.edu/contentm/gen/school_of_pharmacy_generated_pages/Department_Information_m95.html**) invites applications for a full-time, tenure-track faculty position at the **ASSISTANT, ASSOCIATE,** or **FULL PROFESSOR** level for the 2006–2007 academic year. Preference will be given to candidates interested in the broad application of physical or physical-organic chemistry to pharmaceutical problems related to drug formulation, stabilization, delivery, and/or analysis, utilizing state-of-the-art technology including, but not limited to, high resolution nuclear magnetic resonance and mass spectrometry. See **website: http://jobs.ku.edu** for the full announcement. The candidate should demonstrate a strong potential for research and scholarship for appointment at the rank of Assistant Professor, or a proven record of research and scholarship, commensurate with rank, for appointment at the level of Associate or Full Professor. The review process will begin after September 1, 2005, and continue until the position is filled. Complete applications will include: a letter of application, curriculum vitae, a concise summary of past research and future research plans, and three letters of recommendation. Contact: **Dr. Christian Schöneich, Department of Pharmaceutical Chemistry, The University of Kansas, 2095 Constant Avenue, Lawrence, KS 66047-3729. Telephone: 785-864-4880.** *Equal Opportunity/Affirmative Action Employer.*

The Department of Medicine at the University of California San Francisco (UCSF) is recruiting physician-scientists engaged in translational research. Candidates must have an M.D. or M.D./Ph.D. degree and demonstrated potential to lead a first-rate and independent research program. Board certification in internal medicine is required. Appointments will be made at the **ASSISTANT/ASSOCIATE PROFESSOR** level in the In-Residence series, depending upon qualifications. The candidate will also become a member of the graduate program in biomedical sciences. Please send curriculum vitae to:

Joseph M. McCune, M.D., Ph.D.
Chair, Search Committee
Gladstone Institute of Virology and Immunology
1650 Owens Street
San Francisco, CA 94158

UCSF is an Affirmative Action/Equal Opportunity Employer. The University undertakes affirmative action to assure equal employment opportunity for underutilized minorities and women, for persons with disabilities, and for Vietnam-era veterans and special disabled veterans.

ASSISTANT PROFESSOR OF BIOLOGY (IMMUNOLOGY)

Applications are invited for a tenure-track position in biology at the level of Assistant Professor beginning fall 2006. We seek applicants who are committed to excellence in teaching at the undergraduate level and who are dedicated to developing an active research program that engages students. Full ad and details are available at **website: http://www.macalester.edu/provost/positions/.** Send letter of application, curriculum vitae, statement of teaching philosophy and research plans, and three letters of reference to:

Dr. Lin Aanonsen
Chair, Department of Biology
Macalester College
St. Paul, MN 55105
E-mail: aanonsen@macalester.edu

Applications should be received by 15 October 2005. *Macalester is an Equal Opportunity/Affirmative Action Employer that prides itself on providing support for excellence in teaching and in faculty scholarship.*

POSITIONS OPEN

MICROBIOLOGIST
University of Victoria
Victoria, British Columbia, Canada

The Department of Biochemistry and Microbiology invites applications for a tenure-track **ASSISTANT PROFESSOR** position in microbiology. The University of Victoria offers excellent research infrastructure, particularly in proteomics, genomics, ocean sciences, forest biology, and medical research. There are ample opportunities to collaborate with other microbiologists not only in this Department but also in the Biology Department and in the newly established Island Medical Program. Applications are thus welcomed from scientists in any area of molecular microbiology. The appointee will be expected to develop a rigorous, independent research program, funded by external support, and participate in the teaching activities of the Department. The expected start date is July 1, 2006.

Qualifications include a Ph.D., postdoctoral experience, and demonstrated research and teaching excellence. Letters of application, clearly outlining the candidate's expertise and research interests, along with curriculum vitae and names and contact information of at least three references should be sent by September 15, 2005, to:

Dr. C. G. Cupples, Chair
Department of Biochemistry and Microbiology
University of Victoria
P.O. Box 3055 STN CSC
Victoria, BC V8W 3P6
Canada
E-mail: biocmicr@uvic.ca
Website: http://web.uvic.ca/biochem

All qualified applicants are encouraged to apply; however, in accordance with Canadian immigration requirements, Canadians and permanent residents will be given priority.

The University of Victoria is an Equity Employer and encourages applications from women, persons with disabilities, visible minorities, Aboriginal peoples, people of all sexual orientations and genders, and others who may contribute to the further diversification of the University.

ASSISTANT PROFESSOR, BIOLOGY

Applications are invited for a tenure-track position to begin August 2006. Teaching responsibilities will include contributing to introductory/intermediate biology courses and an upper-division course in developmental biology. The successful candidate will be expected to develop an active research program involving Master's level and undergraduate students. Area of research is open but should attract extramural funding. Postdoctoral research and some teaching experience preferred. Applicants should submit a letter of application, curriculum vitae, reprints, statements of research interests and teaching philosophy, and three letters of recommendation, no later than September 9, 2005, to:

Dr. George Mourad
Chair, Search Committee
Department of Biology
Indiana University-Purdue University
Fort Wayne, Fort Wayne, IN 46805-1499
E-mail: mourad@ipfw.edu
Website: http://www.ipfw.edu/bio/

An Affirmative Action/Equal Opportunity/Equal Access Employer.

FACULTY POSITION
Institute of Molecular and Cellular Biology
National Taiwan University

The Institute is seeking an outstanding individual to fill a full-time faculty position available on August 1, 2006. The level of appointment is open. The specific research area is open, but it should be related to molecular and cellular biology. Applicants should send curriculum vitae (including publication list), a brief outline of proposed research and teaching course(s), and three recommendation letters to: **Chair, Faculty Search Committee, Institute of Molecular and Cellular Biology, National Taiwan University, No. 1 Sec. 4 Roosevelt Road, Taipei, Taiwan 10617. Website: http://cell.lifescience.ntu.edu.tw/english/index.htm.** The deadline for receipt of materials is November 15, 2005.

POSITIONS OPEN

FACULTY POSITION IN IMMUNOLOGY/PATHOLOGY

The University of Utah School of Medicine, Department of Pathology, seeks qualified candidates in immunology for a tenure-track position at the **ASSISTANT/ASSOCIATE PROFESSOR** level, with emphasis on host responses to bacterial, viral, or parasitic infections.

Candidates should have a Ph.D. and/or M.D., and a record of scholarly, laboratory-based achievements with strong potential for independent extramurally funded research.

Preference will be given to individuals who submit curriculum vitae and a brief statement of current and future research prior to October 1, 2005. Please include names of three individuals who can provide recommendation letters on your behalf. Contact:

C/o Janis Weis, Ph.D.
Department of Pathology
University of Utah
School of Medicine
30 N 1900 East Room 5C124
Salt Lake City, UT 84132
Website: http://www.path.utah.edu/cbi/index.htm

The University of Utah is an Equal Opportunity/Affirmative Action Employer.

BIOCHEMIST/MOLECULAR BIOLOGIST
Bryn Mawr College

The Department of Biology invites applications for a tenure-track faculty position in biochemistry/molecular biology at the rank of **ASSISTANT PROFESSOR.** We are searching for an individual who will thrive in an environment that combines teaching and research. The successful candidate is expected to teach at all levels of the curriculum and establish an externally funded research program that provides rigorous collaborative research projects for undergraduates. Candidates with research interests that complement the College's interdisciplinary program in environmental studies are particularly encouraged to apply. A Doctorate and at least one year of postdoctoral research experience are required. Submit curriculum vitae, statement of research and teaching interests, and arrange for three letters of recommendation to be sent by October 3, 2005, to: **Chair, Biology Search, Department of Biology, Bryn Mawr College, and 101 N. Merion Avenue, Bryn Mawr, PA 19010-2899.** Located in suburban Philadelphia, Bryn Mawr College is a highly selective liberal arts college for women who share an intense intellectual commitment, a self-directed and purposeful vision of their lives, and a desire to make meaningful contributions to the world. Bryn Mawr comprises an undergraduate college with 1,200 students, as well as coeducational graduate schools in some humanities, sciences, and social work. The College supports faculty excellence in both teaching and research, and participates in consortial programs with the University of Pennsylvania, and Haverford and Swarthmore Colleges. *Bryn Mawr College is an Equal Opportunity/Affirmative Action Employer. Minority candidates and women are especially encouraged to apply.*

POSTDOCTORAL FELLOW

A Postdoctoral Fellowship studying experimental cerebral ischemia is available in the Department of Neurosurgery at Stanford University School of Medicine. Candidates for the fellowship should have a Ph.D. or M.D. degree, with experience in cellular and molecular techniques, apoptosis, and cell signal pathways or cerebral vasculature and angiogenesis research. Experience in the field of stroke research is desirable but not necessary. Please send curriculum vitae and brief description of your interest to: **Heng Zhao, Ph.D., Department of Neurosurgery, Stanford University School of Medicine, Stanford, CA 94305-5327. E-mail: hzhao@stanford.edu.**

FACULTY
CANCER BIOLOGIST AND POSTDOCTORAL POSITIONS

UNIVERSITY OF ILLINOIS

The UIC College of Dentistry in Chicago has recently launched an interdisciplinary program to re-engineer cancer care and dental education utilizing an NIDCR U24 infrastructure grant. We need senior/junior scientists and postdoctoral research associates to join existing strong interdisciplinary cancer and tissue regenerative researchers under this new program. The assembled research teams will develop research to improve the prevention, diagnosis, treatment, quality of life, and reconstruction of patients with oropharyngeal cancer and patients with adverse oral reactions to cancer therapy. For additional information, go to: **http://dentistry.uic.edu/research/u24**.

The College is seeking applicants for **full-time tenure-track researchers at the rank of Assistant/Associate/Full Professor in the area of cancer biology**. Preference will be given to candidates who have, or are willing to develop, a research focus in oral/head and neck cancer, or oral mucositis. Required qualifications include a Ph.D. in basic biomedical sciences (or advanced clinical degree with applicable research training), evidence of high quality research experience and publication in cancer biology, and ability to generate external funding. Clinician-scientists are encouraged to apply. Salary commensurate with experience and qualifications. Two postdoctoral research associate positions are also available. Applications will be accepted until positions are filled. For fullest consideration, respond by August 15, 2005. Applicants should submit a cover letter, C.V., names of three references, and a description of research interests and plans to S. Odmark, UIC College of Dentistry, 801 S. Paulina St. (M/C 621), Chicago, IL 60612. Please reference Job Code **APU24CB** in your cover letter.

AA/EOE.

EXELIXIS™
UNDERSTANDING DISEASE, CREATING CURES

What are the qualities that differentiate a good biotechnology researcher from one who is great? That perfect blend of intelligence, integrity and insight. Boldness balanced by discipline, the ability to set and achieve high personal goals and to thrive on collaboration.

What are the qualities that differentiate a good biotechnology company from a great one? That perfect blend of innovation and pragmatism; an unwavering focus on goals and an unrelenting dedication to execution.

What makes Exelixis a great company? The answer is obvious.

Exelixis Plant Sciences (EPS), based in Portland, Oregon is a wholly-owned subsidiary of Exelixis, Inc. EPS is dedicated to the discovery and production of high value products for improved nutrition and health. We are currently offering exciting career opportunities at our Plant Sciences Division in Portland, OR.

INFORMATICS RESEARCH SCIENTIST I

Working in collaboration with designated leaders program leaders, you'll improve and develop databases and informatics tools for all projects at EPS. Requires Doctoral degree (PhD); and a minimum of six months related experience and/or training plus experience programming in multiple programming languages. Experience analyzing genetic, chemistry, and/or biological data, and experience with software and database design also required.

BIOCHEMICAL ENGINEER

Plan, design, and implement fed-batch high cell density cell culture process development, optimization and scale–up primary recovery operations, and tech transfer. Requires Doctoral degree (PhD) in Biochemical Engineering and a minimum of 2 years of related experience.

We also have the following available at our South San Francisco, CA location:

RESEARCH SCIENTIST II

We are seeking a highly motivated scientist to join a new Exelixis program in stem cell biology. Our ideal candidate will have significant research experience in the fields of hematopoietic, cardiac, endocrine, or neural stem cells, or the role of stem cells in cancer. Requires a Ph.D. in the biological sciences with at least 3 years of postdoctoral experience in mammalian stem cell biology.

EOE

To apply, please visit the careers section of our website at: **www.exelixis.com**.

National Institute on Aging

Department of Health and Human Services
National Institutes of Health
National Institute on Aging
Behavioral and Social Research Program (BSR)

http://www.nia.nih.gov/ResearchInformation/ExtramuralPrograms/BehavioralAndSocialResearch

Health Scientist Administrator Opportunity for Specialist in Behavioral/Population Genetics Vacancy Announcement Number NIA-05-66442A

BSR is seeking an individual with expertise in behavioral/population genetics, or strong genetics/social science research. BSR is an Extramural Research Program, with a strong interdisciplinary focus, that supports basic research and training in a wide variety of disciplines.

The National Advisory Council on Aging, workgroup on genetics (May 2004), advised that BSR continue to expand the integration of genetics with behavioral and social sciences. The successful candidate will take the lead in implementing their recommendations, including:

- Developing criteria for priority setting within the growing genetics and genomics portfolio
- Assembling a small expert group to discuss priority areas that focus on bringing together social sciences and genetics, to produce a more focused statement of what should be pursued
- Exploring specific topics that might be particularly tractable
- Supporting interdisciplinary training programs for behavioral geneticists
- Linking social and behavioral sciences to genomics activity at the NIH and elsewhere.

The successful candidate will demonstrate independent research experience plus progressive responsibility in research program administration. This position will challenge someone with vision, skills and insight to take a growing program to new heights. Responsibilities of this position include:

- Providing scientific leadership, defining short-range and long-term goals for research integrating genetics and the social-behavioral sciences in studies on aging
- Developing areas of scientific research emphasis by inviting grant applications
- Identifying research areas warranting increased or decreased funding emphasis
- Serving as project officer on wide-ranging and cutting-edge behavioral research studies
- Serving as spokesperson for agency programs in dealing with the scientific community, the Congress, and other Federal agencies.

Health Scientist Administrator Opportunity for Specialist in Biodemography Vacancy Announcement Number NIA-05-66442B

BSR is seeking to fill a Health Scientist Administrator position. Interested candidates must have expertise in or knowledge of demography and biological sciences to plan and develop an interdisciplinary portfolio of research and training grants, drawing on the intersection of population sciences, genetics, and evolutionary theories of aging. Experience with biomarkers, clinical physiology, physical anthropology, and performance measures in large scale longitudinal studies and surveys is a plus. Candidates should have doctorate level training in the areas specified, independent research experience, and progressive responsibilities in research program administration. This position will challenge someone with skill, vision and insight to take a growing program to new heights.

Responsibilities of this position include:

- Providing scientific leadership, defining short-range and long-term goals for research integrating genetics and the social-behavioral sciences in studies on aging
- Developing areas of research emphasis by inviting grant applications from the scientific community
- Identifying research areas warranting increased or decreased funding emphasis
- Serving as project officer on wide-ranging and cutting-edge behavioral research studies on aging
- Serving as spokesperson for agency programs in dealing with the scientific community, the Congress, and other Federal agencies.

Salary is commensurate with qualifications and research experience, and time for independent research may be negotiated. For qualifications, evaluation criteria, and application instructions see **http://www.usajobs.opm.gov/**. Search by Vacancy Announcement Number. For info contact **Pat Boyce** at **410-558-8032**. Applications must be received by **September 30, 2005**.

DHHS and NIH are Equal Opportunity Employers.

POSITIONS OPEN

University of Nebraska Medical Center

College of Dentistry, **RESEARCH ASSISTANT PROFESSOR.** The University of Nebraska Medical Center (UNMC) College of Dentistry, Department of Oral Biology, has a full-time, nontenure-track position available October 1, 2005. The successful candidate is expected to establish a strong research program in cell signaling aspects of cancer biology. Superb opportunities for research are available as the Department expands its research programs. Applicants with a research focus compatible with departmental goals are encouraged to apply. Ph.D. or equivalent degree and postdoctoral experience required. Review of applications will continue until the position is filled. Applications for this position, #0755, are being accepted online at **website: http://jobs.unmc.edu.** *The University of Nebraska Medical Center is an Equal Opportunity/Affirmative Action Employer.*

TENURE-TRACK FACULTY
Department of Neurosciences
Medical University of South Carolina, Charleston

Tenure-track faculty position in the Department of Neurosciences (40 percent teaching, 60 percent research). A Ph.D or M.D. in a neuroscience-based program is required with a demonstrated interest in teaching medical neuroscience and maintaining an active research program. Significant experience and success with teaching and research is essential. Prior experience as a course director would be an asset. Applicants must apply online at **website: http://www.musc.edu/hrm/careers/faculty.htm.** Position requisition number is 041783.

Applicants should also submit online a one-page summary outlining research and teaching vision, a current curriculum vitae, three references, and a cover letter expressing their interest and qualifications addressed to: **Dr. Ed Soltis, Department of Neurosciences, Medical University of South Carolina, 173 Ashley Avenue, BSB 403, Charleston, SC 29425.** *The Medical University of South Carolina is an Equal Employment Opportunity/Affirmative Action Employer.*

SIX POSTDOCTORAL FELLOWSHIPS FOR FIELDWORK ON ENDANGERED SPECIES

The Zoological Society of San Diego seeks to fill six Millennium Postdoctoral fellowships for fieldwork in its Department of Conservation and Research for Endangered Species (CRES). Projects will be carried out in Brazil (ecology and behavior of the muriqui), the Caribbean (reintroduction of rock iguanas), Australia (koala population ecology), California (translocation biology of kangaroo rats), New Zealand (kiwi: behavioral ecology), and Zambia (ecology and behavior of African wild dogs).

Appointments will be for three years with the possibility of extension to five years (maximum). Candidates must be Ph.D. qualified with no more than three years postdoctoral experience. Stipends begin at $41,796. Additional funds for travel and field expenses are provided. Applications, including curriculum vitae, reprints, and names and addresses of three referees, should be addressed to: **Zoological Society of San Diego, San Diego Zoo's Wild Animal Park, Attn: Human Resources (Millennium Postdoctoral Fellowship Program), 15500 San Pasqual Valley Road, Escondido, CA 92027-9614, U.S.A.** Closing date: August 31, 2005.

POSTDOCTORAL, MOLECULAR NEUROSCIENCE

Postdoctoral wanted for molecular neuroscience laboratory with focus on sensory transduction and homeostatic regulation. The successful candidate has published at least one highly visible paper and is fluent in molecular biology. Experience with *C. elegans* is a great plus. See latest review article at **website: http://jp.physoc.org/cgi/content/abstract/jphysiol.2005.088963v1. Webpage: http://neurobiology.mc.duke.edu/CTN/faculty/liedtke/. E-mail: wolfgang@neuro.duke.edu.**

POSTDOCTORAL POSITIONS supported by the NIH are available for self-motivated, enthusiastic individuals with Ph.D. degree and experience in molecular biology, cell biology, and/or genetics, to study the mechanism of a novel nuclear protein (we identified very recently) and other cofactors with chromatin remodeling activities in hormone signaling mediated by the nuclear receptors, in control of cell cycle, and in breast cancer and prostate cancer. We currently utilize multiple approaches including functional genomics (expression microarray and chromatin immunoprecipitation-chip) and proteomics, viral vector-mediated gene transfer and RNA interference, and genetically modified mice for tumorigenic study and drug target discovery. Other approaches can be found in publications (see: *Cell* **98:**675, 1999; *Science* **294:**2507, 2001; *Proc. Natl. Acad. Sci.* **100:**2226, 2003; *Mol. Cell. Biol.* **24:**5157, 2004). Our laboratory is at the highly interactive Cancer Center of the University of California at Davis. Annual salary is commensurate with experience. Please send a letter of interest, curriculum vitae, and contact information of three references via e-mail to:

Hongwu Chen, Ph.D.
Department of Medical Biochemistry and Molecular Medicine
UCDMC Research III
University of California at Davis
Davis, CA 95817
E-mail: hwzchen@ucdavis.edu

POSTDOCTORAL POSITION
Microbial Immunology/Cell Signaling

A position is available to study immunological and cell signaling aspects of *Mycobacterium* species relevant to occupational respiratory diseases. Research will involve pathogen-macrophage interactions, in vitro and in vivo cellular immune response, identification of novel protein antigens for investigating pathogenesis, and immunodiagnosis, among other molecular signaling and microbiological techniques. Required qualifications are a Ph.D. degree in microbiology or biological sciences and relevant experience in immunological, proteomic, and molecular techniques. Apply to:

Dr. Jagjit S. Yadav
Department of Environmental Health
University of Cincinnati Medical Center
Cincinnati, OH 45267
Telephone: 513-558-4806
E-mail: jagjit.yadav@uc.edu

A position is available for a **POSTDOCTORAL ASSOCIATE** in the area of signal transduction at SUNY-Buffalo. The regulation of signal transduction (mitogen-activated protein [MAP] kinase) pathways is of central importance to the understanding of cell behavior, development, and human health. Our laboratory is interested in defining connections between Cdc42-coupled receptors and MAP kinase pathway activation. Qualified applicants should have a Ph.D. and experience in molecular, biochemical, and preferably genomics approaches. The successful applicant will have the opportunity for independent project development and should be careful, disciplined, and self-motivated. To apply, please contact: **Dr. Paul J. Cullen** at **e-mail: pjcullen@buffalo.edu.** *The Research Foundation SUNY-Buffalo is an Affirmative Action/Equal Opportunity Employer.*

Physicians' Education Resource (PER) is seeking a Continuing Medical Education (CME) **MEETINGS CONTENT COORDINATOR** to join its team.

Successful candidates will be responsible for developing the scientific content for medical meetings by working closely with program committee members, overseeing the invitation and confirmation of faculty to speak at these meetings, writing CME documentation, reviewing presentations for scientific accuracy/completeness, creating slide sets upon request, and advising faculty on lecture content. This full-time position requires a Ph.D. in a biomedical science and is located in Dallas, Texas. E-mail resume and salary requirements to: **Human Resources Director** at **e-mail: hr@perlp.com.**

POSTDOCTORAL, RESEARCH, AND CLINICAL FELLOWSHIPS
at the
National Institutes of Health
U.S. Department of Health and Human Services

Website: http://www.training.nih.gov

NIH is dedicated to building a diverse community in its training and employment programs.

SCHOLAR SCIENTIST AND ASSOCIATE DIRECTOR
Florida State University Marine Laboratory

The Florida State University Marine Laboratory (FSUML) is recruiting a full-time Scholar Scientist to serve as the Associate Director for Research, Teaching, and Outreach. The position will be based at the facility on the Gulf of Mexico, 45 miles from FSU's main campus in Tallahassee. The successful candidate will be expected to maintain an extramurally funded research program based at the FSUML in an area that is complementary with the missions of the FSUML, which include oceanography, marine biology, coastal ecology, fisheries biology, and marine archeology. In addition, this individual will manage the day-to-day research, education, and outreach operations of the FSUML and be the liaison between FSU main campus faculty and the FSUML. The successful candidate will be expected to work with the Director of the FSUML to define and implement a renewed commitment by FSU to emphasize marine science and will be assisted by a laboratory manager. Minimum qualifications include a Ph.D. in an appropriate science, leadership skills, administration experience, national or international scientific reputation, and a demonstrated ability to attract research funding. A courtesy appointment with the appropriate academic department at Florida State University is expected. Salary and rank will be commensurate with experience. Evaluation of applications will begin August 1, 2005, and continue until the position is filled. More information can be found at **website: http://www.marinelab.fsu.edu/.** Please send cover letter, curriculum vitae, research statement, and the names and contact information of three references to: **Marine Lab Search, 109 Westcott, Florida State University, Tallahassee, FL 32306** or electronically to **e-mail: marinesearch@research.fsu.edu.** Questions can be addressed to: **Don Levitan** (**e-mail: levitan@bio.fsu.edu**). *The Florida State University is an Equal Opportunity/Affirmative Action Employer, committed to diversity in hiring, and a Public Records Agency.*

The College of Sciences and Mathematics at Auburn University located in Auburn, Alabama (**website: http://www.auburn.edu/cosam**) is seeking candidates for the position of **POSTDOCTORAL FELLOW** in the sciences and mathematics. From time-to-time, postdoctoral positions become available under a variety of research grants and projects in the College. We are seeking applications from individuals with a Ph.D. in any one area such as: biology, chemistry, geology, geography, mathematics, statistics, physics, or related fields. Successful foreign applicants must meet eligibility requirements to work in the United States. The positions are available for a minimum of one year as full-time, 12-month, with renewal possible. Salary will be commensurate with education and experience. Review of applications will begin after July 1, 2005, and continue throughout the year as positions become available. Please send curriculum vitae, statement of research interests, along with a list of three references and contact information to:

Dr. Marie Wooten
Associate Dean for Research
COSAM, 315 Roosevelt Concourse
Auburn University, AL 36849
E-mail: wootemw@auburn.edu
Fax: 334-844-5748

Minorities and women are encouraged to apply.
Auburn University is an Affirmative Action/Equal Opportunity Employer.

POSITIONS OPEN

UCLA

POSTDOCTORAL POSITION available at the University of California at Los Angeles (UCLA) to study role of the interleukin-4 receptor signaling pathways in allergic inflammation. Requires strong background in signal transduction and cellular immunology, and in vivo allergic models. Send curriculum vitae and names of three references to: **Dr. Talal Chatila, Department of Pediatrics, UCLA. E-mail: tchatila@mednet.ucla.edu.**

ASSISTANT/ASSOCIATE PROFESSOR

The Department of Comparative Biomedical Sciences is seeking a tenure-track Assistant/Associate Professor (Physiologist). The Department has numerous well-funded investigators in cell and molecular biology. Required qualifications: Ph.D. or equivalent degree in physiology and/or biological/biomedical sciences. Additional qualifications desired: D.V.M. degree; postdoctoral experience; ability to teach comparative vertebrate physiology of multiple-organ systems. Primary responsibilities: coordinates a two-semester, team-taught, physiology course in the veterinary professional curriculum; maintains a competitive, extramurally funded research program. Salary and rank will be commensurate with qualifications. Application deadline is August 26, 2005, or until candidate is selected. Submit letter of application and resume (including e-mail address) to:

Dr. Gary E. Wise, Professor and Head
Comparative Biomedical Sciences
School of Veterinary Medicine
Louisiana State University
Reference #000097
Baton Rouge, LA 70803
Telephone: 225-578-9889
E-mail: gwise@vetmed.lsu.edu

Louisiana State University is an Equal Opportunity/Equal Access Employer.

POSTDOCTORAL POSITIONS: Several Postdoctoral positions funded by the National Institutes of Health are available, to study the roles of insulin, nitric oxide, and protein tyrosine phosphatases in regulation of vascular smooth muscle cell signaling and neointima formation in vascular injury. Our projects address important basic science questions and also have relevance to clinical problems. Experience in molecular biology and/or rat and mouse surgery is essential. Competitive salaries are offered. Please send curriculum vitae and the names of three references to: **Dr. Aviv Hassid, Department of Physiology, University of Tennessee, 894 Union Avenue, Memphis, TN 38163. E-mail: ahassid@tennessee.edu; fax: 901-448-7126.** *The University of Tennessee is an Equal Employment Opportunity/Affirmative Action/Title IV/Title IX/Section 504/ADA/ADEA Institution in the provision of its education and employment programs and services.*

The Division of Endocrinology, Department of Medicine, University of Oklahoma Health Science Center has several **POSTDOCTORAL RESEARCH POSITIONS** available to investigate the role of cellular redox state and reactive oxygen species in vascular cell biology. This work is part of collaborative projects funded by the National Institutes of Health and entails studies on endothelial cell biology and redox-sensitive signal transduction. Candidates should have expertise in transgenic mouse models, molecular biology, and signal transduction. Knowledge in diabetes is a plus. Please send curriculum vitae and three references to: **Ming-Hui Zou, M.D., Ph.D., Department of Medicine Endocrinology, P.O. Box 26901, BSEB 302, Oklahoma City, OK 73190. E-mail: ming-hui-zou@ouhsc.edu.** *University of Oklahoma is an Equal Employment Opportunity/Affirmative Action Employer, Minorities/Females/Persons with Disabilities.*

POSITIONS OPEN

FELLOWSHIP TRAINING IN IMMUNOLOGY AND INFECTIOUS DISEASE RESEARCH
Indiana University School of Medicine

Post- and predoctoral fellowships are available in immunology and infectious diseases research supported by an NIH training grant. Candidates should have an interest in basic or translational research related to cellular and innate immunology, viral and bacterial pathogenesis, vaccine biology, and biodefense. Trainees will be mentored by faculty from microbiology and immunology, biochemistry and molecular biology, medicine, and pediatrics at Indiana University School of Medicine with formal training in grant writing and research ethics. Visit **website: http://www.iupui.edu/~micro/imm_inf_trgn_prog.html** for a list of research areas and mentors. *Candidates must be U.S. citizens or permanent residents.* Applicants are invited to contact faculty listed on the program website and should also send curriculum vitae with three references to:

Janice S. Blum, Ph.D.
Microbiology and Immunology
Indiana University
School of Medicine
420 MS, 635 Barnhill Drive
Indianapolis, IN 46202-5124
E-mail: jblum@iupui.edu

Indiana University is an Affirmative Action/Equal Opportunity Employer. Qualified minority applicants are encouraged to apply.

RESEARCH STAFF SCIENTIST

Applications are invited for a Research Scientist position in the Oncology Research Institute (ORI) at Sioux Falls, South Dakota. ORI is part of the South Dakota Health Research Foundation (SDHRF), which is a partnership between the University of South Dakota School of Medicine and Sioux Valley Hospitals and Health System. This particular position is in the Gynecologic Oncology Laboratory that focuses on human papilloma virus (HPV)/cervical cancer research. An academic appointment with the University of South Dakota School of Medicine is available for this position based on qualifications and experience.

Applicants must have a Ph.D. or equivalent in biomedical sciences with at least three years of postdoctoral research training in molecular biology. Prior experience in HPV research is a plus as well as previous experience doing research with a clinician. Excellent oral and written communication and personnel skills are essential in addition to being highly self-motivated and disciplined.

Applicants should submit a letter of interest, curriculum vitae, and the contact information of three references to: **Human Resources, South Dakota Health Research Foundation, 1100 East 21st Street, Suite 700, Sioux Falls, SD 57105. Fax: 605-328-1355; e-mail: bpoppens@usd.edu.**

Applications will be accepted until the position is filled. Review of applications will begin on July 25, 2005, until a suitable candidate is found.

SDHRF is an Equal Opportunity/Affirmative Action Employer.

SENIOR RESEARCH FELLOW/ INSTRUCTOR POSITION

An excellent opportunity for career development with conversion to a Junior Faculty Appointment. This position will study signal transduction, transformation, and apoptosis in cancer. Ongoing project areas include regulation of cell death by tumor necrosis factor-related apoptosis-inducing ligand and PS-341, transformation by the Pim protooncogene, and the molecular function of TEL/AML1. Individuals should possess a strong background in molecular, cellular biology, or protein chemistry.

Interested candidates should forward a copy of their curriculum vitae and three professional references to: **Andrew S. Kraft, M.D., Director, Hollings Cancer Center, 86 Jonathan Lucas Street, P.O. Box 250955, Charleston, SC 29425. E-mail: recruit@musc.edu. Reference ad #205.**

POSITIONS OPEN

UCLA

POSTDOCTORAL POSITION available at the University of California at Los Angeles (UCLA) to study role of FOXP3 in peripheral tolerance. Requires strong background in molecular biology, cellular immunology, and in vivo transgenic approaches. Send curriculum vitae and names of three references to: **Dr. Talal Chatila, Department of Pediatrics, UCLA. E-mail: tchatila@mednet.ucla.edu.**

FORUM

INDO-U.S. SCIENCE AND TECHNOLOGY FORUM
Fulbright House, 12 Hailey Road, New Delhi 110 001
Second Call for Proposals 2005–2006

The Indo-U.S. Science and Technology Forum (Forum) seeks to support collaborations between U.S. and Indian institutions in frontier areas of science and technology that are of mutual interest. **Website: http://www.indousstf.org.** We aim to facilitate efforts designed to be catalytic in nature by involving the best and brightest investigators in a broad distribution among all science and technology disciplines including science, engineering, biomedical research, and mathematics.

The Forum seeks to support innovative programs aimed to stimulate interactions that have a strong potential for generating follow-on activities and building long-term Indo-U.S. science and technology relationships. We are also mandated to promote contacts between the next generation of scientists and foster active public-private partnership.

The Forum solicits proposals on a four-monthly cycle, jointly submitted by the U.S. and Indian principal investigators from academia, private research, and development entities (including industry/non-governmental organizations) and government-funded institutions/laboratories towards: (A) bilateral workshop, conference, symposium, and round table, etc.; (B) travel grants for joint project-based activities already awarded/supported in U.S. or Indian institutions; support for extended stay up to additional eight to 10 weeks; and for specific exploratory/planning missions aimed at developing large-scale bilateral collaboration; (C) knowledge research and development networked and public-private networked Indo-U.S. centers.

The detailed formats for application can be downloaded from our **website: http://www.indousstf.org** under the title 'call for proposals' or by **e-mails: amitra@indousstf.org** or **mcheetham@si.edu.** Joint proposals may be submitted by 15 September 2005 simultaneously by e-mails to both the mail addresses. We expect the award decision to be made by 10 December 2005.

ANNOUNCEMENTS

Proposal for **RESEARCH COLLABORATION** relating to specific high affinity protein/oligopeptide design (groundbreaking new concept, U.S. provisional patent application). The ideal partner is a company or academic institute with interest for peptide receptor-ligand and antigen-antibody interactions and has access to routine cloning and protein-expression-library screening techniques. All replies will be held in confidence.

E-mail: jan.biro@sbcglobal.net; website: http://www.janbiro.com/Homulus.html.

CONFERENCE

Biotech and Life Sciences Global Venture Congress 2005

Madison Square Garden, August 25 to 26, 2005. Nobel Laureate Dr. Eric Chivian, Plenary Session.

Conference to address the venture capital landscape, identify current trends in innovation, learn key technologies and scientific discoveries, and discover emerging biotech and life sciences companies (**website: http://bio.saeclub.com**).

AWARDS

Rosenstiel Award
Oceanographic Science

The **Rosenstiel School of Marine and Atmospheric Science of the University of Miami** seeks nominations for the **Rosenstiel Award**. The Rosenstiel Award is presented annually to recognize outstanding achievement and distinction in oceanographic science. The intent of the award is to recognize younger, mid-science career individuals who have contributed substantially towards new directions or understanding in their field. The 2006 award (including a prize of $10,000) will be presented for excellence in the field of marine affairs and policy, specifically in integrated coastal zone management, climate change and environmental decision-making, international ocean policy development, and human dimensions of marine resource allocation.

Nominations, including a curriculum vitae and the names of three referees, should be sent by **September 15, 2005** to:

Dr. J.A. Gifford
Rosenstiel Award Search Committee
Division of Marine Affairs and Policy
Rosenstiel School of Marine
and Atmospheric Science
4600 Rickenbacker Causeway
Miami, FL 33149-1098

jgifford@rsmas.miami.edu

GRANTS

Think Mitochondria

UMDF Research Grant Program
♦ Request for Proposals ♦

UMDF Redefining Hope

UNITED MITOCHONDRIAL DISEASE FOUNDATION

The United Mitochondrial Disease Foundation (UMDF) is seeking new, innovative research to continue its mission to find cures and better treatments for mitochondrial illnesses.

Proposals will be considered in basic science and clinical areas and must fall under at least one of the following categories:

- Seed money for new researchers
- Post-doctoral fellowship
- New area of research for experienced investigators

Letter Of Intent (LOI) Application and additional information about the grant process is available on the UMDF web site at www.umdf.org or by contacting the UMDF office.

Deadline: The UMDF must receive LOI by September 16, 2005. Incomplete LOI or those received past the deadline will not be considered. FAX transmittal is not acceptable.

Contact Information: UMDF Research Grant Program, 8085 Saltsburg Rd, Suite 201, Pittsburgh, PA 15239 USA, Tel: (412) 793-8077, Fax: (412) 793-6477, Email: jean@umdf.org

Novagen®

Didn't you know?

GeneJuice®

Transfection Reagent is formulated for minimal cytotoxicity & maximum effectiveness on a vast range of cell lines

Use GeneJuice.
Cells love it.
So will you.

For more information on GeneJuice and Novagen's other transfection reagents visit: **www.novagen.com/transfection**

Germany	0800 6931 000
UK	0800 622935

or contact your local sales office

Merck Biosciences

Calbiochem | Novabiochem | Novagen

DNA TRANSFECTION REAGENTS

What!

You didn't use GeneJuice?

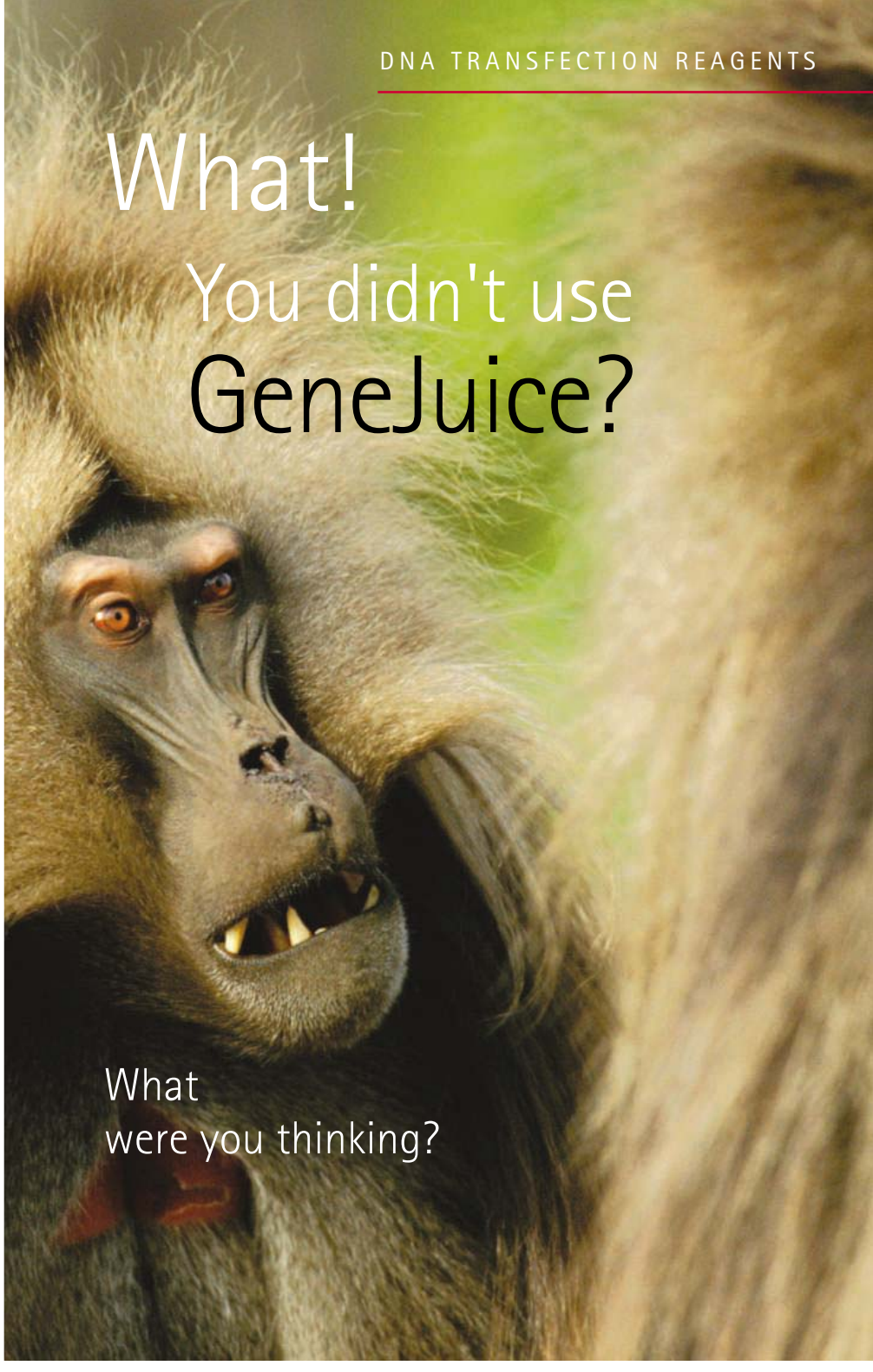

MERCK